



TalentDetector

**TalentDetector2025_Winter
INTERNATIONAL STUDENTS SCIENTIFIC
CONFERENCE**

**Scientific editor:
Mirosław Bonek**

Department of Engineering Materials and Biomaterials,
Faculty of Mechanical Engineering,
Silesian University of Technology
31th January 2025
Gliwice, Poland



Katedra Materiałów
Inżynierskich i Biomedycznych

Katedra Materiałów Inżynierskich i Biomedycznych**Wydział Mechaniczny Technologiczny****Politechnika Śląska**

ul. Konarskiego 18a, 44-100 Gliwice tel. +48 (32) 2371322

Redakcja techniczna i skład komputerowy:

dr h.c. dr hab. inż. Mirosław Bonek, prof. PŚ

Recenzenci:

M. Bonek, W. Borek, A. Czupryński, S. Dinescu, A. Drygała, B. Gitolendia, K. Gołombek, A. Kania, M. Kciuk, A. Kloc-Ptaszna, M. Kremzer, M. Król, B. Krupińska, L. Kuchariková, S. Lesz, G. Matula, C. Meran, M. Musztyfaga-Staszuk, D. Pakuła, O. Polishchuk, M. Polok-Rubiniec, M. Spilka, M. Sroka, M. Staszuk, M. Szindler, A. Śliwa, E. Tillová, M. Uhrčík, A. Włodarczyk-Fligier, B. Ziębowicz

Materiały są opublikowane na podstawie oryginałów dostarczonych przez Autorów, zaopiniowanych przez Zespół Recenzentów.

Wydano za zgodą:

Kierownika Katedry Materiałów Inżynierskich i Biomedycznych
Wydziału Mechanicznego Technologicznego
Politechniki Śląskiej

Wydawca:

Katedra Materiałów Inżynierskich i Biomedycznych
Wydział Mechaniczny Technologiczny
Politechnika Śląska
Gliwice 2025

Wszystkie opublikowane materiały stanowią utwór podlegający ochronie na mocy prawa autorskiego. Utwór ten w całości ani we fragmentach nie może być powielany ani rozpowszechniany za pomocą urządzeń elektronicznych, mechanicznych, kopiujących, nagrywających i innych. Ponadto utwór ten nie może być umieszczany ani rozpowszechniany w postaci cyfrowej zarówno w Internecie, jak i w sieciach lokalnych, bez pisemnej zgody posiadacza praw autorskich.

Seria wydawnicza:

Prace Katedry Materiałów Inżynierskich i Biomedycznych
Wydział Mechaniczny technologiczny
Politechnika Śląska
Publikacja: styczeń 2025

ISBN 978-83-65138-42-2

INTERNATIONAL STUDENTS SCIENTIFIC CONFERENCE
TALENTDETECTOR2024_WINTER
SILESIA UNIVERSITY OF TECHNOLOGY, GLIWICE, POLAND
31TH JANUARY 2025

The International Student Scientific Conference TalentDetector2025_Winter aims to integrate the student and scientific community dealing with topics related to material technologies. It is a place that gives the opportunity to exchange experiences, knowledge, skills and present current scientific achievements, developing and expanding students' interests in the field of materials engineering, surface engineering, biomaterials and biomedical engineering, nanotechnology, pro-ecological technologies and computer materials science. The conference allows for the presentation of projects conducted with the industry as part of the activities of Student Scientific Circles, doctorates, projects implemented in the form of PBL - Project Based Learning as part of the Excellence Initiative - Research University at the Silesian University of Technology, projects in the framework of EURECA PRO/European University in Responsible Consumption and Production and international bilateral cooperation between Universities.

CONFERENCE ORGANIZER

Materials Science Circle of the Association of Alumni of the
Silesian University of Technology, Gliwice, Poland



CONFERENCE CO-ORGANIZER

Department of Engineering Materials and Biomaterials, Faculty
of Mechanical Engineering, Silesian University of Technology,
Gliwice, Poland



INTERNATIONAL SCIENTIFIC COMMITTEE

prof. Mirosław Bonek dr h.c., Silesian University of Technology, Gliwice, Poland - *President of the International Scientific Committee*

prof. Marcin Adamiak, Silesian University of Technology, Gliwice, Poland
prof. Sedat Alkoy, Gebze Technical University, Gebze, Turkey
prof. Rafał Babilas, Silesian University of Technology, Gliwice, Poland
prof. Stela Dinescu, University of Petroșani, Petroșani, Romania
prof. Ahmet Durgutlu, Gazi University, Ankara, Turkey
prof. Boris Gitolendia, Georgian Technical University, Tbilisi, Georgia
prof. Afrim Gjelijaj, University of Pristina, Pristina, Kosovo
prof. Adam Grajcar, Silesian University of Technology, Gliwice, Poland
prof. Alexander Horn, Laserinstitut Hochschule Mittweida, Mittweida, Germany
prof. Volkan Kılıçlı, Gazi University, Ankara, Turkey
doc. Lenka Kuchariková, University of Zilina, Zilina, Slovakia
prof. Martin Kusy, Slovak Technical University in Bratislava, Trnava, Slovakia
prof. Grzegorz Matula, Silesian University of Technology, Gliwice, Poland
prof. Janusz Mazurkiewicz, Silesian University of Technology, Gliwice, Poland
prof. Serhii Matiukh, Khmelnytskyi National University, Khmelnytskyi, Ukraine
prof. Cemal Meran, Pamukkale University, Denizli, Turkey
prof. Oleh Polishchuk, Khmelnytskyi National University, Khmelnytskyi, Ukraine
prof. Mykola Skyba, Khmelnytskyi National University, Khmelnytskyi, Ukraine
prof. Tomasz Tański, Silesian University of Technology, Gliwice, Poland
doc. Miroslava Tavodova, Technical University in Zvolen, Zvolen, Slovakia
prof. Eva Tillova, University of Zilina, Zilina, Slovakia

ORGANIZING COMMITTEE*Chairman*

prof. Mirosław Bonek dr h.c.

prof. Klaudiusz Gołombek	dr. Marek Kremzer
prof. Sabina Lesz	dr. Anna Kloc-Ptaszna
prof. Janusz Mazurkiewicz	dr. Mariusz Król
prof. Małgorzata Musztyfaga-Staszuk	dr. Beata Krupińska
prof. Daniel Pakuła	dr. Magdalena Polok-Rubinić
prof. Marek Sroka	dr. Magdalena Szindler
prof. Marcin Staszuk	dr. Marek Szindler
prof. Agata Śliwa	dr. Anna Włodarczyk-Fligier
prof. Adam Zarychta	dr. Anna Woźniak
dr. Wojciech Borek	dr. Bogusław Ziębowicz
dr. Aleksandra Drygała	Ksenia Czardyban MSc
dr. Rafał Honysz	Amadeusz Dziwis MSc
dr. Aneta Kania	Wojciech Mikotejko MSc
dr. Monika Kciuk	Sichale Worku Fita MSc

TalentDetector HISTORY

The International Student Scientific Conferences TalentDetector from 10 edition (since 2018) have been a place for the exchange of experience, knowledge, skills and presentation of students' current scientific achievements in the field of materials engineering, surface engineering, biomaterials and biomedical engineering since the 8th edition. As part of the conference, two international scientific monographs, TalentDetector_Summer and TalentDetector_Winter, are published annually, which already contain over 600 scientific articles resulting from the implementation of PBL, EURECA PRO, Students Scientific Cycles projects and projects with secondary school students with international authors. Participation in the form of presentations and posters in TalentDetector International Student Scientific Conferences allows members of the project teams to integrate the student and scientific community of the Silesian University of Technology as well as young staff from foreign research centres in Austria, Czech Republic, Ethiopia, Ghana, Georgia, Iran, Romania, Slovakia, Ukraine and Turkey, dealing with topics related to materials technologies.

Scientific monographs are prepared based on articles, mostly with international authors, reviewed by an international scientific committee.

The initiative of the cyclical organization of the International Student Scientific Conference TalentDetector significantly expands activities in the field of student education, organizational and popularization activities for the scientific community related to materials engineering at the national and international level.

Thanks to extensive international cooperation, over 180 articles were published free of charge.

The history of TalentDetector in numbers:

2018

TalentDetector 2019 (Gliwice)

Number of articles: 59

Number of authors: 206

Number of countries: 1

2021

TalentDetector2021_Winter (Gliwice)

Number of articles: 37

Number of authors: 134

Number of countries: 2

TalentDetector2021_Summer (Zawiercie)

Number of articles: 57

Number of authors: 173

Number of countries: 3

2022

TalentDetector2022_Winter (Gliwice)

Number of articles: 79

Number of authors: 179

Number of countries: 4

TalentDetector2022_Summer (Wista)

Number of articles: 79

Number of authors: 176

Number of countries: 4

2023

TalentDetector2023_Winter (Gliwice)

Number of articles: 73

Number of authors: 143

Number of countries: 6

TalentDetector2023_Summer (Brenna)

Number of articles: 105

Number of authors: 173

Number of countries: 9

2024

TalentDetector2024_Winter (Gliwice)

Number of articles: 82

Number of authors: 135

Number of countries: 7

TalentDetector2024_Summer (Gliwice-Zilina)

Number of articles: 84

Number of authors: 147

Number of countries: 8

Number of cooperating universities: 12

Gazi University, Ankara, Turkey

Gebze Technical University, Gebze, Turkey

Georgian Technical University, Tbilisi, Georgia

Khmelnitskyi National University, Khmelnytskyi, Ukraine

Laserinstitut Hochschule Mittweida, Mittweida, Germany

Pamukkale University, Denizli, Turkey

Silesian University of Technology, Gliwice, Poland

Slovak Technical University in Bratislava, Trnava, Slovakia

Technical University in Zvolen, Zvolen, Slovakia

University of Petroșani, Petroșani, Romania

University of Pristina, Pristina, Kosovo

University of Zilina, Zilina, Slovakia



31th January 2025
Gliwice, Poland

DEPARTMENT OF ENGINEERING MATERIALS AND BIOMATERIALS
FACULTY OF MECHANICAL ENGINEERING
SILESIA UNIVERSITY OF TECHNOLOGY

INTERNATIONAL STUDENTS SCIENTIFIC CONFERENCE

Contents

VOLUME 1

Manufacturing Of The NiTi Orthodontoc Arcwire Bahri Can Abaci	1
Zinc Oxide (ZnO) Nanostructures for Dye-Sensitized Solar Cells - A Scientific Review Elizabeth Addae, Wojciech Sitek, Marek Szindler	6
Dislocation Strengthening of PTAW NiCrBSi Coatings by Varying Arc Currents: Insights from EBSD and XRD Augustine Nana Sekyi Appiah, Krzysztof Matus, Evans Atioyire, Pawel Nuckowski, Marcin Adamiak	15
Modern grinding technologies: innovative methods for processing various materials Jennifer Badora, Julia Muszyńska, Mirosław Bonek	21
Assessment of the Anticipated Economic Efficiency of the Sheet Feeder and Turner Device for a Printing Machine Tea Baramashvili, Nini Baidoshvili	27
Impact of Technological Parameters of Steel Laser Cutting on the Quality of Large-Scale Finished Products Piotr Bąk, Mirosław Bonek	32
Topological optimization of the drone frame Natalia Bijok, Sylwia Dziwoki, Kinga Stępska, Martyna Urbańska, Jan Wypiór, Magdalena Hulbój, Emilia Krzystanek, Krzysztof Goczko, Mariusz Król	42
Materials for the automotive industry - characteristics and challenges of the automotive industry Zofia Błaszczuk, Paulina Dymara, Szymon Szczotka, Barbara Grzegorzczuk.....	48

Effects of welding parameters on ferrite-austenite phase balance in RSW of lean duplex stainless steel Zbigniew Brytan, Beatrice N.A. Ardayfio, Afrim Gjelaj, Besart Berisha, Wojciech Pakieła, Tomasz Poloczek, Bernard Wyględacz	56
Application of carbon materials in the production of dye-sensitized solar cells Jakub Budzynowski, Kacper Argalski, Oskar Górka, Szymon Jeż, Aleksandra Drygała, Sabina Lesz, Adam Zarychta, Klaudiusz Gołombek, Janusz Wyrwał, Marek Kremzer, Wojciech Pakieła, Bartosz Drygała, Eva Tillová, Peter Palček.....	62
The impact of laser modification of the surface layer of tool steels on tribological properties Julia Chudy, Bartosz Filip, Julia Haraf, Kacper Krysiak, Katarzyna Furman, Mirosław Bonek, Stela Dinescu, Oleh Polishchuk.....	70
Integration of Laser Technology with Advanced Surface Engineering Methods Julia Chudy, Bartosz Filip, Julia Haraf, Szymon Jędrzejewski, Antonina Olszewska, Mateusz Paluch, Karolina Rogalewska, Wiktoria Wanczura, Mirosław Bonek, Eva Tillova, Oleh Polishchuk, Stela Dinescu.....	76
Classification of structural steel grades using artificial intelligence Anil Can Erbus, Tommaso Giacomelli, Rafał Honysz.....	84
Contemporary Challenges and Opportunities in the Production of Bionic Prosthetics Rafał Gabryś, Jakub Pająk, Julia Dąbrowska, Arkadiusz Górniak, Maksym Cinal, Magdalena Polok-Rubiniec, Anna Włodarczyk-Fligier, Aneta Kania.....	91
Characteristics of steel for automotive industry Jakub Głąbek, Magdalena Koźlik, Jan Parzyk, Łukasz Porwolik, Marek Wojtynek, Paweł Baranek, Gabriela Fojt-Dymara, Barbara Grzegorzczak	95
Wytwarzanie laminatów stosowanych w personalnych osłonach balistycznych Michał Głogowski, Julia Pindur, Karolina Romberg, Klaudiusz Gołombek, Piotr Sakiewicz	102
Galwaniczne nakładanie powłok ochronnych Wojciech Golec, Jakub Zorychta, Amelia Krupińska, Agnieszka Zaleska, Santina Topolska	108
Application of a 3D scanner in the process of designing a hand model for a disabled person Arkadiusz Górniak, Maksym Cinal, Rafał Gabryś, Jakub Pająk, Julia Dąbrowska, Magdalena Polok-Rubiniec, Anna Włodarczyk-Fligier, Aneta Kania.....	118

The impact of vinyl record wear on the quality of the gramophone signal: a frequency band analysis Wiktorija Groelich, Daria Gatner, Maria Bieńkowska, Bogusław Ziębowicz, Michał Kręcichwost.....	122
Application of Advanced Computational Mathematics for Flight Mechanics of Aircraft Luka Guraspashvili, Ramili Zukakishvili	130
Nitinol in aircrafts Samir Haitham Samir Abdelaziz , Givi Sanadze	135
Porovnanie vlastností polotovarov z polymérneho kompozitu používaného pri termoformovaní Rastislav Hanulík, Lenka Markovičová, Mirosław Bonek	140
Comparison of natural and hydroponic farming – advantages, disadvantages, and development prospects Karolina Hanzlik, Monika Kruczyńska, Estera Nawrocka, Paweł Kruczyński, Grzegorz Pośpiech, Aneta Kania, Anna Włodarczyk-Fligier, Magdalena Polok-Rubinić	147
Laser surface treatment Martyna Herman, Eryk Badurski, Jakub Stęplewski, Mirosław Bonek.....	153
Optimization of Urban Transport Systems Based on a Mobility Study Valeri Jajanidze, Boris Gitolendia, Giorgi Mikiashvili	160
Comparison of selected materials used in the manufacture of upper limb prostheses Sebastian Jakubik, Marta Marianek, Mikołaj Micoła, Agata Ociepka, Jakub Osuch, Jakub Painta, Justyna Ryś, Jakub Wieczorek, Anna Włodarczyk-Fligier, Magdalena Polok-Rubinić, Aneta Kania	166
Tribological properties of CrN coating applied to aluminum alloy substrate Justyna Janoszka, Natalia Puchała, Natalia Zaręba, Marcin Staszuk, Daniel Pakuła	171
Eco-friendly technology of laser cutting for engineering materials Bartłomiej Jóźwiak, Nikodem Juszczak, Mirosław Bonek	179
Characterization of the crystalline silicon solar cells using advanced research techniques Ryszard Kała, Jan Czembor, Daniel Foks, Adam Popis, Kacper Kuczera, Janusz Wyrwał, Barbara Grzegorzczak, Aleksandra Drygała	186
Investigating the Hard Tungsten Carbide Coating formed on H13 Steel Surfaces via Electro-Spark Deposition Technique Ahmet Kavukcu, Berke Gültekin, Salim Levent Aktuğ, Metin Usta.....	194

Innovative laser technology for surface treatment of engineering materials Stanisław Kiełkowski, Mateusz Król, Mirosław Bonek.....	202
Characterization of a Fused-Thiophene and Naphthalenediimide-based Polymer for Multilayer Organic Solar Cells Wioletta Klimek, Maciej Gajdemski, Sebastian Gralla, Ammara Aslam, Marek Szindler, Krzysztof Lukaszewicz, Przemysław Ledwoń	209
The temperature and humidity influence on compressive strength of the concrete made of expanded clay and recycled aggregates in time of curing Nicole Kocierz, Barbara Słomka-Słupik	216
Biomimetic Materials in Everyday Products – The Cases of Spider Silk and Velcro. Microscopic investigations Tomasz Kołodziej, Wiktor Rudek, Anna Kloc-Ptaszna, Daniel Pakuła, Marcin Staszuk	224
Research on the structure and chemical composition of PVD coatings deposited on tool ceramics Michał Kopciowski, Krzysztof Hlubek, Marcin Staszuk, Daniel Pakuła	231
Analiza rozkładu naprężenia i odkształcenia haka holowniczego Helena Kordecka, Julia Quaeck, Wojciech Mikołajko, Amadeusz Dziwis, Agata Śliwa, Marek Sroka	237
Stereolithography in the design and manufacturing of Fresnel lenses Emilia Krajewska, Jakub Kuta, Michał Pietruszka, Olaf Sobek, Błażej Łagosz, Michalina Ziółkowska, Marek Szindler, Błażej Tomiczek, Magdalena Szindler	244
Utilization of LIDAR data for PSMNet training Tomasz Kukuczka, Marcin Paszkuta, Dariusz Myszor, Eryk Szmyt, Danel Sobieraj, Paweł Michalski, Krzysztof Pawełczyk, Michał Polończyk	250
Farebné leptanie grafitických liatin Denis Kulas, Alan Vaško	255
ZnO coatings deposited by the ALD method in the application of colored silicon solar cells Dawid Lazaj, Grzegorz Józef Nowak, Sebastian Nowak, Michalina Ziółkowska, Julia Popis, Magdalena Szindler, Marek Szindler	263
Mechanical Recycling of Aluminum Cans Using to Increase the Mechanical Properties of Gypsum Prefabs Bogdan-Ioan Marc, Oana-Denisa Boantă	269

Tribological studies of CrN coating obtained by PVD on austenitic steel surface X2CrNiMo17-12-2 Tobiasz Markowicz, Jakub Pluskota, Benjamin Sobczak, Daniel Pakuła, Marcin Staszuk	275
Development of a computer model and simulation of three-point bending test using the Gleeble 3800 simulator Michał Masoń, Wojciech Borek	283
Technologies for the production of carbon fiber components in the automotive industry Kamil Mazelanik, Bogusław Ziębowicz	289
Korózná odolnosť nehrdzavejúcich ocelí po plazmovej nitridácii Erik Meliš, Viera Zatkaliková	296
Predictive Maintenance on Medium Voltage Cable Production Extrusion Machine Cemal Meran, Berranur Ceker, Sezai Kunan, Murat Mat, Koksai Ilhan	304
Predictive Maintenance on Rod Break Down Machine Cemal Meran, Aysenur Kabukcu, Dilruba Yavas, Mustafa Furkan Orha, Fatih Oztekin	312
Production of Cable That Changes Color at 60 °C Temperature Cemal Meran, Kaan Kucuk, Ali Cagin Hatipoglu, Omer Eren	319
Modelowanie układu nóż stożkowy – uchwyt nożowy do urabiania skał Wojciech Mikołajko, Piotr Cheluszka, Agata Śliwa, Jarosław Mikuła	325
Analiza rozkładu naprężeń występujących w ciernym układzie hamulcowym Mateusz Musialik, Alan Nowak, Łukasz Mann, Daniel Pella, Amadeusz Dziwis, Wojciech Mikołajko, Agata Śliwa	334

VOLUME 2

Structure of CoCrFe, CoFeNi, CoCrNi medium entropy alloys obtained by induction melting Sandra Nadolna, Bartosz Żary, Miłosz Ferdyn, Michał Podgórski, Maxymilian Żukowski, Katarzyna Młynarek-Żak, Monika Spilka, Rafał Babilas	342
Corrosion resistance and hardness of CoCr(Fe,Ni) and CoFeNi medium entropy alloys Sandra Nadolna, Bartosz Żary, Miłosz Ferdyn, Michał Podgórski, Maxymilian Żukowski, Katarzyna Młynarek-Żak, Monika Spilka, Rafał Babilas.....	349

Symbiosis of AI and material science: ChatGPT as a catalytic factor in advanced material processing and analysis Nicoleta Negru	354
Revolutionizing industrial energy management: low-cost IoT solutions for sustainable optimization and enhanced efficiency Nicoleta Negru	363
Stabilization of electric power networks Kamil Oleksy, Bartosz Nikiel, Kajetan Kojm, Łukasz Lomania, Szymon Szeja, Kacper Krysiak, Cezary Zach	372
Möbius strip-shaped track for superconductor levitation: design and prototyping Emil Pająk, Wiktoria Łowczycka, Alicja Jankiewicz, Błażej Tomiczek.....	378
Analysis of the influence of technological parameters of the laser cutting process of steel on the quality of finished large-size products Mateusz Paluch, Piotr Bąk, Szymon Jędrzejewski, Hubert Przybyszewski, Szymon Szeja, Wiktoria Wanczura, Mirosław Bonek, Eva Tillova, Oleh Polishchuk.....	386
Laser cutting Roksana Pałczyńska, Norbert Klęk, Mirosław Bonek	394
Metal determination methods, cyto- and genotoxicity assays for PM _{2.5} Jakub Pawlikowski, Krzysztof Będkowski, Karolina Wołoszyn, Nikola Ochman, Paweł Kolak, Paweł Wranik, Elwira Zajusz-Zubek, Małgorzata Adamiec-Organisiok, Magdalena Węgrzyn, Magdalena Skonieczna, Jacek Nowak, Anna Mainka	400
Characterization of crystalline solar cells using various microscopes Mateusz Pfeifer, Dominik Szendzielorz, Jakub Rusek, Małgorzata Muszyfaga-Staszuk, Aleksandra Drygała, Krzysztof Wiśniewski, Marcin Staszuk	409
Aplikácie ložiskových ocelí Mária Pilarčíková, Igor Gajdáč	417
Computer simulation of marine propeller loading Jakub Polis, Jakub Bicz, Radosław Trojnar, Zuzanna Buchaj, Agata Śliwa, Marek Sroka	425
Computer simulation of dental implant loading Jakub Polis, Jakub Bicz, Radosław Trojnar, Zuzanna Buchaj, Dominik Śliwa, Marek Sroka, Agata Śliwa.....	434

Polymer biocomposites based on biodegradable binders, reinforced with plant-derived fibers for 3D printing Oleg Polishchuk, Mirosław Bonek, Andrii Polishchuk, Serhii Matiukh, Svitlana Lisevich, Artem Tolstiuk.....	443
Technologies for processing carbon fibers into finished products using extrusion Andrii Polishchuk, Mirosław Bonek, Oleg Polishchuk, Serhii Matiukh, Svitlana Lisevich, Yevhen Harbar	455
Design and construction of a hydroponic chamber Grzegorz Pośpiech, Estera Nawrocka, Paweł Kruczyński, Monika Kruczyńska, Karolina Hanzlik, Aneta Kania, Magdalena Polok-Rubinić, Anna Włodarczyk-Fligier	467
History of sound recording - from the phonograph to the digital era Katarzyna Ptasznik, Bogusław Ziębowicz, Anna Ziębowicz.....	473
Investigations of the materials structure and morphology using light microscopy Alicja Rachubka, Magdalena Grabysz, Marta Ostaficzuk, Monika Kciuk	481
Properties of Uncommon Elements Coatings (Ir, Ta, Re): A Comprehensive Overview Karolina Rogalewska, Magdalena Polok-Rubinić	485
Selected research methods for the characterization of photovoltaic materials Bartosz Rybak, Paweł Pietraszek, Tymoteusz Tarnawski, Aleksandra Drygała, Małgorzata Musztyfaga-Staszuk, Jakub Budzynowski, Bartosz Drygała, Marcin Staszuk, Judyta Drygała	493
Activated carbon: Properties, modifications and environmental applications Kinga Rzepiak, Wiktoria Kroczyk, Karol Kukuła, Ewa Puszczała, Anna Marszałek, Gabriela Kamińska, Grzegorz Michalski	499
Analiza wytrzymałościowa klucza imbusowego wykonanego z różnych materiałów inżynierskich Adam Schwarz, Łukasz Buszka, Łukasz Mann, Amadeusz Dziwis, Wojciech Mikołajko, Agata Śliwa	505
Właściwości powłoki miedzianej nakładanej w procesie galwanizacji Jakub Sikora, Krzysztof Michalik, Jakub Hasiński, Michał Nowak, Beata Krupińska, Marcin Staszuk	511
Development of thermal spraying technology for coatings effectively protecting power plant components against high-temperature corrosion Grzegorz Sikorski, Katarzyna Jędrzejczyk, Michał Wnętrzak, Julia Żuławska, Tomasz Haręźlak, Mateusz Dziergas, Artur Czupryński, Waldemar Kwaśny	518

Construction of an electric drive module for wheelchairs and implementation of control systems using AI and BCI Wojciech Sikorski, Dominik Kłaput, Anastasiia Pashko, Julian Koterba.....	526
Effect of steel triboactivation on hardening and relaxation properties of surface layers Yuliia Sokolan, Kateryna Sokolan, Pavlo Maidan, Serhii Matiukh, Oleg Polishchuk, Mirosław Bonek.....	537
Additive Manufacturing of Cobalt-Chromium Dental Implants Using Selective Laser Melting (SLM) Maryam Soleimani, Wojciech Sitek, Magdalena Szindler.....	550
Overview of materials for effective drone construction Kinga Stępska, Martyna Urbańska, Natalia Bijok, Sylwia Dziwoki, Jan Wypiór, Magdalena Hulbój, Emilia Krzystanek, Krzysztof Goczoł, Mariusz Król.....	556
Analysis of reactive power compensation in a 100/15kV station Szymon Szeja.....	565
Analiza numeryczna własności mechanicznych wspornika architektonicznego Mateusz Szojda, Bianka Wyrobek, Wojciech Mikołajko, Amadeusz Dziwis, Agata Śliwa, Marek Sroka	573
Influence of laser modification on structure and properties of hot-work tool steel Dominik Towarnicki, Bartosz Nikiel, Kamil Oleksy, Cezary Zach, Antonina Olszewska, Karolona Rogalewska, Mirosław Bonek, Oleh Polishchuk, Boris Gitolendia	580
Investigation and analysis of electrical and structural parameters of multicrystalline silicon solar cells Julia Urbanek, Kacper Jakubowski, Bartosz Lemański, Mikołaj Wąsik, Christian Sanquedolce, Małgorzata Musztyfaga-Staszuk, Wojciech Filipowski.....	588
Vplyv veľkosti plastickej deformácie na teplotu rekryštalizácie Jozef Vicena, Milan Uhrčík, Mirosław Bonek.....	597
História, stavba kolenných endoprotéz a ich montáž Richard Vidrich, Ronald Bašťovanský, Peter Palček.....	605
Welding of automotive structures made of DOCOL 1100M and DOCOL 1200M steel according to the new recommendations of the European Union Tomasz Węgrzyn, Bożena Szczucka-Lasota, Małgorzata Musztyfaga-Staszuk, Abílio Manuel Pereira da Silva, Wojciech Tarasiuk, Artur Labus, Paweł Piotrowicz, Patrycja Lasota	613

Research on the method of semantic segmentation of objects based on images obtained by multirotor platform Jagoda Więcek, Michał Wieczorek, Kacper Matys, Patryk Mondry, Wojciech Cofalik.....	621
Phase changes induced by corrosion of alkali-activated binders Paulina Wiśniewska, Barbara Słomka-Słupik	626
Characteristic properties decisive for the use of the material in industrial applications Mateusz Woźniak, Borys Lipczyński, Judyta Drygała, Julia Popis, Sabina Lesz	634
Classification of polymer materials used in the manufacture of pressure pipes using computational classification models Filip Ziarkowski, Rafał Honysz	642
Numerical analysis of the thermal strength of electrical insulators Zuzanna Zielińska, Kajetan Kojm, Łukasz Lomania, Agata Śliwa, Marek Sroka, Wojciech Mikołajko.....	648
Numerical analysis of mechanical stresses acting on overhead line power cables Zuzanna Zielińska, Kajetan Kojm, Łukasz Lomania, Agata Śliwa, Marek Sroka, Wojciech Mikołajko.....	653
Key connections between Production Planning and Scheduling, Assembly Systems Organization, and Laser Processing Dominik Towarnicki, Katarzyna Furman, Hubert Przybyszewski, Mirosław Bonek, Oleh Polishchuk, Boris Gitolendia	659
Surface Modification Analysis of Titanium Gyroid Scaffolds for Bone Implant Applications Sichale Worku Fita, Mirosław Bonek, Sebastian Sławski, Anna Woźniak.....	665
Surface Modification Analysis of Titanium Gyroid Scaffolds for Bone Implant Applications M. Grabowska, D. Dziurosz, Sz. Greń, Ł. Kaim, M. Prusko, J. Zarzycki, J. Mytnik, J. Mazurkiewicz, M. Król, W. Kołodziej	673
Recycling opportunities - the second life of metallographic samples for light microscope studies in the form of QR code boards M. Kiczyński, J. Ertel, J. Mazurkiewicz	680
Using 3D FDM printing to build interactive educational models of elementary cells of crystal lattice W. Kołodziej, J. Operskalski, M. Skoniczek, J. Mazurkiewicz, M. Król.....	685



31th January 2025
Gliwice, Poland

DEPARTMENT OF ENGINEERING MATERIALS AND BIOMATERIALS
FACULTY OF MECHANICAL ENGINEERING
SILESIA UNIVERSITY OF TECHNOLOGY

INTERNATIONAL STUDENTS SCIENTIFIC CONFERENCE

Manufacturing Of The NiTi Orthodontic Arcwire

Bahri Can Abaci^a

^a Gazi University, Institute of Science, Metallurgical And Materials Engineering
email: bahrican.abaci97@gmail.com

Abstract: Orthodontic arcwires, which work together with brackets used in orthodontic treatments, are the tools that apply force during the processes of aligning, rotating, and repositioning teeth. These arcwires come in a wide range of options in terms of variations, materials, and coatings. Among them, the most commonly used orthodontic arcwires today are those made from Nickel-Titanium (Ni-Ti shape memory alloy) with round and square forms. In this project, several of the most commonly used arcwire sizes will be selected, and thermal treatment will be applied to give them the most suitable form for the oral environment. The austenitic phase transformation temperature will be determined, and mechanical properties will be tested (tensile, 3-point bending, stiffness, metallographic tests). The forces they apply to the teeth will be optimized, and surface quality studies will be conducted using electro-polishing. The final product will also be compared with existing commercial arcwires as part of the project.

Keywords: Orthodontic arcwire, NiTi, Shape Memory Alloy, Super Elastic

1. INTRODUCTION

Nickel-Titanium (NiTi) shape memory alloys (SMAs) have outstanding properties such as high shape memory effect, flexibility, and corrosion resistance, making them widely used in fields like medical devices, aerospace, and the automotive industry. The properties of SMA wires are closely related to the production process, alloy composition, heat treatment conditions, and thermomechanical processes [1].

In general, the literature indicates that various parameters are optimized to control the austenite transformation temperatures (A_f) of NiTi wires.

When considering alloy composition, even small changes in the Nickel/Titanium ratio significantly affect the austenite and martensite transformation temperatures. Studies have typically focused on alloys containing 50.5-51.5% Nickel. Different annealing temperatures and durations play a critical role in controlling the microstructure and transformation temperatures of these wires. To stabilize transformation temperatures, certain elements have been tested, and their effects on transformation temperatures have been examined. For example, adding small amounts of elements like copper or iron to the alloy has been shown to help control transformation temperatures [2,4,5].

Such studies provide insights into determining appropriate process conditions for producing wires with commonly used austenitic transformation temperatures of 25°C, 37°C, and 40°C. Detailed characterization of the material microstructure (e.g., DSC, XRD, SEM) is recommended during the production process [3].

The NiTi wires used in these studies are often copper-added, but our goal is to achieve similar mechanical and thermal properties without the addition of copper.

Literature studies also include comparisons of the mechanical properties of existing commercial products. Many studies focus on aspects such as the forces applied by the wires on teeth, the mechanical properties of the wires, and the analysis of their austenitic transformation temperatures [6,7].

In addition to these mechanical properties, the final product should have a curve that closely resembles the shape of the oral cavity. Relevant studies have been conducted, and optimal form values for the Turkish jaw structure have been obtained [6,7].

Some studies investigate the effects of coated wires on living cells in the mouth. However, since we will not be using coatings, this topic is outside the scope of our research [8].

2. METODOLOGY

2.1. Tests

• **Since the wires will already come in wire form, the initial shaping process will involve rolling them to the desired dimensions.**

Arcwire shape is so important for the patients. The intercanine distance measured in Turkish volunteers was 29.67 mm, and the canine depth was 6.08 mm. The intermolar distance was 52.35 mm, with a molar depth of 26.85 mm.

In this context, Natural Highland Metal (Franklin, USA) and Bioform III RMO (Denver, USA) were found to be the most compatible wires for the mandibular canine width of the Turkish jaw structure. Regarding molar teeth, the most suitable wires for the mandible were Europa II RMO (Denver, USA) and Form III American Orthodontics (Sheboygan, USA). The authors also noted that the most common arch form in Turkish individuals is the oval (ovoid) arch form, while the conical form is more prevalent in the White American group [12].

Taking these parameters into consideration, the most suitable wire shape for the Turkish jaw structure will be given.

• **The composition of the material will be determined using XRD analysis of the wire.**

This will help define the heat treatment parameters to be applied.

• **Small pieces will be cut from the wire, and the internal structure will be analyzed using techniques such as optical microscopy and SEM.**

• **The wire will be shaped appropriately and subjected to heat treatment in furnaces at approximately 500°C for a specific duration to achieve a fully austenitic microstructure.**

It will then be rapidly cooled to transform it into martensite.

• **Optical microscopy and SEM will again be applied at this stage.**

• **A platform for the three-point bending test will be prepared, and thermal oral conditions will need to be simulated.**

According to Iso 15841 3 point bending test have to be done guideline mentioned below;

The jaw speed should be (1.25 ± 0.75) mm/min.

Samples must be cut to a minimum length of 30 mm.

Wires should be subjected to a symmetrical three-point bending test. A wire 10 mm long should be used between the supports. The deviation should be made with a notch cutter placed in the center. The radius of the support and notch cutter should be (0.10 ± 0.05) mm. Rectangular wires should be tested along the length of the wire. The wires should be tested at a temperature range of 36 ± 1 °C. They should be deflected by 3.1 mm.

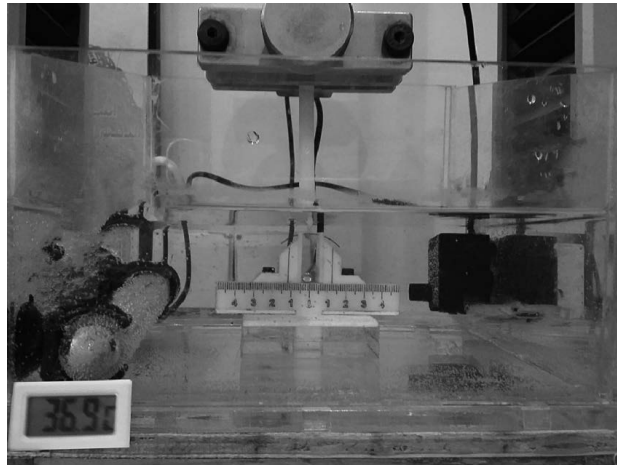


Figure 1. 3 point bending test in 37.5 degrees celcius[10]

- **The mechanical properties of the wire, such as tensile strength, three-point bending, hardness measurements, and surface topography, will be determined.**

The force applied during the optimal unloading force for clinical applications, which is used for tooth alignment, has been reported by Gatto et al. to range between 60-100g when comparing different manufacturers.

Bartzela et al. described this range as 139-239g, and Lombardo et al. reported values between 78.4-109.6g. These values are considered appropriate alignment forces in orthodontic journals, and generally, the range can be evaluated as 60-239g (8.8-234.2cN).

The optimal compression on periodontal tissue should be between 7×10^{-4} MPa (7 g/cm^2) and 2.6×10^{-3} MPa (26 g/cm^2).

Loads exceeding 2.6×10^{-3} MPa can lead to excessive compression of periodontal capillaries, causing local ischemia, which may result in tissue hyalinization. For comparison purposes, based on literature, the optimal initial force to induce physiological cycling on mineralized tissues associated with a maxillary premolar can be assumed to be approximately 50gf (49cN) [11].

- **DSC/TGA tests will be conducted to identify the transformation temperatures.**

With this analysis, we gain information about the Af transformation temperature. The peaks on the graph indicate the starting values of the transformation.

Since we know the approximate value of the transformation temperature, the temperature range selected during the DSC analysis can be kept short, for example, -10 °C to 70 °C. However, one study was conducted between -100 °C and 100 °C, while another was between -30 °C and 100 °C.

According to the ISO15841 definition, a heating rate of 10 °C/min is specified. The Af value indicated by the standard is only acceptable with a tolerance of 1 °C.

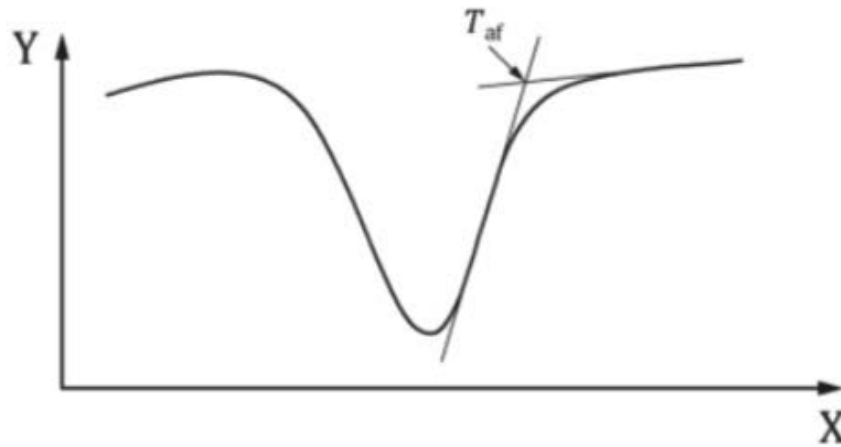


Figure 2. Af transformation graph.

- In the final stage, surface quality will be enhanced through electropolishing.

Between the 13-17 January 2025 all these test will be done.

3. CONCLUSION

As a conclusion, in orthodontic treatments, NiTi arcwires are widely using. The product is a high-value-added item, considering its low production cost and high selling price. Additionally, the knowledge gained here will serve as a foundation for various applications of nickel-titanium wires.

BIBLIOGRAPHY

- [1] Otsuka, K., & Ren, X. (1999). "Recent developments in the research of shape memory alloys." *Materials Science and Engineering: A*, 273–275, 89–105.
- [2] Buehler, W. J., Gilfrich, J. V., & Wiley, R. C. (1963). "Effect of low-temperature phase changes on the mechanical properties of alloys near composition TiNi." *Journal of Applied Physics*, 34(5), 1475–1477.
- [3] Duerig, T. W., Pelton, A., & Stöckel, D. (1999). "An overview of nitinol medical applications." *Materials Science and Engineering: A*, 273–275, 149–160.
- [4] Huang, W. M., Ding, Z., Wang, C. C., Wei, J., Zhao, Y., & Purnawali, H. (2010). "Shape memory materials." *Materials Today*, 13(7–8), 54–61.
- [5] Pelton, A. R., Russell, S. M., & DiCello, J. (2003). "The physical metallurgy of Nitinol for medical applications." *Journal of the Minerals, Metals & Materials Society*, 55(5), 33–37.
- [6] Mechanical properties of NiTi and CuNiTi shape-memory wires used in orthodontic treatment. Part 1: Stress-strain tests
- [7] Mechanical properties of NiTi and CuNiTi wires used in orthodontic treatment. Part 2: Microscopic surface appraisal and metallurgical characteristics

- [8] Comparison of the Nickel Titanium Alloy Archwires' Dimensions with the Mean Arch Dimensions of a Turkish Sample
- [9] Structure, Composition, and Mechanical Properties of Australian Orthodontic Wires
- [10] Evaluating the Elemental Composition, Transformation Behavior, Crystalline Structure, and Mechanical Properties of Three 0.016-Inch by 0.022-Inch Nickel-Titanium Archwires: An In Vitro Study
- [11] Mechanical Performance of Nickel-titanium Archwires, Daniel Jogaib Fernandes, 2015
- [12] Comparison of the Nickel Titanium Alloy Archwires' Dimensions with the Mean Arch Dimensions of a Turkish Sample, Berza Şen Yılmaz, 2021



31th January 2025
Gliwice, Poland

DEPARTMENT OF ENGINEERING MATERIALS AND BIOMATERIALS
FACULTY OF MECHANICAL ENGINEERING
SILESIA UNIVERSITY OF TECHNOLOGY

INTERNATIONAL STUDENTS SCIENTIFIC CONFERENCE

Zinc Oxide (ZnO) Nanostructures for Dye-Sensitized Solar Cells - A Scientific Review

Elizabeth Addae ^a, Wojciech Sitek ^b, Marek Szindler ^c

- a. Scientific and Didactic Laboratory of Nanotechnology and Material Technologies, Faculty of Mechanical Engineering, Silesian University of Technology, Towarowa 7 Str., 44-100 Gliwice, Poland; Elizabeth.Addae@polsl.pl
- b. Scientific and Didactic Laboratory of Nanotechnology and Material Technologies, Faculty of Mechanical Engineering, Silesian University of Technology, Towarowa 7 Str., 44-100 Gliwice, Poland; Wojciech.Sitek@polsl.pl
- c. Scientific and Didactic Laboratory of Nanotechnology and Material Technologies, Faculty of Mechanical Engineering, Silesian University of Technology, Towarowa 7 Str., 44-100 Gliwice, Poland; Marek.Szindler@polsl.pl

Abstract: The revolutionary photovoltaic technology known as dye-sensitized solar cells (DSSCs) has attracted a lot of interest because of its exceptional cost-effectiveness, ease of production, and promise for high energy conversion efficiencies in a variety of environmental settings. Because of its unique structural and electrical characteristics, zinc oxide (ZnO) is a highly effective and adaptable semiconductor that stands out among the other materials being researched for usage as photoanodes in DSSCs. The distinctive characteristics of ZnO nanostructures are thoroughly examined in this study, which also covers their production methods, structural variety, and crucial function in DSSCs. Particular focus is given to clarifying the complex link between morphology and performance, optimizing device efficiency, and resolving the real-world difficulties in using ZnO to optimize DSSC functioning. Additionally, this paper explores the latest developments in hybrid ZnO-based materials, the incorporation of novel dye molecules, and new approaches to get beyond current constraints. By examining these advancements, the research highlights how crucial ZnO will be in determining the direction of sustainable energy solutions in the future and how it may contribute to next-generation energy technology.

Keywords: Zinc Oxide, Nanostructures, Photoanodes, Dye Sensitized Solar Cells

1. INTRODUCTION

One advanced third-generation photovoltaic technology that mimics the natural process of photosynthesis is dye-sensitized solar cells (DSSCs). In order to produce photo-excited electrons and harvest sunlight, they use a dye molecule. This starts a series of charge transfer processes that eventually result in the production of electrical energy. Since the photoanode

material not only provides a scaffold for dye adsorption but also works as a conduit for electron transport to the external circuit, it is closely related to the total efficiency of DSSCs. Zinc oxide (ZnO) is a particularly intriguing contender among prospective photoanode materials because of its unique combination of a broad bandgap (3.3 eV), strong intrinsic electron mobility, and exceptional chemical stability [1]. When combined, these characteristics improve ZnO's capacity to facilitate efficient charge transport by lowering recombination rates and energy losses during electron mobility, both of which are essential for reaching high device efficiency. Its intrinsic chemical stability also guarantees that the material may continue to function for extended periods of time, even in the face of harsh environmental factors like exposure to UV light or changes in humidity and temperature. ZnO is an essential component for dependable and sustainable functioning in DSSC applications because of its dual functionality, which combines durability with efficient electron transport [2].

The intrinsic electron mobility of zinc oxide (ZnO) is superior to that of other well researched semiconductors, such as titanium dioxide (TiO₂), with values reported to be between 200 and 300 cm²/Vs. This high electron mobility minimizes energy losses from electron recombination at defect sites by lowering resistance in the conduction channel, which greatly speeds up charge transfer. The energy conversion efficiency of DSSCs is directly improved by such effective charge collection techniques, which also result in increased photocurrent generation. Apart from its favourable electrical characteristics, ZnO demonstrates exceptional compatibility with a wide variety of dye molecules and electrolyte compositions, rendering it a very adaptable substance for customizing DSSC designs to particular operational and environmental settings [3]. For example, the surface chemistry of ZnO facilitates the efficient adsorption of a range of dye molecules, and its structural flexibility guarantees the best possible interaction with both liquid and solid-state electrolytes. High open-circuit voltages and increased device stability are made possible by this compatibility, which improves interfacial charge transport kinetics. ZnO also has much more to offer in terms of scalability and manufacturing. It may be made in a number of economical ways, including electrodeposition, sol-gel procedures, and hydrothermal development, all of which allow for the fine-tuning of its electrical and morphological properties. Because of these synthesis methods' affordability and excellent scalability, ZnO is a viable option for mass manufacture in commercial applications. The formation of intricate nanostructures such as nanowires, nanoparticles, and hierarchical frameworks by ZnO improves its light-scattering and dye-loading properties and maximizes light absorption throughout the spectrum.

ZnO is positioned as a key component in the creation of next-generation DSSCs due to the combination of these characteristics. ZnO is essential to solving the world's energy problems since it provides a sustainable means to capture solar energy using scalable and eco-friendly production techniques. In an era of rising energy demand, its ability to spur innovation in photovoltaic technology highlights its critical role in improving renewable energy alternatives [4].

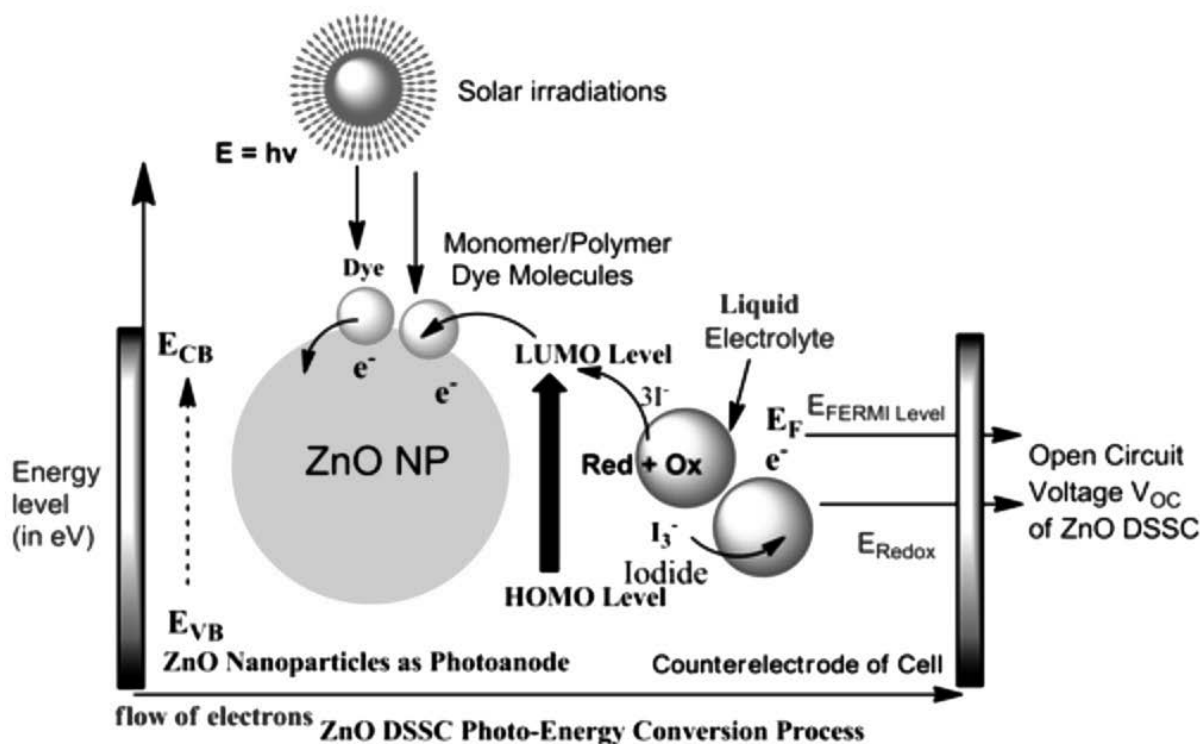


Figure 1: Process for conversion of solar power into electric energy using ZnO-based DSSC [5]

2. SYNTHESIS AND FABRICATION OF ZINC OXIDE NANOSTRUCTURES FOR DYE-SENSITIZED SOLAR CELLS

When creating zinc oxide (ZnO) nanostructures, the synthesis process is crucial in determining the size of the particles, which in turn affects important characteristics like surface area, light absorption, electron mobility, and overall performance in a variety of applications, particularly dye-sensitized solar cells (DSSCs). With their many morphologies—from nanoparticles to nanowires and nanorods—ZnO nanostructures provide special benefits that may be customized for particular uses [6]. Different synthesis techniques have been developed to customize the characteristics and shape of ZnO. The synthesis technique selection has a significant impact on the ZnO nanostructures' size, shape, and crystalline quality, all of which govern their optical, electrical, and surface characteristics that are essential for DSSC performance. For instance, hydrothermal synthesis regulates temperature, reaction duration, and precursor concentration to produce well-aligned nanorods and nanowires. For effective electron transport, one-dimensional structures must have a high degree of crystallinity and homogeneity, which is ensured by this technique. On the other hand, the sol-gel technique produces structures that optimize surface area for dye adsorption by adjusting the pH, concentration, and aging time of the precursor solution, allowing for the creation of ZnO nanoparticles with tunable sizes [7].

3. CATEGORIES OF ZINC OXIDE NANOSTRUCTURES IN DYE-SENSITIZED SOLAR CELLS

3.1 Nanoparticles

ZnO nanoparticles are spherical or nearly spherical structures with sizes that usually range from a few nanometers to hundreds of nanometers. Their main purpose in DSSCs is to offer a large surface area for the adsorption of dye molecules, which is essential for absorbing a large quantity of sunlight and improving the cell's light-harvesting effectiveness. However, because electrons run into barriers when moving between particles, their small size and the associated high density of grain boundaries can cause considerable electron recombination. The DSSC's overall photocurrent and efficiency are decreased by these grain boundaries, which function as traps that obstruct effective charge transfer [8]. The DSSC's light-harvesting efficiency is boosted when more dye molecules are able to adsorb onto the ZnO surface because smaller particles have a higher surface area because of their higher surface-to-volume ratio. But this benefit comes at the expense of increased losses due to electron recombination. Because assemblies of smaller particles have a high density of grain boundaries, there are many trap states where charge carriers can recombine with oxidized species in the electrolyte, lowering the photocurrent and device efficiency overall. Researchers seek to achieve the ideal balance between nanoparticle size and distribution in order to lessen these disadvantages. By lowering the number of grain boundaries, intermediate-sized particles have been demonstrated to strike a balance between optimizing surface area for dye loading and limiting recombination. Additionally, continuous electron routes are ensured by the homogenous dispersion of nanoparticles inside the photoanode layer, improving charge collection. Techniques for surface passivation have been used extensively in addition to size optimization. The application of thin insulating coatings, such Silicon dioxide (SiO_2) or Aluminum oxide (Al_2O_3), to nanoparticles has been shown to effectively inhibit recombination. Because dangling bonds on the ZnO surface are frequently sources of electron trapping, these coatings passivate them, lowering the density of surface defect states [9]. By serving as physical barriers, these layers help enhance charge transfer by preventing direct interactions between the oxidized species in the electrolyte and the photogenerated electrons in ZnO. Crucially, in order to prevent impeding electron transmission from the dye to the ZnO conduction band, these passivation layers need to be thin enough. The creation of homogeneous, ultrathin passivation layers that perfectly combine charge transfer efficiency and recombination suppression has been made possible by developments in atomic layer deposition (ALD) and other precision coating techniques. All of these advancements work together to increase ZnO-based DSSCs' overall stability and performance [10].

3.2 Nanorods and Nanowires

Because they provide continuous and extremely effective electron conduits, they provide direct paths for electron transport, which greatly lowers recombination rates and improves total charge collecting efficiency. In this situation, one-dimensional structures like nanorods and nanowires are essential because they limit electron dispersion and energy losses along the channel while enabling the quick and targeted passage of photo-generated electrons toward the electrode [11]. This is explained by the fact that they are very crystalline and that they do not have grain boundaries, which are frequently linked to electron trapping in other nanostructures. These structures' very small surface area restricts the adsorption of dye molecules, which are

necessary for absorbing sunlight and starting the photovoltaic process, even if they have greater charge transport capabilities [12]. As a result, reaching high light-harvesting efficiency is made more difficult by the smaller surface area. In order to overcome this restriction, scientists have created hybrid structures that combine the increased surface area provided by alternative morphologies, such as nanoparticles, nanosheets, or porous frameworks, with the high electron mobility of one-dimensional ZnO. For instance, increased dye loading capacity is made possible by nanorods combined with hierarchical branching structures or nanoparticle assemblies, all while maintaining the core one-dimensional framework's effective charge transport capabilities [13].

Furthermore, customizing the characteristics of these hybrid designs has been made possible via sophisticated synthesis techniques. For instance, hydrothermal techniques may create adjustable, vertically aligned nanorods that form the framework of composite systems. In a similar vein, complex branching nanowire architectures may be grown more easily via chemical vapor deposition (CVD), which boosts the surface area accessible for dye adsorption without sacrificing electron mobility [14]. Furthermore, post-synthesis changes like doping or surface functionalization strengthen the bond between the dye and the ZnO structure, increasing the stability and effectiveness of charge injection. The viability of these systems for realistic dye-sensitized solar cell applications is ensured by these developments, which highlight the significance of combining morphological and chemical optimizations to strike a balance between light absorption, charge collection, and overall energy conversion efficiency.

Research on improving these hybrid structures using sophisticated characterisation methods and computer modelling is still ongoing. A more logical design of materials that optimize photovoltaic performance has been made possible by in situ research, which have, for example, offered greater insights into the kinetics of electron transport inside solar designs. These creative methods, which combine one-dimensional ZnO with complementary nanostructures, demonstrate how hybrid systems might help close the gap between scalable manufacturing and high efficiency for next-generation solar energy solutions [15].

3.3 Hierarchical Structures

By integrating nanoparticles with one-dimensional ZnO structures, the benefits of effective electron transport and a large surface area are combined in a synergistic way. A large surface area promotes the adsorption of dye molecules, which is essential for dye-sensitized solar cells (DSSCs) to maximize light absorption and photocurrent production. On the other hand, one-dimensional structures like nanorods or nanowires offer direct and continuous electron transport channels, successfully reducing recombination losses that are usually connected to grain boundaries in systems based on nanoparticles [16]. Additionally, by improving light scattering inside the photoanode layer, these hybrid structures lengthen the optical path and boost incident sunlight absorption efficiency. Better photovoltaic performance is a result of the resulting improvements in light harvesting and electron mobility. The morphological and electrical features of these hybrid structures may be optimized thanks to advancements in synthesis techniques like chemical vapor deposition and hydrothermal growth, which provide fine control over these structures. These elements are a viable strategy for next-generation DSSCs as their integration has been demonstrated to greatly enhance important performance parameters, including as photocurrent density, open-circuit voltage, and total energy conversion efficiency[17].

Table 1: Different nanostructure ZnO based DSSCs power conversion efficiency (Giannouli et.al, 2018) [18]

ZnO DSSC Type	V _{oc} (V)	J _{sc} (mA/cm ²)	FF	η (%)
<i>Nanoparticles</i>	0.70 ± 0.02	11.2 ± 1.0	0.54 ± 0.06	6.19 ± 0.60
<i>Nanowires</i>	0.62 ± 0.03	1.2 ± 0.4	0.53 ± 0.04	0.63 ± 0.09
<i>Hierarchical Structures</i>	0.64 ± 0.02	4.8 ± 0.4	0.41 ± 0.03	1.80 ± 0.20

4. RECENT PERFORMANCE ENHANCEMENTS IN ZNO-BASED DYE-SENSITIZED SOLAR CELLS

Recent developments have shown notable increases in performance measures, with ZnO morphology playing a crucial role in influencing the photoanode's surface area and electron transport characteristics. For example, Liu et al. (2021) have shown that the direct paths of nanowire-based ZnO structures have allowed them to attain electron transport efficiencies of up to 85% [19]. Wang et al. (2022) have found a 35% increase in dye loading and a matching rise in photocurrent density in hierarchical structures, such as those that combine nanorods and nanoparticles. These findings highlight the vital role that morphological modification plays in improving the dynamics of charge transport and light-harvesting efficiency in ZnO-based DSSCs [20].

By maximizing the ZnO layer's porosity and thickness, light absorption and effective electron transport are balanced. Research by Kim et al. (2020) indicated that ZnO layers with porosity levels that boost dye adsorption by 40% may be produced via hydrothermal synthesis, according to recent experimental data [21]. Chen et al. (2021) have also reported that atomic layer deposition has enabled the production of uniformly thick, ultra-thin ZnO films, resulting in a 25% decrease in electron recombination losses. In order to get better charge transport characteristics and increased light-harvesting efficiency, these controlled growth approaches have proven essential [22].

Through passivation of defects and reduction of recombination, surface treatments using materials such as Zn(NO₃)₂ or TiCl₄ enhance the surface characteristics of ZnO. According to research by Sakai et al. (2013), for instance, TiCl₄ treatment can enhance overall efficiency by up to 15% and extend electron lifespan by 30% [23]. Similarly, Khan et al. (2023) reported that Zn(NO₃)₂ has improved dye anchoring, which leads to a 20% increase in dye adsorption and a commensurate improvement in photocurrent density. These developments demonstrate how important chemical treatments are to ZnO-based DSSC optimization. At the ZnO-electrolyte contact, protective barriers like SiO₂ or Al₂O₃ coatings have been shown to lessen charge recombination [24]. According to Zhao et al. (2021), recent research has shown that Al₂O₃ coatings can increase the open-circuit voltage (V_{oc}) by as much as 20% by reducing recombination sites and surface traps [25]. Lin et al. (2020) found that SiO₂ coatings may stabilize the ZnO-electrolyte interface and promote charge separation, which can lead to an overall 15% increase in power conversion efficiency.

Dye molecules need to adhere to the ZnO surface effectively and absorb strongly in the visible range. Developments in metal-organic complexes, organic dyes, and co-sensitization techniques have greatly improved the stability and light-harvesting efficiency of ZnO-based DSSCs. Kumar et al. (2021) revealed that the enhanced absorption capabilities and binding durability of ruthenium-based dyes have led to power conversion efficiencies above 8% [26]. According to Tanaka et al. (2020), co-sensitization using organic and inorganic dyes has also enhanced spectrum coverage, resulting in a 20% increase in photocurrent production. These tactics highlight how important dye optimization is, to extending the capabilities of ZnO-DSSCs [27].

Last but not the least, the combination of ZnO and TiO₂ benefits from ZnO's has been proven to enhance electron mobility and TiO₂'s excellent stability. Higher photocurrent densities are frequently the consequence of synergistic effects in hybrid photoanodes. For instance, research by Yadav et al. (2021) showed that ZnO- TiO₂ hybrid systems had a 25% higher photocurrent density than pure ZnO photoanodes. The effective charge separation and decreased recombination made possible by the complimentary qualities of the two materials were credited with this improvement [28]. Similarly, combining ZnO nanowires with TiO₂ nanosheets improved light absorption and increased power conversion efficiency by 18%, according to research by Patel and Singh (2022). These results demonstrate how hybrid systems may surpass the drawbacks of separate parts and produce better photovoltaic results [29].

5. SUMMARY AND CONCLUSION

Because of its remarkable electron mobility, structural adaptability, and simplicity of production, zinc oxide (ZnO) has shown great promise as a photoanode material in dye-sensitized solar cells (DSSCs). Effective electron transport channels and a large surface area for dye adsorption are made possible by ZnO's nanoscale morphology, which includes nanowires, nanorods, nanoparticles, and other nanostructures. These characteristics help to improve the effectiveness of light harvesting and charge collection. Despite their benefits, ZnO-based DSSCs have a number of drawbacks, most notably dye aggregation, charge carrier recombination, and instability after extended use. ZnO and common dyes, namely those with carboxylic acid groups, have an innate chemical interaction that over time may cause dye degradation and reduced efficacy. Further restricting ZnO's ability to attain greater photovoltaics is its modest conduction band location in comparison to other materials, such titanium dioxide (TiO₂). To overcome these constraints, surface alterations, co-sensitization, and the use of buffer layers or substitute dyes to reduce charge recombination and enhance stability are all being considered. Furthermore, it has been demonstrated that improving the ZnO nanostructure can reduce electron scattering and increase light absorption. To sum up, ZnO-based DSSCs show promise as a platform for efficient and affordable solar energy conversion, but further study is required to get over material-specific restrictions and improve their competitiveness versus more well-established systems like TiO₂-based DSSCs. Commercial use of ZnO-based DSSCs may be made possible by future advancements in dye chemistry, interface engineering, and device architecture, which might lead to increased stability and efficiency.

BIBLIOGRAPHY

1. Theerthagiri, J.; Salla, S.; Senthil, R.A.; Nithyadharseni, P.; Madankumar, A.; Arunachalam, P.; Maiyalagan, T.; Kim, H.-S. A Review on ZnO Nanostructured Materials: Energy, Environmental and Biological Applications. *Nanotechnology* 2019, *30*, 392001, doi:10.1088/1361-6528/ab268a.
2. Kumari, P.; Srivastava, A.; Sharma, R.K.; Sharma, D.; Srivastava, S.K. Zinc Oxide: A Fascinating Material for Photovoltaic Applications. In *Nanomaterials for Innovative Energy Systems and Devices*; Khan, Z.H., Ed.; Springer Nature: Singapore, 2022; pp. 173–241 ISBN 978-981-19055-3-7.
3. Zang, Z.; Cai, W.; Zhou, Y. *Metal Oxide Semiconductors: Synthesis, Properties, and Devices*; John Wiley & Sons, 2023; ISBN 978-3-527-84256-8.
4. Lüth, H. *Surfaces and Interfaces of Solid Materials*; Springer Science & Business Media, 2013; ISBN 978-3-662-03132-2.
5. Singh, S.; Raj, T.; Bahadur, I.; Singh, H.; Varma, R.S. Improved Power Conversion Efficiencies of Dye-Capped and Sensitized ZnO Solar Cells. *ChemistrySelect* 2022, *7*, e202202075, doi:10.1002/slct.202202075.
6. Kumar, R.; Umar, A.; Kumar, G.; Nalwa, H.S.; Kumar, A.; Akhtar, M.S. Zinc Oxide Nanostructure-Based Dye-Sensitized Solar Cells. *J Mater Sci* 2017, *52*, 4743–4795, doi:10.1007/s10853-016-0668-z.
7. Szindler, M.; Szindler, M.M.; Boryło, P. ZnO Nanocrystalline Powder Prepared by Sol-Gel Method for Photoanode of Dye Sensitized Solar Cells Application. *Journal of Achievements in Materials and Manufacturing Engineering* 2018, *Vol. 88*, doi:10.5604/01.3001.0012.5866.
8. Nithya, N. Synthesis And Applications Of ZnO Nanocrystalline Materials. *JOURNAL OF OPTOELECTRONICS LASER* 2022, *41*, 291–301.
9. Pokropivny, V.; Löhmus, R.; nova, I.; Pokropivny, A.; Vlassov, S. *Introduction in Nanomaterials and Nanotechnology*; 2007;
10. Wong, K.K.; Ng, A.; Chen, X.Y.; Ng, Y.H.; Leung, Y.H.; Ho, K.H.; Djurišić, A.B.; Ng, A.M.C.; Chan, W.K.; Yu, L.; et al. Effect of ZnO Nanoparticle Properties on Dye-Sensitized Solar Cell Performance. *ACS Appl. Mater. Interfaces* 2012, *4*, 1254–1261, doi:10.1021/am201424d.
11. Baxter, J.B.; Aydil, E.S. Dye-Sensitized Solar Cells Based on Semiconductor Morphologies with ZnO Nanowires. *Solar Energy Materials and Solar Cells* 2006, *90*, 607–622, doi:10.1016/j.solmat.2005.05.010.
12. Baxter, J.B.; Aydil, E.S. Nanowire-Based Dye-Sensitized Solar Cells. *Applied Physics Letters* 2005, *86*, 053114, doi:10.1063/1.1861510.
13. Baxter, J.B.; Walker, A.M.; van Ommering, K.; Aydil, E.S. Synthesis and Characterization of ZnO Nanowires and Their Integration into Dye-Sensitized Solar Cells. *Nanotechnology* 2006, *17*, S304, doi:10.1088/0957-4484/17/11/S13.
14. Cheng, H.-M.; Chiu, W.-H.; Lee, C.-H.; Tsai, S.-Y.; Hsieh, W.-F. Formation of Branched ZnO Nanowires from Solvothermal Method and Dye-Sensitized Solar Cells Applications. *J. Phys. Chem. C* 2008, *112*, 16359–16364, doi:10.1021/jp805239k.
15. Suh, D.-I.; Lee, S.-Y.; Kim, T.-H.; Chun, J.-M.; Suh, E.-K.; Yang, O.-B.; Lee, S.-K. The Fabrication and Characterization of Dye-Sensitized Solar Cells with a Branched Structure of ZnO Nanowires. *Chemical Physics Letters* 2007, *442*, 348–353, doi:10.1016/j.cplett.2007.05.093.

16. Xia, Y.; Wang, J.; Chen, R.; Zhou, D.; Xiang, L. A Review on the Fabrication of Hierarchical ZnO Nanostructures for Photocatalysis Application. *Crystals* 2016, *6*, 148, doi:10.3390/cryst6110148.
17. Wang, X.; Ahmad, M.; Sun, H. Three-Dimensional ZnO Hierarchical Nanostructures: Solution Phase Synthesis and Applications. *Materials* 2017, *10*, 1304, doi:10.3390/ma10111304.
18. Giannouli, M.; Govatsi, K.; Syrokostas, G.; Yannopoulos, S.N.; Leftheriotis, G. Factors Affecting the Power Conversion Efficiency in ZnO DSSCs: Nanowire vs. Nanoparticles. *Materials* 2018, *11*, 411, doi:10.3390/ma11030411.
19. Li, X.; Liu, X.; Li, Y.; Gao, D.; Cao, L. Using Novel Semiconductor Features to Construct Advanced ZnO Nanowires-Based Ultraviolet Photodetectors: A Brief Review. *IEEE Access* 2021, *9*, 11954–11973, doi:10.1109/ACCESS.2021.3051187.
20. ZnO Nanorods Decorated with Ag Nanoflowers as a Recyclable SERS Substrate for Rapid Detection of Pesticide Residue in Multiple-Scenes - ScienceDirect Available online: <https://www.sciencedirect.com/science/article/abs/pii/S1386142522014251> (accessed on 9 January 2025).
21. Kim, H.; Jung, M.J.; Choi, S.; Choi, B.J. ALD Growth of ZnO on P-Si and Electrical Characterization of ZnO/p-Si Heterojunctions. *Materials Today Communications* 2020, *25*, 101265, doi:10.1016/j.mtcomm.2020.101265.
22. Chen, X.; Wan, J.; Wu, H.; Liu, C. Effective Encapsulation of ZnO Thin Film Transistors Controlled by Thermal Energy. *Applied Surface Science* 2021, *548*, 149253, doi:10.1016/j.apsusc.2021.149253.
23. Sakai, N.; Miyasaka, T.; Murakami, T. Efficiency Enhancement of ZnO-Based Dye-Sensitized Solar Cells by Low-Temperature TiCl₄ Treatment and Dye Optimization. *The Journal of Physical Chemistry C* 2013, *117*, 10949–10956, doi:10.1021/jp401106u.
24. Khan, S.A.; Patel, S.; Shukla, P.; Dixit, R.; Kumar, R. A Review on the Incorporation of Nanoparticles in Polymer Based Optoelectronic Devices. *SAMRIDDHI: A Journal of Physical Sciences, Engineering and Technology* 2023, *15*, 109–115, doi:10.18090/10.18090/samriddhi.v15i01.29.
25. Xu, Q.; Liu, F.; Meng, W.; Huang, Y. Plasmonic Nanoparticles Enhanced Dye-Sensitized Solar Cells. *Proceedings of SPIE - The International Society for Optical Engineering* 2013, *8923*, doi:10.1117/12.2033938.
26. Veerakumar, P.; Hung, S.-T.; Hung, P.-Q.; Lin, K.-C. Review of the Design of Ruthenium-Based Nanomaterials and Their Sensing Applications in Electrochemistry. *J. Agric. Food Chem.* 2022, *70*, 8523–8550, doi:10.1021/acs.jafc.2c01856.
27. Tanaka, E.; Robertson, N. Polyiodide Solid-State Dye-Sensitized Solar Cell Produced from a Standard Liquid I⁻/I₃⁻ Electrolyte. *Journal of Materials Chemistry A* 2020, *8*, 19991–19999, doi:10.1039/D0TA07377F.
28. Bhogaita, M.; Devaprakasam, D. Hybrid Photoanode of TiO₂-ZnO Synthesized by Co-Precipitation Route for Dye-Sensitized Solar Cell Using *Phyllanthus Reticulatas* Pigment Sensitizer. *Solar Energy* 2021, *214*, 517–530, doi:10.1016/j.solener.2020.12.009.
29. Understanding the Electronic Structure and Electron Transfer Kinetics of Titanium Dioxide Photoanodes and Analyzing Parameters Affecting Flatband Potentials in Metal Oxides.



31th January 2025
Gliwice, Poland

DEPARTMENT OF ENGINEERING MATERIALS AND BIOMATERIALS
FACULTY OF MECHANICAL ENGINEERING
SILESIA UNIVERSITY OF TECHNOLOGY

INTERNATIONAL STUDENTS SCIENTIFIC CONFERENCE

Dislocation Strengthening of PTAW NiCrBSi Coatings by Varying Arc Currents: Insights from EBSD and XRD

Augustine Nana Sekyi Appiah ^a, Krzysztof Matus ^a, Evans Atioyire ^b, Pawel Nuckowski ^a, Marcin Adamiak ^a

^a Silesian University of Technology, Faculty of Mechanical Engineering, Materials Research Laboratory

^b University of Ghana, CBAS, School of Engineering Sciences, Department of Materials Science and Engineering

email: augustine.appiah@polsl.pl

Abstract: This study examines the influence of arc current on the dislocation strengthening of NiCrBSi coatings deposited via Plasma Transferred Arc Welding (PTAW). Using EBSD, XRD, and Vickers microhardness tests, the relationship between arc current, dislocation density, grain size, and hardness was analyzed. Results showed that lower arc currents produced smaller grains and higher dislocation densities, leading to greater hardness, with a peak of 832 HV_{1.0} at 70 A. Higher arc currents resulted in reduced dislocation strengthening, emphasizing the importance of optimizing process parameters to achieve tailored mechanical properties for advanced applications.

Keywords: microstructure, grain refinement, dislocation density, kernel average misorientation

1. INTRODUCTION

Dislocations are fundamental defects in crystalline materials that play a crucial role in determining their mechanical properties. These linear defects facilitate plastic deformation but can also serve as barriers to further dislocation motion under applied stress, significantly influencing the strength of materials [1]. The interaction between dislocations and microstructural features, such as grain boundaries, is a key mechanism for strengthening materials, commonly referred to as dislocation strengthening. This phenomenon is particularly relevant in metallic coatings, where optimizing dislocation density and microstructure can enhance performance in demanding environments.

NiCrBSi coatings, deposited via Plasma Transferred Arc Welding (PTAW), are well-suited for applications requiring superior wear resistance, high-temperature stability, and corrosion resistance [2]. These coatings benefit from controlled microstructural features such as grain size, crystallographic texture, and dislocation density, which can be tailored by varying process parameters like arc current. Understanding how dislocations contribute to the mechanical

behavior of PTAW-deposited coatings provides valuable insights into optimizing their performance.

This study focuses on the effect of varying arc currents on the dislocation strengthening of PTAW-deposited NiCrBSi coatings. Advanced characterization techniques, including Electron Backscatter Diffraction (EBSD) and X-ray Diffraction (XRD), are employed to investigate the relationship between arc current, dislocation density, and grain size. Vickers microhardness tests are used to assess the mechanical performance of the coatings in relation to their microstructure. By elucidating these relationships, this work aims to provide a deeper understanding of the role of dislocations in strengthening NiCrBSi coatings and offers guidance for optimizing PTAW parameters for enhanced coating performance.

2. METHODOLOGY

The PTAW coatings were prepared following the procedure outlined in reference [3]. Four samples were fabricated at varying arc currents, as detailed in **Table 1**.

Table 1. Sample designation and processing conditions used for the study

Sample ID	Plasma transferred Arc Current [A]
PTA70	70
PTA80	80
PTA90	90
PTA100	100

To analyze grain size and crystallography, Electron Backscatter Diffraction (EBSD) was performed using a Zeiss Evo MA 15 series Scanning Electron Microscope (SEM). The EBSD analysis was conducted at an operating voltage of 20 kV with a step size of 0.2 μm . For further characterization, X-ray Diffraction (XRD) was carried out using a PANalytical X'Pert Pro diffraction system. The XRD measurements were performed with a cobalt anode lamp ($K\alpha\text{Co}$, $\lambda = 0.179 \text{ nm}$) operating at 40 kV and a filament current of 30 mA.

3.0 RESULTS AND DISCUSSION

3.1. Electron Backscatter Diffraction (EBSD) Analysis

The results from EBSD investigations for all samples are presented in Figure 1. The image quality (IQ) map for the PTA70 sample, shown in Figure 1A, highlights visible grain boundaries with an average grain size of approximately 16.4 μm (grain tolerance angle, GTA = 2°). High-angle grain boundaries (HAGBs), characterized by misorientation angles greater than 15°, account for approximately 49% of the total grain boundaries, while low-angle grain boundaries (LAGBs) with misorientation angles below 15° dominate at approximately 61% (Figure 1B). The kernel average misorientation (KAM) map (Figure 1C) reveals KAM values ranging from 1 to 5, indicating dense accumulation of geometrically necessary dislocations (GNDs) within the grain interiors, based on the direct relationship between KAM values and GNDs densities.

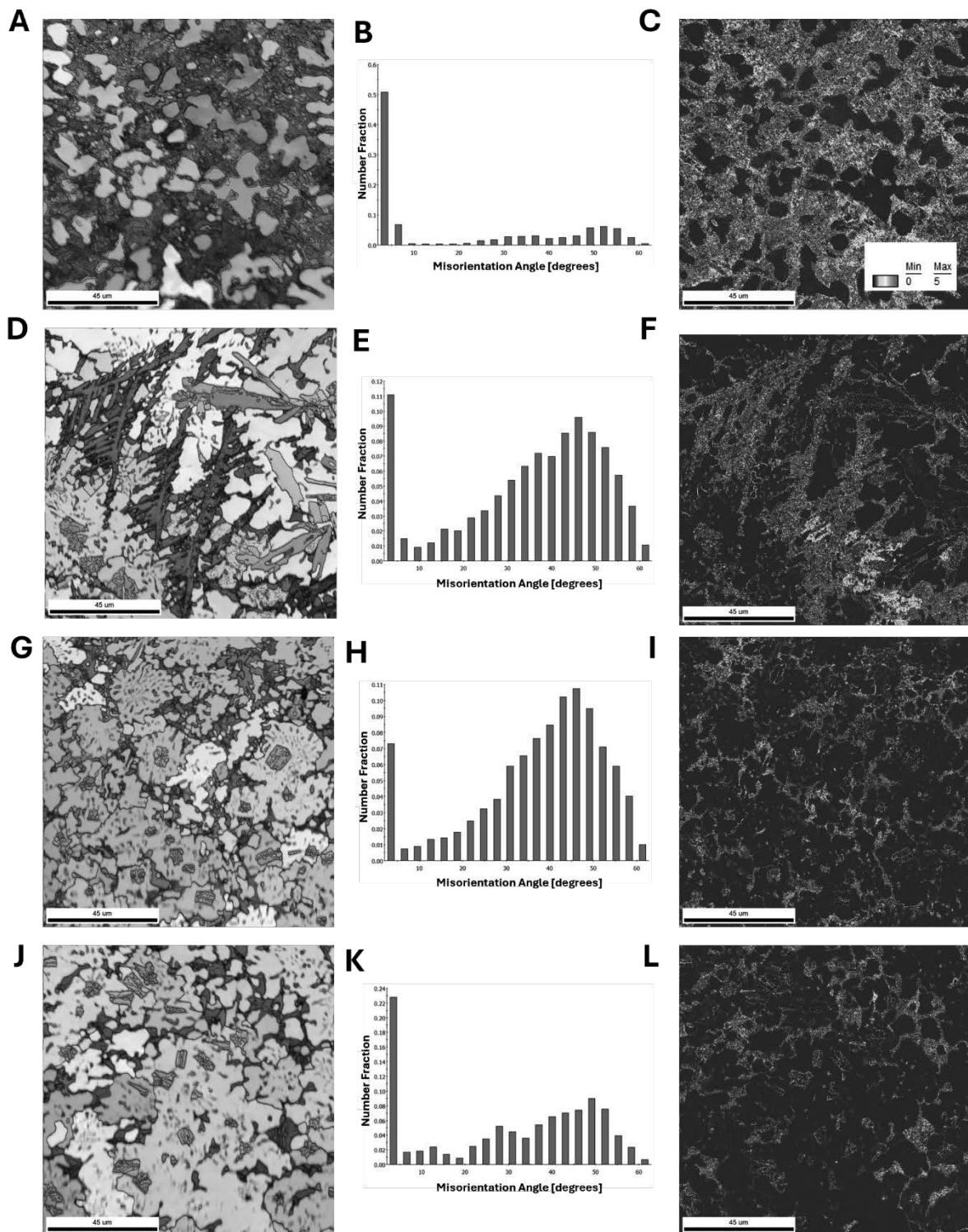


Figure 1. Electron backscatter diffraction (EBSD) analyses results. Image quality (IQ) map, misorientation angle distribution plot and kernel average misorientation (KAM) maps for (A, B, C) PTA70 sample, (D, E, F) PTA80 sample, (G, H, I) PTA90 sample, and (J, K, L) PTA 100 sample

In contrast, the IQ map for the PTA80 sample (Figure 1D) shows a larger average grain size of approximately 28.7 μm (GTA = 2°). This sample exhibits a significant increase in HAGBs volume to approximately 85.1% (Figure 1E) and a corresponding decrease in LAGBs volume to 14.9%. The KAM map (Figure 1F) demonstrates a notable reduction in GNDs density within the grain interiors and around grain boundaries.

Further increasing the arc current to 90 A results in the PTA90 sample having an average grain size of approximately 37.2 μm (GTA = 2°) (Figure 1G). HAGBs increase substantially to 90.3% (Figure 1H), while the KAM map (Figure 1I) reveals a further reduction in GNDs accumulation.

At the highest arc current investigated, 100 A, the PTA100 sample exhibits the largest grains, with an average grain size of approximately 48.1 μm (GTA = 2°), as shown in the IQ map (Figure 1J). Interestingly, the volume of LAGBs increases to approximately 28.7%, while HAGBs decrease to 71.3%. The corresponding KAM map (Figure 1K) shows the lowest density of GNDs observed among all samples, both within the grain interiors and at the grain boundaries.

Overall, the results demonstrate a clear trend: increasing the arc current leads to larger average grain sizes and a corresponding reduction in GND density. To further quantify dislocation density across all samples, XRD analysis was performed.

3.2. X-Ray Diffraction (XRD) Analyses

The XRD spectra of the deposited coatings are presented in Figure 2, showcasing characteristic FCC Ni peaks. Among these, the most prominent is the Ni (200) peak, which exhibits noticeable peak broadening and intensity variations as the arc current increases. Dislocation densities were calculated for the samples using XRD data, based on the crystallite sizes derived at each deposition arc current. The crystallite size (D) was determined using the Scherrer equation (Equation 1).

$$D = K\lambda/\beta\cos\theta \quad (1)$$

Where K is the Scherrer constant (typically 0.9 for spherical grains); λ is the X-ray wavelength (0.1789 nm for Co radiation); β is FWHM in radians; and θ is the Bragg angle in radians. The calculated crystallite size values were then used to estimate dislocation (ρ) using Equation 2.

$$\rho = 1/D^2 \quad (2)$$

At an arc current of 70 A, the smallest crystallite size of 17.05 nm was observed, corresponding to a dislocation density of $5.96 \times 10^{15} \text{ m}^{-2}$. When the arc current was increased to 80 A, the crystallite size grew to 25.42 nm, accompanied by a reduction in dislocation density to $3.77 \times 10^{15} \text{ m}^{-2}$. This trend persisted with further increases in arc current: at 90 A, the crystallite size reached 26.91 nm with a dislocation density of $2.74 \times 10^{15} \text{ m}^{-2}$, and at 100 A, the crystallite size expanded significantly to 53.90 nm, with a corresponding dislocation density of $4.42 \times 10^{14} \text{ m}^{-2}$. These findings reveal a clear inverse relationship between crystallite size and dislocation density: as the arc current increases, the crystallite size enlarges while the dislocation density decreases. This behaviour is consistent with the literature, which suggests that smaller crystallite sizes are more effective at impeding dislocation motion, thereby enhancing material strength [4]. A summary of the XRD derived properties: crystallite size and dislocation density is presented in Table 1.

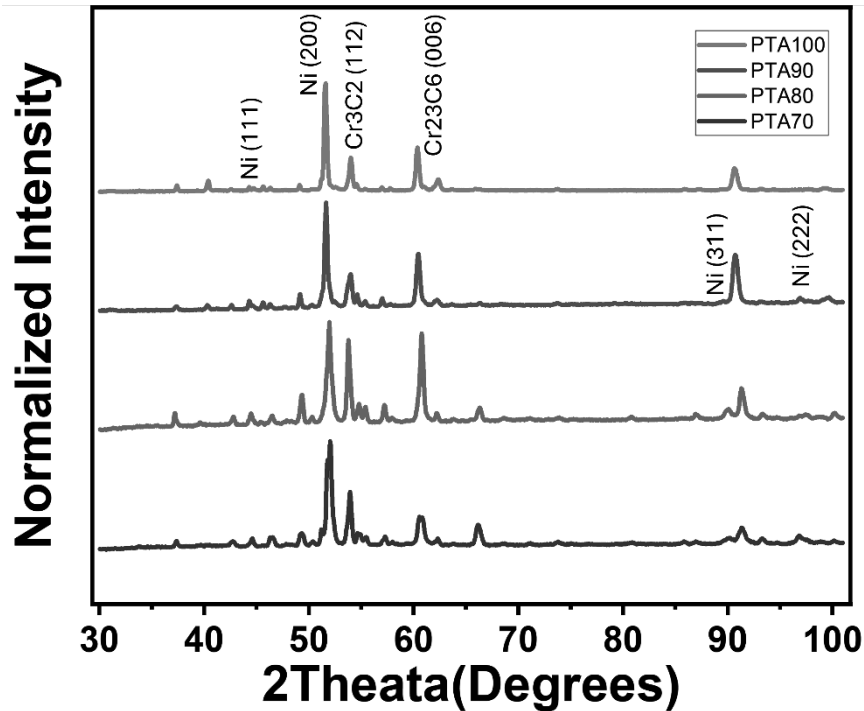


Figure 2. X-ray diffraction (XRD) spectra for the investigated coatings

Table 2. Summary of dislocation density measurements results from XRD.

Sample	Crystallite Size (nm)	Dislocation Density (m^{-2})
PTA70	17.05	5.96×10^{15}
PTA80	25.42	3.77×10^{15}
PTA90	26.91	2.74×10^{15}
PTA100	53.90	4.42×10^{14}

3.3. Hardness

Vickers microhardness tests were performed to evaluate the mechanical behaviour of the coatings under varying arc currents, corresponding to significant differences in dislocation density. Measurements were taken across three regions of the samples: the coatings, the heat-affected zones (HAZ), and the substrate material (Figure 3A). The results are presented in Figure 3B. The hardness of the HAZ and substrate remained relatively consistent across all samples, showing no significant variation. However, in the coatings, where dislocation densities varied substantially, corresponding differences in hardness were observed. The highest microhardness, 832 $HV_{1.0}$, was recorded for the PTA70 sample, which exhibited the highest dislocation density and the smallest grain size. For the PTA80 sample, the microhardness decreased to 552 $HV_{1.0}$. Further increases in arc current led to even lower hardness values of 445 $HV_{1.0}$ and 448 $HV_{1.0}$ for the PTA90 and PTA100 samples, respectively. These results indicate that at higher arc currents, the mechanical response of the coating is influenced not only by dislocation density but also by other factors, such as grain refinement.

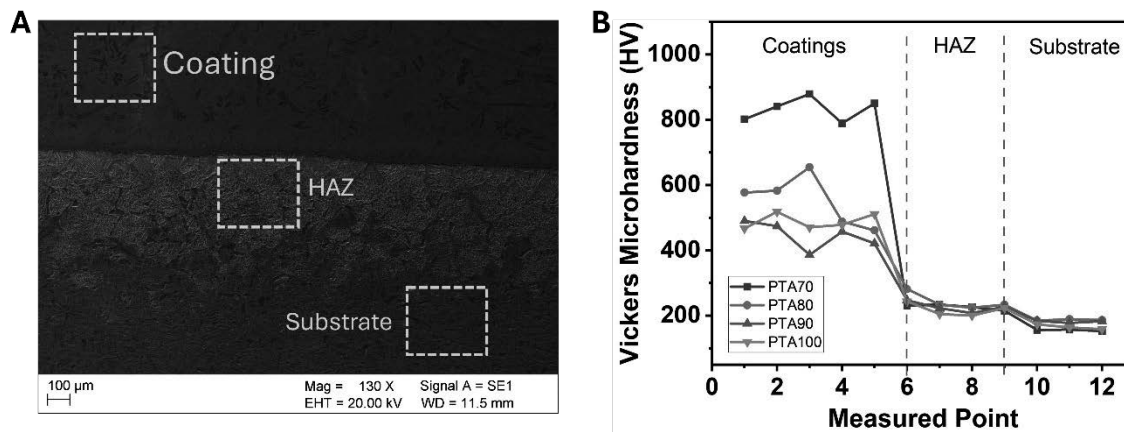


Figure 3. Microhardness measurements. A. SEM image showing the regime of Vickers microhardness measurement taken in three regions consisting of the coating, heat-affected zone (HAZ) and the substrate, and B. Results of Vickers Microhardness measurements.

CONCLUSION

This study demonstrates the significant impact of arc current on the microstructure and mechanical properties of PTAW-deposited Ni-based coatings. Increasing arc current resulted in a consistent increase in grain size and a corresponding decrease in dislocation density, as evidenced by EBSD and XRD analyses. The Vickers microhardness tests revealed that the highest hardness was achieved at lower arc currents, where dislocation density was highest and grain size smallest. However, at higher arc currents, the influence of dislocations alone was insufficient to sustain hardness, highlighting the role of other microstructural factors, such as grain refinement.

BIBLIOGRAPHY

1. Snopiński, P.; Hilšer, O.; Hajnyš, J. Tuning the Defects Density in Additively Manufactured Fcc Aluminium Alloy via Modifying the Cellular Structure and Post-Processing Deformation. *Mater. Sci. Eng. A* 2023, *865*, 144605, doi:10.1016/j.msea.2023.144605.
2. Appiah, A.N.S.; Batalha, G.F.; Adamiak, M. Thermal-Induced Evolution of Microstructure as a Plasma Arc Coating Direction-Dependent Phenomenon. *Appl. Surf. Sci.* 2024, *665*, 160320, doi:10.1016/j.apsusc.2024.160320.
3. Appiah, A.N.S.; Wyględacz, B.; Matus, K.; Reimann, Ł.; Bialas, O.; Batalha, G.F.; Czupryński, A.; Adamiak, M. Microstructure and Performance of NiCrBSi Coatings Prepared by Modulated Arc Currents Using Powder Plasma Transferred Arc Welding Technology. *Appl. Surf. Sci.* 2024, *648*, 159065, doi:10.1016/j.apsusc.2023.159065.
4. Snopiński, P.; Matus, K.; Łagoda, M.; Appiah, A.N.S.; Hajnyš, J. Engineering an Ultra-Fine Grained Microstructure, Twins and Stacking Faults in PBF-LB/M Al-Si Alloy via KoBo Extrusion Method. *J. Alloys Compd.* 2024, *970*, 172576, doi:10.1016/j.jallcom.2023.172576.



31th January 2025
Gliwice, Poland

DEPARTMENT OF ENGINEERING MATERIALS AND BIOMATERIALS
FACULTY OF MECHANICAL ENGINEERING
SILESIA UNIVERSITY OF TECHNOLOGY

INTERNATIONAL STUDENTS SCIENTIFIC CONFERENCE

Modern grinding technologies: innovative methods for processing various materials

Jennifer Badora^a, Julia Muszyńska^a, Mirosław Bonek^b

^a Student of Silesian University of Technology, Faculty of Mechanical Engineering, Department of Engineering Materials and Biomaterials

^b Silesian University of Technology, Faculty of Mechanical Engineering, Department of Engineering Materials and Biomaterials, email: miroslaw.bonek@polsl.pl

Abstract: Surface grinding is a key process in many industrial sectors, requiring precision and efficiency. Technological advancements have introduced modern methods such as advanced abrasive materials, CNC systems, and automation, enhancing the quality of machining. This article will explore the latest techniques and their applications in the industry.

Keywords: materials, laser treatment, polymers, grinding, Surface,

1. INTRODUCTION

Grinding is one of the machining methods that allows for the removal of minor surface irregularities. This process is classified as an abrasive machining technique, in which excess material is removed using abrasive tools. A distinctive feature of grinding is its very precise finishing operations, ensuring smoothness and high-quality surface finishes of components.

Surface grinding using CNC machines ensures much higher repeatability of the smoothing process compared to manual tools or power tools. This technique is particularly useful in the production of large batches of components that need to be manufactured with precise dimensions and minimal tolerances- below 0.02 mm).

2. MODERN METHODS OF GRINDING

2.1. Types of CNC Grinding Based on the Grinding Head Operation:

CNC Profile Grinding- provides high accuracy and surface smoothness. It is used for smoothing profiled components. The grinding head is positioned stationary relative to the workpiece.

CNC Cylindrical Grinding- ensures high smoothness within the hole. It is used for grinding holes or components with circular shape.

CNC Surface Grinding – this method is similar to profile grinding, but the difference is that the workpiece remains stationary while the abrasive element moves.

Advantages of CNC Grinding:

1. High Precision and Accuracy – CNC machines ensure highly precise results, which is crucial when machining components with tight tolerances.
2. Repeatability – The processes are repeatable, ensuring consistent results in mass production, even with large volumes.
3. Automation – With computer control, CNC grinding eliminates human errors and reduces processing time, increasing production efficiency.
4. Complex Shapes – CNC machines allow for the machining of complex shapes and profiles that are difficult to achieve using traditional methods.
5. Error Minimization – Thanks to precise control, CNC grinding reduces the risk of errors during the machining process.
6. Long-term Cost Reduction – Despite higher initial costs, CNC machines can significantly lower unit costs in large production runs.

2.2. Laser grinding

Modern methods of steel processing, such as grinding using laser technology, are revolutionizing contemporary industry by offering unprecedented precision and speed. Laser beams, known for their ability to focus on a small area, enable highly precise control of the grinding process. This allows for perfectly smooth surfaces, even in the case of complex shapes and patterns. As a result, this technology finds applications in fields where traditional methods may fall short, such as the aerospace, automotive, or medical industries, where precision is paramount.

One of the most significant advantages of laser grinding is the considerable reduction in processing time compared to traditional mechanical techniques. Accelerating the production process translates into increased efficiency and lower operational costs. Furthermore, laser technology minimizes the risk of material damage, making it particularly appealing when working with high-quality steels or advanced metal alloys.

The primary benefits of this technology include unparalleled precision and versatility. With the ability to accurately control the depth and intensity of grinding, it is possible to achieve perfect surface parameters while minimizing material waste. Lasers are also versatile—they can effectively handle both soft and highly hardened steels, expanding their range of applications. Additionally, this technology integrates seamlessly with modern automation and robotics systems, enabling full integration within industrial production lines.

However, it is important to note that laser grinding is not without its drawbacks. The main barrier for many companies can be the high initial costs, including the purchase and maintenance of equipment. Moreover, this technology requires trained personnel to operate the machinery and perform precise calibrations. In some cases, such as processing very thick materials, traditional methods may still hold an advantage in terms of efficiency and cost-effectiveness.



Figure 1 Laser grinding



Figure 2 Laser grinding

2.3 Ultrasonic grinding

Ultrasonic grinding technologies are among the most innovative achievements in steel processing, gaining increasing significance in the industry. This method relies on the use of ultrasonic waves generated by devices that convert electrical energy into mechanical vibrations at very high frequencies. This approach to material processing enables exceptionally precise and gentle surface grinding, offering numerous benefits in terms of both quality and efficiency.

One of the greatest advantages of this technology is its ability to achieve exceptional precision. Ultrasonic waves allow for the creation of extremely smooth steel surfaces, which is especially critical in applications requiring flawless finishing, such as the production of surgical tools, precise measuring instruments, or aerospace components. Additionally, this technology significantly reduces the occurrence of surface microdamage, enhancing the durability and quality of finished products.

Another key advantage is the increased efficiency of the process. Ultrasonic waves facilitate faster steel processing by reducing friction between the tool and the material. This shortens production times and minimizes the wear and tear on machines and tools. Consequently, operational costs are lowered, which is particularly valuable for businesses aiming to optimize their industrial processes.

Ultrasonic technology is also far gentler on the processed material compared to traditional mechanical methods. The risk of deformation or structural damage, which can occur with techniques involving high temperatures or significant mechanical force, is minimized in this case. This preserves the material's integrity, which is especially important when working with expensive or specialized steels with high-performance characteristics.

Ultrasonic grinding finds applications across various industrial sectors. In the medical field, it enables the precise processing of elements like surgical tools and implants. In the automotive industry, this technology is used to manufacture components with complex geometries, such as parts of injection systems or drivetrains. In the electronics industry, where high-precision components are required, ultrasonic steel processing proves indispensable.

Despite its many advantages, ultrasonic technologies have certain limitations. The primary challenge is the high initial cost, including the purchase of advanced equipment and staff training. Operating these machines requires specialized knowledge and precise skills, which may necessitate additional investments in workforce training. Moreover, in the case of very large or thick elements, more conventional methods might prove more cost-effective.



Figure 3 Ultrasonic grinding of quartz glass

2.4 Artificial Intelligence in grinding

Artificial intelligence (AI)-based grinding technologies are revolutionizing the steel processing industry, setting new standards for efficiency, precision, and production quality. Powered by advanced algorithms, AI systems enable full automation and real-time optimization

of grinding processes. As a result, these processes become significantly more efficient, eliminating human error and ensuring the highest level of precision.

One of the key advantages of using AI in steel processing is the ability to continuously monitor machine parameters and dynamically adjust them. Intelligent systems analyze real-time data, such as rotational speed, pressure force, and tool wear, which helps maintain process stability. This results in products with an excellent finish, especially critical in industries such as aerospace, healthcare, and automotive, where precision is crucial.

AI also introduces real-time process adaptation. AI-based systems automatically adjust machine settings to changing conditions, such as material hardness variations or tool load levels. In practice, this means that machines can self-correct problems, reducing downtime and minimizing waste. This adaptability not only improves production efficiency but also helps to cut operational costs.

Another benefit of AI usage is the significant reduction in production time. Precise parameter control allows for faster completion of the grinding process while maintaining high consistency in quality. Each element is processed with identical precision, which is especially important in large-scale production, where maintaining uniform standards is essential.

Integrating AI with modern automation and robotics systems further enhances process efficiency. AI enables full synchronization across different production stages, reducing the risk of downtime and losses. As a result, the entire production line operates harmoniously and optimally.

Despite its many advantages, these technologies are not without their challenges. One main issue is the high initial implementation cost, which involves purchasing advanced equipment, software, and staff training. Operating such systems requires specialized knowledge and experience, which translates into additional financial investments. Furthermore, AI systems rely on data, so improper implementation or calibration issues may negatively affect the system's performance.

3. CONCLUSIONS

Modern grinding technologies, such as CNC grinding, laser grinding, ultrasonic grinding, and AI-driven grinding, have significantly advanced the steel processing industry. These methods provide exceptional precision, efficiency, and adaptability, making them essential in fields requiring high-quality machining and the production of complex components. Each method offers unique benefits: CNC grinding excels in repeatability and machining intricate shapes, laser grinding ensures unmatched precision and minimal material waste, ultrasonic grinding is particularly gentle on materials, and AI integration enhances automation, real-time optimization, and production line synchronization.

The advantages of these technologies include improved accuracy, reduced processing times, and consistency in mass production. Their applications span industries such as aerospace, automotive, medical, and electronics, where flawless finishes and intricate geometries are critical. However, these methods also present challenges. High initial costs, the need for specialized knowledge, and limitations in processing large or thick materials are significant barriers. Additionally, training personnel and maintaining advanced equipment require further investments.

Despite these challenges, the future of grinding technologies is promising. With the ongoing development of AI and automation, these methods will likely become even more efficient and accessible, overcoming current limitations and expanding their industrial applications. This

progress will ensure that modern grinding continues to play a vital role in meeting the demands of precision manufacturing.

ACKNOWLEDGEMENTS

The work was created as a result of the project as part of project of Students Scientific Circle of Laser Surface Treatment under the Initiative of Excellence - Research University, Silesian University of Technology, Gliwice, Poland.

BIBLIOGRAPHY

- [1] <https://radmot.com/pl/blog/szlifowanie-cnc>
- [2] <https://akrostal.pl/asortyment/cnc/szlifowanie-cnc-na-czym-polega-i-dlaczego-warto/>
- [3] <https://automatyzacja-adjatech.pl/2025/01/04/jakie-sa-najnowsze-technologie-w-szlifowaniu-stali/>
- [4] <https://www.youtube.com/watch?v=dLL3MtCYZZI>
- [5] https://www.youtube.com/watch?v=dC_rnRdVEH0
- [6] <https://www.youtube.com/watch?v=RXzbreypIV0>



31th January 2025
Gliwice, Poland

DEPARTMENT OF ENGINEERING MATERIALS AND BIOMATERIALS
FACULTY OF MECHANICAL ENGINEERING
SILESIA UNIVERSITY OF TECHNOLOGY

INTERNATIONAL STUDENTS SCIENTIFIC CONFERENCE

Assessment of the Anticipated Economic Efficiency of the Sheet Feeder and Turner Device for a Printing Machine

Tea Baramashvili^a, Nini Baidoshvili^b

^a PhD Degree in Mechanical Engineering and Technology, Professor, at Georgian Technical University, Faculty of Transport Systems and Mechanical Engineering, Georgia
email: baramashvili.t@gtu.ge

^b Vocational student, at Georgian Technical University, Faculty of Transport Systems and Mechanical Engineering, Georgia
email: niinbaidoshvili@gmail.com

Abstract: The article presents a sheet feeder and sheet turner mechanism for a printing machine, which is fully based on inverse transformation and can address the challenges of aligning the machine's operating components. The mechanism integrates two systems into a unified mechanical structure. The article evaluates the expected economic impact of the sheet feeder and sheet turner mechanism's operation, estimating that the economic benefit in a medium-scale printing enterprise could exceed 40 times the initial investment.

Keywords: Mechanism, Enterprise, Economic Effect, Printing Machine.

1. INTRODUCTION

Let us analyze the mechanisms of modern printing machines. We will examine these mechanisms, identify the negative outcomes of the technological processes carried out by them, which include defects caused by improper machine operation on printed materials, and explore ways to eliminate these issues [5].

Figure 1 presents a universal diagram of a sheet feeder mechanism. This mechanism can operate in both single-sided and double-sided printing modes [1].

In the first case, three cylinders perform the function of transferring the front portion of the sheet. The intermediate cylinder (2) has a dual diameter and, accordingly, two gripper bars that receive the sheet from the gripper bar of cylinder (1) and transfer it to the gripper bar of cylinder (3).

In the second case, the same cylinders perform the function of a reversing mechanism, as they operate in a mode that transfers the rear portion of the sheet to the third cylinder.

The transfer of the sheet's rear portion is performed by the grippers of the transfer cylinder, which execute a rotational motion combined with reversal. Afterward, the grippers (4) of the intermediate cylinder (2) grab the rear portion of the sheet at the alignment point of cylinders

(2) and (3). The grippers (5) then release the sheet at the rear portion, while the intermediate cylinder's guides (6) secure it.

During the cylinder's rotation, the grippers (5) carry out a rotational motion, controlling the rear portion of the sheet for a specific period. Upon releasing the grippers (4), the sheet is aligned in the correct direction and delivered from the upper surface of cylinder (2).

From this point onward, the sheet is fixed in a reversed position on cylinder (3), allowing the second side of the sheet to be printed. During the operation of the sheet-turning system, the configuration of the grippers (4) and auxiliary guides is adjusted based on the format. This adjustment can be performed manually or in automatic mode, depending on the requirements.

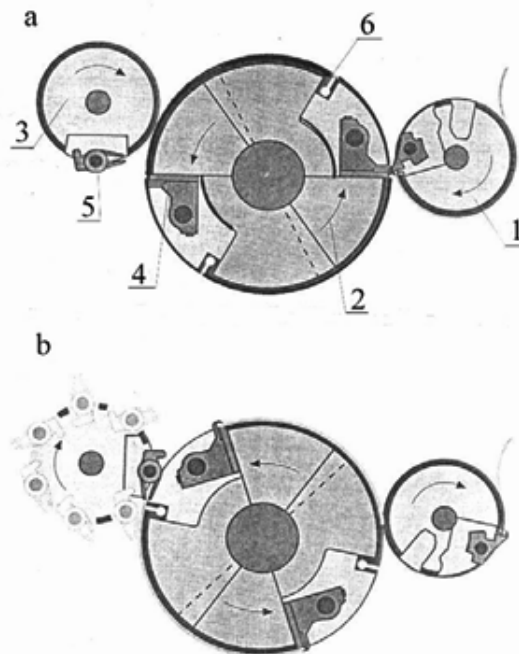


Figure 1. Sheet Feeder Mechanism

As noted, one of the main disadvantages of the sheet feeder mechanism may be the fact that the grippers, which are supposed to operate in synchronized mode, may fail to align properly in certain cases, leading to defective handling of the sheets. It is sufficient for the grippers of one cylinder to deviate by a fraction of a millimeter from the alignment with the grippers of the other cylinder for the mechanism to fail in sheet transfer, resulting in errors or malfunctions.

The mechanisms we developed, based on the principles of inverse kinematics, have successfully solved this issue. The sheet feeder and sheet turner mechanisms are designed with a remarkably simple structure and are protected under Patent P 4980, issued by the National Intellectual Property Center of Georgia, "Sakpatenti." This patent covers a system fully reliant on inverse kinematics and capable of addressing the alignment challenges of machine grippers [4].

The simplified design presented here integrates the operations of the two mechanisms into a single, unified mechanical system [2].

We have calculated the anticipated economic impact of the sheet feeder and sheet turner mechanisms for a printing machine. In a medium-scale printing enterprise, the estimated economic benefit from their implementation could exceed 40 times the initial investment.

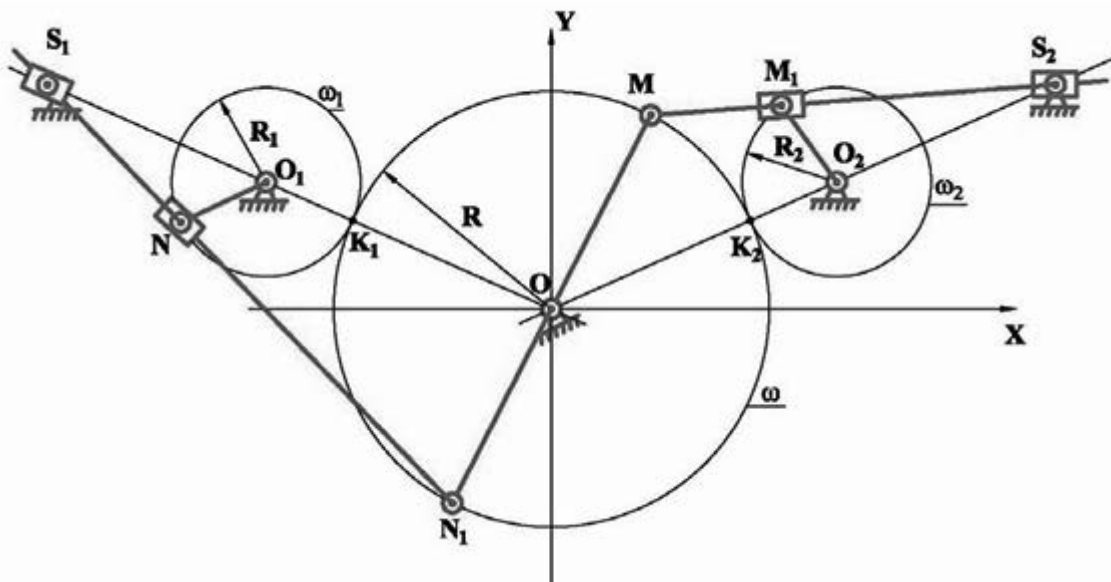


Figure 2. Structural Diagram of the Sheet Feeder and Turner Mechanism

On a national scale, the introduction of our developed sheet feeder mechanism in Georgian printing enterprises not only improves the parameters of double-sided printed products but also offers a tangible economic benefit for printing firms [3].

This benefit is achieved through cost reductions in labor, printing, and binding processes, as well as savings on consumables.

Considering the labor-saving potential of the sheet feeder mechanism, we can extend the evaluation to include the broader economic effect of labor cost reductions. In our case, this effect

$$\Xi = \left[3_1 \frac{B_2}{B_1} \cdot \frac{P_1 + E_n}{P_2 + E_n} + \frac{(U'_1 - U'_2) - E_n(U'_1 - U'_2)}{P_1 + E_n} - 3_2 \right] N$$

Where, Ξ - The annual expected economic effect is denoted;

3_1 and 3_2 - Allocated expenses correspond to market and alternative scenarios;

B_1 and B_2 - Production capacities correspond to market and alternative scenarios;

P_1 and P_2 - Retained operational efficiency over the long term corresponds to market and alternative scenarios;

U'_1 and U'_2 - Annual operational costs correspond to market and alternative scenarios;

E_n - The standard efficiency coefficient in the printing industry is set at 0.15;

N - The annual productivity of labor is measured in natural indicators.

Allocated expenses are limited by the sum of the product of the existing revenues generated through the use of the sheet feeder mechanism and the normative coefficient of the efficiency of additional capital investments

$$3 = C + E_n \Delta K$$

In our case, the revenue generated by the operation of the sheet feeder mechanism amounts to 12,000 GEL per month for an average-sized printing enterprise. Calculated per unit of production (one printed sheet), this equals 0.12 tetri.

The cost of preparing the mechanism we propose is estimated at 2,500 GEL, which, when distributed across unit production, amounts to 0.011 tetri. Taking these figures into account

$$3_2 = 0,12 + 0,15 \cdot 0,011 = 0,12165 \text{ (tetri)}$$

The relevant data for existing options have been increased accordingly, reflecting the values associated with the expansion of the printing line. For the specified case, we propose the following:

$$3_1 = 0,36 + 0,15 \cdot 0,007 = 0,36105 \text{ (tetri)}$$

The use of the sheet feeder mechanism in our proposed and existing options is approximately equivalent.

Therefore,

$$\frac{P_1 + E_n}{P_2 + E_n} = 1$$

Likewise, we can also consider the production capacity of labor resources as equivalent to 1, meaning that:

$$\frac{B_2}{B_1} = 1$$

As for operational costs, our mechanism allows for their reduction. This results in a savings of 0.24 tetri per unit of production, meaning that:

$$U'_1 - U'_2 = 0,24$$

As for the conclusion

$$\frac{(U'_1 - U'_2) - E_n(U'_1 - U'_2)}{P_1 + E_n} = \frac{0,24 + 0,15 \cdot 0,48}{0,1 + 0,15} = \frac{0,24 + 0,072}{0,25} = \frac{0,312}{0,25} = 1,24 \text{ (tetri)}$$

As for the condition, the annual economic effect per unit of production will be

$$3_1 = 0,36105 \cdot 1,248 - 0,12165 = 0,4505904 - 0,12165 = 0,3289404$$

An average-scale printing enterprise annually prints 60,000 conditional printed sheets, meaning that:

$$3 = 0,3289404 \cdot 60000 = 19736,424$$

Approximately 200 GEL per month, or 2,400 GEL annually.

Since the estimated cost of our proposed sheet feeder mechanism is 2,500 GEL, the payback period is:

$$T = \frac{K}{3} = \frac{2500}{2400} = 1,04 \text{ (yaer)}$$

2. CONCLUSION

The implementation of our developed sheet feeder mechanism in an average-scale printing enterprise provides an annual economic benefit of 2,400 GEL.

The initial costs will be recouped within slightly more than one year. On a national scale in Georgia, it can be estimated that the achieved economic effect will be at least 40 times greater.

ACKNOWLEDGEMENTS

The work was created as a result of the project as part of project based learning - PBL, in the 11th competition under the Initiative of Excellence - Research University, Silesian University of Technology.

BIBLIOGRAPHY

1. Research and Modeling of the Label Sticking Mechanism - T. Baramashvili, J. Uplisashvili, "Transport and Mechanical Engineering" – ISSN 1512-3537, No. 2(39) 2017, Tbilisi, p. 5-12.
2. J. Uplisashvili, N. Javakhishvili, T. Baramashvili - Inversion and its use, "Technical University" publishing house, Tbilisi, 2013.
3. Uflisashvili J., Natbiladze N., "Geometrical Foundations of Printing Machine's Movable Spatial Systems," Tbilisi, 2009.
4. J. Uflisashvili, Z. Uflisashvili, I. Ugrekhelidze, T. Baramashvili, "Belt-Pulley Inverter," GE P 2010 4980 B, Filed 04.22.2009.
5. "Offset Printing Machines," Printing Systems of HEIDELBERG, Moscow, MSUP Publishing, 1999.



31th January 2025
Gliwice, Poland

DEPARTMENT OF ENGINEERING MATERIALS AND BIOMATERIALS
FACULTY OF MECHANICAL ENGINEERING
SILESIA UNIVERSITY OF TECHNOLOGY

INTERNATIONAL STUDENTS SCIENTIFIC CONFERENCE

Impact of Technological Parameters of Steel Laser Cutting on the Quality of Large-Scale Finished Products

Piotr Bąk^a, Mirosław Bonek^b

^a Silesian University of Technology, Faculty of Mechanical Engineering, Department of Automation of Technological Processes and Integrated Manufacturing Systems

^b Silesian University of Technology, Faculty of Mechanical Engineering, Department of Engineering Materials and Biomaterials
email: miroslaw.bonek@polsl.pl

Abstract: This article examines the influence of technological parameters in the laser cutting process on the quality of large-scale steel products. Key factors such as laser power, cutting speed, shielding gas type, and focal distance are analyzed to determine their impact on surface quality, dimensional accuracy, and structural integrity. The study integrates literature review, numerical modeling, and experimental research to identify optimal process parameters. The results emphasize the importance of precise parameter adjustment to minimize defects, reduce the heat-affected zone (HAZ), and enhance product durability. Additionally, the article highlights the role of quality management systems and material testing in ensuring high-quality outputs. The findings have practical applications in industries such as construction, automotive, and energy, where precision and efficiency are critical. The article also discusses the life cycle of laser sources and cutting heads, providing insights into their management for improved operational efficiency.

Keywords: Large-scale products, Heat-affected zone (HAZ), Industrial applications, Surface quality

1. INTRODUCTION

This article investigates the relationship between key technological parameters—such as laser power, cutting speed, shielding gas type, and focal distance—and the quality of laser-cut surfaces. The study is structured around three main pillars: theoretical analysis, numerical modeling, and experimental validation. By integrating these approaches, the research aims to provide a comprehensive understanding of how process parameters influence surface quality, dimensional accuracy, and material properties.

A significant focus is placed on the life cycle of laser sources and cutting heads, which directly impacts the efficiency and reliability of the cutting process. The article also discusses the role of quality management systems, including real-time monitoring and material testing, in

optimizing production processes and minimizing defects. Practical applications of the research findings are highlighted, demonstrating their relevance to industries requiring high-precision components.

By combining advanced analytical tools with experimental data, this study contributes to the ongoing effort to enhance the quality and efficiency of laser cutting processes, particularly for large-scale steel products.

2. LIFE CYCLE OF LASER SOURCE AND CUTTING HEAD IN LASER PROCESSING OF LARGE-FORMAT MATERIALS

2.1 The life cycle of a laser source and cutting head can be divided into several key phases:

the run-in phase, the mature life phase and the wear-out phase. Each of these phases has a significant impact on the efficiency of the laser processing, especially in the case of large-format materials, where high precision and system reliability are required [1].

Run-in Phase

During the burn-in phase, the laser source and cutting head undergo intensive testing to detect any manufacturing defects or assembly-related issues. In this period, a relatively high failure rate is observed, which is typical for new equipment. The tests include operation under various load conditions to ensure that the components are ready for long-term use [2].

Mature Life Phase

After successfully passing the burn-in phase, the laser source and cutting head enter the useful life phase. During this period, the failure rate is low, and the system's performance remains consistently high. This is the stage where the laser system is most efficient and cost-effective to operate. For large-format material processing, stable laser operation is crucial for maintaining cutting quality and minimizing downtime [3].

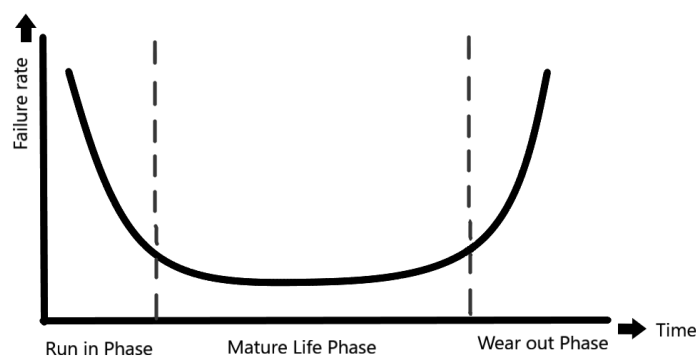


Figure 1. Graphical representation of the laser life cycle

Wear-out Phase

Over time, both the laser source and the cutting head begin to show signs of wear. For the laser source, this may include a decrease in output power, beam instability, or cooling issues. The cutting head, on the other hand, may experience mechanical wear, such as nozzle degradation,

lens wear, or optical system misalignment. In this phase, the risk of failure increases, and maintenance costs rise [4].

2.2 Impact of Cutting Head Wear or Collision on Surface Quality

Wear of the cutting head, especially during the wear-out phase or after a collision, has a direct impact on the quality of the processed material surfaces. The cutting head consists of precision optical components, such as lenses and nozzles, which are critical for focusing the laser beam and effectively removing molten material. If these components become worn or damaged, the following issues may arise:

1. **Deterioration of Cutting Edge Quality:** Worn lenses or nozzles can lead to beam defocusing, resulting in uneven edges and increased surface roughness [5].
2. **Dimensional Inaccuracies:** Mechanical damage to the cutting head, such as after a collision, can cause beam misalignment, leading to errors in the dimensions of the cut parts [6].
3. **Increased Heat-Affected Zone (HAZ):** Worn optical components can cause inefficient removal of molten material, increasing the heat-affected zone and leading to undesirable structural changes in the material [7].

2.3 Management of the Laser Source and Cutting Head Life Cycle

To maximize the efficiency of the laser system, especially in the processing of large-format materials, it is crucial to manage the life cycle of the laser source and cutting head.

This includes:

1. **Regular Technical Inspections:** Systematic checks of the laser source and cutting head allow for early detection of wear and prevention of failures [8].
2. **Monitoring Operational Parameters:** Tracking parameters such as output power, cooling temperature, and beam quality helps assess the system's condition and plan maintenance [9].
3. **Component Replacement Planning:** Replacing the laser source or cutting head before reaching the end-of-life phase minimizes the risk of downtime and production losses [10].

2.4 Conclusions

The life cycle of the laser source and cutting head is crucial for the efficiency of laser processing, especially for large-format materials. Understanding the various phases of the life cycle, from burn-in through useful life to wear-out, allows for optimal management of the laser system. The bathtub curve serves as a useful tool for visualizing this process, aiding in the planning of maintenance and component replacement. Proper life cycle management can significantly extend the effective operational time of the laser system and minimize costs associated with failures [11].

3. QUALITY MANAGEMENT AND UTILIZATION OF MATERIAL TESTING IN A FACILITY SPECIALIZING IN LASER PROCESSING OF LARGE-FORMAT MATERIALS

In facilities specializing in laser processing of large-format materials, quality management and material testing are crucial for ensuring high-quality end products and optimizing production processes. Effective quality management involves not only monitoring process parameters but

also analyzing the impact of laser processing on material properties, which helps minimize errors and increase production efficiency [12].

3.1 Quality Management Strategies in Laser Processing

Real-Time Monitoring Systems:

- Modern facilities use advanced monitoring systems to track key process parameters such as laser power, cutting speed, assist gas pressure, and focal distance. This allows for quick detection of deviations from standards and process adjustments, minimizing the risk of defective products [13].
- Examples of such systems include laser sensors and thermal imaging cameras, which enable continuous assessment of cutting quality and detection of surface defects such as uneven edges or material overheating [14].

1. Surface Quality Control:

- After the cutting process, surface quality is evaluated using measurement tools such as laser profilometers and electron microscopes. These tests determine surface roughness, the presence of burrs, and the heat-affected zone (HAZ) [15].
- For large-format materials, ensuring uniform quality across the entire surface of the processed component is particularly important, requiring precise adjustment of process parameters to the material's thickness and type [15].

2. Analysis of Material Properties:

- Material testing, such as hardness tests, microstructure analysis, and strength testing, is essential for assessing the impact of laser processing on mechanical properties. The results of these tests allow for the optimization of cutting parameters to minimize undesirable changes in the material, such as microcracks or thermal distortions [16].

3.2 Utilization of Material Testing in Process Optimization

Material testing is an integral part of quality management in facilities specializing in laser processing.

It includes:

1. Microstructure Analysis:

- Microscopic examinations allow for the evaluation of changes in the material's structure after laser processing, such as grain size, the presence of intermediate phases, and potential defects. This is particularly important for materials sensitive to high temperatures, such as high-alloy steels [17].

2. Hardness Testing:

- Measuring the material's hardness before and after laser processing helps assess the impact of the process on mechanical properties. For large-format materials, changes in hardness may indicate undesirable phenomena such as overheating or uneven cooling [18].

3. Strength Testing:

- Strength tests, such as tensile or impact tests, are crucial for evaluating the impact of laser processing on material durability. The results of these tests allow for the adjustment of process parameters to ensure optimal strength of the finished components [19].

3.3 Optimization of the Laser Processing Process

The use of material testing results and quality management systems enables the optimization of the laser processing process.

Key steps include:

1. Adjustment of Cutting Parameters:

- Based on material testing results and quality monitoring, cutting parameters such as laser power, cutting speed, and assist gas type are adjusted to meet specific material requirements. This ensures high-quality cutting with minimal thermal impact.

2. Waste Reduction:

- Effective quality management reduces waste by early detection of defective components and process correction. This is particularly important for large-format materials, where material costs are significant.

3. Increased Production Efficiency:

- Continuous quality monitoring and process parameter optimization increase production efficiency while maintaining high-quality end products [20].

4. PRACTICAL APPLICATIONS OF RESEARCH RESULTS

The research findings have broad applications in industries such as construction, automotive, and energy sectors. Optimizing laser cutting parameters enables the production of high-precision and durable components while minimizing production costs. The use of gases such as nitrogen improves surface quality, which is particularly important for components exposed to corrosion. [12]

4.1 Design of a Quality Control System for Large-Format Products After Laser Cutting

As part of the topic "Analysis of the Impact of Technological Parameters of the Laser Cutting Process on the Quality of Large-Format Steel Products," a quality control system for large-format products has been designed. The purpose of this system is to ensure that the cut elements meet quality requirements such as dimensional accuracy, edge quality, and the absence of surface defects. Below is the concept of the system and a description of its operation. [13]

5. CONCEPT OF THE QUALITY CONTROL SYSTEM

The system consists of several key modules that work together to provide comprehensive quality control:

Measurement Module:

- **3D Scanner:** A 3D scanner is used to measure the geometry of the cut elements, allowing for precise mapping of the shape and dimensions of the product. The scanner compares the obtained data with the CAD model, enabling the detection of any deviations. [14]
- **Micrometers and Laser Calipers:** Precise measuring tools such as micrometers and laser calipers are used to measure material thickness and the width of the cut kerf. [15]

Vision Module:

- **High-Resolution Cameras:** The system is equipped with industrial cameras that record the cutting surface in high resolution. These cameras allow for the detection of surface defects such as burrs, unevenness, or signs of overheating.
- **Image Analysis Software:** The collected images are analyzed by specialized software that identifies irregularities based on predefined quality criteria. [16]

Thermal Imaging Module:

- **Thermal Camera:** A thermal camera is used to assess the temperature distribution on the cut edges. This allows for the detection of overheated areas that could lead to microcracks or structural changes in the material.

Reporting Module:

- **Data Management System:** All measurement data is collected in a data management system that generates quality reports. These reports contain information on dimensional deviations, surface defects, and other quality parameters. [19]

5.1 Description of the System Operation

1. Geometry Measurement:

- After the laser cutting process is completed, the product is placed on a measurement station. The 3D scanner scans the entire surface, creating a point cloud that is compared with the CAD model. If dimensional deviations are detected, the system generates an alert.

2. Edge Quality Analysis:

- High-resolution cameras record the cutting surface, and image analysis software identifies defects such as burrs, unevenness, or signs of overheating. The analysis results are compared with quality standards.

3. Thermal Control:

- The thermal camera records the temperature distribution on the cut edges. Areas with elevated temperatures are analyzed for the risk of microcracks or structural changes.

4. Report Generation:

- All data from the measurement, vision, and thermal imaging modules are sent to the data management system, which generates a quality report. The report includes information on dimensional deviations, surface defects, and other quality parameters.

5.2 Precision of Measurements:

- The use of a 3D scanner and precise measuring tools such as micrometers and laser calipers ensures measurement accuracy at the micrometer level. This is crucial for ensuring the dimensional compliance of the cut elements with the design. [14]

Comprehensive Quality Control:

- The system combines geometry measurement, visual analysis, and thermal control, allowing for the detection of both dimensional and structural defects. This ensures high-quality final products.

Automation of the Process:

- The use of CNC systems and image analysis software allows for the automation of the quality control process. This reduces the risk of human error and shortens the time required for inspection.

Flexibility of the System:

- The system can be easily adapted to various production requirements, which is particularly important for mass production and prototyping. The ability to integrate with CAD/CAM systems allows for the quick generation of quality control programs based on 3D models. [17]

Compliance with Quality Standards:

- The system has been designed with international quality standards such as ISO 9001 in mind, ensuring that the cut elements meet customer requirements and industry regulations. [19]

5.3 Conclusions about concept

The designed quality control system for large-format products after laser cutting is a comprehensive solution that ensures high-quality cut elements. By combining precise measuring tools, advanced vision systems, and thermal imaging, the system enables the detection of both dimensional and structural defects. The automation of the quality control process and the ability to integrate with CAD/CAM systems make the system flexible and efficient, leading to increased production efficiency and reduced costs.

6. MANAGEMENT OF THE RESEARCH PROCESS OF LARGE-FORMAT MATERIALS AFTER LASER PROCESSING

The process of researching surfaces after laser processing of large-format materials requires careful management to ensure the reliability of results and their usefulness in optimizing production processes. Managing this process involves planning the research, selecting appropriate measurement methods, analyzing data, and formulating research questions that allow for a deep understanding of the impact of laser processing parameters on surface quality. Below are the key aspects of managing the research process and examples of research questions. [12]

6.1 Management of the Research Process

1. Research Planning:

- **Defining Objectives:** Before starting the research, it is necessary to clearly define the objectives, such as assessing the impact of laser cutting parameters (power, cutting speed, type of assist gas) on surface quality, including roughness, presence of defects, and mechanical properties. [13]
- **Sample Selection:** Large-format materials, such as steel sheets with a thickness of 10-20 mm, should be subjected to laser processing with different parameters to enable comparison of results.
- **Measurement Methods:** Appropriate measurement methods should be selected, such as profilometry for surface roughness evaluation, scanning electron

microscopy (SEM) for microstructure analysis, and hardness tests for assessing mechanical changes [15].

2. Conducting the Research:

- **Process Parameter Control:** During laser processing, parameters such as laser power, cutting speed, and assist gas pressure should be precisely controlled to ensure repeatability of results [16].
- **Surface Measurements:** After processing, surface roughness measurements should be performed using a profilometer, and microstructure should be evaluated using electron microscopy [17].

3. Data Analysis:

- **Statistical Analysis of Results:** Measurement results should be subjected to statistical analysis to determine the significance of the impact of individual processing parameters on surface quality.
- **Interpretation of Results:** Based on the obtained data, conclusions should be drawn regarding the optimal laser processing parameters that ensure the best surface quality. [19]

4. Reporting:

- **Generating Reports:** Research results should be presented in the form of reports containing charts, tables, and conclusions. These reports are crucial for further optimization of production processes. [20]

6.2 Formulation of Research Questions

To effectively manage the research process, it is necessary to formulate relevant research questions that allow for an in-depth analysis of the impact of laser processing on surface quality. Examples of such questions include:

1. Impact of Processing Parameters on Surface Roughness:

- How does changing the laser power affect the surface roughness after laser processing?
- Does increasing the cutting speed lead to a reduction in surface roughness? [14]

2. Impact of Assist Gas Type on Edge Quality:

- How does the type of assist gas (oxygen, nitrogen) affect the formation of defects such as burrs or oxidation?
- Does the use of nitrogen as an assist gas reduce the risk of microcracks on the cut edges? [16]

3. Analysis of Surface Microstructure:

- How does laser processing affect the microstructure of the material surface, including grain size and the presence of intermediate phases?
- Do changes in laser cutting parameters lead to changes in the surface hardness of the material? [17]

4. Assessment of the Impact of Processing on Mechanical Properties:

- How does laser processing affect the tensile strength and impact toughness of the material?

- Can changing laser cutting parameters improve resistance to abrasive wear? [20]

5. Optimization of the Processing Process:

- Which laser cutting parameters (power, speed, type of gas) provide the best surface quality with minimal heat-affected zone (HAZ)?
- Is it possible to develop a mathematical model predicting surface quality based on laser processing parameters? [13]

7. CONCLUSIONS

1. Proper adjustment of laser cutting process parameters ensures high-quality steel products.
2. The choice of shielding gas is crucial for minimizing surface defects.
3. Numerical modeling combined with laboratory experiments allows precise process optimization.
4. Laser cutting of large-scale products requires special attention to dimensional stability and surface quality.
5. Combining computer simulations with advanced experimental analysis enables a deeper understanding of processes occurring during laser cutting.
6. Managing the research process of surfaces after laser processing of large-format materials requires a comprehensive approach, including planning, conducting research, analyzing data, and formulating research questions. This allows for obtaining reliable results that enable the optimization of production processes and improvement of the quality of final products. It is also crucial to consider the impact of laser processing parameters on surface properties, which allows for adapting the process to the requirements of specific industrial applications.

ACKNOWLEDGEMENTS

The work was created as a result of the project as part of project based learning - PBL, in the 11th competition under the Initiative of Excellence - Research University, Silesian University of Technology, Gliwice, Poland and as part of project of Students Scientific Circle of Laser Surface Treatment under the Initiative of Excellence - Research University, Silesian University of Technology, Gliwice, Poland.

BIBLIOGRAPHY

1. J. Powell, "Introduction to Laser Technology," Institute of Physics Publishing, 2004.
2. M. Kowalski, "Numerical Modeling of Laser Cutting Processes," Czasopismo Techniczne, 2020.
3. G. Thompson, "Laser-Assisted Nanostructured Coatings," CRC Press.
4. W. Napadłęk, "3D Technologies in Shape Reconstruction," Autobusy: Technika, 2017.
5. X. Wang, "Computer-Aided Design and Simulation of Laser Processing," Springer, 2018.
6. J. Radziejewska, "Laser Surface Modification," PAN, 2011.
7. B. Stępak, "Impact of Laser Process Parameters on Nanostructured Coatings," Engineering Materials, 2019.

8. M. H. Lee, "Laser Processing of Engineering Materials," Elsevier, 2005.
9. D. Panek, "Laser Treatment of Austenitic Steel," Student Scientific Circles Publications, 2007.
10. Steen, W. M., & Mazumder, J. (2010). Laser Material Processing. Springer.
11. Katayama, S. (2013). Handbook of Laser Welding Technologies. Woodhead Publishing.
12. Li, L. (2008). "Laser Surface Engineering: Processes and Applications." *Journal of Materials Processing Technology*, 208(1-3), 19-25.
13. Ion, J. C. (2005). Laser Processing of Engineering Materials: Principles, Procedure and Industrial Application. Butterworth-Heinemann.
14. Dahotre, N. B., & Harimkar, S. P. (2008). Laser Fabrication and Machining of Materials. Springer.
15. Ready, J. F. (2001). Industrial Applications of Lasers. Academic Press.
16. Powell, J. (1998). CO2 Laser Cutting. Springer.
17. Chryssolouris, G. (1991). Laser Machining: Theory and Practice. Springer.
18. Yilbas, B. S., & Sami, M. (1997). "Laser Cutting Quality Assessment and Thermal Efficiency Analysis." *Journal of Materials Processing Technology*, 70(1-3), 263-273.
19. Schuöcker, D. (1998). High Power Lasers in Production Engineering. World Scientific.
20. Olsen, F. O. (2009). Hybrid Laser-Arc Welding. Woodhead Publishing.



31th January 2025
Gliwice, Poland

DEPARTMENT OF ENGINEERING MATERIALS AND BIOMATERIALS
FACULTY OF MECHANICAL ENGINEERING
SILESIA UNIVERSITY OF TECHNOLOGY

INTERNATIONAL STUDENTS SCIENTIFIC CONFERENCE

Topological optimization of the drone frame

Natalia Bijok^a, Sylwia Dziwoki^b, Kinga Stępska^c, Martyna Urbańska^d, Jan Wypiór^e, Magdalena Hulbójf^f, Emilia Krzystanek^g, Krzysztof Goczoł^h, Mariusz Król^{i*},

^a Studentka kierunku Inżynieria Produkcji i Zarządzania, e-mail: nb309657@student.polsl.pl

^b Studentka kierunku Inżynieria Produkcji i Zarządzania, e-mail: sd309660@student.polsl.pl

^c Studentka kierunku Inżynieria Produkcji i Zarządzania, e-mail: ks309686@student.polsl.pl

^d Studentka kierunku Inżynieria Produkcji i Zarządzania, e-mail: mu309689@student.polsl.pl

^e Student kierunku Inżynieria Produkcji i Zarządzania, e-mail: jw309692@student.polsl.pl

^f Studentka kierunku Inżynieria Produkcji i Zarządzania, e-mail: mh309664@student.polsl.pl

^g Studentka kierunku Inżynieria Produkcji i Zarządzania, e-mail: ek309672@student.polsl.pl

^h Student kierunku Inżynieria Produkcji i Zarządzania, e-mail: kg309663@student.polsl.pl

ⁱ Politechnika Śląska, Wydział Mechaniczny Technologiczny, Katedra Materiałów Inżynierskich i Biomedycznych, e-mail: mariusz.krol@polsl.pl,

Abstract: Drones are uncrewed aerial vehicles that can be either remotely controlled or autonomous. Their increasing range of applications has made them more prevalent. This study focuses on optimizing the topological design of a drone's support structure. To achieve this, we utilized the integrated CAD-CAE system of SolidWorks, which includes a Finite Element Analysis (FEA) module and a specialized topological optimization module. The optimization process led to a significant reduction in the weight of the drone's structure while ensuring that all mechanical criteria for strength and stiffness were met. The findings demonstrate that using numerical methods within CAD software makes optimization not just a theoretical concept, but rather a practical tool that is accessible to any design engineer.

Keywords: *drone, frame, topology optimization, CAD*

1. INTRODUCTION

Quadcopters are among the most popular types of uncrewed aerial vehicles (UAVs) and are used in various fields, including environmental monitoring, rescue operations, parcel delivery, and technical inspections. Their popularity is due to unique capabilities such as hovering, high maneuverability, and the ability to take off and land vertically in confined spaces. Modern applications of quadcopters often involve balancing the need to minimize weight with the requirement for sufficient structural strength.

In the project, we developed an optimized quadcopter frame based on an accurate model. Our goal was to reduce the weight of the original structure while maintaining adequate structural integrity. We utilized SolidWorks CAD software to achieve this. The design and

optimization processes were conducted on actual drones, allowing us to accurately replicate their dimensions and shapes in SolidWorks before optimizing their frames [1-6].

2. AIM OF THE RESEARCH

After thoroughly understanding the design requirements and the specifics of the drone model, the next step was to input this data into CAD software, specifically SolidWorks. This stage was crucial, as accurately mapping the physical model's geometry laid the groundwork for further design and optimization activities. The drone frame was mapped using SolidWorks based on the model's dimensions and shapes.

3. MAIN FEATURES OF THE DRONE FRAME

The first step in transferring dimensions to the CAD software involved accurately measuring the drone that would serve as the starting point for the project. Precision tools, such as calipers and tape measures, were employed for this purpose. Additionally, a 3D scanner was utilized to gather precise data on the shapes and sizes of the main frame components, including the arms, central platform, motor mounts, and openings for other components. The actual weight of the drone was 41 grams (Figure 1). This information was then used to compare the drone's design with the exact model and assess optimization opportunities.



Figure 1. The weight of drone with electronics and battery

Using this data, a basic 3D model that accurately represents the actual drone frame was created in the initial modelling phase. This model served as the foundation for further design

and optimization activities, acting as a reference point for subsequent stages. During this phase, key design features were incorporated, including motor mounting locations, electrical connectors, battery compartments, and other relevant components.

Topological optimization of a quadcopter drone focuses on structuring the materials in the drone's design to create the lightest and most robust framework possible. This process aims to meet essential criteria for strength, stiffness, and aerodynamics. The goal is to enhance flight performance while minimizing weight, which is vital for the effectiveness of drones.

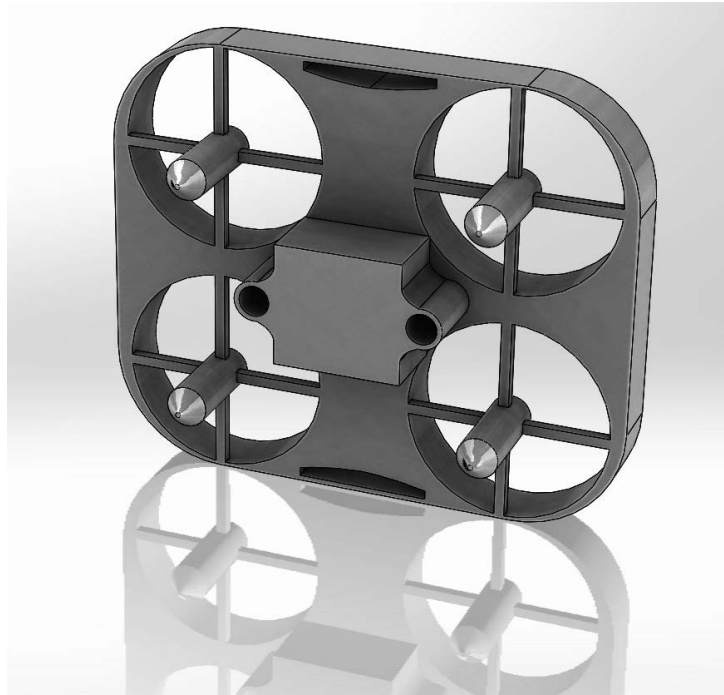


Figure 2. The digital model of drone frame

The 41g drone required optimization of its structure to achieve maximum strength with minimal weight. The process began with the application of topological optimization algorithms, which analyze the distribution of material throughout the structure while considering loads and constraints related to strength and functionality. This topological optimization allowed for a significant reduction in the drone's mass without compromising its structural stability. The focus was placed on key structural components, such as the frame and mounts, where modifications were made to the wall thickness and shape of these elements. This approach effectively reduced weight while ensuring that the components maintained sufficient strength to withstand the necessary loads.

Topographical optimization is carried out in the following steps:

1. Load the created drone model.
2. In SolidWorks, go to the 'Simulation' tab and start a new study. Select the topography test option.
3. Choose the material identified as the most suitable for the structure.
4. Define the external loads to establish the forces acting on the model.
5. Add relationships.

6. Set the test objectives. In this case, select the ‘minimize mass’ command. The program will display the initial mass of the object along with the final mass after optimization.
7. Run the test. The results will be shown on a material mass graph.
8. Based on the solution proposed by the program, create a new design that meets the technological requirements. Once the optimization is complete, the optimized model can undergo further tests, such as a strength test.

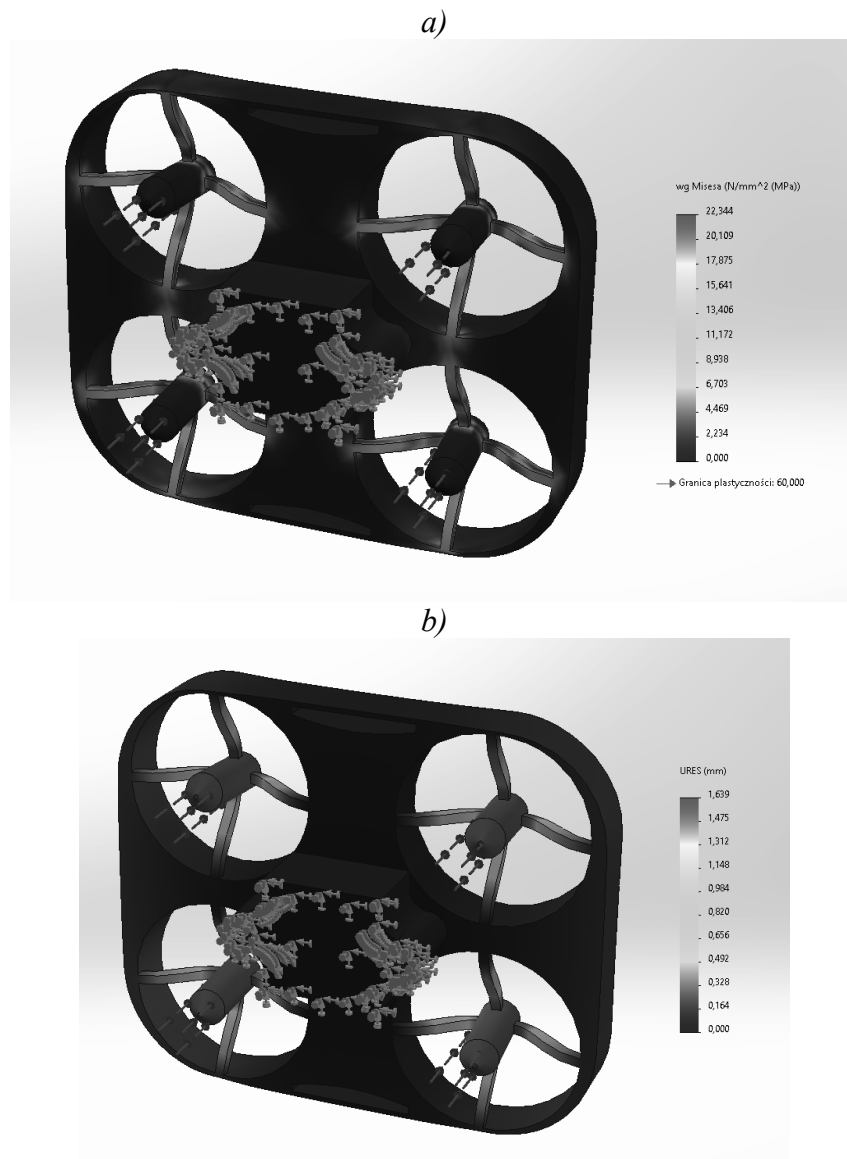


Figure 3. Static structural analysis results of the original quadcopter frame:

a) Von Mises stress state, b) deformation state.

A thrust force of 20 N is applied to the four propeller slots, with a fixed boundary condition placed on the central slot. By employing quarter symmetry, we ensure that the optimized structure is consistently uniform across all four sides after the Finite Element Analysis (FEA).

Using a fine mesh on the geometry significantly enhances the optimization results, leading to improved performance and efficiency. A thorough static structural analysis was performed, revealing significant insights. The results showcased in Figures 3a and 3b highlight a maximum von Mises stress of 22 MPa and a deformation of 1.7 mm, underscoring the reliability and performance of the design.

4. TOPOLOGY OPTIMIZATION

The finite element analysis (FEA) of the drone frame, followed by topology optimization, is essential to achieve the best material distribution by removing excess material. This crucial process not only reduces weight but also enhances the drone's structural efficiency and aerodynamic performance, ultimately leading to a superior thrust-to-weight ratio.

Given that the permissible yield stress of Nylon 101 is 60 MPa, it's vital to limit the stress on the airframe structure to 22 MPa, considering a safety factor of three. Utilizing the SolidWorks topology optimization tool allows us to approximate the most effective design for the quadcopter frame, based on strategically determined preserved regions, as illustrated in Figure 4. The outcome of this optimization is impressive, resulting in an airframe that weighs just 33 grams.

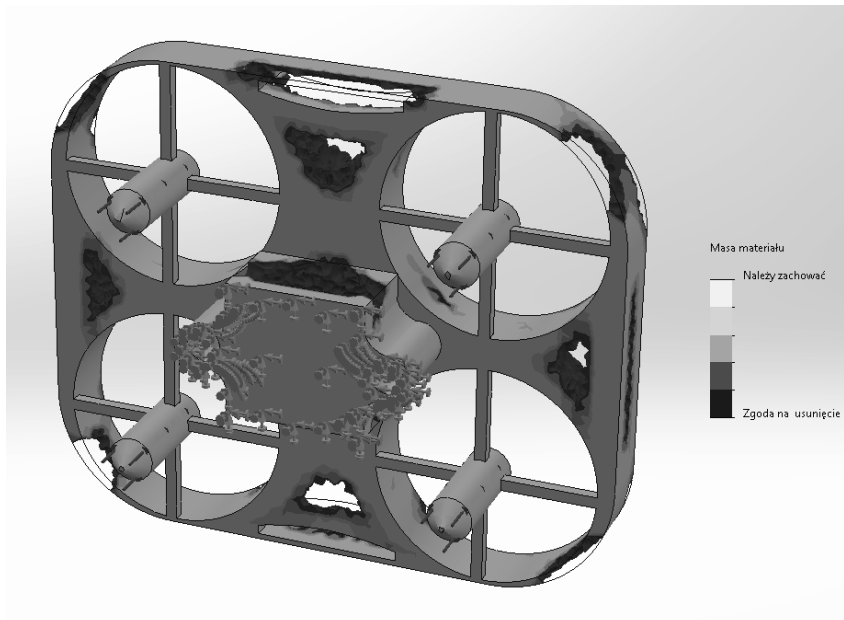


Fig. 4. Airframe topology after optimization

7. SUMMARY

This paper outlines a comprehensive design and topological optimization process for quadcopter frames created using SolidWorks CAD software. Our primary objective was to reduce the weight of the drone while ensuring its structural integrity and strength, both of which are essential for enhancing flight performance.

In summary, this work has demonstrated that combining advanced CAD modeling with topological optimization facilitates the design of lightweight yet sturdy structures for quadcopters. This approach effectively meets the demands of modern applications, enhancing the versatility and efficiency of these devices in various fields, including technical inspection, environmental monitoring, and parcel delivery.

ACKNOWLEDGEMENT

The current study was conducted as part of the collaborative activities of the Student Research Group 'GYROID' at the Department of Engineering and Biomedical Materials, Faculty of Mechanical Engineering, Silesian University of Technology in Gliwice.

This thesis was developed as a result of a project focused on practical, hands-on, project-oriented education (PBL), which was part of competition VI in the Excellence Initiative—Research University program at Silesian University of Technology.

LITERATURE

1. <https://cdotimes.com/2024/05/21/what-is-a-drone-built-in/>
2. https://help.solidworks.com/2021/polish/SolidWorks/cworks/c_generative_design_study.htm
3. B. Pacula, *Optymalizacja masy konstrukcji, Projektowanie i Konstrukcje Inżynierskie*, Listopad 2017
4. K. Mohsin Ali; M. Ali Tawafik; A. Adbulhady Jaber, *Quadcopter 3d-printer frame static optimization*, AIP Conf. Proc. 2977, 020034 (2023)
5. B. Galek, D. Skibicki, *Optymalizacja topologiczna konstrukcji nośnej drona*, *Developments in Mechanical Engineering*, 18(10)2022,
6. <https://www.instructables.com/PROJECT-SOLIDWORK-DRONE-UMP/>



31th January 2025
Gliwice, Poland

DEPARTMENT OF ENGINEERING MATERIALS AND BIOMATERIALS
FACULTY OF MECHANICAL ENGINEERING
SILESIAAN UNIVERSITY OF TECHNOLOGY

INTERNATIONAL STUDENTS SCIENTIFIC CONFERENCE

Materials for the automotive industry - characteristics and challenges of the automotive industry

Zofia Błaszczyk^a, Paulina Dymara^a, Szymon Szczotka^a, Barbara Grzegorzczuk^b

^a Students of the Maria Konopnicka Secondary School with Bilingual Departments in Katowice

^b Silesian University of Technology, Faculty of Mechanical Engineering, Department of Engineering and Biomedical Materials,
email: barbara.grzegorzczuk@polsl.pl

Abstract: The modern automotive industry faces a number of challenges related to the selection of materials that must combine lightness, strength, affordability and environmental friendliness. Among the materials used in car construction, steels play a particularly important role, which still remain the dominant raw material used to build bodies, chassis and many other car components. Higher requirements for fuel efficiency, safety and environmental protection mean that steel must meet increasingly stringent standards and specifications. Increasing the participation of lightweight metals in whole construction is part of efforts to reduce fuel consumption and carbon dioxide emissions into the atmosphere. Considering the aspects of environmental sustainability, sheets are easier to recycle than composite materials. At the same time, in the last decade there has been an increase in research related to plastic forming of sheets from non-ferrous metal alloys. This article presents an overview of the basic applications of construction materials in the automotive industry. The article focuses on the four largest groups of metal materials: steels, aluminum alloys, titanium alloys and magnesium alloys.

Keywords: materials, automotive industry, steels, aluminum alloys, titanium alloys, magnesium alloys.

1. INTRODUCTION

During choosing materials for bodywork components, car manufacturers are guided by technological, material and economic considerations. However, it is often not possible to meet all these requirements at the same time, which is why different materials are currently used, including non-ferrous metal alloys and steel. Historically, steel was the first widely used construction material in the automotive industry. With the advancement of sheet metal production and processing technology, steel replaced wooden components in cars, with mainly low-carbon steel (LC), characterized by moderate mechanical strength and low corrosion resistance, being used. Acting towards reducing the weight of vehicles, and thus reducing fuel consumption and harmful gas emissions, has influenced the development of materials used in the construction of the body and chassis components. Traditional carbon steel sheets and

profiles are gradually being replaced by their lighter counterparts, such as aluminum, magnesium or titanium alloys [1-3].

2. CHARACTERIZATION OF MATERIALS IN THE AUTOMOTIVE INDUSTRY

2.1 Steel

Steels in the automotive industry are crucial and remain irreplaceable in many construction applications. Conventional deep-drawn sheets made of low-carbon steel are used for the construction of car bodies. The carbon content in these steels does not exceed 0.12% by weight, and the yield strength is less than 300 MPa. Low-Strength Steels (LLs) can be divided into two groups: Mild Steels (MSs) and Interstitial Free (IF) steels. High-Strength (HS) steels include Isotropic Steels (ISs), Interstitial Free–High-Strength (IF–HS) steels, Bake Hardening (BH) steels, Carbon–Manganese (CMn) steels, Press Quenched Steels (PQSs), and High-Strength Low Alloy (HSLA) steels. Dual Phase (DP) steels, Ferrite–Bainite (FB) steels, Complex Phase (CP) steels, Transformation Induced Plasticity (TRIP) steels, and martensitic (MS) steels are classified as ultra-high-strength steels (UHS). Development of Advanced High-Strength Steels (AHSS) the third generation introduced new varieties, such as Dual Phase–High Ductility (DH) steels, Complex Phase–High Ductility (CH) steels, TRIP Aided Bainitic Ferrite (TBF) steels, Carbide-Free Bainite (CFB) steels, and Quenching & Partitioning (QP) steels (Fig.1) [4-6].

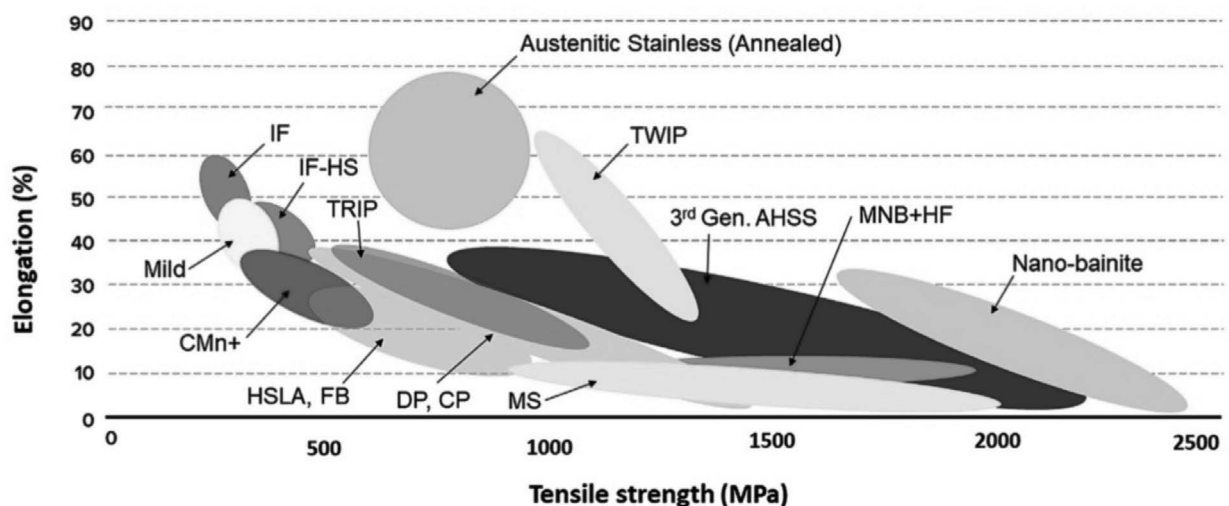


Fig.1. Classification of steels used in the automotive industry [4]

An example of the increasing application of advanced multiphase steels can be observed in the Jeep Grand Cherokee L (2021), where 60% of the body construction consists of Advanced High-Strength Steels (AHSS) and third-generation steels. The development of High-Strength (HS) and Ultra-High-Strength (UHS) steels was driven by the need to reduce vehicle mass while maintaining high stiffness of car bodies. One method to achieve this involves the use of thinner steel sheets with higher tensile strength that retain good ductility. In 2005, low-alloy deep-drawing steels accounted for approximately 85% of vehicle mass, whereas by 2015, their

share had decreased to 40%. According to the Automotive and Transportation Market Research Report (2023), high-strength low-alloy steels currently make up to 60% of modern automotive body constructions [7]. HS steels achieve tensile strengths of up to 550 MPa, while some third-generation steels exceed 1000 MPa while maintaining good formability. Higher quality steels, such as cold and hot rolled, are commonly used for the production of vehicle frames and suspension components. HS steels achieve tensile strengths of up to 550 MPa, while certain third-generation steels exceed 1000 MPa while maintaining excellent plasticity. High-performance steels, such as cold-rolled and hot-rolled varieties, are widely used in the production of vehicle frames and suspension components. The application of HS steels ensures greater vehicle durability and enhanced passenger safety. Stainless steel, on the other hand, is rarely used in passenger car body components due to its high cost. However, it finds application in heavily utilized public transportation vehicles, such as buses, trams, and passenger trains, where stainless steel is used for body construction. The steel industry is witnessing continuous growth in the use of advanced high-strength steels (AHSS) in automotive designs (Fig. 2), making them the fastest-growing materials for future automotive applications. This industrial interest has resulted in the continuation of the ULSAB project (UltraLight Steel Auto Body) by scientific and industrial consortia through projects like ULSAB—Advanced Vehicle Concepts, UltraLight Steel Auto Closure (ULSAC), UltraLight Steel Auto Suspensions (ULSAS), and Future Steel Vehicle (FSV) [8-10].

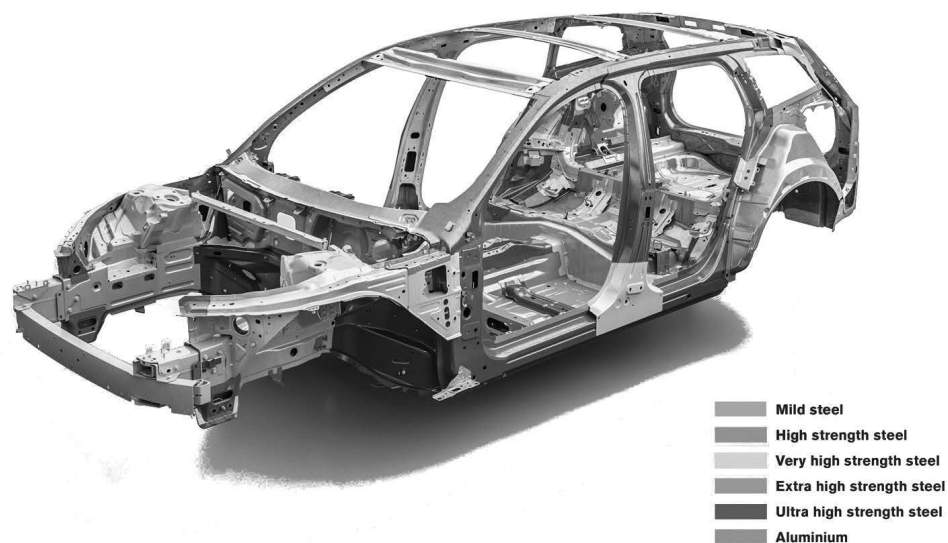


Fig. 2. The use of steel in the construction of the car body Volvo XC90 [7]

The future of the automotive industry will belong to advanced high-performance materials, including modern steel grades that integrate durability, lightweight properties, and environmental sustainability into a single cohesive solution [11,12].

2.2. Aluminum, aluminum alloys

Aluminum currently plays a pivotal role in the production of automotive body constructions. Body cars made from aluminum alloys are significantly lighter than those constructed from steel, as the density of aluminum and its alloys is approximately 65% lower than that of steel. A weight reduction of 300–400 kg in a mid-sized vehicle does not compromise its performance or safety. It is estimated that reducing a vehicle's weight by 100 kg saves approximately 0.6 liters of fuel per 100 km. A 100 kg weight reduction decreases fuel consumption by around 0.4 liters per 100 km and reduces CO₂ emissions by 7.5 to 12.5 g/km. Aluminum alloys are corrosion-resistant and exhibit high mechanical strength. Construction body components such as doors, hoods, roof panels, and trunk lids are commonly produced from aluminum alloys containing copper, magnesium, silicon, nickel, and manganese.

- Al–Mg and Al–Mg–Mn alloys: These offer moderate mechanical strength but exceptional corrosion resistance.
- Al–Mg–Si alloys: These provide good ductility, high corrosion resistance, and moderate mechanical strength.
- Al–Zn–Mg and Al–Zn–Mg–Cu alloys: These deliver strength comparable to steel sheets.

The first car with an aluminum body was the Bugatti 10, and post-war, the Porsche 356 1500 from 1953 featured an aluminum body. Today, aluminum alloys are used in models like the Audi A8, Land Rover Defender, and BMW 5 Series. In 2015, Ford introduced the F-150 with an aluminum body. Aluminum and its alloys are also extensively used in the production of trailers, semi-trailers, delivery vehicles, and automotive tracks. Additionally, aluminum alloys play a key role in composite car body production. Common aluminum-based laminates include: GLARE (glass fiber-reinforced laminates); ARALL (aramid fiber-reinforced laminates); CARALL (carbon fiber-reinforced laminates); CAKRALL (kenaf fiber-reinforced laminates); CAFRALL (flax fiber-reinforced laminates). In sports cars, body constructions are frequently made from aluminum alloys or plastic materials (Fig. 3) [13-15].

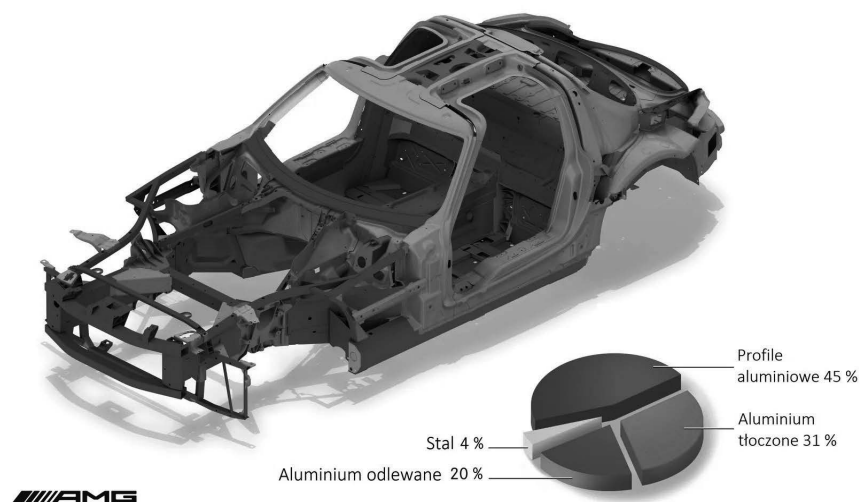


Fig. 3. The use of aluminum alloys in Mercedes SLS AMG [13]

2.3 Titanium, titanium alloys

Titanium and its alloys stand out due to their low density (4.43 g/cm^3) while maintaining high mechanical properties and excellent corrosion resistance. Titanium alloys, such as Ti-6Al-6V-2Sn, exhibit a tensile strength of 1275 MPa. This remarkable combination of properties makes titanium alloys highly versatile and applicable across a wide range of industries, including aerospace, automotive, marine, construction, chemical, and medical sectors. The fundamental properties of titanium alloys make them highly suitable for numerous applications, including but not limited to: springs, bellows, body implants, dental fittings, dynamic marine lifters, drill pipes, sporting equipment. Used in the automotive industry, the density of titanium alloy is only 60% of steel's density, while its strength can exceed 800 MPa. Titanium is known not only for its high strength but also for its good ductility. In cars, components made from titanium alloys are mainly used in exhaust systems, suspension springs, body parts, and body frames (Fig. 4) [16]. Titanium springs allow for a weight reduction of over 70%. Additionally, crash elements made of Ti-6Al-4V titanium are used in car bodies because of their ability to absorb energy through deformation. The use of titanium and its alloys can also be considered in the production of vehicle armor for safety purposes [17-19].

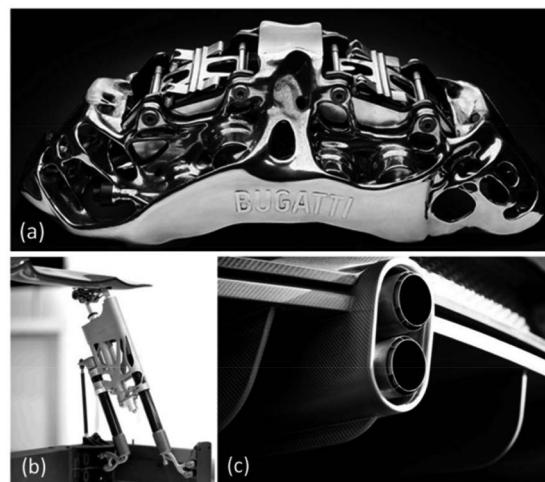


Fig. 4. Titanium components in a Bugatti: (a) eight-piston monobloc brake caliper, (b) active spoiler bracket and (c) exhaust pipe covers [16]

2.4 Magnesium, magnesium alloys

A significant reduction in vehicle weight, and thus a reduction in fuel consumption in internal combustion vehicles or energy consumption in electric vehicles, can be achieved by replacing steel with lightweight magnesium alloys. Magnesium alloys were first used in the automotive industry in 1918, when magnesium-based engine pistons appeared in the Indy 500 race. The use of magnesium and its alloys has been studied since the United States Automotive Materials Partnership (USAMP) was founded in 1993 by Fiat-Chrysler, Ford, and General Motors. These alloys have the highest strength-to-weight ratio among metal alloys. Their high strength and resistance to deformation make them useful for the automotive industry. Currently, magnesium alloys are mostly used in car drivetrains and wheels. While they are less common in body panels and construction parts compared to steel or aluminum, their use is growing. The industry

now focuses on making brackets, profiles and cut-out elements of interior doors. However, shaping magnesium alloys is challenging because they are not very flexible due to their crystal structure. Sheets made from magnesium alloys, like the popular AZ31 alloy, can be shaped better at temperatures above 220°C. However, problems like tool heating during hot forming, limited availability of good lubricants, and the complexity of the process still make it hard to use magnesium alloys widely for making car body panels [20-23].

3. THE FUTURE AND CHALLENGES OF THE AUTOMOTIVE INDUSTRY

The automotive industry is growing quickly, and market demands, changing laws, and new technologies greatly affect the materials used. Manufacturers need to keep up with these changes to stay competitive and meet challenges like sustainability and safety. Advanced driver assistance systems (ADAS) and self-driving cars also need materials that can hold sensors and electronic parts. To make vehicles stronger, safer, and more efficient, new materials are being developed, such as composites and hybrid structures that mix metals with carbon fiber-reinforced plastics. These materials combine high strength, low weight, and lower production costs. Smart materials, like shape memory alloys (SMA) and self-repairing materials, are also being tested. D printing is becoming more common in car manufacturing. This technology creates parts layer by layer from 3D computer designs. It's precise and flexible, making it possible to produce complex parts that traditional methods can't. Today, about 30% of the global 3D printing market is used for cars [24-25].

Still, for most cars, steel will remain the most common material. The future will depend on material costs, advances in production, and the need to reduce vehicle weight and fuel use. Since metals are easy to recycle, replacing them with composites on a large scale might take more time. The growth of the car industry is an exciting mix of technology, ecology, and innovation. While self-driving cars are already being tested by companies like Waymo, Tesla, and BMW, it will take time, new laws, and better infrastructure to make them common. The future is exciting, but it will need teamwork between technology, society, and governments.

ACKNOWLEDGMENTS

The work was created as a result of a project carried out with secondary school pupils as a part of the Excellence Initiative - Research University program (4th competition), Silesian University of Technology. Title: Steel for the automotive industry - the future and challenges of the automotive industry.

BIBLIOGRAPHY

1. F. Czerwinski, Current Trends in Automotive Lightweighting Strategies and Materials, *Materials* 14, 6631, 2021.
2. L. Samek, D. Krizan, Steel—Material of choice for automotive lightweight applications. In *Proceedings of the International Conference Metal'2012* (2012) 1–6.
3. A. Candela, G. Sandrini, M. Gadola, et al, Lightweighting in the automotive industry as a measure for energy efficiency: Review of the Main Materials and Methods. *Heliyon* 2024.

4. A. Kumar, A. Singh, Mechanical properties of nanostructured bainitic steels. *Materialia*, 15, 101034, 2021.
5. S. Yao, H. Zhu, S. Zhang, et al, Green Steel: The Future Path towards Sustainable Automotive Manufacturing. *Resources, Conservation and Recycling*, 200, 107319. 2024.
6. C.D Horvath, Advanced steels for lightweight automotive structures. In *Materials, Design and Manufacturing for Lightweight Vehicles*; Mallick, P.K., Ed.; Woodhead Publishing: Sawston, UK, (2010) 35–78.
7. According to the Automotive and Transportation Market Research Report. Available online: <https://mobilityforesights.com/product/automotive-ahss-market> 2023.
8. A. Grajcar, R. Kuziak, W. Zalecki, Third generation of AHSS with increased fraction of retained austenite for the automotive industry *Archives of civil and mechanical engineering* 12, (2012) 334-341.
9. ULSAB; Final Report; Available online: <https://www.yumpu.com/en/document/view/5349987/ultralight-steel-auto-body-final-report-american-iron-steel-> (accessed on 17 November 2023).
10. ULSAB-AVC. Available online: <https://www.worldautosteel.org/projects/ulsab-avc-2/> (accessed on 16 November 2022).
11. ULSAC. Available online: <https://www.worldautosteel.org/projects/ulsac-2/> (accessed on 16 November 2022).
12. T. B. Hilditch, T. de Souza, P.D. Hodgson, Properties and automotive applications of advanced high-strength steels (AHSS). In *Welding and Joining of Advanced High Strength Steels (AHSS)*, Woodhead Publishing: Sawston, UK, (2015) 9–28.
13. R. Schneider, B. Heine, R.J Grant, Mechanical Behaviour of commercial aluminium wrought alloys at low temperatures, *Light Metal Alloys Applications*; Waldemar, A.M., Ed.; InTech: Houston, TX, USA, 2014; Available online: <https://www.intechopen.com/chapters/46602> (accessed on 16 November 2023).
14. The Application of Aluminum Alloy in Automotive Industry. Available online: <https://www.aluminiummanufacturer.com/blog/the-application-of-aluminum-alloy-in-automotive-industry/> (accessed on 15 December 2023).
15. J. Shin, T. Kim, D. Kim, et al, Castability and mechanical properties of new 7xxx aluminum alloys for automotive chassis/body applications. *J. Alloys Compd.*, 698 2017.
16. P. Nyamekye, S. Rahimpour Golroudbary, et al, Impact of additive manufacturing on titanium supply chain: Case of titanium alloys in automotive and aerospace industries. *Adv. Ind. Manuf. Eng.*, 6, 100112, 2023.
17. L. Wagner, O. Schauerte, Status of titanium and titanium alloys in automotive applications. In *Ti-2007 Science and Technology*, Sendai, Japan, (2007) 1371–1378.
18. T. Furuta, Automobile applications of titanium. In *titanium for consumer applications real world use of Titanium*, Elsevier: Amsterdam, The Netherlands (2019)77–90.
19. Titanium and its alloy used for automotive applications. Available online: <https://energy-ti.com/titanium-and-its-alloy-usedfor-automotive-applications> 2023.
20. F.H. Froes, D. Eliezer, E. Aghion, The science, technology, and applications of magnesium. *JOM* 50, (1998) 30–34.
21. S. Logan, A. Kizyma, C. Patterson, S. Rama, Lightweight Magnesium Intensive Body Structure. *SAE Trans.*, 115, (2006) 469–486.
22. D. Hawke, K Gaw, Effects of chemical surface treatments on the performance of an automotive paint system on die cast magnesium; SAE Technical Paper 920074; SAE International: Warrendale, PA, USA, 1992.

23. D.S. Kumar, C.T. Sasanka, et al, Magnesium and its alloys in automotive applications—A Review. *Am. J. Mater. Sci. Technol.* 4, (2015) 12–30.
24. G. Kajal, M.R. Tyagi, G. Kumar, A review on the effect of residual stresses in incremental sheet metal forming used in automotive and medical sectors. *Mater. Today Proc.*, 78, (2023) 524–534.
25. E. Kubińska-Jabcoń, M. Niekurzak, The use of modern materials in the automotive industry to improve the quality and safety of mechanical vehicles, *Vehicles*, 10–11, (2019) 47–52.



31th January 2025
Gliwice, Poland

DEPARTMENT OF ENGINEERING MATERIALS AND BIOMATERIALS
FACULTY OF MECHANICAL ENGINEERING
SILESIA UNIVERSITY OF TECHNOLOGY

INTERNATIONAL STUDENTS SCIENTIFIC CONFERENCE

Effects of welding parameters on ferrite-austenite phase balance in RSW of lean duplex stainless steel

Zbigniew Brytan ^a, Beatrice N.A. Ardayfio ^b, Afrim Gjelaj ^c, Besart Berisha ^c, Wojciech Pakieła ^a, Tomasz Poloczek ^d, Bernard Wyględacz ^d

^a Silesian University of Technology, Faculty of Mechanical Engineering, Department of Engineering Materials and Biomaterials, Gliwice, Poland, email: zbigniew.brytan@polsl.pl

^b PhD student at Silesian University of Technology, Faculty of Mechanical Engineering, Department of Engineering Materials and Biomaterials, Gliwice, Poland,

^c University of Prishtina, Faculty of Mechanical Engineering, Department of Manufacturing and Industrial Engineering with Management, Prishtine, Republic of Kosovo

^d Silesian University of Technology, Faculty of Mechanical Engineering, Department of Welding Engineering, Gliwice, Poland

Abstract: This study investigates the resistance spot welding (RSW) of lean duplex stainless steel (LDSS) grade 1.4637, focusing on the optimisation of welding parameters to achieve a balanced microstructure in the weld zone. The effects of varying welding current, electrode force and welding time on the microstructure of the weld nugget were investigated. Microstructural analysis showed that cooling rates and electrode pressure significantly influenced the ferrite-austenite phase balance. The study highlights the importance of controlling welding parameters to achieve desired microstructural characteristics in RSW of LDSS, with implications for optimising weld quality and mechanical performance.

Keywords: resistance spot welding, lean duplex stainless steel, phase balance

1. INTRODUCTION

Resistance spot welding (RSW) of duplex stainless steels (DSS) poses distinct challenges owing to their unique metallurgical characteristics (austenitic-ferritic microstructure, specific physical properties related to heat transfer, susceptibility to secondary phase precipitation, etc.). These challenges can significantly impact the weld quality and mechanical performance. The diameter of the electrode tip played a crucial role in determining the nugget size. Smaller diameters can limit nugget formation owing to expulsion phenomena, while larger diameters may lead to increased indentation and reduced tensile shear strength [1]. The welding current is the next critical parameter that directly affects weld quality. Excessive current can lead to larger nugget sizes but may also cause detrimental phase transformations, impacting the mechanical properties of the weld [2,3]. High cooling rates during RSW can lead to phase transformations that affect the hardness and microstructure of the fusion zone, thus

complicating the weldability of DSS [4]. Achieving a balanced austenite-ferrite phase in the fusion zone is challenging. Improper control of the welding parameters can lead to an undesirable phase distribution, affecting the overall strength and ductility of the weld [5].

Duplex stainless steels are known for their unique microstructure that consists of a mixture of austenite and ferrite phases. The ideal phase balance is typically approximately 50% for each phase, which contributes to its strength and toughness. However, during RSW, rapid heating and cooling cycles can lead to an undesirable phase distribution, often resulting in a predominance of the ferritic phase over the austenitic phase. To improve the phase balance in the fusion zone (FZ), changes are made to the welding current and welding parameters, which influence the thermal cycles that the material undergoes. Microstructural changes during RSW have been extensively studied [1-5]. It was observed that the volume fraction of austenite increased with higher welding currents because the increased heat generation allowed more ferrite to transform into austenite. A higher current during RSW can lead to increased heat input, which increases the temperature in the fusion zone (FZ) more rapidly. Conversely, a down-sloping current modification can help control the heat input and cooling rates, thereby promoting a more favourable phase transformation during solidification. Longer welding times can result in more heat accumulation, affecting the cooling rate and the resultant microstructure of the weld. The pressure applied by the electrodes during welding influences the contact resistance and, consequently, heat generation. A higher electrode force can lead to better contact and more efficient heat transfer, thereby affecting the thermal cycling. These parameters are essential for controlling the thermal cycles during RSW, which ultimately influence the phase balance and mechanical properties of DSS [5].

This paper presents an initial investigation into the resistance spot welding of lean duplex stainless steel grade (1.4637), focusing on the optimization of welding parameters to achieve a balanced microstructure in the weld zone. The present study presents a preliminary microstructural assessment of weld nuggets produced for a range of varying RSW parameters.

2. RESEARCH METHODOLOGY

2.1. Materials and welding process

The base metal was lean duplex stainless steel grade 1.4637 / FDX27 / UNS S82031 sheet of 0.57 mm thickness with surface finish 2E manufactured by Outokumpu of composition presented in table 1. The base metal was cut into squares of 35 mm 35 mm in dimension and lap jointed together using a ASPA ZP-40, 50 kVA AC, 50 Hz RSW machine, with a pair of CrCuZr alloy flat electrode caps with a 5 mm diameter. In the experiment following parameters were varied: the weld current (4.08 and 7.7 kA), the electrode force (770, 2300 and 3070 N) and the welding time between 0.1 s, 0.6 s, and (0.1 s current pulse/0.1 s pause) x 20 cycles. Meanwhile, squeeze time of 0.1 s, holding time 0.4 s remained constant.

The objective of the welding parameters was to obtain a range of different cooling rates. The samples were divided into three groups (I – hard, II - soft and III-pulsed), as follows: Group I, which was characterised by a high current and a short time, resulted in the lowest heat generation in the weld zone (I.1 and I.2). Group II, which was defined by a low current and an extended welding time, exhibited higher heat generation than the preceding conditions (II.1 and II.2). Group III, which was distinguished by a low current and an even longer welding time, demonstrated the highest heat generation in the weld zone (III.1 and III.2). Moreover, each configuration employs variable electrode pressure, which can impact the alteration in resistance

throughout the welding process. Lower pressure results in minimal heat generation and a notable reduction in heat transfer to the outer surface (Table 2).

Table 1. Chemical composition of base metal – grade 1.4637 (wt. %)

Grade	C	Cr	Ni	Mo	N
1.4637 / FDX27	≤ 0.04	19.0-22.0	2.0-4.0	0.6-1.4	0.14-0.24

Table 2. Resistance welding parameters

Sample no	Sample designation	Welding current [kA RMS]	Time [(current s/pause s) x cycles]	Electrode pressure [N]	RSW machine setting
1	I.1	7.7	(0.1/0) x 1	3070	40
2	I.2	7.7	(0.1/0) x 1	2300	40
3	II.1	4.08	(0.6/0) x 1	770	10
4	II.2	4.08	(0.6/0) x 1	2300	10
5	III.1	4.08	(0.1/0.1) x 20	770	10
6	III.2	4.08	(0.1/0.1) x 20	3070	10

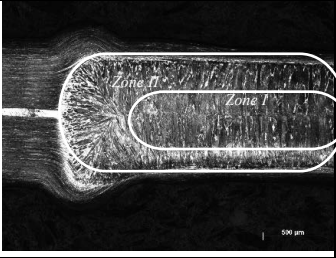
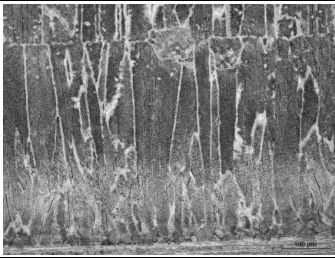
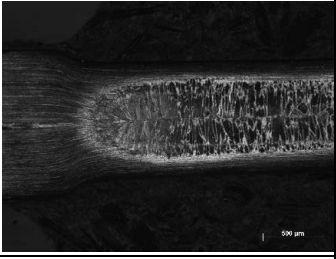
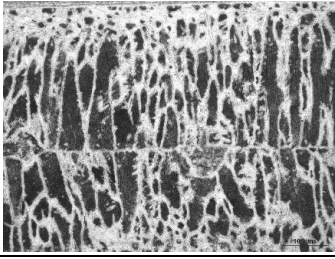
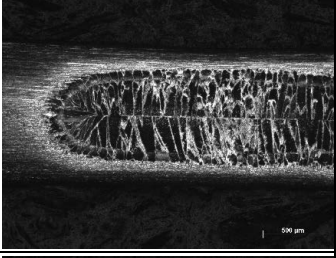
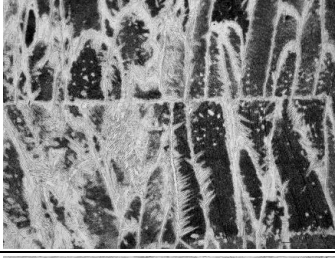

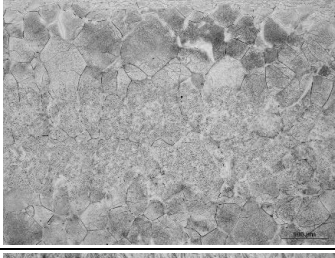
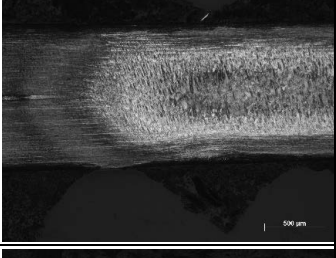
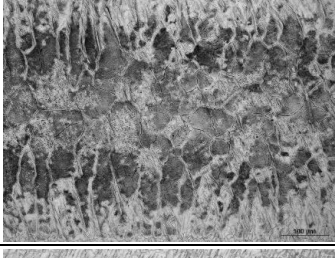
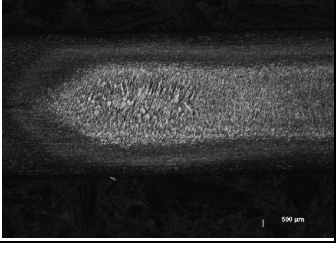
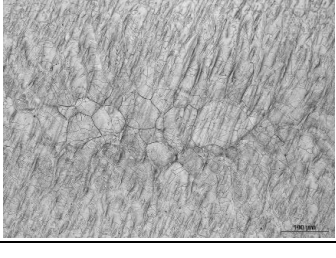
2.2. Microstructure analysis

After spot welding, the lap joint was cross sectioned in a transverse direction. The sectioned specimens were prepared using standard metallographic procedures by polishing and acid electrolytic etching in 10% oxalic acid at 3-6 volts for 5-60 s. The weldment geometry, microstructure of the weld nugget was characterized by optical microscopy (LOM, LEICA MEF4A) and scanning electron microscopy (SEM, Supra 35 from Zeiss Company). The phase content in the weld microstructure was determined by image analysis using ImageJ software. Two zones were considered in the analysis, Zone I - the outermost part of the weld nugget and Zone II - the area close to the centre of the weld nugget. Such zones were clearly identified for each condition and also showed different sizes depending on the conditions applied. For each analysis, 3-5 areas were considered, and the mean phase fraction was estimated.

3. RESULTS AND DISCUSSION

Hard parameters (samples I.1 and I.2) led to rapid heat input and fast cooling, resulting in ferrite-dominated microstructures (Table 3). Sample I.1, which had a higher electrode pressure, exhibited the fastest cooling rate. This enhanced heat dissipation, leaving the weld nugget predominantly ferritic, with approximately 20% austenite in the central zone and 15% in the outer zone. The heat-affected zone (HAZ) of I.1 shows slightly higher austenite content at 25%, but it remains ferrite-dominated overall. In contrast, sample I.2, produced at a lower electrode pressure, exhibited slightly slower cooling due to reduced heat dissipation. This marginally slower cooling allowed for increased austenite formation compared with I.1, resulting in 25% austenite in the central zone, 20% in the outer zone, and 25% in the HAZ. Although both samples retained predominantly ferritic microstructures, I.2 demonstrated a more balanced phase distribution than I.1. The central zone of both samples exhibited columnar ferritic grains due to rapid cooling during solidification, with allotriomorphic austenite precipitation on the grain boundary (GBA) in limited amount due to the short heat retention and fast cooling characteristics of the applied parameters.

Table 3. Macrostructure of RSW joints of 1.4637 grade under different welding parameters

Sample no	Macrostructure of RSW		Austenite content, %		
			Central zone I:	Outer zone II:	HAZ
I.1			20	15	25
I.2			25	20	25
II.1			30	25	30
II.2			35	10	30
III.1			25	30	45
III.2			15	35	45

Sample II.1, with a lower electrode pressure of 770 N, exhibited further reduced cooling, leading to increased austenite formation. In this sample, the central zone contains approximately 30% austenite, with columnar ferritic grains similar to those observed with hard parameters but with more pronounced austenite along the grain boundaries due to the slower cooling rate. The outer zone has a slightly lower austenite content of 25%, reflecting a gradual cooling gradient, while the heat-affected zone shows the highest austenite content at 30%, where extended heat exposure and slower cooling promote significant diffusion and stabilization of austenite.

Sample II.2, processed with a higher electrode pressure of 2300 N, cooled faster than II.1, resulting in slightly reduced austenite formation. The central zone contains 35% austenite, but its microstructure differs markedly from both II.1 and the hard parameter samples. The central zone is composed of equiaxed ferritic grains, and fine intragranular austenite (IGA) is visible. In the outer zone of II.2, the microstructure shifts to massive equiaxed ferritic grains with limited grain boundary austenite, resulting in an austenite content of only 10%. These findings underscore how variations in electrode pressure within the soft parameter regime influence cooling dynamics, phase transformations, and resulting microstructural features.

The pulsed parameters (samples III.1 and III.2) utilized a low current of 4.08 kA combined with a long welding time applied in pulsed cycles. This method introduced cumulative heat into the weld zone while allowing brief cooling intervals between pulses, resulting in the slowest overall cooling rates among the analysed parameters.

Sample III.1, which utilized a lower electrode pressure of 770 N, demonstrated enhanced heat retention due to limited thermal dissipation. This prolonged thermal exposure facilitated significant austenite formation, with the central zone containing approximately 25% austenite. The outer zone exhibited a slightly higher austenite content of 30%, while the heat-affected zone reached the highest austenite content at 45%, owing to the extended heat input and slow cooling that favoured diffusion-controlled phase transformations. In terms of microstructure, the central zone comprises equiaxed ferritic grains with fine intragranular austenite (IGA); however, the IGA content is slightly lower compared to that in sample II.2. In the outer zone, equiaxed ferritic grains are more enriched with grain boundary austenite, reflecting the influence of reduced cooling rates. The HAZ displays a well-balanced microstructure characterized by fine austenitic grains dispersed within a ferritic matrix, achieving an optimal balance of phase distribution.

In contrast, sample III.2, which used a higher electrode pressure of 3070 N, experienced faster cooling due to improved thermal contact with the electrodes. The central zone of III.2 contained about 15% austenite, while the outer zone matched III.1 with 35%. The HAZ also reached 45% austenite, showing a similar level of transformation. Both samples achieved the highest overall austenite content among all parameter sets, largely due to the cumulative heat input from pulsing. However, the slower cooling in III.1 resulted in a more uniform and balanced microstructure, with higher austenite content across all zones compared to III.2. These findings underscore the critical role of electrode pressure in moderating heat dissipation, even under identical pulsed welding conditions.

In addition to phase content, the dimensions of the weld zones (central, outer, and HAZ) represent a crucial element that can exert a considerable influence on the mechanical and corrosion characteristics of the weld. The dimensions of these zones are directly related to the heat input, welding time, and cooling rate, which determine the extent of thermal gradients across the weld.

4. CONCLUSIONS

The study highlights how cooling rates and electrode pressure shape the microstructure of duplex stainless steel welds. Hard parameters (I.1, I.2) produced rapid cooling, resulting in a ferrite-dominated microstructure with columnar ferritic grains in the central zone and limited austenite content on the grain boundaries. Soft parameters (II.1, II.2) facilitated slower cooling, leading to more equiaxed ferritic grains and increased austenite content, particularly in the outer zone and HAZ. The parameters of sample II.2 represent a transition point in the microstructure of the central zone, where the morphology shifts from elongated, massive ferritic grains with grain boundary austenite (GBA) to equiaxed ferritic grains containing intragranular austenite (IGA). This transformation is attributed to the specific combination of cooling rate and electrode pressure. The higher electrode pressure of 2300 N in II.2 promotes faster cooling compared to II.1, while the longer welding time inherent to the soft parameters allows sufficient thermal exposure for partial transformation. Pulsed parameters (III.1, III.2) provided the slowest cooling, enabling a more balanced ferrite-austenite structure with well-distributed grain boundary austenite and refined grains in all zones.

ACKNOWLEDGMENT

The research presented in this paper was partly carried out as part of the International Visegrad Fund Fellowship awarded to Zbigniew Brytan (52410436) in the academic year 2024/2025. This research was made possible by financial support from the European Union's H2020-MSCA-RISE-2018 project (Number 823786), the i-Weld project, and an international project co-financed by the Polish Ministry of Science and Higher Education's "PMW" programme in the years 2020-2023, contract No. 5107/H2020/2020/2. This support is gratefully acknowledged.

BIBLIOGRAPHY

1. V., D., Kalyankar., Gautam, P., Chudasama., Influence of electrode tip diameter on metallurgical and mechanical aspects of spot welded duplex stainless steel, *High Temperature Materials and Processes*, (2020). doi: 10.1515/HTMP-2020-0055
2. K., Vignesh., A., Elaya, Perumal., P., Velmurugan., Optimization of resistance spot welding process parameters and microstructural examination for dissimilar welding of AISI 316L austenitic stainless steel and 2205 duplex stainless steel, *The International Journal of Advanced Manufacturing Technology*, (2017). doi: 10.1007/S00170-017-0089-4
3. M., Prabhakaran, D., Jeyasimman, M., Varatharajulu, Insights and Implications: Unraveling Critical Factors in Resistance Spot Welding of Dissimilar Metals through SS 347 and DSS 2205 Welds, (2023). doi: 10.3390/engproc2023059027
4. M., Pouranvari., M., Alizadeh-Sh., S., P., H., Marashi., Welding metallurgy of stainless steels during resistance spot welding Part I: fusion zone, *Science and Technology of Welding and Joining*, (2015). doi: 10.1179/1362171815Y.0000000015
5. S., H., Arabi., M., Pouranvari., M., Movahedi, Pathways to improve the austenite–ferrite phase balance during resistance spot welding of duplex stainless steels, *Science and Technology of Welding and Joining*, 24 (2019):8-15. doi: 10.1080/13621718.2018.1468949



31th January 2025
Gliwice, Poland

DEPARTMENT OF ENGINEERING MATERIALS AND BIOMATERIALS
FACULTY OF MECHANICAL ENGINEERING
SILESIA UNIVERSITY OF TECHNOLOGY

INTERNATIONAL STUDENTS SCIENTIFIC CONFERENCE

Application of carbon materials in the production of dye-sensitized solar cells

Jakub Budzynowski^a, Kacper Argalski^b, Oskar Górka^a, Szymon Jeż^c, Aleksandra Drygała^d, Sabina Lesz^d, Adam Zarychta^d, Klaudiusz Gołombek^e, Janusz Wyrwał^f, Marek Kremzer^g, Wojciech Pakieła^d, Bartosz Drygała^h, Eva Tillováⁱ, Peter Palčekⁱ

^a Student, Silesian University of Technology, Faculty of Mechanical Engineering, Konarskiego 18a Str., 44-100 Gliwice, Poland

^b Student, Silesian University of Technology, Faculty of Mining, Safety Engineering and Industrial Automation, Akademicka 2 Str., 44-100 Gliwice, Poland

^c Student, Silesian University of Technology, Aeronautical and Space Engineering, 44-100 Gliwice, Poland

^d Silesian University of Technology, Faculty of Mechanical Engineering, Department of Engineering Materials and Biomaterials, Konarskiego 18a Str., 44-100 Gliwice, Poland

^e Silesian University of Technology, Materials Research Laboratory, Silesian University of Technology, 18a Konarskiego St, 44-100 Gliwice, Poland

^f Silesian University of Technology, Faculty of Automatic Control, Electronics and Computer Science, Department of Measurements and Control Systems, Akademicka 16 Str., 44-100 Gliwice, Poland

^g Silesian University of Technology, Faculty of Mechanical Engineering, Nanotechnology and Materials Technology Scientific and Didactic Laboratory, Towarowa 7a Str., Gliwice, Poland

^h Student, Silesian University of Technology, Faculty of Automatic Control, Electronics and Computer Science, Akademicka 16, 44-100 Gliwice, Poland

ⁱ University of Zilina, Faculty of Mechanical Engineering, Department of Materials Engineering, Univerzitná 1 Str., 010 26 Zilina, Slovak Republic

email: aleksandra.drygala@polsl.pl

Abstract: In this work, the influence of carbon material application on the photovoltaic properties of dye-sensitized photovoltaic cells (DSSCs) was presented. The DSSC photoanode, based on titanium dioxide with the addition of carbon fibers in the range of 0-1.5%, was produced. The highest efficiency of solar cells (4.16%) was achieved with a carbon content of 0.5%. With the increase in the carbon content above 0.5%, the number of defects rises, which probably affects the reduction of the efficiency of DSSCs.

Keywords: photovoltaics, dye-sensitized solar cells, carbon materials, fibers

1. INTRODUCTION

The continuously increasing environmental pollution and demand for electricity, motivate people to seek and implement new energy production technologies, that do not negatively impact the surroundings. Currently, renewable energy sources are used for this purpose, with solar

energy - being one of the most rapidly developing fields [1]. According to the Energy Market Agency (ARE), the total capacity of installed photovoltaic panels in Poland amounted to 19,888.7 MW (September 2024), 4,287.3 MW higher than in 2023 [2].

The Sun is a virtually inexhaustible source of energy reaching the Earth. Its emission power is estimated at 3.9×10^{20} MW. The maximum radiation power that can penetrate the outer layer of the atmosphere is 1367 W/m² (known as the solar constant). However, due to the Earth's elliptical orbit, axial tilt, and atmospheric thickness, the amount of energy that actually reaches the Earth's surface is lower. Under ideal conditions, it is about 1000 W/m² [3, 4].

Solar radiation energy can be converted into electricity using solar cells. New types of solar cells, such as perovskite, organic, and dye-sensitized cells, are constantly being developed [5]. In 1988, Brian O'Regan and Michael Grätzel developed innovative dye-sensitized solar cells (DSSCs) [6]. Despite their later application, these cells stand out for their low production costs and relatively long durability, making them increasingly popular. Advanced materials, such as metal oxides (e.g., nanoparticles, nanotubes), organic dyes, and conductive polymers, are used in their manufacturing technology. The production of these cells does not require complex technologies or maintaining high air purity during the manufacturing process. In 2013, research on solid-state DSSCs with perovskite showed an efficiency of 15%. Their low production cost makes DSSCs increasingly used, especially in modern energy solutions and household applications [7]. The name "dye-sensitized solar cells" comes from their unique structure - one layer contains a special dye that plays a key role in the process of converting light into electricity. Unlike typical solar cells, DSSCs are aesthetically pleasing, resembling colourful stained glass or tinted windows. Thanks to their transparency, these devices can be used as decorative elements in interior architecture, where their aesthetic values are significant [8].

To increase efficiency, materials with high light scattering are used in the photoanode of DSSCs. This extends the interaction time of light with the photoanode. One effective approach is the use of one-dimensional nanostructures, such as nanotubes, nanofibers, or nanorods. While these structures significantly improve light scattering, they have limited adsorption capacity due to their small surface area. Hybrid materials combining light scattering properties with high dye adsorption capabilities are used to increase the surface area by integrating various types of nanostructures (1D, 2D, and 3D) [9, 10].

Another enhancement involves noble metals like gold, silver, or platinum. These metals are characterized by high chemical stability and unique optical properties, significantly improving light absorption in DSSCs. Noble metal nanoparticles exhibit a plasmonic effect that increases visible light and near-infrared absorption. Another advantage is improved electron transport, leading to higher DSSC efficiency. Incorporating the mentioned materials into the photoanode also increases the longevity of dye-sensitized solar cells, protecting them from degradation caused by UV radiation and oxygen exposure [11, 12].

Carbon materials such as graphene and carbon nanotubes exhibit high electrical conductivity. Adding them to the metal oxide layer (e.g., TiO₂, a typical photoanode material) reduces electrical resistance and can create a network that improves electron flow while reducing recombination losses. Carbon nanostructures also positively affect the chemical and physical stability of the photoanode. Materials such as graphene are resistant to UV radiation and various degradation processes, which can enhance solar cell performance. Incorporating graphene or other carbon nanostructures into the oxide layer extends the DSSC lifespan while maintaining efficiency over time. Carbon nanostructures can also increase the active surface area of the photoanode, enabling more effective dye adsorption [13, 14, 15, 16]. The use of carbon structures in DSSC photoanodes can be more

advantageous than doping with noble metals due to the economic production process and similar properties to those mentioned metals. This reduces the implementation and production costs [17, 18]. This study analysed the impact of using carbon fibers on the electrical properties of DSSCs.

2. MATERIALS AND METHODS

DSSCs were produced using glass substrates coated with an FTO (Fluorine-doped tin oxide) layer with a resistivity of $7 \Omega/\text{sq}$ and an area of 625 mm^2 . The glass plates were cleaned in a solution of water and detergent using a PS-40A ultrasonic cleaner for 10 minutes. After drying the substrates with compressed air, the process was repeated using 98% ethanol as a cleaning agent.

In the next step, carbon fibers from Velox were added to 18NR-T Titania Paste (GreatCell Solar) in concentrations of 0%, 0.25%, 0.5%, 0.75%, 1%, or 1.5%. The precise amount of carbon material was measured using an AS 310/X scale from RADWAG. The semiconductor layer, with an area of 42 mm^2 , was applied to the FTO-coated side of the prepared substrates using a semi-automatic screen printer (MSR 300 FRO, Printing Machine). The plates were stabilized for 10 minutes, between prints, to ensure uniform paste distribution. Subsequently, the samples were dried in an SLW53STD dryer from Pol-Eko for 5 minutes at 105°C . The deposited layer was then annealed at 500°C for 30 minutes in a P330 furnace from Nabertherm. The semiconductor layers were sensitized with N719 dye (GreatCell Solar) for 24 hours. After removal from the dyeing solution, the photoanode was rinsed with ethanol to remove excess dye.

To examine the surface topography and confirm the chemical composition of the deposited layers, a Zeiss Supra 35 scanning electron microscope (SEM) equipped with an energy-dispersive X-ray spectroscopy (EDS) detector was used. The samples were sputtered with gold, to enhance image quality, using an SCD 050 sputter coater (BAL-TEC) at 540 V, 50 mA, for 40 seconds. Current-voltage characteristics were measured using a testing setup equipped with a solar radiation simulator (Solar Simulator, model # SS150AAA, Photo Emission Tech). Measurements were conducted for AM 1.5 radiation spectra and an intensity of 1000 W/m^2 . For each DSSC, five I-U measurements were performed, and the electrical properties were averaged. DSSCs with varying carbon fibers contents in the TiO_2 layer were analysed.

3. RESULTS

Figures 1 and 2 present the surface topography of the photoanode at magnifications of 75x and 250x, respectively. The images show areas where carbon material is located.

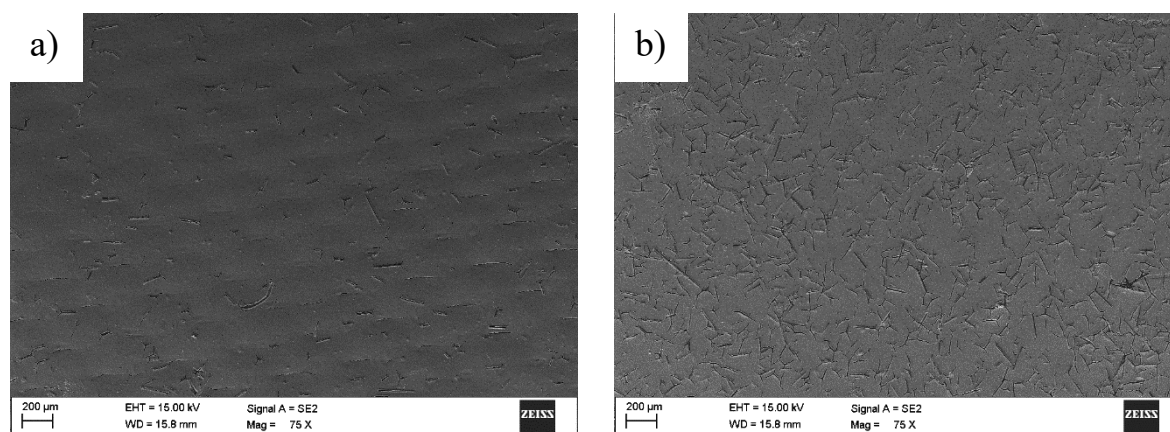


Figure 1. The surface topography of TiO_2 with carbon fiber content a) 0.25%, b) 1.5% at 75x magnification

The carbon fibers are relatively evenly distributed, and their number increases with the C content in the photoanode. The length of the carbon fibers varies but generally does not exceed 100 μm . It was observed that an increase in carbon fibers content corresponds to an increase in surface defects, such as cracks. These cracks appear at the interface between the semiconductor material and the carbon fibers, possibly due to the rapid heating rate of the photoanode. Figure 3 shows an example of a carbon fiber with a length of 62.93 μm and a diameter of 7.73 μm . The results of the EDS chemical composition analysis (Figure 4) in selected regions of the anode confirm the presence of Ti, O, and C elements in the produced dye-sensitized solar cell photoelectrode. The recorded reflexes for tin and ruthenium were from the substrate and the applied dye, respectively.

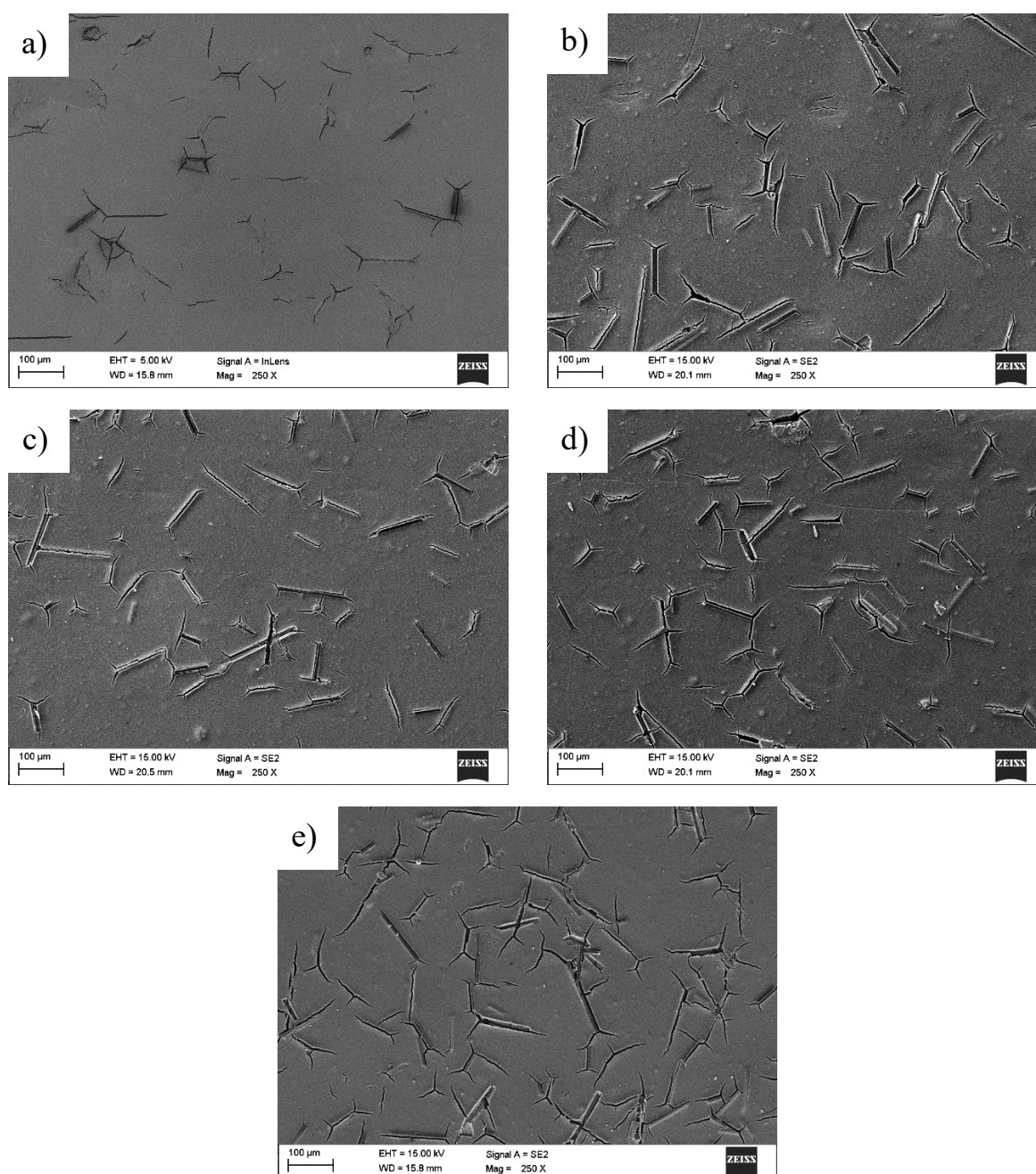


Figure 2. The surface topography of TiO_2 with carbon fibers content a) 0.25%, b) 0.5%, c) 0.75%, d) 1%, e) 1.5% at 250x magnification

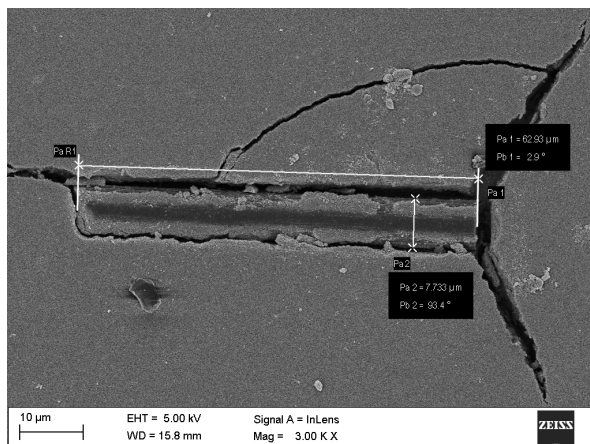


Figure 3. The surface topography of the photoanode with visible carbon fiber at 3 000x magnification

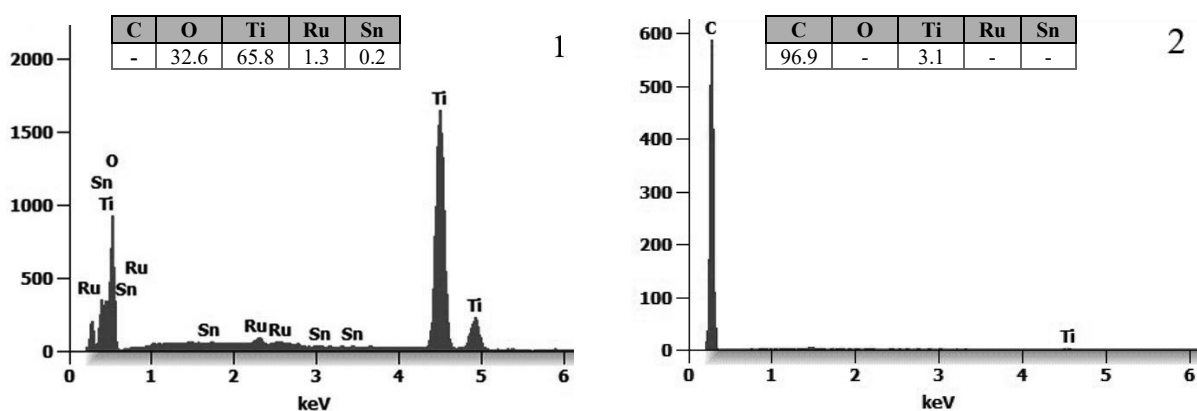
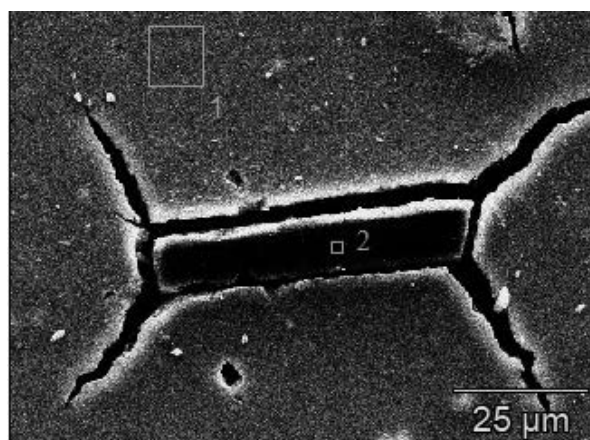


Figure 4. The EDS spectrum and chemical composition analysis of selected DSSC photoanode areas (1 and 2)

Figure 5 presents the current-voltage characteristics of dye-sensitized solar cells with photoanode-containing carbon fiber concentrations of 0%, 0.25%, 0.5%, 0.75%, 1%, or 1.5%.

The solar cell with 0.5% carbon content exhibits the highest current value for voltages in the range of 0–475 mV and an efficiency of 4.16%. At the highest carbon fibers contents (1% and 1.5%), DSSCs show the lowest values of I_{sc} , V_{oc} , FF, and efficiency. As the carbon material content increases (particularly above 0.75%), the short-circuit current decreases, likely due to numerous cracks in the TiO_2 layer. Incorporating carbon fibers into the semiconductor material's structure can improve charge transport and increase solar cell efficiency but simultaneously leads to a higher number of defects that limit their flow.

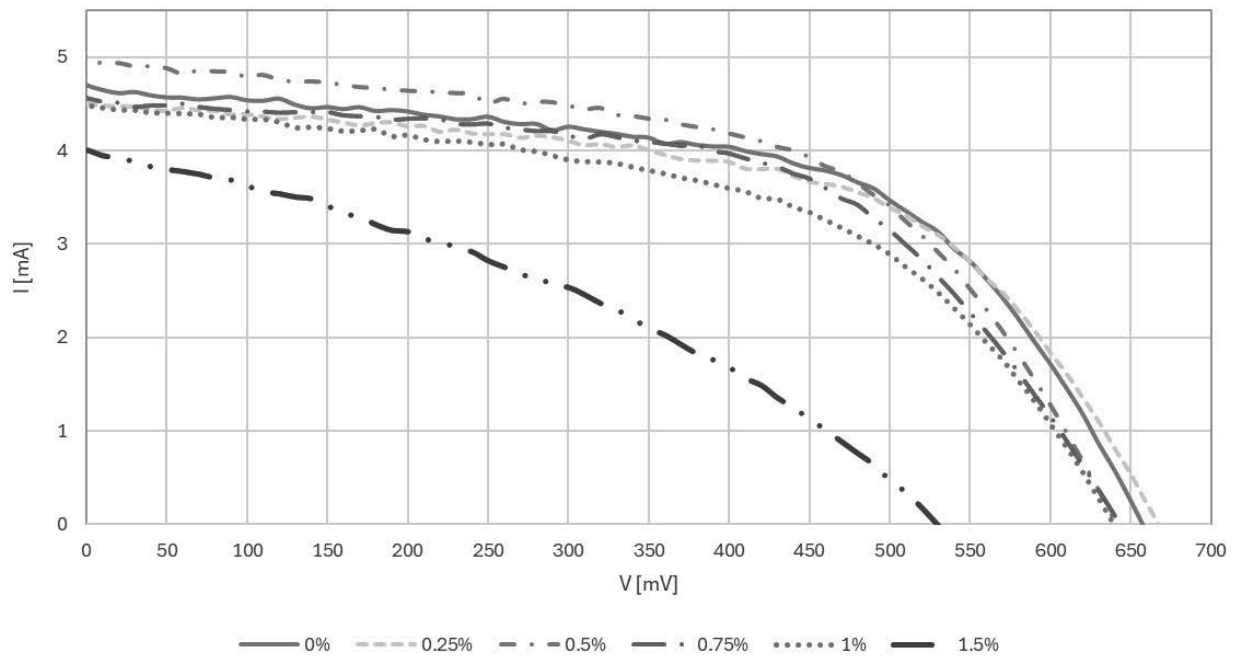


Figure 5. The current-voltage characteristics of dye-sensitized solar cells with different carbon fibers content

Table 1. The averaged electrical properties of DSSCs with different carbon fibers content

Carbon fibers content	Electrical properties				
	I_{sc} [mA]	V_{oc} [mV]	P_m [mW]	FF [-]	Eff [%]
0% C	4.74	651.65	1.74	0.56	3.89
0.25% C	4.42	668.22	1.72	0.58	3.92
0.5% C	4.99	641.97	1.85	0.58	4.16
0.75% C	4.56	640.15	1.66	0.57	3.69
1% C	4.51	641.88	1.56	0.54	3.51
1.5% C	4.21	528.72	0.79	0.36	1.78

4. CONCLUSIONS

Photovoltaic installations provide an environmentally friendly solution for obtaining free electricity from a readily available energy source - the Sun. They are compact, silent, and do not pollute the air. Scientists worldwide strive to improve solar cell efficiency, which would significantly increase their cost-effectiveness. In this study, to the photoanode of dye-sensitized solar cells carbon material was added. The analysis showed that the highest efficiency of 4.16% was achieved for a dye-sensitized solar cell with 0.5% carbon content. Carbon addition can create a network that facilitates electron flow and simultaneously reduces recombination losses. This reduces charge carrier transport losses, leading to increased solar cell efficiency. Moreover, numerous cracks spreading from the locations of carbon fibers were observed on the photoanode surface. As the carbon material content increases (above 0.5%), the number of defects grows, reducing DSSC efficiency. Differences in solar cell efficiency with carbon material content ranging from 0% to 1% are minor (0.65 percentage points), which may serve as a basis for further research on the application of carbon materials in DSSC photoanodes.

ACKNOWLEDGMENTS

The work was created as a result of the project PBL (Project Based Learning) - 11th edition – of the Excellence Initiative - Research University, Silesian University of Technology.

BIBLIOGRAPHY

1. Zapotrzebowanie na energię elektryczną, GLOBENERGIA, <https://globenergia.pl/zapotrzebowanie-na-energie-elektryczna-bedzie-wieksze-niz-kiedykolwiek/>, 2024.
2. H. Mikołajuk, M. Zatorska, E. Stępiak, I. Wrońska, K. Galewski, Informacja Statystyczna o Energii Elektrycznej Vol. 9 (369), Ministerstwo Klimatu i Środowiska, Urząd Regulacji Energetyki, Warszawa, 2024.
3. Energia słoneczna – czym jest i jak powstaje? ,eSOLEO, <https://www.esoleo.pl/co-to-jest-energia-sloneczna-477/>, 2024.
4. M. Ł. Michalski, Światowe zasoby energii słonecznej i kierunki ich wykorzystania, *Czysta Energia* 12 (2006) 16-17.
5. K. Dyndał, G. Lewińska, K. Marszałek, Generacje ogniw fotowoltaicznych, *Fotowoltaika*, Wydawnictwo Akademii Górniczo-Hutniczej, Kraków, 2021.
6. B. O'Regan, M. Grätzel, A low-cost, high-efficiency solar cell based on dye-sensitized colloidal TiO₂ films, *Nature* 353 (1991) 737-740.
7. J. Burschka et al, Sequential deposition as a route to high-performance perovskite-sensitized solar cells, *Nature* 499 (2013) 316–319.
8. Nowinki – barwnikowe ogniwa fotowoltaiczne, *Electrotile*, <https://instalacje.electrotile.com/nowinki-barwnikowe-ogniwa-sloneczne/poradniki/>, 2024.
9. G. Kaur et al, Tailored TiO₂ nanostructures for designing of highly efficient dye sensitized solar cells: A review, *Nano-Structures & Nano-Objects* 36 (2023) 101056.
10. P. Gnida et al, Impact of TiO₂ Nanostructures on dye-sensitized solar cells performance, *materials* 14 (2021) 1633.

11. S. Bera, D. Sengupta, S. Roy, K. Mukherjee, Research into dye-sensitized solar cells: a review highlighting progress in India, *Journal of Physics: Energy* 3 (2021) 032013.
12. M. Ye et al, Recent advances in dye-sensitized solar cells: from photoanodes, sensitizers and electrolytes to counter electrodes, *Materials Today* 18 (2015) 155-162.
13. Y. Kumar, T. Chhalodia, P. K. G. Bedi, P. L. Meena, Photoanode modified with nanostructures for efficiency enhancement in DSSC: a review, *Carbon Letters* 33 (2023) 35-58.
14. E. Muchuweni, B. S. Martincigh, V. O. Nyamori, Recent advances in graphene-based materials for dye-sensitized solar cell fabrication, *RSC Advances* 10 (2020) 44453-44469.
15. S. Bhand, P. K. Jha, N. Ballav, Unusual enhancement in efficiency of DSSCs upon modifying photoanodes with reduced graphene oxide, *RSC Advances* 12 (2022) 30041-30044.
16. H. Lee et al, Effect of graphene incorporation in carbon nanofiber decorated with TiO₂ for photoanode applications, *RSC Advances* 7 (2017) 6574-6582.
17. S. Dou et al, N-, P- and S-tridoped graphene as metal-free electrocatalyst for oxygen reduction reaction, *Journal of Electroanalytical Chemistry* 753 (2015) 21-27.
18. Materials of the future – Graphene and metals, *Graphene Flagship*, <https://graphene-flagship.eu/materials/news/materials-of-the-future-graphene-and-metals>, 2024.



31th January 2025
Gliwice, Poland

DEPARTMENT OF ENGINEERING MATERIALS AND BIOMATERIALS
FACULTY OF MECHANICAL ENGINEERING
SILESIA UNIVERSITY OF TECHNOLOGY

INTERNATIONAL STUDENTS SCIENTIFIC CONFERENCE

The impact of laser modification of the surface layer of tool steels on tribological properties

Julia Chudy ^a, Bartosz Filip ^a, Julia Haraf ^a, Kacper Krysiak ^b, Katarzyna Furman ^a, Mirosław Bonek ^c, Stela Dinescu ^d, Oleh Polishchuk ^e

^a Student, Silesian University of Technology, Faculty of Mechanical Engineering, Department of Engineering Materials and Biomaterials

email: julichu884@polsl.pl, bf313885@polsl.pl, julihar219@polsl.pl

^b Student, Silesian University of Technology, Faculty of Electrical Engineering

email: kacpkry923@student.polsl.pl

^c Silesian University of Technology, Faculty of Mechanical Engineering, Department of Engineering Materials and Biomaterials

^d University of Petroșani, Faculty of Mechanical and Electrical Engineering, Romania

^e Khmelnytskyi National University, Faculty of Engineering, Transport and Architecture, Ukraine

Abstract: This study investigates the impact of remelting parameters on the tribological properties of the surface layer of X40CrMoV5-1 steel using a high-power diode laser (HPDL). The analysis focuses on how remelting parameters influence friction coefficient measurements, as well as wear evaluation through gravimetric analysis, counter-specimen wear area examination, and surface profilography.

Keywords: materials, laser treatment, surface layers of material

1. INTRODUCTION

Laser modification of material surface layers is one of the effective methods for enhancing their performance under harsh conditions. High-power diode lasers (HPDL) have recently gained significant attention in materials engineering due to their advanced capabilities. Unlike continuous CO₂ gas lasers or pulsed Nd:YAG lasers, HPDLs offer a high radiation absorption coefficient for steel (approximately 20-40%), exceptional energy efficiency, and reliability. A notable advantage of HPDLs in surface engineering is their ability to achieve remelting in the form of paths up to 6.8 mm wide, with an almost linear energy density distribution across the laser beam spot.

The primary objective of surface layer remelting is to modify the material's structure, thereby improving its resistance to wear, erosion, and corrosion. This improvement results from rapid crystallization during solidification, which can occur at rates up to 10⁶ °C/s. This process produces a chemically uniform, fine-grained surface layer without altering the material's chemical composition.

The purpose of this study is to establish the technical and technological conditions for remelting the surface layer of X40CrMoV5-1 hot work alloyed tool steel using a high-power diode laser. Additionally, it aims to examine the relationship between laser treatment parameters and the resulting tribological properties.

1.1. High-power diode laser (HPDL)

High-Power Diode Laser (HPDL) is an advanced type of laser widely used in industrial and materials engineering applications due to its unique combination of efficiency, precision, and reliability. It operates by generating coherent light through semiconductor diodes, producing high-intensity laser beams suitable for processes such as welding, cutting, cladding, and surface treatment.

Key Features of HPDL:

- **High Energy Efficiency:** HPDL systems offer exceptional watt-hour efficiency compared to traditional laser types like CO₂ or Nd:YAG lasers, making them cost-effective and environmentally friendly.
- **High Absorption Coefficient:** For metals like steel, HPDLs achieve a high absorption rate (approximately 20-40%), ensuring efficient energy transfer to the material being processed.
- **Broad Beam Width:** These lasers are capable of producing remelting tracks up to 6.8 mm wide, which enhances their utility in surface engineering by providing uniform treatment over larger areas.
- **Near-Linear Energy Distribution:** HPDLs deliver a nearly uniform energy density across the laser beam spot, ensuring consistent heating and material processing.

Applications:

- **Surface Engineering:** HPDLs are used to enhance wear, corrosion, and erosion resistance by remelting surface layers and modifying their structure.
- **Additive Manufacturing:** They are employed for laser cladding and material deposition, enabling precise and durable coatings.
- **Joining and Welding:** Their reliability and precision make HPDLs ideal for welding applications in various industries, including automotive and aerospace.

1.2. X40CrMoV5-1

Steel X40CrMoV5-1 is a hot-work tool steel. It is characterized by high resistance to thermal wear, excellent corrosion resistance, and good resistance to thermal cracking. Thanks to these properties, it is used in the production of die inserts for presses and forging machines, dies and punches for extruding lightweight metal products, components of pressure die-casting molds, and rolls for copper rolling. The chemical composition of this steel includes carbon (0.35–0.42%), silicon (0.80–1.20%), manganese (0.25–0.50%), chromium (4.80–5.50%), molybdenum (1.20–1.50%), and vanadium (0.85–1.15%). In the annealed state, its hardness reaches up to 229 HB, while after hardening and tempering, it can achieve up to 56 HRC. This material is highly durable and ideal for applications requiring significant resistance to high temperatures and variable thermal loads.

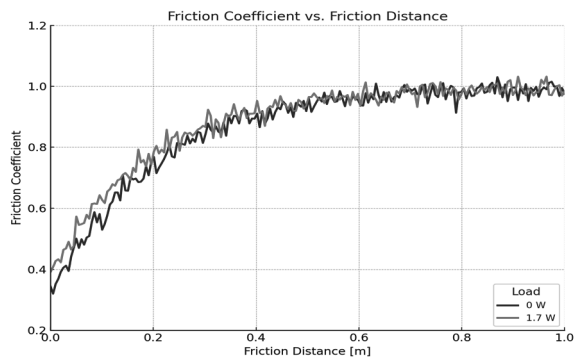


Fig. 1. Friction characteristics of the Al_2O_3 and the X40CrMoV5-1 steel surface layer pair

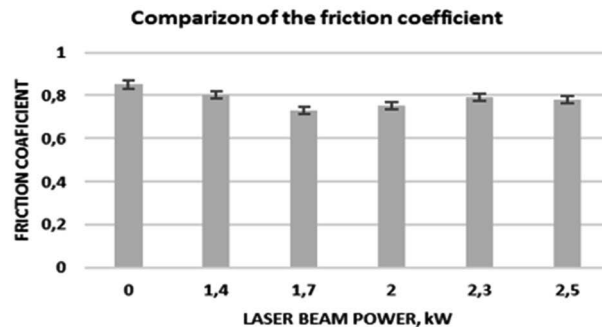


Fig. 2. Comparison of the friction coefficient measurement results depending on the laser beam power used for remelting the steel

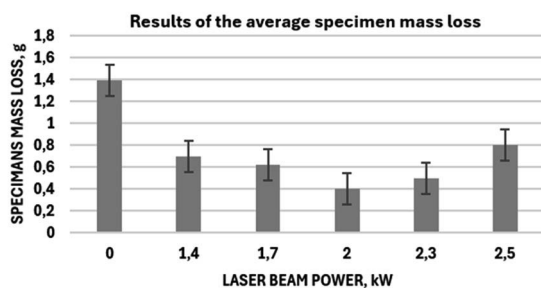


Fig. 3. Measurement results of the average specimen mass loss depending on the laser beam power

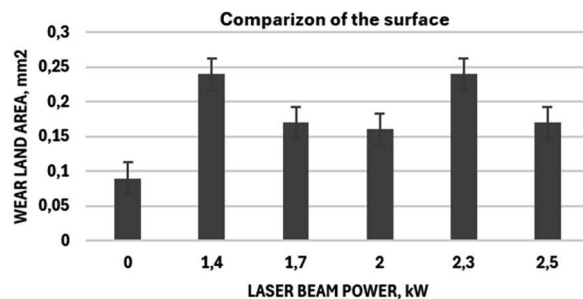


Fig. 4. Comparison of the surface area of the Al_2O_3 counter-specimen wear

2. EXPERIMENT

The specimens from the X40CrMoV5-1 alloy hot work tool steel, obtained from the vacuum melt, and made as O.D. 75 mm bars, featured material for investigation. Specimens with the O.D. 70 mm and 6 mm thick were turned from the material delivered in the soft annealed state, which were next austenitized in the salt bath furnace and tempered in the chamber furnace with the argon protective atmosphere. The specimens were gradually heated to the austenitizing temperature with holding at the temperature of 650°C for 15 min and austenitized for 30 min at a temperature of 1060°C. Cooling was made in hot oil.

After quenching the specimens were tempered twice, each time for 2 hours, in the temperature range from 510 to 660°C with gradation every 30°C. Specimen surfaces were sand blasted and machined on the magnetic grinder. Specimens of the X40CrMoV5-1 steel fixed to the computer controlled welding positioner were remelted with the high power laser beam (HPDL) Rofin DL 020. Remelting of specimens was carried out at the constant remelting rate of 0.5 m/min, changing the laser beam power in the range of 1.4-2.5 kW. Two remelting paths were done on each of the face surfaces of the specimens with radii of 12 and 22 mm. It was determined experimentally that the full shielding of the remelting zone is ensured by argon blow-in with the

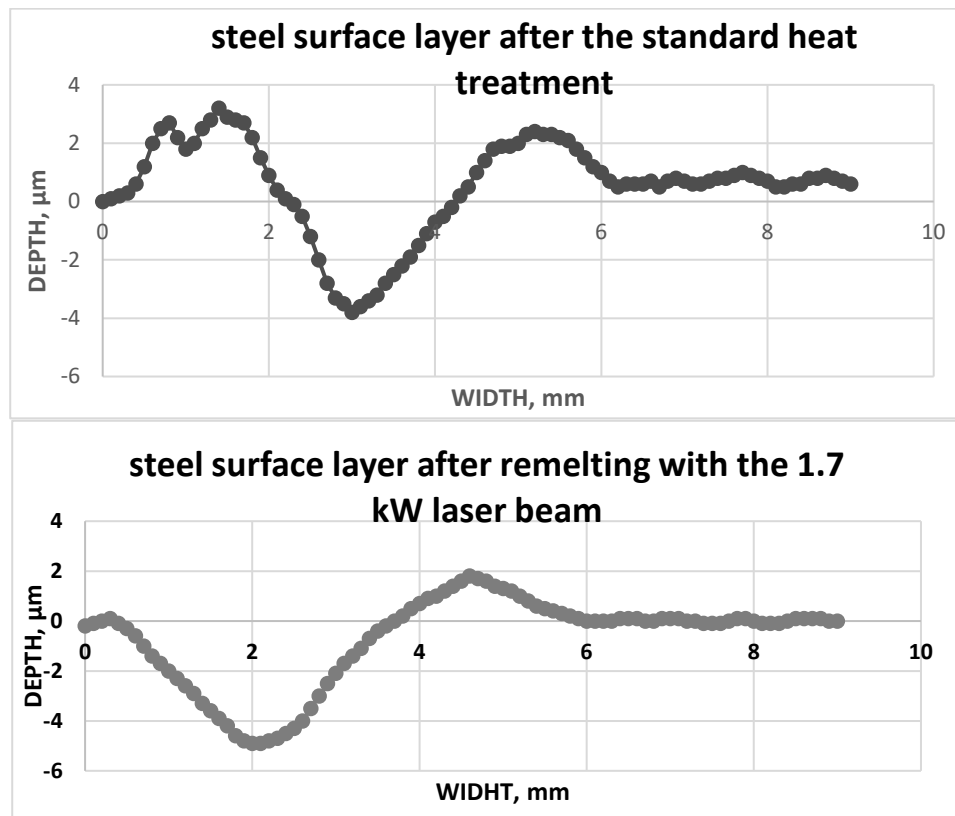


Fig. 5. Exemplary wear profile: a) steel surface layer after the standard heat treatment, b) steel surface layer after remelting with the 1.7 kW laser beam

volume flow of 20 l/min through the circular nozzle of the ϕ 12mm diameter, directed in the direction opposite to the remelting one. The specimens' surfaces were ground after remelting to obtain roughness specified by ASTM G99-90 standard. Test of dry wear resistance with the pin-on-disk method were made on the computer controlled CSEM High Temperature Tribometer. The test friction spot consists of the disk – specimen rotating at the n rotating speed and ball pressed against this disk with a load F at a distance R from the disk centre. Friction force between the ball and the disk was measured during the test run. Basing on the preliminary experiments the following test conditions were assumed: the smallest scatter of results and stable tribological characteristics were obtained for the counter-specimen in the form of the 6 mm diameter ball from the aluminium oxide Al_2O_3 . In this test the stationary ball was pressed against the disk rotating in the horizontal plane with the force of 10N.

The rubbing speed was 0.5 m/sec, friction radius was from 11 to 22 mm, and the optimum friction distance was determined as 1000 m. Environment temperature was assumed as 23°C, and the relative air humidity as 50%. Measurement of the specimens mass loss was made on the Mettler AT 201 electronic weigher, cleaning the specimens from the wear products in the friction zone with the air jet. Analysis of the counter-specimen wear land (Al_2O_3 ball) was made using the light microscope with the Image – Pro Measure Version 1.3 image analysis system at magnification 50x. Wear profiles of the specimens were made on the Taylor – Hobson Form Talysurf 120L laser profile measurement gauge in the depth range from 5 μm to 20 μm and the measurement length from 500 μm to 1755 μm in three planes every 120°. The examined

specimens were tribologically damaged due to action of the counter-specimen with the load of 10 N, along the friction distance of 1000 m. To analyse changes of the friction coefficient, plots of friction coefficient μ as function of friction distance were made. Comparison of the transient part of the friction coefficient plot for the surface layer of steel after heat treatment and after the laser remelting is presented in Figure 1. The value of the friction coefficient was evaluated as the average from the instantaneous values obtained for the part of the characteristics relevant for the stabilized friction (Fig. 2). The significant effect of laser remelting of the surface layer on decrease of friction coefficient, compared to the standard heat treatment only was observed. The tests with the gravimetric method were carried out weighing each specimen three times before the experiment and after the test and their results were statistically analyzed. Confidence intervals calculated with the probability of 95% are marked in the plots. Test results of the average specimens mass loss due to friction in the ball – disk pair for the surface layer obtained at various laser beam power values are presented in figure 3. It turns out from the analysis of the mass loss of specimens, depending on the laser beam power used for remelting of the surface layer, that the mass wear of the remelted specimens was two times smaller and was from 0.4 mg to 0.8 mg in comparison with the material that was not subjected to laser remelting, for which this value was 1.4 mg. The laser beam power does not have any clear effect on the mass wear of the investigated specimens.

The results of the counter-specimen (Al_2O_3 ball) wear land area analysis during the tests of the tribological properties of the ball – disk pair are shown in Figure 4. Increase of the counter-specimen wear land area was observed (0,170 to 0,240 mm^2) in the contact with the laser remelted surface layer. The counter-specimen land wear after the contact with the X40CrMoV5-1 steel after the standard heat treatment is about two times smaller (about 0,094 mm^2). The laser beam power during melting does not have a meaningful influence on the wear land of the counter-specimen from Al_2O_3 .

For the tribological assessment of the examined surface layer the linear wear was measured using the wear profiles. The exemplary surface layer wear profiles of the steel are shown in Figure 5. The influence of laser remelting was found out on the depth of the transverse section of the wear path, which for the non-remelted material was about 4 μm , whereas for the surface layer remelted with the laser beam with the 1.7 kW power it achieved value of 1.8 μm .

3. SUMMARY

The experiments on remelting the surface layer of X40CrMoV5-1 steel using a high-power diode laser (HPDL) demonstrated a reduction of approximately 20% in the friction coefficient in the Al_2O_3 -steel pair with the laser-treated surface. Laser remelting also significantly reduced the mass wear of specimens during testing, attributed to a slower release of wear products. Wear profile analysis of the surface layer showed a decrease in profile depths for the laser-treated materials. Notably, no significant impact of laser beam power on the tribological properties of the remelted surface layer of X40CrMoV5-1 hot work alloy steel was observed. The melting of the surface layer resulted in the formation of a fine-grained dendritic structure and a heat-affected zone. These findings confirm the effectiveness of the laser remelting method in enhancing the tribological properties of the steel's surface layer.

ACKNOWLEDGEMENTS

The work was created as part of project based learning - PBL, in the 11th competition under the Initiative of Excellence - Research University, Silesian University of Technology, Gliwice, Poland and as part of project of Students Scientific Circle of Laser Surface Treatment under the Initiative of Excellence - Research University, Silesian University of Technology, Gliwice, Poland.

BIBLIOGRAPHY

1. M. Bonek: Laser Surface Alloying. In: Wang Q., Chung Y. (Ed.) Encyclopedia of Tribology: SpringerReference, Springer-Verlag Berlin Heidelberg, 2013, pp. 1938-1948
2. M. Bonek: Effect of high power diode laser surface alloying of tool steels, Chiang Mai Journal of Science, 40(5), 2013, pp. 849-856
3. Dobrzański L.A., Tański T., Dobrzańska-Danikiewicz A.D., Jonda E., Bonek M., Drygała A., Structures, properties and development trends of laser-surface-treated hot-work steels, light metal alloys and polycrystalline silicon, in: J. Lawrence, D. Waugh (eds.), Laser Surface Engineering. Processes and Applications, Elsevier Ltd, 2015, pp. 3-32
4. M. Bonek, G. Matula, L.A. Dobrzański: Effect of laser surface melting on structure and properties of a high speed tool steel, Advanced Materials Research Vols. 291-294 (2011) pp 1365-1368
5. J. Kusiński: Laser Applications in Materials Engineering, WN „Akapit”, (2000) Cracow, (in Polish)
6. L.A. Dobrzański, E. Hajduczek, J. Marciniak and R. Nowosielski: Physical metallurgy and heat treatment of tool materials, WNT, Warsaw, (1990), (in Polish)
7. W.M. Steen, J. Mazumder, Laser Surface Treatment, Laser Material Processing, Springer, 2010, pp 295-347.
8. L.A. Dobrzański, E. Jonda, K. Labisz, M. Bonek, A. Klimpel, The comparison of tribological properties of the surface layer of the surface layer of the hot work tool steels obtained by laser alloying, Journal of Achievements in Materials and Manufacturing Engineering 42/1-2 (2010) pp142-147



31th January 2025
Gliwice, Poland

DEPARTMENT OF ENGINEERING MATERIALS AND BIOMATERIALS
FACULTY OF MECHANICAL ENGINEERING
SILESIA UNIVERSITY OF TECHNOLOGY

INTERNATIONAL STUDENTS SCIENTIFIC CONFERENCE

Integration of Laser Technology with Advanced Surface Engineering Methods

Julia Chudy^a, Bartosz Filip^a, Julia Haraf^a, Szymon Jędrzejewski^a, Antonina Olszewska^a, Mateusz Paluch^a, Karolina Rogalewska^a, Wiktoria Wanczura^a, Mirosław Bonek^b, Eva Tillova^c, Oleh Polishchuk^d, Stela Dinescu^e

^a Silesian University of Technology, Faculty of Mechanical Engineering, Department of Engineering Materials and Biomaterials

^b Silesian University of Technology, Faculty of Mechanical Engineering, Department of Engineering Materials and Biomaterials

^c Žilinská univerzita v Žiline, Strojnícka fakulta, Katedra materiálového inžinierstva, Slovakia

^d Khmelnytskyi National University, Faculty of Engineering, Transport and Architecture, Ukraine

^e University of Petroșani, Faculty of Mechanical and Electrical Engineering, Romania

Abstract: This article explores the synergistic integration of laser modification techniques and X-ray methods in modern surface engineering. It highlights the applications of laser processes, such as hardening, texturing, and alloying, in improving wear resistance, reducing friction, and enhancing fatigue strength. Advanced X-ray techniques, including X-ray diffraction (XRD) and computed tomography (CT), are discussed for their role in analyzing the microstructure and properties of laser-modified surfaces. The study also examines the optimization of laser parameters like pulse energy, scanning speed, and exposure time to achieve precise surface characteristics. Additionally, the article underscores the advantages of laser surface modification in industrial applications, its role in addressing corrosion resistance, and its integration with PVD coatings to enhance material performance and durability. These findings provide a robust framework for advancing material engineering solutions in demanding environments.

Keywords: laser surface modification, surface engineering, laser hardening, laser texturing, wear resistance, corrosion resistance, PVD coatings, advanced materials

1. SYNERGY OF LASER MODIFICATION AND X-RAY TECHNIQUES IN SURFACE ENGINEERING

Laser modification of the surface layer of tool steels and X-ray techniques are key elements of modern surface engineering. Processes such as hardening, texturing, or laser alloying enable precise shaping of microstructure and surface properties, leading to increased wear resistance,

reduced friction, and improved fatigue strength. Rapid cooling and the high energy of laser pulses result in the formation of complex structures and phases, which can be analyzed using advanced X-ray techniques such as X-ray diffraction (XRD) and X-ray computed tomography (CT) [1].

1.1 Advanced X-ray Applications in Laser Surface Modification

X-ray diffraction identifies key phases like martensite and austenite, crucial for modified layer properties, and analyzes residual stresses to enhance durability. X-ray computed tomography enables 3D imaging of surface structures, assessing laser texturing effectiveness and its impact on tribological properties. Pulse energy, scanning speed, or exposure time—plays a critical role in optimizing surface modification technology. Pulse energy determines the intensity of the laser beam's interaction with the surface, affecting the depth of thermal transformations and the formation of micro- and nanostructures. Scanning speed controls the energy distribution per unit area, directly influencing the uniformity of the resulting layer. Too low a speed can cause overheating and undesirable effects like thermal cracks, while too high a speed limits modification efficiency. Exposure time impacts crystallization and phase transformation processes, which are essential for achieving desired tribological and mechanical properties. Longer exposure may lead to the formation of harder phases, such as martensite, which enhance wear resistance [1-3].

1.2 Synergistic Development of Surface Engineering through Laser and X-ray Techniques

The integration of laser modification and X-ray techniques enables not only the refinement of existing processes but also the development of new technologies in surface engineering. It allows for the correlation of process parameters, such as laser power, exposure time, or scanning speed, with the properties of the modified surface layer. As a result, surfaces with precisely tailored characteristics can be designed, such as increased durability, higher resistance to extreme operating conditions, and improved functionality. The synergy of these two areas enhances the understanding of mechanisms governing changes in the surface layer, contributing to the creation of advanced materials with optimized functional properties. This approach supports the development of durable, highly functional, and efficient solutions in materials engineering, especially for applications requiring reliability and wear resistance [2].

2. USE OF LASER SURFACE MODIFICATION IN ENGINEERING MATERIALS.

Modern engineering materials must meet increasing industrial demands, including high strength, wear resistance, and durability under challenging operating conditions. One of the advanced solutions for enhancing the properties of surface layers in materials is the use of laser surface modification technology [4,7].

2.1 Principles of Laser Surface Modification

Laser technology relies on the precise delivery of energy in the form of a focused beam of light, allowing controlled microstructural and chemical changes in the surface layers of materials. This process encompasses several techniques, such as: [4-7]

- Laser Hardening – localized heating followed by rapid cooling for surface hardening.
- Laser Cladding – deposition of corrosion- or wear-resistant layers.
- Laser Texturing – micro- and nanoscale surface shaping for improved tribology.

2.2 Applications in Engineering Practice

In industrial practice, laser surface modification finds applications across various fields, such as aerospace, automotive, and energy sectors [4,7]. For example, laser hardening is used to improve the wear resistance of machine components such as shafts and gears [4]. Meanwhile, laser cladding facilitates the repair of costly components, such as gas turbines or tools dulled by use [5].

3. ADVANTAGES OF LASER TECHNOLOGY

Key advantages of laser technology include:

- **Precise Process Control:** Laser systems enable precise control over energy delivery, minimizing thermal damage to base materials and ensuring high-quality results [4,6].
- **Energy Efficiency:** Laser processes are highly energy-efficient, converting a significant portion of input energy into usable output, reducing waste and operational costs [5].
- **Material Versatility:** Lasers can process a wide range of materials, including metals, ceramics, polymers, and composites, making them suitable for diverse industrial applications [7].
- **High Repeatability and Automation:** Laser systems are compatible with modern automation and robotics, ensuring consistent quality and efficiency in high-volume production [5].
- **Customization and Flexibility:** Lasers allow for tailoring surface properties, such as roughness or hardness, to specific requirements, providing flexibility for various engineering challenges [6,7].

4. METHODS OF LASER CUTTING FOR GRADIENTS MATERIALS

Laser cutting methods for gradient materials rely on precise mechanisms, which can be illustrated using the presented diagram. Various cutting techniques, such as melting and blowing, vaporization, exothermic reactions, or pulsed laser cutting, are based on the key components of laser cutting processes.

This diagram perfectly illustrates the principles of the melting and blowing technique, which has been widely applied in gradient materials, such as metals with varying hardness. The ability to adjust optical and gas parameters dynamically enables the process to adapt to the specific layers of the material. For vaporization cutting and other methods, the key components visible in the diagram—such as the focusing system and nozzle—support precise material removal while minimizing the risk of thermal damage to adjacent areas.

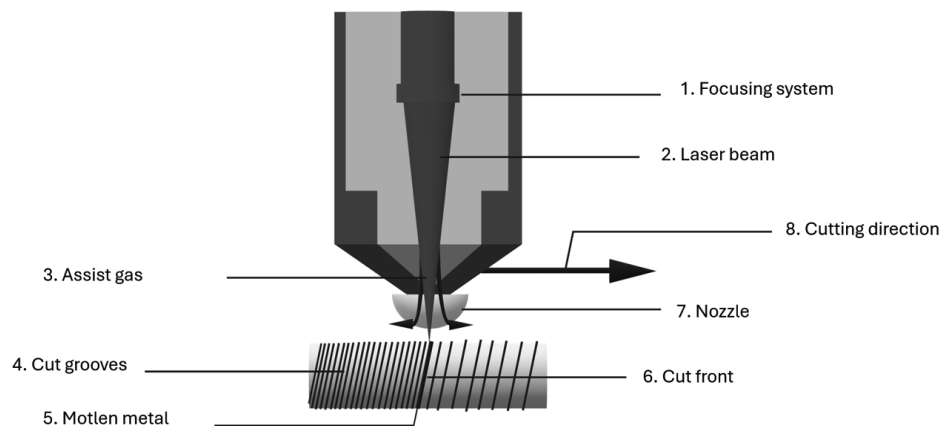


Figure 1 Laser Cutting Diagram

The diagram [Fig. 1] shows the essential elements of the laser cutting process:

1. Focusing System – Lens and mirror optics concentrate the laser beam at the processing point, enabling precise delivery of energy to the material surface.

2. Laser Beam – The focused beam strikes the surface of the material, heating it until it melts or vaporizes.

3. Assist Gas – A stream of gas (e.g., argon, nitrogen, or oxygen) interacts with the laser beam, blowing molten material out of the cutting kerf and ensuring clean and precise edges.

4. Cut Grooves – Grooves are formed due to the laser and gas action, with their pattern depending on process parameters such as cutting speed and beam shape.

5. Molten Metal – The concentrated laser light locally melts the material, allowing selective removal.

6. Cut Front – The cutting kerf is slightly wider than the focused laser beam, enabling precise guidance along the intended contour.

7. Nozzle – The assist gas and laser beam reach the material through the cutting nozzle, allowing control over the process direction and efficiency.

8. Cutting Direction – Movement of the cutting head or material in a specific direction creates a cutting line as per the planned pattern.

4.1 Melting and Blowing Technique

The laser beam melts the material at the cutting site, creating a liquid phase. High-pressure gas removes molten material for precise cuts. This type of cutting is particularly suitable for metallic materials with gradient hardness due to the quality control of the edges achieved through dynamic gas flow adjustments, supported by sensors in automated systems. These sensors analyze the material's thickness and composition across various layers.

4.2 Vaporization Cutting

In vaporization cutting, the high temperature generated by the laser beam plays a key role in transforming the material from solid to gas. The beam's temperature is carefully regulated to avoid overheating adjacent areas. This technique is well-suited for gradient glass and polymers, where the variable property is laser absorption. Laser heat transforms material into gas,

minimizing thermal damage. Femtosecond lasers are used for large property differences in gradient materials, minimizing thermal damage.

4.3 Reactive Cutting

The laser initiates an exothermic reaction between the reactive gas and the material. This results in combustion and additional heat generation, aiding the cutting process.

This method is often used in metal-ceramic materials with a gradient of oxidizability. The presence of oxygen during the process enables uniform and fast cutting. By adjusting the reactive gas proportions, it is possible to obtain clean edges with varying ceramic content.

4.4 Pulsed Cutting

Pulsed cutting relies on ultrashort laser pulses that remove material layer by layer, minimizing the temperature impact generated by the laser beam on adjacent areas. This method is primarily used for gradient polymer materials and allows very precise cutting without damaging delicate layers with lower thermal resistance. An innovation in this method is the ultrasonic-assisted pulse technology, which increases process stability.

5 SYNERGY OF LASER PROCESSING AND PVD COATINGS IN ADVANCED MANUFACTURING

Modern material processing combines laser cutting and PVD coatings to create high-performance components with precise geometries, enhanced durability, and aesthetic appeal. By combining laser machining with PVD coatings, manufacturers can produce parts that not only meet stringent dimensional tolerances but also exhibit superior wear resistance, corrosion protection, and decorative appeal. This synergy between laser processing and PVD coatings opens new possibilities across industries, including aerospace, automotive, and precision engineering.

6 CHARACTERISTICS OF PVD COATINGS

PVD (Physical Vapor Deposition) coatings are thin-layer coatings deposited on the surface of a material through a process of evaporation and deposition in a vacuum chamber. This process include [8,9]:

- **Substrate Cleaning:** Before deposition, the substrate must be thoroughly cleaned of contaminants such as oils, greases, and other residues. Source
- **Pre-treatment:** Methods such as corona or plasma discharge are often used to activate the substrate surface. Source
- **Deposition of Source Material:** The source material evaporates in the vacuum chamber and deposits on the substrate surface, forming a thin coating layer. Source
- **Quality Control:** Coatings are checked for thickness, uniformity, and other quality parameters. Source
- **Surface Finishing:** If necessary, coatings are polished or subjected to other finishing processes to achieve the desired smoothness and appearance. Source

6.1 Properties of PVD Coatings

The main properties of PVD are [8,10]:

- **Durability:** PVD coatings are known for their high durability and wear resistance, making them ideal for applications requiring high mechanical resistance. Source
- **Appearance:** They offer a wide range of decorative possibilities by controlling color and surface finish. They can be used to give metallic surfaces an attractive appearance. Source
- **Functionality:** They significantly increase corrosion resistance, which is crucial for components exposed to aggressive environments. Source
- **Smoothness:** The surface of coated parts is very smooth, reducing friction and improving efficiency in applications where low friction is key. Source

6.2 Applications of PVD Coatings

PVD coatings are used in many industries due to their versatile properties [9,10]:

- **Aerospace and Automotive:** PVD coatings are used for engine parts, gas turbine blades, and suspension components, increasing their durability and wear resistance. Source
- **Metalworking:** Cutting tools, such as drills and milling cutters, are often coated with PVD to increase their durability and wear resistance. These coatings also help improve machining efficiency and precision. Source
- **Optics:** In optics, PVD coatings are used to create anti-reflective ceramic coatings, improving the optical quality of lenses and other optical elements. Source
- **Watchmaking:** In the watchmaking industry, PVD coatings are used to give watches an attractive appearance and increase their scratch resistance. Source

7 LASER PROCESSING AND CORROSION RESISTANCE: A SYNERGISTIC APPROACH

Laser processing not only enables precise cutting and machining of materials but also plays a crucial role in enhancing corrosion resistance through controlled surface modifications. Laser machining reduces surface imperfections and prepares materials for protective coatings, improving corrosion resistance. This method is especially effective in harsh marine or industrial environments, reducing pitting and crevice corrosion. Furthermore, the integration of laser processing with preventive measures like sacrificial anodes or cathodic protection ensures that structures not only maintain mechanical integrity but also withstand aggressive environmental conditions, extending their service life significantly. This synergy between laser technology and corrosion prevention strategies offers a robust framework for durable, high-performance materials in demanding applications.

7.1 Galvanic Corrosion:

Galvanic corrosion occurs when two dissimilar metals with different electrochemical potentials come into contact in the presence of an electrolyte. The less resistant (more active) metal acts as an anode and corrodes more rapidly, while the more resistant (noble) metal serves as the cathode and corrodes less. The rate of galvanic corrosion depends on the potential difference between metals and is influenced by factors such as cathode surface area and the condition of protective films. Incomplete surface films can accelerate localized corrosion, leading to pitting.

Sacrificial anodes, like zinc or magnesium, protect structures by corroding preferentially. Galvanized steel demonstrates this principle, combining a protective barrier with sacrificial properties to reduce corrosion. [11]

7.2 Corrosion in high temperatures:

Hot corrosion is an accelerated form of oxidation that affects surfaces exposed to high-temperature gases containing sulphur and alkali metal salts, typically when heated in the 700–900°C range. The sulphate deposits form due to the reaction between sodium chloride and sulphur compounds in the gas. [12] Superalloys use elements like molybdenum and tungsten for high-temperature strength. However, the oxides of both molybdenum and tungsten (MoO_3 and WO_3) have high vapor pressures at very high temperatures. Molybdenum and chromium provide strengthening through solid solution and carbide formation mechanisms. Silicon effectively improves the oxidation resistance of Cr–Mo. If the chromium content is inadequate, a continuous chromium oxide scale may not form during prolonged service or thermal cycling, resulting in breakaway oxidation [13]

7.3 Atmospheric corrosion:

Atmospheric corrosion varies by exposure and is crucial for system design. A widely accepted classification system, developed by the International Organization for Standardization (ISO), divides outdoor environments into five corrosivity classes:

- Industrial atmospheres are typically rich in sulfur compounds and nitrogen oxides, which contribute to acid rain and smog.
- Temperate marine environments contain fine sea mist particles that can form corrosive salt crusts on exposed surfaces, with the amount of salt varying depending on wind velocity.
- In tropical marine the daily cycle includes high temperatures, high humidity, intense sunlight, and long periods of condensation at night.
- Urban and suburban environments' corrosivity is linked to air quality, which can differ significantly across locations.

Indoor environments, when controlled for humidity and corrosive agents, are typically mild, though specific conditions in storage cabinets, display cases, or galleries can introduce corrosive elements, potentially accelerating the deterioration of metals. [14]

7.4 Guidelines for Corrosion Prevention:

To reduce corrosion, select materials with similar electrode potentials and design structures to minimize moisture accumulation, using butt joints and drip skirts. To further prevent corrosion, resilient sealants should be used to block moisture from entering potential crevices, and cathodic protection, such as galvanized steel or alclad aluminum, should be applied to protect areas prone to crevice corrosion. The electrode potential between electrically interfering structures exposed to the same electrolyte, such as in underground systems or large tanks, should be equalized through methods like cross-bonding, cathodic protection, and proper grounding. Minimize fluid turbulence by optimizing flow patterns and pressure management. Use compatible materials and conduct pretesting for critical applications. Redundant systems, such as spare heat exchanger bundles or replaceable spools, should be implemented for high-risk applications, and nonmetallic materials should be used when necessary to further mitigate corrosion risks. [15]

ACKNOWLEDGEMENTS

The work was created as a result of the project as part of project based learning - PBL, in the 11th competition under the Initiative of Excellence - Research University, Silesian University of Technology, Gliwice, Poland and as part of project of Students Scientific Circle of Laser Surface Treatment under the Initiative of Excellence - Research University, Silesian University of Technology, Gliwice, Poland.

BIBLIOGRAPHY

1. W Paszkowicz, *Synchrotron Radiation in Natural Science Vol. 5, No 3 (2006) Rentgenowskie techniki dyfrakcyjne stosowane w wysokociśnieniowych badaniach materiałów polikrystalicznych*, Warszawa 2006,
2. Sozańska M, Roskosz S, *Metody i techniki badań*, Wydawnictwo Politechniki Śląskiej, Gliwice 2020,
3. Labisz K, *Kształtowanie struktury i własności powierzchni odlewniczych stopów Al-Si-Cu*, Gliwice 2013
4. Steen, W. M., & Mazumder, J. (2010). *Laser Material Processing*. Springer.
5. Katayama, S. (2013). *Handbook of Laser Welding Technologies*. Woodhead Publishing.
6. Li, L. (2008). "Laser Surface Engineering: Processes and Applications." *Journal of Materials Processing Technology*, 208(1-3), 19-25.
7. Ion, J. C. (2005). *Laser Processing of Engineering Materials: Principles, Procedure and Industrial Application*. Butterworth-Heinemann.
8. <https://at-machining.com/pl/pvd-coating-explained/>
9. <https://sacher-cnc.com/pl/blog/powloki-pvd-dlaczego-warto-o-nich-wiedziec/>
10. <https://pl.aziocorp.com/blogs/blog/what-is-pvd-coating>
11. Zhang, X. G., Galvanic Corrosion. *Uhlig's Corrosion Handbook* 123–143 (2011) 1.
12. Prakash, S., Hot corrosion of alloys and coatings. *Developments in High Temperature Corrosion and Protection of Materials* 164–191 (2008).
13. Sequeira, C. A. C., High-Temperature Oxidation. *Uhlig's Corrosion Handbook*, 247–280 (2011).
14. Roberge, P. R., Atmospheric Corrosion. *Uhlig's Corrosion Handbook*, 299–326 (2011)
15. Ion, J. C. (2005). *Laser Processing of Engineering Materials: Principles, Procedure and Industrial Application*. Butterworth-Heinemann



31th January 2025
Gliwice, Poland

DEPARTMENT OF ENGINEERING MATERIALS AND BIOMATERIALS
FACULTY OF MECHANICAL ENGINEERING
SILESIA UNIVERSITY OF TECHNOLOGY

INTERNATIONAL STUDENTS SCIENTIFIC CONFERENCE

Classification of structural steel grades using artificial intelligence

Anil Can Erbus^a, Tommaso Giacomelli^a, Rafał Honysz^b

^a Student of Mechanical Engineering, Silesian University of Technology, Faculty of Mechanical Engineering, Department of Engineering Materials and Biomaterials, email: anilerb273@student.polsl.pl, tommgia112@student.polsl.pl

^b Silesian University of Technology, Faculty of Mechanical Engineering, Department of Engineering Materials and Biomaterials, email: rafal.honysz@polsl.pl

Abstract: The aim of the work was to develop a computational model based on artificial neural networks that allows for the classification of unalloyed and low-alloy structural steel grades based on their chemical composition. This is not an easy task, because the steels have very similar chemical compositions, and the concentration ranges of individual chemical elements overlap in different grades.

Keywords: computer science of materials, artificial neural networks, computational model, structural steel, classification

1. INTRODUCTION

Artificial intelligence is a broad topic and widely discussed in the scientific, journalistic and political spheres. These are activities based on modeling knowledge, data and developing algorithm systems and computing power, which in the current state of technology allows for obtaining a relatively automated system for acquiring, processing and analyzing data, which gives the possibility of autonomous improvement of the system or predicting behaviors and actions based on the analysis of collected data and correlations between them.

One of the artificial intelligence algorithms is artificial neural networks. These are computational systems with connected nodes that work similarly to the neurons in the human brain. The use of algorithms allows them to recognize hidden patterns and correlations in raw data, group and classify them, and (over time) continuously learn and improve. Neural networks are also suitable for supporting humans in solving complex everyday problems. They can learn and model nonlinear and complex connections between inputs and outputs, make generalizations and inferences, reveal hidden connections, patterns and predictions, and model highly variable data.

This algorithm was used to create a computational model that allows for determining the steel grade based on its chemical composition. The problem in the case of structural steels is the small ranges of variation in the concentrations of chemical elements that often overlap, making it difficult to classify steel into a specific grade. The developed tool is to solve this problem and is to help the engineer determine which steel grade corresponds to a given chemical composition.

2. MATERIAL

For research and creation of a set of training data based on them, twelve unalloyed and low-alloy structural steels were selected:

- E295
- E335
- E360
- P255G1
- P265GH
- P355N
- P355NL1
- S235J2G3
- S235JR
- S235JRG2
- S275JR
- S355J2G3

Variability ranges of ten selected chemical elements (alloying elements and impurities) included in the above-mentioned steels were obtained from metallurgical certificates, online databases and cooperation with companies producing steel elements. These are:

- carbon (C)
- manganese (Mn)
- silicon (Si)
- chromium (Cr)
- nickel (Ni)
- molybdenum (Mo)
- copper (Cu)
- aluminium (Al)
- sulphur (S)
- phosphorus (P)

This data allowed us to build a database used to teach an artificial neural network to recognize the type of steel based on the concentrations of chemical elements. Thanks to cooperation with one of the companies producing steel elements from the above-mentioned types of steel, it was possible to obtain as many as 1000 training records. They were saved in a CSV file that served as the input for training the artificial neural network.

3. METHODOLOGY FOR BUILDING A CLASSIFICATION MODEL

JustNN is a neural network system for Microsoft Windows. It makes the creation of neural networks easy. It allows the user to produce multilayer neural networks from a grid or from text files and images. The user can produce training, validating and querying files using the facilities in JustNN or using any editor, word processor or spreadsheet that supports text files. JustNN can learn from training data and can self-validate while learning. It can be queried from a file or interactively. JustNN can produce txt or csv output and results files. JustNN is a free software published in the Science list of programs, part of education.

First create an empty grid and import the data from csv file. Then indicate if the first words (as in our case) contain the name of the rows of the grid. In the second dialog box, click Set names to create the columns and go forward till the last one. When you are on the last column, remember to change the type in Output click OK. After successfully importing data, a table with the data will be displayed (fig. 1).

After data import, the next step is to create an artificial neural network From Action menu chose New Network to create the ANN (fig. 2). At this stage, you can choose the complexity of the network, with one, two or three hidden layers. The number of neurons in the hidden layer will be selected automatically. You can obtain a better ANN selecting the value 1 as grow layer number, allowing, in this way, to JustNN to automatically detect the optimum number of nodes and connections. Only in really few cases, in fact, we could need more than one level of hidden nodes, but JustNN (selecting the values 2 or 3) can generate more levels. Click OK button.

After defining the network architecture in the control dialog you can set the parameters for learning rate and momentum. Additionally, you can check optimize or decay either for Learning Rate and for Momentum. Put 200 in Select examples at random to create some validation examples (randomly selected by JustNN). Check “Stop on cycle” and put the value 100000. Then click OK (fig. 3)

- Answer YES to optimize the controls and YES to start the learning. Once done the learning phase will start. You have to wait for the training phase to end (fig. 4)

Once the learning process is complete, select the Information option from the View menu to see the details of the network. Click on the Refresh button to be sure that the details are all shown. Validation results: from 60 to 80% indicates, that the “predicted” results are correct (fig. 5).

The training process was repeated for networks with different values of the Learning rate, momentum and decay parameters and for networks with two and three hidden layers. The best turned out to be the network with one hidden layer with six neurons (fig 6).

	Symbol	C	Mn	Si	P	S	Cr	Ni	Mo	Cu	Al
#740	P355N	0.1800	1.4000	0.3900	0.0240	0.0110	0.1600	0.0900	0.0400	0.1000	0.0360
#741	E335	0.4200	0.3000	0.2500	0.0180	0.0120	0.2400	0.1300	0.0400	0.1600	0.0000
#742	S235JR	0.1200	0.4900	0.3000	0.0270	0.0350	0.1700	0.0600	0.0000	0.1700	0.0000
#743	P355N	0.1800	1.2900	0.3200	0.0180	0.0320	0.1000	0.0600	0.0190	0.1200	0.0550
#744	S275JR	0.1900	0.4600	0.3800	0.0150	0.0110	0.0600	0.0700	0.0000	0.0900	0.0180
#745	P355N	0.1800	1.2500	0.3100	0.0170	0.0100	0.2500	0.1000	0.0000	0.1100	0.0370
#746	S355J2G3	0.1600	1.2300	0.3100	0.0130	0.0090	0.2700	0.1500	0.0500	0.2000	0.0000
#747	S235JR	0.1500	0.5100	0.2500	0.0100	0.0300	0.0400	0.0500	0.0100	0.1100	0.0000
#748	S235JR	0.0900	0.5100	0.2700	0.0320	0.0330	0.1600	0.1000	0.0000	0.2000	0.0000
#749	P355NL1	0.1600	1.3200	0.3200	0.0250	0.0060	0.2000	0.1100	0.0300	0.0500	0.0480
#750	S355J2G3	0.1700	1.3700	0.4000	0.0100	0.0080	0.0800	0.0400	0.0400	0.1100	0.0570
#751	S355J2G3	0.1700	1.2900	0.3500	0.0170	0.0220	0.1000	0.0800	0.0200	0.1700	0.0000

Figure 1. Program screen showing correctly imported data

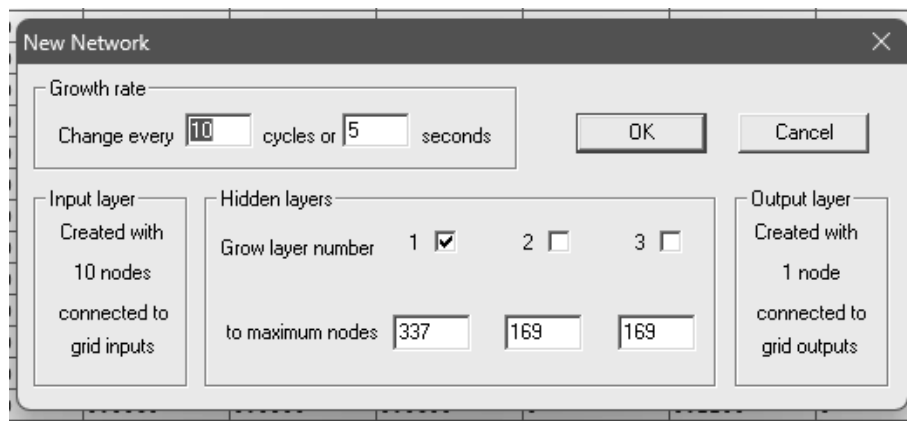


Figure 2. New Network window

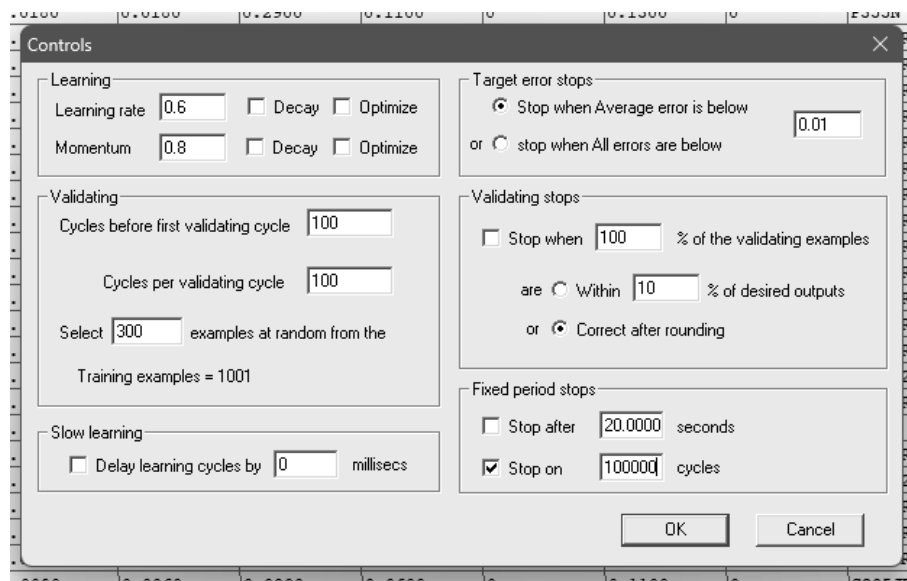


Figure 3. Controls window

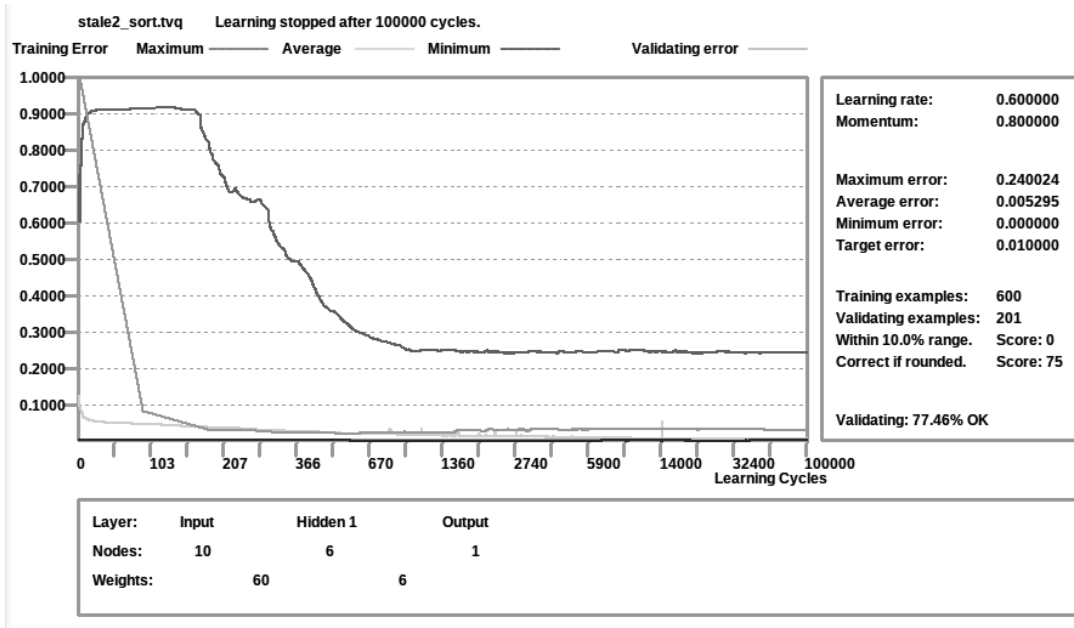


Figure 4. Learning process chart

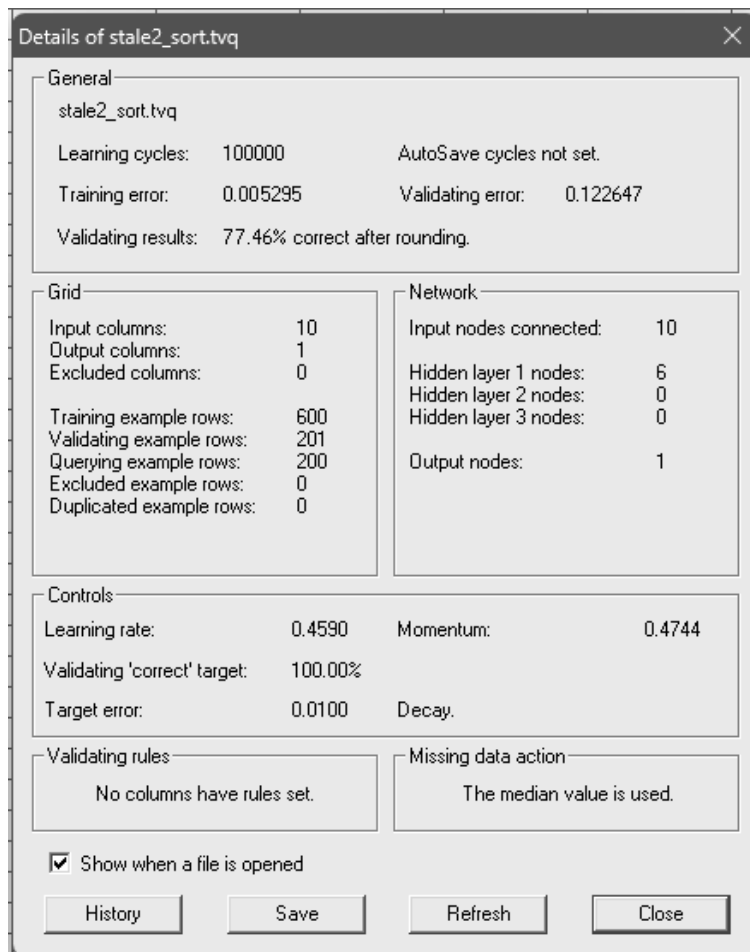


Figure 5. Information window

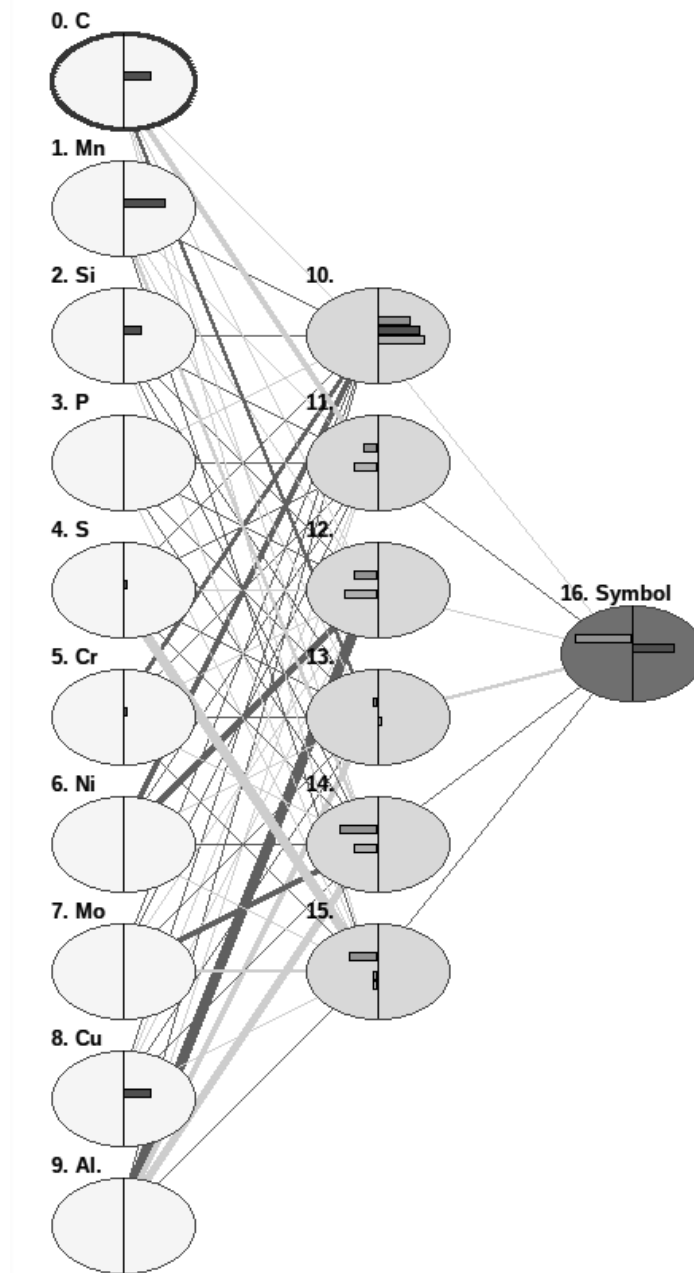


Figure 6. Artificial neural network architecture

4. EVALUATION OF THE DEVELOPED CLASSIFICATION MODEL

From Insert Menu you can add a Querying Example Row. If an 'Example Presets' dialog appears, click OK to set the values to unknown (you will see '?' in the grid). This row allows you to enter independent values and check whether the artificial neural network works correctly and correctly shows the steel grade based on the concentrations of chemical composition elements. These rows, there may be several of them, allow you to verify whether the network works correctly and whether the steel classifications are correct (fig. 7).

	Symbol	C	Mn	Si	P	S
Query	~~~~S275JR	0.3450	0.9500	0.3250	0.1130	0.05
Query	~~~~P255G1	0.2209	0.9567	0.2787	0.0184	0.01

Figure 7. Querying Example Rows

For checking the correctness of the network operation, twenty steels were selected, which did not participate in either the network development or its validation. The concentration values of chemical elements were entered into the query rows. Sixteen steels, whose chemical compositions were entered into the query rows, were correct. In four cases, the artificial neural network returned an incorrect result.

5. SUMMARY

Classification of unalloyed and low-alloy structural steels turned out to be a difficult task. Very small differences in chemical compositions and overlapping concentration ranges of chemical elements did not make the task easier. Some of the developed neural networks were not suitable for use due to their low parameters. However, the results achieved allow us to state that based on the concentration values of chemical elements it is possible to detect the grade of steel that was produced. The error scale of the neural network at the level of 4 errors on twenty types of steel coincides with the parameters of the trained network.

BIBLIOGRAPHY

1. L. A. Dobrzański, Podstawy nauki o materiałach i metaloznawstwo: materiały inżynierskie z podstawami projektowania materiałowego, Wydawnictwo Naukowo-Techniczne WNT, 2006
2. Sztuczna Inteligencja - <https://www.sztucznainteligencja.org.pl/>
3. Neural Planner Software - <https://neural-planner-software-ltd1.software.informer.com/>
4. Y. Liang, B. J. Fugère, Getting Start with JustNN. Computer Science, Université du Québec, Chicoutimi, May 2003
5. R. Folgieri, ANN in JustNN how to... - http://www.mtcube.com/EPS/topic7_ANN_JustNN.pdf
6. O.S. Al-Madhoun, A. Hasira, S. Hegazy, S. Abu-Naser, Low Birth Weight Prediction Using JNN, International Journal of Academic Health and Medical Research (IJAHMR) 4 (11):8-14 (2020)
7. MatWeb, Your Source for Materials Information - <https://www.matweb.com/>
8. European Steel and Alloy Grades - <https://steelnumber.com/>



31th January 2025
Gliwice, Poland

DEPARTMENT OF ENGINEERING MATERIALS AND BIOMATERIALS
FACULTY OF MECHANICAL ENGINEERING
SILESIA UNIVERSITY OF TECHNOLOGY

INTERNATIONAL STUDENTS SCIENTIFIC CONFERENCE

Contemporary Challenges and Opportunities in the Production of Bionic Prosthetics

Rafał Gabryś^a, Jakub Pająk^a, Julia Dąbrowska^b, Arkadiusz Górniak^c, Maksym Cinal^c, Magdalena Polok-Rubinić^d, Anna Włodarczyk-Fligier^d, Aneta Kania^d

^a Students of Industrial Mechatronics, Silesian University of Technology, Faculty of Mechanical Engineering

^b Student of Biotechnology, Silesian University of Technology, Faculty of Automatic Control, Electronics and Computer Science

^c Students of Automation and Robotics/Production Engineering and Management Silesian University of Technology, Faculty of Mechanical Engineering

^d Silesian University of Technology, Faculty of Mechanical Engineering, Department of Engineering Materials and Biomaterials

email: rg302613@student.polsl.pl

Abstract: The article discusses the application of bionic hands, highlighting their rehabilitative, social, and technological functions that help amputees regain independence and engage in professional and recreational activities, while also addressing patient compatibility, precise fitting through 3D scanning technologies, and the use of advanced materials for comfort and durability, and emphasizes challenges such as high costs and the need for further development of feedback systems.

Keywords: Prosthetics, Bionic Arms, 3D Printing, Filaments

1. INTRODUCTION

Bionic arms are applied in various fields, combining rehabilitative, social, and technological functions. They enable individuals with amputations to regain independence, allowing them to perform everyday activities such as grasping objects, writing, or operating devices [1]. In professional environments, these prosthetics facilitate the reintegration of people with disabilities, enabling them to return to work, even in physically demanding roles. Furthermore, advanced prosthetics are used in research on human-machine interfaces, neurostimulation testing, and experiments with artificial intelligence algorithms [2]. Their application in sports and recreation allows individuals with disabilities to actively participate in various sports disciplines, contributing to improved quality of life and increased self-confidence. While challenges remain, such as high costs and the need for further development of sensory feedback, bionic arms hold immense potential to transform the lives of many people [1,3].

2. PATIENT COMPATIBILITY IN THE CONTEXT OF BIONIC ARMS

The compatibility of a bionic arm with the patient is a key aspect of its effectiveness and acceptance (Figure 1). It requires the integration of advanced biomechanical, neurological, and material technologies to ensure that the prosthetic is not only functional but also comfortable for daily use [2,4].

Bionic arms must be precisely tailored to the individual characteristics of the user, which is achieved through imaging and spatial modeling technologies. Using 3D scanning of the residual limb, prosthetics are designed to accommodate the unique geometry of the stump. This approach minimizes pressure points and enhances the stability of the prosthetic during use [5].



Fig.1. An Example of an Advanced Prosthetic [6]

3. NEUROMUSCULAR INTERFACES

Control interfaces are crucial for the intuitive use of bionic prosthetics. The utilization of electromyographic (EMG) signals enables the detection of the patient's muscle activity. Surface electromyography (EMG) has evolved from merely recording muscle activity to neural interfacing technology, facilitating the study of the nervous system and the control of prosthetics (Figure 2). These technologies are applied in neuroengineering and the development of human-machine interfaces. Their key advantages include non-invasiveness and the ability to record large amounts of data under natural conditions [1].

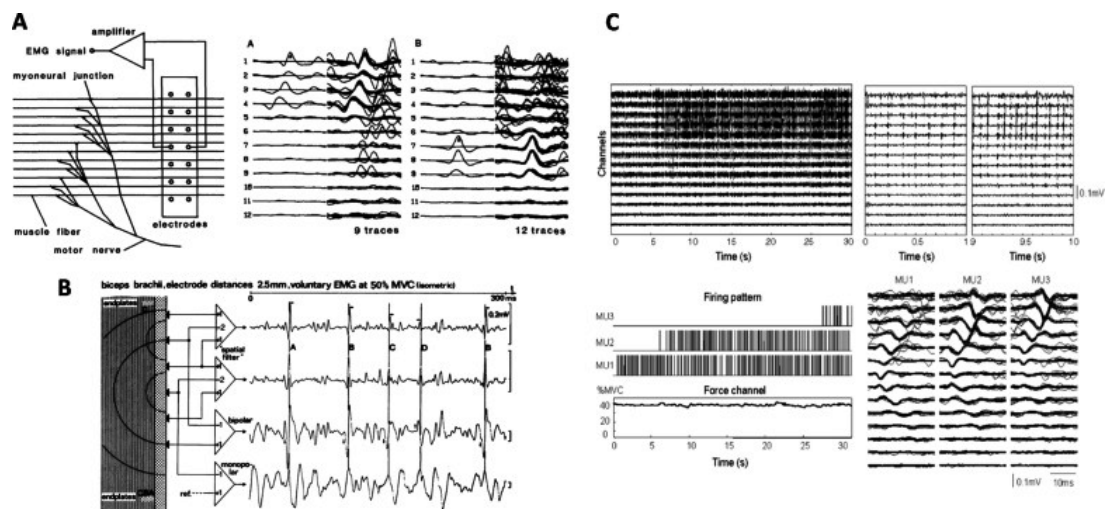


Fig. 2. Example EMG Signals [1]

4. MATERIALS AND FINISHING

User comfort also depends on the materials used. The internal linings of the prosthetic socket are made from flexible materials such as silicone or thermoplastic polymers, which reduce friction and protect the skin from injuries. At the same time, the use of lightweight carbon composites and metal alloys, such as titanium, helps maintain a low prosthetic weight, which reduces the user's load and enhances comfort [3].

Polymers and elastomers, including silicone, polyurethanes (PU), and TPE rubber, are the primary materials used in the production of prosthetic liners due to their exceptional mechanical and physical properties. Silicone, characterized by high elasticity and resistance to compression, provides good protection for the residual limb by effectively distributing pressure. Polyurethanes offer better mechanical properties compared to thermoplastic elastomers, particularly in terms of volumetric elasticity and thermal conductivity. TPE rubber, while cheaper and more flexible, has lower durability under intense use, which may limit its long-term longevity [3].

The use of innovative foam constructions, such as "sandwich" foams with polyurethane and EVA layers, enhances tensile strength, increasing resistance to mechanical damage and providing better comfort. Modern technologies also utilize phase change materials (PCMs) that regulate the surface temperature of the limb, significantly improving prosthetic comfort by extending the time it remains at an optimal temperature [3,5].

3D printing is gaining significance, enabling the design of personalized prosthetic liners that perfectly fit the irregular shapes of the limb. This method not only allows for precise fitting of the prosthetic but also minimizes production waste, making the process more efficient and environmentally friendly [3].

These materials are used in bionic prosthetics, where their primary function is to improve user comfort, ensure durability, and provide effective load distribution. Additionally, modern prosthetics incorporate sensors that monitor stress and improve the fit of the prosthetic to meet the user's individual needs [3,5].

5. PSYCHOLOGICAL AND SENSORY ADAPTATION OF THE PATIENT

An important aspect of compatibility is psychological adaptation. Patients must not only learn how to operate the new device but also accept it as part of their body. The introduction of haptics,

or the simulation of touch sensations, contributes to improving this acceptance. Touch sensors provide feedback on pressure force and temperature, allowing for a better perception of the external environment. Systematic therapy, based on therapeutic strategies aimed at improving these areas, significantly contributes to the patient's functional improvement. This includes exercises with and without the prosthetic. Exercises involve using a 3D prosthetic for tasks such as grasping, waving, and turning pages of a book, as well as activities supporting sensory integration without the prosthetic. Progress in functionality is significantly improved with a higher frequency of therapy [2,5].

6. SUMMARY

Both prosthetic liners and bionic hands represent groundbreaking solutions in the fields of rehabilitation and medical technology. Technologies such as 3D scanning and spatial modeling play a key role in ensuring optimal fit, minimizing pressure points, and improving user comfort. Modern solutions utilize advanced materials that contribute to tissue protection and increased comfort [2,3].

An essential element of bionic hands is neuromuscular interfaces, which enable intuitive control of the device based on EMG signals, significantly enhancing device acceptance among patients and improving their functional abilities [1].

Despite the dynamic development, these technologies still face challenges. However, interdisciplinary collaboration and technological progress offer hope for significantly reducing these limitations in the future [2,5].

BIBLIOGRAPHY

1. D. Farina, M. Roger, *Journal of Electromyography and Kinesiology*, Evolution of surface electromyography: From muscle electrophysiology towards neural recording and interfacing, Elsevier, September 2023.
2. Thomas, T. Muñecas, A rehabilitation protocol for the use of a 3D-printed prosthetic hand in pediatrics, Florida International University, Miami, USA, November 2022.
3. X. Yang, R. Zhao, D. Solav, X. Yang, D. R.C. Lee, B. Sparrman, Y. Fan, H. Herr, *Medicine in Novel Technology and Devices*, Material, design, and fabrication of custom prosthetic liners for lower-extremity amputees, Elsevier, september 2023.
4. Hrushikesh Sayar, Jayant Karajagikar, Sojwal Deshmukh, Prosthetic limb arm for armless human, Department of Manufacturing Engineering and Industrial Management, COEP, Pune 411005, MS, India, September 2022.
5. J. T. Belter, J. L. Segil, A. M. Dollar, R. F. Weir, Mechanical design and performance specifications of anthropomorphic prosthetic hands, *J. Rehabil. Res. Develop. (JRRD)* (2020).
6. Smodin editorial team, What is grounding in artificial intelligence, Smodin, 2024 (in polish)

This paper is the result of a Project Based Learning (PBL) project entitled Development and 3D printing of a prosthetic hand model with software for a disabled person



31th January 2025
Gliwice, Poland

DEPARTMENT OF ENGINEERING MATERIALS AND BIOMATERIALS
FACULTY OF MECHANICAL ENGINEERING
SILESIA UNIVERSITY OF TECHNOLOGY

INTERNATIONAL STUDENTS SCIENTIFIC CONFERENCE

Characteristics of steel for automotive industry

Jakub Głabek^a, Magdalena Koźlik^a, Jan Parzyk^a, Łukasz Porwolik^a, Marek Wojtynek^a, Paweł Baranek^b, Gabriela Fojt-Dymara^c, Barbara Grzegorzczak^d

^a Students of the Silesian University of Technology, Faculty of Mechanical Engineering.

^b Student of the Nicolaus Copernicus School Complex No. 6 in Ruda Śląska

^c Silesian University of Technology, Faculty of Mechanical Engineering, Department of Engineering Processes Automation and Integrated Manufacturing Systems

^d Silesian University of Technology, Faculty of Mechanical Engineering, Department of Engineering and Biomedical Materials

email: barbara.grzegorzczak@polsl.pl

Abstract: The modern automotive industry faces numerous challenges related to the selection of materials that must be characterized by strength, lightness, affordability and environmental friendliness at the same time. Among the various materials used in car production, steel plays a particularly important role, which still dominates as a raw material used in the construction of car bodies, chassis and many other vehicle components. Increasingly high demands on fuel economy, safety and environmental protection mean that steel must meet increasingly stringent standards and specifications. This article presents the basic characteristics of selected steels used for car body construction elements.

Keywords: materials, steels, automotive industry, AHSS (Advanced High-Strength Steel), UHSS (Ultra High Strength Steel)

1. INTRODUCTION

Due to the requirements, two groups of high-strength multi-phase steels (AHSS - Advanced High-Strength Steel) were created. The first group consists of steels belonging to the first generation – low-alloy high-strength steels. They are characterized by favorable mechanical properties (tensile strength R_m up to 900 MPa, elongation A up to 25%), and their additional advantage is a relatively low production price. The second group consists of steels classified as second generation – high-alloy multi-phase steels. They combine high strength with exceptional plasticity (R_m up to 1000 MPa, A up to 50%), but their production is associated with high costs. This results from the need to use a significant amount of alloying elements, such as 20-30% manganese, 1-3% aluminum and 1-3% silicon, which limits their use on a large scale. Recently, a new, third generation of AHSS steel has been developed, the task of which is to fill the gap between the first two groups. This generation includes modern steels, such as martensitic steels QP with retained austenite and bainitic steels with the TRIP effect (Transformation Induced Plasticity). Among them, a new category has distinguished itself -

medium manganese steels, which have the potential to meet the strict requirements of the automotive industry, offering a favorable compromise between strength, ductility and production costs. Additionally, steels with improved corrosion resistance are being developed, such as steels coated with aluminum-zinc coatings, which extend the service life of vehicles and reduce the need for expensive maintenance. Thanks to innovations in processing technology, new steels help vehicle manufacturers achieve better results in terms of fuel efficiency and compliance with emission standards, while maintaining price competitiveness [1-4].

2. CHARACTERIZATION OF STEEL FOR CAR BODY CONSTRUCTION ELEMENTS

Materials used in the construction of car bodies must meet a number of criteria, such as:

- high mechanical strength – body elements must withstand high dynamic and static loads, protecting passengers during a collision.
- low weight – reducing the weight of the car translates into reduced fuel consumption and improved performance.
- corrosion resistance – steel must be durable in contact with moisture, road salt and atmospheric factors.
- plasticity and formability – easy forming of elements with complex shapes is required without losing strength.
- ability to absorb energy – steel must effectively absorb impact energy during a collision, minimizing its effects on passengers [5-7].

Modern cars are constructed from various types of steel (Fig. 1), appropriately selected for the individual construction elements of the car (Fig. 2).

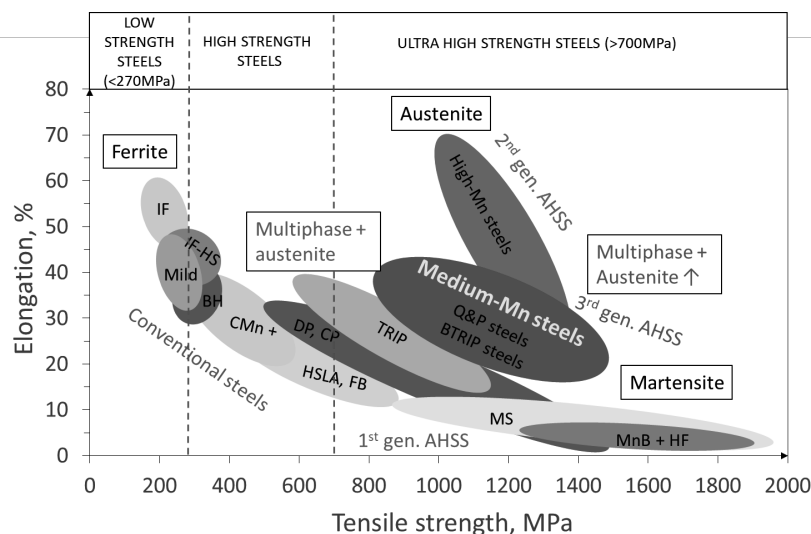


Fig.1. Classification of steels used in the automotive industry [8]

We can distinguish, among others:

MILD Steel – this is a steel containing a low percentage of carbon, usually less than 0.3% by weight. It is easy to twist and weld, but has a low tensile strength, usually less than 200 MPa. It

is one of the most commonly used structural steels, used in many areas, from the automotive industry to construction, suitable for structures not loaded with high stress. Due to its low carbon content, it is easy to process mechanically and thermally. According to [9], as recently as 2005, mild steel accounted for about 85% of the weight of a typical car body, with the rest being high-strength steel. As of 2015, typical car bodies were made of about 40% mild steel and over 50% high-strength steel [9-11].

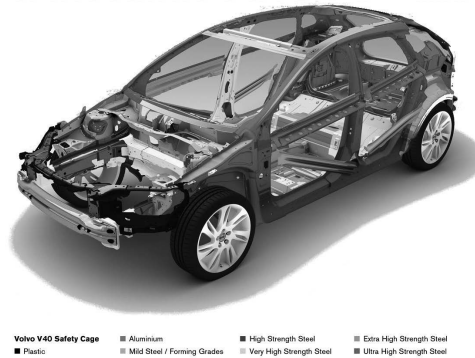


Fig. 2. The use of steel in the body construction of the Volvo V40 Safety Cage [12]

- **Strength Low-Alloy Steel (HSLA)** – it is a low-alloy steel with higher mechanical strength and good corrosion resistance while maintaining a relatively low content of alloying elements. Unlike conventional carbon steels, HSLA steels contain small amounts of alloying elements such as copper, vanadium, niobium, chromium or titanium. High tensile strength ranging from 300 MPa to 800 MPa makes HSLA steels the right choice for structures requiring high mechanical resistance. Some HSLA grades are additionally enriched with elements such as copper, which increases their resistance to atmospheric factors. In the automotive industry, these steels are used in body panels and other elements that require lightness and good resistance to dynamic loads, e.g. bumpers and reinforcement beams that protect passengers in the event of a collision [13,14].
- **Advanced High-Strength Steels (AHSS)** – they are advanced third-generation high-strength steels. They have been developed to achieve an even better balance between strength and plasticity. The AHSS steel group includes dual-phase steels DP (Dual Phase), DP-CP (Dual Phase - Complex Phase), steels with a martensitic structure (MS - Martensitic Steel), which enable the creation of thin-walled components that simultaneously maintain high resistance to deformation and impact. TRIP (Transformation Induced Plasticity), TWIP (Twinning Induced Plasticity) steels and TRIPLEX steels characterized by exceptional ductility, are also increasingly used, especially in places critical to safety (Fig. 3). AHSS steels are the basic material in elements such as body panels, door frames or structural reinforcements. They combine high bearing capacity with low mass, which allows for reducing the weight of the vehicle while maintaining the required stiffness and durability [15-17,18].
- **Ultra High Strength Steel, (UHSS)** - they are characterized by exceptionally high tensile strength from 800 to even 1800 MPa. This strength makes them an ideal material for use in the construction of modern vehicles, especially in elements that require maximum strength

and minimum weight. They are used in key places, such as A, B and C pillars or roof reinforcements. They are extremely resistant to deformation, thanks to which they effectively protect passengers in the event of a collision. They also allow for a reduction in the thickness of components, which has a positive effect on the weight of the car [11, 17,19]

- **Extra High Strength Steel (EHSS)** is a class of steel with very high mechanical strength, reaching R_m up to 2000 MPa, designed for applications requiring special durability, resistance to deformation and the ability to transfer extreme loads. Despite very high strength, some EHSS grades retain sufficient plasticity to be used in stamping and forming, but require special production technologies. EHSS is a development of high-strength steel technology (HSS and UHSS), offering even higher mechanical parameters while maintaining appropriate plasticity. In car bodies, EHSS steels are used for safety elements, e.g. bumper beams, A, B, C pillars, roof and crumple zones [11,20].

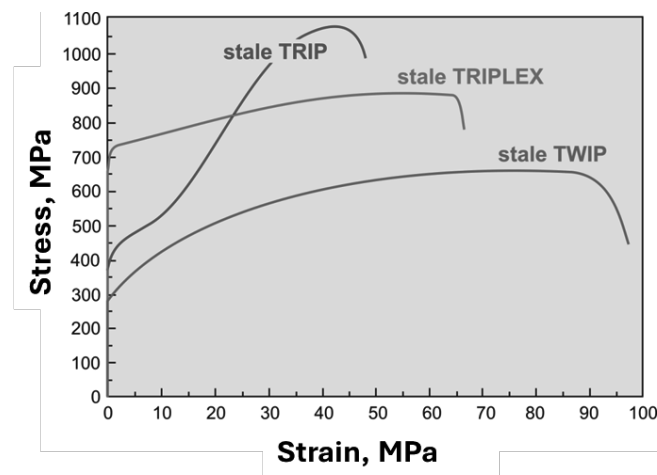
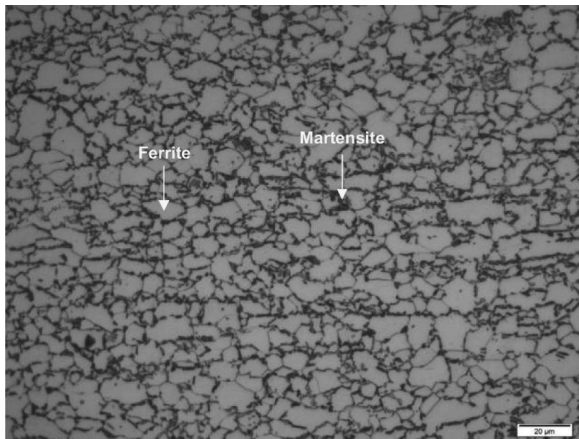


Fig. 3. Curves of strengthening of TRIP, TWIP and TRIPLEX steels [16]

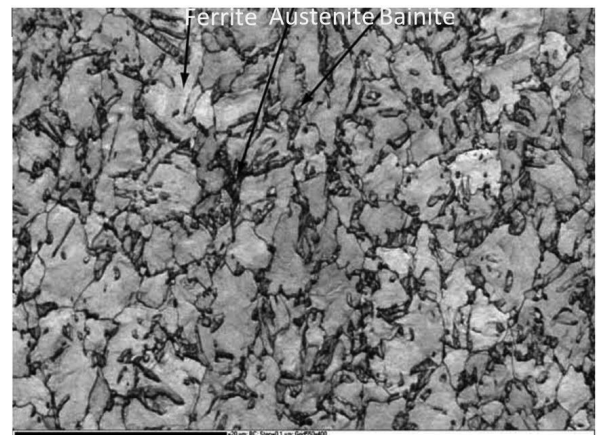
The properties of steel depend on the share of individual structural components, such as ferrite, pearlite, bainite, austenite and martensite, which affect its strength, hardness, plasticity and endurance limit and wearability to a varying degree. Ferrite gives steel good plasticity, but limits its strength. Pearlite provides higher strength and hardness, while maintaining relatively good plasticity. Bainite is an intermediate structure that combines good strength with a certain degree of plasticity. Austenite has a high deformability, which increases the plasticity of steel and allows the use of effects such as TRIP (transformation of austenite into martensite during deformation). Martensite is the hardest structural component, providing high strength, but at the cost of reduced plasticity. By controlling the proportions and arrangement of these components, it is possible to design steels with properties tailored to specific applications – from plasticity, easy-to-form body parts to ultra-strong bearing capacity structures or crumple zones that must absorb energy during a collision [2,10,15]. The microstructures of selected steels are shown in Fig 4.

a)



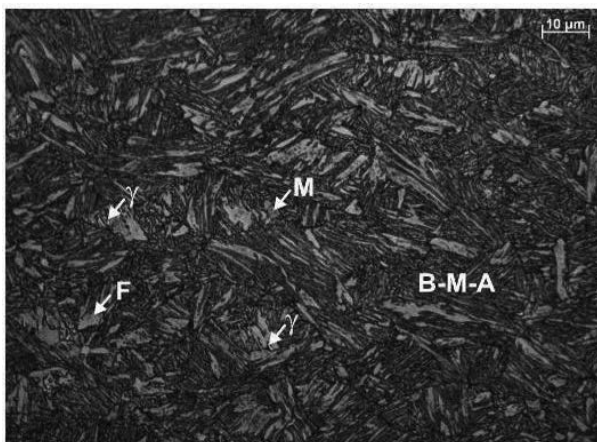
$1.3Mn0.12Si0.92Al0.14Mo$ [18]

b)



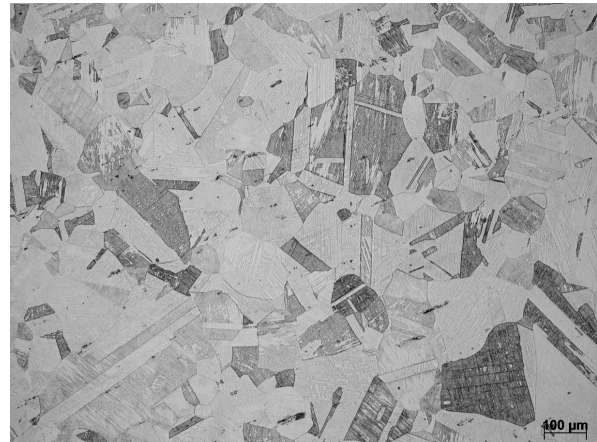
$1.75Mn1.6Si$ [4]

c)



$3Mn1.5Al0.Si$ [1]

d)



$24Mn3Si1.5AlNbTi$

Fig. 4 . Microstructure: a) DP steel, b) TRIP steel, c) Medium manganese steel, d) TWIP steel

3. MODERN TECHNOLOGIES AND DEVELOPMENT OF AUTOMOTIVE STEEL

The automotive industry is constantly developing new steel production technologies and steel processing processes. Increasingly lighter and stronger materials are being introduced, which simultaneously meet ecological and safety standards. New hot stamping technologies are being developed and optimized, which allow for the forming of elements with complex shapes and high strength. Nano-technological coatings are being applied to provide additional protective properties with reduced thickness of the protective layer. Increasingly often, steel composites are being used in cars, which combine traditional steel with other materials, such as plastics, ceramics or carbon fibers, in order to improve their mechanical properties, strength, rigidized or

fatigue resistance. Although steel itself is very versatile, adding reinforcing elements allows its use in modern, lightweight vehicle constructions. [2,3,5,21].

4. SUMMARY

Steel remains a fundamental material in the automotive industry, irreplaceable in many construction applications. However, dynamic market changes, technological development and growing ecological pressure require steel and car manufacturers to constantly adapt to new challenges. In addition, the automotive industry's transition to electric vehicles will place new requirements on steel. This material must meet specific needs, e.g. in the construction of battery housings or electric drive components. The future of the automotive market is advanced high-performance materials, including modern steels that combine durability, lightness and ecology in one. Steel is not only one of the strongest materials in the world, it is also the best automotive material in terms of design flexibility, cost-effectiveness, low emissions during production, recyclability, and affordable price. An important aspect is the design of the chemical composition of steel. Properly selected elements affect the final properties of the finished product. They improve plasticity, strength, and have an impact on the correct production process. The introduction of additives such as Si, Al, Ti can improve the hot ductility of steel, leading to the avoidance of cracks during the manufacturing process, e.g. the operation of straightening the ingot or rolling the sheets. The automotive industry pays attention to reducing the weight of the vehicle, which reduces fuel consumption and harmful exhaust emissions. Additionally, low-density steels are desirable to reduce the weight of the steel construction of the vehicle, due to the installation in modern cars of a large number of sensors, automatic systems and electronic systems, as well as high-class finishing materials - causing an increase in the weight of the final vehicle [2,3,21].

ACKNOWLEDGMENTS

The work was carried out as part of project-oriented education – PBL (Project-Based Learning) – 11th edition. The title: “Modern construction materials used in the automotive industry”.

BIBLIOGRAPHY

1. A. Grajcar, R. Kuziak, W. Zalecki, Third Generation of AHSS with Increased Fraction of Retained Austenite for the Automotive Industry, *Archives of Civil and Mechanical Engineering* 12 (3), (2012) 334–341.
2. C. Scott, S. Allain, M. Faral M, N. Guelton, The development of a new Fe-Mn-C austenitic steel for automotive applications, *Revue de Métallurgie*, 6 (2006) 293-302.
3. Collective work: ULSAB-AVC Body structure materials, TTS 4, 2001.
4. K. Choi, W.N. Liu, X. Sun, M.A. Khaleel, Microstructure-Based Constitutive Modeling of TRIP Steel: Prediction of Ductility and Failure Modes under Different Loading Conditions. *Acta Materialia*, 57 (8), (2009) 2592–2604.
5. F. Czerwinski, Current Trends in Automotive Lightweighting Strategies and Materials. *Materials* 14, 6631, 2021.

6. L. Samek, D. Krizan, Steel—Material of choice for automotive lightweight applications. In Proceedings of the International Conference Metal'2012, Brno, (2012) 1–6.
7. A. Candela, G. Sandrini, M. Gadola, D. Chindamo, P. Magri, Lightweighting in the Automotive Industry as a Measure for Energy Efficiency: Review of the Main Materials and Methods. *Heliyon*, 10 (8), 2024.
8. <https://www.worldautosteel.org>.
9. N. McGuire, Automotive industry lightens up, *Tribology & Lubrication Technology*, Nov. 73,11, (2017) 30-42.
10. R. Mendoza, J. Huante, M. Alanis, et.all, Processing of Ultra Low Carbon Steels with Mechanical Properties Adequate for Automotive Applications in the As-Annealed Condition. *Materials Science and Engineering: A*, 276, (2000)203–209.
11. A.M. Sherman, A. Krause, P. Friedman, Automotive Body Materials. In *Encyclopedia of Materials: Science and Technology*; Elsevier, (2001) 415–421.
12. <https://www.media.volvocars.com/>
13. C.I. Garcia, High Strength Low Alloyed (HSLA) steels, Elsevier, (2017) 145–167.
14. Q. Lu, Q. Lai, Z. Chai, et all, Revolutionizing Car Body Manufacturing Using a Unified Steel Metallurgy Concept. *Sci. Adv.* 2021,
15. O. Grässel, G. Frommeyer, Effect of martensitic phase transformation and deformation twinning on mechanical properties of Fe-Mn-Si-Al steels, *Material Science Technology*, 14, 12, (1998) 1213-1217.
16. M. Jabłońska, Structure and properties of austenitic high-manganese steel strengthened by mechanical twinning in dynamic deformation processes, Silesian University of Technology Publishing House, Gliwice 2016.
17. O. Grässel, L. Kruger, G. Frommeyer, L.W. Meyer, High strength Fe-Mn-(Al,Si) TRIP/TWIP steels development – properties – application, *International Journal of Plasticity*, 16, 2000.
18. I.A. Soomro, S. Pedapati, R. Awang, et all, Effects of Double Pulse Welding on Microstructure, Texture, and Fatigue Behavior of DP590 Steel Resistance Spot Weld. *Int J Adv Manuf Technol*, 125 (3–4), (2023) 1271–1287.
19. H. Ding, G. Zhu, C. Xiang, et all, Excellent combination of plasticity and ultra-high strength in a low-alloy automotive steel treated by conventional continuous annealing. *Materials Science and Engineering A* 791, 139694, 2020.
20. T. Liu, Z. Cao, H. Wang, et all, New 2.4 Gpa Extra-High Strength steel with good ductility and high toughness designed by synergistic strengthening of nano-particles and high-density dislocations. *Scripta Materialia*, 178, (2020) 285–289.
21. M.K. Banerje, Surface and heat treatment processes, *Comprehensive Materials Finishing*, 2017.



31th January 2025
Gliwice, Poland

DEPARTMENT OF ENGINEERING MATERIALS AND BIOMATERIALS
FACULTY OF MECHANICAL ENGINEERING
SILESIA UNIVERSITY OF TECHNOLOGY

INTERNATIONAL STUDENTS SCIENTIFIC CONFERENCE

Wytwarzanie laminatów stosowanych w personalnych osłonach balistycznych

Michał Głogowski^a, Julia Pindur^b, Karolina Romberg^b, Klaudiusz Gołombek^c, Piotr Sakiewicz^d

^a Politechnika Śląska, Wydział Automatyki, Elektroniki i Informatyki, Informatics
mg317553@student.polsl.pl

^b Politechnika Śląska, Wydział Mechaniczny Technologiczny, Inżynieria Produkcji
i Zarządzania

kr316746@student.polsl.pl

jp316730@student.polsl.pl

^c Politechnika Śląska, Wydział Mechaniczny Technologiczny, Laboratorium Badania
Materiałów

email: klaudiusz.golombek@polsl.pl

^d Politechnika Śląska, Katedra Materiałów Inżynierskich i Biomedycznych, Wydział
Mechaniczny Technologiczny

email: piotr.sakiewicz@polsl.pl

Streszczenie: W pracy przedstawiono wyniki badań oraz analizę własności wytrzymałościowych laminatów, które mogą pełnić funkcję personalnych osłon balistycznych. Laminaty te zostały wykonane z kompozytów opartych na papierze i żywicy oraz dodatkowo wzmocnione tkaniną „Poliamid 6”. W ramach badań przeanalizowano ich właściwości mechaniczne oraz zachowanie podczas prób użytkowych, co pozwoliło na ocenę ich potencjalnej skuteczności w zastosowaniach balistycznych.

Abstract: This study presents the results of tests carried out and an analysis of the strength parameters of laminates that act as a personal ballistic shields. These laminates were made of paper and resin-based composites and additionally reinforced with Polyamide 6 fabric. As part of the research, their mechanical properties and behaviour during use tests were analysed, allowing their potential effectiveness in ballistic applications to be assessed.

Słowa kluczowe: laminaty, osłony balistyczne

1. WSTĘP

W obecnym świecie środki ochrony osobistej są nieodzownym elementem wyposażenia żołnierzy, policjantów, innych służb mundurowych, czy też VIP-ów, bądź dziennikarzy znajdujących się поблизу działań wojennych. Najpowszechniej stosuje się kamizelki ochronne wyposażone w kieszenie na płytki z wkładów balistycznych. Aktualnie najbardziej popularne jest zastosowanie kieszeni w okolicy klatki piersiowej z przodu i tyłu, mających na celu ochronić

najwrażliwsze miejsca. Zastosowanie dodatkowego wkładu jako elementu opcjonalnego, umożliwia personalizację wyposażenia, ułatwia wymianę lub dostosowanie kamizelki do nowych wymagań. Na rynku dostępne wkłady balistyczne wytwarzane są z polimerów, ceramiki, metali czy kompozytów. Wielowarstwowe kompozyty-laminaty należą do grupy kompozytów powszechnie stosowanych na wkłady kamizelek kuloodpornych. Tworzenie laminatu odbywa się za pomocą tworzenia warstw składających się z: składnika wzmacniającego, zwanego zbrojeniem oraz wypełnienia, który układa się pomiędzy warstwy. Wypełnienie tworzy formę lepiscza. Warstwy wzmocnienia występują w postaci włókien ciągłych, które ułożone są w jednym kierunku, tkanin albo mat z włókna ciętego [1-8].

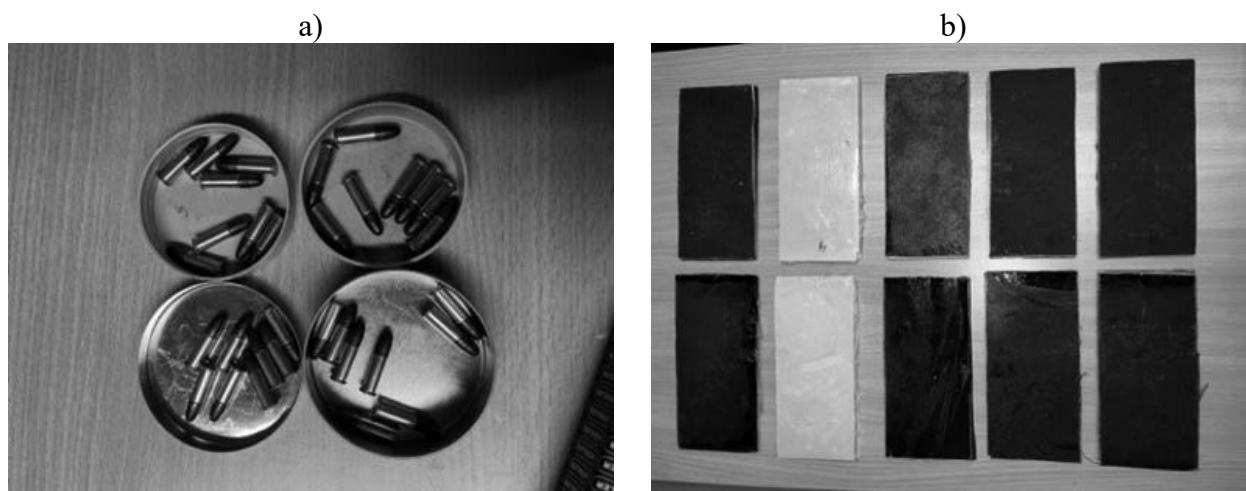
Główne prace badawcze polegały na: doborze żywicy epoksydowej jako osnowy laminatu do wytworzenia wkładów balistycznych; doborze sposobu ułożenia tkanin oraz ilości warstw przy założeniu, że sumaryczna grubość wszystkich warstw nie powinna przekroczyć 10 mm; wytworzeniu laminatów opartych na żywicy epoksydowej i tkaniny poliamidowej; badaniu struktury i wybranych własności np. odporności na udarowe przebicie.

Celem badań jest opracowanie i wytworzenie wielowarstwowych kompozytów-laminatów opartych na osnowie żywicy epoksydowych wzmacnianych tkaniną poliamidową oraz wypełnianych dodatkowo papierem celulozowym.

2. MATERIAŁ I METODYKA BADAŃ

2.1 Materiał i metodyka badań

Do wytworzenia laminatów wykorzystano warstwy papieru i poliamidu, które nasączono żywicą epoksydową, a następnie poddano procesowi utwardzania. Gotowe próbki zostały poddane testom balistycznym, podczas których oceniano ich odporność na działanie pocisków (rys.1). Struktura laminatów została przeanalizowana za pomocą mikroskopii skaningowej i świetlnej, co umożliwiło ocenę rozkładu makro- i mikrouszkodzeń w badanych materiałach.



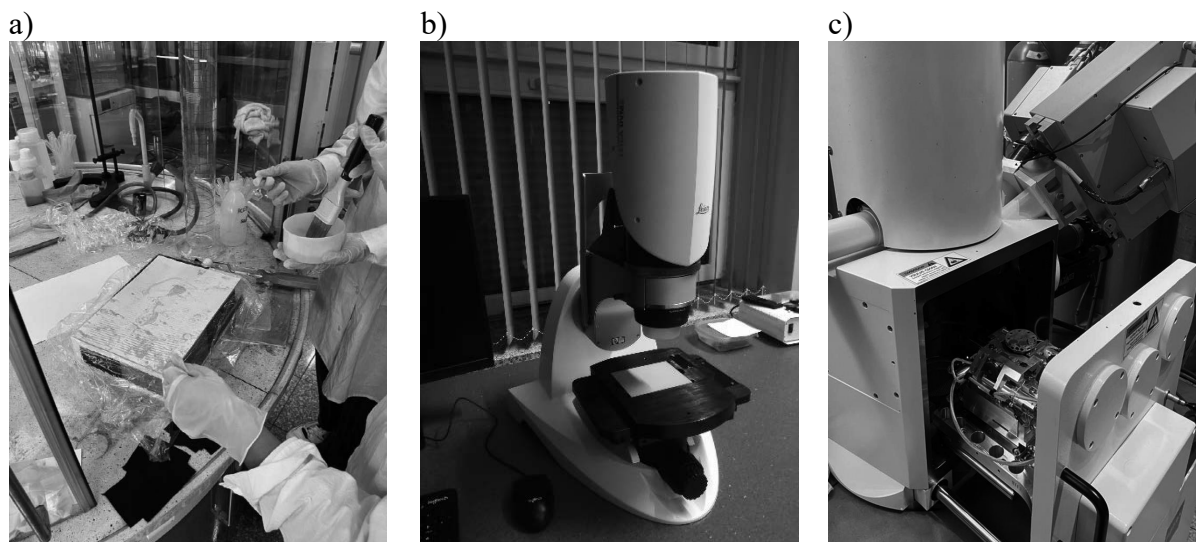
Rysunek 1. Materiały: a) naboje wykorzystane do próby wytrzymałościowej; b) wielowarstwowe kompozyty-laminaty;

Figure 1. Materials: a) bullets used for the endurance test; b) multi-layer composite-laminates;

W pierwszym etapie prac przygotowano składniki do wytworzenia laminatów. Żywicę epoksydową zmieszano z utwardzaczem. Następnie odważono odpowiednie proporcje żywicy oraz wzmocnienia (papier i/lub tkanina poliamidowa „Poliamid 6”) przy użyciu precyzyjnej wagi laboratoryjnej firmy Radwag. Wzmocnienie w postaci papieru zostało odpowiednio ułożone warstwami, natomiast tkaninę przycięto do odpowiednich wymiarów. Tak przygotowane materiały wzmocnienia zostały stopniowo nasączone przygotowaną żywicą, a następnie ułożone w formie warstwowej, z zachowaniem założonej grubości całkowitej, nieprzekraczającej 10 mm. Wszystkie elementy zostały skompresowane w celu usunięcia nadmiaru żywicy oraz uzyskania jednorodnej struktury laminatu. W ramach pracy przeprowadzono następujące badania:

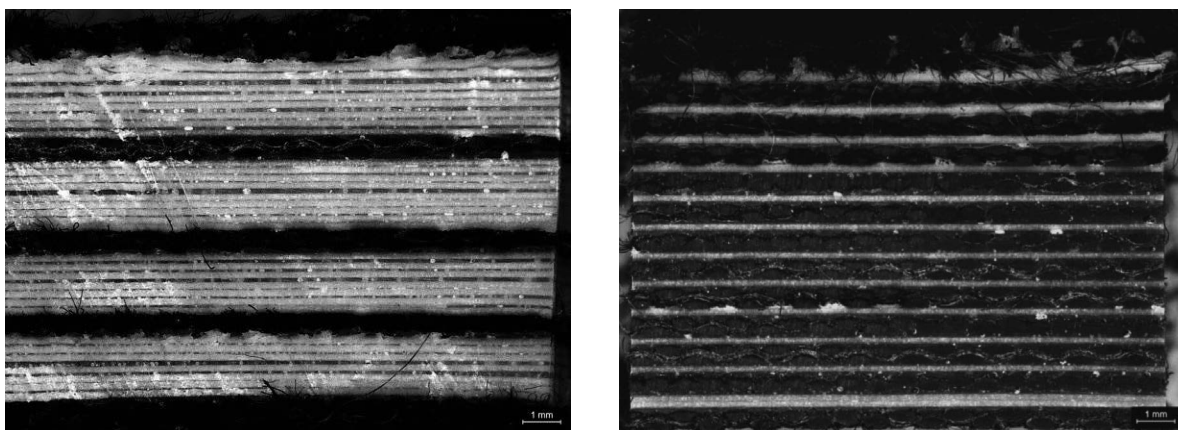
- dobrano żywicę epoksydową jako osnowę laminatów, uwzględniając jej właściwości mechaniczne i przydatność w zastosowaniach balistycznych,
- określono optymalny sposób układania warstw tkaniny „Poliamid 6” oraz dobrano odpowiednią ilość warstw, przy założeniu, że całkowita grubość laminatu nie przekracza 10 mm,
- wytworzono laminaty z zastosowaniem żywicy epoksydowej jako lepiszcza, papieru jako wypełnienia oraz tkaniny „Poliamid 6” jako elementu wzmacniającego,
- przeprowadzono badania struktury laminatów z wykorzystaniem mikroskopu świetlnego i skaningowego mikroskopu elektronowego,
- zbadano podstawowe właściwości mechaniczne, takie jak odporność na przebicie udarowe oraz inne parametry wytrzymałościowe, porównując laminaty wykonane z papieru i laminaty wzmacniane tkaniną „Poliamid 6”.

W celu porównania własności użytkowych wykonano serię pomiarów dla każdego typu próbek, zarówno dla papieru, jak i kompozytów wzmacnianych tkaniną. Obserwację struktury przeprowadzono za pomocą stereoskopowego mikroskopu świetlnego Leica DVM6 A oraz skaningowego mikroskopu elektronowego ZEISS SUPRA 35 (rys. 2) oraz wykonano analizę składu chemicznego z wykorzystaniem detektora EDS. Przykładowe przekroje wytworzonych laminatów przedstawiono na rysunku 3.



Rysunek 2. a) przygotowanie laminatów, b) stereoskopowy mikroskop świetlny Leica, c) skaningowy mikroskop elektronowy

Figure 2. a) preparation of laminates, b) Leica stereo light microscope, c) scanning electron microscope



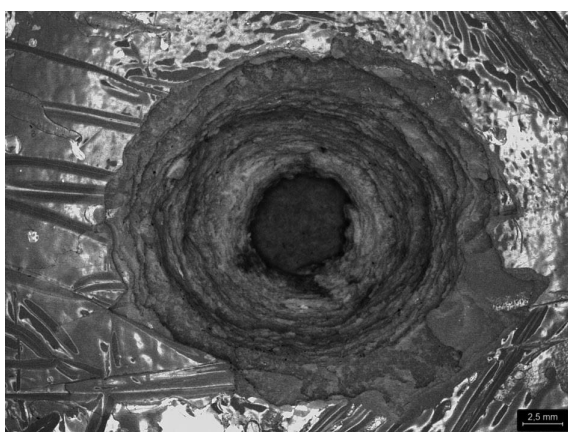
Rysunek 3. Przykładowe przekroje wytworzonych laminatów złożone z papieru oraz żywicy
Figure 3. Examples of cross-sections of laminates made of paper and resin

3. WYNIKI BADAŃ

Przeprowadzone badania wykazały, że laminaty charakteryzują się wysoką odpornością na przebite udarowe i efektywnie zatrzymują pociski o małej i średniej energii kinetycznej. Wielowarstwowa struktura, wzmocniona tkaniną „Poliamid 6”, zapewniła skuteczne rozpraszanie energii pocisku w całej objętości laminatu.

Analiza mikroskopowa wykazała charakterystyczne uszkodzenia w postaci mikropęknięć oraz deformacji lokalnych, co potwierdza mechanizm pochłaniania energii przez poszczególne warstwy kompozytu. Zastosowanie tkaniny poliamidowej, jako warstwy wzmocniającej, znacząco zwiększyło wytrzymałość laminatów w porównaniu do kompozytów opartych jedynie na papierze i żywicy (rys. 4-6).

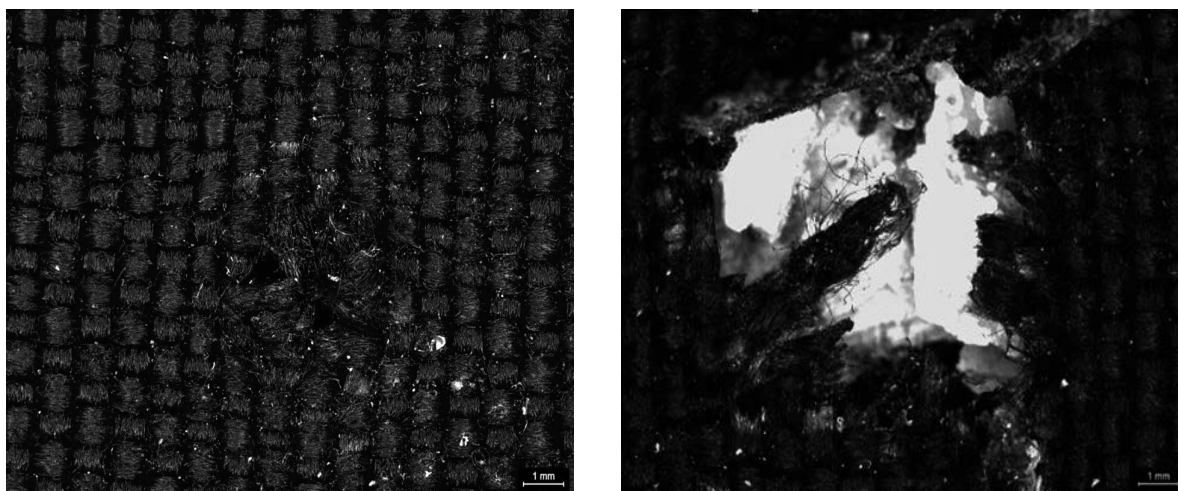
Optymalizacja układu warstw pozwoliła na zmniejszenie masy laminatu bez utraty jego właściwości ochronnych, co czyni go bardziej praktycznym rozwiązaniem w zastosowaniach balistycznych (rys. 7).



Rysunek 4. Prześlona na wylot osłona złożona z papieru oraz żywicy
Figure 4. Shot through cover composed of sheets of paper and resin

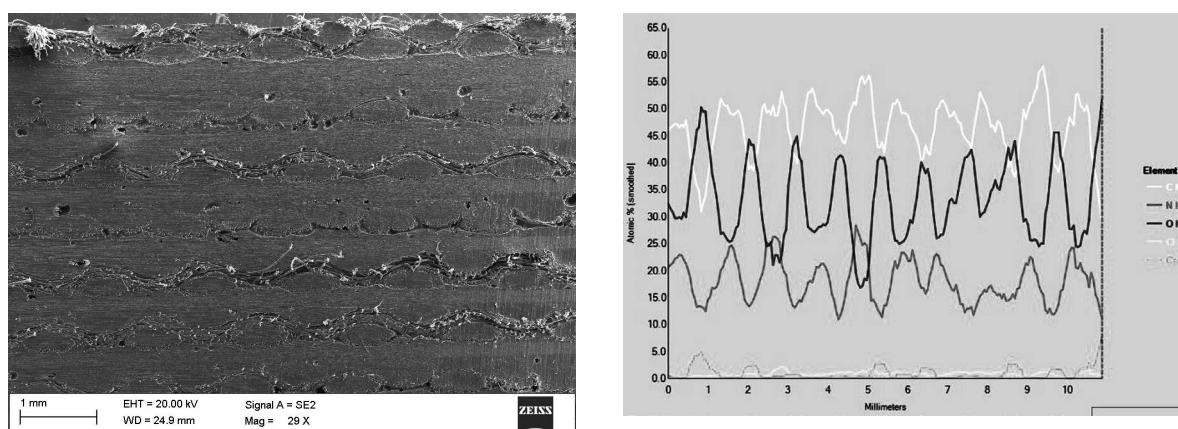


Rysunek 5. Odkształcony nabój
Figure 5. Deformed bullet



Rysunek 6. Uszkodzenie osłony złożonej z kartek papieru, poliamidu oraz żywicy – schemat ułożenia warstw: 1 papier / 1 tkanina

Figure 6. Damaged sheath composed of sheets of paper, polyamide and resin - layering scheme: 1 paper / 1 fabric



Rysunek 7. Struktura laminatu oraz analiza liniowa zmian składu chemicznego osłony złożonej z kartek papieru, poliamidu oraz żywicy – schemat ułożenie warstw 1 kartka papieru / 1 tkanina poliamidowa

Figure 7. Laminate structure and linear analysis of chemical composition changes of a sheath composed of sheets of paper, polyamide and resin - layering scheme 1 sheet of paper / 1 polyamide fabric

4. WNIOSKI

W ramach badań określono różnicę parametrów wytrzymałościowych laminatów – personalnych osłon balistycznych – wytworzonych z papieru i żywicy oraz wzmocnionych tkaniną „Poliamid 6” podczas prób własności użytkowych. Na podstawie badań stwierdzono, że osłony modyfikowane warstwami tkaniny wykazują znacznie większą odporność na pociski w porównaniu do osłony z papieru. Dla porównania: do zatrzymania pocisku widocznego na

zdjęciu 4, przebywającego drogę 20 metrów potrzebne jest 90 kartek papieru 80g/m², w przypadku zastosowania osłony jest potrzebne o połowę mniej. Wytwarzanie osłon balistycznych przy użyciu zaproponowanych materiałów jest możliwe i korzystne, ze względu na niską cenę, niewielką masę oraz powszechność wykorzystywanych surowców.

LITERATURA

1. PN-V-87000:2011, Osłony balistyczne lekkie. Kamizelki kulo- i odłamkoodporne. Wymagania ogólne i badania.
2. National Institute of Standards and Technology, Ballistic Resistance of Body Armor, NIJ Standard-0101.06, National Institute of Justice, 2008.
3. NATO - STANAG 2920 - Classification of personal armour, Ed.2, 2003.
4. M. Madej, D. Ozimina, A. Wdowin, Tworzywa sztuczne i materiały kompozytowe, Politechnika Świętokrzyska, Kielce, 2010.
5. W. Królikowski, Polimerowe kompozyty konstrukcyjne, Wydawnictwo Naukowe PWN, Warszawa, 2012.
6. J.E. Seppala, Y. Heo, P.E. Stutzman, J.R. Sieber, C.R. Snyder, K.D. Rice, G.A. Holmes, Characterization of clay composite ballistic witness materials, *Journal of Materials Science*, 50(21), 2015, 7048–7057, <https://doi.org/10.1007/s10853-015-9259-7>
7. A. Engelbrecht-Wiggans, F. Burni, A. Krishnamurthy, A.L. Forster, Tensile testing of aged flexible unidirectional composite laminates for body armor, *Journal of Materials Science*, 55(3), 2020, 1035–1048, <https://doi.org/10.1007/s10853-019-04063-w>
8. R. Tao, F. Zhang, H.G. Nguyen et al., Temperature-insensitive silicone composites as ballistic witness materials: the impact of water content on the thermophysical properties *Journal of Materials Science*, 56, 2021, 16362–16375, <https://doi.org/10.1007/s10853-021-06334-x>

PODZIĘKOWANIA

Badania wykonano w ramach III edycji projektów badawczych zorientowanych projektowo – PBL (Project Base Learning), realizowanych na Politechnice Śląskiej z uczniami szkół ponadpodstawowych w programie Inicjatywa Doskonałości – Uczelnia Badawcza.



31th January 2025
Gliwice, Poland

DEPARTMENT OF ENGINEERING MATERIALS AND BIOMATERIALS
FACULTY OF MECHANICAL ENGINEERING
SILESIA UNIVERSITY OF TECHNOLOGY

INTERNATIONAL STUDENTS SCIENTIFIC CONFERENCE

Galwaniczne nakładanie powłok ochronnych

Wojciech Golec^a, Jakub Zorychta^b, Amelia Krupińska^c, Agnieszka Zaleska^d, Santina Topolska^e

^a Politechnika Śląska, Wydział Elektryczny, Inżynieria Ogólna
email: wg285400@student.polsl.pl

^b Politechnika Śląska, Wydział Mechaniczny Technologiczny, Mechanika i Budowa Maszyn

^c Zespół Szkół Chemiczno-Medycznych i Ogólnokształcących w Tarnowskich Górach

^d I Liceum Ogólnokształcące im. Stefanii Sempołowskiej w Tarnowskich Górach

^e Politechnika Śląska, Wydział Mechaniczny Technologiczny, Katedra Spawalnictwa

Streszczenie: W pracy zastosowano modyfikację powierzchni profili stalowych poprzez nakładanie cienkich powłok Cu w procesie galwanizacji. Badania wykonano na profilach ze stali konstrukcyjnej S235, które poddano miedziowaniu galwanicznemu w kąpeli siarczanowej, w celu analizy wpływu przygotowania powierzchni oraz warunków procesu na jakość powłok metalicznych. Przeanalizowano wpływ sposobu przygotowania powierzchni uwzględniającego szlifowanie, odtłuszczenie i trawienie, a także parametrów procesu między innymi jego czasu trwania i gęstości prądu, na jakość powłok miedzianych. Przedstawiono także charakterystykę najczęściej stosowanych powłok galwanicznych, wraz z ich zastosowaniami. Wyniki badań wykazały, że jakość powłok zależy od parametrów takich jak chropowatość powierzchni, temperatura odtłuszczenia i trawienia, a także warunków prądowych galwanizacji. Optymalne właściwości adhezyjne uzyskano dla próbek o umiarkowanej chropowatości poddanych procesowi galwanizacji przy wyższych temperaturach kąpeli przygotowawczych.

Abstract: In the study, the surface of steel profiles was modified by applying thin Cu coatings in the galvanization process. Electroplating is an electrochemical process that modifies material properties by applying thin metallic coatings to enhance their properties. The study was conducted on S235 structural steel profiles subjected to copper electroplating in a copper sulfate bath to analyze the impact of surface preparation as well as process conditions on the quality of obtained metallic coatings. The influence of surface preparation methods, including grinding, degreasing, and etching, together with process parameters such as its duration and current density, on the quality of copper coatings was examined. Additionally, the study presented the characteristics of commonly used electroplated coatings along with their applications. The results showed that the quality of the coatings depends on parameters like the surface roughness, degreasing and etching temperature, and electrical conditions. Optimal adhesion properties were achieved for samples with moderate roughness, subjected to electroplating at higher preparatory bath temperatures.

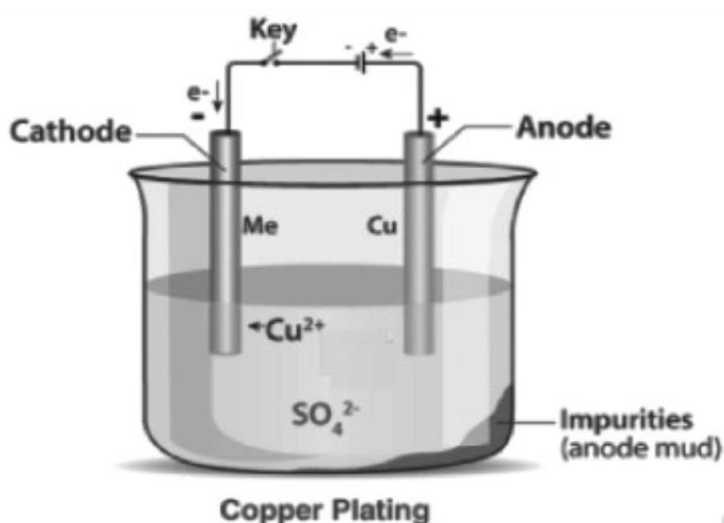
Słowa kluczowe: galwanizacja, miedziowanie, stal S235

1. WSTĘP

Galwanizacja jest wszechstronnym procesem, który umożliwia modyfikację właściwości powierzchni materiałów, odpowiadając na rosnące wymagania współczesnego przemysłu. Głównym celem powlekania elektrolitycznego jest ochrona metali przed korozją oraz poprawa ich odporności na uszkodzenia mechaniczne, a także działanie czynników zewnętrznych [1]. Podstawą tego procesu jest osadzanie cienkiej warstwy metalu na powierzchni innego materiału przy wykorzystaniu prądu stałego oraz elektrolitu. Dzięki zdolności do poprawy przewodności cieplnej i elektrycznej galwanizacja znajduje szerokie zastosowanie w branży elektrotechnicznej [2,3]. Możliwość dostosowania parametrów procesu w tym dokładna grubość powłoki, jej struktura i stan wykończenia powierzchni, a zarazem minimalne obciążenie termiczne obrabianych elementów sprawiają, że proces ten jest powszechnie stosowany [4]. Dodatkowo proces ten charakteryzuje się wysoką skutecznością oraz możliwością odzysku surowców, co obniża koszty [3,4].

1.1. Galwanizacja

Galwanizacja to proces polegający na elektrochemicznym pokrywaniu powierzchni materiału, zazwyczaj metalowego, cienką warstwą metalu. Proces ten zachodzi w roztworze elektrolitycznym, w którym zanurzone elektrody poddawane są działaniu prądu stałego. W efekcie powstaje różnica potencjałów między katodą a anodą, co prowadzi do przemieszczania się jonów metalu zawartych w elektrolicie oraz ich osadzania na powierzchni galwanizowanego elementu [1,2].



Rys. 1. Schemat procesu galwanizacji [3]
Fig. 1. Electroplating process diagram [3]

1.2. Parametry procesu galwanizacji

W procesie galwanicznego nakładania powłok ochronnych kluczową rolę odgrywają parametry, które bezpośrednio wpływają na strukturę oraz właściwości otrzymywanych powłok. Do czynników tych zalicza się: gęstość prądu, temperatura procesu, intensywność mieszania, stężenie elektrolitu oraz zastosowanie substancji powierzchniowo czynnych na efektywność galwanizacji.

Gęstość prądu to stosunek całkowitego natężenia prądu do całkowitej powierzchni. Mała gęstość prądu powoduje, że wyładowanie jonów przechodzi wolno. Istniejące już zarodki rosną szybciej niż powstają nowe, przez to powłoka będzie grubokrystaliczna. Wraz z zwiększaniem gęstości prądu powłoka będzie coraz bardziej drobnoziarnista [3]. Jednak przy bardzo dużych gęstościach prądu może dojść do powstania narostów, inaczej dendrytów. Nie mniej istotnym czynnikiem, obok gęstości prądu, jest jego charakter – może być stały lub pulsacyjny, co wpływa na przebieg procesu. Stosując określone pulsacje można uzyskać mniejsze porowatości nakładanych w ten sposób powłok [1,3].

Poza gęstością prądu, istotnym parametrem kształtującym strukturę oraz jakość powłok galwanicznych jest również temperatura kąpieli. Wzrost temperatury kąpieli może mieć korzystny lub niekorzystny wpływ na strukturę powłoki. Sprzyja on dyfuzji, co zapobiega powstawaniu struktury gruboziarnistej lub powłok gąbczastych przy dużych gęstościach prądu. Dodatkowo wyższa temperatura powoduje spadek nad napięcia wodoru, co ułatwia wydzielenie wodoru gazowego. To z kolei zmniejsza kwasowość roztworu i prowadzi do powstawania soli zasadowych. W umiarkowanych temperaturach przewyższa korzystny wpływ dyfuzji, natomiast w wyższych temperaturach jakość powłok ulega pogorszeniu [1,3].

Parametry takie jak mieszanie i stężenie elektrolitu w znacznej mierze się uzupełniają - zwiększając stężenie elektrolitu lub wprowadzając jego mieszanie, można stosować wyższe gęstości prądu bez ryzyka tworzenia struktury grubokrystalicznej lub wydzielania wodoru. Stosując kąpiele o wyższym stężeniu oraz równomiernemu mieszanii, uzyskiwane powłoki charakteryzują się większą zwartą strukturą. Ponadto większa przewodność kąpieli skutkuje spadkiem napięcia w układzie oraz poprawia zdolność kąpieli do równomiernego pokrywania powierzchni.

Elektrolit wywiera istotny wpływ na charakter powłoki, determinuje również jej jakość oraz charakter osadzonej warstwy. Dostarcza on jony metalu, które następnie zostaną osadzone na powierzchni katody. Do jego kluczowych parametrów należą pH, przewodność i czystość. Zanieczyszczenia mogą powodować różne defekty, a źle dobrane pH - wytrącanie się wodorotlenków metali [1,2].

Oprócz podstawowych parametrów elektrolitu, istotny wpływ na proces galwanizacji mają także dodatki modyfikujące jego właściwości fizykochemiczne w tym substancje powierzchniowo czynne. Substancje te obniżają napięcie powierzchniowe, co ułatwia odrywanie pęcherzyków wodoru od powierzchni katody, dzięki czemu zmniejsza się ryzyko powstawania wad takich jak pitting. Działanie podanych substancji opiera się na ich adsorpcji na zarodkach kryształów, co hamuje dalszy wzrost tych kryształów. W konsekwencji wyładowujące się jony zmuszone są do tworzenia nowych zarodków, co sprzyja powstawaniu drobnokrystalicznych powłok. Brak tych substancji w identycznych warunkach elektrolizy powoduje powstawanie powłok o strukturze grubokrystalicznej. Niemniej jednak zbyt wysokie stężenie tych dodatków może prowadzić do powstania powłok kruchych oraz słabo przyczepnych do podłoża [1].

1.3. Rodzaje powłok galwanicznych

Powłoki galwaniczne, w zależności od rodzaju użytego metalu i technologii nakładania, mogą pełnić funkcje ochronne, dekoracyjne lub techniczne. Wybór powłoki zależy od oczekiwanych cech końcowego produktu, takich jak odporność na korozję, przewodność elektryczna czy wytrzymałość mechaniczna. Najczęściej stosowane rodzaje powłok galwanicznych-stosowane w przemyśle to chromowanie, cynkowanie, niklowanie, srebrzenie, miedziowanie i złocenie.

Chromowanie jest procesem elektrochemicznym, w którym na powierzchniach metalowych osadzana jest warstwa chromu w celu poprawy ich twardości, odporności na korozję i ścieranie oraz nadaniu im estetycznego wyglądu. Najczęściej stosowanymi rodzajami kąpiele do chromowania są kąpiele siarczanowe, fluorokrzemianowe, czterochromianowe oraz wodne roztwory kwasu chromowego [2].

Cynkowanie galwaniczne polega na elektrochemicznym pokrywaniu powierzchni metalowych cienką warstwą cynku. Wytwarzanie powłok cynkowych odbywa się w roztworach zawierających sole cynku o różnych odczynach - kwaśnych, obojętnych lub alkalicznych. Proces ten znacząco wydłuża żywotność metalowych konstrukcji i komponentów, które są narażone na działanie wilgoci i innych czynników atmosferycznych, dzięki czemu znajduje zastosowanie w przemyśle, zwłaszcza w budownictwie oraz motoryzacji [2,4].

Niklowanie polega na nanoszeniu warstwy niklu na powierzchnię metali lub tworzyw sztucznych, gdzie wykorzystuje się między innymi kąpiele typu Watta, fluoroboranowe, czy amidosulfonianowe. W zależności od przeznaczenia, niklowanie może być stosowane jako warstwa ochronna, dekoracyjna, a także jako podkład pod inne powłoki z chromu lub złota. W przypadku stali często stosuje się miedziowanie jako warstwę pośrednią, która poprawia przyczepność niklu do podłoża. Niklowanie jest mniej kosztowne od chromowania, ale charakteryzuje się mniejszą trwałością i odpornością na korozję, co ogranicza jego zastosowania [1,3,4].

Srebrzenie, czyli pokrywanie metali powłokami srebrnymi w wyniku procesów elektrochemicznych. Mają one szerokie zastosowanie jako powłoki dekoracyjno-ochronne, głównie dla wyrobów jubilerskich oraz nakryć stołowych, a także jako powłoki ochronne i techniczne w elektronice. Powstała warstwa srebra charakteryzuje się doskonałym przewodnictwem elektrycznym oraz odpornością na korozję, choć ze względu na niewielką grubość jest podatna na ścieranie. Proces srebrzenia jest stosunkowo kosztowny, co ogranicza jego zastosowanie do produktów wymagających najwyższej jakości [5].

Złocenie galwaniczne to skuteczny sposób na uzyskanie estetycznych i funkcjonalnych złotych powłok. Cienkie powłoki (do 1 μm) nakładane na podwarstwie błyszczącego niklu wykorzystywane są w celach ozdobnych w jubilerstwie i zegarmistrzostwie. Z kolei grubsze powłoki stosuje się w aparaturze laboratoryjnej i elektronice, dzięki doskonałym własnościom przewodzącym. Powłoki złote osadzane są w oparciu o kąpiele o odczynie zasadowym, obojętnym oraz słabo kwaśnym, wykorzystując zespolone związki cyjankowe złota lub czyste złoto [1-4].

Miedziowanie to proces galwaniczny polegający na osadzaniu warstwy miedzi na elementach metalowych lub wykonanych z materiałów przewodzących prąd elektryczny. Technologia miedziowania opiera się na wykorzystywaniu kąpiele siarczanowych oraz cyjankowych. Elektrolityczne powłoki miedziane wykorzystywane są w celu poprawy przewodności elektrycznej, zabezpieczeniu przed korozją, ochrony przed nawęglaniem i azotowaniem lub jako część wielowarstwowych powłok [6].

1.4. Przygotowanie powierzchni do procesu galwanizacji

Przed galwanizacją należy poddać obrabiany element odpowiednim procesom służącym nadaniu powierzchni odpowiedniej chropowatości, oczyszczeniu i jej aktywacji, aby zapewnić wymaganą przyczepność i estetykę powłoki [7].

Pierwszym etapem przygotowania elementu do procesu galwanizacji jest obróbka mechaniczna. Celem tego etapu jest usunięcie większych nierówności, pozostałości korozji oraz

innych powłok, które mogłyby negatywnie wpłynąć na przyczepność i jednorodność warstwy galwanicznej. Do obróbki mechanicznej zalicza się takie procesy obróbki ubytkowej jak piaskowanie, szlifowanie oraz polerowanie [1].

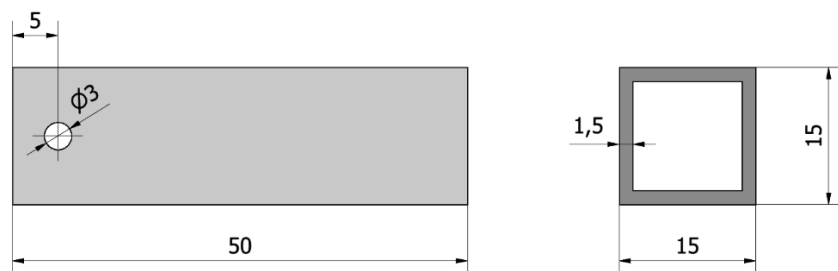
Niezbędnym działaniem po każdym etapie przygotowawczym jest płukanie elementu w wodzie i jego suszenie przy pomocy sprężonego powietrza. Zapobiega to zarówno przenoszeniu się zanieczyszczeń, jak i mieszanii się roztworów następnymi kąpielami, co przedłuża ich efektywność [8].

Kolejnym etapem jest odtłuszczenie, którego celem jest usunięcie z powierzchni tłuszczów, smarów oraz innych substancji mogących osłabić przyczepność powłoki galwanicznej. Do tych procesów należy odtłuszczenie chemiczne oraz elektrochemiczne. Proces odtłuszczenia chemicznego polega na zanurzeniu elementu w odpowiednim rozpuszczalniku, często podgrzanym w celu zwiększenia skuteczności działania. W przypadku odtłuszczenia elektrochemicznego mogą być stosowane te same związki, ale dodatkowo element pełni rolę elektrody (anody lub katody), co wspomaga proces usuwania zanieczyszczeń [4].

Trawienie ma na celu usunięcie mikrozanieczyszczeń, takich jak tlenki metali czy zgorzelina. Proces ten znacząco poprawia przyczepność i jednorodność osadzonej warstwy galwanicznej. Trawienie chemiczne realizowane jest przy użyciu roztworów kwasów między innymi kwasu siarkowego lub azotowego. Dodatkowo w przypadku trawienia aktywacyjnego, stosuje się specjalne kąpiele chemiczne, które oczyszczają powierzchnię, a także zwiększają jej aktywność, co sprzyja lepszemu przyleganiu powłoki [4,9].

2. MATERIAŁ I METODYKA BADAWCZA

Badania zostały wykonane na profilach stalowych, których wymiary podano na rys. 2, wykonanych ze stali konstrukcyjnej S235, zgodnej z normą EN 10025, której skład chemiczny podano w tabeli 1. Przygotowanie próbek do procesu elektrochemicznego obejmowało obróbkę mechaniczną powierzchni, odtłuszczenie i trawienie. Pomiedzy każdym etapem obróbki przygotowawczej próbki płukano w wodzie i suszono. Proces miedziowania galwanicznego przeprowadzano w kąpeli z siarczanem miedzi o temperaturze pokojowej (rys.3). Określono wpływ warunków prądowych oraz czasu galwanizacji na wyniki badań.



Rys. 2. Wymiary próbek
Fig. 2. Sample dimensions

Tabela 1. Skład chemiczny stali S235, %wag. (EN 10025)

Table 1. Chemical composition of S235 steel in wt% (EN 10025)

Fe	C	Mn	P	S	N
reszta	<0,17	<1,4	<0,045	<0,045	<0,012

Proces szlifowania wykonano z użyciem papierów ściernych o stopniowo zmieniającej się ziarnistości, począwszy od 800, przez 1200, 1500, 2000, aż do 2500, przy użyciu ręcznej szlifierko-polerki. Próbki oznaczone numerami 1, 2, 3 oraz 5 zostały wyszlifowane papierem ściernym o ziarnistości 1200, próbka nr 4 – papierem o ziarnistości 800, natomiast próbki 6 i 7 – papierem o ziarnistości 2500. Po zakończeniu procesu szlifowania wszystkie próbki wypolerowano, w celu uzyskania gładkiej powierzchni. Z kolei próbki oznaczone numerami od 8 do 10 zostały oszlifowane ręcznie za pomocą papieru ściernego o gradacji wynoszącej 220. Po zakończeniu szlifowania próbki poddano kąpeli odtłuszczającej w 5% roztworze wodorotlenku sodu, a następnie przeprowadzono proces trawienia w 10% roztworze kwasu solnego. W przypadku próbek 1 i 2 kąpiele odtłuszczające i trawiące przeprowadzono w temperaturze 20°C, natomiast dla próbek od 3 do 10 roztwory zostały podgrzane do 60°C.

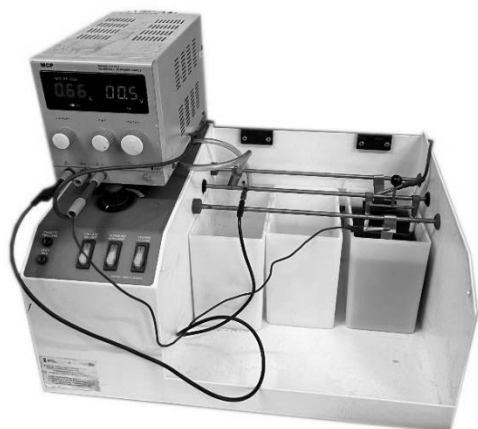
Celem badań było porównanie wpływu temperatury kąpeli na jakość uzyskanej powłoki. Stąd proces galwanicznego miedziowania wykonano w kąpeli kwaśnej produkcyjnej zawierającej między innymi roztwór siarczanu miedzi(II). Miedziowanie przeprowadzono przy różnych natężeniach prądu, mieszczących się w zakresie od 0,6 do 2,5 A oraz różnym czasie zanurzenia w kąpeli elektrolitycznej, co przedstawiono w tabeli 2.

Próbki zostały zbadane pod względem grubości warstwy. Do pomiaru parametrów powłoki użyte zostały: miernik grubości powłok Defelsko PosiTector 6000 F90S (rys. 4).

Tabela 2. Parametry procesu galwanizacji

Table 2. Parameters of the electrochemical copper plating process

Nr próbki	Natężenie prądu [A]	Czas galwanizacji [min]
1	2,5	1
2	1	1
3	1	1
4	1	0,5
5	1	1,5
6	0,6	1,5
7	0,6	2,5
8	0,6	2,5
9	0,6	4
10	1	1



Rys. 3. Stanowisko do galwanizacji
Fig. 3. *Electroplating station*



Rys. 4. Miernik Defelsko PosiTector 6000 F90S
Fig. 4. *Defelsko PosiTector 6000 F90S gauge*

3. WYNIKI BADAŃ

Wykonane badania wykazały, że jakość powłoki miedzianej znacząco zależy od sposobu przygotowania powierzchni. Próbki nr 1 i 2, które zostały wyszlifowane papierem o gradacji 1200, a następnie odtłuszczone i trawione w roztworach o temperaturze pokojowej. Otrzymana powłoka była nietrwała i dosyć łatwo schodziła z powierzchni, co może wskazywać na słabe właściwości adhezyjne. Z kolei próbka nr 3, przygotowana w identyczny sposób co próbka nr 2, ale odtłuszczana i trawiona w wyższej temperaturze równej 60°C, wykazała znacznie lepsze przyleganie powłoki. Zjawisko to wskazuje na to, że zwiększenie temperatury podczas procesu odtłuszczania i trawienia może poprawiać właściwości adhezyjne. Próbka nr 4, wyszlifowana z mniejszą dokładnością papierem o gradacji 800, charakteryzowała się matową powierzchnią powłoki, co może wskazywać na jej gruboziarnistą strukturę. Próbkę nr 5 wyszlifowano papierem o ziarnistości 1200 i poddano procesowi galwanizacji przez 1,5 minuty, przez co osiągnięto grubą i jednorodną powłokę. Próbki nr 6 i 7, szlifowane papierem o bardzo drobnej gradacji 2500 oraz wypolerowane, cechowały się gładką powierzchnią, jednak uzyskana powłoka schodziła już przy lekkim potarciu, co może o wskazywać na całkowity brak adhezji. Podane wyniki sugerują, że nadmierne wygładzenie powierzchni może ograniczać przyczepność powłoki miedzianej, co może być związane ze zmniejszeniem mikroskopijnej chropowatości niezbędnej do prawidłowego wiązania miedzi z podłożem. Próbki nr 8,9 i 10 oszlifowano papierem o najmniejszej gradacji wynoszącej 220. Chropowata powierzchnia przyczyniła się do bardzo dobrego przylegania powłoki.

Kolejnym czynnikiem wpływającym na jakość uzyskanej powłoki była temperatura procesu. Próbki nr 1 i 2, odtłuszczone i wytrawione w temperaturze 20°C, charakteryzowały się znacznie gorszą jakością powłok w porównaniu do próbek o numerach od 3 do 10, przygotowanych w temperaturze 60°C. Wyższa temperatura kąpeli poprawiała zarówno adhezję, jak i grubość powłoki, co można tłumaczyć bardziej efektywnym usunięciem zanieczyszczeń z powierzchni oraz lepszym przygotowaniem jej do procesu galwanizacji.

Analiza wyników wskazuje, że zarówno natężenie prądu, jak i czas trwania procesu elektrochemicznego wywierają istotny wpływ na grubość uzyskanej powłoki miedzianej.

Szczegółowe parametry galwanizacji przedstawiono w tabeli 2, a średnie grubości uzyskanych powłok w tabeli 3. Próbka nr 1, poddana galwanizacji przy wysokim natężeniu prądu wynoszącym 2,5 A przez 1 minutę, osiągnęła stosunkowo cienką powłokę o grubości 2,78 μm , która charakteryzowała się słabą trwałością. Sugeruje to, że zbyt wysoka gęstość prądowa ma negatywny wpływ na jakość powłok. W przypadku próbek nr 2 i 3, galwanizowanych przy natężeniu 1 A przez 1 minutę, grubości powłok wynosiły odpowiednio 2,46 μm oraz 3,90 μm . Skrócenie czasu galwanizacji przy zachowaniu natężenia 1 A, jak w próbce nr 4, prowadziło do znacznego wzrostu grubości powłoki do 7,58 μm , co może wynikać z bardziej skoncentrowanego osadzania miedzi na powierzchni w krótkim czasie. W przypadku próbki nr 5, przy tym samym natężeniu, ale wydłużeniu czasu do 1,5 minuty, uzyskano jeszcze grubszą powłokę o grubości 7,71 μm . Próbki nr 8 i 9 były galwanizowane przy niższym natężeniu prądu wynoszącym 0,6 A przez odpowiednio 2,5 oraz 4 minuty. Wyniki wskazują na uzyskanie powłok o podobnych grubościach, wynoszących odpowiednio 6,99 μm i 6,96 μm , co sugeruje, że przy dłuższym czasie galwanizacji niskie natężenie może zapewnić równomierne osadzanie powłoki. Ostatnia badana próbka nr 10, galwanizowana przy natężeniu prądu 1 A przez 1 minutę, uzyskała powłokę o grubości 7,49 μm . Podane wyniki wskazują, że wyższe natężenie prądu pozwala szybciej osiągnąć powłoki o określonej grubości, jednak wydłużenie czasu galwanizacji przy niższym natężeniu prądu prowadzi do bardziej jednorodnych i trwałych warstw galwanicznych.



Rys. 5. Próbka nr 2
Fig. 5. Sample no. 2



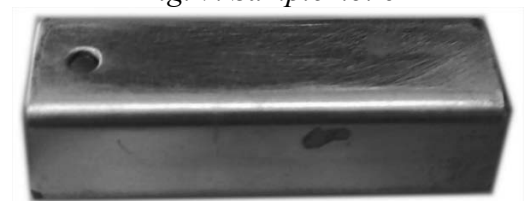
Rys. 6. Próbka nr 3
Fig. 6. Sample no. 3



Rys. 7. Próbka nr 6
Fig. 7. Sample no. 6



Rys. 8. Próbka nr 7
Fig. 8. Sample no. 7



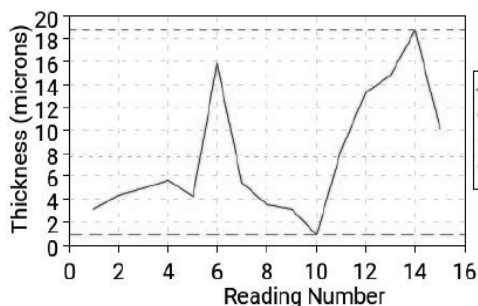
Rys. 9. Próbka nr 8
Fig. 9. Sample no. 8



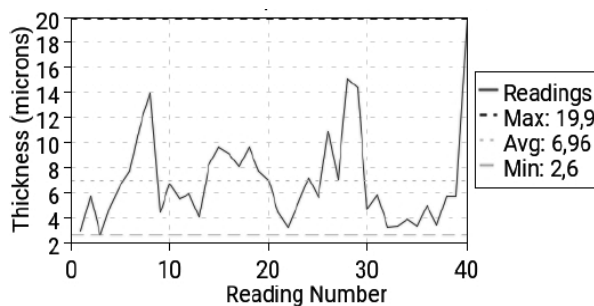
Rys. 10. Próbka nr 9
Fig. 10. Sample no. 9

Tabela 3. Wpływ parametrów przygotowania próbek na średnią grubość powłoki
 Table 3. Influence of sample preparation on average layer thickness

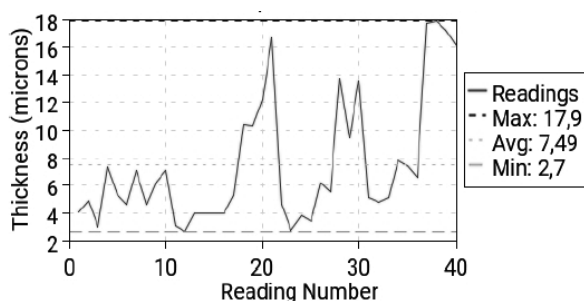
Nr próbki	Średnia grubość [μm]	Gęstość prądowa [A/dm^2]
1	2,78	4,49
2	2,46	1,8
3	3,90	1,8
4	7,58	1,8
5	7,71	1,8
6	–	1,08
7	–	1,08
8	6,99	1,08
9	6,96	1,08
10	7,49	1,8



Rys. 11. Wykres grubości warstwy próbki 5
 Fig. 11. Coating thickness graph of sample 5



Rys. 12. Wykres grubości warstwy próbki 9
 Fig. 12. Coating thickness graph of sample 9



Rys. 13. Wykres grubości warstwy próbki 10
 Fig. 13. Coating thickness graph of sample 10

Na wykresach (rys. 11-13) przedstawiających pomiary grubości powłok uzyskanych za pomocą miernika Defelsko PosiTector 6000 F90S można zaobserwować, że grubość powłoki w poszczególnych próbkach mieści się w przedziale od 0,9 μm do 19,9 μm . Biorąc pod uwagę średnie arytmetyczne grubości powłok ze wszystkich pomiarów zauważyć można, iż średnia grubość powłoki naniesionej na próbkę nr 9 jest najmniejsza. Jednocześnie zanotowano w niej największą maksymalną grubość. W próbce 5 odnotowano najmniejszą ze wszystkich grubość powłoki wynoszącą 0,9 μm .

4. PODSUMOWANIE

W ramach badań wytworzono powłoki miedziane na elementach stalowych przy zastosowaniu procesu galwanizacji elektrochemicznej. Wyniki badań potwierdzają, że jakość powłok miedzianych zależy od kilku kluczowych parametrów procesu galwanizacji. Wysoka chropowatość powierzchni sprzyja uzyskaniu grubych powłok o dobrej adhezji. Dłuższy czas galwanizacji prowadzi do uzyskania ciemniejszego koloru powłoki. Dodatkowo, wyższa temperatura odtłuszczenia i trawienia zapewnia lepsze oczyszczenie powierzchni, co przekłada się na wyższą jakość powłoki. Z kolei optymalizacja parametrów galwanizacji, takich jak natężenie prądu i czas procesu, umożliwia kontrolę grubości oraz trwałości powłok, co jest istotne w kontekście ich zastosowań w różnych gałęziach przemysłu.

PODZIĘKOWANIA

Praca powstała w wyniku realizacji projektu „*Elektrochemiczne tworzenie powłok ochronnych na metalach*” w ramach kształcenia zorientowanego projektowo – PBL, w konkursie XI w ramach programu Inicjatywa Doskonałości – Uczelnia Badawcza, Wydział Mechaniczny Technologiczny, Politechnika Śląska.

LITERATURA

1. Poradnik Galwanotechnika – Praca zbiorowa, Wydawnictwa Naukowo-Techniczne, Warszawa, 1985.
2. L.A. Dobrzański, A.D. Dobrzańska-Danikiewicz, *Obróbka powierzchni materiałów inżynierskich*, Open Access Library, Volume 5, 2011.
3. Gugua, E. C., Ujah, C. O., Asadu, C. O., Von Kallon, D. V., Ekwueme, B. N. (2024). Electroplating in the modern era, improvements and challenges: A review. *Hybrid Advances*, 7, Article 100286. <https://doi.org/10.1016/j.hybadv.2024.100286>
4. Giurlani, W., Zangari, G., Gambinossi, F., Passaponti, M., Salvietti, E., Di Benedetto, F., Caporali, S., Innocenti, M. (2018). Electroplating for Decorative Applications: Recent Trends in Research and Development. *Coatings*, 8(8), 260. <https://doi.org/10.3390/coatings8080260>
5. Srebrzenie, Galvano-Aurum, 2015, <https://www.galvanoaurum.com/srebrzenie/>
6. Dini, J. W., Snyder, D. D. (2010). Electrodeposition of copper. In M. Schlesinger (Ed.), *Modern Electroplating* (5th ed., pp. 33-78). Wiley. <https://doi.org/10.1002/9780470602638.ch2>
7. Ravai-Nagy, S., Titu, A. M., Pop, A. B. (2023). The Influence of Galvanizing on the Surface Quality and Part Precision of S235J0 Alloy Machined by Turning. *Coatings*, 13(4), 701. <https://doi.org/10.3390/coatings13040701>
8. Durney, L. J. (Ed.). (1984). *Graham's electroplating engineering handbook*. Springer Science & Business Media
9. Choi, J.-C., Lee, Y.-S., Lee, J., Kwon, H.-W., & Lee, J.-H. (2018). Etching behaviors of galvanic coupled metals in PCB applications. 2018 Pan Pacific Microelectronics Symposium (Pan Pacific), Big Island, HI, USA, 1–4. <https://doi.org/10.23919/PanPacific.2018.8319019>



31th January 2025
Gliwice, Poland

DEPARTMENT OF ENGINEERING MATERIALS AND BIOMATERIALS
FACULTY OF MECHANICAL ENGINEERING
SILESIA UNIVERSITY OF TECHNOLOGY

INTERNATIONAL STUDENTS SCIENTIFIC CONFERENCE

Application of a 3D scanner in the process of designing a hand model for a disabled person

Arkadiusz Górniak^a, Maksym Cinal^a, Rafał Gabryś^b, Jakub Pająk^b, Julia Dąbrowska^c, Magdalena Polok-Rubinić^d, Anna Włodarczyk-Fligier^d, Aneta Kania^d

^aAutomation and Robotics/Production Engineering and Management Silesian University of Technology, Faculty of Mechanical Engineering

^bIndustrial Mechatronics Silesian University of Technology, Faculty of Mechanical Engineering

^c Silesian University of Technology, Faculty of Automatic Control, Electronics and Computer Science, Biotechnology

^d Silesian University of Technology, Faculty of Mechanical Engineering, Department of Engineering Materials and Biomaterials

email:arkagor919@student.polsl.pl

Abstract: The article describes the use of the Shining3D EinScan Pro HD 3D scanner in the process of designing 3D models for prosthetic applications. It focuses on the device's capabilities in accurately reproducing details essential for prosthetic modeling. In the conducted study, the hand of a healthy individual was scanned, a digital model was developed, and it was subsequently adjusted for 3D printing requirements. The results highlight the potential of 3D scanning technology in prosthetics and the process of prosthetic personalization.

Keywords: 3D scanner, 3D printing, hand prosthesis, 3D modeling, scanning technologies

1. INTRODUCTION

1.1. Introduction to the topic of 3D scanning

3D scanning is an advanced technology enabling precise digital representation of the shape and structure of objects. The utilization of this method is gaining increasing importance in various fields, including medicine and prosthetics, where accurate adaptation of designed solutions to the specific needs of patients is crucial. 3D scanners facilitate the rapid and precise acquisition of data, such as object geometry, enabling the creation of high-quality 3D models. These models can subsequently be applied in design and manufacturing processes, for instance, through 3D printing technology [1].

In prosthetics, 3D scanning allows a transition from traditional, time-intensive methods to digital modeling, offering higher precision, time efficiency, and the possibility of customizing prostheses and medical devices. Acquiring precise data on the shape of a patient's limb enables the creation of perfectly fitted prostheses, enhancing user comfort and functionality. This

technology also supports advancements in prototyping and simulation, allowing for the testing of innovative solutions before their final implementation [2].

The aim of this article is to present the technological capabilities of the Shining3D EinScan Pro HD 3D scanner and its practical application in the creation of 3D hand models that can be utilized in the 3D printing process. Owing to its modular design, high resolution, and ability to capture intricate details even on challenging surfaces, this scanner finds applications across a wide range of fields, from industry and design to medicine and prosthetics [2].

The paper illustrates how the EinScan Pro HD scanner can be employed to scan the hand of a healthy individual to create a precise digital model. This model is then edited and prepared for 3D printing. Conducting this process demonstrates the potential of 3D scanning technology for personalizing prostheses, optimizing their design, and creating high-quality, accurate anatomical models [2].

2. SHINING3D EINSCAN PRO HD SCANNER

2.1. Characteristics and applications of the 3D scanner

The Shining3D EinScan Pro HD scanner stands out for its versatility, offering various operating modes such as handheld HD scanning, rapid scan mode, automatic, and fixed modes. This makes it suitable for both small and medium-sized objects, enabling precise reproduction of intricate shapes, such as hands or other limbs. Its advanced light projection algorithms and accuracy of up to 0.045 mm allow for faithful replication of even challenging surfaces, such as skin or materials with dark or metallic finishes. Its modular design and different scanning modes provide flexibility to adapt the process to the object's size and specific requirements [3].

These features make the device widely applicable in prosthetics, where individual customization and high precision in reproducing object geometry are crucial. The scanner excels in modeling small details and larger components, making it an indispensable tool in designing personalized prostheses and anatomical models [3].

3. SCANNING AND MODEL PREPARATION PROCESS

3.1. Description of the hand scanning process for a healthy individual

During the scanning process, the hand is captured from various perspectives to create a complete 3D model. In handheld mode, the EinScan Pro HD scanner allows the operator to freely move the device around the hand, enabling precise capture of all details, such as skin folds, nails, and spaces between fingers. Thanks to structured light technology and the optional use of color reference markers, the device ensures high accuracy in reproducing even the most complex shapes [4].

The scanner can process up to 3,000,000 points per second in handheld mode, making the scanning process both fast and highly efficient. Furthermore, its modular design allows for enhanced functionality through optional accessories, such as the Color Pack module. This enables the scanner to capture full-color textures, which is particularly useful for creating realistic 3D models of hands [4].

3.2. Editing and processing the 3D model

The obtained model was edited using Meshmixer, where the model's surfaces were smoothed, and errors from the scanning process, such as unwanted deformations or irregularities, were corrected. Meshmixer is a tool particularly suitable for preparing models for printing, especially organic objects like hands, where details must be accurately represented [5].

The next step involves processing the model in Fusion 360, which allowed the 3D model to be divided into smaller parts. This enabled adjustment of individual component dimensions to meet 3D printing requirements and ensured that the final model was well-suited to the production technology [5].

3.3. Final model ready for printing and potential applications in prosthetics



Figure 1. Hand Model After Processing

Upon completing the scanning and data processing, a 3D hand model ready for printing is generated, which can be utilized in additive manufacturing technologies such as FDM, SLA, or SLS. This model can be printed using various materials, including biocompatible plastics or resins, enabling customization for specific prosthetic needs. It finds extensive application, particularly in the design of cosmetic prostheses that accurately replicate the shape, texture, and proportions of a natural hand, providing a realistic and aesthetically pleasing appearance [6].

The model can also be used to create personalized fitting components, such as prosthetic sleeves, tailored precisely to the patient's anatomy. Additionally, the 3D model serves as a template or mold for producing prostheses from advanced materials such as silicones or composites. A significant application is the digital inversion of a healthy hand model to design a symmetrical prosthesis for a missing limb.

Moreover, the model is valuable for biomechanical analyses and functional tests, allowing for the evaluation and optimization of prostheses in a virtual environment before their physical production. Advanced 3D scanning and printing technologies make these models a critical tool in developing modern, personalized, and functional prosthetic solutions [6].

4. SUMMARY

This article presents the application of 3D scanning technology, exemplified by the Shining3D EinScan Pro HD scanner, in the design of personalized hand prostheses. The high precision in capturing details and the flexibility of modeling enable the creation of realistic and functional prostheses tailored to the patient's anatomy. The process of scanning a healthy hand and digitally processing the model in Meshmixer and Fusion 360 software was discussed, leading to project optimization for 3D printing technologies such as FDM, SLA, and SLS. The developed models have applications in the production of cosmetic prostheses, casting molds, fitting components, and biomechanical analyses.

In the future, 3D scanning could support the development of dynamic prostheses responsive to muscle signals, advanced biomechanical simulations, and personalized rehabilitation devices, offering precise and innovative medical solutions that enhance patient comfort and quality of life.

BIBLIOGRAPHY

1. J. Bochnia, The use of 3D scanning in reverse engineering. *Mechanics* [in Polish]. 2019, 3.
2. Skanery 3D shining3D, Global 3D, https://global3d.pl/pl/skanery-3d-shining3d/348-skaner-3d-shining3d-einscan-pro-hd-6970163080956.html?_gl=1*k7bf5
3. Morena, S., Barba, S., & Álvaro-Tordesillas, A. (2019). Shining 3D EinScan-Pro, application and validation in the field of cultural heritage, from the Chillida-Leku museum to the archaeological museum of Sarno. *The International Archives of the Photogrammetry, Remote Sensing and Spatial Information Sciences*, 42, 135-142.
4. Skaner 3D SHINING 3D EinScan Pro HD, <https://center3dprint.com/pl/einscan-pro-hd>
5. Schmidt, R., & Singh, K. (2010). Meshmixer: an interface for rapid mesh composition. In *ACM SIGGRAPH 2010 Talks* (pp. 1-1).
6. 3D Printing for Medicine, <https://rapidmade.com/3d-printing/in-the-medical-industry>

This paper is the result of a Project Based Learning (PBL) project entitled Development and 3D printing of a prosthetic hand model with software for a disabled person



31th January 2025
Gliwice, Poland

DEPARTMENT OF ENGINEERING MATERIALS AND BIOMATERIALS
FACULTY OF MECHANICAL ENGINEERING
SILESIA UNIVERSITY OF TECHNOLOGY

INTERNATIONAL STUDENTS SCIENTIFIC CONFERENCE

The impact of vinyl record wear on the quality of the gramophone signal: a frequency band analysis

Wiktoria Groelich^a, Daria Gatner^b, Maria Bieńkowska^c, Bogusław Ziębowicz^b, Michał Kręcichwost^c

^a Faculty of Biomedical Engineering, Department of Biomaterials and Medical Device Engineering, Silesian University of Technology, Roosevelta 40, 41-800 Zabrze, Poland; email: wg301436@student.polsl.pl

^b Faculty of Mechanical Engineering, Department of Engineering Materials and Biomaterials, Silesian University of Technology, Konarskiego 18A, 44-100 Gliwice, Poland; email: boguslaw.ziebowicz@polsl.pl

^c Faculty of Biomedical Engineering, Department of Medical Informatics and Artificial Intelligence, Silesian University of Technology, Roosevelta 40, 41-800 Zabrze, Poland; email: michal.krecichwost@polsl.pl

Abstract: Despite the widespread availability of music via radio and the internet, vinyl records remain highly popular. Enthusiasts, collectors, and artists who release their work in this traditional format make up a large part of the vinyl audience. A gramophone operates through the physical interaction of a needle with the record's grooves, which naturally wears down over time with use, potentially impacting the quality of the music reproduced. This study investigates the effect of repeated vinyl playback on the quality of gramophone signals. Researchers conducted a band-frequency analysis to determine the harmonic distribution of signals across various frequency ranges. The study compared the playback signals of both new and worn records using statistical analysis. Initial findings indicate that within the analysed range, the differences between the signals of new and worn records are not statistically significant.

Keywords: phonograph needle, vinyl record, tribological wear, sound analysis, cleaning agents.

1. INTRODUCTION

In today's world, access to music is virtually limitless. Thanks to the internet and especially streaming services, you can listen to nearly any artist globally for a relatively low fee. Numerous devices are available for playing music, with smartphones remaining the most popular. With the continuous advancements in headphone and speaker technology, music now accompanies us virtually everywhere.

Despite this, a growing number of people prefer traditional methods of playing music at home, such as using a gramophone. More artists are also releasing singles on vinyl records, ensuring high sound quality [8]. Enthusiasts of turntables firmly believe that the audio experience from analog output is vastly superior to that of digital devices [1].

The operation of a gramophone relies on the movement of the needle along the grooves of the record. A vinyl phonograph record serves as a sound carrier, where the most crucial component is the spirally arranged groove, which forms the embossed sound track [9].

During music playback, the needle traces the groove of the record, creating vibrations that are transmitted to a sensor at the end of the gramophone arm. This sensor generates an electrical signal proportional to the mechanical vibrations. The signal is then sent to the amplifier, which boosts its level and converts it into sound. The process of reading sound from a vinyl record is entirely analog, meaning the signal produced by the needle accurately reflects the mechanical vibrations within the groove of the record [10].

Vinyl records are susceptible to surface scratches and electrostatic forces, which make them easily charged and prone to attracting stubborn dust particles. Additionally, the playback of sound involves friction, which can alter the groove's irregularities over prolonged use. As a result, the sound reproduced may differ from the original recording [11, 12]. Given the concern for sound quality reproduction from gramophone records, the question of their longevity arises – specifically, how long they can continue to faithfully replicate the original recording. [13].

A literature review on gramophone sound reproduction technology and the impact of wear on both the needle and record reveals studies examining the overall effect of these components' wear on the quality of the reproduced signal [2]. In particular, the wear of the gramophone needle is analyzed for its impact on sound distortion, especially the decline in the quality of high-frequency reproduction [14].

However, much of the available information comes from internet forum discussions, like those on The Vinyl Press, where users share their experiences about the impact of needle wear on sound quality. These discussions often focus on high-frequency distortions and suggest replacing the needle after approximately 600–800 hours of use [15, 16, 17].

Despite numerous discussions on audiophile forums about the effects of record wear on sound quality, there is a lack of scientific studies specifically analyzing the frequency-band characteristics of the signal in relation to both needle and record wear. Most available analyses focus on general effects of wear, such as micro-scratches or record contamination, rather than examining how these changes affect the accuracy of audio signal reading across different frequency ranges [3, 4, 5].

The primary objective of this article is to conduct preliminary studies and evaluate the extent of wear on phonograph records under home usage conditions, employing frequency-band analysis and statistical methods.

2. MATERIALS AND METHODS

2.1 Measurement station

The experiments were conducted using an Argon Audio TT turntable equipped with an Ortofon 2M Bronze needle. For the recordings, two identical vinyl records were employed. Prior to recording, one of the records was played 100 times, while the other was unwrapped from its protective foil immediately before the recording. The audio signal from the

gramophone was captured via the line output using a Zoom F8n recorder at a sampling rate of 196 kHz. The data was saved in WAV format on an SD card. Recordings were performed multiple times for each record to ensure a representative sample. Figure 1 shows the measurement site, and Figure 2 presents photos of the individual components of the setup.

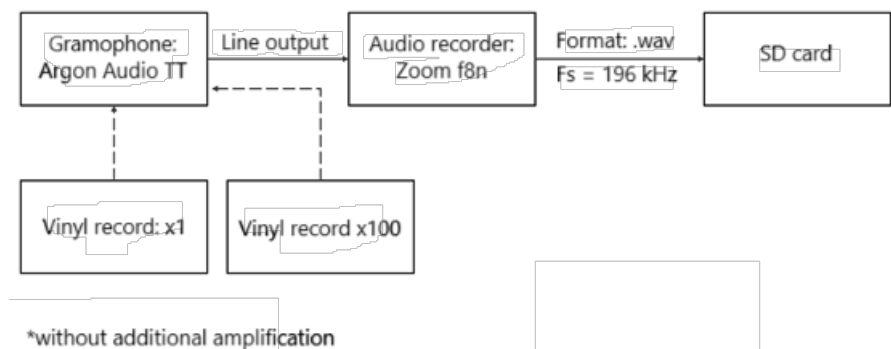


Figure 1. Measurement station diagram



Figure 2. a) gramophone Argon Audio TT, b) vinyl record, c) Ortofon 2M Bronze gramophone needle, d) Zoom F8n audio recorder

2.2 Dataset

The dataset comprised six recorded fragments of the analyzed track. For each of the two vinyl records – one new and one worn – three files were recorded and then shortened to 80 seconds. The chosen fragment covered the track's full frequency range.

To analyze the data, a Fourier transform was applied to each file to extract the signal spectrum. The amplitude spectrum components were then summed within predefined frequency ranges: 100-599 Hz, 600-3599 Hz, 3600-8099 Hz, and 8100-12000 Hz [6,7]. This process resulted in numerical values representing the contribution of sounds from these frequency ranges within the track. Frequencies above 12,000 Hz were excluded from the analysis because their amplitude spectrum values were significantly lower .

To enhance the visualization of the results and account for the non-linear nature of human hearing, the amplitude values were converted to a logarithmic scale, expressed in decibels (dB). This decibel scale facilitated the comparison of signal components across different frequency bands [6,7].

2.3 Data analysis

The statistical analysis aimed to evaluate significant differences between the amplitude spectra of signals from two types of recordings: new and worn records.

The initial step of the analysis involved checking the normality of data distribution within each group (new record, worn record) using the Shapiro-Wilk test. Since the data did not follow a normal distribution, the Mann-Whitney U test was selected. This test enables the comparison of medians between two independent groups (new record vs. worn record) across the entire frequency spectrum.

Subsequently, after categorizing the data into frequency bands (100-500 Hz, 600-3500 Hz, 3600-8000 Hz, 8100-12000 Hz), an analysis was performed using the Kruskal-Wallis test. This test facilitated the evaluation of significant differences between groups within each frequency band. The entire statistical analysis was performed using the JASP software [18].

3. RESULTS

The initial step in the results analysis was to perform a normality test on the data distribution. The results, shown in Table 1, reveal a significant deviation from normal distribution for both the new and worn record data.

Table 1 Test of Normality (Shapiro-Wilk)

		W	p
Harmonic sum [dB]	record-worn	0.886	< .001
	record-new	0.886	< .001

To evaluate the differences in signal power between the new and worn record data, the Mann-Whitney U test was performed. The results, presented in Table 2, indicate that there were no significant differences in the power spectrum of the signal ($p = 0.095$). Furthermore, the Brown-Forsythe test for equality of variances, conducted to compare the variance distributions between the two groups, also did not reveal significant differences ($p = 0.493$) [Table 3].

Table 2 T-test for independent samples (Mann-Whitney U test)

	U	df	p
Harmonic sum [dB]	1699	79.000	0.095

Table 3 Test of Equality of Variances (Brown-Forsythe)

	F	df ₁	df ₂	p
Harmonic sum [dB]	0.004	1	1198	0.493

The harmonic sum of the signal for each type of recording (all analyzed frequencies) is presented on the Figure 3.

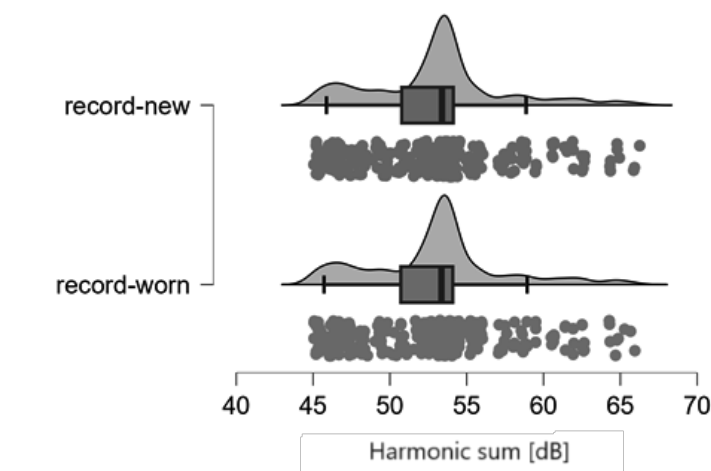


Figure 3. Harmonic sum of the signal for new and worn record

The next step of the analysis was to compare the power spectrum of the signals in different frequency ranges using the Kruskal-Wallis test. Table 4 presents the test results for each frequency band. The values from Dunn's post hoc analysis suggest that for all analyzed bands, there are no significant differences between the signals from the new and worn records (all $p > 0.05$). Figure 4 shows the harmonic sums for different frequency bands the two types of recordings.

Table 4 Dunn's post hoc comparison – Frequency band (N – record-new, S – record-worn)

Comparison	z	W _i	W _j	r _{rb}	p
100-500Hz (N) - 100-500Hz (S)	-0.017	700.067	701.333	0.084	0.987
600Hz-3.5kHz (N) - 600Hz-3.5kHz (S)	-0.015	569.678	570.156	0.002	0.988
3.6kHz-8kHz (N) - 3.6kHz-8kHz (S)	0.030	390.274	389.519	0.005	0.976
8.1kHz-12kHz (N) - 8.1kHz-12kHz (S)	-0.063	127.000	128.683	0.012	0.950

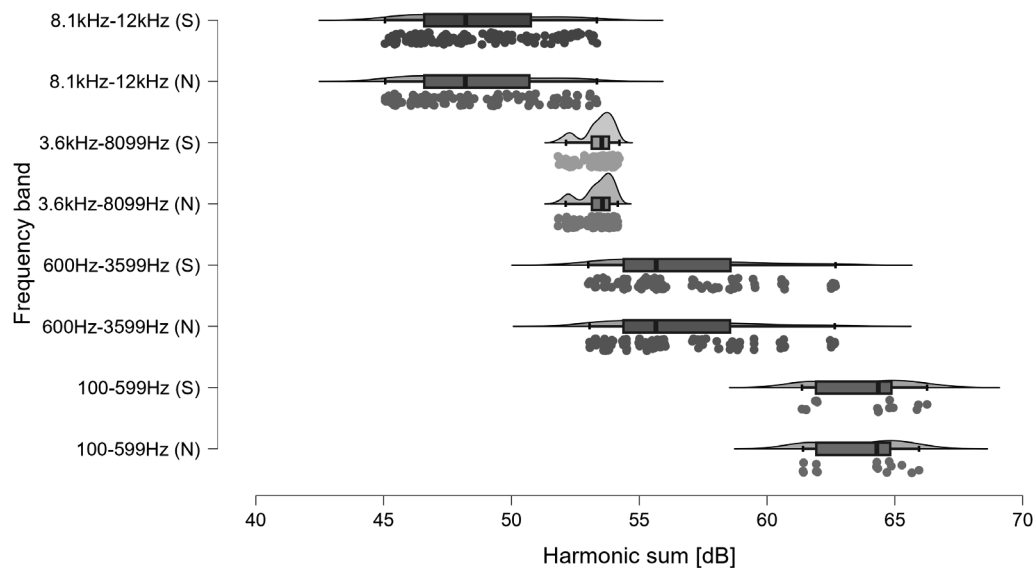


Figure 4. Harmonic sum for different frequency bands for the two types of recordings (*S* – worn record and *N* – new record)

4. DISCUSSION

The analysis revealed that there are no statistically significant differences between the signals recorded from new and worn records, both within the entire frequency spectrum and within individual bands (100-599 Hz, 600-3599 Hz, 3600-8099 Hz, 8100-12000 Hz). The results of the statistical analysis indicate that after 100 plays, the wear on the vinyl record does not cause significant changes in sound quality.

5. CONCLUSION

The findings of this study could be beneficial for vinyl record collectors and gramophone users. They demonstrate that despite numerous plays, which cause wear on both the needle and the record, the sound quality recorded in the groove remains largely unchanged. The statistical analysis conducted shows no significant differences in sound quality between new and worn records, even after 100 plays.

There is a clear need for further research into the macro and microscopic changes affecting both records and phonograph needles. Comparing frequency analysis data with microscopic or tribological observations could provide insights into the effects of use and storage on sound quality during playback. This is especially relevant considering the increasing popularity of vinyl records and the expanding community of collectors and enthusiasts. Understanding how records wear during use could encourage more mindful practices, including regular cleaning with specialized products, careful handling, and limiting playback of particularly valuable records. Such knowledge could help extend the lifespan of records and improve their quality of use over the long term.

ACKNOWLEDGMENTS

This work is part of a Project Based Learning (PBL) project titled 'Analysis of the sound quality recorded on a vinyl record depending on its usage and the wear level of the phonograph needle,' conducted in the 2024/25 academic year at the Silesian University of Technology.

BIBLIOGRAPHY

1. Bartmanski, D., & Woodward, I. (2016). Vinyl record: A cultural icon. *Consumption Markets & Culture*, 21(2), 171–177. Doi: 10.1080/10253866.2016.1212709
2. Bastiaans, C. R. (1967). Factors affecting the stylus/groove relationship in phonograph playback systems. *Journal of the Audio Engineering Society*, 15(4), 389–396.
3. Hensman, A., & Casey, K. (2007). Optical reading and playing of sound signals from vinyl records. *The Annual International Conference on Information Technology and Telecommunication (ITT07)*. Institute of Technology Blanchardstown, Dublin.
4. Tian, B., & Barron, J. L. (2007). Sound from gramophone record groove surface orientation. *2007 IEEE International Conference on Image Processing (ICIP)*, San Antonio, TX, USA, 84–91. Doi: 10.1109/icip.2007.4379641
5. Tian, B., & Barron, J. L. (n.d.). Reproduction of sound signal from gramophone records using 3D scene reconstruction. Department of Computer Science, The University of Western Ontario, London, Ontario, Canada, N6A 5B7.
6. Zwicker, E., & Fastl, H. (2007). *Psychoacoustics*. Berlin, Heidelberg: Springer Berlin Heidelberg.
7. Alessio, S. M. (2019). *Digital signal processing and spectral analysis for scientists: Concepts and applications*. Springer.

NETOGRAPHY

1. Recording and Playing Music [PL: Zapis i odtwarzanie muzyki]. Retrieved from <https://mlodytechnik.pl/eksperymenty-i-zadania-szkolne/wynalazczosc/30029-zapis-i-odtworzanie-muzyki> [Accessed 29 November 2024].
2. Guide to Vinyl Record Sizes. Retrieved from <https://blog.discmakers.com/2023/07/guide-to-vinyl-record-sizes/> [Accessed 29 November 2024].
3. From Vinyl to Sound in Speakers – How Does a Vinyl Record Play? [PL: Od winylu do dźwięku w głośnikach - jak gra płyta winylowa]. Retrieved from <https://rms.pl/baza-wiedzy/2885-od-winylu-do-dzwieku-w-glosnikach-jak-gra-plyta-winylowa> [Accessed 29 November 2024].
4. How do you take care of your vinyl records? Retrieved from https://www.reddit.com/r/vinyl/comments/23l21j/how_do_you_take_care_of_your_vinyl_records/ [Accessed 29 November 2024].
5. How to Care for Vinyl Records: A Comprehensive Guide. Retrieved from <https://vinyl.ae/blogs/news/how-to-care-for-vinyl-records-a-comprehensive-> [Accessed 29 November 2024].

6. How Many Times Can a Vinyl Record Be Played? Retrieved from <https://myvinylpassion.com/how-many-times-can-a-vinyl-record-be-played/> [Accessed 29 November 2024].
7. Vinyl High-Frequency Distortion. Retrieved from <https://allforturntables.com/2023/06/23/vinyl-high-frequency-distortion/> [Accessed 29 November 2024].
8. The Finish Line for Your Phonograph Stylus. Retrieved from <https://thevinylpress.com/the-finish-line-for-your-phonograph-stylus/> [Accessed 29 November 2024].
9. How Many Times Can You Play a Vinyl Record Without Worrying About Its Wear and Tear? Retrieved from <https://x-disc.pl/en/blog-en/how-many-times-can-you-play-a-vinyl-record-without-worrying-about-its-wear-and-tear/> [Accessed 29 November 2024].
10. Three-Way Vinyl Record Wear Test. Retrieved from https://www.reddit.com/r/vinyl/comments/1dvv5k6/threeway_vinyl_record_wear_test/?rdt=62889 [Accessed 29 November 2024].
11. Source: Website – JASP Stats Download [PL: Źródło: Strona internetowa: JASP Stats Download]. Retrieved from <https://jasp-stats.org/download/> [Accessed 29 November 2024].



31th January 2025
Gliwice, Poland

DEPARTMENT OF ENGINEERING MATERIALS AND BIOMATERIALS
FACULTY OF MECHANICAL ENGINEERING
SILESIA UNIVERSITY OF TECHNOLOGY

INTERNATIONAL STUDENTS SCIENTIFIC CONFERENCE

Application of Advanced Computational Mathematics for Flight Mechanics of Aircraft

Luka Guraspashvili^a, Ramili Zukakishvili^b

^a Georgian Technical University, Faculty of Transport Systems and Mechanical Engineering, Department of Mechanical Engineering and Industrial Technology,
Email: guraspashvili.luka24@gtu.ge

^b Georgian Technical University, Faculty of Transport Systems and Mechanical Engineering, Department of Mechanical Engineering and Industrial Technology, Associate professor.
Email: r.zukakishvili@gtu.ge

Abstract: Computational Mathematics has been a huge advancement in engineering industry. It allows engineers to solve complex equations with maximum accuracy and efficiency. It is used to analyse material strength, construction strength, aerodynamics and so on. This paper describes the use of computational mathematics in combination with Python and OpenVSP to model, simulate and analyse flight and its applications in aircraft engineering. The advantages of using computational methods in aircraft engineering, compared to traditional methods, are also presented.

Keywords: Computational Mathematics, Differential Equations, CFD, Numerical Methods, Numerical Analysis, Python, NumPy, SciPy, Mathematical Modelling.

1. INTRODUCTION

Computers have revolutionized our everyday lives, from transforming how we communicate to enabling self-driving cars. However, their most profound impact lies in their ability to solve complex problems faster and more accurately than ever before.

In the field of aeronautical engineering, flight analysis is one of the most challenging areas, often involving differential equations that are impossible to solve analytically. Traditionally, engineers relied on expensive and time-consuming physical experiments, such as wind tunnel testing and real flight tests, to gather data and validate designs.

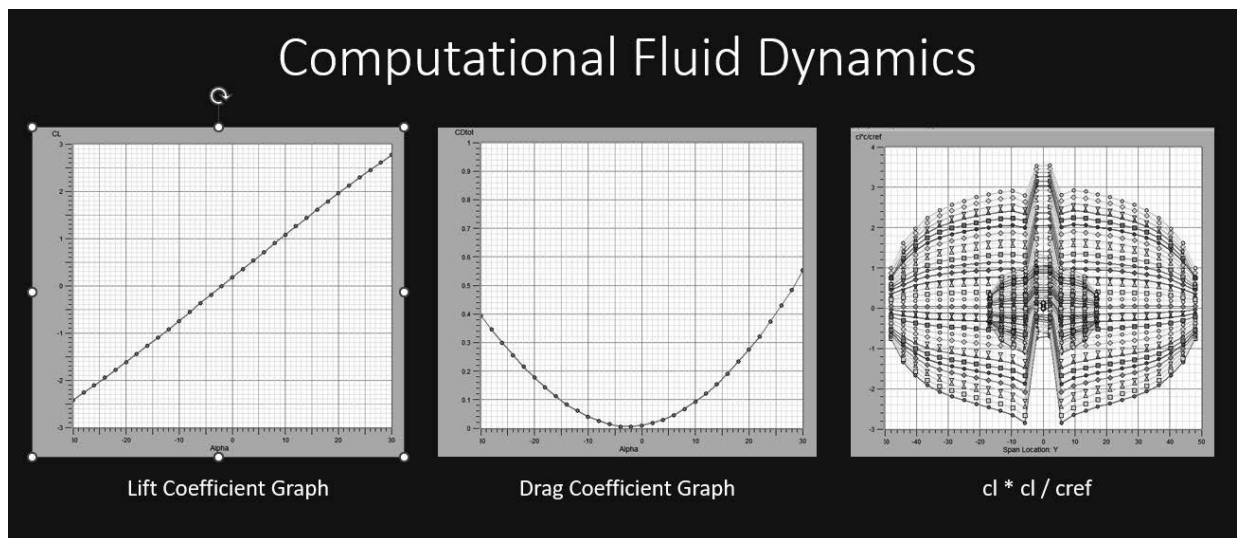
With advancements in computational technology, many of these experiments can now be conducted virtually. By creating detailed models and running simulations, engineers can analyze aerodynamic performance, predict flight behavior, and optimize designs, all from within a computer. This shift not only reduces costs and time but also opens new possibilities for innovation in aircraft development.

2. COMPUTATIONAL FLUID DYNAMICS

Understanding an aircraft's aerodynamics is one of the first and most crucial tasks for an aeronautical engineer, as it directly determines the aircraft's performance in the air. Traditionally, wind tunnels were used to study aerodynamic behavior by simulating airflow around a model. However, with recent advancements in Computational Fluid Dynamics (CFD) technology, engineers can now accurately analyze an aircraft's aerodynamic characteristics in a virtual environment.

One of the tools widely used for this purpose is **OpenVSP (Open Vehicle Sketch Pad)**, an open-source parametric modeling tool developed by NASA. OpenVSP allows engineers to quickly create detailed 3D models of aircraft and analyze their aerodynamic properties. The tool provides a wide range of features to modify key parameters, such as wing shape, fuselage dimensions, and airfoil profiles, enabling rapid exploration of various designs.

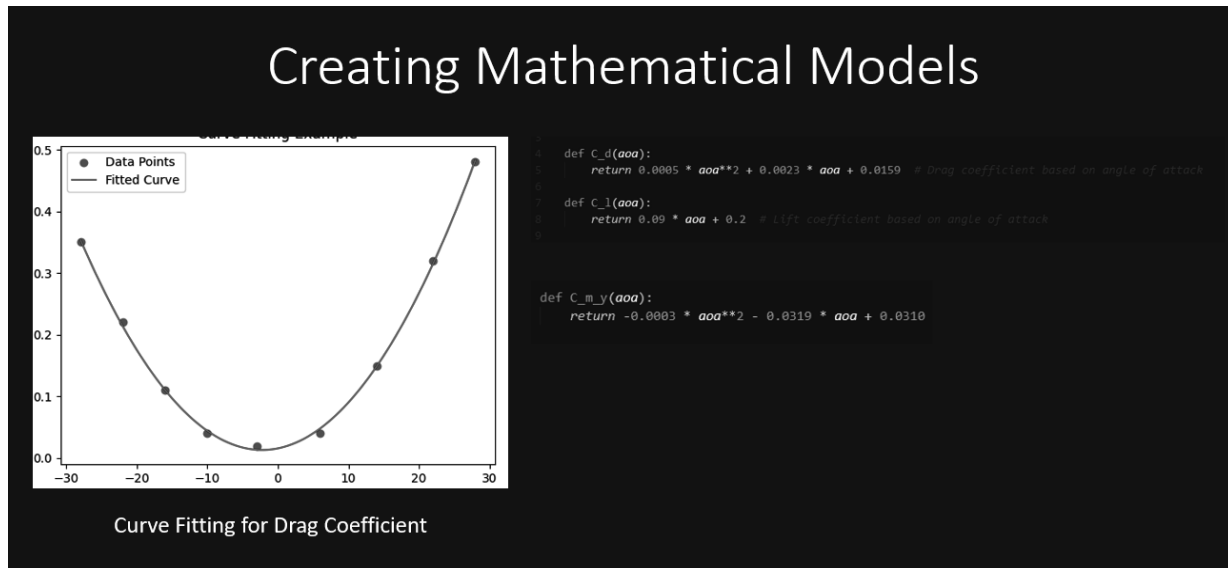
An important feature of OpenVSP is its ability to generate aerodynamic data in **CSV format**, which can be used for mathematical modeling and simulations. After running a virtual analysis, OpenVSP can output a file containing key characteristics such as **lift, drag, moment coefficients, pressure distribution, and stability derivatives**. This data can then be imported into numerical models to study an aircraft's behavior under different flight conditions, allowing engineers to predict performance, optimize designs, and reduce the need for expensive physical experiments.



3. MATHEMATICAL MODELLING WITH PYTHON

After obtaining the results from OpenVSP, mathematical models can be created to better understand the aerodynamic behavior of an aircraft. For this purpose, the **Python programming language** and its scientific library **SciPy** are commonly used. By applying the **least squares method**, engineers can fit mathematical functions to the data for **drag, lift, and moment coefficients**, creating models that describe how these forces vary with different flight parameters.

These functions can then be integrated into **flight simulations**, allowing for more accurate predictions of an aircraft's performance under various conditions. By building such simulations, engineers can study stability, efficiency, and control characteristics, reducing the need for costly real-world testing and accelerating the design process.



3. SIMULATION WITH THE MATHEMATICAL MODEL

After creating the mathematical models, we are ready to use them for simulating flight. Essentially, we are solving a differential equation that describes the plane's trajectory. To do this, we will employ the **Euler method**.

In mathematics and computational science, the **Euler method** (also known as the forward Euler method) is a first-order numerical technique used to solve ordinary differential equations (ODEs) with a given initial condition. It is the simplest explicit method for numerically integrating ODEs and is considered the most basic of the Runge–Kutta methods. The method is named after the Swiss mathematician **Leonhard Euler**, who first introduced it in his work *Institutionum calculi integralis* (published between 1768 and 1770).

We implement this numerical method in Python using the **NumPy** library for efficient numerical calculations, which helps us solve differential equations iteratively. For visualizing and plotting the results, we use **matplotlib**, a powerful Python plotting library. This enables us to visualize the plane's trajectory over time as well as other important variables such as **velocity** and **forces**.

By plotting the **velocity over time**, we can observe how the plane's speed changes during the flight. Similarly, plotting **aerodynamic forces** (such as lift, drag, and thrust) helps us understand the forces acting on the aircraft at different stages of the simulation. These plots allow for a comprehensive analysis of the flight dynamics.

```
def eulers_method(aaa, X_pos, Y_pos, mass, air_density, wing_area, dt, initial_time, final_time, T_m, chord_length, moment_of_inertia):
    x_velocity = 0
    y_velocity = 0
    angular_velocity = 0

    n_steps = int((final_time - initial_time) / dt)

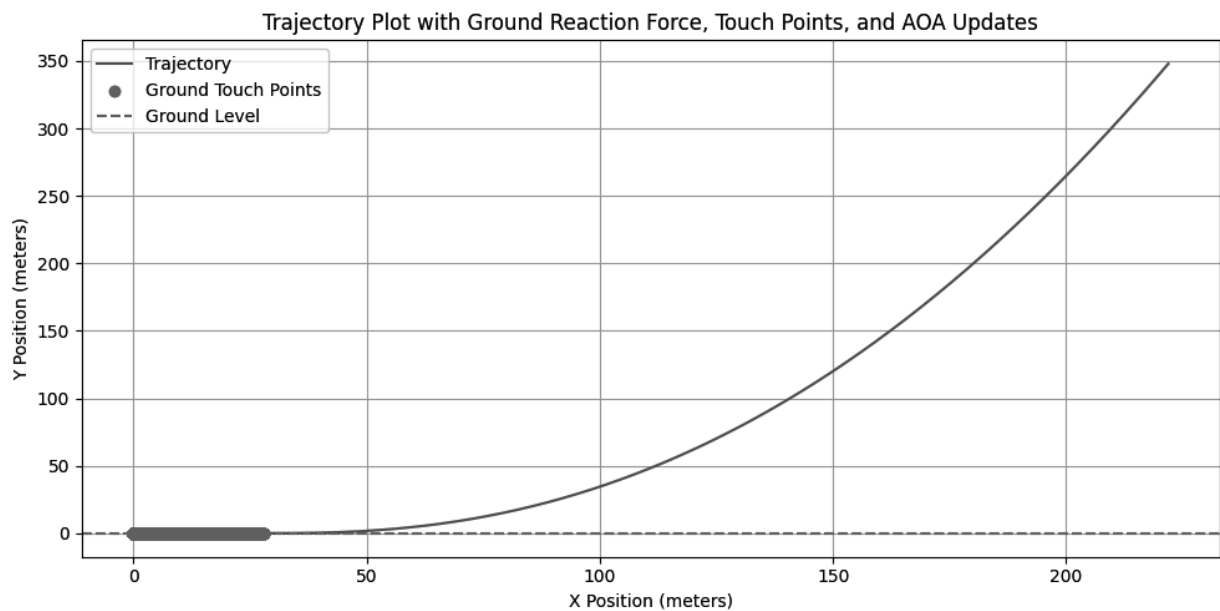
    time = np.linspace(initial_time, final_time, n_steps + 1)
    x_values = np.zeros(n_steps + 1)
    y_values = np.zeros(n_steps + 1)
    aaa_values = np.zeros(n_steps + 1)
    velocity_values = np.zeros(n_steps + 1)

    x_values[0] = X_pos
    y_values[0] = Y_pos
    aaa_values[0] = aaa
```

4. THE RESULT AND PRACTICAL USE OF THE DATA OBTAINED

In conclusion, leveraging simulations and mathematical models in aircraft design brings numerous benefits to the industry. These tools enhance efficiency, safety, and cost-effectiveness in various aspects of aircraft development.

- **Optimizing aircraft design for performance:** Improving aerodynamics, wing geometries, and airfoil profiles to boost fuel efficiency and speed.
- **Designing highly maneuverable aircraft:** Refining control surface placement for superior maneuverability.
- **Cutting costs and time for testing:** Reducing the need for expensive wind tunnel tests and flight trials.
- **Developing autopilot systems:** Using flight dynamics models to design and test accurate autopilot systems.
- **Pilot training:** Creating realistic virtual environments for effective pilot training without the risks of actual flight



ACKNOWLEDGEMENTS

The work was created as a result of the project as part of project based learning - PBL, in the 11th competition under the Initiative of Excellence - Research University, Silesian University of Technology, Gliwice, Poland.

BIBLIOGRAPHY

1. R. H. Barnard and D. R. Philpott. Aircraft Flight. A description of the physical principles of aircraft flight. Fourth edition. Pearson Education Limited. 2010. 385 pages.
2. Ranjan Vepa. Flight Dynamics, Simulation, and Control For Rigid and Flexible Aircraft. CRC Press Taylor & Francis Group. 2015. 678 pages.
3. A. C. Kermode. Mechanics of Flight. 11th edition. Pearson Education Limited 2006. 513 pages.
4. C. Pozrikidis. Fluid Dynamics Theory, Computation, and Numerical Simulation. Third Edition. Springer. 2017. 912 pages.
5. Atul Sharma. Introduction to Computational Fluid Dynamics Development, Application and Analysis. Wiley. Athena Academic. 2017. 399 pages.
6. How to do Mathematical Modeling in Python? <https://www.geeksforgeeks.org/how-to-do-mathematical-modeling-in-python/>.
7. Sastry S.S. Introductory methods of numerical analysis. Fifth edition. PHI Learning Private Limited, New Delhi. 2012. 455 Pages.



31th January 2025
Gliwice, Poland

DEPARTMENT OF ENGINEERING MATERIALS AND BIOMATERIALS
FACULTY OF MECHANICAL ENGINEERING
SILESIA UNIVERSITY OF TECHNOLOGY

INTERNATIONAL STUDENTS SCIENTIFIC CONFERENCE

Nitinol in aircrafts

Samir Haitham Samir Abdelaziz^a, Givi Sanadze^b

^a Georgian Technical University, Faculty of Transport Systems and Mechanical Engineering, Department of Mechanical Engineering and Industrial Technology, email: samir.samir@gtu.ge

^b Georgian Technical University, Faculty of Transport Systems and Mechanical Engineering, Department of Mechanical Engineering and Industrial Technology, Professor Email: sanadzegivi05@gtu.ge

Abstract: Nitinol, a memory alloy made of nickel-titanium, a material that has significant potential in aerospace industry. Nitinol has unique properties like shape memory super elasticity, and it is a corrosion resistant material, which allow it to be used in varies parts in aircrafts. This paper describes the applications of nitinol in aircraft's components like actuators, sensors, and structural components. this paper describes the advantages and the challenge accompanying the use of nitinol in aircrafts, focusing on nitinol potential to improve aircrafts performance, efficiency, and safety.

Keywords: Nitinol, shape memory alloy (SMA), aerospace, aircraft, materials, wing morphing, super elasticity, shape memory effect, landing gear, sensors, actuators, NASA, Boeing.

1. INTRODUCTION

The aerospace industry is committed to developing new technologies and material to make aircrafts more efficient and ensure safety, that is why nitinol an nickel-titanium alloy was researched to be used in aircrafts, nitinol has very interesting properties such as shape memory effect and super elasticity, additionally, nitinol is corrosion resistant material an important property for a material that will be used in an aircraft.

Nitinol properties are interesting because of the various ways in which it can be applied to aircrafts as the shape memory effect property allows the material to remember it is original shape even after the metal is deformed to a totally different shape by just heating the metal above a certain degree the metal will return to it is original shape, additionally super elasticity allows the metal to deform as many times without having any permanent damage to the metal by just heating the metal it will return to the original shape, finally the metal is corrosion resistant which is a very important property for a metal to have in case of aerospace applications.

2. WAYS OF USING NITINOL IN AIRCRAFTS

Nitinol can be used in numerous ways in aircrafts such as actuators, sensors, and structure.

- **Actuators:** Nitinol can be used as an actuator in aircrafts to operate and control systems, for example it can be used to deploy the landing gears of an aircraft and even control the flaps, aileron, and the slats in an aircraft wing, the advantage of using a nitinol actuator is that it uses low amount of energy but still provide reliable and precise actuation.
- **Sensors:** Nitinol can be used to detect changes in environment such as temperature and pressure during the flight of an aircraft. The reasoning behind that is the metal ability to change shape with increase of temperature using this property it is possible to set triggers that control specific systems based on the amount of change in the shape.
- **Structure:** Nitinol can be used as structural components such as wings, spars, ribs, and fuselage. Nitinol ability to return is beneficial to such components as it allows the components to return to the intended shape after impact or deformation that may happened during the flight without the need for complex repairs.

3. ADVANTAGES OF NITINOL IN AIRCRAFT

Using nitinol in aircraft comes with various benefits such as:

- **Lightweight:** Nitinol is lighter than steel which make it a suitable candidate to use in aircraft where weight reduction is essential for improving the aircraft performance and efficiency.
- **Corrosion Resistance:** Nitinol is highly resistant to corrosion making it suitable for the hostile environment that aircrafts experience during flights.
- **Durability:** Nitinol is resistant to fatigue which is a needed property for a metal that will be using in an aircraft that will experience cyclic loads each flight.
- **Simplified Design:** Using nitinol allows engineers to eliminate complex machines allowing aircraft to be lighter and make the aircraft easier to maintain reducing cost of operation.
- **Morphing Aerostructures:** Nitinol enables morphing aerostructures, which allows control of the aircraft aerodynamics by changing the shape of the wings improving the aircraft efficiency and performance.

4. CHALLENGES OF NITINOL IN AIRCRAFT

Despite the advantages of nitinol, nitinol also has challenges that make it hard to adopt in the aerospace industry such as:

- **Cost:** Nitinol is more expensive than currently used metals like steel and aluminium, which is the main barrier preventing the adoption of nitinol in aircrafts.
- **Manufacturing Complexity:** Nitinol manufactures need to use overly complex techniques to manufacture the metal, manufacturers must control temperature and parameters of the production precisely to ensure that the nitinol have the desired properties and performance, increasing the cost of production.
- **Predictability:** Nitinol needs advanced modelling to predict the behaviour of the shape memory effect in every environment requiring heavy simulation and testing to ensure the desired effect is achieved.

5. APPLICATIONS OF NITINOL IN AIRCRAFTS

5.1. Adaptive Wing Structures

- **Smart Vortex Generators:** NASA is working with Boeing to utilize nitinol in creating smart vortex generators that can change shape according to altitude, temperature, and speed for more effective airflow around the airplane. Using the vortex generator can enhance the aircraft aerodynamics help reducing drag and noise allowing for increased fuel efficiency.



Figure 1. Smart Vortex Generators in closed position



Figure 2. Smart Vortex Generators in open position

- **Morphing Wings:** Nitinol can be used to allow wings to change shape which is achieved using nitinol wires or actuators inside the wing structure when heated they can deform wing shape allowing for adjustment in the shape, which allows pilots to use the most optimal wing shape for each situation, they can use a wing shape that can make take-off easier and faster then change it to a shape that allow for faster and more comfortable cruise.

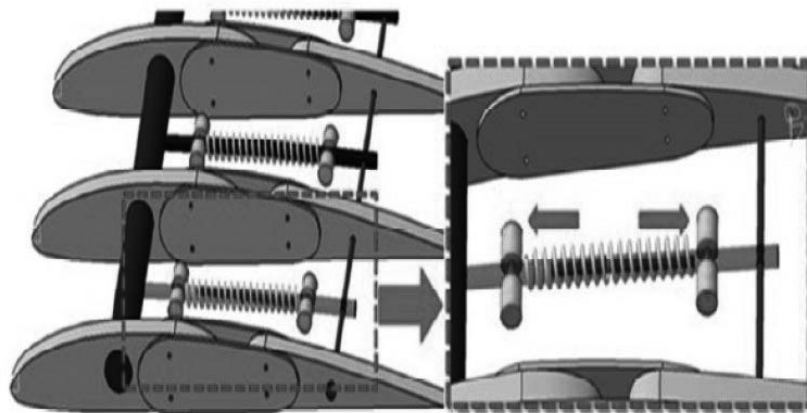


Figure 3. showing morphing wing mechanism concept

- **Folding wings:** Nitinol was used by NASA and Boeing to develop nitinol actuators for folding the wings of F/A-18 which is beneficial for aircrafts with limited storage area in this case aircraft carriers, this also shows the possibility of using nitinol for large wings morphing.

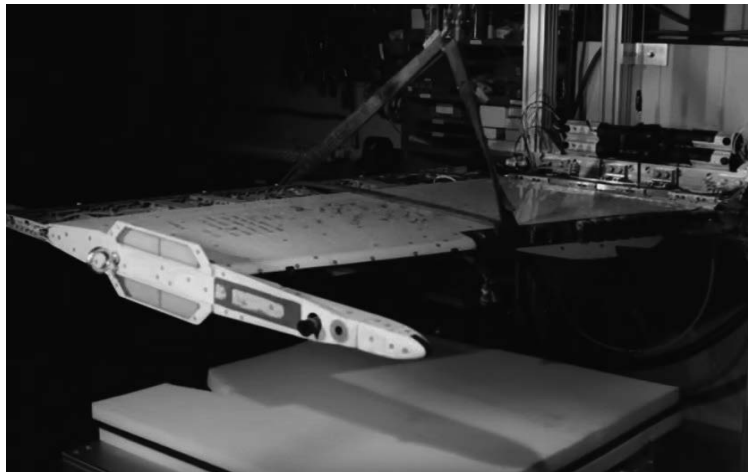


Figure 4. NASA folding wing experiment

5.2. Aircraft Control Systems

Nitinol can be used in aircraft control systems such as landing gear deployment, wing morphing, and flight control surfaces. The shape memory effect of nitinol allows it to have precise and reliable actuation with minimal energy consumption. For example, Nitinol wire can be used for landing gear deployments allowing reliable use even in extreme conditions and environment. Also using nitinol actuators will allow for control over the flight surfaces in an aircraft such as flaps and slats.

5.3. Aircraft Bearings

60NiTi, Made by NASA Glenn research center, is a type of nitinol that can be used as aircraft bearing, it is lighter than traditional bearings with a corrosion resistance property that make it very good for use in aircrafts, what is more interesting in this type of bearing is that it is made of nitinol meaning by heating the bearing it will return to original shape so in case of damage caused by debris to the bearing it can be fixed easily enhancing the reliability of the bearing and most importantly the longevity of it.

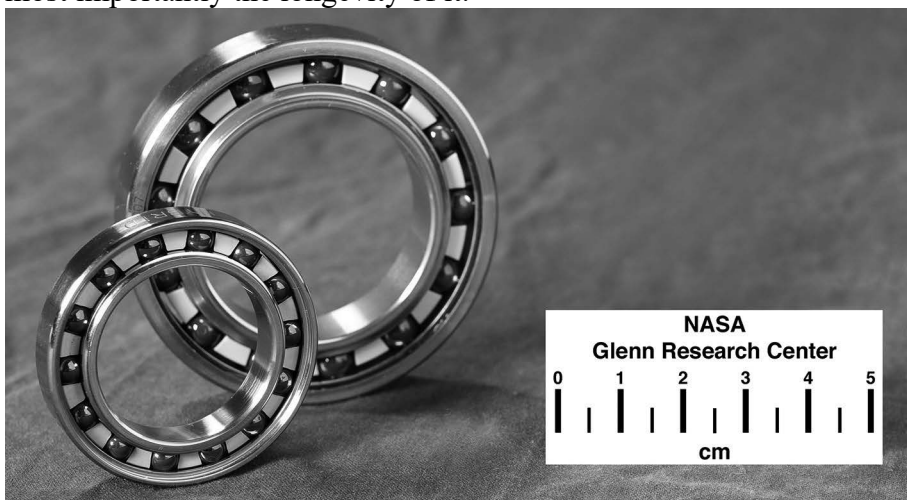


Figure 5. 60NiTi Made by NASA Glenn research center

6. CONCLUSION

Nitinol, with its unique properties of shape memory, super elasticity, lightweight, and corrosion resistance, makes it a suitable metal to be used in aerospace industry which demands high performance and lightweight metals to ensure performance and efficiency. Nitinol applications as actuators, sensors and structure in aerospace can improve safety, performance, and efficiency.

Development of innovative applications of nitinol is crucial to build the future of aircrafts, despite the challenges of nitinol from cost and complexity of manufacturing, the industry needs to continue the research on nitinol to develop new manufacturing process that can reduce the cost of production, allowing for massive adoption of the metal in aircraft manufacture which can reshape the industry allowing for new innovative aircraft designs which are not always possible with current materials. NASA and Boeing have proved the potential nitinol has in their research, so the main barrier for nitinol mass adoption is cost of production which with more research can lead to new cost-effective manufacturing process.

ACKNOWLEDGEMENTS

The work was created as a result of the project as part of project based learning - PBL, in the 11th competition under the Initiative of Excellence - Research University, Silesian University of Technology, Gliwice, Poland.

BIBLIOGRAPHY

1. DellaCorte, C. Ni-Ti Alloys for Aerospace Bearing Applications. 6th World Tribology Congress. 2017.
2. NASA. Memory Metals are Reshaping the Evolution of Aviation. 2019.
3. NASA. Shape Memory Alloys Activity. National Aeronautics and Space Administration. 2022.
4. Costanza, G., & Tata, M. E.. Shape Memory Alloys for Aerospace, Recent Developments, and New Applications: A Short Review. 2020.



31th January 2025
Gliwice, Poland

DEPARTMENT OF ENGINEERING MATERIALS AND BIOMATERIALS
FACULTY OF MECHANICAL ENGINEERING
SILESIA UNIVERSITY OF TECHNOLOGY

INTERNATIONAL STUDENTS SCIENTIFIC CONFERENCE

Porovnanie vlastností polotovarov z polymérneho kompozitu používaného pri termoformovaní

Rastislav Hanulík^a, Lenka Markovičová^a, Mirosław Bonek^b

^a Žilinská univerzita v Žiline, Strojnícka fakulta, Katedra materiálového inžinierstva, Univerzitná 8215/1, 010 26 Žilina, Slovak Republic

^b Silesian University of Technology, Faculty of Mechanical Engineering, Department of Engineering Materials and Biomaterials

email: hanulik3@stud.uniza.sk, lenka.markovicova@fstroj.uniza

Abstrakt: Práca je zameraná na plasty - ako plasty používať a súčasne chrániť životné prostredie. Cieľom práce je identifikovať možný činiteľ, ktorý negatívne vplyva v procese termoformovania na výsledný produkt vyrobený z polymérneho materiálu plneného talkom. Zhrnuté sú poznatky o polypropyléne, kompozitných materiáloch a výrobných technológiách, kde sú vysvetlené poznatky z oblasti termoformovania, extrúzie a valcovania.

Kľúčové slová: polymér, kompozit, polymérne kompozity, polypropylén, termoformovanie

1. ÚVOD

Plasty a ich kompozity sa už pomerne dlhý čas využívajú v leteckom priemysle, zároveň však predstavujú novú generáciu alternatívnych materiálov aj pre automobilový priemysel, vzhľadom na ich nízku hmotnosť, vysokú odolnosť a lepšie mechanické vlastnosti v porovnaní s tradičnými materiálmi.

Kompozit je materiál, ktorý vznikol kombináciou jednoduchých materiálov s využitím poznatkov fyzikálnej metalurgie. Pozostáva z matrice, ktorá má funkciu pojiva a zložky, ktorá má spevňujúci účinok. Túto spevňujúcu fázu môžu tvoriť vlákna alebo častice, líšiace sa morfológiou a veľkosťou. Matrica obklopuje a chráni výstuž pred poškodením a okolitým prostredím, má relatívne nízku pevnosť v ťahu, ale vysokú tvrdosť a zároveň aj húževnatosť. Materiál matrice zároveň určuje pracovnú teplotu a podmienky spracovania kompozitu. Pre tieto materiály je typický tzv. synergizmus, čo znamená, že vlastnosti kompozitu sú vyššie, ako vlastnosti jednotlivých zložiek, z ktorých kompozit pozostáva, dokopy. Kompozity môžeme klasifikovať z hľadiska rôznych parametrov, napríklad podľa povahy matrice, tvaru spevňujúcej fázy, atď. [1].

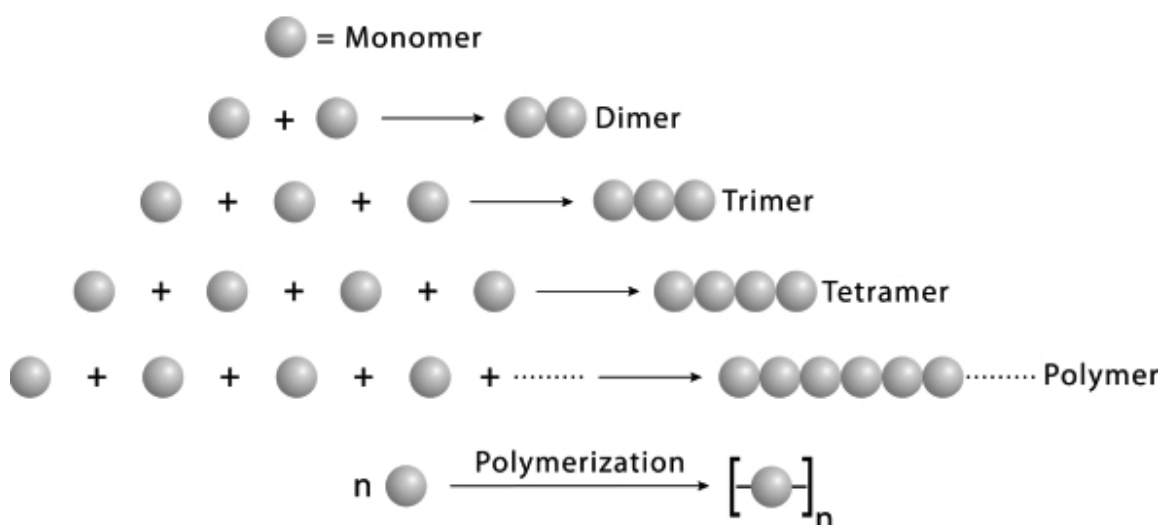
Polymérne kompozity predstavujú špičkovú triedu materiálov, ktoré spôsobujú revolúciu v mnohých priemyselných odvetviach na celom svete. Tieto kompozity sú skonštruované kombináciou polymérnej matrice s vystuženými materiálmi ako sú vlákna alebo častice, aby sa dosiahli zlepšené mechanické, tepelné a elektrické vlastnosti. Oproti kovovým a keramickým

kompozitom majú polymérne kompozity niekoľko výhod, ako napríklad ľahká výroba a spracovanie, dobré tlmiace vlastnosti, lepšie dynamické vlastnosti, odolnosť voči korózii. Medzi ich dobré vlastnosti patrí aj vysoká tvarová stálosť a fakt, že z nich možno vyrábať zložité diely jednorazovo alebo ich skladať z celkovo menšieho počtu dielov. Ich najdôležitejšou vlastnosťou je vysoká špecifická pevnosť, a to je aj jeden z dôvodov, prečo sú vystužené plasty vhodné pre aplikácie, ktoré musia vydržať nárazy. Ako výskum neustále napreduje, polymérne kompozity sú príslubom pre ešte rozmanitejšie a inovatívnejšie aplikácie, ktoré poháňajú pokrok v rôznych oblastiach [1].

2. ZÁKLADNÉ POJMY

Základná stavebná jednotka - Makromolekulové látky majú vysokú molárnu hmotnosť (desiatky tisíc až niekoľko miliónov), čo im dáva unikátne vlastnosti odlišné od nízkomolekulových zlúčenín. Ich štruktúra je charakterizovaná pravidelne sa opakujúcimi stavebnými blokmi, ktoré sú známe ako stavebná jednotka (mer) a súvisia s monomérmi použitými pri ich syntéze. Štrukturálna jednotka je najmenšia časť molekuly, ktorá sa pravidelne opakuje; niekedy je totožná so stavebnou jednotkou, ako pri polyvinylchloride (PVC) [1 - 4].

Monomér je organická molekula schopná chemicky reagovať s ďalšími molekulami za vzniku polymérov prostredníctvom procesu polymerizácie (obr. 1). Kľúčovou vlastnosťou monomérov je polyfunkčnosť, teda schopnosť vytvárať väzby aspoň s dvoma ďalšími molekulami, čím vznikajú buď lineárne reťazce, alebo zosieťované štruktúry. Monoméry s adičnými reakciami obsahujú dvojité väzby (napr. styrén) alebo cykly, zatiaľ čo kondenzačné polymerizácie sa vyskytujú medzi zlúčeninami s alkoholovými a kyslými skupinami, čo vedie k vzniku polyesterov či nylonu-6,6. Monoméry sú stavebné bloky polymérov, pričom ich usporiadanie a reakcie určujú vlastnosti výsledných materiálov [5-7].



Obr. 1 Polymerizácia [8].

Figure 1. Polymerization [8].

Polymér je molekula tvorená opakujúcimi sa jednotkami (monomérmi), ktoré tvoria dlhý reťazec. Tieto reťazce môžu byť jednoduché (napr. polyetylén) alebo zložité (napr. proteíny). Polyméry tvoria veľkú časť živých organizmov (proteíny, celulóza, nukleové kyseliny) a priemyselných materiálov (betón, sklo, plasty, guma). Kategorizácia polymérov je zložitá kvôli ich variabilnej štruktúre a vlastnostiam, preto sa delia podľa rôznych kritérií, ako sú pôvod, chemické zloženie alebo vlastnosti pri zaťažení [9 - 13].

Polyméry podľa elasticko-plastických vlastností delíme na [9 - 13]:

- **Termoplasty**, ktoré možno opakovane taviť a tvarovať, pričom si zachovávajú pôvodné vlastnosti. Medzi najznámejšie patria polypropylén (PP), polyetylén (PE) a polyvinylchlorid (PVC).
- **Reaktoplasty**, ktoré po vytvrdnutí nereagujú na opätovné zahrievanie. Tieto materiály sú známe svojou vysokou pevnosťou a odolnosťou, avšak majú obmedzenú pružnosť.
- **Elastoméry** sú primárne lineárne polyméry charakterizované nízkou úrovňou zosieťovania, ktorá spôsobuje prerušenie sekundárnych väzieb aj pri izbovej teplote. Elastoméry ako syntetický kaučuk, sú mimoriadne pružné a využívajú sa napríklad pri výrobe pneumatík či tesnení.

3. KOMPOZITY

Kompozitné materiály sú anizotropné a nehomogénne, vznikajú kombinovaním dvoch alebo viacerých materiálov s odlišnými vlastnosťami. Ich vlastnosti závisia od faktory ako typ vlákien, matrice, orientácia vlákien a spôsob výroby.

Kompozity majú vysoký pomer pevnosti k hmotnosti a ich zložky sú dobre rozlíšiteľné. Príkladom prírodného kompozitu je drevo, kde celulózové vlákna drží lignín, ktorý poskytuje väčšiu odolnosť [1, 13-14].

Medzi príklady kompozitných materiálov patria cement, betón, vystužené plasty, kovové a keramické kompozity. Sú široko využívané v inžinierskom priemysle, najmä v letectve, energetike a stavebníctve. Využívajú sa napr. aj v kozmických lodiach, ktoré musia odolávať extrémnym podmienkam [15].

Vystužujúce vlákna pre kompozity zahŕňajú:

- **Uhlíkové vlákna:** Vysoký pomer pevnosti k hmotnosti, používané v letectve a automobilovom priemysle.
- **Sklenené vlákna:** Efektívne a nákladovo dostupné, používané v lodných trupoch a automobilových komponentoch.
- **Armaidové vlákna (Kevlar):** Výnimočná pevnosť a odolnosť, používané v balistickej ochrane a letectve.
- **Prírodné vlákna:** Ekologické možnosti, ako ľan a konope, využívané v aplikáciách so zameraním na životné prostredie.
- **Čadičové vlákna:** Dobrá pevnosť a odolnosť voči teplote, používané v stavebníctve.
- **Polyetylenové vlákna:** Vysoká pevnosť, nízka hmotnosť, odolnosť voči chemikáliám, používané v lanách a ochranných prostriedkoch.
- **Kompozity s kovovou maticou:** Zlepšujú tuhosť a tepelnú vodivosť, používané v letectve a automobilovom priemysle.

- **Keramické matricové kompozity:** Odolnosť voči vysokým teplotám, používané v letectve a obrane.

3.1 Kompozity s polymérou matricou

Kompozity s polymérou matricou (PMC) pozostávajú z polymérov, ktoré tvoria spojitú matricu a vyztužené vlákna. Tieto materiály majú kľúčovú úlohu v zvyšovaní pevnosti a tuhosti kompozitov. Matrica zabezpečuje rovnomerné rozloženie vlákien a prenáša zaťaženie medzi nimi [17].

PMC sa delia na pokročilé a vyztužené kompozity, ktoré sa líšia pevnosťou a tuhosťou. PMC nachádzajú široké využitie, najmä v letectve, automobilovom priemysle a stavebníctve. Pokročilé kompozity, ako tie používané v leteckom priemysle, poskytujú vynikajúcu pevnosť a odolnosť voči korózii, ale ich vysoká cena a náročné výrobné procesy obmedzujú ich širšie použitie. Hlavnými výzvami PMC sú zlepšiť náklady na výrobu, odolnosť proti nárazu a problémy s delamináciou. Pri výrobe PMC je dôležité vyvinúť efektívnejšie výrobné metódy a zlepšiť ich mechanické vlastnosti.

3.2 Polypropylén

Polypropylén (PP), objavený v roku 1954, je ľahký lineárny polymér s nízkou hustotou. Vzniká polymerizáciou propylénového plynu a patrí do skupiny polyolefinov [1]. PP má podobné vlastnosti ako polyetylén, ale líši sa nižšou hustotou, vyššou prevádzkovou teplotou, väčšou tvrdosťou, odolnosťou voči praskaniu a chemickému napadnutiu, ale je náchylnejší na oxidáciu. Vyznačuje sa vynikajúcou odolnosťou voči priepustnosti plynov a vody, mechanickými vlastnosťami a tepelnou odolnosťou, čo ho robí vhodným pre výrobky, ktoré musia byť sterilizované, ako vedrá a fľaše. Je najuniverzálnejší plast používaný v priemysle, najmä v automobilovom sektore. PP je odolný voči atmosférickej oxidácii, ale podlieha fotodegradácii pri vystavení svetelnému žiareniu [1].

4. VÝROBNÉ TECHNOLOGIE

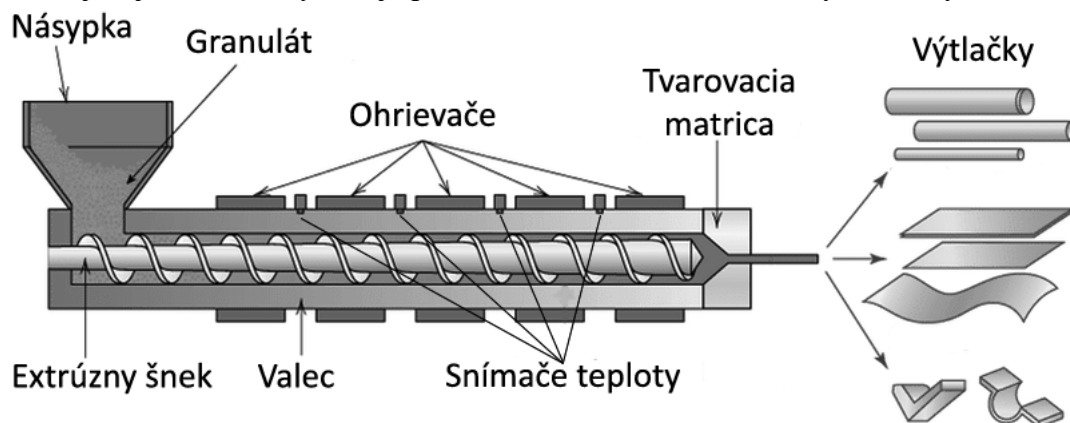
Termoformovanie - je proces, pri ktorom sa plastová fólia zahrieva na tvárnu teplotu, natiahne cez formu a po ochladení sa vytvára požadovaný tvar [18, 19]. Tento proces zahŕňa rôzne techniky, ako vákuové tvarovanie, tvarovanie rúšok, alebo tlakové tvarovanie.

Termoformovanie sa rýchlo rozvíja v plastikárskom priemysle vďaka pokrokom v materiáloch a výrobných metódach. Hlavné výhody sú nízke náklady na stroje, flexibilita v spracovaní rôznych materiálov a široké použitie v obalovom priemysle, doprave a medicíne. Nevýhodou je nerovnomerné zahrievanie a vysoké náklady na materiál. Používané materiály zahŕňajú PVC, PS, PET, PP, LDPE, HDPE, PC, PMMA a ABS, ktoré majú rôzne vlastnosti vhodné pre rôzne aplikácie, od obalov po automobilové diely a optické médiá.

Extrúzia je proces, pri ktorom sa materiál pod tlakom pretláča cez formu, čím vzniká kontinuálne tvarovaný produkt. Tento proces sa používa nielen na kovy a plasty, ale aj na potraviny, ako cestoviny alebo žuvačky [20].

Pri výrobe plastových strún sa plastový granulát taví a vytláča, pričom sa používajú vyhrievané valce a šnekový dopravník (obr. 2), ktorý zabezpečuje rovnomerné roztavenie

plastu a zabraňuje jeho úniku. Hlavné vlastnosti extrúzných strojov zahŕňajú vysoký výkon, rovnomerný transport taveniny a zabezpečenie jej fyzikálnych vlastností. Dôležité je tiež zabrániť korózii a degradácii materiálu, preto sú komponenty ako valec a šnek vyrobené z nehrdzavejúcej ocele. Pri výrobe je potrebné udržiavať konštantnú rýchlosť vytlačania.

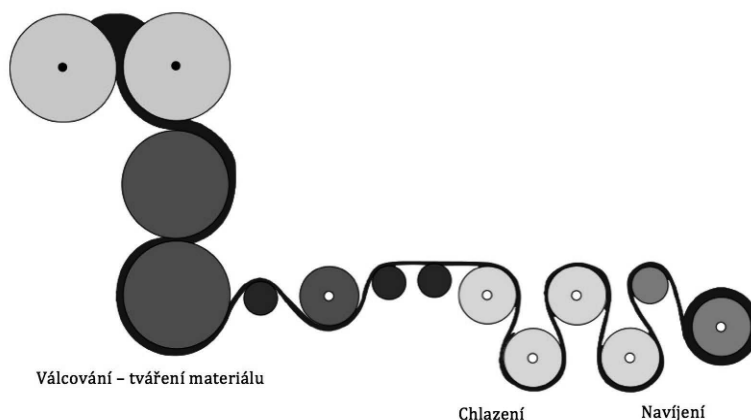


Obr. 2 Extrúzný stroj

Figure 2. Extrusion machine

Valcovanie, alebo kalandrovanie, je proces výroby súvislých pásov fólií, typicky s hrúbkou od 0,17 mm do 0,6 mm (pre PVC-U). Používa sa pri termoplastoch ako PVC-U, PVC-P a gumové materiály. Materiál sa spracováva medzi vyhrievanými valcami (obr. 3), ktoré vytvárajú rovnomernú hrúbku a povrch s možným vzorom [21-22].

Tento proces je menej tepelne náročný ako extrúzia, čo ho robí ideálnym pre výrobu PVC fólií s nižším obsahom stabilizátorov a kaučukových zmesí. Kalandrovacie linky, vybavené štyrmi valcami, sú jednými z kapitálovo náročnejších zariadení v priemysle a sú efektívne pri výrobe fólií, kože a podobných materiálov.



Obr. 3 Kaladrovacia linka [21].

Figure 3. Calendering line [21].

POĎAKOVANIE

Príspevok vznikol v rámci riešenia spoločného slovensko-poľského projektu Project Based Learning ako výsledok spolupráce medzi Politechnikou Slaskou, Gliwice a Žilinskou univerzitou v Žiline a projektov KEGA č. 004ŽU-4/2023 a KEGA č.016ŽU-4/2023.

BIBLIOGRAPHY

1. Liptáková, Tatiana, a iní. Polymérne konštrukčné materiály. 2012.
2. Běhálek, Luboš. Polymery. s.l. : Code Creator, s.r.o., 2016.
3. Fričová, Oľga. Polymérne materiály. Košice : s.n., 2019.
4. Macuráková, Viktória. PŮDNÍ HYDROGELY FUNGUJÍCÍ NA PRINCIPU ŘÍZENÉHO UVOLŇOVÁNÍ. Brno : s.n., 2017.
5. McMahon, Bryan. What is monomer? study.com. [Online] 14. 4 2022. <https://study.com/learn/lesson/monomer-types-examples.html>.
6. Augustyn, Adam. Monomer. www.britannica.com. [Online] 2023. <https://www.britannica.com/science/monomer>.
7. What is Monomer? <https://byjus.com>. [Online] 2019. <https://byjus.com/chemistry/monomers/>.
8. Smith, Sophia. Polymerization Monomers and Polymers Quiz. <https://www.proprofs.com/quiz-school/quizzes/polymerization-monomers-and-polymers-quiz>. [Online] 16. 8 2023. <https://www.proprofs.com/>.
9. Švorčík, Václav. Struktura a vlastnosti polymerů.
10. Perkins, Sid. Explainer: What are polymers? <https://www.snexplores.org>. [Online] 13. 10 2017. <https://www.snexplores.org/article/explainer-what-are-polymers>.
11. Cosmos. What is polymer? <https://cosmosmagazine.com>. [Online] 2. 6 2021. <https://cosmosmagazine.com/science/explainer-what-is-a-polymer/>.
12. Britannica. Polymer. <https://www.britannica.com>. [Online] 5. 3 2024. <https://www.britannica.com/science/polymer/Synthetic-polymers>.
13. Bradford, Alina. What is a Polymer? <https://www.livescience.com>. [Online] 14. 10 2017. <https://www.livescience.com/60682-polymers.html>.
14. Williams, Jim. The science and technology of composite materials. <https://www.science.org.au>. [Online] <https://www.science.org.au/curious/technology-future/composite-materials>.
15. Krizberg, Juris a Gutakovskis, Viktors. KOMPOZITNÉ MATERIÁLY. 2016.
16. Jawaid, Mohammad, Thariq, Mohamed a Saba, Naheed. Durability and Life Prediction in Biocomposites, Fibre-Reinforced Composites and Hybrid Composites. s.l. : Copyright © 2019 Elsevier Ltd. All rights reserved, 2019. 978-0-08-102290-0.
17. Brabazon, Dermont. Encyclopedia of Materials: Composites. s.l. : Copyright © 2021 Elsevier Inc. All rights reserved, 2021. 978-0-12-819731-8.
18. Kutz, Mayer. Applied Plastics Engineering Handbook. s.l. : Copyright © 2011 Elsevier Inc. All rights reserved, 2011. 978-1-4377-3514-7.
19. Nasim, Uddin. Developments in Fiber-Reinforced Polymer (FRP) Composites for Civil Engineering. s.l. : Copyright © 2013 Woodhead Publishing Limited. All rights reserved, 2013. 978-0-85709-234-2.

20. Török, Jozef. NÁVRH A VÝROBA EXTRUZNÍHO STROJE PRO VÝROBU. <https://dspace.vut.cz>. [Online] 2020.
<https://dspace.vut.cz/server/api/core/bitstreams/7b853f6a-8001-4af8-afed-d740bf2be510/content>.
21. Ausperger, Aleš. Technologie zpracování plastů. s.l. : © Code Creator, s.r.o.; distribuce publi.cz; 2016, 2016. 978-80-88058-77-9.
22. Sova, Miloš. Charakteristika kalandrování termoplastů. 2015.



31th January 2025
Gliwice, Poland

DEPARTMENT OF ENGINEERING MATERIALS AND BIOMATERIALS
FACULTY OF MECHANICAL ENGINEERING
SILESIA UNIVERSITY OF TECHNOLOGY

INTERNATIONAL STUDENTS SCIENTIFIC CONFERENCE

Comparison of natural and hydroponic farming – advantages, disadvantages, and development prospects

Karolina Hanzlik^a, Monika Kruczyńska^a, Estera Nawrocka, Paweł Kruczyński, Grzegorz Pośpiech, Aneta Kania^b, Anna Włodarczyk-Fligier, Magdalena Polok-Rubiniec

^a Student of Silesian University of Technology, Faculty of Chemistry
email: kh301171@student.polsl.pl, mk304249@student.polsl.pl

^b Silesian University of Technology, Faculty of Mechanical Engineering, Department of Engineering Materials and Biomaterials
email: aneta.kania@polsl.pl

Abstract: In the face of a growing global population, climate change, and environmental degradation, the search for alternative plant cultivation methods is becoming crucial. In response to these challenges, hydroponics – a method of growing plants without soil – is emerging as a promising alternative to traditional agricultural methods. The aim of this document is to compare hydroponics and conventional farming in terms of cultivation technologies, water and energy efficiency, environmental impact, and crop productivity. It also addresses the challenges associated with initial investment and maintenance costs, as well as the future role of both approaches in agriculture.

Keywords: hydroponics, conventional agriculture, sustainable development

1. INTRODUCTION

Agriculture is a key and indispensable sector of the economy, forming the basis of humanity's food supply [1]. Conventional farming requires large areas of land specifically designated for cultivation, as well as soil, and is associated with intensive water consumption and a negative impact on human health and the environment due to excessive use of fertilizers, pesticides, and herbicides [1,2].

In light of the projected population growth, expected to reach 9.8 billion by 2050, the challenge of ensuring sufficient food and living space for this population arises [3]. Current issues such as hunger in many regions of the world, limited availability of fertile land, environmental degradation, climate change, and ongoing urbanization drive the search for alternative farming methods. To address these challenges, it is necessary to implement modern agricultural technologies that maximize resource utilization, increase production efficiency, and reduce the environmental footprint [1,3].

One solution gaining importance is hydroponics – a system of growing plants using soilless substrates. In hydroponic farming, plants are nourished with water-based solutions rich in nutrients essential for their growth. By eliminating the need for soil, the "farming" area required is significantly smaller compared to traditional farming, leading to reduced water demand. Additionally, an advantage of this method is the ability to continuously monitor environmental conditions, allowing for year-round cultivation. Circulatory systems not only save up to 90% of water but also keep nutrients within the system, reducing their consumption and preventing nitrates and phosphates from fertilizers from entering the environment [4].

2. TECHNOLOGY AND ENVIRONMENTAL COMPARISON

2.1. Cultivation technology

Traditional farming relies on soil as the primary medium for plant growth. It requires regular irrigation, fertilization, and pest control [1]. Additionally, it is more vulnerable to changing climatic conditions, which can negatively affect the quality and quantity of crops as well as the stability of production [5]. Furthermore, traditional agriculture demands large areas of land, and using soil as a source of nutrients necessitates crop rotation to maintain its fertility [3].

In contrast, hydroponics involves growing plants in a nutrient-rich water solution tailored to their needs, without the use of soil. This method utilizes advanced control systems that allow precise monitoring and regulation of key parameters, such as temperature, humidity, and water levels, providing optimal conditions for plant growth [1]. Moreover, cultivation in controlled environments enables plant growth in any climate, eliminating the adverse effects of unfavorable weather conditions on crop quality and yield [5]. Hydroponics also allows for more efficient use of space by utilizing both horizontal and vertical surfaces [3].

2.2. Water usage

Conventional agriculture accounts for approximately 70% of global freshwater consumption, primarily due to the need for crop irrigation. Unfortunately, this water is not reused, as traditional farming systems lack water recirculation, leading to significant losses and waste [5]. This is a critical drawback, especially in the face of a growing population and intense urbanization, which increase the volume of wastewater. Such wastewater cannot be fully treated and reintroduced into the cycle, further depleting potable water resources [1].

Despite the enormous water consumption, irrigated land constitutes only 17% of the total agricultural area, yet it provides 30–40% of the world's food supply. In the context of the increasing water deficit and United Nations (UN) forecasts indicating that by 2025 approximately 40% of the global population will live in water-scarce areas, such high usage is disproportionate to the yields achieved [1].

In response to these challenges, hydroponics emerges as a far more water-efficient alternative. Hydroponic systems enable water recirculation, reducing water usage by up to 95% compared to conventional farming [1]. By delivering water directly to plant roots and using closed containers, losses due to soil absorption and evaporation are eliminated [5]. Moreover, water used in hydroponics can come from treated wastewater, further alleviating pressure on freshwater resources [1].

2.3. Energy consumption

In traditional agriculture, energy consumption is relatively low, amounting to approximately 1,100 kJ/kg annually for lettuce cultivation. Most of this energy is derived from fuels used to power agricultural machinery and irrigation pumps [6].

Higher energy consumption is observed in traditional greenhouse farming, where energy is primarily used to maintain appropriate temperature and lighting conditions. For instance, a 1,050 m² greenhouse in Mexico required 32,228.76 kWh of energy annually for heating when temperatures dropped below 12 °C [1].

Compared to the energy demand of hydroponics, this consumption is not as significant. In hydroponic systems, most energy is used to maintain optimal temperature, provide artificial lighting, and power water pumps that ensure water circulation and nutrient delivery to plants [1,6].

For example, in the case of lettuce cultivation over an area of 866.56 m² in a hydroponic system, the annual energy consumption was approximately 90,000 kJ/kg. Such systems require greater energy inputs than traditional farming, primarily due to the more intensive management of the microclimate within greenhouses [6].

2.4. Environmental impact

Traditional agriculture has numerous negative effects on the environment, primarily due to the intensive use of pesticides, herbicides, and fertilizers. These practices lead to ecosystem degradation, loss of biodiversity, and soil quality deterioration. Additionally, the intensive use of agricultural land, combined with excessive chemical inputs, contributes to soil erosion and water pollution as runoff carries these substances into water bodies [1].

In contrast, hydroponics offers a more sustainable method of plant cultivation. The absence of soil eliminates the need for pesticides and herbicides, reducing the risk of environmental contamination [3]. Furthermore, hydroponic systems enable precise management of water and fertilizers, while water recirculation minimizes resource use and reduces the risk of environmental pollution. Hydroponics also avoids soil erosion and degradation since it does not rely on traditional land use. This is a significant advantage for environmental conservation, especially given the increasing pressure on land resources [1].

2.5. Cultivation efficiency

Hydroponic farming demonstrates a clear advantage in terms of efficiency compared to traditional plant cultivation. Hydroponic systems allow for significantly higher yields per unit area due to increased plant density and the optimization of growth conditions. For many crops, such as lettuce or tomatoes, the hydroponic method can deliver yields that are several times higher than those achieved through traditional farming, often exceeding a tenfold increase [1,6].

For instance, hydroponic lettuce cultivation yields are 11 times higher than those from conventional farming, reaching 41 ± 6.1 kg/m²/year compared to 3.9 ± 0.21 kg/m²/year in traditional cultivation [6].

3. ECONOMIC ASPECTS

3.1. Investment and maintenance costs

Soilless cultivation methods, such as hydroponics, require the purchase of specialized equipment and suitable space for cultivation. However, finding space can be simpler than with agricultural land, as hydroponics requires up to five times less space, which does not necessarily need to be agricultural land. Urban farming, gaining popularity through initiatives such as Parisian Garden Cultures (rooftop farming), Krakow's Community Gardens, and vertical farms in Moscow, allows for efficient use of space. An example is the Pasona company in Tokyo, which transformed an office building into an urban farm, allowing employees to grow plants like rice and tomatoes. Thus, hydroponics, as a method of plant cultivation in a controlled environment, significantly reduces the need for transporting food over long distances. In urban agriculture or cultivation near consumption centers, such solutions reduce greenhouse gas emissions associated with transportation, thereby lowering the carbon footprint of the entire food production process. This also allows for harvesting plants at their peak ripeness, enhancing their nutritional value and quality [7].

Limiting transportation also directly impacts logistical costs, such as fuel, storage fees, and the cost of refrigeration during transport. Moreover, the freshness of locally delivered products reduces the risk of losses due to spoilage during transport or storage [7,8].

Despite these benefits, hydroponics also has its drawbacks. Production generates significant waste (e.g., plastic), consumes large amounts of energy, particularly due to year-round artificial lighting. Hydroponic systems incur high costs and require advanced infrastructure, which comes with the risk of system failures. This necessitates the involvement of properly trained personnel to manage and maintain these systems in optimal condition [7,8].

On the other hand, conventional agriculture involves high investment costs, including the purchase of land, agricultural machinery, fertilizers, pesticides, herbicides, and irrigation systems. Land prices rise depending on the region, land availability, and its quality. Additionally, maintaining large agricultural areas entails management costs and regular expenses for fuel for machinery and irrigation systems. Fertilizers and plant protection products also become significant expenses on large fields. Traditional agriculture also requires crop rotation and pest and disease control measures, which incur additional investments. Climate change, soil erosion, and environmental pollution can significantly affect these crops, thereby increasing production costs [9].

3.2. Perspectives and future of both methods

Hydroponics, a modern method of soil-free plant cultivation, is gaining importance in the context of the future of agriculture. Its development is driven by increasing urbanization, climate change, and the need for sustainable use of natural resources. Thanks to its high resource efficiency, particularly in cities and regions with limited natural resources, hydroponic systems use up to 95% less water, eliminate losses associated with soil erosion, and allow for year-round production independent of weather conditions. Examples of vertical farms in Tokyo, London, and New York demonstrate that hydroponics can effectively meet the needs of urban populations, reducing transportation emissions and food waste [7,8].

In contrast, conventional agriculture, despite its crucial role in global food supply, faces challenges such as soil degradation, intensive water usage, and negative environmental impacts. Traditional methods still dominate, but in order to meet the growing population, innovations

such as mechanization, regenerative agriculture, and precise resource management are necessary [9,10].

The future of agriculture will likely involve the integration of both approaches. Hydroponics will become a key solution in cities, while traditional methods, supported by modern technologies, will remain the foundation in rural areas. Hybrid solutions, like those used in the Netherlands, demonstrate the tremendous potential for synergy, enhancing efficiency and sustainability in the global food system [10].

4. SUMMARY

Hydroponics represents a promising alternative to traditional agriculture, offering numerous economic and environmental benefits. With its lower water consumption and more efficient use of space, it can be particularly advantageous in cities and regions with limited natural resources. Additionally, cultivation in controlled conditions allows for year-round production, regardless of changing climatic conditions. On the other hand, conventional agriculture, despite its dominant role in global food supply, involves significant water, fertilizer, and pesticide usage, as well as intensive land use, leading to soil degradation and environmental pollution. While hydroponics comes with higher initial costs and greater energy consumption, its ecological benefits and water-use efficiency make it a more sustainable option. The future of agriculture will likely involve the integration of both methods, ensuring a sustainable food production system where hydroponics supports urban development, while traditional agriculture, enhanced by modern technologies, remains essential in rural areas.

BIBLIOGRAPHY

1. D.I. Pomoni, M.K. Koukou, M.G Vrachopoulos, L. Vasiliadis, A Review of Hydroponics and Conventional Agriculture Based on Energy and Water Consumption, Environmental Impact, and Land Use, *Energies* 16(4) (2023) 1690.
2. M. Farvardin, M. Taki, S. Gorjian, E. Shabani, J.C. Sosa-Savedra, Assessing the Physical and Environmental Aspects of Greenhouse Cultivation: A Comprehensive Review of Conventional and Hydroponic Methods, *Sustainability* 16(3) (2024) 1273.
3. R.S Velazquez-Gonzalez, A.L. Garcia-Garcia, E. Ventura-Zapata, J.D.O. Barceinas-Sanchez, J.C. Sosa-Savedra. A Review on Hydroponics and the Technologies Associated for Medium- and Small-Scale Operations, *Agriculture* 12(5) (2022) 646.
4. A. Shouf, A. Alshrouf, Hydroponics, Aeroponic and Aquaponic as Compared with Conventional Farming, *American Scientific Research Journal for Engineering, Technology, and Sciences (ASRJETS)* 27(1) (2017) 247-255.
5. M. Kannan, G. Elavarasan, A. Balamurugan, B. Dhanusiya, D. Freedom, Hydroponic farming – A state of art for the future agriculture, *Materials Today: Proceedings* 68(6) (2022) 2163-2166.
6. G.L. Barbosa, F.D.A. Gadelha, N. Kublik, A. Proctor, L. Reichelm, E. Weissinger, G.M. Wohlleb, R.U. Halden, Comparison of Land, Water, and Energy Requirements of Lettuce Grown Using Hydroponic vs. Conventional Agricultural Methods, *International Journal of Environmental Research and Public Health* 12(6) (2015) 6879-6891.

7. A. Rutkowska-Gurak, Rolnictwo w mieście przyszłości? *Myśl Ekonomiczna i Polityczna* 1(76) (2023) 167-185.
8. Ł.M. Sokołowski, Uprawy i Hodowle Bezglebowe a Potrzeba Ochrony Gruntów Rolnych z Perspektywy Zapewnienia Bezpieczeństwa Żywnościowego, *Przegląd Prawa Rolnego* 1(28) (2021) 167-183.
9. B. Gołębiowska, Externalities of Aricultural Production and Their Influence on Farm Income, *Stowarzyszenie Ekonomistów Rolnictwa i Agrobiznesu, Roczniki Naukowe, Vol. XIII, No. 4.*
10. N. Nina, L. Lucas, K. Sridar, Vertical Farming Innovation in Urban Netherlands: Sustainable Solutions with Modern Hydroponics, *Techno Agriculturae Studium of Research* 1(1) (2024) 102-112.

This paper is the result of a Project Based Learning (PBL) entitled Development of a chamber for hydroponic plant cultivation and comparison of its efficiency to natural cultivation.



31th January 2025
Gliwice, Poland

DEPARTMENT OF ENGINEERING MATERIALS AND BIOMATERIALS
FACULTY OF MECHANICAL ENGINEERING
SILESIA UNIVERSITY OF TECHNOLOGY

INTERNATIONAL STUDENTS SCIENTIFIC CONFERENCE

Laser surface treatment

Martyna Herman^a, Eryk Badurski^a, Jakub Stęplewski^a, Mirosław Bonek^b

^aSilesian University of Technology, Faculty of Mechanical Engineering,
email: mh307613@student.polsl.pl, eb308177@student.polsl.pl, js308313@student.polsl.pl

^bSilesian University of Technology, Department of Engineering and Biomedical Materials,
Faculty of Mechanical Engineering
email: miroslaw.bonek@polsl.pl

Abstract: The article explores various laser surface modification techniques, including laser surface cladding, hardening, and shock peening, emphasizing their applications in improving wear resistance, mechanical properties, and durability of materials. It presents the underlying principles, benefits, and limitations of these methods while highlighting their use in industries like automotive, aerospace, and tool manufacturing. The study also includes examples of microstructural transformations and improved material properties achieved through these laser-based processes.

Keywords: laser surface cladding, laser surface hardening, laser shock peening

1. INTRODUCTION

Surface modification is a frequently used solution to improve the wear resistance of materials. It is a topic of significant importance according to current realities. It provides savings on strategic materials while helping to design superior components with desired surfaces and bulk properties. Many techniques are available for coating and modifying substrate surfaces, such as electrodeposition, physical vapor deposition, chemical vapor deposition, thermal spraying, laser surface treatment, etc. [1]

Each of these methods has its limitations, related to the substrate material, its geometry, film adhesion, and the possibility of thermal deformation, among others. Laser surface treatment (LST) overcomes most of these difficulties. It can be used on different types of geometries and materials, guaranteeing excellent coating adhesion and a limited heat-affected zone. In addition, the process is characterized by high repeatability and controllability, making it possible to precisely adjust the parameters to the requirements of the material being processed [2].

The laser beam, thanks to its excellent spatial resolution, is particularly suitable for precise deposition of coatings on miniature components. Various techniques are used in laser surface modification, such as laser surface remelting, laser surfacing, and laser surface alloying. The high power of the laser makes it possible to achieve temperatures sufficient to melt both the substrate and the reinforcing material, leading to strong metallurgical bonding [3].

Laser surface processing makes it possible to generate high heating and cooling rates and large thermal gradients. Such conditions promote the formation of meta-stable phases and the development of microstructures with unique properties that cannot be obtained using conventional processing techniques. As a result, it is possible to significantly increase the mechanical and corrosion resistance of the surface layers while maintaining the volumetric properties of the material [3].

Laser beams are used in surface modification of many materials. They are used to improve the properties of titanium [4], steel [5], copper [6], magnesium [7], and even polymers [8].

Laser surface treatment is widely used across industries where enhanced surface durability and wear resistance are critical. In the automotive industry, it is applied to components such as gears, camshafts, and crankshafts to improve their fatigue strength and extend operational life [9]. The aerospace sector utilizes its capabilities to protect high-stress components like turbine blades and landing gear against wear and surface degradation [10]. In aviation, it is used to repair and strengthen turbine blades and rotors, increasing the durability of these components under demanding operating conditions [11]. In the tool and die industry, it is used to harden cutting tools, molds, and dies, ensuring they withstand high pressures and abrasive environments [12]. Additionally, in heavy machinery and agricultural equipment, laser hardening reinforces parts like hydraulic cylinders and tillage tools, which endure significant mechanical stress [13].

2. EXAMPLES OF LASER SURFACE TREATMENT METHODS

2.1 Laser surface cladding

Laser Surface Cladding (LSC) is a method of modifying the surface of materials to significantly improve their properties by forming permanent metallurgical bonds between the coating and the substrate. LSC is widely used in cases requiring dissimilar surface and core material properties [2]. The process uses a laser beam to simultaneously melt the coating material and the surface of the substrate, resulting in a homogeneous, compact layer of high microstructure quality. High cooling rates in this process result in dense and homogeneous microstructures [14]. Figure 1 shows an example of this method [fig 1].

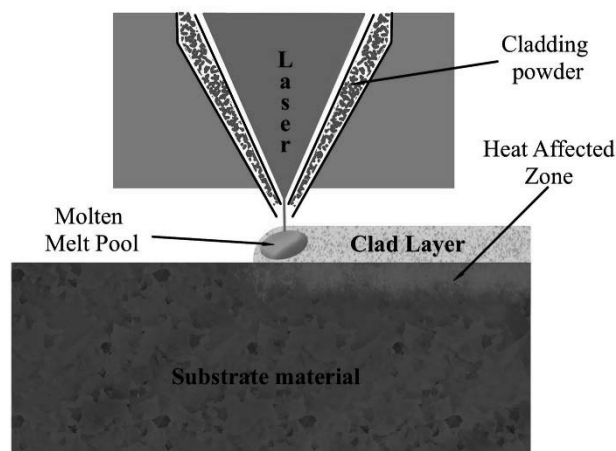


Figure 1. Scheme of laser surface cladding

The LSC process consists of several steps. The first step is surface preparation by removing contaminants and degreasing to ensure good adhesion of the coating material [15]. The powder is then uniformly applied to the surface using a nozzle, directing it precisely into the laser zone [16].

The laser beam melts the powder material and the top layer of the substrate forming strongly bonded layers with a homogeneous structure [17]. The final step is cooling the material and quality control to eliminate defects and ensure coating consistency.

There are two main powder feeding techniques for this process. The first involves applying powder to the surface in advance, which is then melted using a laser beam. The second method uses powder blown into the laser's point of influence on the surface, where it is melted and fuses with the substrate [4, 8].

Among the most important advantages of the technology is its high precision, which allows the formation of thin, homogeneous layers with minimal thermal effects on the base material [19]. Precise powder material dispensing reduces material losses, making the process more economical [20]. The versatility of the technology allows the use of a variety of powder materials, such as nickel alloys, cobalt, or ceramics [21].

The process also has limitations. It requires expensive, specialized laser equipment and is energy-intensive [21]. Making small parts using LSC is problematic [15]. Keeping the powder in place during laser operation is also a considerable problem [22].

2.2 Laser hardening

This multi-step process results in enhanced wear resistance and mechanical properties while preserving the material's core toughness. Laser hardening induces significant microstructural changes in the surface layers of treated materials, primarily transforming the existing structure into a martensitic phase. The rapid heating and self-quenching process caused by the laser beam results in the formation of fine-grained martensite, which significantly enhances the hardness and wear resistance of the material. [23]. Additionally, the process refines the grain structure at the surface, leading to residual compressive stresses, which improve the fatigue life of the component. [24]. The localized nature of laser hardening ensures minimal impact on the core microstructure, preserving its toughness while achieving a hardened surface layer with depths ranging from 0.1 to 2 mm [25]. These microstructural changes make laser hardening a highly effective surface treatment for improving the performance of components in demanding environments.

Laser hardening enables precise and localized treatment, allowing targeted hardening of specific areas without affecting surrounding material, thus minimizing thermal distortion [23]. Additionally, it is an environmentally friendly process, as it eliminates the need for quenching media and hazardous chemicals, reducing waste and energy consumption [26]. The method also enhances mechanical properties, such as surface hardness and fatigue resistance, through martensitic transformation [25]. However, laser hardening is not without limitations. The cost of the initial systems is high [23]. Furthermore, it has material limitations, as its effectiveness diminishes with non-ferrous or low-carbon steels, and the hardened layer depth is generally limited to 0.1–2 mm [24]. Despite these challenges, advancements in automation and laser technology continue to expand its applicability in modern manufacturing processes.

Laser hardening is a precise process involving several critical steps. The process begins with surface preparation, where the material is cleaned to remove contaminants, ensuring optimal laser energy absorption [27]. The next step involves adjusting the laser parameters, which are tailored to the specific material and desired hardening depth [28].

During the heating phase, the laser raises the material surface temperature. For steel the austenitization range [29]. This is immediately followed by self-quenching, where heat dissipates into the cooler core, rapidly cooling the surface and forming a hardened martensitic layer as shown in Figure 2 (fig2.) below

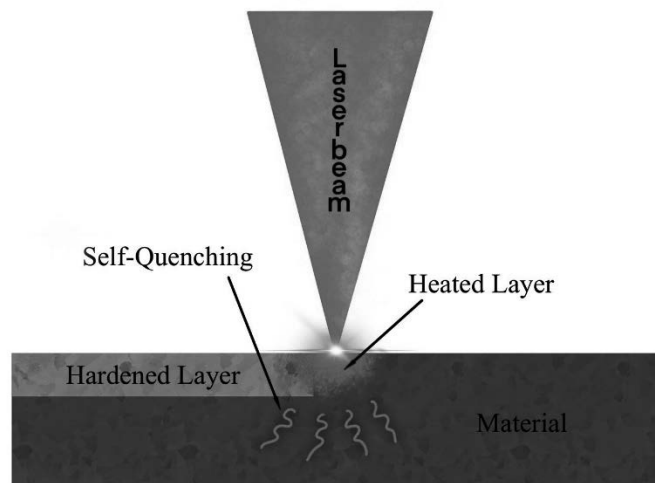


Figure 2. Principle of laser hardening

2.3 Laser Shock Peening

The Laser Shock Peening (LSP) method is a modern surface treatment technique that uses laser pulses to introduce compressive residual stresses into the surface of metallic materials. LPS involves applying high-energy short-pulse laser treatment to the metal surface, generating a powerful shock wave pressure. This process results in ultra-high strain rate plastic deformation and introduces deeper residual compressive stresses, inducing grain refinement and nanosizing [31].

Using LSP leads to enhance wear resistance, corrosion resistance, and mechanical strength [32]. However, the process has some limitations. The generation of high-energy laser beams and the associated systems involve substantial costs, which restrict the widespread industrial adoption of LSP [33]. Additionally, precise control over laser power, pulse duration, and optical systems is required, increasing the risk of errors and limiting productivity [34]. Excessive laser energy can also result in localized overheating or microstructural damage [35].

LSP is particularly effective for improving the properties of materials such as aluminum [36], titanium [37], high-strength steels [38], and various other metals [39]. The first step involves applying a protective coating to the surface of the target material. This layer prevents thermal damage and aids in generating effective shock waves. Following this, a transparent medium, typically water, is introduced to contain the plasma formed during the laser pulse. This containment amplifies the pressure of the shock wave on the material's surface. A high-energy pulsed laser beam is then aimed at the target area, with laser parameters adjusted based on the specific properties of the material [40]. Scheme of LSP can be seen below – Fig. 3.

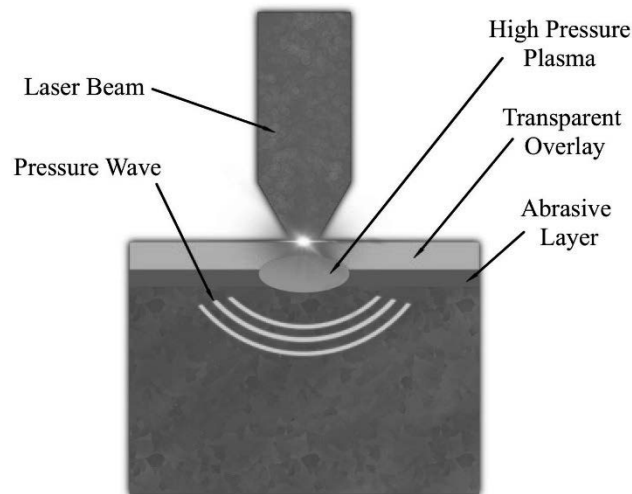


Figure 3. Principle of laser shock peening

When the laser energy strikes the material's surface, it rapidly heats the area, causing plasma formation. The rapid expansion of this plasma produces high-pressure shock waves that penetrate the material, inducing compressive residual stresses beneath the surface. These stresses mitigate tensile stresses, thereby improving the material's fatigue resistance. The localized plastic deformation enhances the material's mechanical characteristics, such as its resistance to fatigue and cracking. Maintaining precise control of laser parameters is essential to prevent unwanted effects, such as melting or surface damage [41].

Once the LSP process is complete, the treated surface is examined to verify the desired improvements. Advanced evaluation techniques, including X-ray diffraction (XRD) and ultrasonic testing, are frequently utilized to assess the results [42].

Main advantages of LSP: modifies the inherent properties of the base material without adding external material, ensuring homogeneity and avoiding potential issues like layer delamination [43]. Unlike traditional peening methods that use media, LSP is a clean process with no risk of surface contamination [44] and also can treat intricate shapes and hard-to-reach areas effectively [45].

3. CONCLUSIONS

Laser surface modifications, such as surfacing, hardening and peening, enable significant improvements in the mechanical and chemical properties of materials while maintaining their volumetric integrity. Due to their precision and control, these processes are used in sectors such as automotive and aerospace, where they increase the durability and wear resistance of components. Laser surfacing creates homogeneous, metallurgically bonded layers, while hardening strengthens the surface by introducing martensite, and peening introduces compressive stresses, improving fatigue and corrosion resistance.

ACKNOWLEDGEMENTS

The work was created as a part of project of Students Scientific Circle of Laser Surface Treatment under the Initiative of Excellence - Research University, Silesian University of Technology, Gliwice, Poland.

BIBLIOGRAPHY

1. Dziarski, P., et al., The Impact of Laser Beam Power on the Microstructure and Some Mechanical Properties of Laser-Alloyed Inconel®600 with WC Particles, *Materials*, 2023.
2. Qiu, J., et al., Applications of Surface Technologies, *Progress in Surface Science*, 2020.
3. Thakur, P., Microstructural Analysis in Manufacturing, *Wear*, 2017.
4. Blažek, S., Effects of Surface Coatings, *Thin Solid Films*, 2005.
5. Steen, W. M., et al., Laser Surface Treatment of Tool Steels, ResearchGate Publication, 2002.
6. Singh, P., Nanostructured Coatings: Advances in Thin Films, *Applied Surface Science*, 2011.
7. Wang, T., et al., Innovations in Chemical Surface Engineering, *Frontiers in Chemistry*, 2022.
8. Harris, B., Novel Theoretical Models in Composite Formation, arXiv Preprint, 2021.
9. Trzepieciński, T., et al., New Advances in Forming Technology of Hybrid Composites, *Journal of Composites*, 2021.
10. Wang, J., et al., Applications of Laser Surface Treatment in Gears, *Journal of Materials Engineering and Performance*, 2024.
11. Costa, M. M., Surface Science in Engineering Applications, *Materials Chemistry and Physics*, 2024.
12. Ion, J., Laser Processing of Engineering Materials, Elsevier, 2005.
13. La Rocca, A. V., Laser Applications in Manufacturing, *Scientific American*, 1982.
14. Marquez, J., Photonics and its Technological Impact, *Optics and Laser Technology*, 2023.
15. Kumar, V., et al., Laser Surface Alloying Techniques, *International Journal of Surface Engineering*, 2024.
16. Lee, H. J., Protective Coatings for Engineering Applications, *Coatings*, 2024.
17. Anderson, M., Material Characterization Studies, SSRN Preprint Paper, 2025.
18. Costa, M. M., Laser-Induced Surface Hardening Studies, *Journal of Materials Science*, 2024.
19. Sharma, R., Advanced Techniques in Surface Engineering, *Applied Sciences*, 2024.
20. Lee, H. J., Corrosion Resistance Studies, *Coatings*, 2024.
21. Kumar, V., et al., Surface Strengthening Techniques, *Surface Engineering Advances*, 2024.
22. Gupta, P. K., Microscopic Investigation of Advanced Surfaces, *Optics and Laser Technology*, 1994.
23. Schübler, P., et al., Comparison of Multiline Laser Surface Hardening and Induction Hardening, *NETSUSHORI*, 2024.
24. But, A., et al., Material Challenges in Laser Hardening, *Key Engineering Materials*, 2024.

25. Vindokurov, I., et al., Effects of Laser Surface Hardening, ResearchGate, 2024.
26. Wang, Z., et al., Laser Cutting Technology Routes for Integrated Hot Stamping, Atlantis Press, 2024.
27. Gómez-Ortega, A., et al., The Scratch Resistance of Plasma-Assisted DUPLEX-Treated Stainless Steel, Coatings, 2024.
28. Yang, H., et al., Effect of Laser Remelting on Microstructure and Properties, Surface and Coatings Technology, 2024.
29. Mondragon Rodriguez, G., et al., The Effect of Temperature on Plasma Nitriding Properties, SSRN, 2024.
30. Nemani, A. V., et al., Advancements in Additive Manufacturing for Copper-Based Alloys, ProQuest, 2024.
31. Li, J., et al., Molecular dynamics simulation of microstructural evolution and mechanical behavior of titanium alloy subjected to laser shock peening, Opt Laser Technol, 175, Article 110748, 2018.
32. Raad M., Abed: "Vol. 23 No. 1 (2024): THE IRAQI JOURNAL FOR MECHANICAL AND MATERIALS ENGINEERING".
33. Amegadzie, M., Fatigue Strength Improvement of an Aluminium Powder Metallurgy Alloy Using Ultrasonic Pulsed Waterjet Peening, Proceedings of the 63rd Conference of Metallurgists, SPRINGER INTERNATIONAL PU, 2024.
34. Qin, R., Laser Shock Peening: Performance and Process Simulation, Deciphering Laser Shock Peening Quality Monitoring, Woodhead Publishing, 2006.
35. Wang, D., et al., Effect of Layer-Wise Femtosecond Laser Shock Peening on Cracking Growth, Springer Berlin Heidelberg, 2015.
36. Liu, P., et al., Control and Modelling of Laser Shock Peening without Coating (LSPwC) Texture of AISI 9310 Steel, PubMed, 2024.
37. Khanigi, A.F., et al., Effect of Power Density on Microstructure Characterization and Fatigue Behavior of Laser Shock Peened Rene-80 Ni-Based Superalloy, Optics & Laser Technology, 2024.
38. Yu, W., et al., Simulation and Analysis of Residual Stress in 17-7 PH Stainless Steel Welded Joints Using Laser Shock Peening Technology, Front. Mater., 2024.
39. Wakchaure, M. B., et al., A Comprehensive Review on Finite Element Analysis of Laser Shock Peening, University of Nevada, Reno, NV 89557, USA 2024.
40. Verezhak, M., et al., Application of Deep Learning for Technological Parameter Optimization of Laser Shock Peening of Ti-6Al-4V Alloy, Frattura ed Integrità Strutturale, 2024.
41. Maharjan, N., et al., Post-processing of cold sprayed Ti6Al4V coating by laser shock peening, Journal of Materials Processing Technology, Volume 330, 2024.
42. Maleki, E., et al., Surface Post-Treatments for Metal Additive Manufacturing: Progress, Challenges, and Opportunities, Post-Processing Techniques for Additive Manufacturing, 2023.
43. Zheng, M., et al., Microstructure Evolution and Mechanical Properties of Refractory High-Entropy Alloy Nitride Film, Surface and Coatings Technology, Volume 483, 2024.
44. Cheng, W., et al., FEM-ANN Coupling Dynamic Prediction of Residual Stresses Induced by Laser Shock Peening of TC4 Titanium Alloy, Optics & Laser Technology Volume 179, 2024.
45. Bowen, Z., et al., Applications of Laser Surface Treatment in Gears: A Review, ASM International, 1998.



31th January 2025
Gliwice, Poland

DEPARTMENT OF ENGINEERING MATERIALS AND BIOMATERIALS
FACULTY OF MECHANICAL ENGINEERING
SILESIA UNIVERSITY OF TECHNOLOGY

INTERNATIONAL STUDENTS SCIENTIFIC CONFERENCE

Optimization of Urban Transport Systems Based on a Mobility Study

Valeri Jajanidze^a, Boris Gitolendia^a, Giorgi Mikiashvili^b

^a Georgian Technical University, Faculty of Transport Systems and Mechanical Engineering Associate Professor; E-mail: vl.jajanidze@gtu.ge

^a Georgian Technical University, Faculty of Transport Systems and Mechanical Engineering Associate Professor E-mail: boris.gitolendia@gtu.ge

^b Georgian Technical University, Faculty of Business Engineering E-mail: giorgi.mikiashvili@gtu.ge

Abstract: The efficient functioning of an urban transport system is determined by the quantitative, qualitative, and interdependent parameters of available transportation means and infrastructure. The effective use of moving assets is influenced by the cause-and-effect relationship in transport system development and the "transport psychology" of its users, including passengers, drivers, and pedestrians. This includes decisions on transport modes, duration of use, trends in and frequency of alternative transport modes, specific route parameters, and more.

This paper examines a modern model for studying urban transport systems and presents the results of conducted research. Based on these findings, the current state, developmental trends, and potential future scenarios for urban transport systems are identified. The implementation of these findings will enhance the optimization of urban transport systems and improve the convenience of their use for citizens.

Keywords: Transport; Mobility; Household; Public Transport; Questionnaire.

1. INTRODUCTION

The primary function of an urban transport system is to fully meet the mobility needs of the population, which necessitates ensuring its optimal functioning. The design and operation of modern urban transport systems differ significantly from the approaches of the 20th century, which prioritized the seamless movement of motor vehicles, metros, trams, trolleys, and private cars, demanding infrastructure development accordingly.

Today, the focus has shifted toward integrating non-traditional modes of transport such as bicycles, mopeds, scooters, electric skateboards, and motorcycles, alongside promoting shared and rental transportation services. Urban transport systems are analysed for their efficiency in linking all areas of a city. However, the systems must also address problems such as traffic congestion and environmental safety.

Given these challenges, optimizing urban transport systems through the development of sustainable urban mobility plans has become increasingly relevant. Such plans prioritize transportation efficiency, safety, environmental impact, and equitable conditions for all types of transport users.

Traditional vs. Sustainable Urban Mobility Planning:

Traditional transport system planning involves:

- Defining a dominant mode of transport;
- Developing infrastructure exclusively for the dominant mode;
- Aligning road infrastructure to cater to the dominant mode;
- Influencing user behavior to favor the dominant mode.

This approach often overlooks the needs of users of other transport modes, leading to infrastructure overload and operational inefficiencies.

In contrast, sustainable urban mobility planning includes:

- Equal development of all transport modes;
- Infrastructure development for all types of transport;
- Encouraging the use of non-traditional transport modes;
- Studying urban mobility needs of the population;
- Reducing the negative impacts of transport systems on the environment and users.

The key criterion for optimizing urban transport systems in the modern era is the development and implementation of a sustainable mobility plan. However, in cases where mobility needs are still met using traditional approaches, it may be necessary to evolve traditional transport models incrementally to align with sustainable mobility goals.

One of the advantages of a sustainable mobility plan is the elimination of discriminatory approaches among transport modes and population groups. This requires comprehensive research into urban mobility needs, the preparation of appropriate methodologies, and their practical implementation.

The first step in studying urban mobility involves developing a relevant questionnaire, defining interview methods, and determining delivery methods. For this research, focused on Tbilisi residents, mass surveys were chosen as the method.

The mass survey process includes:

1. Developing research hypotheses and selecting tools (questionnaires or interviews);
2. Conducting a pilot study;
3. Sampling participants;
4. Data collection;
5. Statistical analysis of data;
6. Preparing a research report detailing findings and their interpretation.

The questionnaire topics include:

- Household information: family size, vehicle ownership (quantity and type), income, mobility with or without private cars;
- Personal information of respondents and family members: occupation, education, vehicle ownership, mobility with and without private cars;
- Survey day characteristics: selected day, its similarities or differences from a standard day, and mobility patterns;
- Mobility details: travel duration, purpose, direction, transport modes used, and whether travel involved companions.

For a comprehensive household study, Tbilisi was divided into 10 districts, further subdivided into 30 study zones. The target was to survey 1,000 individuals (approximately 330-350 households), with the proportional distribution of respondents across zones presented in Tab. 1.

Table 1

#	District	Population	percentage Distribution	Number of Respondents per District	Number of Households to Survey per District
1	Samgori	168801	14%	140	47
2	Gldani	164229	14%	140	47
3	Nadzaladevi	161088	14%	140	47
4	Saburtalo	151060	13%	130	43
5	Isani	137588	12%	120	40
6	Vake	113215	10%	100	33
7	Chugureti	78060	7%	70	23
8	Didube	73227	6%	60	20
9	Mtatsminda	61194	5%	50	17
10	Krtsanisi	56734	5%	50	17
სულ		1165196	100%	1000	334

Although the number of individuals and families to be surveyed in the city's districts was predetermined, the study was conducted using a **random sampling method**. This involved selecting random points on Google Maps and surveying participants in the surrounding area, which significantly enhanced the reliability of the research results.

During the research process, a **histogram of the primary data** was developed and used to assess the alignment of the actual survey count with the targeted numbers.

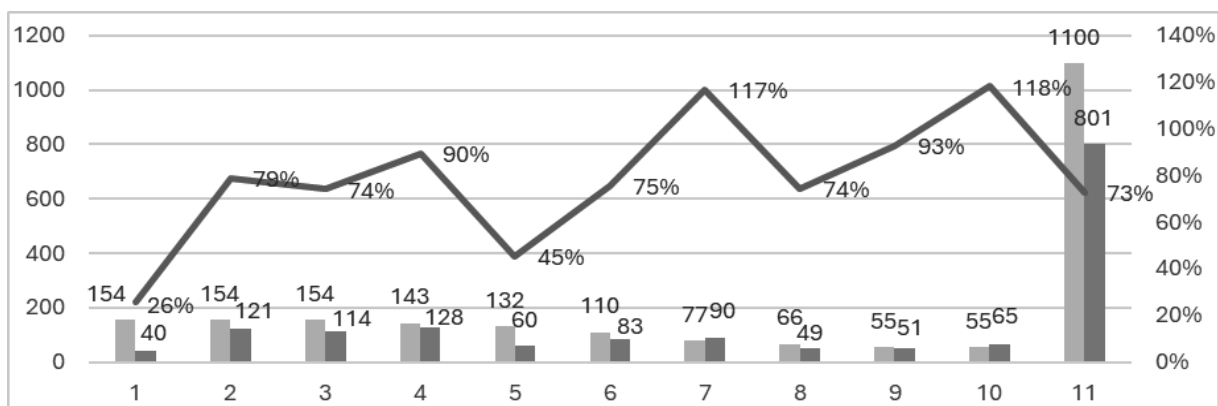


Fig. 1. Histogram of Processed Current Data

The purpose of the study was to identify the demand for transport mobility among the population of Tbilisi and the preferred transport modes for meeting their mobility needs, considering traffic and environmental safety of the surveyed households:

- 30% own 1 vehicle,
- 6% own 2 vehicles, and
- only 0.5% own 3 vehicles.

Additionally, 5% of the surveyed households use corporate vehicles. Approximately 9% of households own motorcycles, mopeds, or scooters.

Thus, it can be inferred that the remaining households rely on shared/rented transport services or public transport to meet their mobility needs. Therefore, it is important to study the accessibility of public transport in the context of geographical location, specifically the distance between boarding/disembarking points and residential areas. The study of this parameter is presented in Histogram 2.

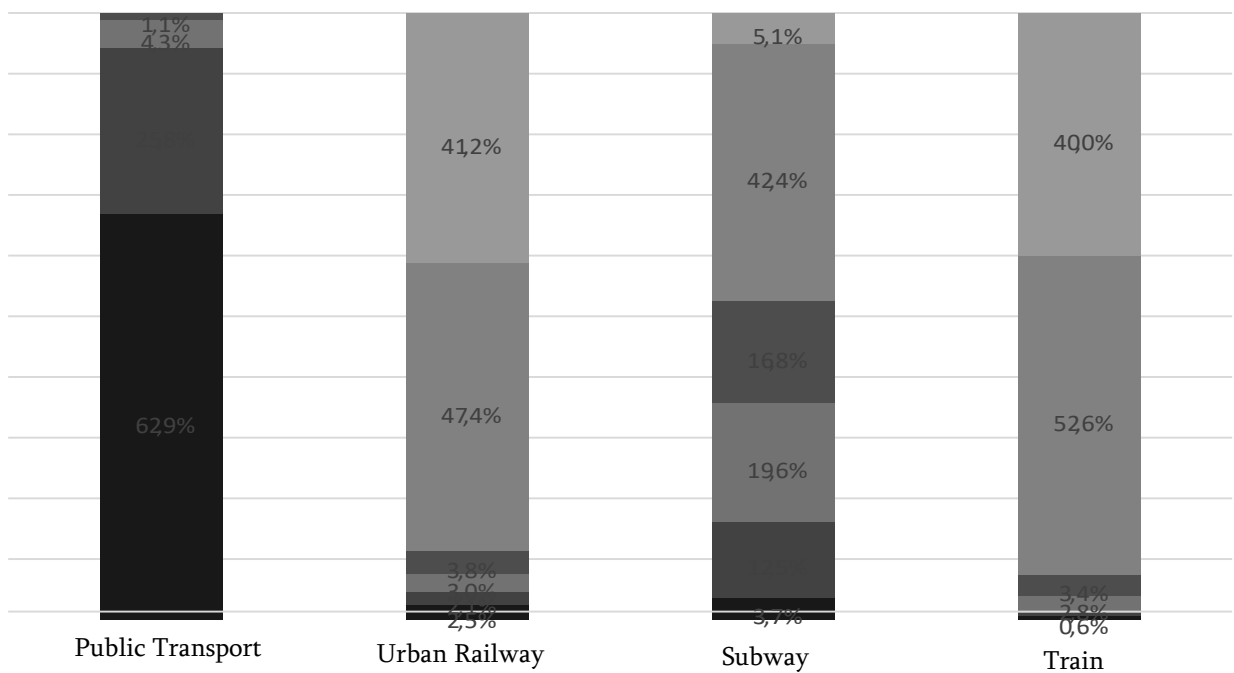


Fig. 2. Distance of public transport boarding/disembarking points from residential areas, based on travel time: 1-5 minutes, ■ 6-10 minutes, ■ 11-15 minutes, ■ 16-20 minutes, ■ 20 minutes or more.

It should be noted that the location of urban bus stops is convenient in 94% of cases, with residents needing an average of 3-7 minutes to reach the stop. Only 4.3% require 11-15 minutes to reach a stop, and an even smaller percentage, 1.1%, need 20 minutes or more. This allows us to conclude that, from the perspective of urban planning, this mode of transport is favorable for fulfilling the mobility needs of the population.

Based on the study's objectives, the demand for various modes of transport within the city's transport system to facilitate mobility was determined. A questionnaire covering relevant topics was developed, and the results of the study are presented in the form of the corresponding histogram.

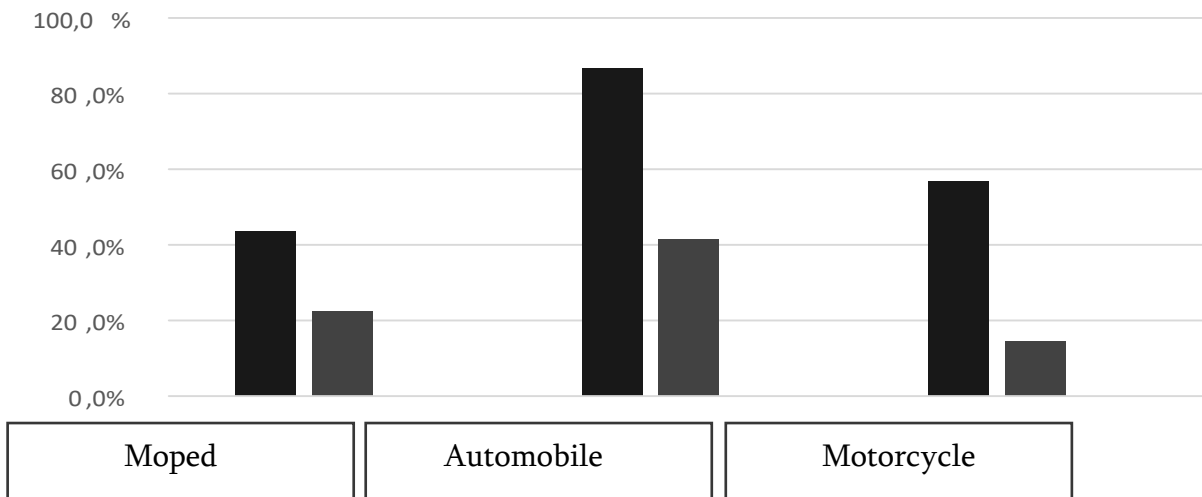


Fig. 3. Percentage of Population with Driving Licenses in Households, by Gender:
 ■Male, ■Female.

Based on the presented histogram, it can be concluded that in addition to motor vehicles, it is essential to prioritize the development of infrastructure required for the safe use of mopeds, bicycles, and motorcycles. This is particularly important because the analysis of research results revealed that over 30% of the city's population makes at least three trips a day in different directions and using different modes of transportation. Of these, the third trip is often a short-distance circular movement on foot or using bicycles, scooters, or electric skateboards.

CONCLUSION

Meeting the mobility needs of modern urban residents requires approaches that simultaneously reduce pollution levels in the city's ecosystem and ensure mobility with high safety and comfort standards. Such objectives cannot be achieved using traditional methods of urban transport system management. Therefore, the focus must be on modifying the existing transport system in line with the requirements of sustainable mobility planning.

The key starting point is the study of the city's residents' capabilities and needs, which serves as one of the most effective means of identifying so-called stable and generated mobility indicators.

Based on the study conducted in Tbilisi in 2022, the main indicators of a sustainable urban mobility plan were identified, including:

- Preferred types of transport;
- Types and number of vehicles owned by residents;
- Residents' readiness and ability to operate specific types of transport;
- Accessibility and comfort of public transport;
- Mobility behavior of residents during the day.

From these indicators, it can be concluded that optimizing the city's transport system should involve the development of a sustainable urban mobility plan. This approach will allow for the development of infrastructure for all types of transport citywide and eliminate discriminatory practices among transport modes.

ACKNOWLEDGEMENTS

The work was created as a result of the project as part of project based learning - PBL, in the 11th competition under the Initiative of Excellence - Research University, Silesian University of Technology.

BIBLIOGRAPHY

1. Tbilisi Household Survey, 2022;
2. Sustainable Mobility Handbook, Author Group, GIZ, 2023;



31th January 2025
Gliwice, Poland

DEPARTMENT OF ENGINEERING MATERIALS AND BIOMATERIALS
FACULTY OF MECHANICAL ENGINEERING
SILESIA UNIVERSITY OF TECHNOLOGY

INTERNATIONAL STUDENTS SCIENTIFIC CONFERENCE

Comparison of selected materials used in the manufacture of upper limb prostheses

Sebastian Jakubik^a, Marta Marianek^a, Mikołaj Micuła^a, Agata Ociepka^a, Jakub Osuch^a, Jakub Painta^a, Justyna Rys^a, Jakub Wieczorek^a, Anna Włodarczyk-Fligier^b, Magdalena Polok-Rubinić^b, Aneta Kania^b

^a Students of Mechanical Engineering and Industrial Automation and Robotics at the Faculty of Mechanical Engineering and Technology of the Silesian University of Technology, a Student of Electronics and Telecommunications at the Faculty of Automatics, Electronics and Informatics of the Silesian University of Technology and a Student of Mechatronics Types at the Faculty of Electrical Engineering of the Silesian University of Technology.

email: ao307638@student.polsl.pl

^b Silesian University of Technology, Faculty of Mechanical Engineering, Department of Engineering and Biomedical Materials

email: anna.wlodarczyk@polsl.pl

Abstract: In the article, the types of prostheses are described. Selected materials for the production of prostheses are analysed in terms of their features, advantages, and disadvantages.

Keywords: prosthesis, prosthesis materials, PLA

1. INTRODUCTION

A prosthesis is an artificial part that commonly replaces missing body parts and organs. The advantages of the use of prostheses are comfort, improved quality of life and their natural appearance. Nowadays, with the help of technology, it is possible to restore original mobility through the use of a prosthesis [1]. The disadvantage of prostheses is that they need to be individually adapted to the patient's needs depending on congenital defects or mechanical damage. Personalisation of the prosthesis influences its cost through the use of differently priced materials, which ultimately affects the cost of the finished product. The field of science dealing with the manufacture and use of prostheses is prosthetics, which also deals with material selection. The selection of a suitable prosthetic material is one of the key tasks to which specialists must pay attention. Unfortunately, a large proportion of materials are oxidised or corroded by interaction with human tissues or body fluids [2].

The most common materials for prostheses are titanium and silicone, but developments in incremental (additive) technology are spreading polymeric materials such as PLA and PETG [3].

2. UPPER LIMB PROSTHESES

Upper limb prostheses are divided into two types: cosmetic [4] and functional. The purpose of cosmetic prostheses is to naturally reflect the lost limb. They have no internal mechanisms and are used as a camouflage for the missing limb. When deciding on a cosmetic prosthesis, the user should be aware that the prosthesis will not restore full mobility.

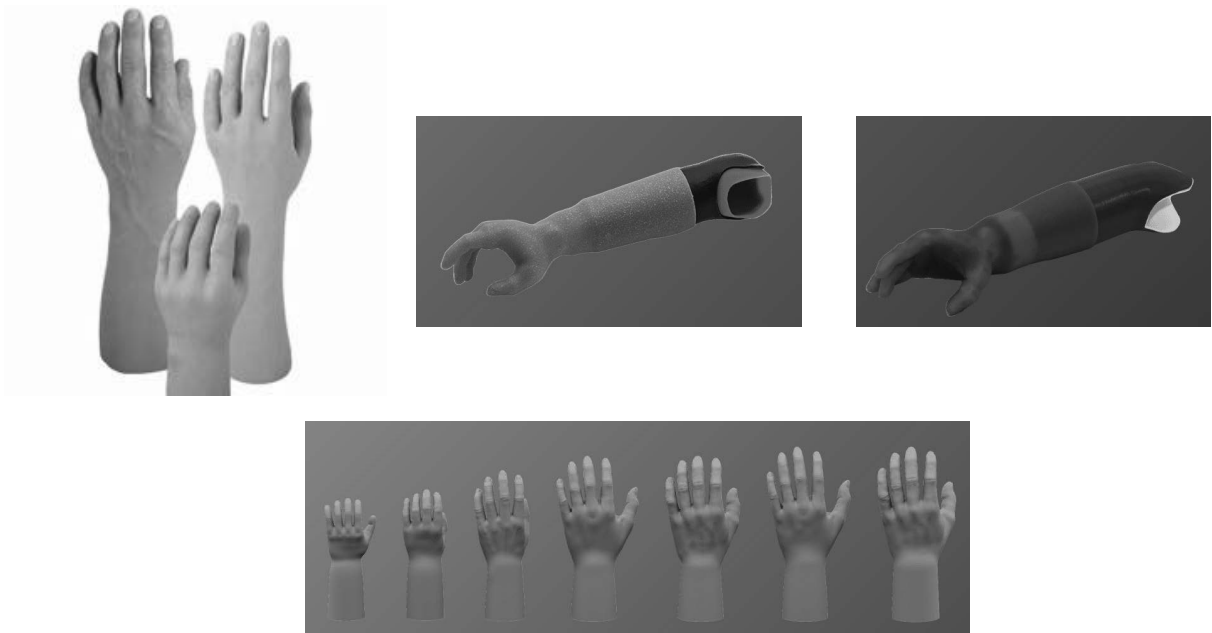


Figure 1. Cosmetic prosthesis [5,8].

A functional prosthesis, as opposed to a cosmetic prosthesis, has moving parts that allow basic simple activities of daily living to be performed. For example, a hand that can be controlled mechanically or by electrical energy, which requires the development of special and appropriate tools for this purpose [5].

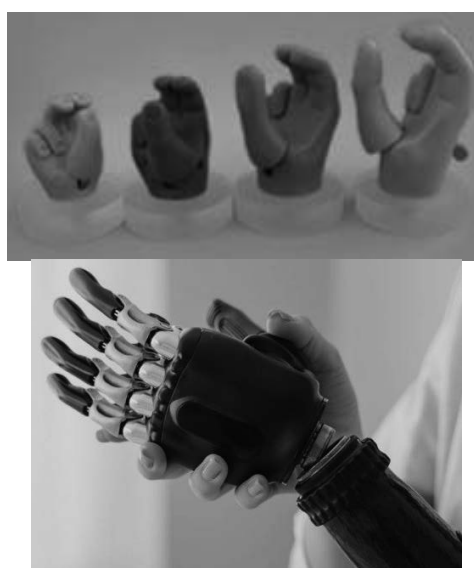


Figure 2. Functional prosthesis [5,9].

The use of functional prostheses is more demanding compared to cosmetic prostheses, requiring appropriate training to teach the user how to use the prosthesis fully, leading to independence. The selection of a suitable prosthesis depends mainly on the interview conducted with the prosthetist and the patient's daily needs.

3. MATERIALS USED IN THE MANUFACTURE OF PROSTHESES

3.1 Titan

Titanium (Fig.3) is a metal with very similar strength properties comparable to human bones. The main advantages of titanium are its light weight, biocompatibility with the human body and resistance to corrosion. It is characterised by high fatigue resistance to alternating loads, which is particularly important in the manufacture of internal and external prostheses. Due to its hardness, it is very demanding in technological processing, which increases the cost of producing a prosthesis [6].



Figure 3. Titanium [10].

3.2 Silicon

Silicone is a type of polymer based on silicon, characterised by high elasticity and durability. It is biologically inactive and therefore does not react with human tissues. It is commonly used in medicine as a material for implants in plastic surgery, orthotics and cosmetic prostheses, due to its ability to mirror a missing limb and match the patient's skin colour. However, using only medical silicone, it is not possible to produce a functional prosthesis [4].

3.3 PLA

Poly lactide (PLA) is an almost odourless polymer that uses raw materials of natural origin, mainly from corn and rice, which makes it biodegradable. It is neither toxic nor does it pollute the environment, due to its biodegradability. It is not flammable (Fig.4) and has a low melting point. It becomes liquid at temperatures between 150°C and 160° C, indicating its thermoplastic properties. It is mainly used in 3D printing technology due to its availability. Its wide application extends to the extensive medical field of prosthetics, in the manufacture of prostheses, orthoses and stabilisers, for example [7].



Figure 4. Polylactide PLA [11].

4. SUMMARY

Manufactured prostheses that replace missing body parts, improve quality of life and restore the patient's mobility. Depending on his or her needs, they are divided into cosmetic and functional, which influences the selection of the most favourable material.

Different materials are used in the manufacture of prostheses, depending on their application and therefore their properties. In the case of functional prostheses, the most commonly used material is the polymer PLA, which is particularly advantageous through its ease of production using 3D printing technology. Low cost, easy availability and also colour variety are further advantages of this material.

Despite many important advantages, PLA also has disadvantages. One of them is the inability to use this material at higher temperatures. In addition, polylactide is not very durable and cannot be subjected to high stresses.

LITERATURE

1. I. Chudawska "Methodology of design and rapid manufacturing of upper limb prosthesis components". - Master's thesis Poznan University of Technology Chair of Management and Production Engineering, Poznan 2017
2. D. Biela, D. Szalaty, A. Kania, A. Włodarczyk-Fligier, M. Polok-Rubiniec, "Biomaterials for implantology applications", Faculty of Mechanical Engineering and Technology, Department of Engineering and Biomedical Materials, Silesian University of Technology, Gliwice, 2021
3. Edutech Expert "PETG-HF Filament the Ideal Material for 3D Printing" <https://edutech.expert/pl/blog/filament-petg-hf-idealny-material-do-druku-3d-1722417121>, 2024
4. Gerwin Smit, Dick H. Plettenburg "Comparison of mechanical properties of silicone and PVC (polyvinylchloride) cosmetic gloves for articulating hand prostheses", Department of Biomechanical Engineering, Delft Institute of Prosthetics and Orthotics, Delft University of Technology, Delft, the Netherlands, 2013
5. Ortho Centre "Upper limb prostheses" <https://www.ortocentrum.com.pl/protezy-konczyn-gorych>, 2014
6. Auremo "Use of titanium in medicine" <https://auremo.pl/reference/titan-v-mediczine>, no date

7. Vincent DeStefano, Salaar Khan, Alonzo Tabada "Applications of PLA in modern medicine", Department of Biomedical Engineering, Stony Brook University, Stony Brook, USA, 2020
8. <https://vbionic.com/tolka-proteza-kosmetyczna/>
9. <https://www.inovamed.pl/jak-dziala-proteza-mioelektryczna-reki-ulatwienie-dla-pacjentow-po-amputacjach/>
10. Wikipedia
11. <https://www.agro-chemistry.com/news/corbion-and-total-to-build-first-world-scale-plant-in-europe/>

This paper is the result of a Project Based Learning (PBL) project entitled Comparison of selected materials used in the manufacture of upper limb prostheses.



31th January 2025
Gliwice, Poland

DEPARTMENT OF ENGINEERING MATERIALS AND BIOMATERIALS
FACULTY OF MECHANICAL ENGINEERING
SILESIA UNIVERSITY OF TECHNOLOGY

INTERNATIONAL STUDENTS SCIENTIFIC CONFERENCE

Tribological properties of CrN coating applied to aluminum alloy substrate

Justyna Janoszka^a, Natalia Puchała^a, Natalia Zaręba^b, Marcin Staszuk^c, Daniel Pakuła^c

^a Student of Engineering Production and Management, Faculty of Mechanical Engineering, Silesian University of Technology, ul. Konarskiego 18A, 44-100 Gliwice, Poland

^b Student of Geodesy and Cartography, Faculty of Mining, Safety Engineering and Industrial Automation, Silesian University of Technology, ul. Akademicka 2A, 44-100 Gliwice, Poland
Engineering Production and Management

^c Silesian University of Technology, Faculty of Mechanical Engineering, Department of Engineering Materials and Biomaterials, ul. Konarskiego 18A, 44-100 Gliwice, Poland

*email: daniel.pakula@polsl.pl

Abstract: The work was realized within the framework of the PBL project (11th edition) at the Faculty of Mechanical Engineering of the Silesian University of Technology in Gliwice. The aim of the research project was to get an understanding of the methodology of tribological testing of engineering materials. The paper presents the results of the study of tribological properties of CrN coating applied by physical vapor deposition (PVD) on AlSi9Cu3 aluminum alloy substrate. The paper primarily investigates how the linear velocity of the counterspecimen affects the wear resistance of both uncoated and CrN-coated aluminum alloy.

Keywords: AlSi9Cu3 aluminum alloy, PVD, CrN coating, wear resistance

1. INTRODUCTION

The demand for materials that combine light weight and high strength is growing significantly, which is particularly noticeable in various areas of the automotive and aerospace industries. One solution to this challenge is aluminum alloy AlSi9Cu3, which contains silicon and copper in its composition. AlSi9Cu3 has good corrosion resistance, and the combination of silicon and copper in the alloy guarantees high mechanical strength. This alloy also includes lead, which has lubricating properties that reduce wear in mechanical parts, and chromium, which improves ductility, strength and corrosion resistance, including stress corrosion cracking. This can be particularly important in chemically aggressive environments or under high mechanical stresses. Chromium stabilizes the structure of the metal, reducing the risk of micro-cracking due to stress and corrosive environments [1].

Thanks to these properties, the alloy is widely used in the production of advanced machine and engine components, such as cylinder heads, engine blocks, transmission housings, crankshafts, and other parts requiring precise, durable castings, but also in 3D printing

solutions. Aluminum alloys, however, due to their light weight and strength, are prone to wear under high loads or friction, requiring the use of appropriate lubrication technologies and protective coatings [2].

To further improve the properties of these materials, protective coatings obtained by PVD physical vapor deposition technology are used. This process takes place under vacuum conditions, where the material to be coated is, among other things, vaporized and then deposited on a suitably prepared substrate, forming a thin but very strong layer. PVD coatings applied to aluminum improve its resistance to abrasion, scratching and corrosion, thus increasing the durability of the material. In addition, they provide an aesthetically pleasing appearance and do not significantly affect weight, which is important in various industries. In research work, it was shown that PVD coating - AlCrN, as well as PVD+ALD hybrid coatings - TiO₂/nanoTiO₂, CrN/TiO₂ significantly improved the corrosion resistance of Al-Si-Cu alloys coated with them. These coatings also helped to improve the tribological properties of the materials studied [3-6]. The improvement of functional properties including especially tribological properties through the application of PVD coatings (e.g. CrN, WC-C, Cr-DLC) on various types of engineering materials was presented in research papers [7-12].

The purpose of this work is to evaluate the tribological properties of a CrN coating applied by physical vapor deposition (PVD) to an AlSi9Cu3 aluminum alloy substrate.

2. MATERIALS AND METHODOLOGY

AlSi9Cu3 aluminum alloy was used for the study. Specimens with a diameter of 20 mm were properly prepared (ground, polished), and then CrN coating was applied to their surface by PVD physical vapor deposition. Subsequently, ball-on-disk tests were carried out, where the test sample performed rotational motion at a specified speed, and a counter-sample in the form of a tungsten carbide ball with a diameter of 6 mm pressed against the surface of the test piece with a constant load. These tests were performed at room temperature and 50% humidity. The parameters of the tribological tests are shown in Table 1.

Table 1. Tribological test parameters

Sample number	Substrate	Coating	Parameters				
			Number of cycles	Load [N]	Radius [mm]	Reading frequency [Hz]	Linear velocity [cm/s]
1	AlSi ₉ Cu ₃	-	20 000	5	5	10	5
2		CrN					
3		-					20
4		CrN					

The resulting abrasion was examined using a Taylor Hobson Surtronic contact profilometer. The traces of the abrasion (damage formed) were also examined using a ZEISS SEM SUPRA 35 scanning electron microscope with a high electron voltage EHT of 15 kV at a magnification of 40 to 5,000 times using secondary electrons (SE). In addition, chemical composition analysis was performed on the same device using EDS energy dispersive spectroscopy.

3. RESULTS

The coefficient of friction of the tested materials ranged from 0.4 to 0.8. For the uncoated material (Fig. 1a), the coefficient of friction in the first cycles was high, then remained constant. At a wiping speed of $V=5$ cm/s, the averaged coefficient of friction was 0.4216 and the standard deviation was 0.0434, while at a wiping speed of $V=20$ cm/s it was 0.4245 and the standard deviation was 0.0442. For CrN-coated aluminum alloy (Fig. 1b), the averaged coefficient of friction was 0.5226 and the standard deviation was 0.1125 for a wiping speed of $V=5$ cm/s. In contrast, for a wiping speed of $V=20$ cm/s, the averaged coefficient of friction was 0.4862 and the standard deviation was 0.0671. Before reaching these values until the coating rubbed off, the coefficient of friction gradually increased to a level of 0.7-0.8. At the lower linear wiping speed, the CrN coating rubbed off after about 7980 cycles, and at the higher speed after 4117 cycles. On the friction coefficient graphs, a dodge indicating the moment when the protective coating wiped off is clear. To sum up, based on the friction coefficient studies, it can be concluded that the use of a higher linear test speed causes faster wear of aluminum alloy without coating as well as with CrN coating (Fig. 1, Table 2).

Table 2. Average coefficient of friction and standard deviation for coated and uncoated Al-Si-Cu alloy

Sample number	Coating	Linear velocity [cm/s]	Average coefficient of friction	Standard deviation
1	-	5	0,421596	0,043383
2	CrN		0,522617	0,112501
3	-	20	0,424494	0,044208
4	CrN		0,48619	0,067088

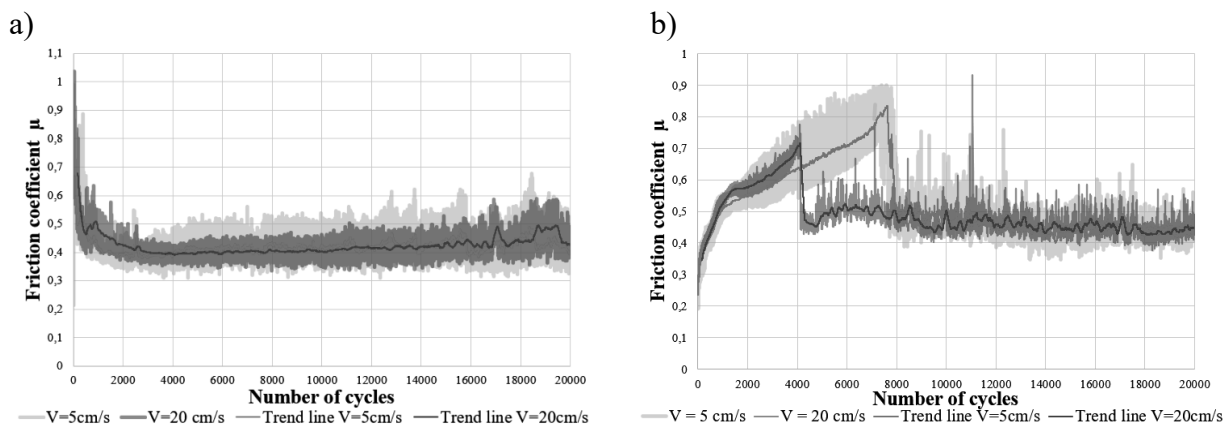
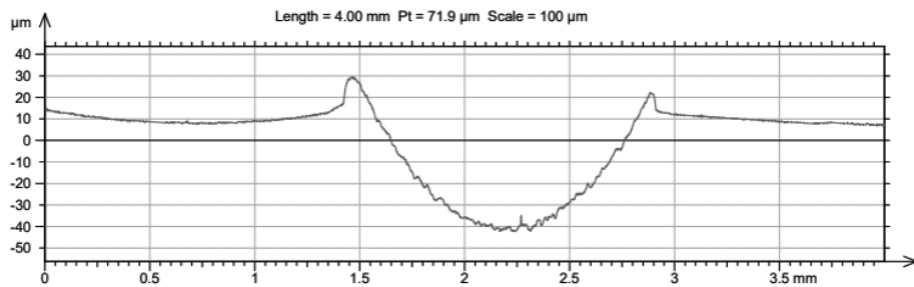


Figure 1. friction coefficient as a function of the number of cycles for Al-Si-Cu alloy (a) coated, (b) uncoated

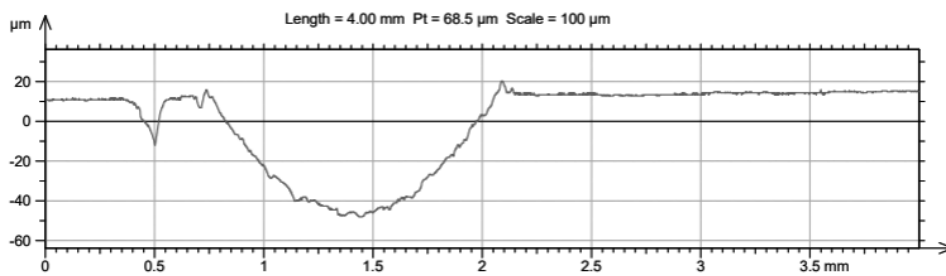
The abrasion profiles measured with the contact profilometer are shown in Figure 2. For the uncoated material - aluminum alloy, the abrasion profiles are characterized by a symmetrical shape and uniform indentation. For a linear wiping speed of 5cm/s, the maximum indentation was 40 μm and for a speed of 20 cm/s it was about 50 μm . In contrast, the wipe marks of CrN-coated aluminum alloy are characterized by irregular indentation and sharp edges. The depth of the wipe profile of coated samples is similar to that of uncoated samples. The application of

CrN coating on this substrate material did not significantly affect the depth of abrasion. On the other hand, the abrasive wear character of the coated samples was more irregular due to the formation of fine particles of the abraded coating additionally in the wiping process.

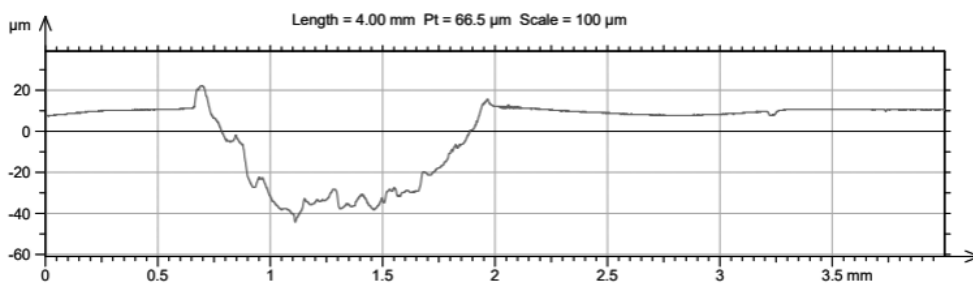
a)



b)



c)



d)

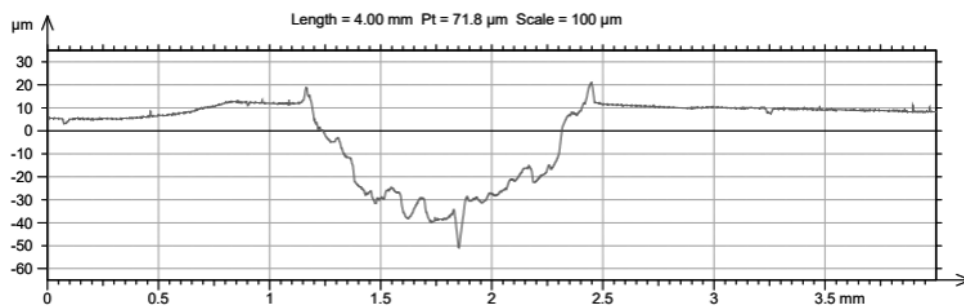


Figure 2. Profiles received from contact profilometer measurements: a) Al-Si-Cu alloy without coating (5cm/s), b) Al-Si-Cu alloy without coating (20cm/s) c) Al-Si-Cu alloy with coating (5cm/s), d) Al-Si-Cu alloy with coating (20cm/s)

Table 3. Average surface area and abrasion volume of Al-Si-Cu alloy with and without coating

Coating	Linear velocity [cm/s]	Area [mm ²]	Volume [mm ³]
-	5	0,0144	0,4519
-	20	0,0094	0,2940
CrN	5	0,0081	0,2534
CrN	20	0,0073	0,2302

On the basis of the abrasion profiles, the surface area and abrasion volume of the tested materials were calculated (Table 3). The reduction in the abrasion volume of PVD-coated Al-Si-Cu alloy is due to the higher abrasion resistance typical of this type of hard protective coating. For coated and uncoated aluminum alloys, a higher linear velocity of wiping leads to a reduction in abrasion volume, which may be due to more intense initial wear at the lower velocity, as well as differences in abrasion mechanisms for the two velocities. As a result, the presence of a coating on this substrate material significantly reduces the abrasive wear of the tested materials, as indicated by the calculated abrasion volume (Fig. 3).

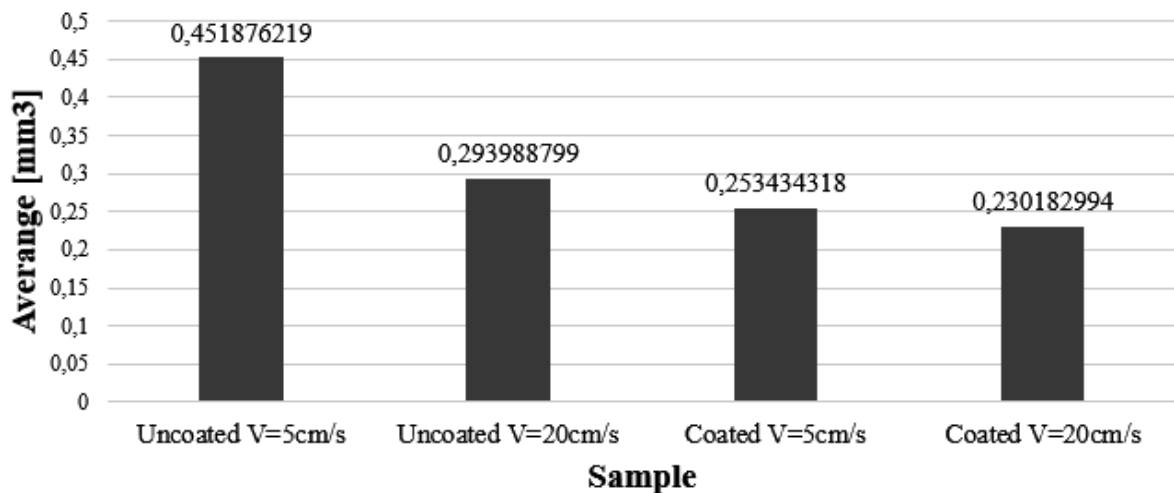


Figure 3. Average abrasion volume of CrN-coated and uncoated Al-Si-Cu alloy at different linear test speeds

Interpreting the values of the abrasion volume, differences can be observed between the tested materials with and without PVD coating. Aluminum alloy without coating shows a larger abrasion volume for both linear velocities - about 0.452 mm³ (V=5 cm/s) and about 0.294 mm³ (V=20 cm/s). On the other hand, Al-Si-Cu alloy with CrN coating exhibit a lower abrasion volume of - about 0.253 mm³ (V=5 cm/s) and about 0.230 mm³ (V=20 cm/s).

Observations of the abrasion traces were made by scanning electron microscopy SEM (Fig. 4) and the chemical composition was analyzed using energy dispersive spectroscopy EDS in the indicated areas of the sample (Fig. 5). Based on the study of the abrasion traces, it was concluded that the primary mechanism of the resulting damage in the materials studied was abrasion. In the case of CrN-coated aluminum alloys, as a result of abrasion regardless of the linear velocity of the test, the substrate was completely exposed and the surface of the substrate

material was partially oxidized (as confirmed by chemical composition analysis (Fig 5)). In some places, the loss of abraded material is significant - delaminations, discontinuities and inhomogeneities of the abraded surface are visible. In turn, as a result of intensive flaking (deformation) of the coating during the test, the rubbing edges of CrN-coated aluminum alloy have an irregular shape.

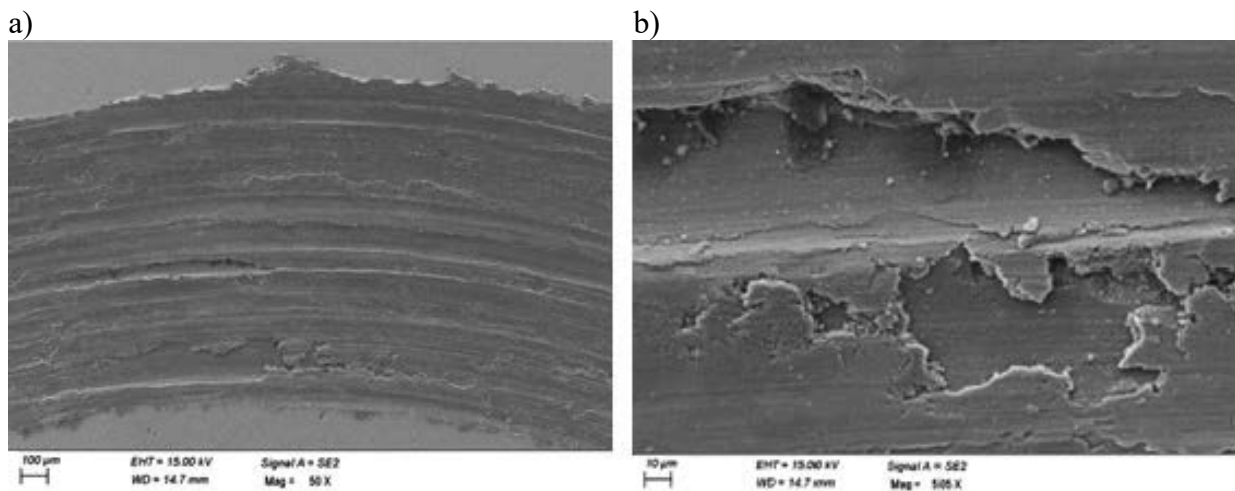


Figure 4. a) Wear trace of CrN-coated Al-Si-Cu alloy (20cm/s), b) magnification of the wear edge

In the chemical composition determined by EDS energy dispersive spectroscopy, no elements were found that would indicate material from the counter-sample (WC) material. In addition, the chemical composition examined in the indicated areas confirmed complete abrasion of the CrN coating applied to the aluminum alloy substrate. (Fig. 5).

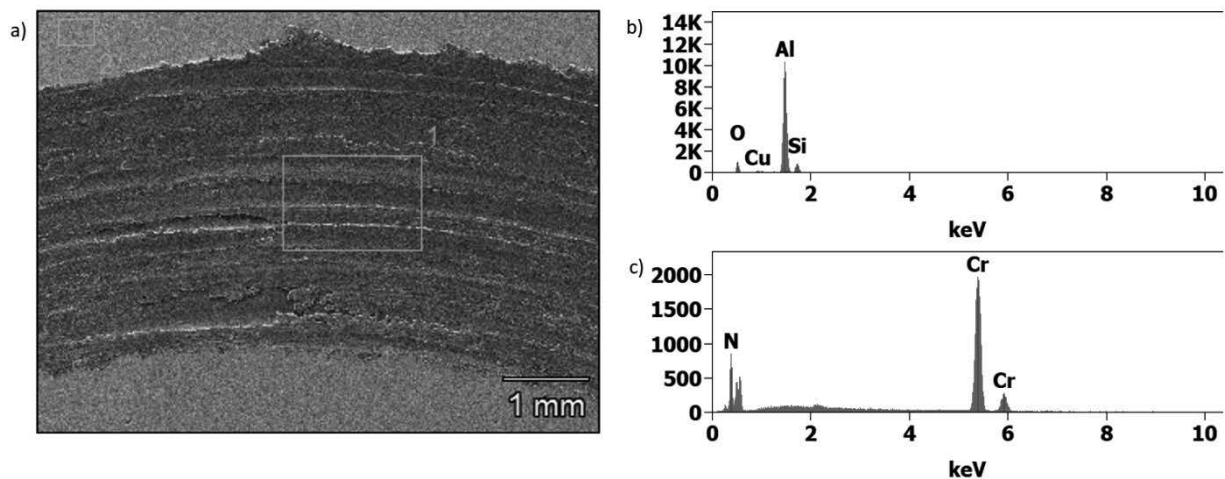


Figure 5. a) Al-Si-Cu alloy with CrN coating (20 cm/s), b) EDS analysis from area 1, c) EDS analysis from area 2

4. CONCLUSIONS

Based on the study, it was found that:

- The use of CrN coating on Al-Si-Cu alloy substrate improves abrasion resistance, but its life depends on the linear speed of the wear test. For a lower linear velocity of abrasion, the coating wiped off after about 7980 cycles, and at a higher velocity - after 4117 cycles. The lower the linear speed of abrasion, the longer the protection provided by the CrN coating.
- CrN-coated Al-Si-Cu alloy has a lower abrasion volume than the uncoated one. The abrasion volume was smaller for Al-Si-Cu alloy, for which the linear velocity of abrasion was higher. Al-Si-Cu alloy with CrN coating had the smallest abrasion volume for $V=5\text{cm/s}$ it was 0.253 mm^3 , and for $V=20\text{cm/s}$ it was 0.230 mm^3 .
- The average coefficient of friction for uncoated Al-Si-Cu alloys was 0.4216 ($V=5\text{cm/s}$) and 0.4245 ($V=20\text{cm/s}$). In contrast, it was 0.5226 ($V=5\text{cm/s}$) and 0.4862 ($V=20\text{cm/s}$) when CrN coating was applied.
- The main wear mechanism of uncoated and CrN-coated Al-Si-Cu alloy was abrasive.

ACKNOWLEDGEMENTS

This work was produced as part of the project implemented within the framework of project-oriented education – PBL, in the XI competition under the Excellence Initiative – Research University program, at the Silesian University of Technology

BIBLIOGRAPHY

1. K. Przybyłowicz, *Metaloznawstwo*, Wydawnictwa Naukowo-Techniczne, Warszawa, 2007.
2. F.P. Bowden, D. Tabor, *The Friction and Lubrication of Solids*, Oxford Clarendon Press, USA, 1954.
3. M. Staszuk, Ł. Reimann, D. Pakuła, M. Pawlyta, M. Musztyfaga-Staszuk, P. Czaja, P. Beneš, Investigations of $\text{TiO}_2/\text{NanoTiO}_2$ Bimodal Coatings Obtained by a Hybrid PVD/ALD Method on Al Si–Cu Alloy Substrate, *Coatings* vol. 12, (2022), 338-339.
4. M. Staszuk, Investigations of CrN/ TiO_2 coatings obtained in a hybrid PVD/ALD method on Al–Si–Cu alloy substrate, *Bulletin of The Polish Academy of Sciences Technical Sciences* vol. 71, (2023), 7-8.
5. M. Staszuk, Application of PVD and ALD Methods for Surface Treatment of Al-Si-Cu Alloys, *Solid State Phenomena* vol. 293, (2019), 108-109.
6. J. Leppaniemi, P. Sippola, A. Peltonen, J.J. Aroma, H. Lipsanen, J. Koskinen, Effect of surface wear on corrosion protection of steel by CrN coatings sealed with Atomic Layer Deposition., *ACS Omega* vol. 12, (2018), 1791–1800.
7. C.X. Shan, X. Hou, K.L. Choy, P. Choquet, Improvement in corrosion resistance of CrN coated stainless steel by conformal TiO_2 deposition, *Surface & Coatings Technology* vol. 202, (2008), 2147–2151.
8. S.C. Demirtas, E. Yeten, PVD coating application on aluminum alloys”, *Güncelleme Tarihi Bursa* vol.9, (2020), 8-9.

9. T. S. Kumara, A.V. Jebaraja, Metallurgical characterization of CrN and AlCrN physical vapour deposition coatings on aluminium alloy AA 6061, *Materials Today: Proceedings* vol.22, (2019), 1479-1488.
10. G.G. Fuentes, M.J. D'iaz de Cerio, R. Rodriguez, J.C. Avelar-Batista, E. Spain, J. Housden, Y. Qin, Investigation on the sliding of aluminium thin foils against PVD-coated carbide forming-tools during micro-forming, *Journal of Materials Processing Technology* vol. 177, (2006), 644-648.
11. R. Ferreira , Ó. Carvalhoa, L. Sobralb, S. Carvalhoc, F. Silvaa, Influence of morphology and microstructure on the tribological behavior of arc deposited CrN coatings for the automotive industry, *Surface & Coatings Technology* vol. 397, (2020), 126-127.
12. F.D. Duminica, R. Belchi, L. Libralesso, D. Mercier, Investigation of Cr(N)/DLC multilayer coatings elaborated by PVD for high wear resistance and low friction applications, *Surface & Coatings Technology* vol. 337, (2028), 52-54.



31th January 2025
Gliwice, Poland

DEPARTMENT OF ENGINEERING MATERIALS AND BIOMATERIALS
FACULTY OF MECHANICAL ENGINEERING
SILESIA UNIVERSITY OF TECHNOLOGY

INTERNATIONAL STUDENTS SCIENTIFIC CONFERENCE

Eco-friendly technology of laser cutting for engineering materials

Bartłomiej Józwiak^a, Nikodem Juszczak^a, Mirosław Bonek^b

^a- V Liceum Ogólnokształcące z Oddziałami Dwujęzycznymi im. Andrzeja Struga email: jozwiakbartek50@gmail.com

^b- Politechnika Śląska, Wydział Mechaniczny Technologiczny, Katedra Materiałów Inżynierskich i Biomedycznych email: miroslaw.bonek@polsl.pl

Abstract: This article discusses the operating principle of lasers, their applications in cutting engineering materials, highlights the eco-friendly benefits of their use, and presents the challenges and prospects in the development of this technology.

Keywords: Laser, surface engineering, ecology

1. INTRODUCTION

Modern industrial technologies are increasingly focused on improving energy efficiency and minimizing their impact on the natural environment. In this context, laser cutting of engineering materials stands out as a technology that meets the demands of modern, eco-friendly production. The use of lasers in materials engineering has been recognized as key to enhancing product competitiveness through advanced repeatability, efficiency, and automation capabilities.

Cutting is a process in which the material's cohesion is disrupted. Depending on the desired outcome, cutting can be complete, resulting in separation into two distinct parts, or partial, where the material is only incised. Energy application is essential in the cutting process to disrupt the material's integrity. Depending on the energy source used, four cutting methods can be distinguished:

- **Laser cutting**, where a focused laser beam acts as the cutting tool, is widely used due to numerous advantages, including excellent surface quality of the cut and high productivity. This method can cut materials up to 20 mm thick.
- **Gas cutting**, which utilizes oxygen or plasma to melt and then oxidize the metal being cut, is suitable for cutting materials with significant dimensions (over 300 mm).
- **Mechanical cutting**, the oldest method, involves dividing the material with a moving cutting tool that induces stress on the surface of the material, leading to cracking at the desired location and subsequent separation.
- **Water jet cutting**, where highly compressed water at a pressure of approximately 4,150 bar presses against the material, removing it from the cutting gap through erosion and abrasive fatigue of the processed material.

Laser cutting is a process in which the energy of a continuous or pulsed (impact) laser beam is applied to a specific area of a workpiece. Depending on the cutting technique and material type, this energy causes the material to melt within the cutting gap and either be expelled, synchronously melted and vaporized, or melted and burned. Although laser cutting can be performed manually (nowadays very rarely), it is most often automated and robotized, widely used in various industrial applications. This process is effective for cutting a wide range of engineering materials, such as metals, cermets, ceramics, wood, and plastics.

An essential aspect of laser cutting is the use of an auxiliary gas, which flows coaxially with the laser beam through the nozzle, removing molten and vaporized material from the cutting gap. This gas may be chemically inert or reactive, depending on the material being cut. During the process, the power density of the laser beam should range between 10^4 – 10^6 W/mm², adjusted based on the material to be processed.

The laser beam's radiation acts as a linear energy source that melts the material across its entire thickness. Beam polarization is critical to process efficiency and cut quality, with the laser's design determining whether the polarization is linear, random, circular, or elliptical. Circular polarization is often preferred, as it ensures consistent cut quality in all directions, making it widely used in laser cutting machines.

Selecting the appropriate working gas is crucial in laser cutting. The choice depends on factors such as the material being cut and the desired processing outcome. The main working gases include:

- **Oxygen**, used for cutting unalloyed or low-alloy steel sheets.
- **Nitrogen**, applied for cutting tool steels and non-metallic materials.

Laser cutting has numerous advantages that make it superior to other cutting methods in various aspects, leading to its widespread industrial adoption. These benefits include:

- High cutting speeds.
- Excellent surface quality after cutting, often eliminating the need for finishing processes.
- The ability to cut a wide range of materials.
- Minimal heat-affected zones on the material.
- Reduced material distortion.
- High material efficiency due to narrow cutting gaps.
- Compatibility with automation and robotization.
- Low production costs.

Despite its many advantages, laser cutting has certain limitations, such as:

- High initial investment costs.
- A thickness limitation of up to 20 mm for the materials being cut.
- Hazardous, invisible electromagnetic radiation.
- Specific surface quality requirements after cutting.

Key factors that influence laser cutting include the power and quality of the beam, the type of working gas, and the cutting speed. In addition to the three primary cutting methods (melting and blowing, melting and vaporization, and melting and burning), alternative techniques are used in special cases. For instance, thermal fracture generation is applied when cutting glass, while scribe-and-break techniques are employed for shaping corundum plates, where the material is incised with a laser and then mechanically broken. The graph in Figure 1 illustrates the relationship between cutting speed and beam power for the three main laser cutting methods.

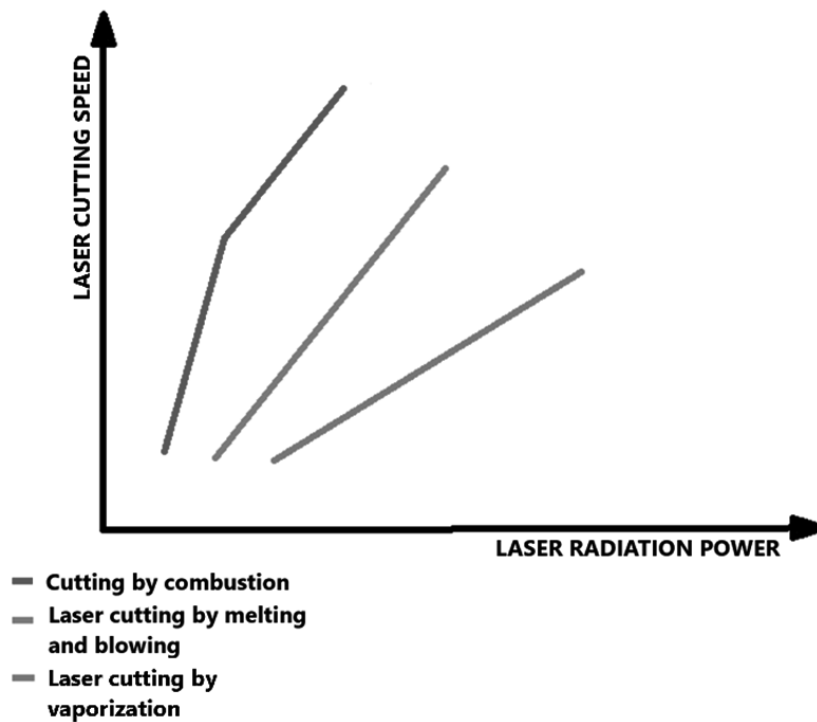


Figure 1. Relationship between cutting speed and beam power for the three main laser cutting methods

Laser cutting involving material combustion occurs when oxygen is used as the working gas. This process resembles oxyacetylene torch cutting, as the material being cut burns within the cutting gap, producing liquid slag as a byproduct, which is then expelled from the cutting area. The process begins with the laser beam heating the material in the cutting gap to its ignition temperature, approximately 1200°C for structural steel. Subsequently, oxygen is introduced through the gas nozzle to enhance the combustion process dynamically. This type of laser cutting enables relatively high cutting speeds but is limited to processing unalloyed and low-alloy steels. The speed of the laser beam's movement directly depends on the laser power and the dimensions of the workpiece. The quality of the cut is also significantly influenced by the nozzle diameter, which increases with the material's thickness, and the oxygen pressure, which decreases as the nozzle diameter grows. Figure 2 illustrates this method of laser cutting.

In the method of cutting by melting and subsequently blowing out the molten material, energy is generated exclusively by laser radiation, with power densities ranging from 10^1 to 10^2 kW/mm². The working gas does not participate in energy generation, as it does not react exothermically with the material being cut. The process begins with melting the material at the cutting site, achieved through the high power of the laser beam. Next, a technical gas, such as nitrogen or argon, removes the molten material from the cutting gap. This eliminates combustion within the process and prevents the formation of oxides on the material's surface. This characteristic is particularly advantageous in processes involving non-ferrous metals and high-alloy steels. To achieve maximum surface purity, it is essential to use a gas at high pressure, typically ranging from 8 to 29 [bar], depending on the material. The use of such high-pressure gas requires specially designed cutting heads. Figure 3 illustrates this cutting process.

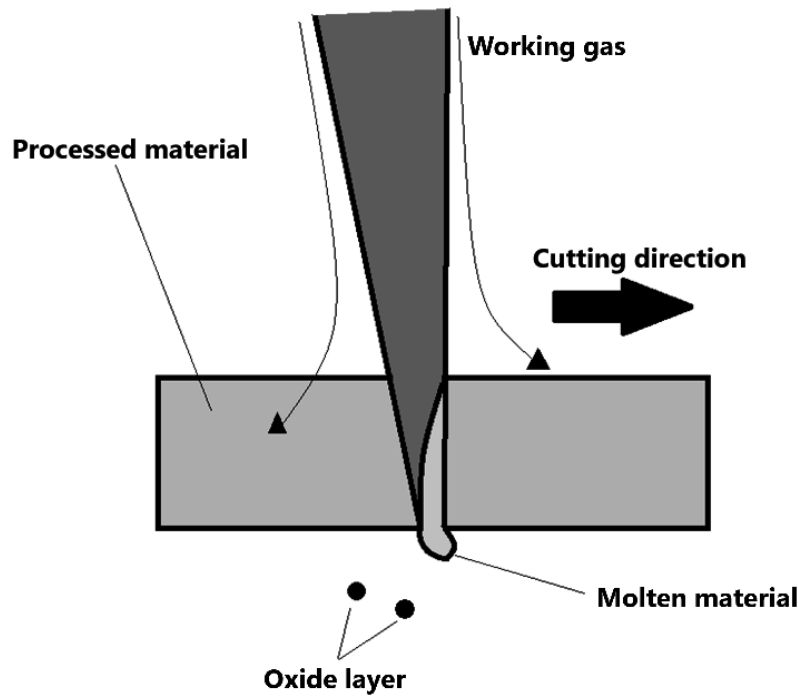


Figure 2. Diagram of laser cutting, where material combustion occurs

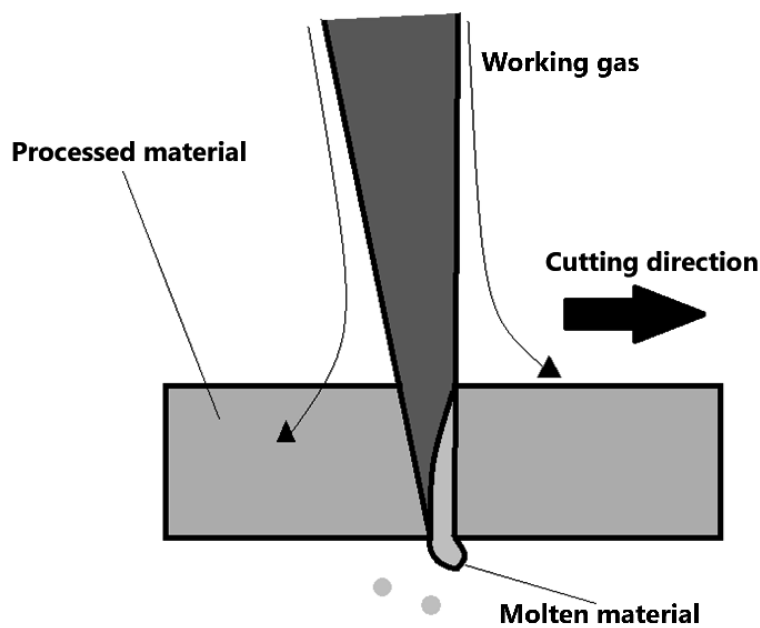


Figure 3. Diagram of laser cutting, where melting and blowing out of the material occur

The laser cutting method involving material vaporization operates at extremely high power densities, ranging from 10^2 to 10^3 kW/mm². Such intense radiation heats the material in the cutting zone to a very high temperature, causing part of the material to transition into a gaseous state. Within the cutting gap, a capillary forms, with its center filled with the material's vapor.

These vapors collide with the capillary walls, enhancing absorption and facilitating the penetration of the cutting channel into the material. This process results in full perforation. Intense gas-dynamic processes inside the cutting gap further enhance the removal of cutting byproducts. This method is primarily used for cutting non-metallic materials, such as plastics, leather, and ceramics, with thicknesses limited to a maximum of 6 mm. For metals with high thermal conductivity, the recommended material thickness should not exceed 3 mm. When processing highly flammable materials, the use of inert gases (argon or nitrogen) is essential for safety. Figure 4 illustrates this laser cutting method.

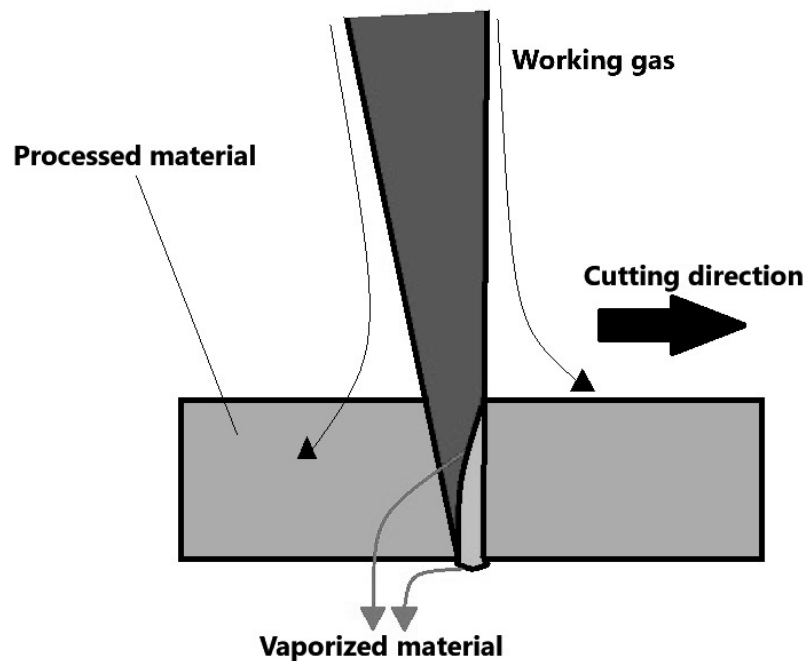


Figure 4. Diagram of laser cutting with the material vaporization process occurring

The energy of highly concentrated radiation used in laser cutting enables the production of components with exceptional speed and precision. This method is increasingly applied in both single-item and mass production, primarily because it delivers materials of outstanding quality that often require no further processing. These advantages are driving the replacement of other cutting methods, while continuous advancements in this technology are expanding the range of laser-compatible materials and broadening the scope of laser cutting applications.

2. ENVIRONMENTAL ASPECTS OF LASER CUTTING TECHNOLOGY

Laser cutting of materials offers not only precision but also numerous environmental benefits, such as:

- **Waste minimization** – The precision of the laser beam significantly reduces production waste compared to traditional cutting methods.
- **Energy efficiency** – Modern lasers are more energy-efficient than mechanical cutting machines.

- **No chemicals required** – The laser cutting process does not require cooling fluids or other chemicals, minimizing the risk of environmental contamination.
- **Recyclability** – Lasers enable the cutting of materials that are difficult to process, such as composites or coated metals, facilitating recycling efforts.

3. CHALLENGES AND DEVELOPMENT PROSPECTS

Challenges in Using Eco-friendly Laser Cutting Technology:

- **High Cost:** The purchase of advanced laser equipment can be a barrier for smaller companies. However, these costs are often recouped through higher efficiency and material savings.
- **Energy Demand:** Processing thick materials requires higher laser power, which increases energy consumption.
- **Technological Progress:** Innovations are needed toward more eco-friendly solutions, such as ultrashort pulse lasers or hybrid laser systems.

Development Prospects Include:

- Integration with Industry 4.0 systems (e.g., Artificial Intelligence, Internet of Things).
- Utilization of lasers in the recycling of advanced materials.
- Continued improvement of energy efficiency and cost reduction.

4. CONCLUSION

This article presented laser cutting technology, which stands out for its significant eco-friendly efficiency compared to traditional methods. Laser cutting of engineering materials, due to its precision, minimizes production waste, thus reducing its negative environmental impact. Furthermore, this process does not require the use of chemicals or cooling fluids, eliminating the risk of environmental contamination. These technologies are also applied in industries where they enable the processing of difficult-to-recycle materials, such as composites. As a result, laser cutting plays a crucial role in sustainable development within material engineering, combining precision with environmental efficiency.

ACKNOWLEDGEMENTS

The work was created as a result of a project carried out with secondary school pupils as a part of the Excellence Initiative - Research University program, Silesian University of Technology.

BIBLIOGRAPHY

- [1] website bud-expert: <http://ciecielaserem.info>
[dostęp 22/04/2014].
- [2] P. Kołodziejczak.: Rodzaje cięcia laserowego. Przegląd spawalnictwa, 2015/7 vol.87.
- [3] B. Józwiak, N. Jusczyk, M. Bonek, Zastosowanie nowoczesnej technologii cięcia laserowego stali w przemyśle samochodowym.

-
- [4] A. Klimpel.: Technologia spawania i cięcia metali, Wydawnictwo Naukowo-Techniczne, Warszawa 1999.
- [5] O.S. Sirotkin, V.V. Blinkov, J. Michalski, A. Nakonieczny, P. Wach, Technologie laserowe obróbki powierzchniowej części stosowanych w przemyśle lotniczym, Inżynieria Powierzchni 2 (2010)
- [6] J. Kusiński, Technologie laserowe. Problemy Eksploatacji 3 (2004)
- [7] The impact of the Fourth Industrial Revolution on the services innovation
monika.wodnicka@uni.lodz.pl



31th January 2025
Gliwice, Poland

DEPARTMENT OF ENGINEERING MATERIALS AND BIOMATERIALS
FACULTY OF MECHANICAL ENGINEERING
SILESIA UNIVERSITY OF TECHNOLOGY

INTERNATIONAL STUDENTS SCIENTIFIC CONFERENCE

Characterization of the crystalline silicon solar cells using advanced research techniques

Ryszard Kała^a, Jan Czembor^b, Daniel Foks^b, Adam Popis^c, Kacper Kuczera^c, Janusz Wyrwał^d, Barbara Grzegorzczak^e, Aleksandra Drygala^e

^a Student, Silesian University of Technology, Faculty of Automatic Control, Electronics and Computer Science, Akademicka 16 Str., 44-100 Gliwice, Poland

^b Student, Silesian University of Technology, Faculty of Mechanical Engineering, Konarskiego 18a Str., 44-100 Gliwice, Poland

^c Student, Silesian University of Technology, Faculty of Mining, Safety Engineering and Industrial Automation, Akademicka 2 Str., 44-100 Gliwice, Poland

^d Silesian University of Technology, Faculty of Automatic Control, Electronics and Computer Science, Department of Measurements and Control Systems, Akademicka 16 Str., 44-100 Gliwice, Poland

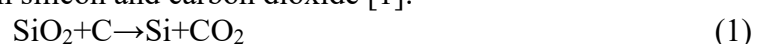
^e Silesian University of Technology, Faculty of Mechanical Engineering, Department of Engineering Materials and Biomaterials, Konarskiego 18a Str., 44-100 Gliwice, Poland
email: aleksandra.drygala@polsl.pl

Abstract: Continuous improvement in the performance of solar cells requires an in-depth understanding of their operation and the knowledge of their various properties. In this work, crystalline silicon solar cells were characterized using advanced research techniques. Surface topography of monocrystalline silicon was studied using scanning electron microscopy. The influence of chemical treatment and antireflective coating deposition on optical properties of monocrystalline silicon was investigated applying a UV-Vis spectrophotometer. Electrical properties of mono- and polycrystalline solar cells were studied using a system for measuring current-voltage characteristics equipped with a solar radiation simulator.

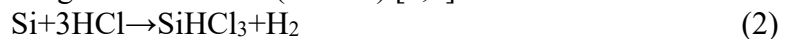
Keywords: photovoltaics, solar cells, research techniques, spectrophotometer, current-voltage characteristics, SEM

1. INTRODUCTION

The production of silicon solar cells involves several stages. Pure silicon is obtained from silicon dioxide (SiO₂), which is a commonly occurring chemical compound on Earth, mainly found in sand and silicates. Silicon dioxide is reduced with carbon in large arc furnaces at temperatures of 1500–2000°C to form silicon and carbon dioxide [1]:



Silicon obtained in this way is referred to as metallurgical grade silicon, and its purity ranges from 98% to 99%. It must be purified to be used in electronics during the Siemens process. Silicon is converted into a volatile compound, which is purified through fractional distillation. This is done by dissolving metallurgical silicon in hydrochloric acid (HCl) at 300°C, in the presence of copper as a catalyst, forming trichlorosilane (SiHCl₃) [2,3]:



In this reaction, iron, aluminum, and boron are removed, forming FeCl₃, AlCl₃, and BCl₃, respectively. The gaseous reaction products condense, and the resulting liquid is distilled. The product is purified SiHCl₃, which is then mixed with gaseous hydrogen in a reaction furnace at 1100°C for 200–300 hours [3]:



This process produces a high-purity silicon [2,3].

Monocrystalline silicon is obtained by the Czochralski method. In this process, polycrystalline silicon is melted in a quartz crucible with the addition of other elements. These elements are added to obtain n-type or p-type silicon. The process takes place at 1410°C in an argon atmosphere. A seed crystal is dipped into the molten silicon and then slowly pulled and rotated around its axis. The temperature and pulling speed must be strictly controlled to achieve the desired crystal diameter [3,4].

Semiconductors are elements which possess the ability to radically change their conductivity in response to external influences like temperature, potential difference or light. Their structure is described as band, with layers of different energetic states [5].

Creating useful semiconductor requires doping intrinsic semiconductor (e.g. silicon or germanium). This allows to obtain semiconductors with surplus (n-type) or lack of the electrons (p-type). Intrinsic semiconductors are elements of the fourth main group of the periodic table. By doping them with an element of the fifth group (e.g. phosphorus, antimony, or arsenic) one excess (from the crystal structure point of view) electron will be released to the structure. On the other hand, adding elements from the third group (e.g. boron, gallium, aluminum, or indium) causes structure to lack electrons. In room temperature of 300K number of free electrons and holes is equal to the number of doped atoms [6].

Connecting both types of semiconductors makes p-n junction, which has useful applications thanks to effects that happen between them. In 300K diffusion current in such junction has the same value as drift current, but they flow in opposite directions. First one is caused by lack of balance of electric charges. The second is an effect of electric field existing due to barrier layers. Lack of balance (potential difference) creates voltage which will push electrons when layers are connected by conductor or when gap between them in junction is minimized [7,8]. When solar radiation with appropriate energy acts upon semiconductor electron jumps from the valence to conductive energetic layer, which creates electron-hole pair. This causes movement of electrons to negative layer and enhances potential difference between front and back electrodes [9].

Solar cells consist of p-type and n-type layers. Most often, p-type silicon is obtained by adding appropriate dopants during its crystallization (e.g. boron). Then, such a p-type silicon wafer is subjected to diffusion (e.g. phosphorus), as a result of which an n-type area is created in the surface layer. Diffusion is carried out in a furnace about 850°C in the presence of POCl₃. At high temperatures, the concentration of donors (phosphorus) increases at the surface of the wafer, phosphorus atoms begin to diffuse into the wafer surface, and the layer becomes an n-type semiconductor [6]. Edge isolation is an important step in silicon solar cell production to prevent electrical shunting of the front and back electrode at the edges. This is done for example by plasma etching. The wafers are stacked so that only the edges are in contact with the plasma.

Reactive gases ($\text{CF}_4 + \text{O}_2$) activated by the plasma aggressively etch the wafer edge, creating a clean connection between the p and n layers [6,10].

In solar cells, a passivation layer (e.g. SiO_2 , Si_3N_4) is a thin material layer that is applied to reduce surface recombination of charge carriers. To increase solar cell efficiency, an anti-reflective coating is applied to the wafers, usually made of titanium dioxide (TiO_2) or SiN_xH . The coating is deposited from the vapor phase of $(\text{C}_2\text{H}_5)_4\text{Ti}$ or from $\text{NH}_3 + \text{SiH}_4$ in a vacuum at 400°C [7]. The final step of solar cell production is the fabrication of electrodes. The bottom and top electrode is usually made of aluminium and silver, respectively, using the screen printing method. The electrodes are then heated at temperature above 850°C [7]. The prepared solar cells are tested and assembled into modules, and then into photovoltaic panels, which are used to generate electricity [8,11].

Solar cells' layers have usually great difference in size. Most often n-type layer is facing light, while it is much thinner than the p-type layer. Such difference occurs because thicker layer of silicon with phosphorus would cause element to generate less electron-holes pairs [12]. The structure of a silicon solar cell is shown in Figure 1.

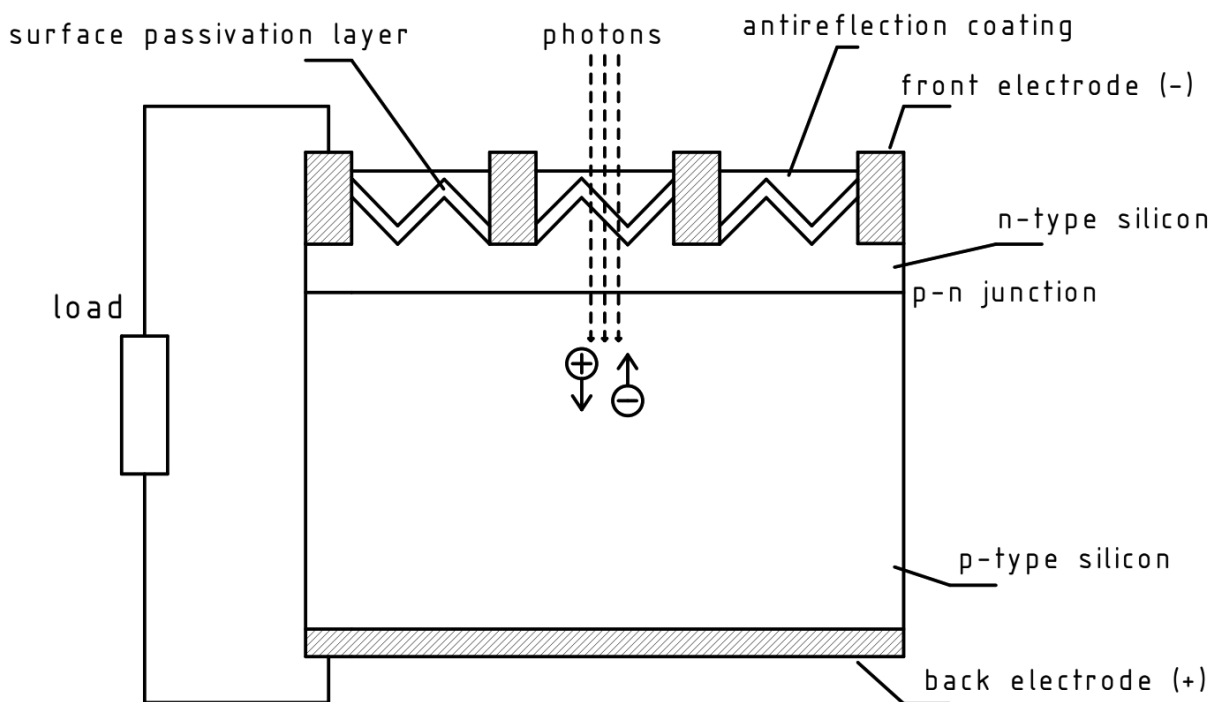


Figure. 1. Solar cell structure [7,8,13]

Solar cells are an ecological alternative to traditional energy sources. Their research is aimed at developing and improving technology that allows for the efficient conversion of solar radiation energy into electrical energy. In this work, photovoltaic cells were characterized using advanced research methods. The surface topography of monocrystalline silicon was assessed and the optoelectrical properties of crystalline silicon solar cells were determined.

2. MATERIALS AND METHODOLOGY

The materials used for experiments were:

- boron doped p-type monocrystalline silicon of thickness of $200\pm 30\ \mu\text{m}$ with crystallographic orientation (100),
- monocrystalline and polycrystalline silicon solar cells of area $10\ \text{cm} \times 10\ \text{cm}$ (Fig. 2). All of them were produced using the same technology.

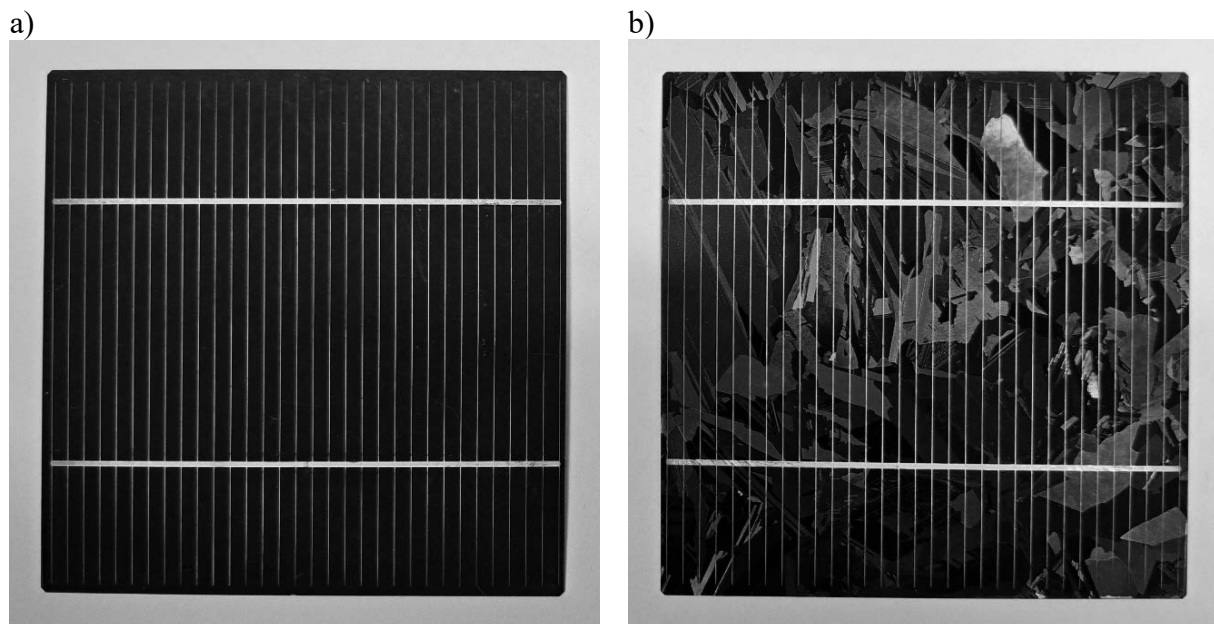


Figure 2. Silicon solar cells a) monocrystalline b) polycrystalline

The topography of monocrystalline silicon surface was investigated by Zeiss Supra 25 scanning electron microscope (SEM). The reflectance of the monocrystalline silicon surfaces (without texture, with texture, with texture and Si_3N_4 antireflection coating (ARC) was measured with Thermo Scientific UV-Vis spectrophotometer (Fig. 3) in the wavelength range from 400 to 1000 nm.

The electrical properties of monocrystalline silicon solar cells were determined based on measured current-voltage characteristics using a PV Test Solutions Tadeusz Źdanowicz system equipped with a Solar Simulator model #SS150AAA from Photo Emission Tech (Fig. 4). The measurements were conducted under the illumination intensity of $1000\ \text{W}/\text{m}^2$ with an AM 1.5 solar spectrum and a temperature of 25°C . Prior to the measurements, the system was calibrated using a reference cell.



Figure 3. Thermo Scientific UV-Vis spectrophotometer



Figure 4. System for measuring the current-voltage characteristics of solar cells equipped with an SS150AAA solar radiation simulator

3. RESULTS

Figure 5a shows the surface topography of monocrystalline silicon "as cut" - not subjected to chemical-mechanical treatments. The surface is rough, uneven and defective, which, according to literature [8], increases surface recombination and consequently reduces the efficiency of the solar cell. In order to improve the surface quality, the silicon is subjected to cleaning and texturing. The purpose of texturization is to increase the surface area and reduce light reflection. This is often done using wet chemical etching (such as with sodium or potassium hydroxide and isopropyl alcohol). As a result of alkaline etching, unevenly distributed "pyramids" are formed on the surface of single-crystalline silicon (100), not exceeding $10\ \mu\text{m}$ at the base (Fig. 5b).

To confirm effectiveness of produced textures and deposited ARC reflectance was measured with spectrophotometer UV-Vis (Fig.6). Monocrystalline silicon before texturization through the entire range of the test area reflects above 27% of the light. The applied to monocrystalline silicon with crystallographic orientation (100) alkaline texturization significantly enhances absorption of the light. In the range of $500\div 1050\ \text{nm}$ reflectance index decreases below 13.5%. Textured monocrystalline silicon with antireflective coating shows the best outcomes with the lowest values of the reflectance reached.

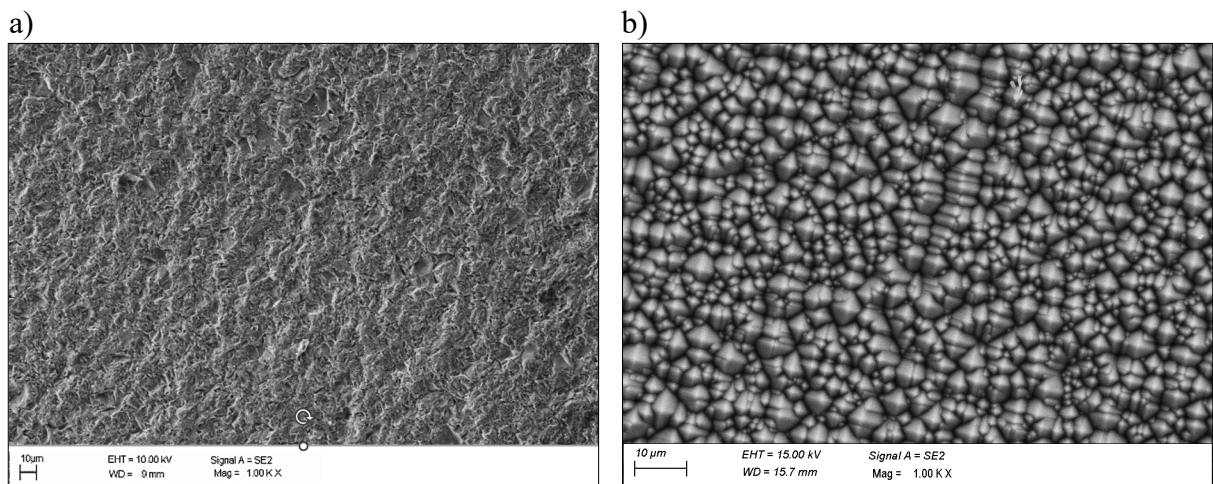


Figure 5. Monocrystalline silicon surface (100) a) before, b) after texturization

The reflection for the surface of textured monocrystalline silicon is significantly reduced compared to the non-textured substrate, while the nature of the curve is very similar. On the other hand, the application of an antireflection coating of silicon nitride causes a significant reduction in reflection in the wavelength range of 580÷680 nm, reaching a minimum of 2.41% (at 627 nm). Most of the solar energy that reaches the earth is in the visible light range (approx. 400 nm to 700 nm). Optimizing the absorption of light in this range is crucial for the solar cells to generate as much electrical energy as possible.

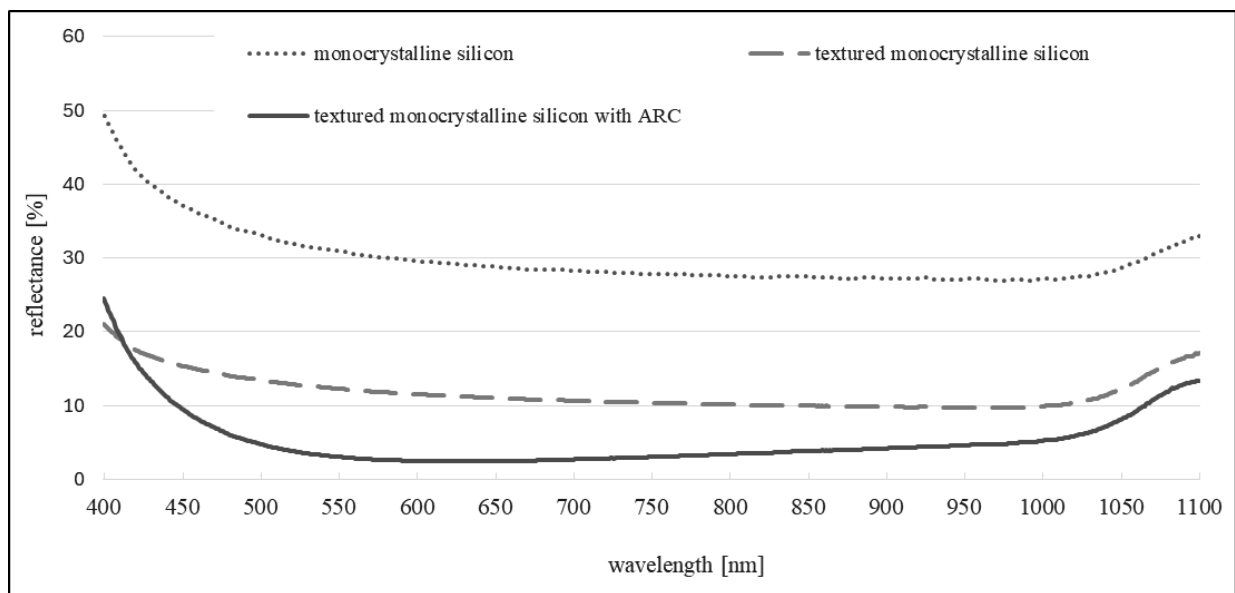


Figure 6. Dependence of the light reflectance on the light wavelength of the monocrystalline silicon surface for different stages of processing

Comparison of the I–V characteristics of the monocrystalline and polycrystalline silicon solar cells are shown in Figure 6. The electrical properties of silicon solar cells such as: conversion efficiency (E_{ff}), fill factor (FF), short circuit current (I_{sc}), open-circuit voltage (V_{oc}), current (I_m) and voltage (V_m) for which the power (P_m) reaches its maximum value are summarized in Table 1. It was found that the monocrystalline silicon solar cell exhibit higher short-circuit current, open-circuit voltage, fill factor and efficiency by 0.4 A, 0.025 V, 0.01 and 2.37 percentage points, respectively, compared to the device made of polycrystalline silicon. A monocrystalline silicon has a uniform crystal structure, meaning that the silicon atoms are arranged in a regular manner throughout the material. This regularity allows an electron to move freely within a single crystal lattice, leading to lower electrical resistance. Moreover, the texturing of polycrystalline silicon in alkaline solutions is not as effective as for monocrystalline silicon due to the different etching rates of grains with different crystallographic orientations. This leads to a decrease in the efficiency of solar cells made of polycrystalline silicon.

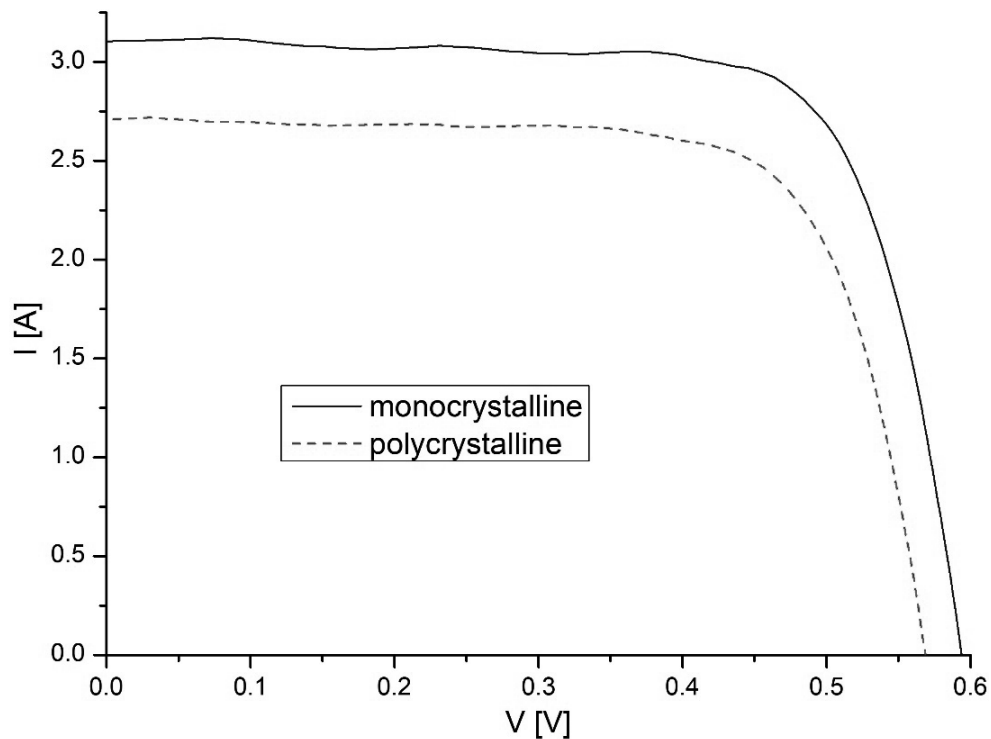


Figure 7. Current-voltage characteristics of polycrystalline and monocrystalline silicon solar cells

Table 1. Electrical properties of polycrystalline and monocrystalline silicon solar cells

Type of silicon solar cell	Electrical properties						
	I_{sc} [A]	V_{oc} [V]	I_m [A]	V_m [V]	P_m [W]	FF	E_{ff} [%]
polycrystalline	2.71	0.569	2.47	0.454	1.12	0.73	11.21
monocrystalline	3.11	0.594	2.86	0.477	1.36	0.74	13.58

4. CONCLUSIONS

The solar cells characteristics are important factors to take into account when designing photovoltaic systems expected to depend on the solar energy. Knowing them allows to optimize the operation of devices. Despite the fact that the devices were made using the same technology, the efficiency of the monocrystalline silicon photovoltaic cell is higher by 2.37 percentage points compared to the device based on polycrystalline silicon. This is due, among other things, to the different efficiency of silicon surface texturing. The use of potassium or sodium base for etching monocrystalline silicon with crystallographic orientation (100) results in the formation of a characteristic pyramidal structure on the surface. Unfortunately, this method of texturing polycrystalline silicon is not as effective due to the presence of grains with different crystallographic orientation, which reduces the efficiency of the solar cell. In addition, in the case of monocrystalline silicon, the entire material is made up of a single crystal, which means that electrons can move freely throughout the material, minimizing energy loss. In polycrystalline silicon, there are grain boundaries, which makes it difficult for charge carriers to move and leads to energy loss.

ACKNOWLEDGMENTS

The work was created as a result of the project PBL (Project Based Learning) - 11th edition – of the Excellence Initiative - Research University, Silesian University of Technology.

BIBLIOGRAPHY

1. H. Zhao, L. Zhang, Silicon production technology, *Journal of Materials Processing Technology*, 146/1-3 (2004) 1-9.
2. T. Petzold, Advances in Silicon Processing: From the refining to the purification, *Journal of Materials Science & Technology*, 32/1 (2016) 10-18.
3. J. A. Bergman, T. Norberg, Silicon production and refining techniques. *Materials Science and Engineering Reports*, 35/3 (2001) 1-35.
4. L. A. Dobrzański, *Materiały inżynierskie z podstawami technologii procesów materiałowych*, Wydawnictwo Naukowe PWN, 2024.
5. M. D. Sabatino, R. Hendawi and A. S. Garcia, Silicon Solar Cells: Trends, Manufacturing Challenges, and AI Perspectives, *Crystals*, 14/2 (2024) 167.
6. T. Markvart, L. Castaner, *Solar Cells – Materials, manufacture and operation*, Elsevier, 2004.
7. P. Panek, M. Lipiński, E. Beltowska-Lehman, Industrial technology of multicrystalline silicon solar cells, *Opto-Electronics Review*, 11/4 (2003) 269-275.
8. A.S. Al-Ezzi, M.N.M. Ansari, Operation and physics of photovoltaic solar cells: an overview, *Applied System Innovation*, 5 (2022) 67.
9. S. Ranjan, S. Balaji, R. A. Panella, B. E. Ydstie, Silicon solar cell production, *Computers & Chemical Engineering*, 35/8 (2011) 1439-1453.
10. A. Machin, F. Marquez, Advancements in photovoltaic cell materials: silicon, organic, and perovskite solar cells, *Materials*, 17/5 (2024) 1165.
11. P. K. Nayak, G. Garcia-Belmonte, A. Kahn, J. Bisquert and D. Cahen, Photovoltaic efficiency limits and material disorder, *Energy Environmental Science*, 5 (2012) 6022-6039.
12. K. Krykowski, *Energoelektronika*, Wydawnictwo Politechniki Śląskiej, Gliwice, 2007.
13. L. A. Dobrzański, A. Drygała, Surface texturing of multicrystalline silicon solar cells, *Journal of Achievements in Materials and Manufacturing Engineering*, 31/1 (2008) 77-82.



31th January 2025
Gliwice, Poland

DEPARTMENT OF ENGINEERING MATERIALS AND BIOMATERIALS
FACULTY OF MECHANICAL ENGINEERING
SILESIA UNIVERSITY OF TECHNOLOGY

INTERNATIONAL STUDENTS SCIENTIFIC CONFERENCE

Investigating the Hard Tungsten Carbide Coating formed on H13 Steel Surfaces via Electro-Spark Deposition Technique

Ahmet Kavukcu^{a,b}, Berke Gültekin^a, Salim Levent Aktuğ^a, Metin Usta^a

^a Gebze Technical University, Faculty of Engineering, Department of Materials Science and Engineering, Aluminum Research Center
email: akavukcu@gtu.edu.tr

Abstract: This study explores the application of hard tungsten carbide (WC) coatings on H13 steel using the Electro-Spark deposition (ESD) technique to enhance its hardness and wear resistance. Structural and mechanical characterization of the WC-coated samples was conducted using scanning electron microscopy (SEM), energy dispersive spectroscopy (EDS), X-ray diffraction (XRD), and microhardness testing, providing both qualitative and quantitative analyses. Additionally, dry sliding wear and microhardness tests were conducted to evaluate the friction coefficient, wear behavior, and hardness of the samples. The results showed the successful formation of WC and W₂C phases, leading to a significant increase in hardness (approximately 400%, from 290 HV to 1400 HV), a reduction in the coefficient of friction (CoF) by 80-85%, and a decrease in wear volume by 80%. These findings demonstrate that WC coatings applied via ESD significantly improve the mechanical properties of H13 steel, offering enhanced durability and wear resistance for applications subjected to high loads and mechanical stress in demanding industrial settings.

Keywords: Tungsten Carbide, Electro-Spark Deposition, Hot Work Tool Steels

1. INTRODUCTION

For many years, hot work die steels have been widely used in industries requiring materials capable of withstanding high loads and mechanical stresses, such as those experienced by hot forging dies, hot extrusion dies, and pressure casting dies [1,2]. H-series steels, in general, are primarily employed in die manufacturing due to their exceptional ability to withstand the high loads and elevated temperatures involved in forging. The demand for materials capable of withstanding severe thermal and mechanical stresses has positioned AISI H13 steel as a preferred choice in the tooling industry [3]. Although H13 steel exhibits excellent mechanical properties and is widely utilized in various applications, prolonged usage under excessive mechanical stresses and abrasive conditions can lead to surface degradation and wear-related challenges. Surface modification techniques play a crucial role in overcoming these issues. Various surface modification techniques have been developed in order to improve the performance of H13 steel and to extend its service life. Among these surface modification techniques are physical vapor deposition (PVD), laser cladding, gas and plasma nitriding,

powder-pack boriding, hot-dip aluminizing (HDA), and high velocity oxy-fuel (HVOF) coating, with various studies and publications having been conducted on their applications and effects [4–9].

WC (Tungsten Carbide), TiC (Titanium Carbide), CrC (Chromium Carbide), and NiC (Nickel Carbide) are advanced ceramic materials widely used in industrial applications for their exceptional hardness, wear resistance, and ability to withstand extreme thermal and mechanical stresses [10–13]. Within surface modification techniques, the electro-spark deposition (ESD) method is notable for its versatility, portability, and efficiency in improving surface properties, enhancing wear resistance, and boosting performance in demanding conditions, allowing for the application of cermets [14]. Electro-spark deposition (ESD) is a micro-welding process that utilizes a potential difference to create rapid electrical discharges, transferring material from an electrode to a substrate. This phenomenon can be visually represented in Figure 1. The process generates high-temperature and high-stress zones through pulsed micro-arcs, enabled by the potential difference, facilitating alloying and the formation of high-melting-point composite coatings. This precise process minimizes heat affected zone (HAZ) compared to conventional welding methods, making it ideal for repairing and improving steel surface properties in demanding applications [15].

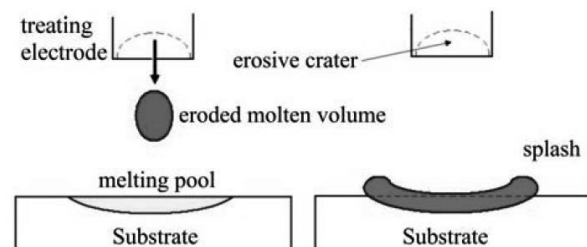


Figure 1: Illustration of the transfer of eroded molten volume from the anode (electrode) to the cathode (substrate).

The motivation behind this study stems from the need to enhance the durability and performance of steel components, particularly in demanding industrial applications. The findings could significantly contribute to improving the wear resistance, hardness, and overall durability of steel components, thus advancing the field of surface coating technologies for industrial applications.

In this study, a tungsten carbide (WC) coating was applied to an AISI H13 steel substrate using the electro-spark deposition (ESD) technique. The coating layers were characterized structurally and mechanically through both qualitative and quantitative analyses, while dry sliding wear and microhardness tests were conducted to evaluate the friction coefficient, wear behavior, and hardness of the samples.

2. EXPERIMENTAL PROCEDURES

2.1 Sample Preparation

For the experimental studies, H13 (ASTM A681- DIN 1.2344) hot work tool steel plates were cut as rectangular prism-shaped plates with dimensions of 15 mm x 6 mm x 10 mm.

The chemical composition of H13 steel, determined using a SpectroMaxx optic emission spectrometer, includes 0.37 wt% carbon (C), 5.18 wt% chromium (Cr), 1.37 wt% molybdenum (Mo), 0.9 wt% silicon (Si), and 1.0 wt% vanadium (V), with the remainder comprising iron (Fe). All samples were ground using SiC grinding paper up to 1000 grit, then cleaned in an ultrasonic bath containing alcohol. Afterward, samples were rinsed with distilled water and dried using a heat gun. Detailed information about the ESD coating system can be found in previous studies [16,17].

2.2. Coating System and Parameters

Elitron-16 type computer assisted electro-spark deposition device was used. WC (92)-Co(8) electrode was used to conduct deposition. In the present investigation, the ESD coating experiments were conducted in air with a series of pulses of a certain duration by hand-held applicator. Mass changes in coated samples are measured by analytical balance before and after deposition process. The electro-spark deposition process utilized a WC (92)-Co (8) coating electrode with a pulse energy of 1.32 J, an electric charge of 3000 mC, a pulse current of 200 A, a pulse duration of 390.25 μ s, and a frequency of 38.437 Hz.

2.3. Characterization Methods

Rigaku D/Max 2200 model XRD device was used for the XRD analyses, conducted with Cu-K α radiation at 40 mA current and 40 kV generator voltage, over a scanning angle range of 30° to 90°. The SEM-EDS analyses of the samples were conducted with Scanning Electron Microscope using a Philips XL 30 SFEG scanning electron microscope equipped with an integrated energy dispersive spectrometer (EDS). A Mitutoyo HM-112 microhardness tester was used to measure the microhardness. Vickers microhardness indentations were made on all samples by applying a 25-gram load for 10 seconds. To determine the effect of coatings on wear characteristics, CSM Tribometer branded a “ball on disc” wear test method was applied to the samples with alumina ball. The wear tests were conducted under conditions of 200 meter, a 10N load, and a speed of 10 cm/s for all samples.

3. RESULTS AND DISCUSSIONS

3.1. Characterization of Coating Layer

The graph shown in Figure 2 illustrates the relationship between the number of passes, along with the increase in mass (in milligrams) and the percentage increase in mass of the substrate. It can be observed that as the number of passes increases, the mass gain initially rises, but the percentage increase in mass becomes limited. As a characteristic of Electro-Spark Deposition (ESD), an increase in the substrate material's weight was expected. However, as the number of passes increased, the rate of mass gain decreased due to the insufficient formation of an adequate spark between the anode and cathode [18]. This trend highlights the efficiency of material deposition during the initial passes, with the increase in mass becoming less pronounced in the later passes.

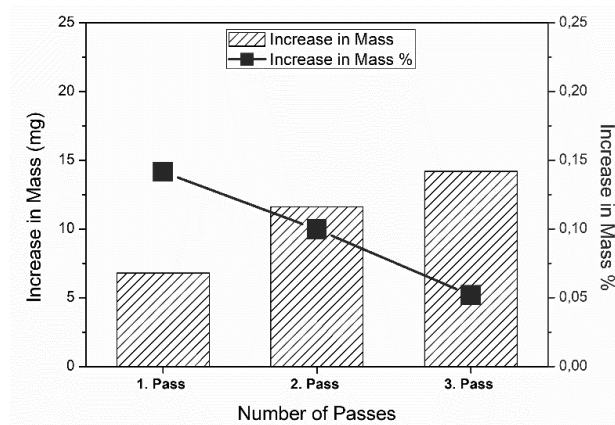


Figure 2. The number of passes, along with the increase in mass (in milligrams) and the percentage increase in mass of the substrate.

X-ray diffraction (XRD) patterns of WC-coated sample and H13 steel are given in Figure 3. XRD patterns analysis indicates the formation of tungsten carbide phases, primarily WC and W₂C, on the WC-coated sample surface. These phases are known for their high hardness and wear resistance. The diffraction peaks corresponding to Fe-based phases are thought to originate from signals emitted by the substrate metal.

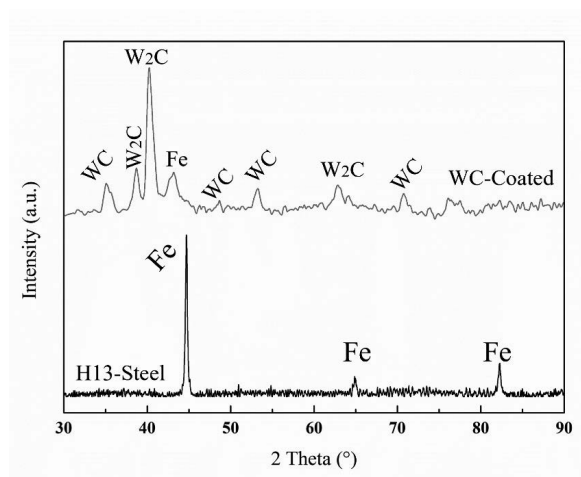


Figure 3. X-ray diffraction (XRD) patterns of WC-coated sample and H13 steel

Top view Scanning Electron Microscopy (SEM) images of the WC-coated steel surfaces at different magnifications, along with the Energy Dispersive Spectroscopy (EDS) analysis results, are presented in Figure 4. The SEM images reveal a heterogeneous and rough microstructure, which is characteristic of the Electro-Spark Deposition (ESD) process. The surface displays distinct solidified regions, with microcracks and porosities observed in certain areas. These features are indicative of the rapid solidification processes typical of ESD. Additionally, regions showing splat-like structures suggest localized melting and resolidification, consistent with the high-energy discharge inherent to the ESD method [19,20]. The droplet-like materials part, eroded from the electrode, fall on top of each other and form a layered structure, contributing to the creation of small peaks on the surface. This stacking effect is a direct result of the spark interactions during the electro-spark deposition process [21]. Energy Dispersive Spectroscopy (EDS) analysis confirms the tungsten carbide successfully deposited on the H13 steel substrate. The primary elements detected include tungsten, carbon,

iron. This morphological structure, formed by stacked droplets that create micro-scale elevations, yielded a result consistent with expectations, showing the tungsten content to be higher in the uppermost droplet.

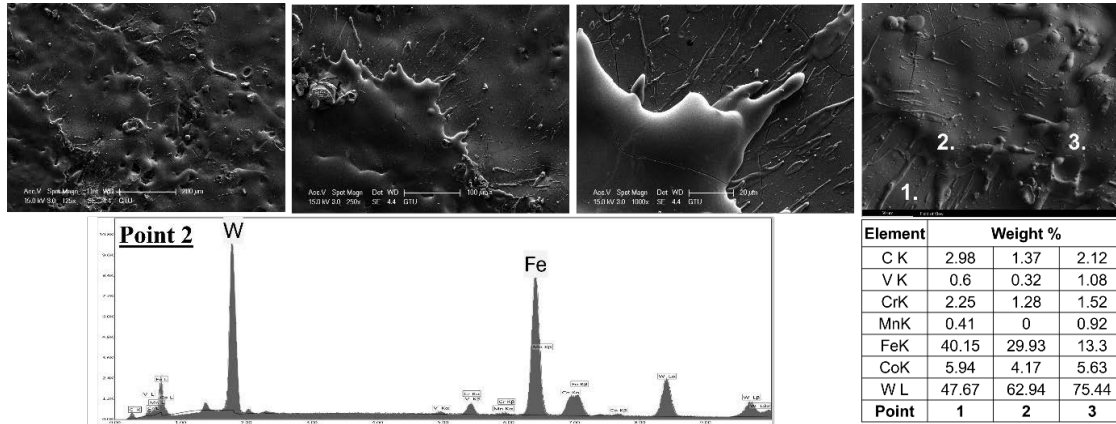


Figure 4. Scanning Electron Microscopy (SEM) top-view images of the WC-coated steel surfaces at different magnifications, along with the Energy Dispersive Spectroscopy (EDS) analysis.

Cross-sectional SEM images of the WC-coated steel surfaces at different magnifications and the EDS analysis results are presented in Figure 5. The coating thickness varies between 15 μm and 25 μm , showing relatively consistent deposition across the surface with satisfactory adherence to the substrate. On the other hand, defects in the coating layer, including cavities and cracks, are evident, mainly due to the evaporation and accumulation of eroded materials during the ESD process. This accumulation leads to the heterogeneous dispersion of phases throughout the coating layers [22]. The EDS results show bright spots on the surface, corresponding to high atomic number, which confirms the presence of tungsten phases in the coating layers. The atomic percentages of tungsten and carbon indicate that the phases are predominantly tungsten carbide.

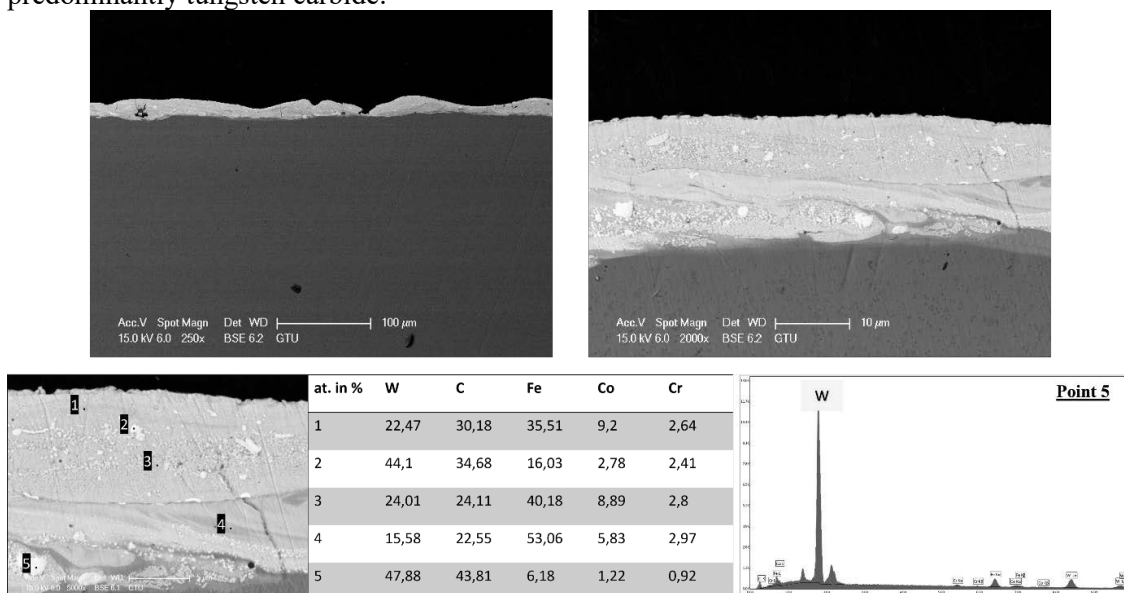


Figure 5. SEM cross-sectional images of the WC-coated steel surfaces at different magnification with EDS analysis results

3.2. Mechanical and Tribological Properties

As shown in Figure 6, the coefficient of friction (CoF) comparison between uncoated H13 steel and the WC-coated sample is presented, along with a column graph highlighting the significant increase in hardness of the WC-coated sample compared to H13 steel. Additionally, optical images of the hardness track demonstrate the differences in the hardness profiles of the two materials. Friction coefficient for uncoated H13 steel ranges between 0.8 and 0.9, exhibiting fluctuations. In contrast, the WC-coated sample maintains a stable CoF of approximately 0.15, reflecting superior frictional stability and reduced sliding resistance. Wear resistance is markedly improved, with the WC-coated sample achieving an 80–85% reduction in wear compared to the uncoated H13 steel, as evidenced by CoF and wear analysis. The average hardness of the WC-coated layers is significantly enhanced, reaching 1400 HV, nearly five times higher than the 290 HV of uncoated H13 steel. The increase in hardness and the decrease in CoF can be correlated with the presence of WC phases on the surface [13,23].

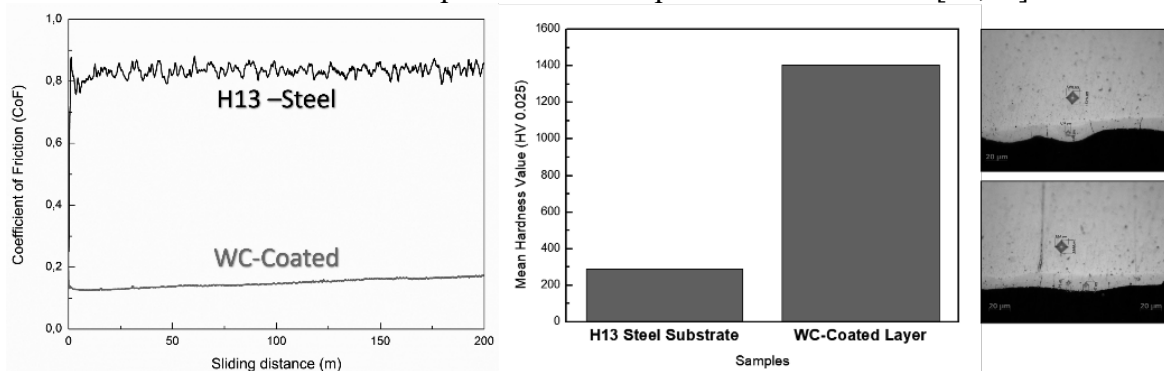


Figure 6. Graph of sliding distance, coefficient of friction and Vickers hardness value with hardness track images

Figure 7 illustrates the wear rates graph, 3D profiles images, and SEM images of the worn surfaces of the materials. The wear rate analysis indicates a significant improvement with the WC coating. The wear volume of uncoated H13 steel is approximately 12.32 mm³, with a wear rate of 12.5×10^{-6} mm³/N·m. In comparison, the WC-coated sample shows a drastically lower wear volume of approximately 2.38 mm³, with a wear rate of 2.5×10^{-6} mm³/N·m. This demonstrates a substantial reduction in material wear, indicating the effectiveness of the WC coating in enhancing wear resistance, as expected [24,25]. Given these results, it is recommended to use WC coating for applications where reduced wear and enhanced durability are critical, as it significantly reduces the wear volume by approximately 80–85%, improving the wear performance of H13 steel. The worn trace images of uncoated H13 steel typically show deeper grooves, cracks, and surface damage, with detached material particles (such as small fragments or debris) visible around the wear track. The surface may exhibit signs of plastic deformation, wear ridges, and micro-cracks, indicative of high friction and stress during wear. The overall appearance often reflects a rougher and more severely worn surface compared to coated materials, with signs of material loss concentrated in specific areas. In contrast, the WC-coated surface exhibits shallower grooves and a less extensive worn area, with abrasive wear patterns, further confirming its superior wear resistance [26,27].

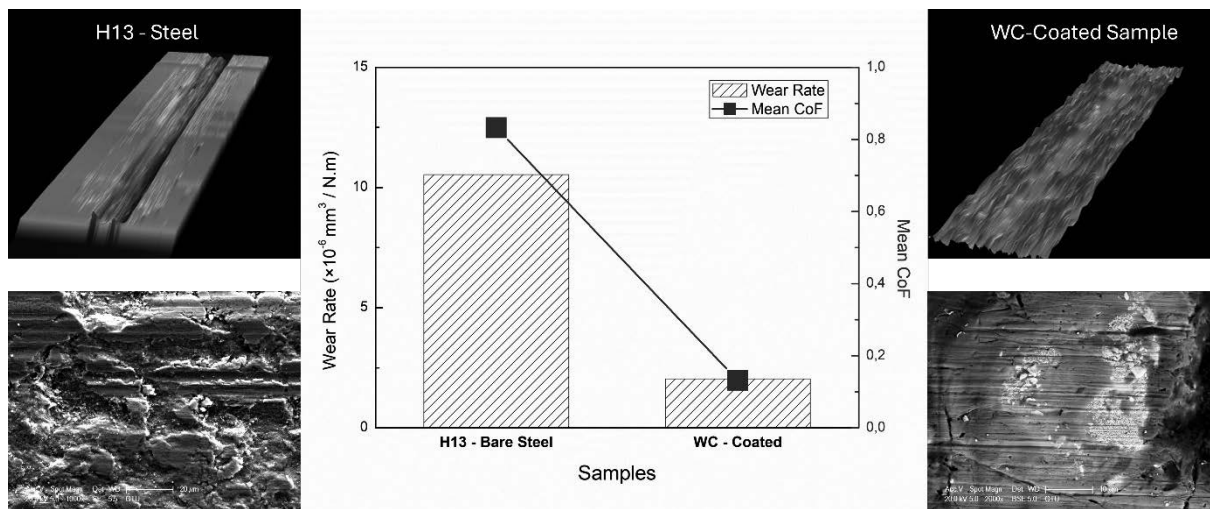


Figure 7. Wear rates and mean CoF graph, 3D profiles images, and SEM images of the worn surfaces of the materials.

4. CONCLUSION

Deposition was successfully achieved with reasonable coating parameters and a consistent coating process, as evidenced by the increase in mass. XRD analysis confirmed the formation of WC and W_2C phases on the surface, which are known for their high hardness and wear resistance. In accordance with the EDS results, these phases were detected in the coating layers, further supporting the presence of tungsten carbide compounds in the deposited material.

The hardness of the WC-coated H13 steel improved by approximately 400%, increasing from 290 HV (uncoated H13 steel) to 1400 HV (WC-coated steel). The coefficient of friction (CoF) was reduced by around 80-85%, with the WC-coated sample exhibiting a CoF of approximately 0.15, compared to range of 0.8-0.9 observed in uncoated H13 steel. The wear volume of the WC-coated sample decreased by approximately 80%, with the wear volume of the uncoated H13 steel at 12.32 mm^3 and the WC-coated sample at 2.38 mm^3 . The wear rate of the WC-coated sample was reduced by 80%, with a wear rate of $2.5 \times 10^{-6} \text{ mm}^3/\text{N}\cdot\text{m}$ for the WC-coated sample, compared to $12.5 \times 10^{-6} \text{ mm}^3/\text{N}\cdot\text{m}$ for the uncoated H13 steel.

These mechanical improvements can be attributed to the presence of tungsten carbide (WC) phases dispersed within the coating layers, which contribute significantly to the enhanced hardness, wear resistance, and reduced friction.

REFERENCES

- [1] Q. Zhou, X. Wu, N. Shi, J. Li, N. Min, *Materials Science and Engineering: A*, 528 (2011) 5696–5700.
- [2] J.-Y. Li, Y.-L. Chen, J.-H. Huo, *Materials Science and Engineering: A*, 640 (2015) 16–23.
- [3] J. Marashi, E. Yakushina, P. Xirouchakis, R. Zante, J. Foster, *Journal of Materials Processing Technology*, 246 (2017) 276–284.
- [4] Q.Y. Zhang, Y. Zhou, J.Q. Liu, K.M. Chen, J.G. Mo, X.H. Cui, S.Q. Wang, *Wear*, 344–345 (2015) 22–31.

- [5] R.C. Morón, I. Hernández-Onofre, A.D. Contla-Pacheco, D. Bravo-Bárceñas, I. Campos-Silva, *Journal of Materials Engineering and Performance*, 29 (2020) 4529–4540.
- [6] A.A. Candido Recco, A.P. Tschiptschin, *Journal of Materials Research and Technology*, 1 (2012) 182–188.
- [7] H. Li, B. Li, C. Deng, Y. Wang, *Journal of Physics: Conference Series*, 1213 (2019) 52020.
- [8] J.Z. Lu, J. Cao, H.F. Lu, L.Y. Zhang, K.Y. Luo, *Surface and Coatings Technology*, 369 (2019) 228–237.
- [9] R. Rodríguez-Baracaldo, J.A. Benito, E.S. Puchi-Cabrera, M.H. Staia, *Wear*, 262 (2007) 380–389.
- [10] X.C. Zhang, B.S. Xu, F.Z. Xuan, S.T. Tu, H.D. Wang, Y.X. Wu, *Wear*, 265 (2008) 1875–1883.
- [11] V.I. Kalita, A.A. Radyuk, D.I. Komlev, A.B. Mikhailova, A. V Alpatov, D.D. Titov, M.I. Alymov, *Inorganic Materials: Applied Research*, 12 (2021) 461–467.
- [12] E. Celik, O. Culha, B. Uyulgan, N.F. Ak Azem, I. Ozdemir, A. Turk, *Surface and Coatings Technology*, 200 (2006) 4320–4328.
- [13] L. Qiao, Y. Wu, S. Hong, W. Long, J. Cheng, *Ceramics International*, 47 (2021) 1829–1836.
- [14] W. Wang, M. Du, X. Zhang, C. Luan, Y. Tian, *Materials*, 14 (2021).
- [15] M. Rukanskis, *Surface Engineering and Applied Electrochemistry*, 55 (2019) 607–619.
- [16] K. Korkmaz, A. Ribalko, *Metallic Materials*, 49 (2011) 265–270.
- [17] A. V Ribalko, K. Korkmaz, O. Sahin, *Surface and Coatings Technology*, 202 (2008) 3591–3599.
- [18] K. Korkmaz, *Surface and Coatings Technology*, 272 (2015) 1–7.
- [19] S.K. Tang, (2009) 69.
- [20] Y. Xie, M. Wang, *Surface and Coatings Technology*, 201 (2006) 691–698.
- [21] Y. Liu, Q. Su, S. Zhang, J. Qu, S. Zhang, *Coatings*, 13 (2023).
- [22] A. Lešnjak, J. Tušek, [Http://Dx.Doi.Org/10.1179/136217102225006886](http://Dx.Doi.Org/10.1179/136217102225006886), 7 (2013) 391–396.
- [23] R.N. Johnson, G.L. Sheldon, *Journal of Vacuum Science & Technology A: Vacuum, Surfaces, and Films*, 4 (1998) 2740.
- [24] S. Buytoz, M. Ulutan, M.M. Yildirim, *Applied Surface Science*, 252 (2005) 1313–1323.
- [25] B. Song, J.W. Murray, R.G. Wellman, Z. Pala, T. Hussain, *Wear*, 442–443 (2020) 203114.
- [26] N. Vashishtha, S. Sapate, *Materials Research*, 22 (2018).
- [27] J. Xu, X.-C. Zhang, F.-Z. Xuan, Z. Wang, S.-T. Tu, *Journal of Materials Engineering and Performance*, 21 (2011).



31th January 2025
Gliwice, Poland

DEPARTMENT OF ENGINEERING MATERIALS AND BIOMATERIALS
FACULTY OF MECHANICAL ENGINEERING
SILESIA UNIVERSITY OF TECHNOLOGY

INTERNATIONAL STUDENTS SCIENTIFIC CONFERENCE

Innovative laser technology for surface treatment of engineering materials

Stanisław Kielkowski^a, Mateusz Król^a, Mirosław Bonek^b

^a- V Liceum Ogólnokształcące z Oddziałami Dwujęzycznymi im. Andrzeja Struga

^b- Politechnika Śląska, Wydział Mechaniczny Technologiczny, Katedra Materiałów Inżynierskich i Biomedycznych

Abstract: This article discusses the principle of operation of lasers, their use in cutting engineering materials, highlights the innovative features resulting from their use, and presents challenges and prospects in the development of this technology.

Keywords: Laser, surface engineering, innovation

1. INTRODUCTION

Physicists had been working for generations toward controlling ever shorter wavelengths. After radio (meters) and radar (centimeters, then millimeters), the logical next step would be far-infrared waves. Masers had been modestly useful, more for scientific research than for military or industrial applications. Only a few scientists thought an infrared maser might be important and pondered how to make one. Infrared rays could not be manipulated like radar, and indeed were hard to manage at all.

Schawlow found the key put the atoms you wanted to stimulate in a long, narrow cavity with mirrors at each end. The rays would shuttle back and forth inside so that there would be more chances for stimulating atoms to radiate. One of the mirrors would be only partly silvered so that some of the rays could leak out. This arrangement (the Fabry-Pérot etalon) was familiar to generations of optics researchers.

The same arrangement meanwhile occurred to Gordon Gould, a graduate student at Columbia University who had discussed the problem with Townes. For his thesis research, Gould had already been working with "pumping" atoms to higher energy states so they would emit light. As Gould elaborated his ideas and speculated about all the things you could do with a concentrated beam of light, he realized that he was onto something far beyond the much-discussed "infrared maser". In his notebook he confidently named the yet-to-be-invented device a LASER (for Light Amplification by Stimulated Emission of Radiation).

Schawlow, Gould and Townes now understood how to build a laser in principle. To actually build one would require more ideas and a lot of work. Some of the ideas were already in hand. Other physicists in several countries, aiming to build better masers, had worked out various ingenious schemes to pump energy into atoms and molecules in gases and solid crystals. In a way they too were inventors of the laser. So were many others clear back to Einstein.

2. HISTORICAL DEVELOPMENT OF LASER

1960s

The first medical treatment using a laser on a human patient is performed by Dr. Charles J. Campbell of the Institute of Ophthalmology at Columbia-Presbyterian Medical Center and Charles J. Koester of the American Optical Co. at Columbia-Presbyterian Hospital in Manhattan. An American Optical ruby laser is used to destroy a retinal tumor.

Groups at GE, IBM and MIT's Lincoln Laboratory simultaneously develop a gallium-arsenide laser, a semiconductor device that converts electrical energy directly into infrared light but which must be cryogenically cooled, even for pulsed operation.

Nick Holonyak Jr., a consulting scientist at a General Electric Co. lab in Syracuse, N.Y., publishes his work on the "visible red" GaAsP (gallium arsenide phosphide) laser diode, a compact, efficient source of visible coherent light that is the basis for today's red LEDs used in consumer products such as CDs, DVD players and cell phones.

Extreme nonlinear optical techniques have succeeded in upconverting visible laser light into x-rays, making a tabletop source of coherent soft x-rays possible. (University of Colorado)

Bell Labs reports the first yttrium aluminum garnet (YAG) laser. Logan E. Hargrove, Richard L. Fork and M.A. Pollack report the first demonstration of a mode-locked laser; i.e., a helium-neon laser with an acousto-optic modulator. Mode locking is fundamental for laser communication and is the basis for femtosecond lasers.

Herbert Kroemer of the University of California, Santa Barbara, and the team of Rudolf Kazarinov and Zhores Alferov of A.F. Ioffe Physico-Technical Institute in St. Petersburg, Russia, independently propose ideas to build semiconductor lasers from heterostructure devices. The work leads to Kroemer and Alferov winning the 2000 Nobel Prize in physics.

After two years working on HeNe and xenon lasers, William B. Bridges of Hughes Research Labs discovers the pulsed argon-ion laser, which, although bulky and inefficient, could produce output at several visible and UV wavelengths.

Townes, Basov and Prokhorov are awarded the Nobel Prize in physics for their "fundamental work in the field of quantum electronics, which has led to the construction of oscillators and amplifiers based on the maser-laser-principle."

The carbon dioxide laser is invented by Kumar Patel at Bell Labs. The most powerful continuously operating laser of its time, it is now used worldwide as a cutting tool in surgery and industry.

The Nd:YAG (neodymium-doped YAG) laser is invented by Joseph E. Geusic and Richard G. Smith at Bell Labs. The laser later proves ideal for cosmetic applications, such as laser-assisted in situ keratomileusis (lasik) vision correction and skin resurfacing. Two lasers are phase-locked for the first time at Bell Labs, an important step toward optical communications. Jerome V.V. Kasper and George C. Pimentel demonstrate the first chemical laser, a 3.7- μm hydrogen chloride instrument, at the University of California, Berkeley.

Charles K. Kao, working with George Hockham at Standard Telecommunication Laboratories in Harlow, UK, makes a discovery that leads to a breakthrough in fiber optics. He calculates how to transmit light over long distances via optical glass fibers, deciding that, with a fiber of purest glass, it would be possible to transmit light signals over a distance of 100 km, compared with only 20 m for the fibers available in the 1960s. Kao receives a 2009 Nobel Prize in physics for his work. French physicist Alfred Kastler wins the Nobel Prize in physics for his method of stimulating atoms to higher energy states, which he developed between 1949 and 1951. The technique, known as optical pumping, was an important step toward the creation of

the maser and the laser. Bernard Soffer and Bill McFarland invent the tunable dye laser at Korad Corp. in Santa Monica, Calif. In California, Maiman and other laser pioneers found the laser advocacy group Laser Industry Association, which becomes the Laser Institute of America in 1972. Gould buys back his patent rights for \$1 plus 10 percent of future profits when TRG is sold.

Basov, V.A. Danilychev and Yu. M. Popov develop the excimer laser at P.N. Lebedev Physical Institute. Alferov's group at Ioffe Physico-Technical Institute and Mort Panish and Izu Hayashi at Bell Labs produce the first continuous-wave room-temperature semiconductor lasers, paving the way toward commercialization of fiber optic communications.

At Corning Glass Works (now Corning Inc.), Drs. Robert D. Maurer, Peter C. Schultz and Donald B. Keck report the first optical fiber with loss below 20 dB/km, demonstrating the feasibility of fiber optics for telecommunications.

A laser in operation at the Electronics Resource Centers Space Optics Laboratory is checked by Lowell Rosen and Dr. Norman Knable. They investigated energy levels of atoms in very excited states as a step to improving the laser's efficiency in space.

The ERC opened in September 1964, taking over the administration of contracts, grants and other NASA business in New England from the antecedent North Eastern Operations Office (created in July 1962), and closed in June 1970. It served to develop the space agency's in-house expertise in electronics during the Apollo era. A second key function was to serve as a graduate and postgraduate training center within the framework of a regional government-industry-university alliance. Research at the ERC was conducted in 10 different laboratories: space guidance, systems, computers, instrumentation research, space optics, power conditioning and distribution, microwave radiation, electronics components, qualifications and standards, and control and information systems. Researchers investigated such areas as microwave and laser communications; the miniaturization and radiation resistance of electronic components; guidance and control systems; photovoltaic energy conversion; information display devices; instrumentation; and computers and data processing. Although the only NASA center ever closed, the ERC actually grew while NASA eliminated major programs and cut staff in other areas. Between 1967 and 1970, NASA cut permanent civil service workers at all centers with one exception, the ERC, whose personnel grew annually until its closure in June 1970. (NASA Archives)

1970s

Arthur Ashkin of Bell Labs invents optical trapping, the process by which atoms are trapped by laser light. His work pioneers the field of optical tweezing and trapping and leads to significant advances in physics and biology. Izu Hayashi and Morton B. Panish of Bell Labs design the first semiconductor laser that operates continuously at room temperature.

Charles H. Henry invents the quantum well laser, which requires much less current to reach lasing threshold than conventional diode lasers and which is exceedingly more efficient. Holonyak and students at the University of Illinois at Urbana-Champaign first demonstrate the quantum well laser in 1977. A laser beam is used at Bell Labs to form electronic circuit patterns on ceramic. A pack of Wrigley's chewing gum is the first product read by a bar-code scanner in a grocery store.

Engineers at Laser Diode Labs Inc. in Metuchen, N.J., develop the first commercial continuous-wave semiconductor laser operating at room temperature. Continuous-wave operation enables transmission of telephone conversations. First quantum-well laser operation

made by Jan P. Van der Ziel, R. Dingle, Robert C. Miller, William Wiegmann and W.A. Nordland Jr. The lasers actually are developed in 1994.

First demonstration, at Bell Labs, of a semiconductor laser operating continuously at room temperature at a wavelength beyond 1 μm , the forerunner of sources for long-wavelength lightwave systems.

John M.J. Madey and his group at Stanford University in California demonstrate the first free-electron laser (FEL). Instead of a gain medium, FELs use a beam of electrons that are accelerated to near light speed, then passed through a periodic transverse magnetic field to produce coherent radiation. Because the lasing medium consists only of electrons in a vacuum, FELs do not have the material damage or thermal lensing problems that plague ordinary lasers and can achieve very high peak powers.

The first commercial installation of a Bell Labs fiber optic lightwave communications system is completed under the streets of Chicago.

Gould is issued a patent for optical pumping, then used in about 80 percent of lasers. The LaserDisc hits the home video market, with little impact. The earliest players use HeNe laser tubes to read the media, while later players use infrared laser diodes. Following the failure of its videodisc technology, Philips announces the compact disc (CD) project. Gould receives a patent covering a broad range of laser applications.

1980s

Schawlow and Bloembergen receive the Nobel Prize in physics for their contributions to the development of laser spectroscopy.

Peter F. Moulton of MIT's Lincoln Laboratory develops the titanium-sapphire laser, used to generate short pulses in the picosecond and femtosecond ranges. The Ti:sapphire laser replaces the dye laser for tunable and ultrafast laser applications.

The audio CD, a spinoff of LaserDisc video technology, debuts. Billy Joel fans rejoice, as his 1978 album "52nd Street" is the first to be released on CD.

Bell Labs' Steven Chu (now US Secretary of Energy) and his colleagues use laser light to slow and manipulate atoms. Their laser cooling technique, also called "optical molasses," is used to investigate the behavior of atoms, providing an insight into quantum mechanics. Chu, Claude N. Cohen-Tannoudji and William D. Phillips win a Nobel Prize for this work in 1997.

David Payne at the University of Southampton in the UK and his team introduce erbium-doped fiber amplifiers. These new optical amplifiers boost light signals without first having to convert them into electrical signals and then back into light, reducing the cost of long distance fiber optic systems. Gould begins receiving royalties from his patents.

1990s

The first semiconductor laser that can simultaneously emit light at multiple widely separated wavelengths – the quantum cascade (QC) laser – is invented at Bell Labs by Jérôme Faist, Federico Capasso, Deborah L. Sivco, Carlo Sirtori, Albert L. Hutchinson and Alfred Y. Cho. The laser is unique in that its entire structure is manufactured a layer of atoms at a time by the crystal growth technique called molecular beam epitaxy. Simply changing the thickness of the semiconductor layers can change the laser's wavelength. With its room-temperature operation and power and tuning ranges, the QC laser is ideal for remote sensing of gases in the atmosphere.

The first demonstration of a quantum dot laser with high threshold density is reported by Nikolai N. Ledentsov of A.F. Ioffe Physico-Technical Institute. The first pulsed atom laser, which uses matter instead of light, is demonstrated at MIT by Wolfgang Ketterle.

Shuji Nakamura, Steven P. DenBaars and James S. Speck at the University of California, Santa Barbara, announce the development of a gallium-nitride (GaN) laser that emits bright blue-violet light in pulsed operation.

An engineer at the Marshall Space Flight Center (MSFC) Wind Tunnel Facility uses lasers to measure the velocity and gradient distortion across an 8-in. curved pipe with joints and turning valves during a cold-flow propulsion research test, simulating the conditions found in the X-33's hydrogen feedline.

Lasers are used because they are nonintrusive and do not disturb the flow like a probe would. The feedline supplies propellants to the turbo pump. The purpose of this project was to design the feedline to provide uniform flow into the turbo pump. (NASA Archives)

2000s

A team of researchers from NASA's Marshall Space Flight Center in Huntsville, Ala., from NASA's Dryden Flight Research Center at Edwards Air Force Base in California and from the University of Alabama in Huntsville successfully flies the first laser-powered aircraft. The plane, its frame made of balsa wood, has a 1.5-m wingspan and weighs only 311 g. Its power is delivered by an invisible ground-based laser that tracks the aircraft in flight, directing its energy beam at specially designed photovoltaic cells carried onboard to power the plane's propeller.

The international inertial confinement fusion community, including LLNL researchers, uses the OMEGA laser at the University of Rochester's Laboratory for Laser Energetics to conduct experiments and test target designs and diagnostics. The 60-beam OMEGA laser at the University of Rochester has been operational since 1995.

Electronic switching in a Raman laser is demonstrated for the first time by Ozdal Boyraz and Bahram Jalali of the University of California, Los Angeles. The first silicon Raman laser operates at room temperature with 2.5-W peak output power. In contrast to traditional Raman lasers, the pure-silicon Raman laser can be directly modulated to transmit data.

John Bowers and colleagues at the University of California, Santa Barbara, and Mario Paniccia, director of Intel Corp.'s Photonics Technology Lab in Santa Clara, Calif., announce that they have built the first electrically powered hybrid silicon laser using standard silicon manufacturing processes. The breakthrough could lead to low-cost, terabit-level optical data pipes inside future computers, Paniccia says.

Bowers and his doctoral student Brian Koch announce that they have built the first mode-locked silicon evanescent laser, providing a new way to integrate optical and electronic functions on a single chip and enabling new types of integrated circuits.

At the University of Rochester in New York, researcher Chunlei Guo announces a new process that uses femtosecond laser pulses to make regular incandescent lightbulbs superefficient. The laser pulse, trained on the bulb's filament, forces the surface of the metal to form nanostructures that make the tungsten become far more effective at radiating light. The process could make a 100-W bulb consume less electricity than a 60-W bulb, Guo says.

The largest and highest-energy laser in the world, the National Ignition Facility (NIF) at Lawrence Livermore National Laboratory in Livermore, Calif., is dedicated. In a few weeks, the system begins firing all 192 of its laser beams onto targets.

The hohlraum cylinder, which contains the fusion fuel capsule, is just a few millimeters wide, about the size of a pencil eraser, with beam entrance holes at either end. The fuel capsule is the

size of a small pea. Credit is given to Lawrence Livermore National Security LLC, Lawrence Livermore National Laboratory and the US Department of Energy, under whose auspices this work was performed.

NASA launches the Lunar Reconnaissance Orbiter (LRO). The Lunar Orbiter Laser Altimeter on the LRO will use a laser to gather data about the high and low points on the moon. NASA will use that information to create 3-D maps that could help determine lunar ice locations and safe landing sites for future spacecraft.

Lasers get ready to enter household PCs with Intel's announcement of its Light Peak optical fiber technology at the Intel Developer Forum. Light Peak contains vertical-cavity surface-emitting lasers (VCSELs) and can send and receive 10 billion bits of data per second, meaning it could transfer the entire Library of Congress in 17 minutes. The product is expected to ship to manufacturers in 2010.

Industry analysts predict the laser market globally for 2010 will grow about 11 percent, with total revenue hitting \$5.9 billion.

The National Nuclear Security Administration announces that NIF has successfully delivered a historic level of laser energy – more than 1 MJ – to a target in a few billionths of a second and demonstrated the target drive conditions required to achieve fusion ignition, a project scheduled for the summer of 2010. The peak power of the laser light is about 500 times that used by the US at any given time.

The artist's rendering features an NIF target pellet inside a hohlraum capsule with laser beams entering through openings on either end. The beams compress and heat the target to the necessary conditions for nuclear fusion to occur. Ignition experiments on NIF will be the culmination of more than 30 years of inertial confinement fusion research and development, opening the door to exploration of previously inaccessible physical regimes. Credit is given to Lawrence Livermore National Security LLC, Lawrence Livermore National Laboratory and the US Department of Energy, under whose auspices this work was performed.

Rainer Blatt and Piet O. Schmidt and their team at the University of Innsbruck in Austria demonstrate a single-atom laser with and without threshold behavior by tuning the strength of atom/light field coupling.

4. CONCLUSION

Before any other application, lasers were used for scientific research. At first, like masers, they were used to study atomic physics and chemistry. But uses were soon found in many fields. For example, focused laser beams are used as "optical tweezers" to manipulate biological samples such as red blood cells and microorganisms. Five researchers have shared Nobel Prizes for using lasers to cool and trap atoms and to create a strange new state of matter (the Bose Einstein condensate) that probes the most fundamental physics. Over the long run, none of the uses of lasers is likely to be more important than their help in making new discoveries, with unforeseeable uses of their own.

ACKNOWLEDGEMENTS

The work was created as a result of a project carried out with secondary school pupils as a part of the Excellence Initiative - Research University program, Silesian University of Technology.

REFERENCES

Book References

1. Laser Material Processing – William M. Steen Jyotirmoy Mazumder
2. Steen, W. M. "Laser Materials Processing", 2nd Ed. 1998.
3. Siegman, Anthony E. (1986). Lasers. University Science Books. p. 4
4. University Physics, Wolfgang Bauer and Gary D. Westfall, 2011 (Specifically Chapter 38.5 on Lasers)

Internet References

1. www.aip.org/history/exhibits/laser/
2. www.bell-labs.com/about/history/laser/laser_def.html
3. http://www.press.uchicago.edu/Misc/Chicago/284158_townes.html
4. <http://www.national-laser.com/laser-history.htm>



31th January 2025
Gliwice, Poland

DEPARTMENT OF ENGINEERING MATERIALS AND BIOMATERIALS
FACULTY OF MECHANICAL ENGINEERING
SILESIA UNIVERSITY OF TECHNOLOGY

INTERNATIONAL STUDENTS SCIENTIFIC CONFERENCE

Characterization of a Fused-Thiophene and Naphthalenediimide-based Polymer for Multilayer Organic Solar Cells

Wioletta Klimek^a, Maciej Gajdemski^b, Sebastian Gralla^b, Ammara Aslam^{a,c}, Marek Szindler^b, Krzysztof Lukaszewicz^b, Przemysław Ledwoń^a,

^a Silesian University of Technology, Faculty of Chemistry, Department of Physical Chemistry and Technology of Polymers, Strzody 9, 44-100 Gliwice, Poland

email: przemyslaw.ledwon@polsl.pl

^b Silesian University of Technology, Faculty of Mechanical Engineering, Department of Engineering Materials and Biomaterials, Konarskiego 18A, 44-100 Gliwice, Poland

email: marek.szindler@polsl.pl

^c Silesian University of Technology, PhD School, 2A Akademicka str., 44-100 Gliwice, Poland

Abstract: The article describes the characteristics of compounds and layers for multilayer organic solar cells. We are particularly focusing on a donor-acceptor polymer consisting of a fused-thiophene and naphthalenediimide-based units. The procedure of fabrication of organic solar cells with bulk heterojunction is described. The bulk heterojunction is based on two structures. The first one is the standard fullerene/polymer system forming organic bulk heterojunction PCBM:P3HT. The second one is all-polymer bulk heterojunction consisting of donor-acceptor polymer PThNDI and P3HT. Atomic Layer Deposition process was included to obtain intermediate ZnO layers.

Keywords: photovoltaics, conjugated polymers, ALD, AFM

1. INTRODUCTION

The device that can absorb light and provide the electrical current as a response is known as a solar cell. Solar cells are widely used in fabricating solar panels, that can be cast off for renewable energy. Their working mechanism is based on the photovoltaic effect. When the photons strikes the material it excites the electrons. The positive and negative charges are generated. There are various types of solar cells like monocrystalline and polycrystalline silicon solar cells, thin film silicon, dye-sensitised solar cells (DSSCs), perovskite solar cells, organic solar cells (OSC) [1,2]. Current trends include scientific research aimed at obtaining of new eco-friendly, less toxic, low cost, and environmentally friendly solar cells [3,4].

π -Conjugated polymers gain significant importance in the field of OSC. They are attracting researchers' attention because of their light absorbance ability to convert into electrical current. They can be an alternative to silicon solar cells where low weight and flexibility are important. The advantages of OPV also include low-cost fabrication, low-temperature working, and roll-

to-roll solution-processed fabrication. Several properties like mechanically flexible modules, large-area, transparent and colored sheets, lightweight, etc. present new research possibilities to work on it [5–7].

Among the π -conjugated polymers, the most interest has recently been aroused by those with a donor-acceptor structure. It is a type of polymer consisting of at least two different repeating units, one of which is electron-rich and the other is electron-poor.

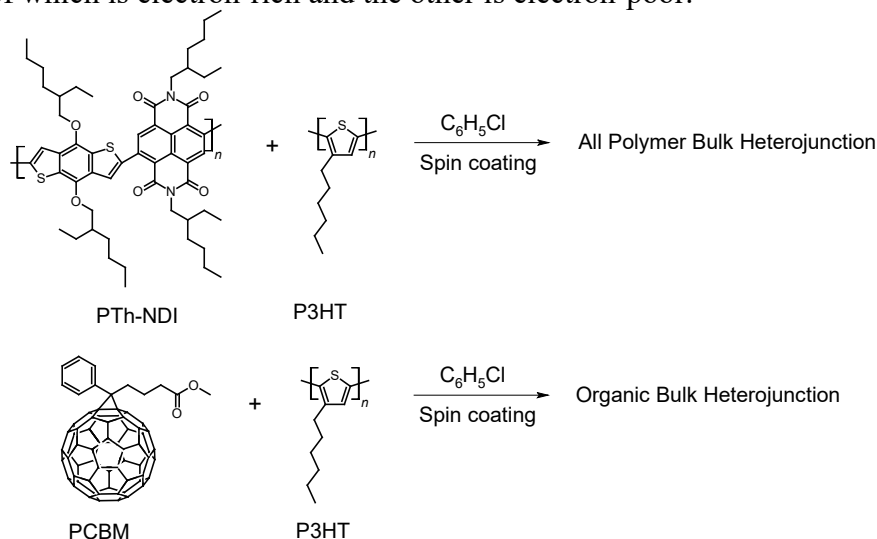


Figure 1. Structure of the studied heterojunctions

2. EXPERIMENTAL

The synthesis of polymer PTh-NDI was described previously in article [8]. 97.6% regioregular poly(3-hexylthiophene) (P3HT) and 6 pixel ITO substrates were provided by Ossila B.V. [6,6]-Phenyl C61 butyric acid methyl ester 99.5% (PCBM) was provided by Solaveni GmbH.

UV-Vis-NIR measurements were performed on a HP 8453 Spectrophotometer. Cyclic Voltammetry measurements were performed on a CH 660 potentiostat. Solid films were deposited using Spin Coater Laurell. Metallic layers were deposited using Lesker SPECTROS150 Organic Thin Film Deposition & Metallization System. ITO electrodes were prepared according to Ossila procedure [9].

The surface topography of the analyzed samples was evaluated utilizing the Park Systems XE100 atomic force microscope (Park Systems, Suwon, South Korea). The investigation was conducted in non-contact mode over regions measuring $2 \times 2 \mu\text{m}^2$. Both two-dimensional images and their three-dimensional representations were recorded. Furthermore, essential roughness parameters were calculated. The cantilever operated at a vibration frequency of 300 kHz. The acquired data were processed using the Park Systems XEI 4.3.1 software.

Thin films zinc oxide (ZnO), along with their combinations, were deposited using an ALD Picosun R-200 reactor (Espoo, Finland). Organometallic precursors, such as trimethylaluminum (TMA) and diethylzinc (DEZ), were employed in the process. Deposition was carried out at a temperature of 250 °C, with precursor pulse durations of 0.1 seconds for TMA/DEZ and 4 seconds for water. Between pulses, a 4-second nitrogen purge step was applied to eliminate residual precursors and by-products from the reaction. Deionized water

served as the reactant throughout the process, with thermal ALD being utilized for the selected materials.

3. RESULTS AND DISCUSSION

3.1. Polymer characterization

Electrochemical properties of PTh-NDI were estimated using Cyclic Voltammetry in order to check the LUMO energy (Fig. 2a). The estimated LUMO energy is -4.04 eV indicates that the polymer can be checked as a n-type semiconductor with complementary p-type polymer such as P3HT in a bulk heterojunction photovoltaic cells.

The optical properties of polymers P2Th-NDI, P3HT and its mixture were characterized with the use of UV-Vis-NIR spectroscopy, illustrated in Figure 2. The polymers were compared in solution and as solid layers. The analysis reveals differences in light absorption for different measurement conditions and polymer compositions. In the case of P3HT a sharp peak at 458 nm is observed for solution in C_6H_5Cl . For the solid layer of P3HT, a bathochromic shift is observed up to 551 nm. Analysis of the P2Th-NDI spectra indicates only a slight absorption shift. Their values are 366 nm, 384 nm, 458 nm, 606 nm for solution in C_6H_5Cl and 365 nm, 385 nm, 464 nm, 608 nm for solid film. There are also significant differences observed between the absorption of the solution containing the polymer mixture and their layer forming the P2Th-NDI:P3HT heterojunction. Analysis of the spectra recorded in C_6H_5Cl indicates a predominant absorption by P3HT (peak at 456 nm) while the absorption of P2Th-NDI has a much smaller influence on the recorded spectrum (small peak at 623 nm). The spectrum of P2Th-NDI:P3HT heterojunction show multicomponent spectrum with a maximum at 556 nm. This effect indicates strong π - π interactions between polymer chains and aggregations among polymer chains [10–12].

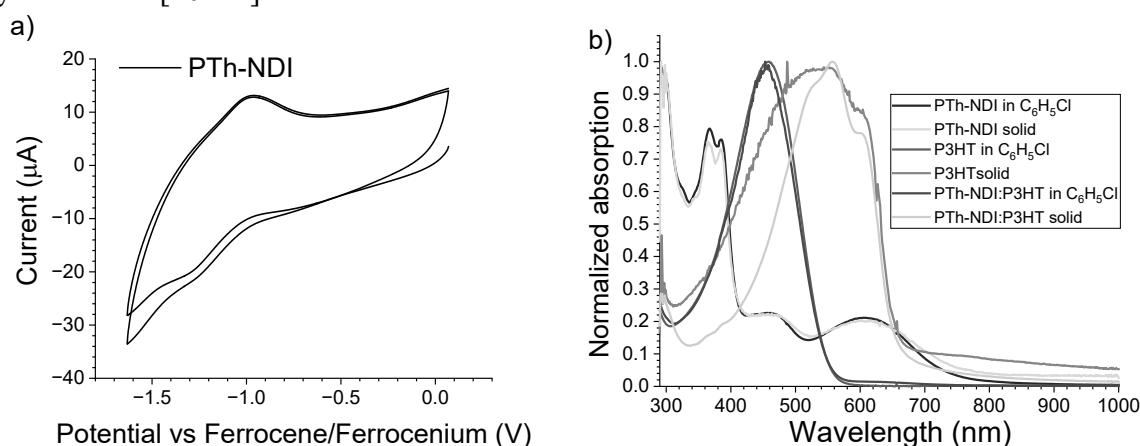


Figure 2. Cyclic Voltammetry of PTh-NDI (a) and UV-Vis-NIR characterization in solid state and solution in chlorobenzene of polymers (b)

3.2. AFM film characterization

In the surface morphology analysis, topographical images and their corresponding 3D representations were obtained (Fig. 3). A $4 \mu m^2$ area was examined. Thin layers of PTh-NDI spin-coated from $CHCl_3$ and $C_6H_5Cl/CHCl_3$ solutions, and PTh-NDI:P3HT blend were investigated. In all cases, uniform layer thicknesses with minimal irregularities were achieved. No significant impurities or large aggregates were observed. Each layer exhibited a granular structure characterized by repeating small atomic clusters. The observed uniformity and

absence of defects suggest good compatibility and homogeneity in the polymer layers, which is critical for ensuring optimal performance in their intended applications. Based on the images obtained using XEI software, key roughness parameters were calculated and are summarized in Table 1. The PTh-NDI film spin-coated from CHCl_3 exhibited lower roughness compared to the polymer spin-coated from $\text{C}_6\text{H}_5\text{Cl}/\text{CHCl}_3$ (5:95%). This difference in roughness influences the final morphology of the blend surface, with the roughness values of the blend falling between those of the individual polymers. These results highlight the interplay between the polymers and the role of solvents, which directly impacts the surface characteristics and may influence the material's performance in practical applications.

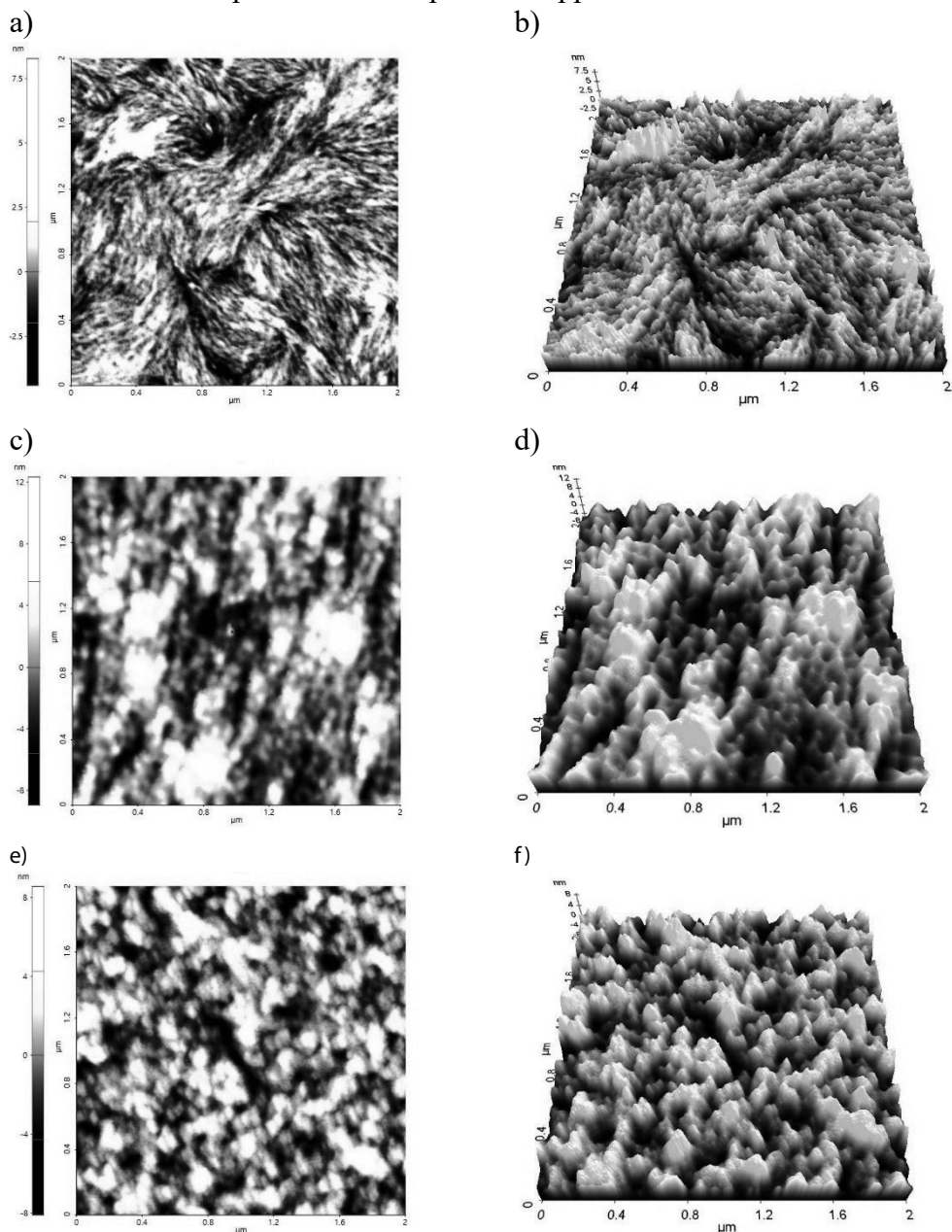


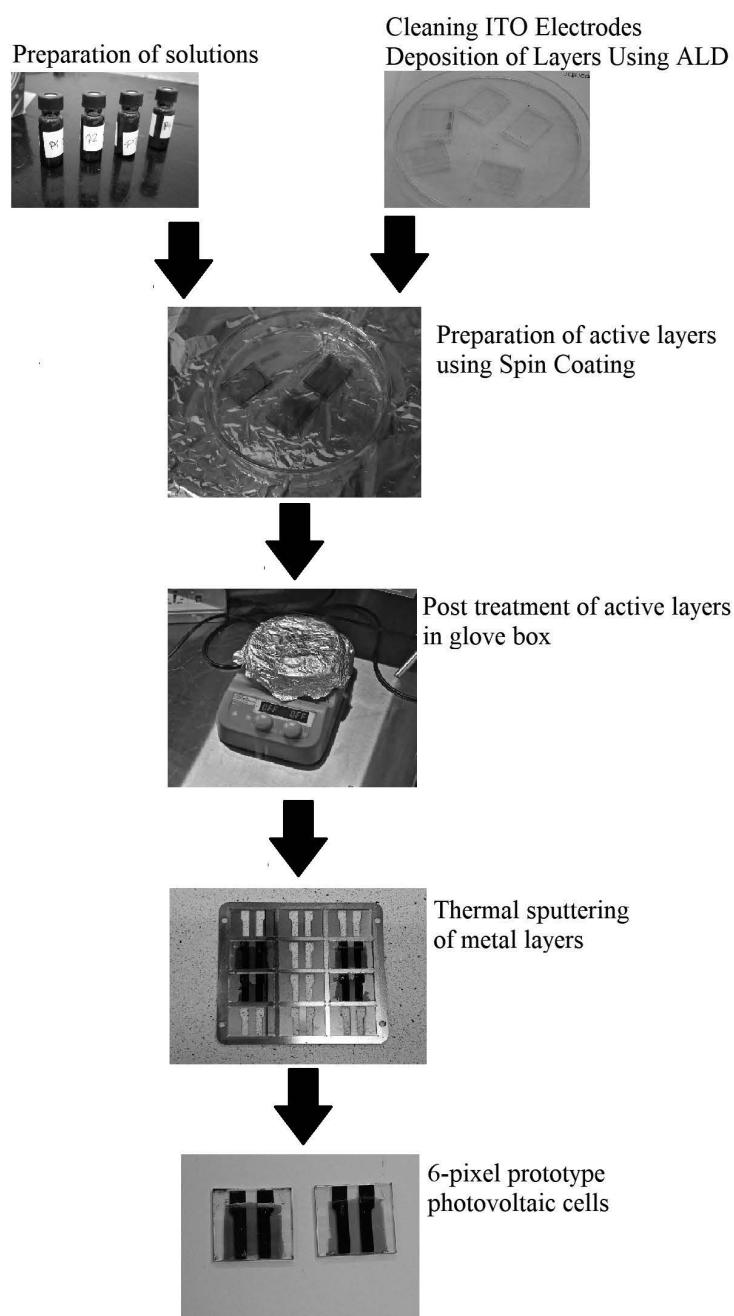
Fig. 3. Surface topography image and its 3D representation for: a-b) PTh-NDI from CHCl_3 , c-d) PTh-NDI, e-f) PTh-NDI:P3HT polymer blend

Tab. 1 Summary of roughness parameters

Sample	Rq [nm]	Ra [nm]	Max irregularity [nm]
PTh-NDI from CHCl ₃	1.01	0.73	8.3
PTh-NDI from C ₆ H ₅ Cl/CHCl ₃	2.84	2.20	12.30
Polymer Blend	2.18	1.73	8.56

3.3. Fabrication of bulk heterojunction photovoltaic cells

The schematic process of preparing P2Th-NDI:P3HT heterojunctions and photovoltaic cells based on them is shown in Scheme 1.



Scheme 1. Schematic of the preparation of organic solar cells (OPV)

Additionally, devices PCBM:P3HT heterojunctions were used as standards. Two different device schemes were used, the first with standard architecture ITO/PEDOT:PSS/P2Th-NDI:P3HT/Al and ITO/PEDOT:PSS/PCBM:P3HT/Al. The second one had an ITO/ZnO/P2Th-NDI:P3HT/Al and ITO/ZnO/PCBM:P3HT/Ag reverse architecture.

ITO was cleaned using 5% Hellmanex solution, 10 % NaOH and isopropanol.

Depending on the photovoltaic cell architecture, appropriate layers are applied. PEDOT:PSS was used as hole transport layer (HTL) in the case of normal structure. PEDOT:PSS was deposited by Spin Coating. ZnO was used as electron transport layer (ETL) in the case of reverse structure. ZnO was deposited using Atomic Layer Deposition. Depending on the application of the layer to the ITO electrodes.

Appropriate P2Th-NDI, P3HT and PCBM were prepared in C_6H_5Cl and stirred for at least 18h. Then, the solutions were filtered. A solution created from a combination of PCBM and P3HT polymers was deposited on the ETL or HTL electrodes using spin-coating. The time of depositing the layer was set to 40 seconds. The violet P2Th-NDI:P3HT and orange PCBM:P3HT layers were obtained. The obtained multilayer structures were transferred to a glove box. They were heated at 140 °C for 15 minutes. Then the multilayer structures were transferred to the sputtering apparatus. A layer of Al and MoO_3 was applied and left in the apparatus overnight. The finished devices were removed from the sputtering apparatus and then tested for conductivity which indicated the need for detailed optimization of devices.

4. SUMMARY AND CONCLUSIONS

The surface morphology analysis of PTh-NDI and its blend with P3HT demonstrated the formation of uniform thin layers with minimal irregularities, free from significant impurities or large aggregates. The granular structure observed in each layer, consisting of repeating small atomic clusters, indicates good material compatibility and homogeneity. Roughness analysis revealed that PTh-NDI spin-coated from $CHCl_3$ exhibited lower roughness compared to the polymer film spin-coated from $C_6H_5Cl/CHCl_3$ solution, with the blend displaying intermediate roughness values. These findings underscore the role of solvents and interplay between polymers, which significantly impacts the surface morphology and may influence the functional properties of the material in practical applications. The observed uniformity and controlled roughness suggest promising potential for these polymers in advanced technologies requiring precise surface characteristics. Additionally the electrochemical and optical properties of the P2Th-NDI polymer were investigated to evaluate its potential as an n-type semiconductor for use in bulk heterojunction photovoltaic cells. Cyclic Voltammetry analysis revealed that the LUMO energy level of -4.04 eV confirms the suitability of P2Th-NDI to pair with p-type semiconductors, such as P3HT. UV-Vis-NIR spectroscopy showed differences in light absorption between solutions and solid layers of P2Th-NDI, P3HT, and their mixtures. The absorption spectra of the P2Th-NDI:P3HT mixture revealed significant differences between the solution and the solid heterojunction layer. The results indicates strong π - π interactions and aggregation among polymer chains in the solid state.

ACKNOWLEDGMENTS

The research was financially supported by the PBL-IDUB project entitled "Wpływ struktury ogniw słonecznych opartych na polimerach typu donor-akceptor na ich właściwości fotowoltaiczne".

BIBLIOGRAPHY

- [1] J. Dhilipan, N. Vijayalakshmi, D.B. Shanmugam, R. Jai Ganesh, S. Kodeeswaran, S. Muralidharan, Performance and efficiency of different types of solar cell material – A review, *Mater. Today Proc.* 66 (2022) 1295–1302. doi:10.1016/j.matpr.2022.05.132.
- [2] J. Pastuszak, P. Węgierek, Photovoltaic Cell Generations and Current Research Directions for Their Development, *Materials (Basel)*. 15 (2022) 5542. doi:10.3390/ma15165542.
- [3] M. V Dambhare, B. Butey, S. V Moharil, Solar photovoltaic technology: A review of different types of solar cells and its future trends, *J. Phys. Conf. Ser.* 1913 (2021) 012053. doi:10.1088/1742-6596/1913/1/012053.
- [4] W.B. Tarique, A. Uddin, A review of progress and challenges in the research developments on organic solar cells, *Mater. Sci. Semicond. Process.* 163 (2023) 107541. doi:10.1016/j.mssp.2023.107541.
- [5] A. Colsmann, A. Puetz, A. Bauer, J. Hanisch, E. Ahlswede, U. Lemmer, Efficient Semi-Transparent Organic Solar Cells with Good Transparency Color Perception and Rendering Properties, *Adv. Energy Mater.* 1 (2011) 599–603. doi:10.1002/aenm.201000089.
- [6] C.-C. Chen, L. Dou, R. Zhu, C.-H. Chung, T.-B. Song, Y.B. Zheng, S. Hawks, G. Li, P.S. Weiss, Y. Yang, Visibly Transparent Polymer Solar Cells Produced by Solution Processing, *ACS Nano*. 6 (2012) 7185–7190. doi:10.1021/nm3029327.
- [7] V. Shrotriya, Polymer power, *Nat. Photonics*. 3 (2009) 447–449. doi:10.1038/nphoton.2009.130.
- [8] K. Dang Anh, P.L. dos Santos, M. Saeed, M.U. Chaudhry, I.H. Bechtold, A. Batycki, A. Drewniak, A. Szlapa-Kula, P. Ledwon, The role of fused thiophene and naphthalene diimide (NDI) in shaping the optical and electrical properties of donor-acceptor polymers, *Org. Electron.* 129 (2024) 107058. doi:10.1016/j.orgel.2024.107058.
- [9] OPV and OLED Fabrication Guide, (n.d.). https://www.ossila.com/pages/organic-photovoltaic-opv-and-organic-light-emitting-diode-oled-fabrication-manual?_pos=1&_sid=714c3cd30&_ss=r.
- [10] J. Royakkers, K. Guo, D.T.W. Toolan, L. Feng, A. Minotto, D.G. Congrave, M. Danowska, W. Zeng, A.D. Bond, M. Al-Hashimi, T.J. Marks, A. Facchetti, F. Cacialli, H. Bronstein, Molecular Encapsulation of Naphthalene Diimide (NDI) Based π -Conjugated Polymers: A Tool for Understanding Photoluminescence, *Angew. Chemie Int. Ed.* 60 (2021) 25005–25012. doi:10.1002/anie.202110139.
- [11] V. Singh, S. Kwon, Y. Choi, S. Ahn, G. Kang, Y. Yi, M.H. Lim, J. Seo, M. Baik, H.R. Byon, Controlling π - π Interactions of Highly Soluble Naphthalene Diimide Derivatives for Neutral pH Aqueous Redox Flow Batteries, *Adv. Mater.* 35 (2023). doi:10.1002/adma.202210859.
- [12] P. Ledwon, D. Ovsianikova, T. Jarosz, S. Gogoc, P. Nitschke, W. Domagala, Insight into the properties and redox states of n-dopable conjugated polymers based on naphthalene diimide units, *Electrochim. Acta.* 307 (2019) 525–535. doi:10.1016/j.electacta.2019.03.169.



31th January 2025
Gliwice, Poland

DEPARTMENT OF ENGINEERING MATERIALS AND BIOMATERIALS
FACULTY OF MECHANICAL ENGINEERING
SILESIA UNIVERSITY OF TECHNOLOGY

INTERNATIONAL STUDENTS SCIENTIFIC CONFERENCE

The temperature and humidity influence on compressive strength of the concrete made of expanded clay and recycled aggregates in time of curing

Nicole Kocierz, Barbara Słomka-Słupik ^a

^a Silesian University of Technology, Faculty of Civil Engineering, Department of Building Structures, email: barbara.slomka-slupik@polsl.pl

Abstract: The work refers to the influence of temperature and humidity, in time of the lightweight concrete curing time, on compressive strength and density. Comparative samples of expanded clay concrete and samples with the addition of aggregates, gypsum plaster and autoclaved cellular concrete, were made. The samples were cured in air at 5°C, 20°C and 35°C, in water in temperature 20°C, and partially in water and air. The volumetric densities of each sample were determined, and their compressive strengths after 28 days were determined. Based on the results, it was found that humidity has no effect on the strength of some samples, while it has a significant effect on sample with recycled porous aggregate. On the other hand, in the case of samples cured at different temperatures, then significant differences can be seen only at 35°C, and at 5°C and 20°C there are only small variations in strength between samples.

Keywords: lightweight concrete, lightweight aggregate, circular economy, recycling, construction waste

1. INTRODUCTION

Expanded clay concrete is an innovative building material that is made by mixing expanded clay, sand, water and cement, and sometimes various additives and admixtures. It belongs to lightweight aggregate concretes and has a dry density between 800 kg/m³ and 2000 kg/m³. It is used to make a variety of structural elements either on site or as precast. Thanks to the lightness of this concrete, it is possible to reduce the dimensions of these elements due to the lower self-weight of the entire structure [1]. Expanded clay is included in the group of artificial lightweight aggregates for concrete, which is derived from mineral resources [1].

Today's society is faced with the challenge of environmental protection, use of natural resources and waste management. The way to sustainable development is the Circular Economy and the currently very important recycling of construction materials, which in 2022 in Poland was only 47%, with 736 thousand tons of construction and demolition waste produced. This is a huge drop in the recycling rate, which was at 85% in 2020-2021 [2]. In their work, Adamczyk and Dylewski [3] point out that in order to stop environmental degradation, ecological criteria should also be taken into account when choosing materials, and traditional technologies should be changed to preserve natural resources for future generations. This means that all building

materials will have to be reusable, easily recyclable or should contain little virgin materials in their composition. This will significantly reduce the environmental impact of building materials and consequently, the entire construction sector. Currently, it is possible to measure the environmental impact of building materials, as described by Golanski [4] in his work, proposing as main factors, for example: the energy required for production, CO₂ emissions, the possibility of obtaining locally, and the life cycle of the material and its potential for recycling.

There is an effect of temperature and humidity on the compressive strength of concrete, which has been repeatedly confirmed in normal concretes. It is estimated that this effect is negative up to 85°C and above 3% moisture content, but there are no conclusive studies confirming either hypothesis. With high-strength concretes, changes could only be seen at 120°C [5].

During the concreting of elements at the construction site, various weather conditions can occur. The temperature is often between 5 and 35 degrees, and the weather can vary from full sun to heavy rain. It is not uncommon to forget that everything affects the strength of concrete, and even the smallest change can lead to a reduction in concrete grade. In this article we decided to check whether the variation of temperature and humidity during the hardening of this concrete will have a significant effect on its compressive strength.

The research results described in this article will be part of the author's (N. Kocierz) master's thesis and are part of the work in the student's research club "SKN Build Green" [6]. The main purpose of the master thesis is to show what effect recycled filler aggregates have on expanded clay concrete. Among other things, the research included compressive strength and water sorption tests. The work also discusses issues related to ecology in construction industry and circular economy-

2. MATERIALS AND METHODS

The concrete specimens were made using tap water taken from the laboratory building of the Silesian University of Technology's Faculty of Civil Engineering, and Heidelberg Materials Poland (Góraźdże) Portland multicomponent CEM II 52,5N. The cement used had a declared compressive strength after 28 days of at least 52,5 MPa, and "N" meant normal strength buildup dynamics. The main aggregate was 0-4 mm anti-skid expanded clay from Weber (A-I) and 0-2 mm quartz sand from Kreisel (A-II). Additional aggregates were used in the form of gypsum plaster aggregate (A-III) and autoclaved cellular concrete (A-IV) made by ourselves by crushing. Figure 1 shows the aggregates used for the concrete mixtures.

The composition of the first mix, which is also the reference mix, was selected on the basis of the estimated values of the bulk densities of the filling aggregates and the concrete integrity formula. A w/c (water/cement mass) ratio of 0.5 was assumed, and then, based on previous studies, the additional water was assumed to be 50% by weight of the additional aggregate, which is the same as the estimated absorbability of additional aggregates. The amounts of cement, sand, expanded clay and water remained the same, however, due to the different volumes of the mixture obtained, the percentages of each component are shown in Table 1. Mixture K_1 is a reference mixture and does not contain additional aggregate. Mixture TG_05_14 contains 5% filler aggregate by weight of cement. It was prepared using aggregate from gypsum plaster which was crushed 14 days after it was made. Mixture ABK_05_12 also contains 5% filler aggregate by weight of cement, and it was from autoclaved cellular concrete (ACC) of 1-2 mm fraction.

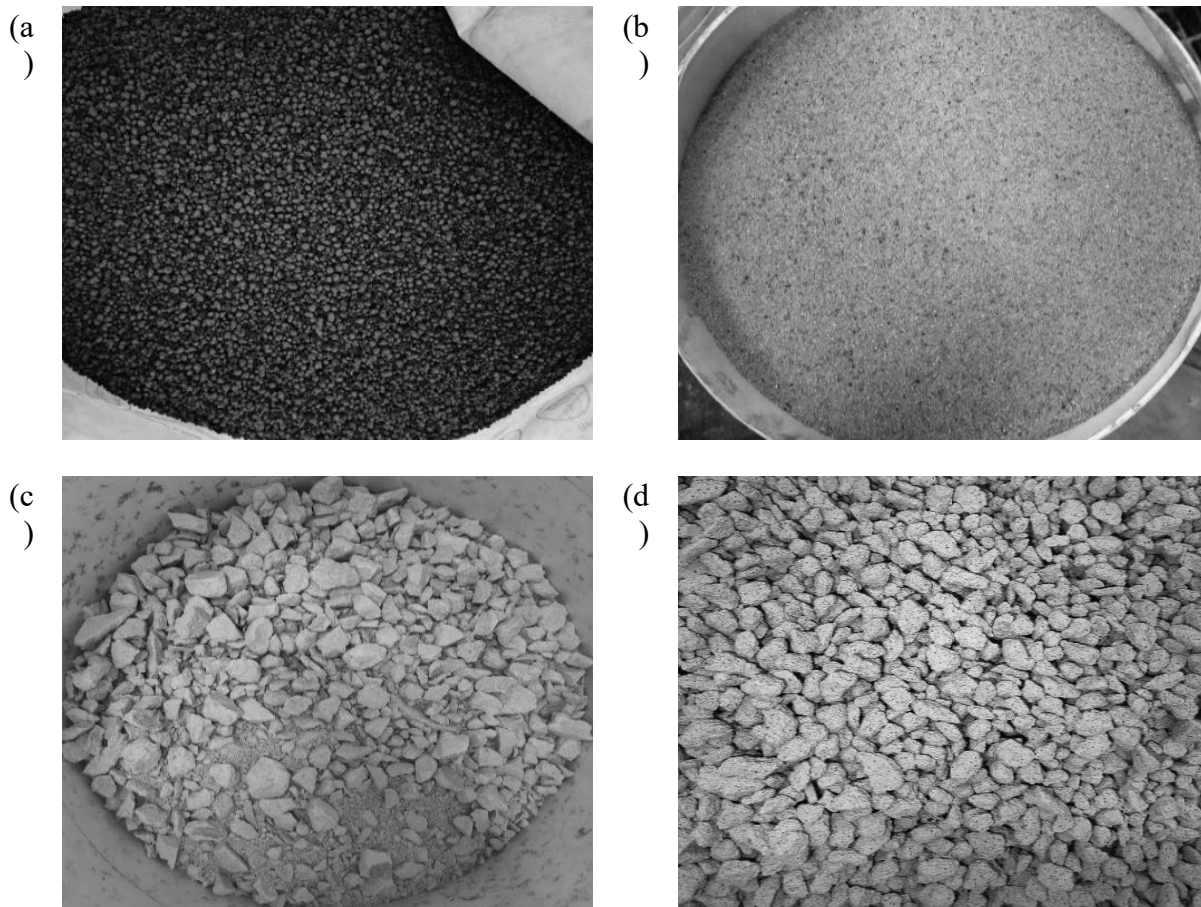


Figure 1. Aggregate A-I (a), A-II (b), A-III (c), A-IV (d)

Table 1. Percentage content of concrete mixture components

Name of mixture	Cement 52,5 N	Crushed gypsum plaster or ACC	Water	Additional water	Sand	Expanded clay
K_1	34.5%	0.0%	17.2%	0.0%	37.9%	10.3%
TG_05_14	33.6%	1.7%	16.8%	0.8%	37.0%	10.1%
ABK_05_12	33.6%	1.7%	16.8%	0.8%	37.0%	10.1%

Figure 2 shows the preparation steps of the mixtures and consistency of the K_1 mixture. During the preparation of the mixtures, half of the base water was added to the expanded clay and left for 5 min to saturate the aggregate. Sand, cement, and additional aggregate were added then. Finally, the rest of the base water and additional water were added. The mixture was mixed after adding each ingredient until they were thoroughly mixed. The consistency of the made mixtures can be described as plastic, but in order to maintain its rheological properties it required mixing until the molds were filled.

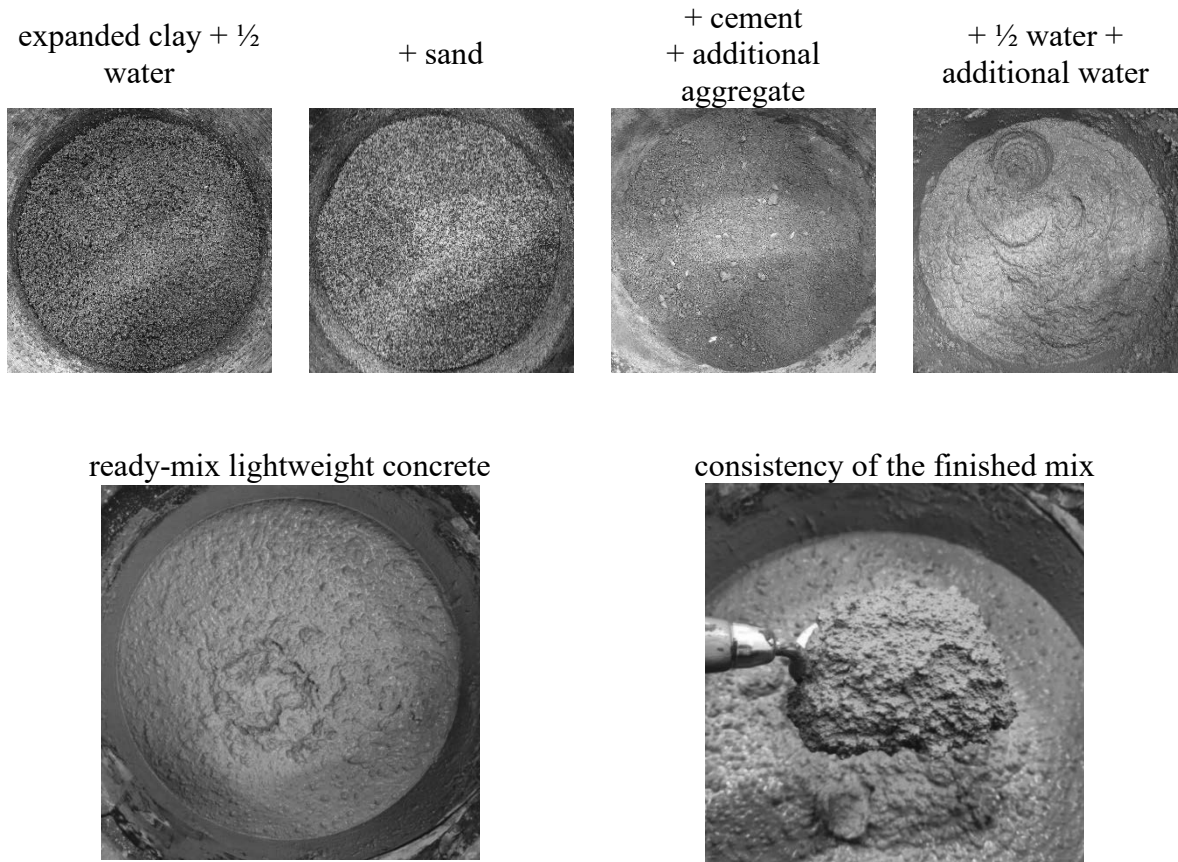


Figure 2. Preparation stages of the concrete mixture

Figure 3 shows how samples are cared for during curing. Samples 1/2/3 were curing in the refrigerator at 5°C (a), samples 4/5/6/7 were curing in the air at 20°C (b and c), samples 8/9/10 were curing in a drying cabinet (d), samples 11/12/13 were in water all the time (e), and samples 14/15/16 matured in the air, but once every 3-5 days were put in water for 5 minutes (f). All concrete cubes were unmolded after 1 day and immediately moved to proper temperature and humidity conditions.



samples 10x10x10cm curing in air in 5°C



samples 10x10x10cm curing in air in 20°C



a) samples 15x15x15cm curing in air in 20°C



b) samples 10x10x10cm curing in air 35°C



c) samples 10x10x10cm curing in water in 20°C



d) samples 10x10x10cm curing in air and water in 20°C

Figure 3. Methods of care for concrete samples during hardening

3. RESULTS WITH ANALYSIS

Table 2 lists the density of made concrete cubes, counted for five different conditions of care in time of hardening. The lowest density was for sample K_1 cured at 35°C in air and its density was 1677 kg/m³. The reason for this result was most likely due to the lack of additional aggregates, which increase the saturation of the entire sample, and thus, sample K_1 gave up water faster than samples TG_05_14 and ABK_05_12. On the other hand, the ABK_05_12 sample cured in water had the highest density and it was 1854 kg/m³. This may be due to the very high sorption capacity of the autoclaved cellular concrete aggregate, caused by its high porosity. All samples matured at 35°C had the lowest density of the entire mixture, and the highest density was for those stored in water. All cubes had density of less than 2000 kg/m³, so they can be classified as lightweight concretes.

Table 2. The density of concrete cubes

Name of mixture	K_1	TG_05_14	ABK_05_12
Curing in 5°C, air, kg/m ³	1702	1732	1732
Curing in 20°C, air, kg/m ³	1735	1744	1725
Curing in 35°C, air kg/m ³	1677	1709	1684
Curing in 20°C, water, kg/m ³	1844	1822	1854
Curing in 20°C, air and water, kg/m ³	1758	1740	1722

Figure 4 shows the change in densities of the samples depending on the thermal and humidity conditions during curing. The graph clearly illustrated the finding described earlier that the samples immersed in water had the highest density, while those dried in a dryer had the lowest density. It was also observed that in samples matured in air at different temperatures or water and air, sample K_1 always had the lowest density, followed by sample ABK_05_12 and sample TG_05_14 with the highest density. Only in the samples matured in water it can be seen that sample ACC had the higher density than TG, most likely due to the higher absorbability of the additional aggregate.

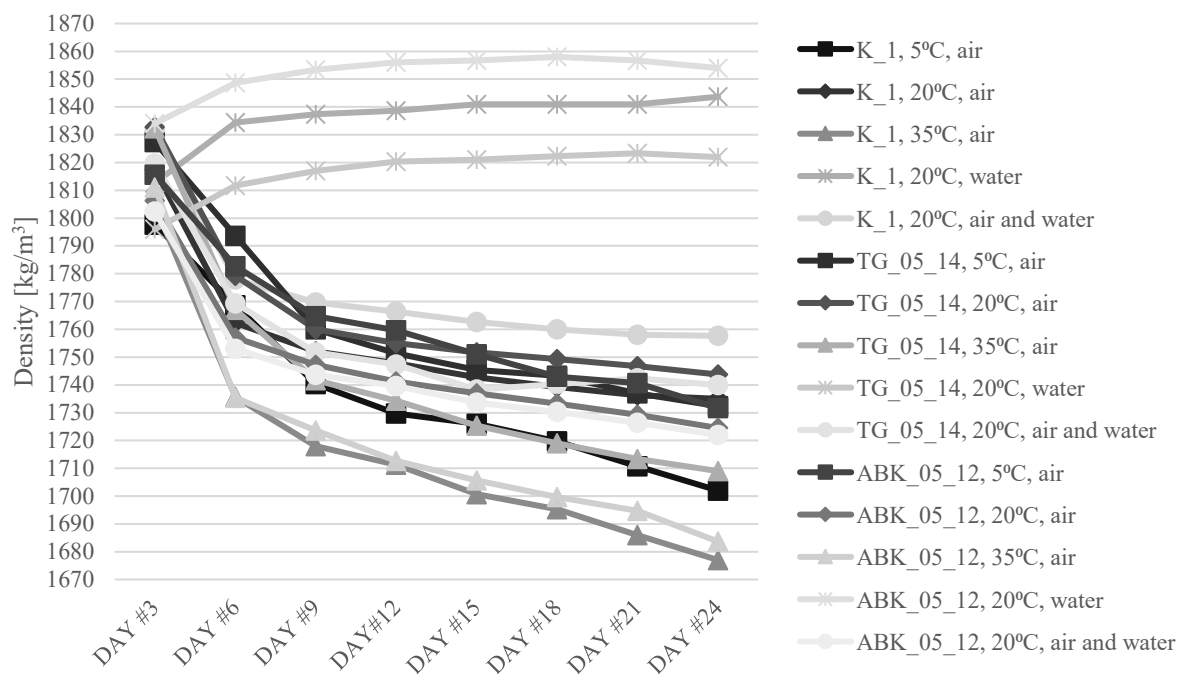


Figure 4. Density of concrete cubes in different temperature and humidity in time of curing

Table 3 and Figure 5 show average compressive strength values after 28 days of hardening under different temperature conditions. Sample K_1 cured at 20°C had the highest compressive strength, while cured at 35°C had the lowest compressive strength from all of the samples. This may be due to the lack of the additional aggregate to absorb water, which may have been released during curing, nurturing the concrete from the inside. The smallest difference between curing at different temperatures was observed in samples ABK_05_15, where the strength ranged between 39 – 42 MPa. Sample TG_05_14 showed a slight decrease in strength when cured at 35°C, which is 36 MPa, compared to 39 – 40 MPa for samples cured at 20°C and 5°C. The largest decrease in strength was observed in sample K_1 cured at 35°C, where the strength was 31 MPa, which is as much as about 10 MPa less compared to samples matured at 20°C and 5°C.

Table 3. Average values of compressive strength of concrete cured in different temperatures

Name of mixture	K 1	TG 05 14	ABK 05 12
Curing in 5°C, air, MPa	39.66	39.77	40.42
Curing in 20°C, air, MPa	42.15	38.94	41.87
Curing in 35°C, air, MPa	31.02	36.18	39.49

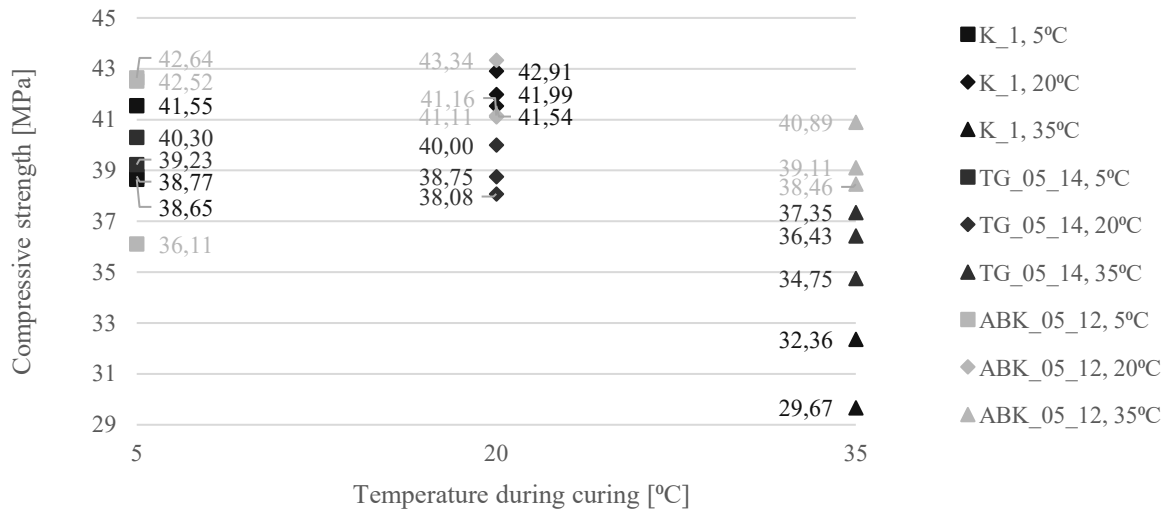


Figure 5. Relationship between temperature and compressive strength of concrete

Table 4 and Figure 6 show average compressive strength values after 28 days of specimens cured under different humidity conditions. Sample K_1 cured in air and water had the highest compressive strength, while sample ABK_05_12 cured in the same conditions had the lowest compressive strength of all samples. Samples K_1 and TG_05_14 had about the same strength regardless of the conditions under which they cured. Whereas, in the ABK_05_12 sample, it was observed that even the small amount of water significantly reduced the strength by almost 8 MPa, and by 5 MPa when fully saturated.

Table 4. Average value of compressive strength of concrete cubes (humidity)

Name of mixture	K 1	TG 05 14	ABK 05 12
Curing in 20°C, water, MPa	42.15	38.93	36.63
Curing in 20°C, air and water, MPa	42.47	38.18	34.04
Curing in 20°C, air, MPa	41.45	37.97	41.87

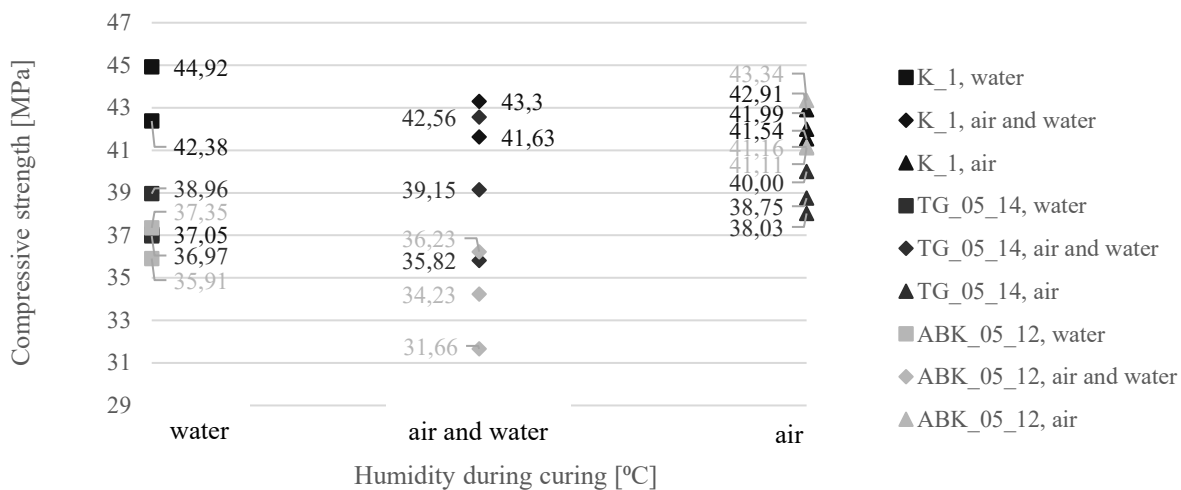


Figure 6. Relationship between humidity and compressive strength of concrete

4. SUMMARY AND CONCLUSIONS

All samples had the highest volumetric density after curing in water and the lowest density while cured in air at 35°C. In all samples matured in air, regardless of temperature, K_1 samples had the lowest density, then there were ABK_05_12 samples, and the highest density had TG_05_14, which may be related to the saturation of the additional aggregate.

Samples cured at 5°C and 35°C, the ABK_05_12 had the highest compressive strength, the K_1 sample had the highest strength at 20°C. Thus may be due to the amount of water that was absorbed in the additional aggregate and slowly returned to the sample during curing. This is the most evident with samples matured at 35°C, where the difference between consecutive samples (K_1, TG_05_14 and ABK_05_12) in compressive strength was 5 MPa and 3 MPa, respectively.

Samples K_1 and TG_05_14 had almost the same strength regardless of humidity conditions, while in case of sample ABK_05_12, a significant difference can be seen even with a small amount of water.

Lightweight concretes with waste aggregate are among the materials of the future that will be widely used to maintain a low carbon footprint and low environmental impact. Research on them should be ongoing, especially on concretes with low-carbon cement or even cement-free concretes.

BIBLIOGRAPHY

1. L. Domagała, Konstrukcyjne lekkie betony kruszywowe, Monografia 462, 2014.
2. Główny Urząd Statystyczny, <https://bdl.stat.gov.pl/bdl/dane/podgrup/tablica>, (access date 09/02/2024)
3. J. Adamczyk, R. Dylewski, Recykling odpadów budowlanych w kontekście budownictwa zrównoważonego, Problemy Ekorozwoju, 2010, vol. 5, no 2, 125-131
4. M. Golański, Wybór materiałów budowlanych w kontekście efektywności energetycznej i wpływu środowiskowego, Budownictwo i inżynieria środowiskowa, 2012, nr 3, 39-53
5. M. Deutscher, M. Markert, S. Scheerer, Influence of temperature on the compressive strength of high performance and ultra-high performance concretes, Structural Concrete, 2022, 23:2381-90
6. B. Słomka-Słupik, T. Kruczek, N. Kocierz, Betony lekkie z kruszywem z materiałów odpadowych. Praca zbiorowa 1006, red: S. Werle, J. Ferdyn-Grygierek: Ochrona Klimatu i Środowiska. Nowoczesna Energetyka, s.135-150. Wyd. Politechniki Śląskiej, Gliwice 2023



31th January 2025
Gliwice, Poland

DEPARTMENT OF ENGINEERING MATERIALS AND BIOMATERIALS
FACULTY OF MECHANICAL ENGINEERING
SILESIA UNIVERSITY OF TECHNOLOGY

INTERNATIONAL STUDENTS SCIENTIFIC CONFERENCE

Biomimetic Materials in Everyday Products – The Cases of Spider Silk and Velcro. Microscopic investigations

Tomasz Kołodziej ^a, Wiktor Rudek ^a, Anna Kloc-Ptaszna ^b, Daniel Pakuła ^b, Marcin Staszuk ^b

^a Students of the 5th Secondary School named after Andrzej Struga in Gliwice, ul. Górnych Wałów 29, 44-100 Gliwice, Poland

^b Silesian University of Technology, Faculty of Mechanical Engineering, Department of Engineering Materials and Biomaterials, ul. Konarskiego 18A, 44-100 Gliwice, Poland
email: anna.kloc@polsl.pl, daniel.pakuła@polsl.pl, marcin.staszuk@polsl.pl

Abstract: This article was produced within the scope of a PBL project between high school students. The aim of the study is to illustrate biomimetic materials inspired by nature using a scanning electron microscope. The research focused on two examples of biomimetic inspiration: spider silk as a prototype for dental floss and the structure of the *Arctium lappa* fruit as the blueprint for Velcro. The results indicate that mimicking natural solutions can lead to the development of more durable and environmentally friendly technologies [12].

Keywords: biomimetics, spider silk, dental floss, *Arctium lappa*, Velcro, scanning electron microscopy (SEM).

1. INTRODUCTION

Biomimetics, the science of emulating solutions observed in nature, gained popularity in the early 20th century and has since been applied in various fields, from materials engineering to medicine. The earliest and one of the most cited examples of biomimetics was Velcro invented by George de Mestral in 1941, based on the mechanism of the *Arctium lappa* fruit. Observing how the fruit adheres to clothing and animal fur, de Mestral developed the fastening system [1], which has become one of the most popular products on the market. This technology constituted the birth of biomimetics as an independent scientific discipline.

Spider silk as a model system for dental floss and the organisation of *Arctium lappa* fruit as a template for Velcro. The tested materials were characterised for their structural characteristic by scanning electron microscopy (SEM). The results demonstrate that biomimetics has great amount of potential to develop stronger, functional, and environmentally friendly alternatives.

2. MATERIALS AND METHODOLOGY

2.1. Sample Preparation

Spider Silk:

Spider silk was obtained from natural sources. After collection, it was cleaned of organic impurities and trimmed to the required size to allow SEM analysis. The collected spider silk was stored under controlled conditions before analysis to preserve its natural structure.

Dental Floss:

Dental floss was purchased from the market, selecting a standard commercial product. The chosen floss was made of synthetic materials such as Teflon or nylon, which are commonly used in commercial products. The floss was cleaned of any impurities and prepared in the same manner as the spider silk, trimming it to the required size.

Arctium Lappa:

The inflorescence of arctium lappa was obtained from natural sources. After collection, it was cleaned of organic impurities and trimmed to the required size to allow SEM analysis. The collected inflorescences were stored under dry and controlled conditions prior to analysis to preserve their natural structure.

Velcro:

The Velcro was sourced from the market, and a standard commercial product. The Velcro chosen was made from synthetic materials such as nylon and polyester, which are commonly used in commercial products. The Velcro was cleaned of any impurities and prepared in the same manner as the *Arctium lappa* inflorescences by trimming it to the required size.

2.2 Sample preparation for SEM

All samples were subjected to drying to remove moisture, preventing distortion during microscopic analysis. Spider silk, dental floss, arctium lappa, and velcro samples were placed in a sputter coater to ensure proper electrical conductivity. A thin layer of gold was applied to the surface of the samples to improve conductivity and achieve clearer images during scanning.

2.3 SEM Analysis

All materials – spider silk, dental floss, arctium lappa and velcro – were analysed using a scanning electron microscope (SEM) [Zeiss Supra 35]. Images were obtained at various magnifications, depending on the level of detail required for the analysis. SEM investigations allowed for an in-depth structural analysis of both threads, particularly focussing on the arrangement of the fibres and any microscale elements that might affect their strength and flexibility properties.

3. RESULTS

3.1 Spider Silk as inspiration for Dental Floss

Spider silk is one of the most fascinating natural materials, known for its exceptional strength, flexibility, and lightweight properties. These characteristics make it a remarkable example of biomimicry, inspiring the design of many modern materials [2]. One such application is dental floss, which draws from the strength and thinness of spider silk. Just like spider silk, dental floss must exhibit high tensile strength, flexibility, and the ability to navigate narrow spaces, making it an effective tool for oral hygiene.

3.1.2 Spider silk SEM analysis of spider silk (Fig. 1) revealed a unique fibre structure characterised by a homogeneous surface with small irregularities and microscopic protrusions.

At a magnification of 5000x, the natural layered construction of the fibre is visible, which may contribute to its elasticity and high tensile strength. The surface of the spider silk does not show irregular defects, indicating the high quality of the material produced by spiders.

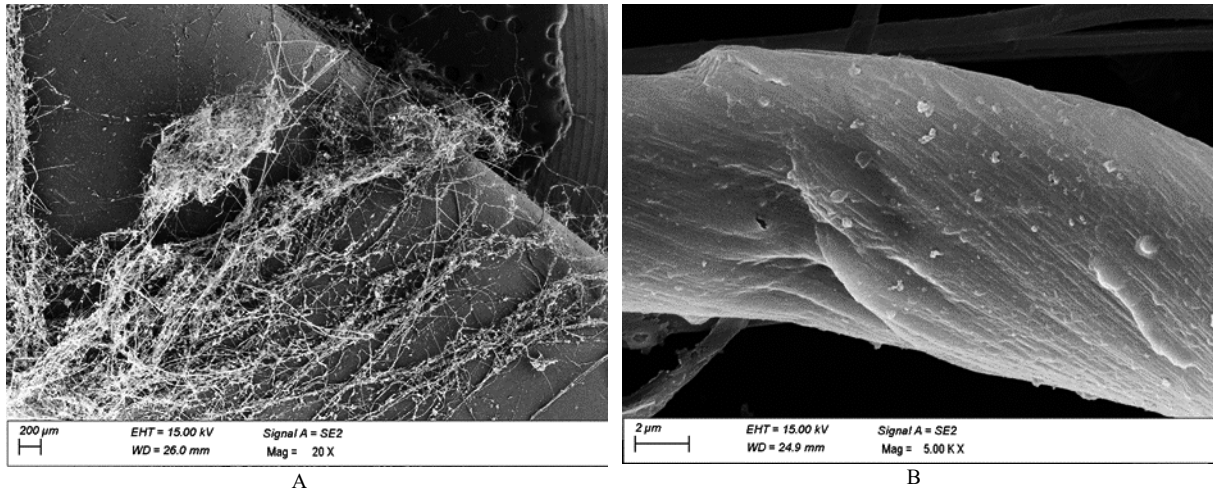


Fig. 1. Spider silk: A) 20 X , B) 5000X

3.1.3 Analysis of dental floss

Dental floss, examined with SEM (Fig. 2), shows a significantly different structure compared to spider silk. At a magnification of 101x, layers of synthetic fibres that form the final structure of the floss are visible. The surface of the floss is uneven, with numerous irregularities resulting from the manufacturing process, distinguishing it from the smoother structure of spider silk. The interwoven fibres are also visible, providing mechanical strength during usage.

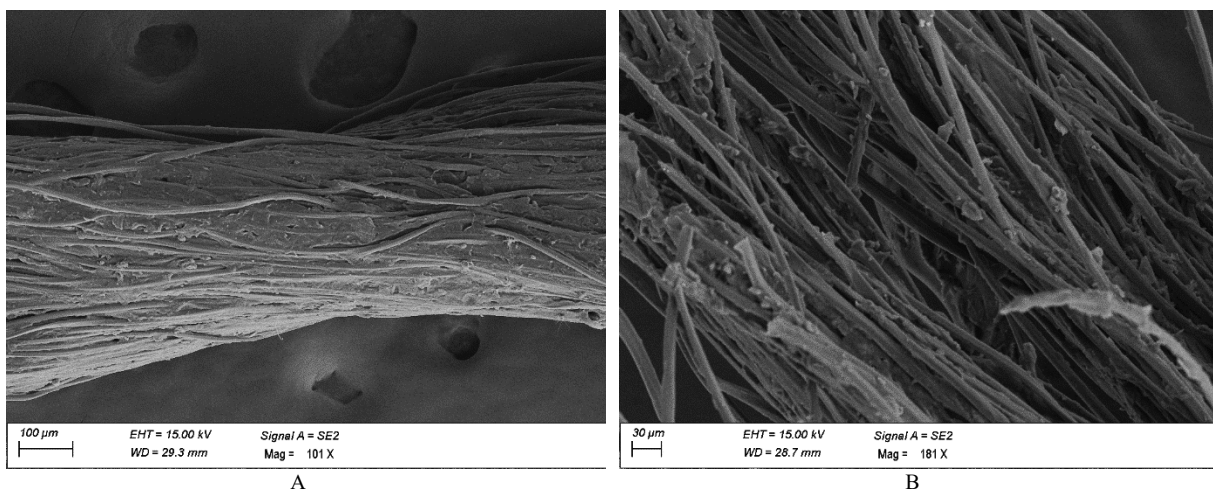


Fig. 2. Dental floss : A) 101 X, B) 181 X

3.1.4 Similarities Between Spider Silk and Dental Floss

Despite differences in origin and structure, an analysis revealed certain similarities between spider silk and dental floss. Both materials exhibit fibrous structures that are crucial for their properties. Spider silk consists of proteins with a high content of specific amino acids, which form fibres with remarkable tensile strength [3]. Dental floss, originally made of silk, is now manufactured using nylon fibres or other synthetic materials such as Teflon or polyethylene [4]. Both materials have microscopic surface irregularities that influence their elasticity and load-bearing capacities. Additionally, the layered construction of spider silk and dental floss enables them to withstand multidirectional stresses, making them effective in their respective natural and practical applications.

3.1.5 Interpretation of results

The results obtained through SEM analysis demonstrate that spider silk and dental floss differ primarily in their origin and microscopic structure but share common features that could inspire biomimetic engineering. The smoothness and exceptional tensile strength of spider silk, derived from its hierarchical microstructure with crystalline β -sheet regions, could serve as an inspiration for the development of advanced synthetic fibres [5]. Meanwhile, the layered construction of dental floss, composed of multiple wound filaments, highlights the efficiency of current manufacturing techniques in creating materials highly resistant to stress [6].

3.2 *Arctium Lappa* as inspiration for Velcro

The inflorescence of *Arctium lappa* is an extraordinary example of a natural hook-and-loop mechanism that inspired one of the most innovative inventions of the twentieth century Velcro. The characteristic hook-like spines of the burdock inflorescence allow it to attach to fibres, animal fur, or clothing, which in 1941 inspired Swiss engineer Georges de Mestral to create the system we now know as Velcro. As with the inflorescence of *Arctium lappa*, Velcro is based on a hook-and-loop principle that makes it simple to attach and detach. This biomimetic technology has been used extensively in textiles, medicine, industry, and even personal life. By observation of a natural mechanism, the burdock has evolved into a brand of innovation powered by nature, a marriage of effectiveness and simplicity in a perfectly applicable solution. Mestral innovation is often cited as a classic case of biomimicry. According to Barthlott et al. (1997), "Velcro is a remarkable example of biomimetic design, directly inspired by the hooks of burdock spines that naturally evolved for seed dispersal." Furthermore, Vincent et al. (2006) discuss how natural mechanisms such as burdock attachment properties continue to inspire engineering solutions in modern design [9,10].

3.2.1 Principle of *Arctium Lappa* Attachment

The flower head of *Arctium lappa* has numerous small hooks on its surface (Fig. 3), which are flexible and durable. When the flower head comes into contact with surfaces such as clothing, animal fur, or plant fibres, the hooks latch onto protruding elements such as threads, fibres, or other irregularities. The hooks are irregular in shape and arrangement, which influences their attachment efficiency. Their natural flexibility allows them to adapt to

various surfaces. This mechanism enables the seeds of the flower head to spread as they attach to moving animals, which is critical for the plant's reproduction.



Fig. 3. *Arctium lappa* hooks: A) 109 X, B) 85 X

3.2.2 Principle of Velcro Attachment

Velcro, inspired by the flower head of *Arctium lappa*, is an enhanced version of this natural hooking system (Fig. 4). It consists of two layers: one with synthetic hooks and the other with soft loops. [8] Unlike *Arctium lappa* hooks, synthetic hooks are more uniform in shape and arrangement. This provides a larger active surface for attachment and greater durability. The Velcro hooks latch onto the loops, creating a temporary bond. Separating the two layers requires mechanical force to bend the hooks and release the loops. Due to the precise design and durable materials, Velcro is reusable, making it more effective for everyday use compared to natural *Arctium lappa* mechanism [7].

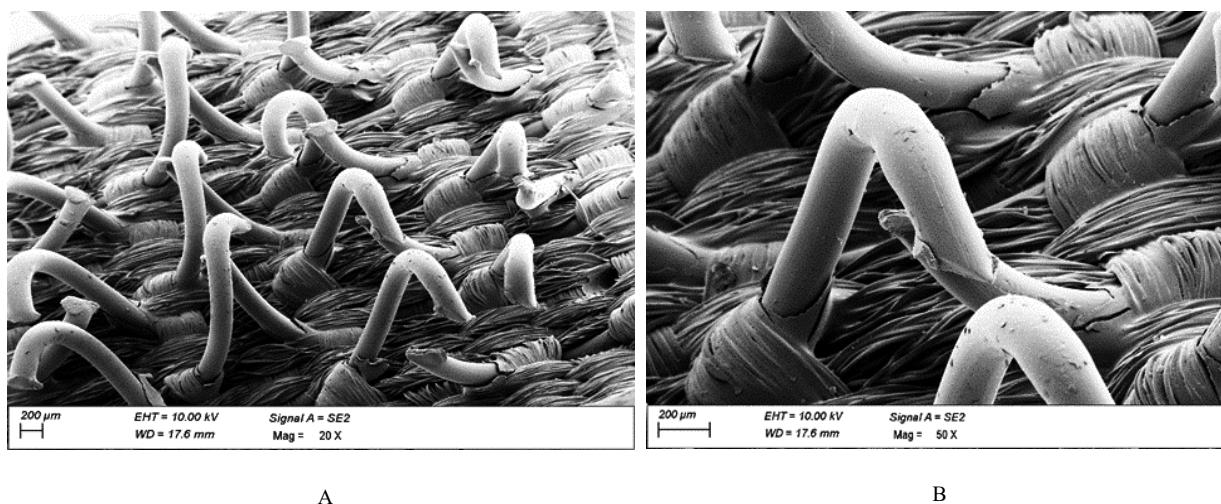


Fig. 4. Velcro structure: A) 20 X, B) 50 X

3.2.3 Similarities Between *Arctium lappa* and Velcro

- **Structure and Efficiency of Attachment:** SEM analysis revealed that *Arctium lappa* hooks are more irregular and less durable than synthetic Velcro hooks. However, natural hooks possess enough flexibility to fulfil their biological purpose. Synthetic hooks, optimised for uniformity and material properties, offer greater efficiency and durability.
- **Hook arrangement:** The uneven distribution of hooks on *Arctium lappa* flower heads limits the number of active attachment points, whereas Velcro's evenly distributed hooks create more contact points, which can enhance bonding strength.
- **Adaptation to Different Surfaces:** The natural mechanism of *Arctium lappa* is adapted to grip natural fibres like fur or clothing, but is less effective on synthetic surfaces. Velcro, with its flexible materials, performs equally well on natural and artificial fibres.
- **Durability and Reusability:** **Arctium lappa hooks** degrade after a limited number of attachment cycles, restricting their long-term functionality. In contrast, Velcro's synthetic hooks are designed to maintain their properties even after repeated use, making them a significantly more practical and durable solution. Studies such as Bhushan (2009) highlight how advances in synthetic materials have optimised natural mechanisms for enhanced longevity and efficiency in technological applications [11].

3.2.4 Interpretation of results

The SEM examination confirmed that the synthetic Velcro, inspired by the flower head of *Arctium lappa*, is a significant improvement over the natural attachment mechanism. The study highlights how nature provided a brilliant template, which, after optimisation, found widespread applications in technology and daily life. This example demonstrates the power of biomimicry in translating natural designs into improved technological solutions, offering improved functionality and durability (Bhushan, 2009).

4. CONCLUSIONS

4.1 Clear connection with research findings

Studies on spider silk and *Arctium lappa* burrs demonstrate that nature provides patterns that can be successfully adapted to technology. SEM analyses revealed unique features of these materials, such as the layered structure of spider silk, inspiring the design of strong and flexible fibres, and the hook mechanism of *Arctium lappa*, which formed the basis for Velcro. The similarities between natural and synthetic materials confirm the effectiveness of biomimetics in the development of practical solutions.

4.2 Theoretical implications

The findings confirm that biomimetics is a promising direction in materials engineering, combining biological and technological advances. Structural analysis of spider silk and *Arctium lappa* provides new insights into natural mechanisms, expanding knowledge of their

microstructures. This supports the potential of biomimetics to serve as a foundation for new material design theories that prioritise performance and ecological considerations.

ACKNOWLEDGEMENTS

This work was produced as part of the project implemented within the framework of project-orientated education, the PBL project implemented with secondary school students, in the IV competition under the Excellence Initiative - Research University programme, at the Silesian University of Technology.

BIBLIOGRAPHY

1. “The Complete History of Biomimicry (with Examples)”, Dec.10.2024
<https://www.learnbiomimicry.com/blog/history-of-biomimicry>
2. S. Kang, “Biomimetics: Engineering Spider Silk”, Nov.1.2009,
<https://illuminate.usc.edu/biomimetics-engineering-spider-silk>
3. M. Maniecka, “Mały krawiec, wielkie umiejętności: jedwab pajęczy”,
<https://laboratoria.net/artukul/12636.html>
4. “Dental floss”, Jan.1.2025,
https://en.wikipedia.org/wiki/Dental_floss
5. H. Sogawa, K. Nakano, A. Tateishi, K. Tajima, K. Numata, “Surface Analysis of Native Spider Draglines by FE-SEM and XPS”, *Front Bioeng Biotechnol* (2020) Mar.20.8.231,
6. Z. Huang, J.M. Broadbent, J. Jung Eun Choi, “Comparison of dental flosses – an investigation of subjective preference and mechanical properties”, Sep.22.2023,
<https://pubmed.ncbi.nlm.nih.gov/articles/PMC10519255>
7. “Our Innovation Story - Velcro Companies”, (2022)
<https://www.velcro.com/our-story>
8. “A Brief History of: Velcro”, June.15.2010
<https://time.com/archive/6916217/a-brief-history-of-velcro>
9. W. Barthlott, C. Neinhuis, G. Kerner, *Biomimetic Innovations in the Natural World*, Oxford University Press. (1997).
10. J.F.V. Vincent, O.A. Bogatyreva, A.-K. Pahl, A. Bowyer, "Biomimetics: Its Practice and Theory." *Journal of the Royal Society Interface*, 3(9) (2006) 471–482.
11. B. Bhushan, *Biomimetics: Lessons from Nature – An Overview*. *Philosophical Transactions of the Royal Society A: Mathematical, Physical and Engineering Sciences*, 367/1893 (2009)1445–1486.
12. Yoseph Bar-Cohen, *Biomimetics: Biologically Inspired Technologies*. CRC Press. (2006).



31th January 2025
Gliwice, Poland

DEPARTMENT OF ENGINEERING MATERIALS AND BIOMATERIALS
FACULTY OF MECHANICAL ENGINEERING
SILESIA UNIVERSITY OF TECHNOLOGY

INTERNATIONAL STUDENTS SCIENTIFIC CONFERENCE

Research on the structure and chemical composition of PVD coatings deposited on tool ceramics

Michał Kopciowski^a, Krzysztof Hlubek^a, Marcin Staszuk^b, Daniel Pakuła^{b, *}

^a Students of the 5th Secondary School named after Andrzej Struga in Gliwice, ul. Górnych Wałów 29, 44-100 Gliwice, Poland

^b Silesian University of Technology, Faculty of Mechanical Engineering, Department of Engineering Materials and Biomaterials, ul. Konarskiego 18A, 44-100 Gliwice, Poland

*email: daniel.pakula@polsl.pl

Abstract: This article has been made as a part of the PBL project (4th edition) conducted with high school students, titled: "Electron Microscopy? Who Needs It? Applications of Microscopy in Surface Engineering." The aim of this study was to examine the structure of single-layer nitride coatings such as TiZrN, TiAlN, TiCN, and TiBN deposited using Physical Vapor Deposition (PVD) on tool material surfaces. The cross-sectional structure and surface morphology of the coatings were investigated using Scanning Electron Microscopy (SEM). The chemical composition analysis was performed with an Energy Dispersive X-ray Spectrometer (EDS).

Keywords: SEM, Tool materials, PVD coatings

1. INTRODUCTION

Physical Vapor Deposition (PVD) is a method of applying thin coatings (with about a few micrometers of thickness) on engineering materials, utilizing certain physical phenomena such as evaporation and spraying the coated material. Ever since the 1960s this method has been successfully implemented in the process of forming coatings on tool materials, simultaneously greatly contributing to the increase of overall tool durability. The first commercially used coatings were single-layer TiN and TiC type coatings. They were followed by multi-component, multi-layered, gradient and hybrid coatings that were brought onto the market next. Among the most important advantages of PVD coatings there are for example: improved microhardness of the surface (2400-4000 HV), high abrasive resistance (against grinding), low friction ratio, low thermal conductivity, chemical resistance or preventing the parts of the workpiece from sticking onto the tool surface (grease layers). However the most important property of PVD coatings is the fact that they significantly improve upon the efficiency of the tool that they are layered on by delaying the process of its deterioration, which as a result leads up to a 300% of an increase in their work time when compared to an uncoated tool [1-9].

Despite all the advantages listed above, PVD coatings have one significant drawback – structural defects, such as grain boundaries or discontinuities in the form of craters (a side effect of the deposition process), which in some cases can lead to a deterioration of the functional properties of the coated materials. Therefore, it is crucial to conduct quality control of the structure and surface morphology of the produced materials during the implementation stage or innovative research on the designed coatings. For this purpose, a scanning electron microscope (SEM) is often used. By utilizing a scanning electron beam at very high magnification, it enables the examination of the quality of the produced surface layers. Moreover, this microscope is equipped with an energy-dispersive spectrometer (EDS), which, based on the emission of characteristic X-ray radiation, identifies the chemical composition of the examined areas [1-9].

The aim of this study is to present the results of structural, surface morphology, and chemical composition analyses of TiZrN, TiAlN, TiCN, and TiBN coatings deposited on tool ceramics substrates using PVD technology.

2. MATERIALS AND METHODOLOGY

The research materials consisted of nitride and sialon tool ceramics covered with single-layer coatings using the Physical Vapor Deposition technology. The nitride coatings TiZrN, TiAlN, TiCN, and TiBN were applied to appropriately prepared tool materials using the Cathode Arc Evaporation (CAE) process.

The structure of the fractures and the surface topography of the examined materials were investigated using Scanning Electron Microscopy (SEM). The study was conducted using an HRSEM SUPRA 35 microscope at a voltage range of 10 to 20 kV for SE mode and magnifications between 1000 and 70000x. For InLens mode, the voltage was set to 7 kV, with magnifications of 100000 and 200000x. The chemical composition was analyzed in selected micro-areas of the coatings using an Energy Dispersive X-ray Spectrometer (EDS).

3. RESULTS

Based on the research conducted with Scanning Electron Microscopy (SEM), it was confirmed that the observed TiZrN, TiAlN, TiCN, and TiBN coatings were uniformly applied to the substrate material. Minor cracks and indentations were observed, but aside from them the coatings adhered closely to the substrate material. In the case of TiAlN and TiCN coatings, slight delaminations (discontinuities and inhomogeneities) were visible in the zone between the substrate material and the coating. According to the theory presented in the literature [2], it can be concluded that TiZrN and TiCN coatings exhibit a dense columnar grain structure consistent with Zone II of Thornton's model, whereas the (Ti,Al)N coating also has a columnar structure resembling Zone I of Thornton's model (Fig. 1). The thickness of the produced coatings, measured using a SEM microscope, ranged from 0.7 to 1.8 μm (Table 1).

Table. 1. Coating thickness.

Coating	TiZrN	TiAlN	TiCN	TiBN
Thickness, μm	1.8	0.7	1.8	0.8

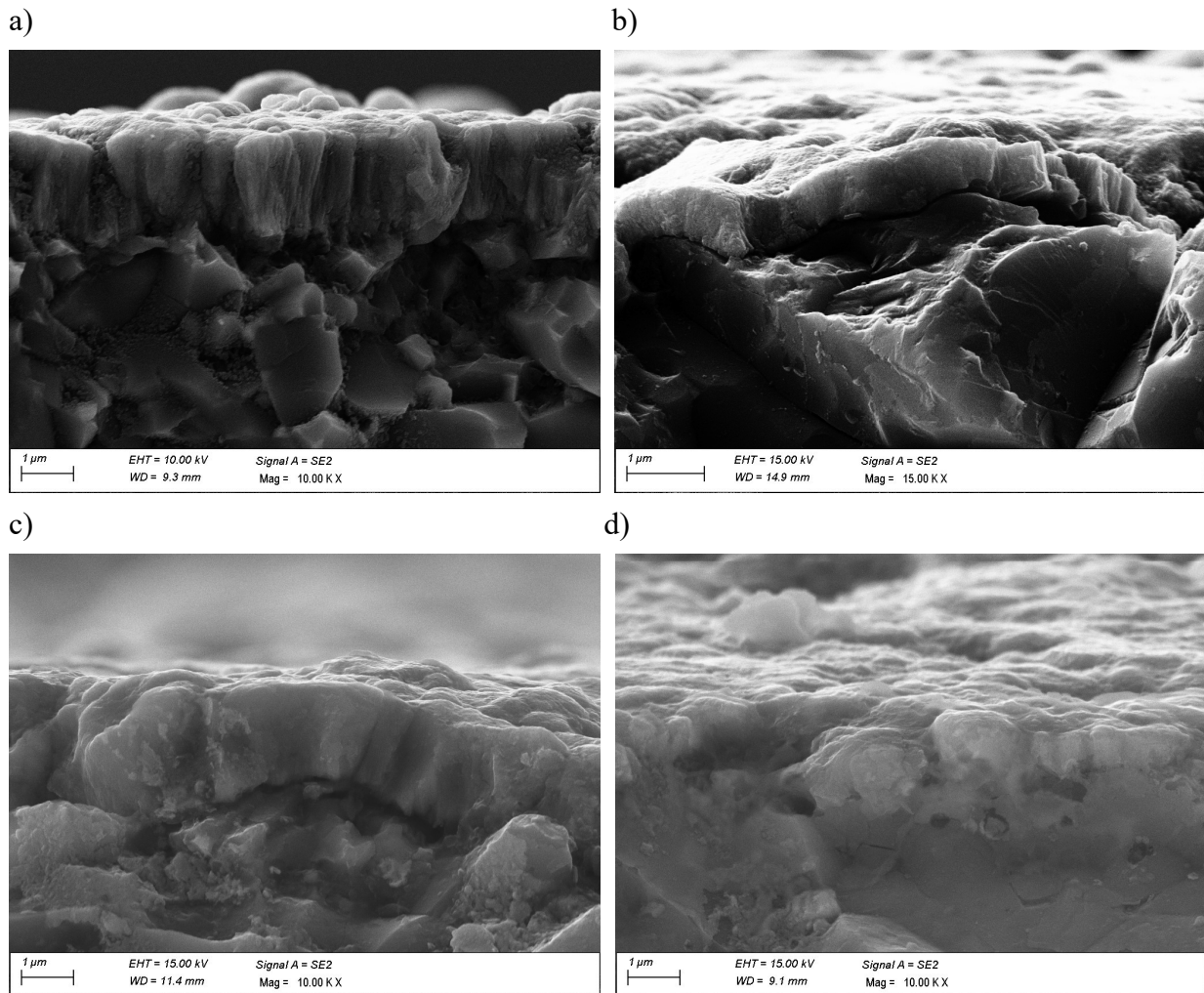


Fig. 1. Structure of the: a) TiZrN coating, b) TiAlN coating, c) TiCN coating, d) TiBN coating

Based on the fractographic analysis of the surface topography of the coatings, a structure typical of coatings applied by Physical Vapor Deposition (PVD) was identified [1,3,4]. The surface of the examined TiZrN, TiAlN, TiCN, and TiBN coatings is characterized by inhomogeneity and a presence of discontinuities in the form of micropores and cracks. Analysis using the Scanning Electron Microscopy (SEM) showed the presence of numerous microdroplets on the coating surfaces, which are remnants of the PVD coating process. This type of defect is associated with the nature of the CAE process used for coating deposition. It was also noted that craters formed in some areas where previously the solidified droplets had been located, which is also a characteristic feature of this process, as confirmed by previous research [1,3,4] (Fig. 2).

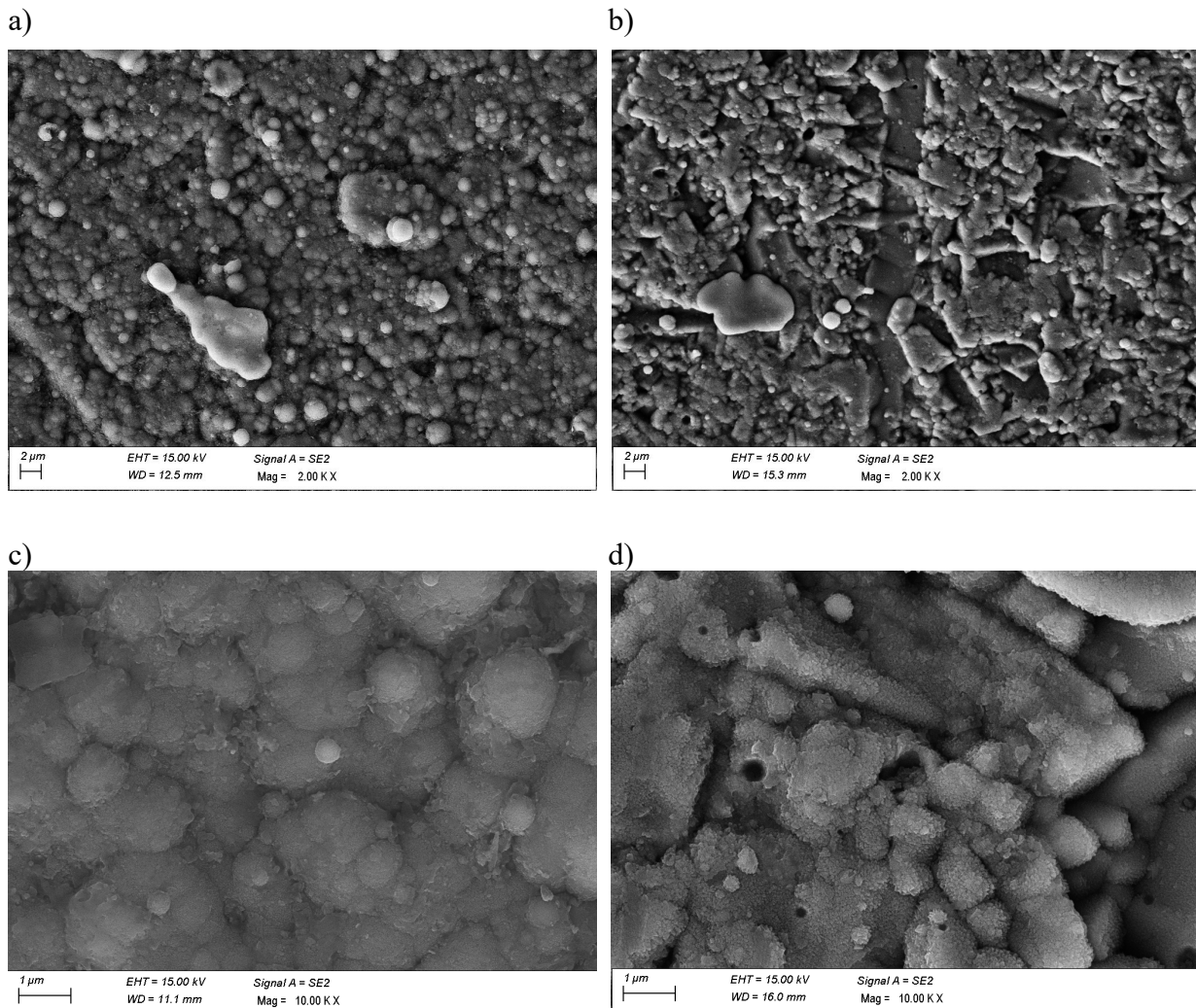


Fig. 2. Surface topography of the coating, a) TiZrN coating, b) TiAlN coating, c) TiCN coating, d) TiBN coating

The chemical composition microanalysis conducted with the Energy Dispersive X-Ray Spectrometer (EDS) confirmed the correct distribution of elements in both the coatings and the substrate material. All elements present in the TiZrN, TiAlN, TiCN, and TiBN coatings were identified solely within the coatings area (except for boron, which cannot be detected using this method). In the substrate area, elements typical of tool ceramics were found (Fig. 3).

4. CONCLUSIONS

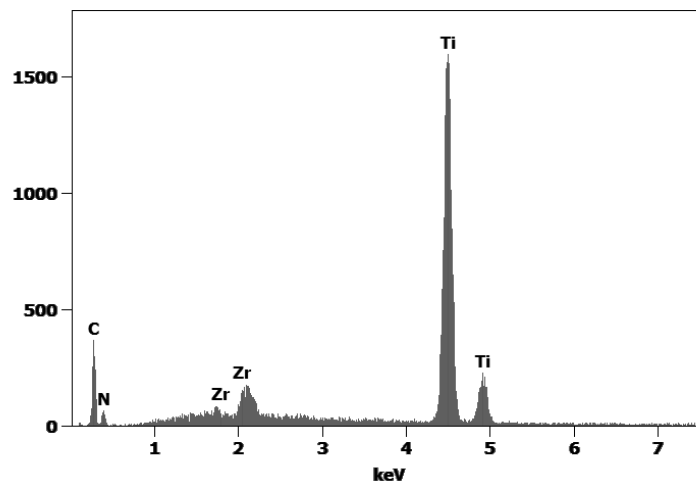
Based on the conducted research, the following conclusions were drawn:

- The thickness of the coatings applied to the tool ceramics ranged from 0.7 to 1.8 μm .
- The TiZrN, TiAlN, TiCN, and TiBN coatings were uniformly applied and adhered closely to the substrate material—tool ceramics. In the case of TiAlN and TiCN coatings, slight

delaminations and cracks were observed in the zone between the substrate material and the coating.

- TiZrN and TiCN coatings exhibit a structure resembling Zone II of Thornton's model, while the TiAlN coating structure corresponds to Zone I of Thornton's model [2].
- Surface analysis of the PVD coatings revealed inhomogeneity associated with the presence of micromolecules in the shape of droplets, which is inherent to the used CAE coating deposition process.
- The EDS chemical composition analysis confirmed the presence of expected elements in both the coatings and the substrate material.

a)



b)

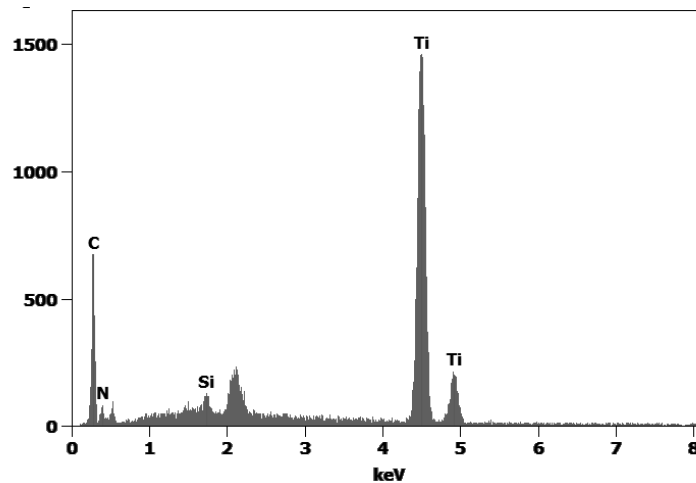


Fig. 3. EDS analysis from the: a) area TiZrN coating, b) area TiCN coating

ACKNOWLEDGEMENTS

This work was produced as part of the project implemented within the framework of project-oriented education - PBL project implemented with secondary school students, in the IV competition under the Excellence Initiative - Research University program, at the Silesian University of Technology.

BIBLIOGRAPHY

1. D. Pakuła, Forming of the surface structure and properties of tool's ceramic inserts with improved abrasion resistance, *Archives of Materials Science and Engineering* 62/2 (2013) 55-96.
2. J.A. Thornton, *Journal of Vacuum Science and Technology*, A4, (6) 3059-3065 (1986).
3. D. Pakuła, M. Staszuk, K. Gołombek, A. Śliwa, J. Mikuła, Structure and properties of the tool ceramics with hard wear resistant coatings, *Archives of Metallurgy and Materials* 61/3 (2016) 1265-1270.
4. L.A. Dobrzański, D. Pakuła, M. Staszuk, A.D. Dobrzańska-Danikiewicz, Structure and properties of multicomponent coatings on cemented carbides and nitride and sialon ceramics, *Open Access Library, Annal (V)* (1), 2015 (in Polish)
5. M. Staszuk, D. Pakuła, M. Pancielejko, T. Tański, L.A. Dobrzański, Investigations on wear mechanisms of PVD coatings on carbides and sialons, *Archives of Metallurgy and Materials* 62/4 (2017) 2095-2100.
6. J. Mikuła, D. Pakuła, L. Żukowska, K. Gołombek, A. Križ, Wear resistance of (Ti,Al)N metallic coatings for extremal working conditions. *Coatings* 2021, 11, 157.
7. M. Staszuk, D. Pakuła, G. Chladek, M. Pawlyta, M. Pancielejko, P. Czaja, Investigation of the structure and properties of PVD coatings and ALD+PVD hybrid coatings deposited on sialon tool ceramics, *Vacuum* 154 (2018) 272-284.
8. Lianchang Qiu, Du Yong, Zhong Zhiqiang, Shi Haidong, Albir Layyous, Influence of annealing on the microstructure and mechanical properties of MTCVD TiC_{0.79}N_{0.21} coating, *Vacuum* 148 (2018) 88–97.
9. Wei Liu, Quanquan Chu, Rongxuan He, Meipeng Huang, Haidong Wu, Qiangguo Jiang, Jian Chen, Xin Deng, Shanghua Wu, Preparation and properties of TiAlN coatings on silicon nitride ceramic cutting tools, *Ceram. Int.* 44 (2018) 2209-2215.



31th January 2025
Gliwice, Poland

DEPARTMENT OF ENGINEERING MATERIALS AND BIOMATERIALS
FACULTY OF MECHANICAL ENGINEERING
SILESIA UNIVERSITY OF TECHNOLOGY

INTERNATIONAL STUDENTS SCIENTIFIC CONFERENCE

Analiza rozkładu naprężenia i odkształcenia haka holowniczego

Halina Kordecka ^a, Julia Quaeck ^a, Wojciech Mikołajko^b, Amadeusz Dziwis^b, Agata Śliwa^b, Marek Sroka^b

^a V Liceum Ogólnokształcące im. Andrzeja Struga w Gliwicach
email: helena.k783@gmail.com, juliaquaeck@icloud.com

^b Silesian University of Technology, Faculty of Mechanical Engineering, Department of Engineering Materials and Biomaterials
email: wojciech.mikolajko@polsl.pl, amadeusz.dziwis@polsl.pl, agata.sliwa@polsl.pl, marek.sroka@polsl.pl

Streszczenie: Tematem niniejszego artykułu było przeprowadzenie analizy odkształceń haka kulowego holowniczego oraz przedstawienie jego dopuszczalnych wartości. Model wyjściowy 3D został wykonany za pomocą metod elementów skończonych w programie SolidWorks.

Abstract: The theme of this article was to analyze deformation tow ball hitch and to provide its permissible values. The output 3D model was made using Finite Element Methods in SolidWorks.

Słowa kluczowe: hak holowniczy, MES, rozkład naprężenia, odkształcenie

1. WPROWADZENIE

Haki holownicze mogą pełnić w samochodzie kilka funkcji. Wykorzystywane są głównie do ciągnięcia przyczep lub innych uszkodzonych samochodów, ale mogą zostać również użyte do montażu dodatkowego bagażnika, za pośrednictwem którego można bezpiecznie przewozić różne elementy np. rowery. Hak holowniczy bez wątpienia nie dodaje uroku samochodowi, w którym jest montowany, ale daje komfort psychiczny w razie wystąpienia jednej z powyższych sytuacji. Niestety sam montaż jest nie lada problemem, gdyż w wielu przypadkach konieczne jest cięcie zderzaka [1].

Hak dobiera się na podstawie podstawowych parametrów auta, takich jak: marka, model, rok produkcji czy wersja nadwozia. Zakupiony hak powinien być więc dedykowany do poszczególnego rodzaju pojazdu, dzięki czemu będziemy mieli ułatwiony montaż, ponieważ mocowanie będzie wykorzystywać otwory fabryczne. Unikać należy zakupu najprostszych haków, które montowane są do auta na stałe, z powodu braku możliwości ich zdemontowania, a także tego że nie spełniają one wymogów Unii Europejskiej. Zdecydowanie większym zainteresowaniem cieszą się haki, które mocuje się za pomocą kilku śrub wraz z systemem

automatycznego wypinania. Poniżej przedstawiono przykładowe mocowanie haka holowniczego [1,4].



Rysunek 1. Przykładowe mocowanie haka holowniczego [5]

Figure 1. Examples of mounting the tow bar in car [5]

2. PARAMETRY HAKA HOLOWNICZEGO

Podstawowym parametrem, który decyduje o funkcjonalności haka jest jego maksymalny udźwig. Każdy hak powinien zawierać wyszczególnione zalecenia dotyczące ciężaru, jaki jest w stanie udźwignąć. Należy przy tym pamiętać, że tonaż haka nie może przekraczać masy całkowitej pojazdu, do którego będzie zamontowany. Drugim parametrem jest materiał z jakiego jest wykonany. Haki holownicze wykonuje się najczęściej ze stali konstrukcyjnej S215 (st3) [2].

Tablica 1. Podstawowe własności stali S215 [3]

Table 1. Basic properties of steel S215 [3]

Oznaczenie stali	Re [MPa]	Rm [MPa]	Twardość [HB]	A ₅ [%]	Zawartość C [%]
S215/st3	235	375	120	23÷26	0,22

Największą uwagę należy zwrócić na kwestię homologacji haku, ponieważ bez niej narazimy się na kłopoty podczas przeglądu rejestracyjnego czy kontroli policji. Dodatkowo wybierając hak warto sprawdzić czy jest wykonany ze stali ocynkowanej, która cechuje się większą odpornością korozyjną niż stal bez powłoki [2].

3. PRZYGOTOWANIE MODELU I WYKONANIE SYMULACJI KOMPUTEROWEJ

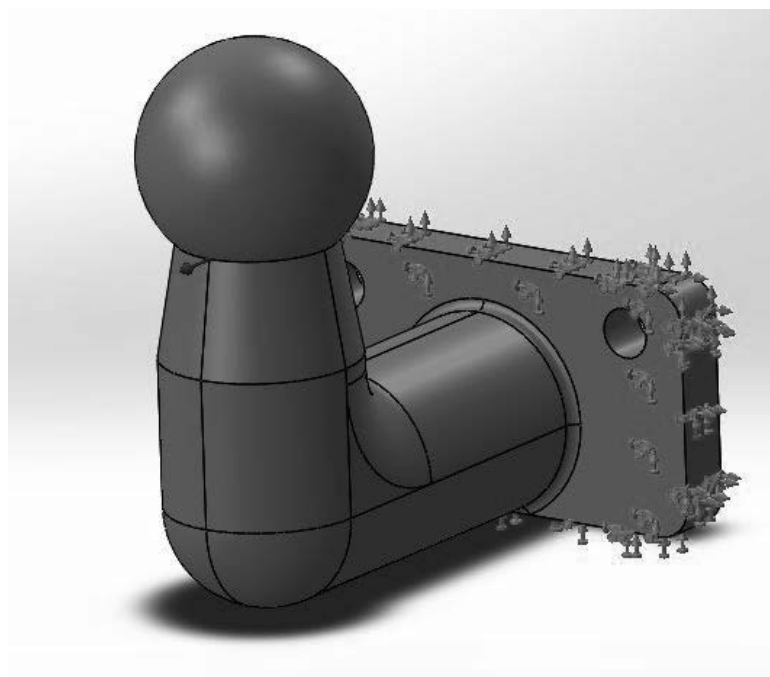
W niniejszej pracy poddano analizie hak holowniczy z wykorzystaniem metod elementów skończonych (MES) przy użyciu programu SolidWorks. Celem analizy było otrzymanie symulacji naprężeń, odkształceń i przemieszczeń występujących w elemencie podczas pracy.

Głównym założeniem MES jest podział modelu geometrycznego ciągłego na elementy skończone, czego efektem jest utworzenie modelu geometrycznego dyskretnego. Podczas

dyskretyzacji dąży się do maksymalnego zbliżenia postaci dyskretnej i ciągłej. Na modelu 3D zostały dobrane punkty podparcia od strony mocowania do samochodu danego haka oraz obciążono go dwoma różnymi siłami – 11000 N oraz 20000 N (Rysunek 3). Dokonano dwóch symulacji, ponieważ przedstawiono hak holowniczy dla ford galaxy, który posiada masę własną około 1700 kg, jak podano wcześniej samochód ten powinien holować elementy poniżej jego własnej masy, właśnie dlatego dokonano dwóch symulacji. Geometryczny model został przedstawiony na rysunku 2. Model zdyskretyzowano za pomocą 18528 węzłów (Rysunek 4).



Rysunek 2. Model geometryczny haka holowniczego
Figure 2. Geometric model of towbar



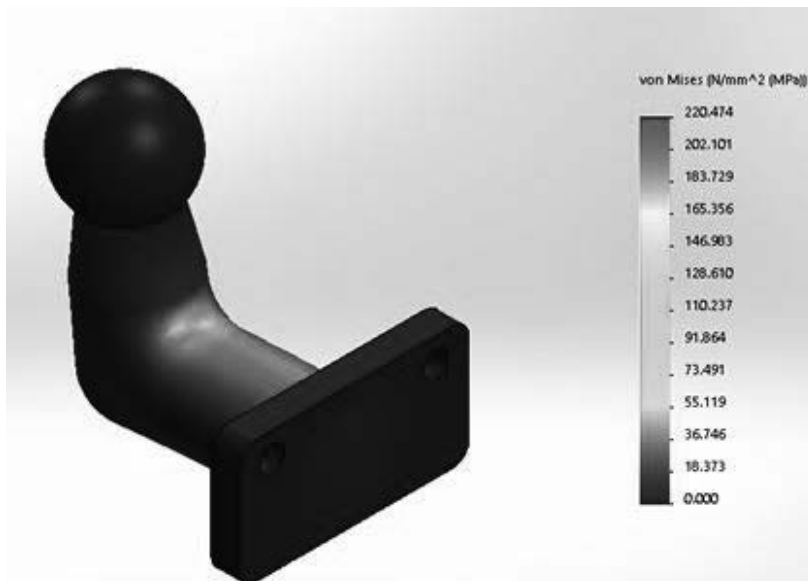
Rysunek 3. Nadanie utwierdzenia oraz obciążenia zewnętrznego
Figure 3. Giving restraint and external load



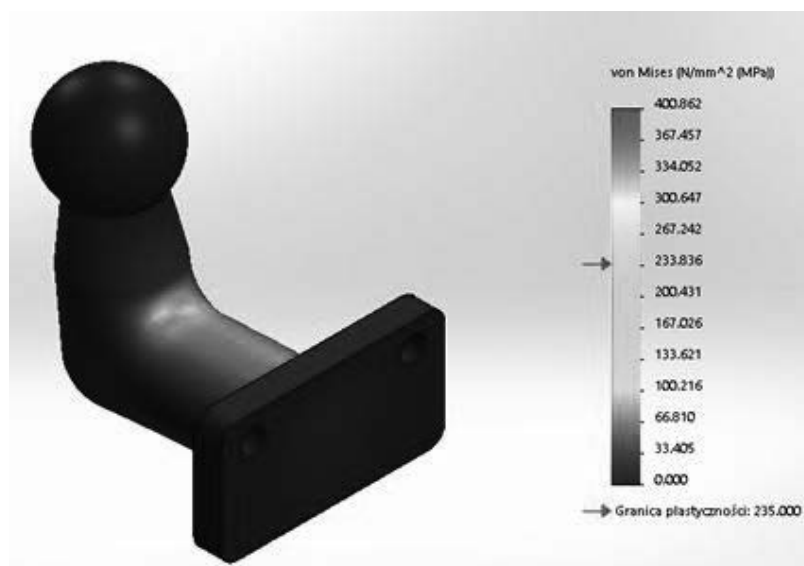
Rysunek 4. Model haka z naniesioną siatką (zdyskretyzowany)
Figure 4. Numerical model of towbar

4. ANALIZA WYNIKÓW

W pracy przeanalizowano wpływ obciążeń o dwóch różnych wartościach. W pierwszym przypadku element został obciążony siłą równą 11000 N, natomiast w drugim siłą 20000 N. Pierwszą analizą rozkład naprężeń von Misesa (Rysunek 5 i 6). Na podstawie analizy można stwierdzić, że największe naprężenia powstają na zgięciu haka oraz górnej powierzchni poziomej części.



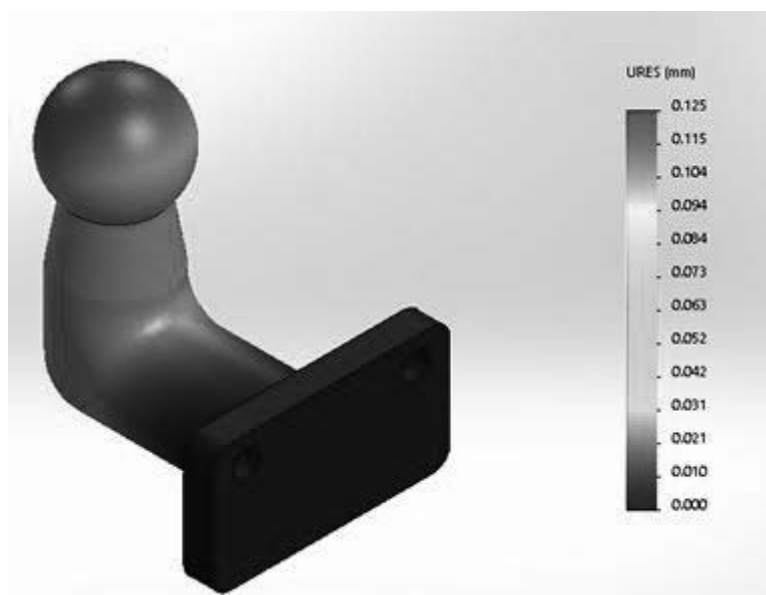
Rysunek 5. Rozkład naprężeń von Misesa przy obciążeniu 11000 N
Figure 5. Von Mises stress distribution for 11000 N load



Rysunek 6. Rozkład naprężeń von Misesa przy obciążeniu 20000 N

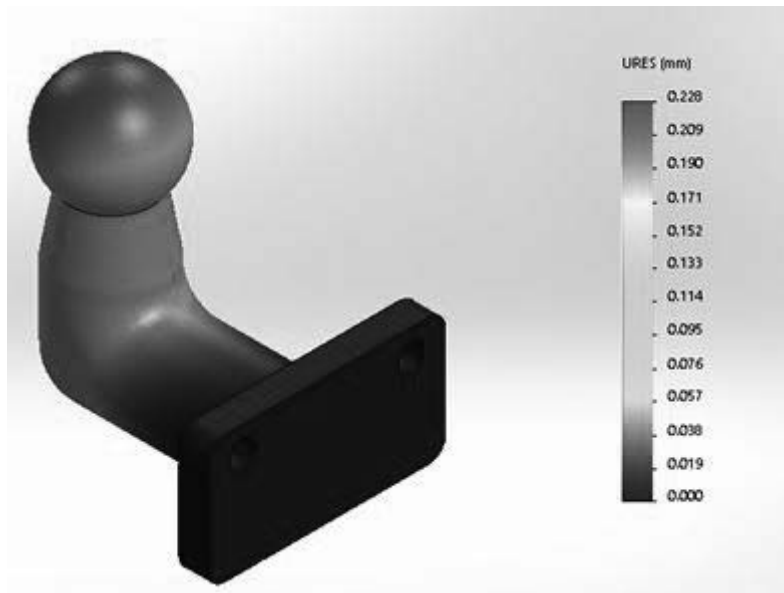
Figure 6. Von Mises stress distribution for 20000 N load

Druga analiza dotyczyła rozkładu przemieszczeń. W obu przypadkach największe przemieszczenia zachodziły na kuli haka. Największe wynosiły kolejno: dla 11000 N – 0,125mm, a dla 20000 N – 0,228mm (Rysunek 7 i 8).



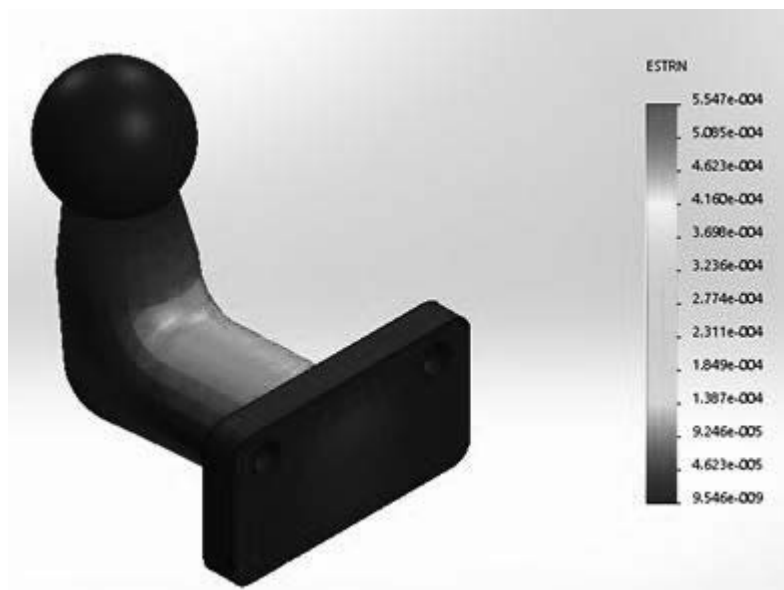
Rysunek 7. Rozkład przemieszczeń dla siły 11000 N

Figure 7. Displacement distribution for 11000 N load

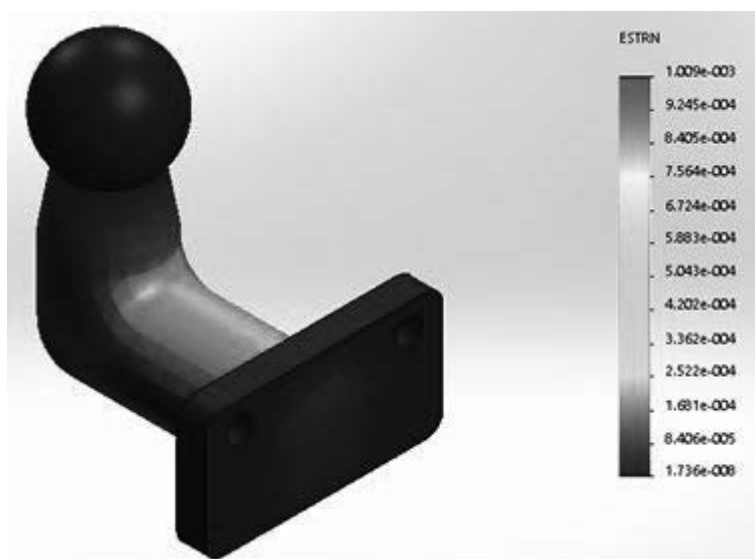


Rysunek 8. Rozkład przemieszczeń dla siły 20000 N
Figure 8. Displacement distribution for 20000 N load

Ostatnią przeprowadzoną analizą był rozkład odkształceń w badanym elemencie. W obu przypadkach największe odkształcenie występuje na wewnętrznym zgięciu haka (Rysunek 9 i 10).



Rysunek 9. Rozkład odkształceń dla siły 11000 N
Figure 9. Deformation distribution for 11000 N load



Rysunek 10. Rozkład odkształceń dla siły 20000 N
Figure 10. Deformation distribution for 20000 N load

5. PODSUMOWANIE

Jak widać na powyższych rysunkach punkt maksymalnego przesunięcia w obu przypadkach, znajduje się na kuli. Maksymalne przesunięcie dla pierwszego przypadku (11000 N) wyniosło 0,125 mm, a dla drugiego przypadku (20000 N) wyniosło 0,228 mm. Dla obciążenia 1100 kg jest to odkształcenia bardzo małe i ma znikomy wpływ na żywotność tego elementu. Dla drugiego obciążenia 2 ton jest to odkształcenie prawie dwa razy większe, więc już należy uważać z zwiększaniem masy. Ogólna zasada mówi, aby holowany samochód był lżejszy od holującego pojazdu, co pierwsza symulacja potwierdza możliwość bezpiecznego używania haka holującego. Jeżeli obciążenia byłyby rzędu kilku milimetrów, wtedy element posiada wadę konstrukcyjną i jest niesprawny do użycia.

LITERATURA

1. „Hak holowniczy” [Online], <http://www.iparts.pl/czesci-samochodowe/hak-holowniczy,100607.html>
2. „Parametry haka holowniczego” [Online], <http://allegro.pl/artukul/na-co-zwrocic-uwage-wybierajac-hak-holowniczy-jakie-parametry-powinien-posiadac-41939>
3. „Własności stali” [Online], <http://www.pkm.edu.pl/index.php/07/stale/63-07010201>
4. „Haki holownicze” [Online], <http://www.swistak.pl/poradniki/313-Jak-wybrac-haki-holownicze.html>
5. „Hak holowniczy” [Online], <http://old.skoda-auto.pl/modele/octavia-combi/akcesoria/turystyka>



31th January 2025
Gliwice, Poland

DEPARTMENT OF ENGINEERING MATERIALS AND BIOMATERIALS
FACULTY OF MECHANICAL ENGINEERING
SILESIA UNIVERSITY OF TECHNOLOGY

INTERNATIONAL STUDENTS SCIENTIFIC CONFERENCE

Stereolithography in the design and manufacturing of Fresnel lenses

Emilia Krajewska^a, Jakub Kuta^a, Michał Pietruszka^a, Olaf Sobek^a, Błażej Łagosz^a, Michalina Ziółkowska^b, Marek Szindler^c, Błażej Tomiczek^c, Magdalena Szindler^d

^a Student of Silesian University of Technology, Faculty of Mechanical Engineering, Production Engineering and Management, Gliwice

^b Student of Silesian University of Technology, Faculty of Mining, Safety Engineering and Industrial Automation, Automatic Control and Industrial Informatics, Gliwice

^c Silesian University of Technology, Faculty of Mechanical Engineering, Scientific and Didactic Laboratory of Nanotechnology and Material Technologies, Gliwice

^d Silesian University of Technology, Faculty of Mechanical Engineering, Department of Engineering Materials and Biomaterials; Gliwice

Abstract: This article explores the application of stereolithography in the design and production of Fresnel lenses. It discusses the structural differences between traditional lenses and Fresnel lenses, highlighting their advantages, such as reduced weight and thickness while maintaining the ability to focus light. The manufacturing process of the lens using 3D printing and resin-based materials is presented. The results of tests conducted with various types of lasers are analyzed, demonstrating significant differences in light-focusing capabilities depending on the surface treatment. These findings confirm the practical potential of stereolithography in producing precise optical components.

Keywords: Optics, Fresnel lens, 3D printing, stereolithography

1. INTRODUCTION

A lens, as an optical instrument made of a transparent material (e.g., glass or plastic), is bounded by two spherical surfaces or one spherical and one flat surface. Its purpose is to focus or disperse light rays through double refraction: first when transitioning from the surrounding medium into the lens, and then upon exiting back into the same medium. A key geometric element of a lens is its principal optical axis, a line passing through the centers of the bounding surfaces, which also serves as the symmetry axis of the lens [1, 2].

Typically, the medium surrounding the lens is air or another medium with a refractive index lower than that of the lens material. Lenses can be classified as either converging or diverging (Figure 1). Converging lenses have a thickness at the edges that is smaller than at their optical axis. Examples include convex, plano-convex, and concave-convex lenses. Diverging lenses, on the other hand, have greater edge thickness than at the optical axis. Examples include concave, plano-concave, and convex-concave lenses [3].

The real focus (F) of a converging lens is the point on its optical axis where all parallel light rays meet after passing through the lens. The virtual focus (F') of a diverging lens is the point where the extensions of dispersed light rays intersect. The focal length (f) of a lens is the distance between its focus (F) and the center of the lens (O). For virtual foci, this value is negative. The paths of light rays through both types of lenses are shown in Figure 2. In a converging lens, parallel rays focus at a point on the optical axis, whereas in a diverging lens, the rays spread out, and their extensions meet at the virtual focus [4].

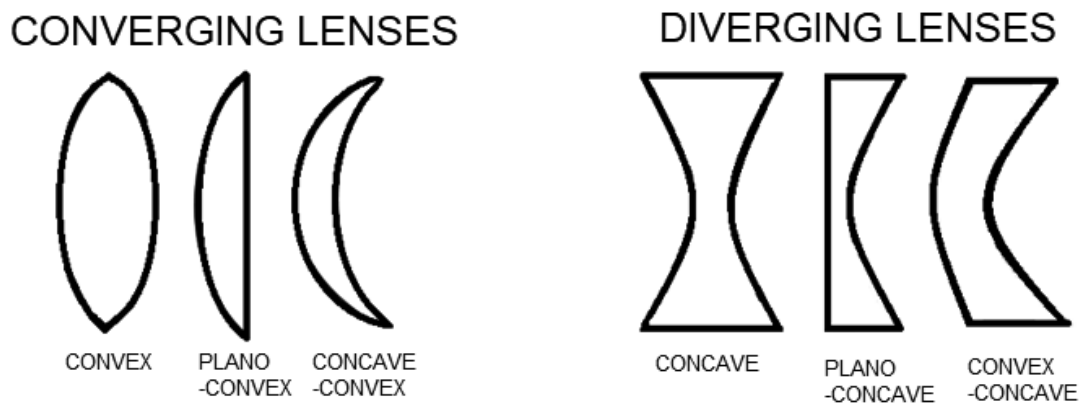


Figure 1. Classification of lenses

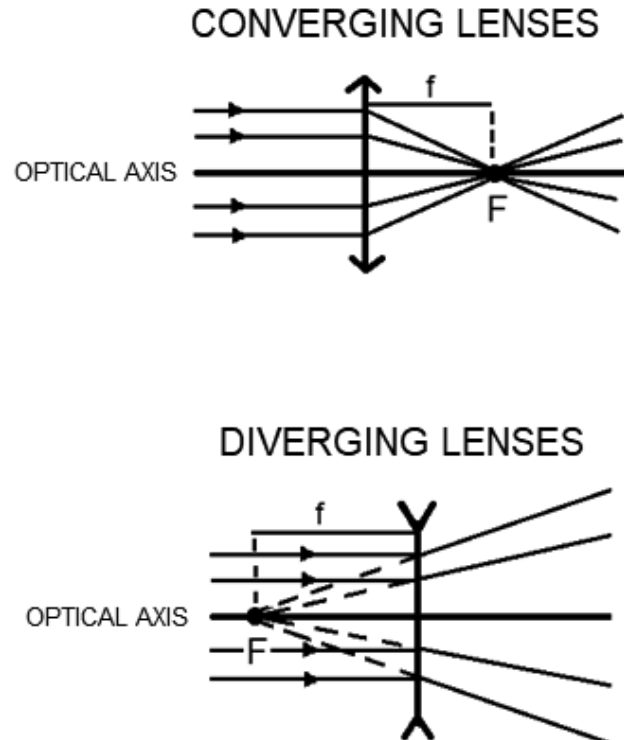


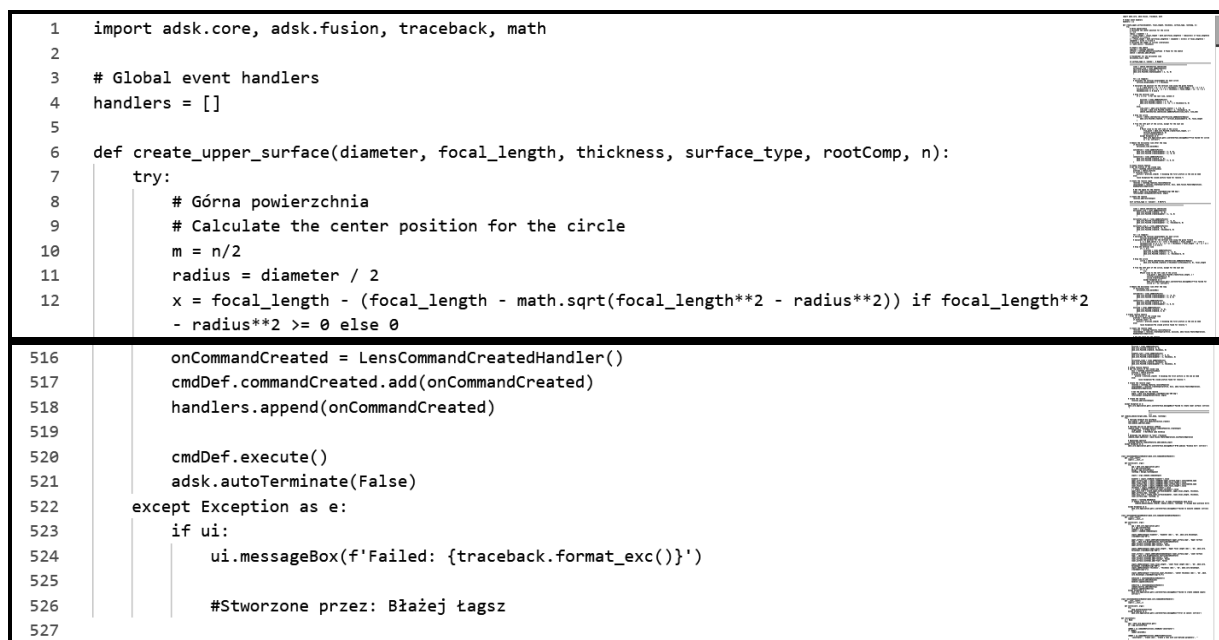
Figure 2. Light ray paths through both types of lenses

Traditional lenses with large diameters are heavy and difficult to manufacture, while Fresnel lenses minimize material usage by dividing the optical surface into concentric rings. Each ring acts as an independent prism, maintaining the ability to focus light while significantly reducing thickness and weight. Each Fresnel lens segment directs light based on refraction principles, reducing optical aberrations compared to flat lenses of the same diameter. Fresnel lenses are particularly useful in systems where long-distance light focusing is critical, such as lighthouses, theatrical lighting, or projectors. Modern applications include solar concentrators and cameras. When designing Fresnel lenses, both precision requirements and practical limitations are considered. Their ability to control light propagation depends on precisely engineered surfaces and their geometric arrangement [5-9].

2. MATERIALS AND METHODS

The Fresnel lenses were designed using CAD software, specifically Fusion 360 by Autodesk. However, before the design process in Fusion 360, a custom Python script (Figure 3) was developed to calculate the diameter, thickness, and the number of rings for the Fresnel lenses. This script ensured precise specifications and optimized the geometry for the desired optical performance. Once the designs were finalized, several lenses were 3D printed using a Formlabs SLA printer with clear resin (Figure 4a). After printing, the lenses were carefully cleaned to remove uncured resin using an isopropyl alcohol bath. To complete the process, the outer layer of the lenses was cured in a UV curing chamber for 60 minutes at a temperature of 60°C (Figure 4b).

This combination of computational precision, advanced CAD tools, and SLA printing resulted in high-quality Fresnel lenses, ready for further application and testing.

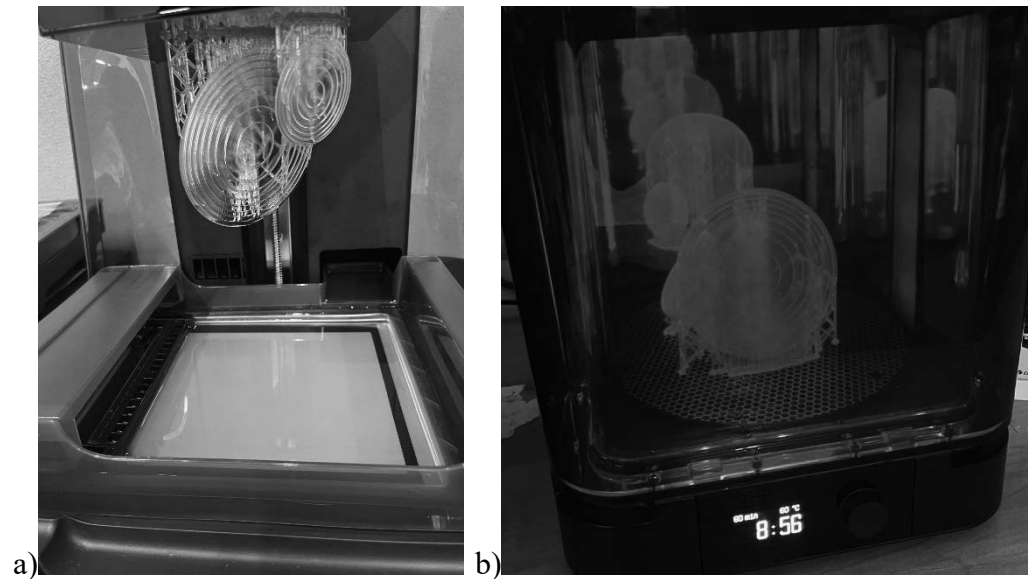


```

1  import adsk.core, adsk.fusion, traceback, math
2
3  # Global event handlers
4  handlers = []
5
6  def create_upper_surface(diameter, focal_length, thickness, surface_type, rootComp, n):
7      try:
8          # Górna powierzchnia
9          # Calculate the center position for the circle
10         m = n/2
11         radius = diameter / 2
12         x = focal_length - (focal_length - math.sqrt(focal_length**2 - radius**2)) if focal_length**2
           - radius**2 >= 0 else 0
516        onCommandCreated = LensCommandCreatedHandler()
517        cmdDef.commandCreated.add(onCommandCreated)
518        handlers.append(onCommandCreated)
519
520        cmdDef.execute()
521        adsk.autoTerminate(False)
522    except Exception as e:
523        if ui:
524            ui.messageBox(f'Failed: {traceback.format_exc()}')
525
526        #Stworzone przez: Błażej tagsz
527

```

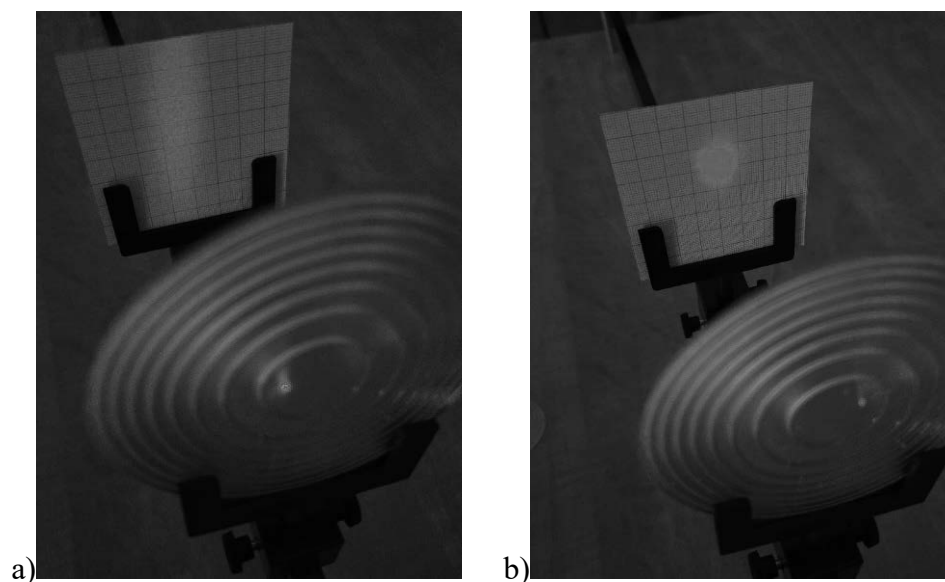
Figure 3. The beginning and the end of Python script that computes the key dimensions of a Fresnel lens, serving as the foundation for its CAD design in Fusion 360



*Figure 4. The Fresnel lenses:
a) printed with clear resin using a Formlabs SLA printer; b) cured in a UV curing chamber*

3. RESULTS AND DISCUSSION

The lens with a diameter of 70 mm was partially covered with a brush with a thin layer of clear resin from which it was printed. Then, the outer layer of the lenses was cured in a UV curing chamber for 60 minutes at a temperature of 60°C again. Several tests were conducted using different lasers: red-point, red-horizontal, and green-horizontal. All results were compared on graph paper. By covering a thin layer with a brush and hardening it, improved its ability to focus light, what is shown on Figure 5 and Figure 6. The other half was left without an additional layer.



*Figure 5. The Fresnel lens with:
a) point laser on uncovered surface; b) point laser on covered surface*

Significant differences in the focus of the laser beam can be observed, particularly with the red laser. For the red-point laser, the focus improved from 6 cm (untreated surface) to 2 cm (treated surface). Similar improvements were observed with the red-horizontal laser. The green laser showed smaller improvements in focus, from 4 cm (untreated) to 2 cm (treated).

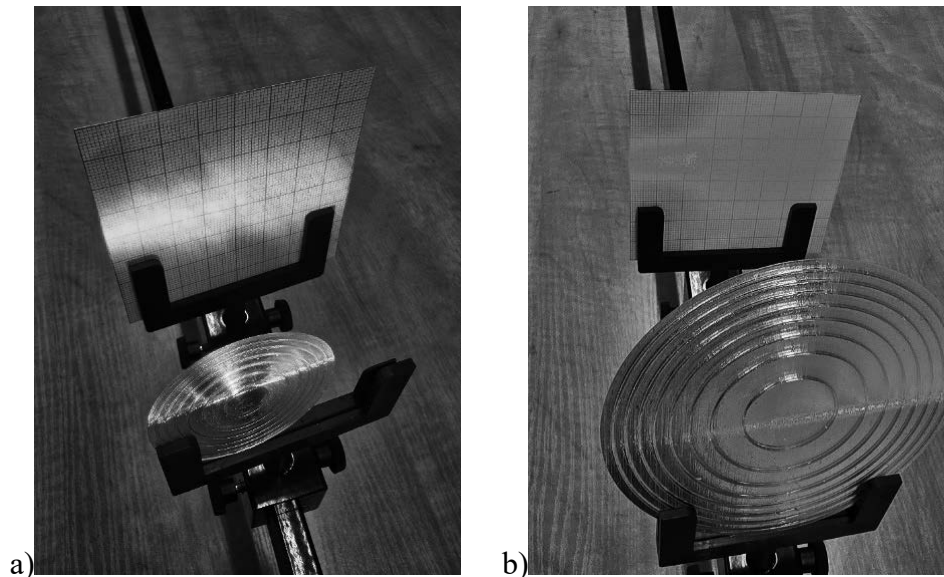


Figure 6. The Fresnel lens with partially covered and partially uncovered surface with: a) horizontal green laser; b) horizontal red laser

4. SUMMARY

Lenses are optical instruments designed to focus or disperse light through refraction, achieved by their unique geometry composed of spherical or flat surfaces. They are classified as converging or diverging, with their functionality determined by thickness distribution and refractive properties. While traditional lenses are bulky and challenging to manufacture, Fresnel lenses revolutionize optics by dividing the optical surface into concentric rings, significantly reducing material and weight while maintaining light-focusing capabilities. These features make them ideal for applications requiring precise light control, such as lighthouses, solar concentrators, and projectors.

In this study, Fresnel lenses were designed using a combination of computational and additive manufacturing techniques. A custom Python script was first developed to calculate the dimensions and number of concentric rings, forming the basis for CAD modeling in Autodesk Fusion 360. The lenses were then 3D printed using a Formlabs SLA printer with clear resin and underwent cleaning and curing processes to enhance optical quality.

Experimental results demonstrated the lenses' effectiveness in focusing light, particularly when an additional resin layer was applied and cured. Tests with red and green lasers showed significant improvements in focus, confirming the precision and practicality of the combined computational and manufacturing methods. These findings highlight the potential of Fresnel lenses for advanced optical applications, showcasing the synergy of modern design tools and manufacturing technologies.

ACKNOWLEDGMENTS

The research was financially supported by the PBL-IDUB project entitled "Stereolitografia w konstruowaniu i wytwarzaniu soczewek Fresnela".

BIBLIOGRAPHY

1. D. Halliday, R. Resnick, J. Walker: *Fundamentals of Physics. Volume 3*, Wydawnictwo Naukowe PWN, 2013.
2. <https://ilf.fizyka.pw.edu.pl/podrecznik/3/8/11>
3. E. Hecht: *Optics*, Wydawnictwo Naukowe PWN, 2018.
4. website acces 10.01.2025 r.: <https://zpe.gov.pl/a/bieg-promieni-w-soczewce-skupiajacej-i-rozpraszajacej-konstrukcja-obrazow-powstajacych-przy-uzyciu-soczewek/DqC9wrI18>
5. J. Goodman: *Introduction to Fourier Optics*, Roberts and Company Publishers, 2005.
6. N. Yew Jin Tan, X. Zhang, D. Wee Keong Neo, R. Huang, K. Liu, A. Senthil Kumar: *Journal of Manufacturing Processes - A review of recent advances in fabrication of optical Fresnel lenses (113-133)*, 2021.
7. K. Zhang, Y. Su, H. Wang, Q. Wang, K. Wang, Y. Niu, J. Song: *Highly Concentrated Solar Flux of Large Fresnel Lens Using CCD Camera-Based Method*, 2022.
8. F. Lafta Rashid, M. A. Al-Obaidi, A. Jafer Mahdi, A. Ameen: *Advancements in Fresnel Lens Technology across Diverse Solar Energy Applications: A Comprehensive Review*, 2024.
9. W. Sum Choong, Z. Yong Ho, R. Bahar: *Solar Desalination Using Fresnel Lens as Concentrated Solar Power Device: An Experimental Study in Tropical Climate*, 2020.



31th January 2025
Gliwice, Poland

DEPARTMENT OF ENGINEERING MATERIALS AND BIOMATERIALS
FACULTY OF MECHANICAL ENGINEERING
SILESIA UNIVERSITY OF TECHNOLOGY

INTERNATIONAL STUDENTS SCIENTIFIC CONFERENCE

Utilization of LIDAR data for PSMNet training

Tomasz Kukuczka^a, Marcin Paszkuta^b, Dariusz Myszor^c, Eryk Szmyt^d, Danel Sobieraj, Paweł Michalski^e, Krzysztof Pawełczyk^f, Michał Polończyk^f

^a Silesian University of Technology, Faculty of Automatic Control, Electronics And Computer Science, Department of Graphics, Department of Cybernetics, Nanotechnology and Data Processing

^b Silesian University of Technology, Faculty of Automatic Control, Electronics And Computer Science, Department of Graphics, Computer Vision and Digital Systems

^c Silesian University of Technology, Faculty of Automatic Control, Electronics And Computer Science, Department of Algorithmics and Software

^d Silesian University of Technology, Virtual Flying Student Research Club

^e Opole University of Technology, Department of Informatics

^f Autonomos Systems Sp. z o. o.

email: Tomasz.Kukuczka@polsl.pl

Abstract: This article presents the integration of LIDAR data with PSMNet, focusing on data preparation and a custom DataLoader for converting LIDAR depth maps into disparity maps required by the network. These methods enable accurate depth estimation and open new possibilities for multimodal applications in challenging conditions.

Keywords: Artificial Neural Networks, Machine Learning, Depth Map

1. INTRODUCTION

Contemporary technologies in image processing and spatial analysis play a significant role in developing fields such as autonomous vehicles, robotics, and monitoring systems. Among these technologies, LIDAR systems and advanced neural networks, such as PSMNet, serve as the foundation for precise spatial analysis and depth estimation.

The LIDAR system, based on laser technology, enables precise environmental mapping regardless of lighting conditions. Utilizing the time-of-flight (ToF) of laser beams allows the generation of accurate 3D point clouds that can be transformed into depth maps [4,9].

Simultaneously, the development of neural networks like PSMNet allows the use of stereoscopic images to generate depth maps based on disparity differences between images. PSMNet, leveraging cost volumes and 3D convolutions, delivers precise depth maps applicable in numerous applications, including vehicle automation and spatial modeling.

Combining LIDAR data with neural networks creates broad opportunities for spatial analysis[2]. This article presents methods of their integration, the process of preparing data, and adapting it to the needs of the PSMNet model. Additionally, it discusses the structure and application of a custom DataLoader program, which enables transforming depth maps generated by LIDAR into formats used by neural networks.

2. LIDAR

The LIDAR system emits laser beams in various directions, creating a 360-degree depth map [2]. The LIDAR detector receives light reflected from objects in the environment. For each emitted beam, the time of flight (ToF) is recorded, and the distance is calculated using the formula:

$$d = \frac{c \cdot ToF}{2},$$

based on the calculated distances, the system generates a three-dimensional map of the environment in the form of a point cloud. Each point represents spatial coordinates (x,y,z)[1].

LIDAR operates independently of external light sources, allowing data collection in challenging lighting conditions, including total darkness. This makes the system an ideal data source for training neural networks in extreme conditions. It is also possible to combine LIDAR with other technologies, such as GPS and RGB cameras, enhancing the system's versatility[3,8].

Data collected by LIDAR can be transformed into a depth map - a two-dimensional representation containing information about the distance of each point within the sensor's field of view. In such a map, each pixel corresponds to a point in space and is represented by brightness, reflecting the distance from the sensor.

LIDAR operates independently of external light sources, allowing data collection in challenging lighting conditions, including total darkness[8,10]. This makes the system an ideal data source for training neural networks in extreme conditions. It is also possible to combine LIDAR with other technologies, such as GPS and RGB cameras, enhancing the system's versatility (see Figure 1).



Figure 1. A frame captured from the camera image with the corresponding points from the LIDAR projected onto it. The LIDAR points are overlaid on the image in a way that aligns with the camera's perspective, providing a combined view of the scene.

3. PSMNET

PSMNet is a neural network utilizing a pyramidal architecture to analyze information at multiple scales[5]. The processing involves several stages. Initially, input images from the left and right cameras are analyzed separately. Then, a cost volume is generated by combining feature maps extracted from both images. This volume reflects the matching costs of image fragments for various disparity values.

The next step is analyzing the cost volume using 3D convolutions, which account for spatial dimensions and disparity, enabling the understanding of pixel relationships. The network's output is a disparity map generated relative to one of the cameras (left or right). This map represents differences in pixel positions between images, which can be transformed into a depth map indicating actual distances to objects.

The transformation requires knowledge of the camera parameters and the distance between cameras in a stereoscopic setup. Such an approach enables precise depth estimation of a scene based on stereoscopic images.

4. DATALOADER

The PSMNet architecture was implemented in Python using the PyTorch library and is available in the PSMNet GitHub repository. The default loader program supports KITTI[7] and Scene Flow[6] datasets.

To enable training and validation of PSMNet on LIDAR data, a custom loader class was developed. This class handles PNG files containing RGB images and depth maps generated by LIDAR, which are dynamically converted into disparity maps.

Overlaying the point cloud onto images requires transforming points from the LIDAR coordinate system to the camera system using a transformation matrix. Depth maps are then encoded, scaled, and stored. To obtain a normalized depth map, PNG files are converted to float32 arrays scaled by dividing by 256.

PSMNet requires disparity maps for the training process. Since no ready-made data exists in this format, an algorithm was developed to convert depth maps into disparity maps using the formula:

$$disp = \frac{focal \cdot baseline}{depth_{norm}},$$

the baseline is the distance between cameras in the stereoscopic pair (expressed in meters). For data collected from the LIDAR system, the focal length is described by the equation:

$$focal = \frac{width}{2 \cdot \tan\left(\frac{FOV \cdot \pi}{360}\right)}.$$

In the above equation, width represents the number of pixels, while FOV refers to the horizontal field of view of the camera, determined using calibration tables. Additional conditions have been applied to prevent unwanted errors in the neural network:

$$disp = \begin{cases} 0, & disp < 0.5 \\ disp, & disp \geq 0.5 \end{cases}$$

Minor shifts between corresponding points in the left and right images are misinterpreted by the neural network, negatively affecting the learning process.

The data loading class for the model was designed to accept the following arguments:

- a list of paths to images from the left camera,
- a list of paths to images from the right camera,
- a list of paths to depth maps.

The elements in the lists correspond to each other, meaning that the data from the left camera, right camera, and the associated depth maps should be linked by the same index. The PIL library was used for data loading: images are loaded in RGB format, and depth maps are converted into disparity maps using appropriate formulas.

Before processing, the data is cropped to dimensions 256×512, converted to tensors, and passed to the model. The DataLoader class inherits from data.Dataset, allowing integration with PyTorch and efficient data management.

5. CONCLUSION

The integration of the LIDAR system and neural networks such as PSMNet enables precise spatial analysis and depth estimation. Thanks to LIDAR-generated data, independent of lighting conditions, and advanced processing in PSMNet, it is possible to develop applications in autonomous vehicles, robotics, and monitoring systems. The described solutions, including the data adaptation process, provide a solid foundation for further research and implementation in modern future technologies.

6. ACKNOWLEDGEMENTS

The publication/paper was based on the results of the project no. POIR.01.01.01-00-0123/20 co-financed by the European Union under the European Regional Development Fund - Smart Growth program 2014-2020.



BIBLIOGRAPHY

1. LI, You; IBANEZ-GUZMAN, Javier. Lidar for autonomous driving: The principles, challenges, and trends for automotive lidar and perception systems. *IEEE Signal Processing Magazine*, 2020, 37.4: 50-61.
2. LI, Ying, et al. Deep learning for lidar point clouds in autonomous driving: A review. *IEEE Transactions on Neural Networks and Learning Systems*, 2020, 32.8: 3412-3432.
3. MOU, Shenyu, et al. An optimal lidar configuration approach for self-driving cars. arXiv preprint arXiv:1805.07843, 2018.
4. RAJ, Thinal, et al. A survey on LiDAR scanning mechanisms. *Electronics*, 2020, 9.5: 741.
5. CHANG, Jia-Ren; CHEN, Yong-Sheng. Pyramid stereo matching network. In: *Proceedings of the IEEE conference on computer vision and pattern recognition*. 2018. p. 5410-5418.
6. M. Menze and A. Geiger, "Object scene flow for autonomous vehicles," 2015 IEEE Conference on Computer Vision and Pattern Recognition (CVPR), Boston, MA, USA, 2015, pp. 3061-3070, doi: 10.1109/CVPR.2015.7298925.
7. Mayer, Nikolaus et al. "A Large Dataset to Train Convolutional Networks for Disparity, Optical Flow, and Scene Flow Estimation." 2016 IEEE Conference on Computer Vision and Pattern Recognition (CVPR) (2015): 4040-4048.
8. BEHROOZPOUR, Behnam, et al. Lidar system architectures and circuits. *IEEE Communications Magazine*, 2017, 55.10: 135-142.
9. RORIZ, Ricardo; CABRAL, Jorge; GOMES, Tiago. Automotive LiDAR technology: A survey. *IEEE Transactions on Intelligent Transportation Systems*, 2021, 23.7: 6282-6297.
10. ZHANG, Yihuan, et al. An efficient LiDAR-based localization method for self-driving cars in dynamic environments. *Robotica*, 2022, 40.1: 38-55.



31th January 2025
Gliwice, Poland

DEPARTMENT OF ENGINEERING MATERIALS AND BIOMATERIALS
FACULTY OF MECHANICAL ENGINEERING
SILESIA UNIVERSITY OF TECHNOLOGY

INTERNATIONAL STUDENTS SCIENTIFIC CONFERENCE

Farebné leptanie grafitických liatin

Denis Kulas^a, Alan Vaško^a

^a Žilinská univerzita v Žiline, Strojnícka fakulta, Katedra materiálového inžinierstva, Univerzitná 8215/1, 010 26 Žilina, Slovak Republic
email: kulas2@stud.uniza.sk, alan.vasko@fstroj.uniza.sk

Abstrakt: Článok sa zameriava na aplikáciu a využitie farebného leptania pri štruktúrnej analýze grafitických liatin, s cieľom priniesť nové detailnejšie poznatky o ich štruktúre. Medzi tieto zistenia patria napr. schopnosť zvýrazniť rozdiely v chemickom zložení mikrolokalít, alebo rozlíšenie fáz v matici grafitických liatin, ktoré sú pri použití čiernobieleho kontrastu ťažko rozlíšiteľné, prípadne úplne neidentifikovateľné. Ďalej sa článok zaoberá charakteristikou a rozdelením grafitických liatin a metodikou leptania.

Kľúčové slová: liatina, grafit, leptanie, matrica

1. ÚVOD

Liatina sa vyrábala už v 4. storočí pred našim letopočtom na území dnešnej Číny, kde sa z nej vyrábali rôzne poľnohospodárske predmety. Aj keď je tento materiál pomerne starý, stále nachádza široké uplatnenie v rôznych priemyselných oblastiach. V priebehu času sa poznatky o metalografii a výrobe liatin neustále prehľbovali a zdokonaľovali. Dnes síce výroba a produkcia zliatin železa a liatin klesá, keďže sa vyvíjajú nové materiály so značne lepšími vlastnosťami, avšak tieto kovové materiály stále zostávajú dôležitou súčasťou priemyselnej výroby. Jednou z najstarších a najbežnejších metód na skúmanie štruktúry kovov a zliatin je svetelná metalografická mikroskopia, ktorá je založená na fotodokumentácii vnútornej štruktúry kovov a zliatin získanej odrazom svetelných lúčov od povrchu špeciálne pripravených vzoriek. Na rozlíšenie štruktúrnych fáz metalografických vzoriek sa často používa čiernobiely kontrast medzi rôznymi štruktúrnymi mikrolokalitami.

Farebná metalografia je súbor metodík svetelnej metalografickej mikroskopie, ktorý využíva farebný kontrast fáz ako zdroj nových informácií o štruktúre v porovnaní s klasickými postupmi. V rade prípadov je možné vyvolať farebný kontrast tam, kde sa klasickými postupmi vôbec nezíska identifikovateľný fázový kontrast. Pomocou farebného kontrastu získavame nové informácie o štruktúre, v čom je prínos jeho využitia v metalografii. Farebný modro-žltý kontrast je rozhodne výraznejší ako tmavosivo-svetlosivý kontrast. Pritom nie je podstatná celkom presná reprodukovateľnosť farieb, pretože nie je podstatné, či dve fázy rozlíšime podľa modro-žltého alebo zeleno-okrového kontrastu. Tento farebný kontrast je možné dosiahnuť buď použitím špeciálnych prídavných zariadení mikroskopu, alebo úpravou povrchu vzoriek [1 - 2].

1.1 Charakteristika grafitických liatin

Liatina je zliatina železa, uhlíka a ďalších prvkov, pričom obsah uhlíka presahuje maximálnu rozpustnosť v austenite, teda 2,14 %. Liatiny sa rozdeľujú na biele a grafitické na základe svojej štruktúry, pričom z technického hľadiska sú dôležitejšie grafitické liatiny, pretože sú v praxi používané častejšie. Pri grafitických liatinách prebieha eutektická premena v stabilnej rovnováhe a jedným z jej produktov je grafit. Grafit je čistý uhlík, ktorý kryštalizuje v hexagonálnej sústave. Typickým znakom grafitických liatin je prítomnosť grafitu, ktorý vzniká tvorbou grafitického eutektika pri stabilnej rovnováhe [3 - 4].

1.2 Rozdelenie grafitických liatin

Grafitické liatiny sa rozdeľujú podľa tvaru grafitu, ktorý vzniká kryštalizáciou z taveniny. Medzi tieto liatiny patrí liatina s lupienkovým grafitom, liatina s červíkovitým grafitom, liatina s guľôčkovým grafitom a tiež temperovaná liatina, keďže grafit môže vzniknúť grafitizáciou cementitu v tuhom stave [3 - 5].

Medzi kľúčové faktory, ktoré ovplyvňujú veľkosť a tvar grafitu, patria očkovanie a modifikovanie. Očkovanie znamená pridávanie cudzích látok do taveniny, ktoré podporujú vznik grafitizačných zárodkov a tým aj znižujú veľkosť grafitu. Modifikovanie podporuje rast grafitu, čím sa zabezpečuje jeho výhodnejší tvar. Modifikátor spôsobuje, že grafit sa stáva globulárnym, buď čiastočne (v prípade červíkovitého grafitu), alebo úplne (v prípade guľôčkového grafitu) [3].

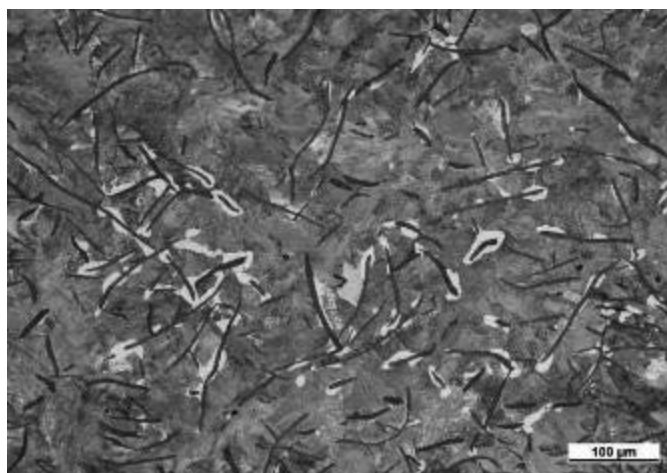
Štruktúru základnej kovovej matrice grafitických liatin môžu tvoriť ferit, perlit a ich kombinácia, cementit, fosfidové eutektikum alebo inklúzie. Perlit má lamelárny tvar a jeho prítomnosť zlepšuje pevnostné vlastnosti, ako je pevnosť v ťahu (R_m) a tvrdosť (HB), avšak znižuje tvárne vlastnosti liatiny, ako sú ťažnosť a húževnatosť. Ferit v štruktúre grafitických liatin znižuje pevnosť, ale zlepšuje tvárnosť. Cementit je nežiaduca fáza, ktorá zvyšuje tvrdosť a krehkosť, čím zhoršuje obrábatelnosť. Fosfidové eutektikum sa vyskytuje v liatinách s vyšším obsahom fosforu a tvorí sa na hraniciach eutektických buniek, pričom je považované za tvrdú a krehkú štruktúrnu zložku. Inklúzie v grafitických liatinách môžu byť v podobe oxidov, kremičitanov, hlinitanov, hlinitokremičitanov, karbidov, karbonitridov, nitridov a sulfidov [3].

Pri opise vlastností grafitických liatin je potrebné zohľadniť veľkosť, rozloženie, množstvo a tvar grafitu, ako aj štruktúru základnej kovovej matrice. Grafit môže byť vylúčený v rôznych formách, od lupienkového až po pravidelne guľôčkový tvar [4 - 5].

1.2.1 Liatina s lupienkovým grafitom

Liatina s lupienkovým grafitom (obr. 1) sa vyznačuje lupienkovým grafitom v štruktúre a obvykle obsahuje 2,5 až 3,5 % C, do 3,5 % Si, 0,4 až 0,8 % Mn, 0,2 až 1,2 % P a 0,08 až 0,12 % S. Očkovaním sa dosahuje nízky stupeň eutektickosti, čo vedie k zníženiu obsahu grafitu v štruktúre, ale zároveň sa zvyšuje pevnosť liatiny. Najčastejšie používané očkovadlo je ferosilícium, ktoré sa pridáva v množstve približne 0,5 %. Základnú kovovú maticu tvoria perlit, perlit-ferit alebo ferit. Mikroštruktúra liatiny s lupienkovým grafitom je zobrazená na obrázku 1.

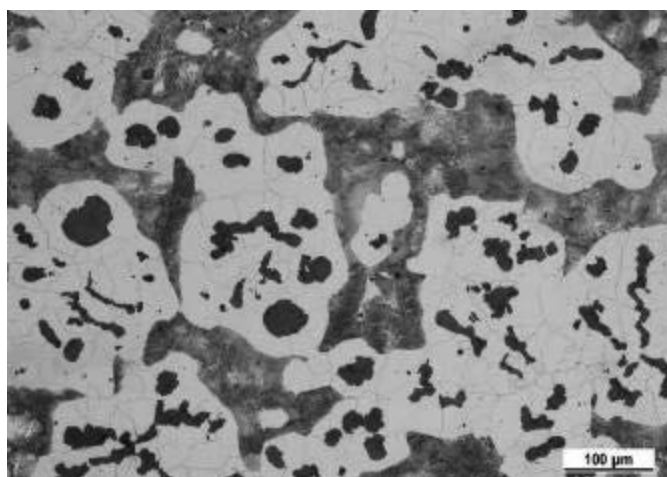
Táto liatina dosahuje pevnosť v ťahu do 250 MPa, pričom po očkovaní sa pevnosť zvyšuje na 250 až 350 MPa. Je to krehký materiál, ktorý má takmer nulovú ťažnosť, ale vyniká výbornými zlievarenskými vlastnosťami pri nízkych nákladoch. Liatina s lupienkovým grafitom sa využíva na výrobu ložísk, valcov kompresorov, ozubených kolies, vačiek, závitových kolies, hydraulických piestov, remeník a rôznych častí motorov [5].



Obr. 1. Mikroštruktúra perliticko-feritickej liatiny s lupienkovým grafitom, lept. 3 % Nital
Figure 1. Microstructure of pearlite-ferritic lamellar cast iron, etch. 3 % Nital

1.2.2 Liatina s červíkovitým grafitom

Pri výrobe liatiny s červíkovitým grafitom je požiadavkou približne eutektické zloženie s obsahom síry do 0,02 %. Modifikovaním sa dosahuje neúplná sferoidizácia grafitu a teoretické zníženie nečistôt, ako sú kyslík a siera, na rozhraní tavenina-grafit počas rastu grafitu. V štruktúre liatiny s červíkovitým grafitom sa môže vyskytovať aj guľôčkový grafit, pričom jeho podiel by nemal presiahnuť 20 %. Štruktúra matrice liatiny s červíkovitým grafitom v liatom stave závisí od chemického zloženia východiskového tekutého kovu, typu a množstva modifikátora a rýchlosti ochladzovania. Pre optimálne modifikované odliatky je charakteristická feriticko-perlitická matrica, ktorá obsahuje 40 - 70 % feritu [5]. Mikroštruktúra liatiny s červíkovitým grafitom je dokumentovaná na obr. 2.



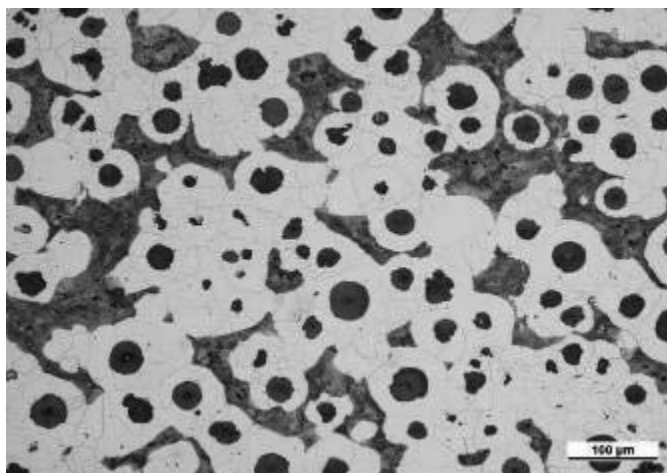
Obr. 2. Mikroštruktúra feriticko-perlitickej liatiny s červíkovitým grafitom, lept. 3 % Nital
Figure 2. Microstructure of ferrite-pearlitic vermicular cast iron, etch. 3 % Nital

Táto liatina obvykle kryštalizuje s vysokým podielom feritu v matrici (zvyčajne 40 - 80 %), pričom pevnosť v ťahu sa pohybuje v rozmedzí 500 - 350 MPa, modul pružnosti je 160 - 140

GPa a ťažnosť A_5 je 2 - 6 %. Mechanické vlastnosti tejto liatiny je možné zlepšiť tepelným spracovaním, ktoré sa môže, ale nemusí použiť. Ak sa použije, môže to viesť k zvýšeniu pevnosti, ťažnosti a húževnatosti. Liatina s červíkovitým grafitom sa využíva pri výrobe tvarovo zložitejších odliatok a súčiastok, ktoré sú vystavené vyšším mechanickým zaťaženiám a tepelným rázom, aj keď jej výroba nie je veľmi častá [5 - 6].

1.2.3 Liatina s guľôčkovým grafitom

Chemické zloženie liatiny s guľôčkovým grafitom obvykle obsahuje 3,2 až 4,2 % C, 1,5 až 4 % Si, 0,4 až 0,8 % Mn, menej ako 0,1 % P a menej ako 0,02 % S. Na dosiahnutie guľôčkového tvaru grafitu sa liatina modifikuje, pričom ako modifikátor sa používa horčík alebo zliatiny horčíka. Keďže horčík zvyšuje stabilitu karbidov, následne sa vykonáva grafitizačné očkovanie. Matrica liatiny býva tvorená perlitom, zmesou feritu a perlitu alebo feritom, pričom jej zloženie závisí od chemického zloženia a rýchlosti ochladzovania. Pri výbere chemického zloženia je dôležité, aby mikroštruktúra neobsahovala voľné karbidy, ktoré negatívne ovplyvňujú zlievarenské vlastnosti. Uhlík a kremík sú dva kľúčové grafitotvorné prvky, ktoré zabraňujú vylúčeniu voľných karbidov. S narastajúcim obsahom kremíka sa zvyšuje podiel feritu alebo perlitu, zvyšuje sa tvrdosť feritu, znižuje sa rázová húževnatosť a zvyšuje sa prechodová teplota. Mikroštruktúra liatiny s guľôčkovým grafitom je zobrazená na obr. 3.



Obr. 3. Mikroštruktúra feriticko-perlitickej liatiny s guľôčkovým grafitom, lept. 3 % Nital
Figure 3. Microstructure of ferrite-pearlitic nodular cast iron, etch. 3 % Nital

Liatina s guľôčkovým grafitom patrí medzi najpoužívanejšie materiály na výrobu odliatok. Pevnosť v ťahu dosahuje hodnoty od 400 do 800 MPa, tvrdosť je v rozmedzí 150 až 300 HB a ťažnosť sa pohybuje od 20 % do 2 % [6].

1.3 Leptanie grafitických liatin

Leptanie je najpoužívanejšou metódou na rozlíšenie štruktúry grafitických liatin pomocou svetelnej metalografickej mikroskopie, ktorá umožňuje pozorovanie štruktúrnych zložiek na rovinnom reze vzorky a kontrolu kvality odliatok. Pre rozlíšenie jednotlivých fáz a rozhraní sa používa leptanie, ktoré vytvára na povrchu vzorky mikrorelief. Kľúčovou požiadavkou je, aby

medzi štruktúrnymi útvarmi vznikol optický kontrast, čo sa dosahuje buď čiernobielym, alebo farebným leptaním.

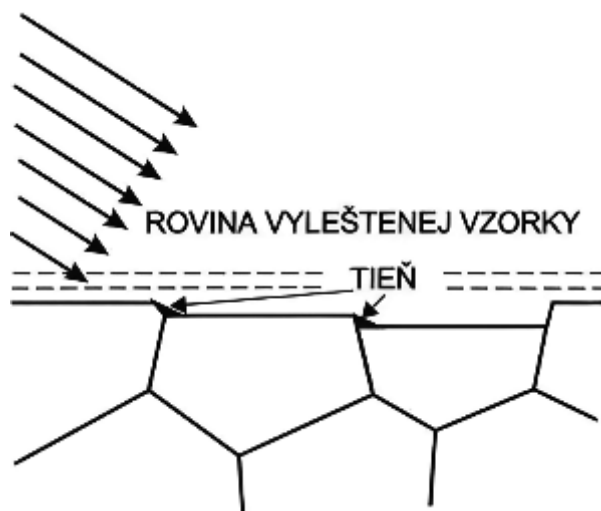
Pomocou leptania sa zviditeľní štruktúra matrice metalografickej vzorky. Po leštení sa na povrchu vzorky vytvára tzv. Beilbyho vrstva, ktorú je potrebné odstrániť chemickou cestou, a to leptaním vzorky v kyselinách, zásadách, ich alkoholických roztokoch alebo elektrolyticky. Leptanie môže prebiehať rôznymi spôsobmi, pričom leptadlo môže pôsobiť buď na plochu zŕn, na hranice zŕn, alebo len na určité štruktúrne zložky či fázy. Podľa toho sa leptanie delí na plošné leptanie, leptanie na hranice zŕn a selektívne leptanie.

Najčastejšie sa leptanie vykonáva ponorením vzorky do leptadla, pričom vzorkou sa pohybuje, aby sa leptadlo premiešalo a leptanie prebiehalo rovnomerne. Ďalšou metódou je leptať pomocou vaty namočenej v leptadle, pričom povrch vzorky sa vatou potiera. Stupeň naleptania sa posudzuje podľa zmatnenia povrchu, a podrobne sa sleduje pomocou svetelného mikroskopu. Po leptaní je potrebné vzorku dôkladne opláchnuť destilovanou vodou a alkoholom a následne osušiť horúcim vzduchom.

Po leptaní sa pozoruje a hodnotí druh, tvar, veľkosť, množstvo a rozloženie jednotlivých štruktúrnych zložiek vzorky. Tento proces umožňuje detailné posúdenie mikroštruktúry materiálu, čo je rozhodujúce pre analýzu jeho vlastností a kvality [1].

1.3.1 Čiernobiele leptanie

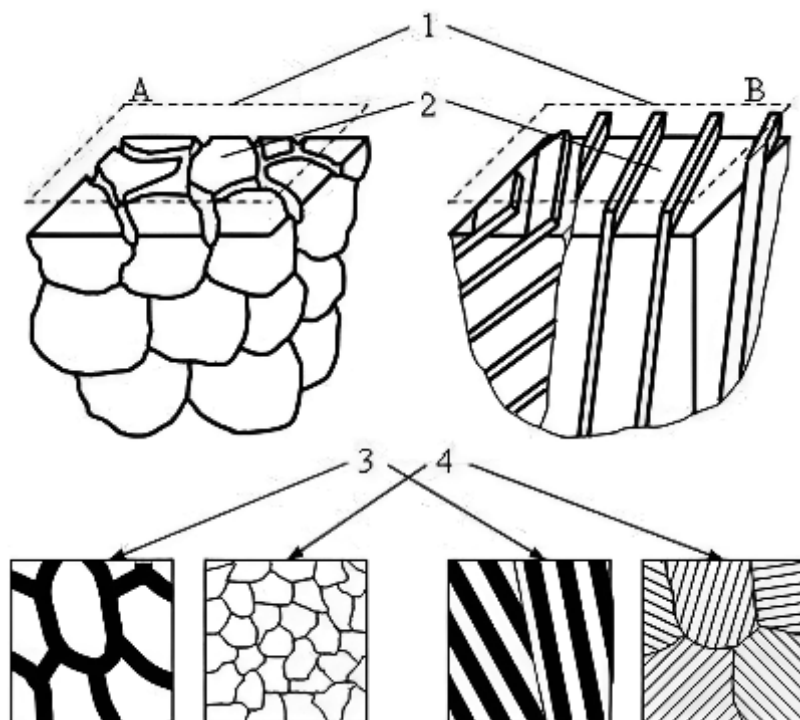
Leptaním sa na pôvodnom rovnom povrchu výbrusu vzorky vytvára reliéf, ktorého stupne pri šikmom osvetlení vrhajú tieň, ktorý zobrazuje tvar hraníc zŕn (obr. 4).



Obr. 4. Vytvorenie mikroreliéfu plošným leptaním jednofázovej štruktúry a vytvorenie tieňa po osvetlení [1]

Figure 4. Creation of microrelief by surface etching of a single-phase structure and creation of a shadow after illumination

Na obr. 5 sú zobrazené modely naleptaných plôch výbrusov s polyedrickou a lamelárnou štruktúrou. Polyedrická štruktúra môže byť tvorená kryštálmi ľubovoľnej homogénnej fázy, zatiaľ čo lamelárna štruktúra je typická pre eutektoidné zmesi. Tento povrchový reliéf, ktorý vznikne pri leptaní, je podstatou zviditeľnenia štruktúry materiálu.



Obr. 5. Schéma leptania: 1 - neleptaný povrch, 2 - reliéf po naleptaní, 3 - tieňe na reliéfe, 4 - charakter mikroštruktúry: A - polyedrická štruktúra, B - lamelárna štruktúra [1]

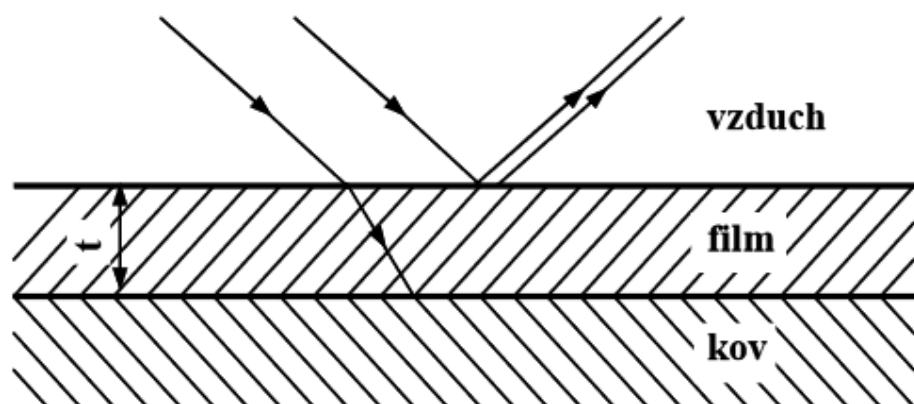
Figure 5. Etching scheme: 1 - unetched surface, 2 - relief after etching, 3 - shadows on the relief, 4 - character of the microstructure: A - polyhedral structure, B - lamellar structure

Pri čiernobielych leptaní sa najčastejšie ako leptadlo používa Nital. Nital sa môže tiež kombinovať s inými leptadlami, ako je napr. kyselina pikrová, aby sa dosiahol požadovaný kontrast a zviditeľnenie štruktúrnych detailov na povrchu vzorky.

1.3.2 Farebné leptanie

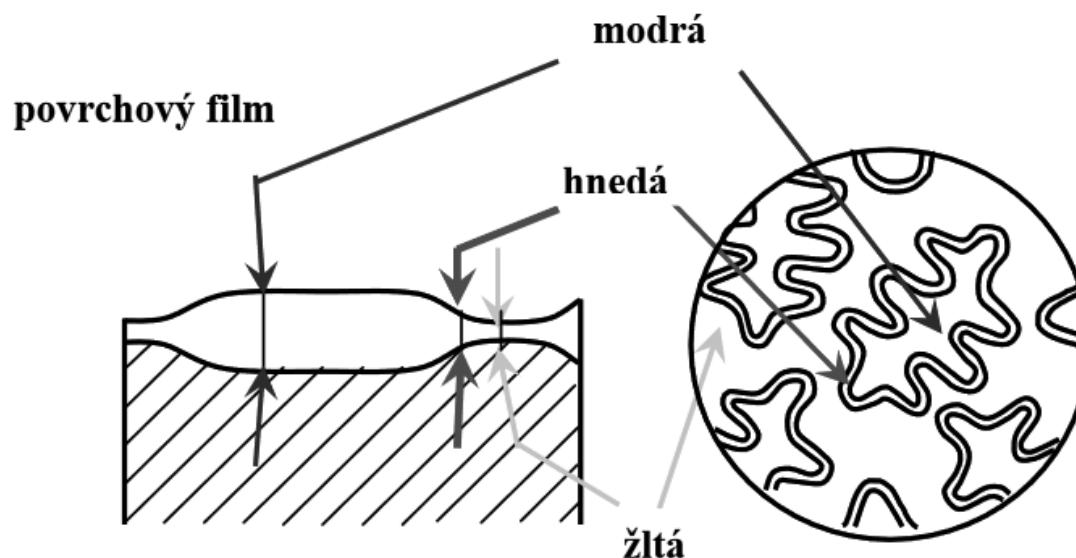
Farebným leptaním sa zvyrazňujú rozdiely v chemickom zložení mikrolokalít, tepelne ovplyvnených zón alebo difúzných vrstiev. Farebné leptadlá reagujú s povrchom výbrusu, čím vzniká sulfidový, chromátový, oxidický alebo iný transparentný film, ktorý pôsobí ako interferenčný povlak. Tento film spôsobuje interferenciu svetla, keď sa odrazené svetlo rozdelí na zložky, ktoré sa odrážajú na rozhraní vzduch-vrstva a na rozhraní kov-vrstva (obr. 6). Týmto spôsobom vzniká farebný kontrast, ktorý umožňuje podrobnejšie skúmanie mikroštruktúry materiálu [4].

Vznik interferenčného javu závisí od vlnovej dĺžky svetelného zdroja (λ), hrúbky filmu (t) a indexu lomu svetla v ňom. Ak sa skutočná dráha svetla odrazeného od oboch povrchov líši o nepárny násobok $\lambda/2$, dochádza k interferencii. Najviditeľnejší farebný kontrast sa dosahuje pri najtenšej hrúbke povlaku, ktorá zabezpečuje interferenciu ($t = \lambda/4$). Pri splnení tejto podmienky, keď je vzorka osvetlená bielym svetlom, sa objaví komplementárna farba pre niektorú zložku svetla (napríklad modrá-žltá, zelená-ryšavohnedá). Tento jav umožňuje vizualizovať rozdiely v chemickom zložení alebo štruktúre materiálu [4, 7].



Obr. 6. Schéma interferencie lúčov odrazených od vzorky s povlakom [1]
 Figure 6. Scheme of the interference of rays reflected from a coated sample

Hrúbka povlaku je závislá od chemického zloženia materiálu výbrusu, pričom pri výraznej zmene chemického zloženia mikrolokality sa bude meniť aj farba jednotlivých mikrolokality. Tento efekt je obzvlášť zreteľný pri osvetlení v svetlom poli (obr. 7), kde rôzne mikrolokality reagujú na svetlo a vykazujú odlišné farby v dôsledku interferenčných javov.



Obr. 7. Podstata farebného leptania [7]
 Figure 7. The essence of colour etching

Chemické zloženie farebných leptadiel je navrhnuté tak, aby umožnilo vytvorenie povlakov s meniacou sa hrúbkou v rozmedzí približne 100 - 150 nm [1].

Najdôležitejšie farebné leptadlá sa delia do troch hlavných skupín:

- a) Pyrosiričitanové leptadlá: Tieto leptadlá majú pyrosiričitanový ión ($S_2O_5^{2-}$) ako základnú zložku, ktorá je prítomná vo forme draselnej soli. Pyrosiričitanové leptadlá sa ďalej delia podľa typu základného roztoku, v ktorom sa rozpúšťa prísada pyrosiričitanu draselného.

- b) Molybdénové leptadlá: Pri použití týchto leptadiel sa vytvára transparentný film, keď sa molybdén (Mo) redukuje z oxidačného stavu Mo^{6+} na Mo^{4+} pôsobením štruktúrnych zložiek, ktoré fungujú ako mikrokatódy.
- c) Horúce leptadlá: Tieto leptadlá sú na báze chrómanu sodného alebo pikrátu sodného. Pri varení sa vytvárajú zložité chromátové alebo oxidické transparentné vrstvy, ktoré spôsobujú farebný kontrast [4].

POĎAKOVANIE

Príspevok vznikol v rámci riešenia spoločného slovensko-poľského projektu Project Based Learning ako výsledok spolupráce medzi Politechnikou Slaskou, Gliwice a Žilinskou univerzitou v Žiline a projektov KEGA č. 004ŽU-4/2023 a KEGA č.009ŽU-4/2023.

BIBLIOGRAPHY

1. Konečná, R., Fintová, S., 2010. *Praktická metalografia*. [ONLINE]. Žilinská univerzita v Žiline - Katedra materiálového inžinierstva, [cit. 22.11.2024] Dostupné na internete: http://kmi2.uniza.sk/wp-content/uploads/2010/10/Prakticka_Metalografia.pdf
2. Skočovský, P., Podrábský, T., 2001. *Farebná metalografia zliatin železa*. EDIS, 68 s., ISBN 80-7100-911-3.
3. Skočovský, P., Podrábský, T., 2005. *Grafické liatiny*. EDIS, 168 s., ISBN 80-8070-390-6.
4. Skočovský, P., Bokůvka, O., Konečná, R., Tillová, E., 2014. *Náuka o materiáli*. EDIS, 349 s., ISBN 978-80-554-0871-2.
5. Skočovský, P., Vaško A., 2007. *Kvantitatívne hodnotenie štruktúry liatin*. EDIS, 73 s., ISBN 978-80-8070-748-4.
6. Moravec J., Koňár R., Pastirčák R., Fabian P., 2020. *Technológia I*. EDIS, 411 s., ISBN 978-80-554-1731-8.
7. Vaško, A., 2022. *Advantages of colour etching in quality control of graphitic cast irons*. In: Production Engineering Archives. vol. 28, issue 4, p. 319-324, ISSN 2353-7779.



31th January 2025
Gliwice, Poland

DEPARTMENT OF ENGINEERING MATERIALS AND BIOMATERIALS
FACULTY OF MECHANICAL ENGINEERING
SILESIA UNIVERSITY OF TECHNOLOGY

INTERNATIONAL STUDENTS SCIENTIFIC CONFERENCE

ZnO coatings deposited by the ALD method in the application of colored silicon solar cells

Dawid Lazaj^a, Grzegorz Józef Nowak^{bc}, Sebastian Nowak^d, Michalina Ziółkowska^d, Julia Popis^e, Magdalena Szindler^e, Marek Szindler^f

^a Graduate of the Silesian University of Technology

^b Łukasiewicz Research Network – Krakow Institute of Technology, Centre of Biomedical Engineering, Zabrze, Poland

^c Silesian University of Technology, Faculty of Biomedical Engineering, Department of Biomaterials and Medical Devices Engineering, Zabrze, Poland

^d Student of the Silesian University of Technology

^e Silesian University of Technology, Faculty of Mechanical Engineering, Department of Engineering Materials and Biomaterials, Gliwice, Poland

^f Silesian University of Technology, Faculty of Mechanical Engineering, Didactic Laboratory of Nanotechnology and Material Technologies, Gliwice, Poland

email: marek.szindler@polsl.pl

Abstract: With the increasing interest in photovoltaic technologies, the number of manufacturers offering innovative solutions in this field and the level of market competition are both on the rise. To thrive as a manufacturer or technologist in this industry, it is essential to provide services that are distinctive and competitive. One way to differentiate products in the photovoltaic cell market is by producing cells in non-traditional colors, which are uncommon for this type of technology. The study investigates the influence of ZnO layer thickness on the color variation of polished silicon wafers. The ZnO layer was characterized and applied using the ALD (Atomic Layer Deposition) method to produce solar cells, resulting in unique, colored silicon cells. Additionally, the electrical properties of the fabricated cells were analyzed.

Keywords: thin films, ZnO, Solar cells, Photovoltaic

1. INTRODUCTION

Silicon-based photovoltaic (PV) cells are among the most common and efficient solutions for converting solar energy into electricity. This is primarily due to their ability to achieve high efficiency levels—up to 25%—at a relatively low production cost. These attributes have made silicon-based cells dominant in the photovoltaic market, accounting for over 80% of its share. While continuous advancements are being made to improve the electrical properties of solar cells, increasing attention is being directed toward enhancing their utility and adaptability for diverse applications. One of the key areas of focus is the aesthetic aspect of solar panels,

particularly the ability to customize the shape and color of the cells [1-4]. This is especially relevant for installations on buildings under conservation protection, where the integration of modern technologies must respect architectural and historical constraints. The possibility of producing photovoltaic cells in non-standard shapes and colors broadens their application potential, making them suitable for use in heritage sites or architecturally unique structures. To achieve this, research efforts are being directed toward the deposition of specialized layers, such as ZnO (zinc oxide), on silicon wafers. These layers can modify the visual appearance of the cells while maintaining or even enhancing their electrical performance. Techniques such as Atomic Layer Deposition (ALD) have proven effective in achieving consistent, thin, and uniform coatings, enabling a wide range of optical effects. By combining advancements in efficiency with innovations in aesthetics, the photovoltaic industry is moving toward a future where solar panels are not only functional but also seamlessly integrated into their surroundings, meeting both energy and design requirements [5-9].

2. EXPERIMENTAL

High-purity polished silicon wafers, commonly used in electronics, were cut into fragments with dimensions of $20 \times 20 \text{ mm}^2$ using a diamond scribe. The silicon pieces were then thoroughly cleaned using an ultrasonic bath. The cleaning process involved sequential rinsing for several minutes in water with detergent, acetone, and isopropyl alcohol to ensure the removal of any contaminants. Zinc oxide (ZnO) layers were deposited onto the cleaned silicon substrates using the Atomic Layer Deposition (ALD) method. Diethylzinc (DEZ) served as the precursor, while water (H_2O) was used as the reactant. The deposition process was carried out under controlled temperature conditions, with the thickness of the ZnO layers being determined by varying the number of deposition cycles. The deposition was performed using the R200 Basic system manufactured by Picosun, which is specifically designed for precision ALD applications. This setup ensured uniform and high-quality ZnO coatings, critical for further analysis and applications in photovoltaic technologies.

The thickness of the prepared thin films was determined using a FR-pRo-UV/VIS spectroscopic reflectometer (ThetaMetrisis SA., Peristeri, Greece). The tests were performed in the reflective mode.

Current-voltage characteristics of polycrystalline solar cells with ITO layers deposited with various parameters were recorded using a solar simulator SS150AAA type. The measurements were conducted under standard test conditions (STC) ($P_{\text{in}} = 1000 \text{ W/m}^2$, AM1.5G spectrum, $T = 25^\circ\text{C}$). The most important electrical properties of the solar cells were computed by using the software I-V Curve Tracer

3. RESULTS AND DISCUSSION

In parallel with the measurement of the thickness of the deposited layers (Fig. 1), detailed color measurements were conducted. The specialized software utilized in the study allowed for the determination of the color's position within several color spaces, including RGB, HUE, and CIE Lab. The change in the RGB color values in a two-dimensional representation as a function of the number of ALD cycles is shown in Figure 2 and summarized in Table 1. However, it should be emphasized that the RGB color space does not faithfully represent the

actual colors observable by the human eye when viewing the examined substrates. This is because RGB does not align with the human visual system's perception of color and fails to account for factors such as chromaticity and light source properties. These limitations can lead to discrepancies between numerical representations and perceived colors. To address this issue and provide a more accurate depiction of color variation, the study also analyzed the color changes in the CIE Lab color space. Unlike RGB, the CIE Lab model incorporates parameters that reflect human visual perception, including lightness and chromaticity.

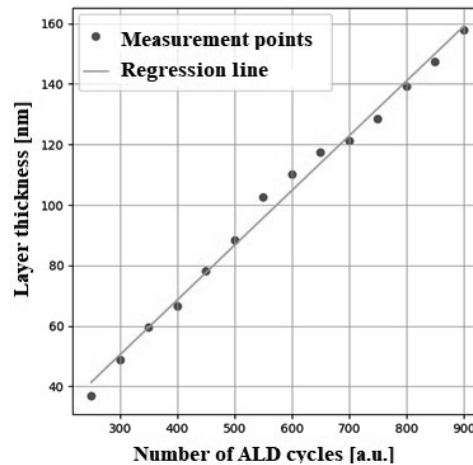


Figure 1. Dependence of the thickness of the applied ZnO coating on the number of ALD cycles performed

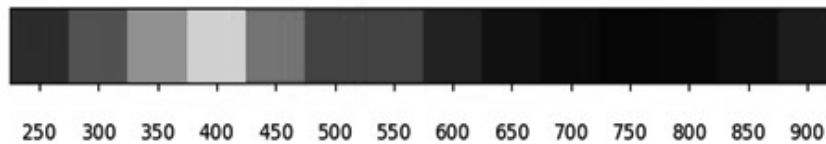


Figure 2. The color change of the cell in the 2-stage RGB color space depending on the number of ALD cycles performed

The results of CIE lab analysis, highlighting the dependence of color on the number of ALD cycles, are illustrated in Figure 3. This approach ensures a more precise understanding of the optical properties of the deposited ZnO layers. The colors represented in the two-dimensional CIE Lab color space provide a more precise depiction of human visual perception when observing the obtained samples. Unlike simpler color models such as RGB, the CIE Lab space is designed to align with the way the human eye perceives color, accounting for variations in lightness, chromaticity, and the nuances of color tones under different lighting conditions. This model's ability to separate color dimensions (lightness, a^* for green-red, and b^* for blue-yellow) makes it particularly valuable for analyzing subtle differences in the visual properties of the deposited layers. By offering a perceptually uniform representation, the CIE Lab space ensures that changes in the coatings' appearance whether due to variations in thickness, material composition, or ALD processing parameters can be interpreted in a manner consistent with human visual experience. As a result, the application of the CIE Lab color space in this study enhances the accuracy and relevance of the color analysis, providing critical insights into the optical effects achieved through advanced material deposition techniques.

Tab. 1 Summary of color parameters

Number of ALD cycles	R	G	B
250	45	71	127
300	71	112	197
350	119	184	183
400	168	242	119
450	0	189	60
500	0	128	28
550	175	66	3
600	116	34	2
650	74	13	2
700	53	3	7
750	23	2	37
800	7	2	71
850	2	2	110
900	2	16	180

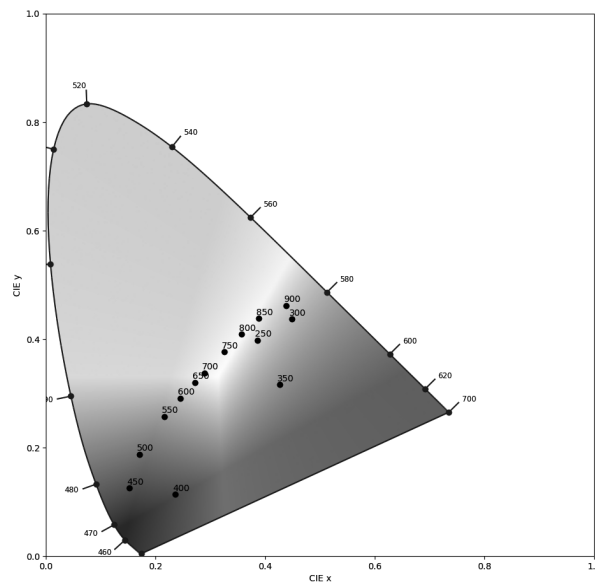


Figure 3. The color change of the cell in the CIE Lab 2-level color space depending on the number of ALD cycles

Following an initial analysis of the obtained results for the thickness and colors of the deposited layers, the ALD process was reproduced on three monocrystalline silicon solar cells. The process was carried out for 500, 750, and 1000 cycles, resulting in a sequential change in color from navy blue to gold, purple, and green. The electrical properties of the modified silicon solar cells were evaluated using a solar simulator Tab. 2. This method allowed for precise characterization of the cells' performance under standardized light conditions, providing insights into the impact of the deposited ZnO layers on their photovoltaic efficiency and functionality.

Tab. 1 Summary of the current-voltage characteristics of the cells before and after the ALD process

Parameters	Solar cell before modification			Solar cell after modification		
	1	2	3	1+ZnO	2+ZnO	3+ZnO
V_{OC} [V]	0,632	0,633	0,632	0,620	0,619	0,618
I_{SC} [A]	5,604	5,628	5,682	5,294	5,237	5,302
V_{MPP} [V]	0,475	0,471	0,470	0,465	0,466	0,470
I_{MPP} [A]	5,004	4,981	5,038	4,520	4,474	4,469
M_{PP} [W]	2,377	2,350	2,371	2,102	2,089	2,103
FF	0,670	0,658	0,659	0,640	0,644	0,641
η [%]	15,267	15,040	15,153	13,491	13,347	13,407

4. SUMMARY AND CONCLUSIONS

This study examined the optical of ZnO thin film on the silicon substrate by ALD method and its application on the silicon solar cells. The investigation focused on the relationship between the number of ALD cycles and the resulting layer thickness, color, and photovoltaic performance. To achieve a precise depiction of color changes, measurements were conducted using RGB, HUE, and CIE Lab color spaces. The study highlighted the superiority of the CIE Lab model in representing human visual perception, accounting for factors such as lightness, chromaticity, and nuanced color tones. This approach allowed for an accurate analysis of the optical properties of ZnO layers, demonstrating how variations in ALD cycles influenced color transitions from navy blue to gold, purple, and green. The process was replicated on monocrystalline silicon photovoltaic cells for 500, 750, and 1000 ALD cycles, and their electrical properties were subsequently evaluated using a solar simulator. The results showed that the ZnO layers not only altered the cells' visual appearance but also impacted their photovoltaic performance. These findings underscore the potential of ALD as a versatile tool for customizing both the aesthetic and functional properties of photovoltaic materials, paving the way for broader applications in building-integrated photovoltaics and other design-sensitive technologies.

ACKNOWLEDGMENTS

The research was financially supported by the SKN-IDUB project entitled "Opracowanie kolorowych krzemowych ogniw słonecznych".

BIBLIOGRAPHY

1. S. Ranjan, S. Balaji, R.A. Panella, and B.E. Ydstie, "Silicon solar cell production" *Comput. Chem. Eng.*, vol. 35, pp. 1439–1453, 2011, doi: 10.1016/j.compchemeng.2011.04.017

2. M. Szindler, M.M. Szindler, J. Orwat, and G. Kulesza-Matlak, "The Al₂O₃/TiO₂ double antireflection coating deposited by ALD method," *Opto-Electronics Review*, vol. 30, p. e141952, 2022, doi: 10.24425/opelre.2022.141952.
3. G. Kulesza-Matlak et. al., "Black Silicon Obtained in Two-Step Short Wet Etching as a Texture for Silicon Solar Cells – Surface Microstructure and Optical Properties Studies," *Arch. Metall. Mater.*, vol. 62, pp. 1009–1017, 2018, doi: 10.24425/amm.2018.122436.
4. Mousa, H. M., Shabat, M. M. & Karmoot, M. R. Double layer antireflection coating design for conductive solar cells. *Rom. Rep. Phys.* 72, 1–18 (2020). <https://rrp.nipne.ro/2020/AN72416.pdf>.
5. Dobrzański, L. A., Szindler, M., Drygala, A. & Szindler, M. M. Silicon solar cells with Al₂O₃ antireflection coating. *Cent. Eur. J. Phys.* 12, 666–670 (2014). <https://doi.org/10.2478/s11534-014-0500-9>.
6. Sarkar, S. & Pradhan, S. K. Silica-based antireflection coating by glancing angle deposition. *Surf. Eng.* 35, 98.
7. Yin, S., Wang, J., Li, Z. & Fang, X. State-of-the-art short-term electricity market operation with solar generation: A review. *Renew. Sustain. Energy Rev.* 138, 110647 (2021). <https://doi.org/10.1016/j.rser.2020.110647>.
8. Gall, S. et. al. Polycrystalline silicon thin-film solar cells on glass. *Sol. Energy Mater. Sol. Cells* 93, 1004–1008 (2009). <https://doi.org/10.1016/j.solmat.2008.11.029>.
9. A. Drygala, L.A. Dobrzański, M. Szindler, M.M. Szindler, M. Prokopiuk vel Prokopowicz, and E. Jonda, "Influence of laser texturization surface and atomic layer deposition on optical properties of polycrystalline silicon," *Int. J. Hydrog. Energy*, vol. 41, no. 18, pp. 7563–7567, 2016, doi: 10.1016/j.ijhydene. 2015.12.180.



31th January 2025
Gliwice, Poland

DEPARTMENT OF ENGINEERING MATERIALS AND BIOMATERIALS
FACULTY OF MECHANICAL ENGINEERING
SILESIA UNIVERSITY OF TECHNOLOGY

INTERNATIONAL STUDENTS SCIENTIFIC CONFERENCE

Mechanical Recycling of Aluminum Cans Using to Increase the Mechanical Properties of Gypsum Prefabs

Bogdan-Ioan Marc^a, Oana-Denisa Boantă^a

^a University of Petrosani, Faculty of Mechanical and Electrical Engineering
email: bogdanmarc94@yahoo.com

Abstract: In this paper, we have shown how important the mechanical recycling of aluminum cans is in increasing the mechanical properties of gypsum prefabricated products. For this purpose, we have made an aluminum grid for reinforcing a gypsum brick and we have tested the compressive and bending resistance of 2 samples, namely a simple gypsum brick and a brick reinforced with 3 aluminum grids, using a hydraulic press.

Keywords: recycling, aluminum, cans, gypsum, prefabs.

1. INTRODUCTION

Aluminum is a resource that makes up about 8% of the Earth's crust. It is mined and extracted from bauxite, which contains the compound alumina, in an energy-intensive electrolytic process. Four tons of bauxite contain two tons of alumina, which produces one ton of valuable aluminum. The metal is used in buildings, transportation and other industrial applications, as well as in packaging. Aluminum is the most cost-effective material to recycle, using about 5% of the energy and emissions required to make it from the raw material bauxite. In addition, all scraps left over from the aluminum production process can be melted down and used again and again. For this reason, recycling is part of the normal life cycle of large industrial products - about 75% of all aluminum ever produced is still in circulation.

The aluminum recycling industry has set an impressive standard for other recycling industries to follow. Long-term efforts to promote the recycling and reuse of aluminum have paid off handsomely, and no product material is returned to recycling plants more frequently (on a percentage basis) than aluminum [8].

Globally, approximately 67% of all consumer-grade aluminum cans are recycled, making them the most recycled container in the world. To put this into perspective, only nine percent of plastic bottles are currently recycled, despite the popularity of community recycling programs and the wide availability of recycling containers in public areas. The modern aluminum recycling process is fast and efficient, and this is vitally important as much of this eminently practical metal is now available for reprocessing and reuse.

Aluminum may be the most versatile product and building material on the planet. It is light and extremely flexible, but also very strong when combined with other metals such as magnesium,

copper, molybdenum and silicon. It is non-magnetic, has high thermal conductivity and is extremely resistant to corrosion. It can be cast, machined, bent, welded, tapered and alloyed easily and does not degrade with repeated reuse. Aluminum is widely used in the construction, manufacturing and consumer goods industries to make items large and small [9,10].

2. MECHANICAL RECYCLING COMPARED TO THERMAL RECYCLING

Molten aluminum is produced from alumina by the Hall-Heroult electrolysis process. This process involves two steps: the dissolution of the previously obtained alumina in a bath with cryolite and the passage of electric current through this bath, which has the effect of decomposing the alumina into aluminum and oxygen.

The aluminum obtained is removed from the cell for electrolysis and the oxygen is used to obtain carbon dioxide and monoxide. Aluminum smelters are generally equipped with monitoring and emission reduction systems. The most used purification systems are scrubbers, whether with a dry or wet process. However, unlike the scrubbers with a dry process, those with a wet process more efficiently capture carbon dioxide, nitrogen and sulfur oxides. The operations associated with this process consist of: recovery, preparation and handling of the raw material; control operations; equipment maintenance and repair; water and waste air treatment [1].

Beverages packaged in aluminum cans are bought by millions of consumers around the world every day. The life cycle of a dose of drink lasts up to 60 days. In this short period of time, a can of drink arrives from the shelves of a store in the possession of consumers and then enters a recycling cycle. Within this cycle, it can be remelted and reused as raw material to obtain another dose with the same physical characteristics as the one that was used as raw material in the recycling process.

Aluminum cans are usually recycled according to the following steps:

In a first phase, the doses are separated from the municipal waste through an eddy current separator, and then, to reduce the volume, they are crushed with the help of a crusher. The doses are then subjected to a chemical or mechanical treatment in order to avoid the oxidation of aluminum in contact with oxygen. The shredded cans are then placed in furnaces and heated to temperatures of up to 750°C to produce molten aluminum. The slag is removed and the dissolved hydrogen is degassed (cast aluminum easily dissociates on a hydrogen basis from water vapor and hydrocarbons as contaminants). This is usually done with chlorine and nitrogen gas. Hexachloroethane tablets are normally used as a chlorine source. Ammonium perchlorate can also be used, which decomposes mainly into chlorine, nitrogen and, if heated, into oxygen. Samples are taken for spectroscopic analysis. Depending on the desired end product: high purity aluminum or alloys, copper, zinc, manganese, silicon and/or magnesium are added to modify the composition of the melt according to the alloy specifications. The furnace is exploited, the molten aluminum is poured out, and the process is repeated again for the next batch [2].

Depending on the final product, it can be cast into ingots, blocks or rods, formed into large rolling slabs, atomized into powder, sent to an extruder, or transported in a molten state to manufacturing facilities for further processing. Unlike recycling by melting aluminum cans, mechanical recycling requires lower costs without having to reach the melting point with the material, only a cutting device is needed to the dimensions that are desired to be achieved. The

energy consumption by cutting the doses into strips is much lower, and the phases of this process are fewer than in the case of melting.

3. TEST RESULTS AND DATA DISCUSSIONS

In order to highlight the applicability of the work, two types of samples were made with and without aluminum insertion. The first reference sample was made without insertion, called sample 0 and the other type of sample with three rows of insertion, (Figure 1). When plaster is mixed with water, the water reacts with the semi-hydrated calcium sulfate in a solid state, which it turns into dehydrated calcium sulfate, which begins to crystallize.

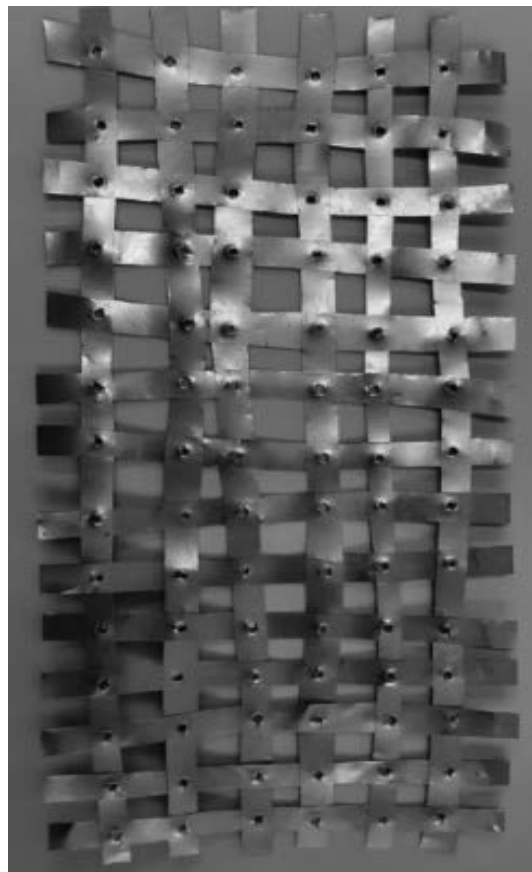


Figure 1. Aluminum grid used to reinforce the bricks

At first, the crystals being very small, the mixture of plaster and water acquires the plasticity necessary for the work. Through the continuous growth of the crystals, they solidify and form a rigid mass, completely devoid of plasticity. The precision and accuracy with which one works will later determine the quality of the sample. The mold must have all perfectly straight surfaces and must be designed in such a way that no mechanical shocks occur when the sample is removed, which can damage the integrity of the sample. The mold must be reusable so that later cast samples have the same dimensions [1].

The dimensions of the sample are 250x120x60 mm. After finishing the casting, the mold is placed on a perfectly horizontal surface so that the paste hardens uniformly in the mold, with equal dimensions over its entire surface. The accuracy of the tests to which the sample is

subjected depends on the quality of the sample manufacturing process. The samples were dried for 28 days, after which they were subjected to mechanical tests, to determine the different resistance values [2].



Figure 2. Compression testing of brick with hydraulic press

The figure below shows the simple brick that broke very quickly after compression testing using a hydraulic press.

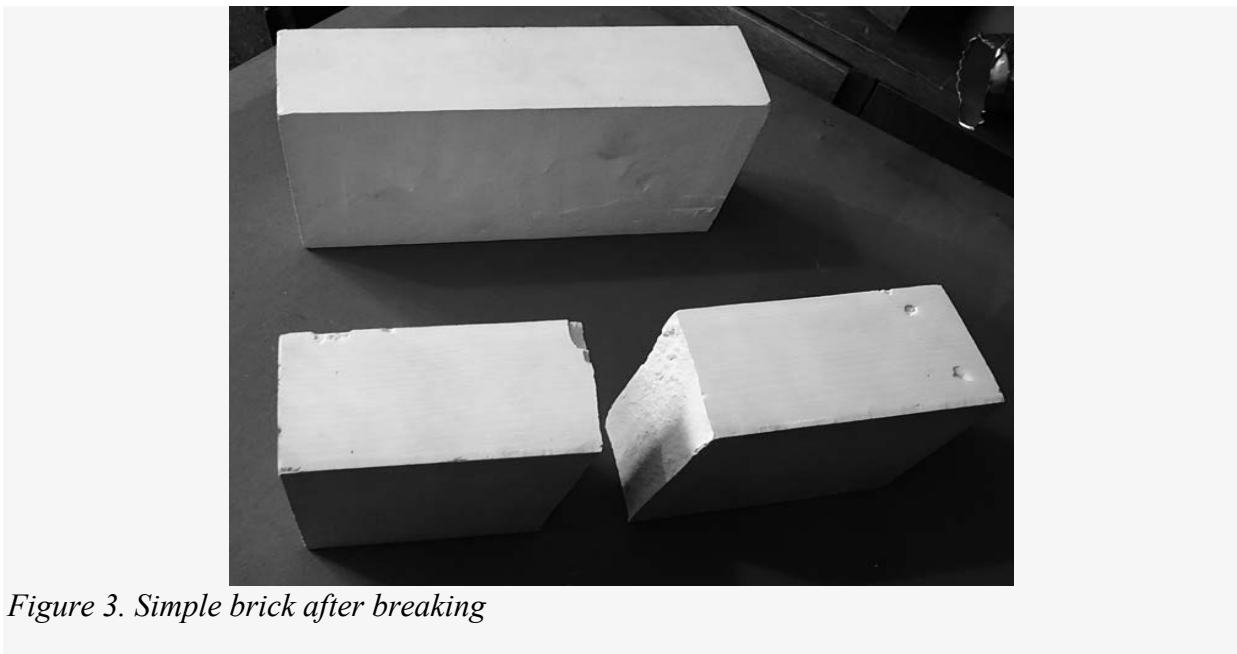


Figure 3. Simple brick after breaking

The graph below shows the axial deformation of a brick reinforced with three layers of aluminum grid. Compared to simple unreinforced brick, the mechanical properties of reinforced brick are superior in terms of resistance to compression and bending.

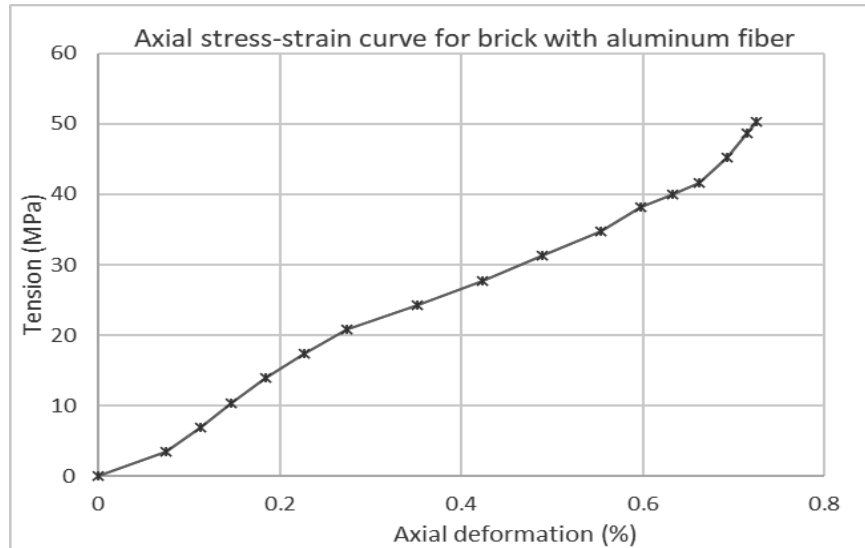


Figure 4. Axial strain graph for aluminum brick

4. CONCLUSIONS

Following the tests of the two samples, we found that the mechanical properties of reinforced brick are superior in terms of compressive and bending resistance compared to plain unreinforced brick.

The process of mechanical recycling of aluminum cans and the use of reinforcement from the product resulting from this process in the reinforcement of gypsum prefabs provides a new economically advantageous recycling method that provides better resistance to mechanical demands.

ACKNOWLEDGEMENTS

The work was created as a result of the project as part of project based learning - PBL, in the 11th competition under the Initiative of Excellence - Research University, Silesian University of Technology.

BIBLIOGRAPHY

1. Bolunduț, I. L.: Tehnologia materialelor plastice și compozite, Editura Junimea, Iași (2011), Tsicura C., Csedreki I.
2. T. Suntola, Tsicura A.: Cartea Ipsosarului, Editura Tehnica, București (1989).

3. L.A. Lushnikova N., Dvorkin L.: Sustainability of gypsum products as a construction material, Woodhead Publishing Series in Civil and Structural Engineering, Pages 643-681 (2016).
4. Zong, L.; Fei, Z.; Zhang, S. Permeability of recycled aggregate concrete containing fly ash and clay brick waste. *J. Clean. Prod.* 2014, 70, 175–182.
5. Aliabdo, A.; Abd-Elmoaty, A.-E.M.; Hassan, H.H. Utilization of crushed clay brick in concrete industry. *Alex. Eng. J.* 2014, 53, 151–168.
6. Saikrishnan, S.; Jubinville, D.; Tzoganakis, C.; Mekonnen, T.H. Thermo-mechanical degradation of polypropylene (PP) and low-density polyethylene (LDPE) blends exposed to simulated recycling. *Polym. Degrad. Stab.* 2020, 182, 109390.
7. Di, L.; Yang, Y. Towards closed-loop material flow in additive manufacturing: Recyclability analysis of thermoplastic waste. *J. Clean. Prod.* 2022
8. Atomic Layer LNCS Homepage, <https://www.aluminum.org/Recycling>.
9. LNCS Homepage, <https://climate.selectra.com/en/recycling/aluminium>.
10. LNCS Homepage, <https://www.recyclenow.com/how-to-recycle/can-recycling>



31th January 2025
Gliwice, Poland

DEPARTMENT OF ENGINEERING MATERIALS AND BIOMATERIALS
FACULTY OF MECHANICAL ENGINEERING
SILESIA UNIVERSITY OF TECHNOLOGY

INTERNATIONAL STUDENTS SCIENTIFIC CONFERENCE

Tribological studies of CrN coating obtained by PVD on austenitic steel surface X2CrNiMo17-12-2

Tobiasz Markowicz ^a, Jakub Pluskota ^a, Beniamin Sobczak ^a, Daniel Pakuła ^b, Marcin Staszuk ^b

^a Student of Silesian University of Technology, Faculty of Mechanical Engineering, ul. Konarskiego 18A, 44-100 Gliwice, Poland

email: tm307633@student.polsl.pl, jp307654@student.polsl.pl, bs308653@student.polsl.pl

^b Silesian University of Technology, Faculty of Mechanical Engineering, Department of Engineering Materials and Biomaterials, ul. Konarskiego 18A, 44-100 Gliwice, Poland

email: daniel.pakula@polsl.pl, marcin.staszuk@polsl.pl

Abstract: The article was written as part of the PBL project. It investigates the tribological properties of CrN coating deposited by physical vapor deposition (PVD) on 316L austenitic steel. The tribological properties were examined using the ball-on-disc method. Wear mechanisms were analyzed with a contact profilometer and scanning electron microscopy (SEM). Studies on topography of coating were conducted using atomic force microscopy (AFM).

Keywords: 316L, Tribology, PVD, CrN, SEM, AFM

1. INTRODUCTION

Stainless steel is one of the most popular metal materials used in such fields as cookware, medical devices and also in high-end engineering applications. This kind of steel has several advantages ranging from excellent corrosion resistance even in diverse harsh engineering environments, high ductility and shapeability to high and stable across a broad temperature spectrum impact strength and sufficient mechanical strength [1,2].

One type of stainless steel is 316L (X2CrNiMo17-12-2). This grade of steel due to its mechanical properties, great corrosion resistance and sufficient biocompatibility is extensively used in sectors like transportation or petrochemistry, as well as in biomedical engineering. In the later field, 316L steel has an application because it is the most popular representative of stainless steel in this range and it is used for surgical implants like bone screws and plates or even joint endoprosthesis [3,4].

However, 316L steel has low hardness which could cause a predisposition to galling and scratch the surface and makes it susceptible to wear. Other disadvantages are poor tribological properties and also limited lifespan in high temperature applications. Various types of coatings are used to remedy this type of defect [3,5,6].

Chemical composition of 316L steel is shown in Table 1.

Table 1. Chemical composition of 316L steel [7]

	Chemical composition [%]											
	Cr	Ni	Mo	C	Mn	Cu	P	S	Si	N	Fe	
Min	17	13	2.25	-	-	-	-	-	-	-	-	Balance
Max	19	15	3	0.03	2	0.5	0.025	0.01	0.75	0.1		

Coatings applied by physical vapor deposition (PVD) increases surface microhardness, reduces friction coefficient and also enhance aesthetic values and electrochemical properties. The improvement of specific properties depends on the type and chemical composition of the coating applied to the material [2].

PVD coating finds use in a wide variety of situations, improving surface properties of material without the need of making whole parts out of high-end materials, greatly decreasing costs and often allowing for easier manufacturing. PVD or physical vapor deposition is a process in which solid materials are vaporized and deposited on the surface of a part making a coat with desired mechanical, chemical or esthetical properties most often higher than the material of the coated part. Such coatings can increase corrosion resistance and protect against wear, those properties are extremely important among medical instruments and prosthetic implants. Combining great surface properties of PVD coating with relatively low cost 316L stainless steel would make tools that could be used in many fields where degradation of material is critical. Most commonly used coatings are titanium-based Ti/TiN and chrome based CrN/CrAlN [8].

Ti/TiN were extensively studied showing considerable increase in corrosion resistance of coated steels as well as hardness, conducted test on tribocorrosion showed ability of coating to repair passive film affected area after sliding stops, that passive film also shows some lubricating abilities helping with wear degradation [9].

Other commonly used coatings CrN/CrAlN, studies conducted on those coatings showed significant increase in microhardness and good adhesion to base material. What is more, those kinds of coatings had great surface roughness and small friction coefficient leading to good tribological wear resistance and contributing to increase in corrosion resistance [10].

The study of sliding surface interaction is known as tribology. It consists of friction, wear and lubrication. The resistance exerted on a solid body by another body in contact is called friction. Wear occurs as a consequence of the mechanical action exerted by a solid body removing material from the surface of another body. A significant part of the energy and objects generated by humanity is wasted due to friction and wear. Introducing intended substances between the surfaces of two bodies to reduce friction and wear is lubrication [11].

Wear resistance can be tested with a tribometer, e.g. in the ball-on-disc mode. Parameters affecting wear are type of counter-sample, wear diameter, linear speed, normal force and number of cycles [4].

The purpose of this research is to present the results of tribological and structural studies of PVD coating deposited on 316L austenitic steel samples.

2. MATERIALS AND METHODOLOGY

The material used to conduct the tests was 316L stainless steel. Samples with a diameter of 20 mm were subjected to grinding and polishing. Subsequently, the CrN coating was applied to the samples.

Tribological properties (e.g. friction coefficient) of samples with and without coating were examined by a tribometer using ball-on-disc method. Study parameters are presented in Table 2.

Table 2. Parameters used for the study of tribological properties

Sample number	Substrate	Coating	Parameters				Linear speed $\left[\frac{\text{cm}}{\text{s}}\right]$
			Number of cycles	Normal load [N]	Radius [mm]	Acquisition rate [Hz]	
1	316L	-	20000	5	5	10	5
2		CrN					
3		-					20
4		CrN					

The studies were conducted at temperature of 25°C and 50% humidity. The tungsten carbide (WC) ball with 6 mm diameter was used as a counter-sample.

Paths created by counter-sample were measured by Taylor Hobson Surtronic profilometer. Topography of coatings surface and wear mechanisms were analyzed using atomic force microscopy AFM and scanning electron microscopy SEM using EHT voltage of 15 kV at magnifications ranging from 40 to 5000 times and using secondary electron (SE) detectors. Chemical composition of certain micro areas was conducted using X-ray energy dispersive spectroscopy EDS.

3. RESULTS

The surface topography at the microscale shows a topographical structure of CrN coating obtained by PVD method (Fig. 1). Some morphological defects in form of pores appear on the surface of coatings as well as visible scratches, which are residues from process of mechanical preparation of samples by grinding and polishing.

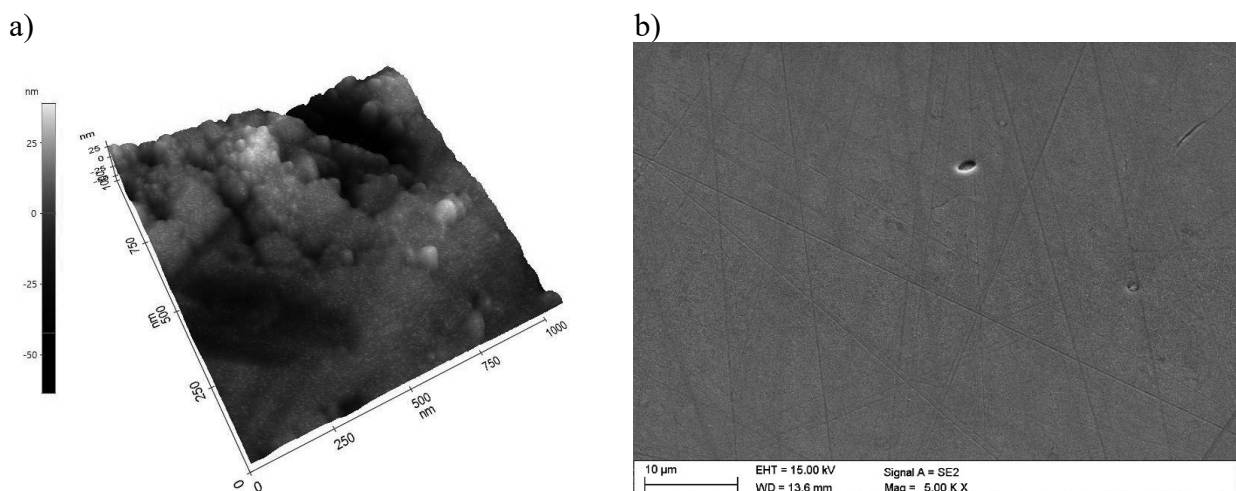


Fig. 1. CrN coating topography a) AFM, b) SEM.

Tribological measurements showed the difference between coated and uncoated. Average coefficient of friction and standard deviation are shown in Table 3. For uncoated samples, the

coefficient of friction slowly increased as the test continued. Measurements showed that the friction coefficient value was lower at higher speeds, averaging at $\mu = 0.71$ for $v = 5$ cm/s and $\mu = 0.67$ for $v = 20$ cm/s.

For the CrN-coated samples, the coefficient of friction was lower than for the uncoated samples. For $v = 5$ cm/s, the average coefficient of friction reached $\mu = 0.51$, and for $v = 20$ cm/s it was $\mu = 0.49$. These differences are small and may be due to the test conditions and surface purity. The lack of abrupt changes indicates a lack of abrasion to the surface (Fig. 2).

Table 3. Average coefficient of friction and standard deviation for steel samples

Sample number	Coating	Linear speed $\left[\frac{\text{cm}}{\text{s}}\right]$	Average friction coefficient	Standard deviation
1	-	5	0.71	0.12
2	CrN		0.51	0.06
3	-	20	0.67	0.05
4	CrN		0.49	0.03

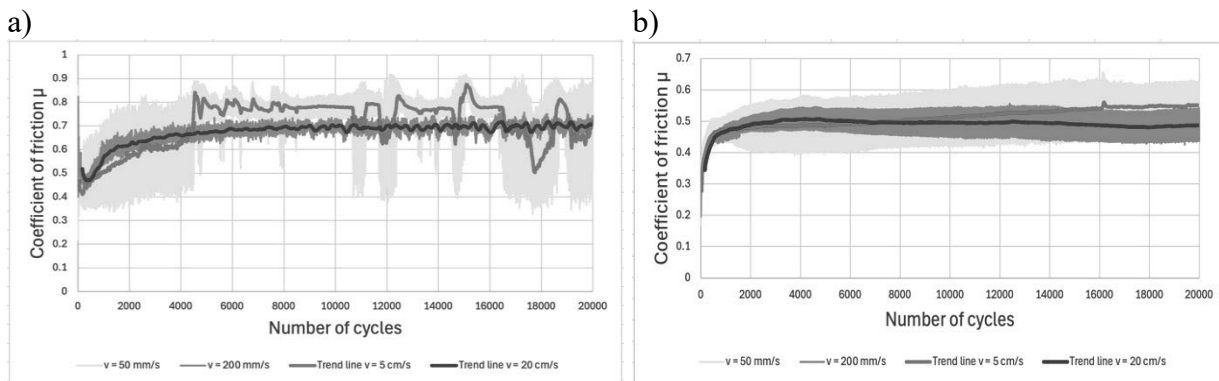


Fig. 2. Friction coefficient as a function of the number of cycles for the steel sample a) uncoated, b) coated.

Measurements conducted using contact profilometer showed that in case steel with no coating raising linear speed at which tests were conducted from 5 cm/s to 20 cm/s affected the amount of lost material increasing it by more than four times (Table 4). As to samples with CrN coating, the cavities that appeared on them during tests were so small that they were immeasurable proving effectiveness of coatings (Fig. 3, Fig. 4).

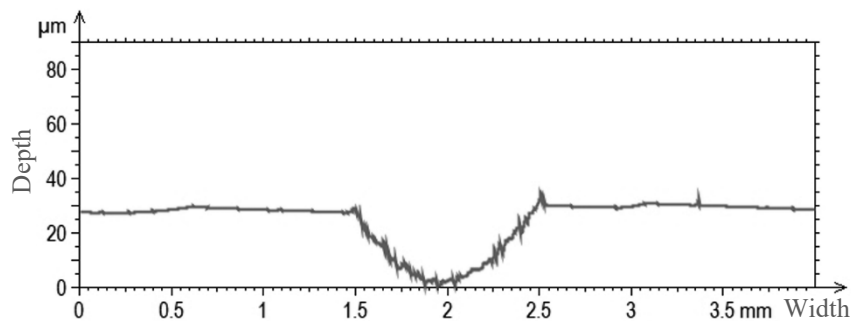


Fig. 3. Profile of steel with no coating received from contact profilometer measurements, linear speed 5 cm/s.

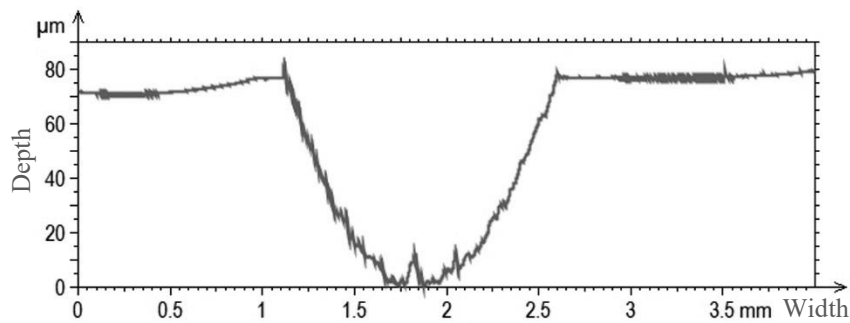


Fig. 4. Profile of steel with no coating received from contact profilometer measurements, linear speed 20 cm/s.

Samples with CrN coating don't show any visible signs of wear and give back results with which it is impossible to calculate the amount of material lost to wear damage. With results from measuring samples of raw 316L steel we can calculate area of the profile of cavities and then calculate volume of lost material. This is shown in Table 4.

Table 4. Average area and volume of cavities created on samples with no coating

Coating	Linear speed $\left[\frac{\text{cm}}{\text{s}}\right]$	Area $[\text{mm}^2]$	Volume $[\text{mm}^3]$
-	5	0.017	0.557
-	20	0.072	2.276
CrN	5	Unmeasurable	Unmeasurable
CrN	20	Unmeasurable	Unmeasurable

The wear area and volume are significantly greater in the steel sample tested at $v = 20$ cm/s than in the sample tested at $v = 5$ cm/s (Fig. 5).

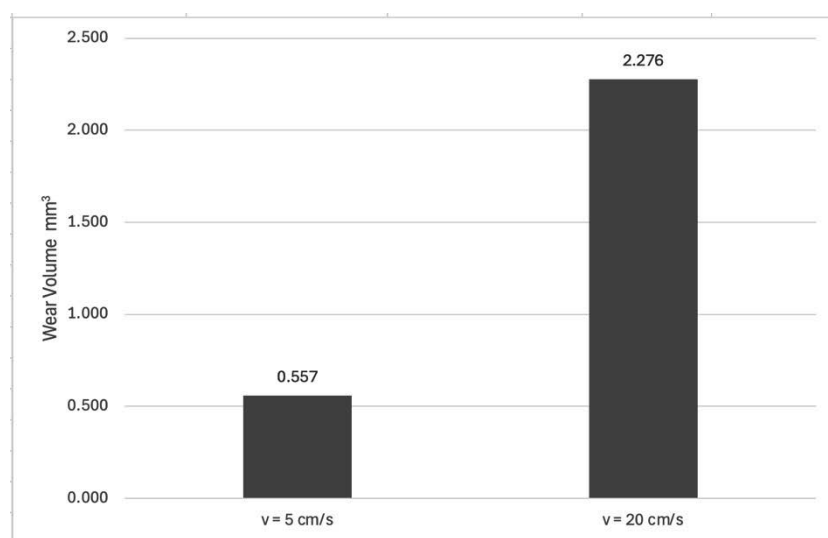


Fig. 5. Comparison of surface wear volume of uncoated samples for different linear speeds.

Conducted SEM topography studies confirmed severe but expectable wear on an uncoated sample, also EDS results didn't show any unexpected elements that shouldn't be present in 316L stainless steel.

As to coated samples the wear traces were hardly as noticeable, SEM studies showed that in neither case did the coatings fail, small cases of delamination were visible. EDS study showed mostly chromium and nitrogen confirming that the counter-sample didn't wear through the coating, what's more study showed traces of tungsten which might have come from the tungsten carbide counter-sample (Fig. 6, Fig. 7, Fig. 8).

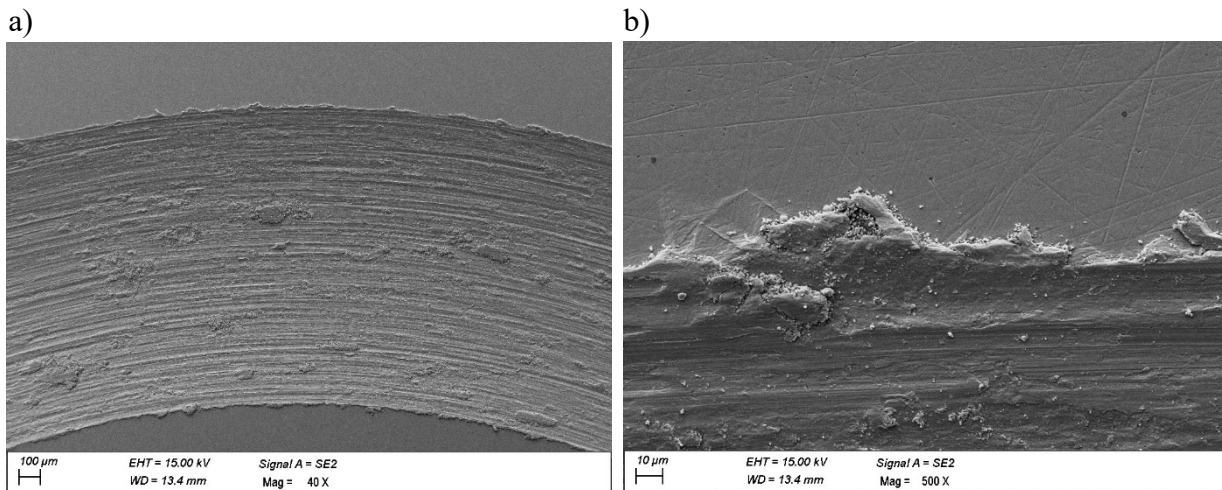


Fig. 6. a) Wear trace after the ball-on-disc test at linear speed $v = 20$ cm/s for 316L steel without coating, b) Close-up of the wear edge.

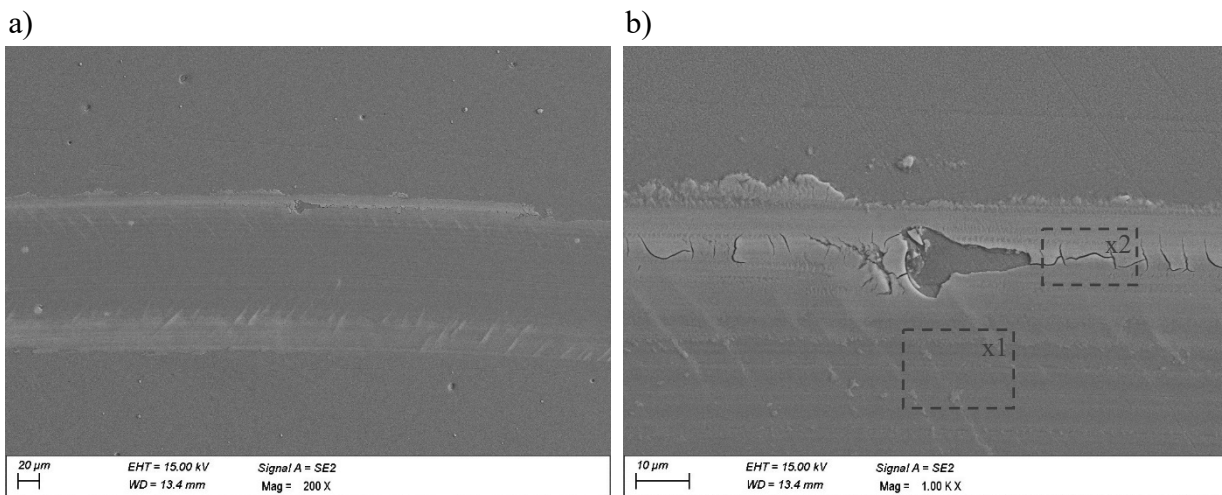


Fig. 7. a) Wear trace after the ball-on-disc test at linear speed $v = 20$ cm/s for 316L steel with CrN coating, b) Close-up of the damage on the coating surface.

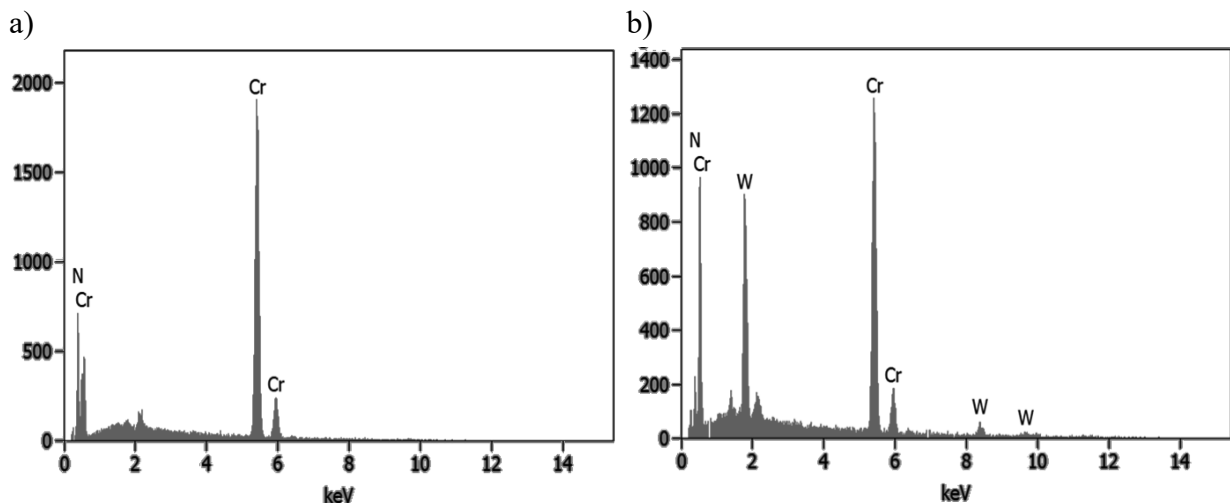


Fig. 8. EDS analysis a) from the x1 micro-area as in fig. 7b, b) from the x2 micro-area as in fig. 7b.

Average wear width depends on whether the sample was coated or not and on linear speed at which tests were conducted, wear width was smaller on coated samples and in both cases increased with higher linear speed. Average wear width for all samples is shown in Table 5.

Table 5. Average wear width for all samples

Sample number	Wear width [μm]
1	987.3
2	185.5
3	1394.3
4	145.8

4. CONCLUSIONS

Based on the conducted research, it has been determined that:

- Higher linear velocity, at which tribological tests are conducted, results in more wear on the samples.
- The CrN coating greatly increases the wear resistance of the material.
- The presence of tungsten on the surface of the test sample indicates that the strength of the CrN coating is greater than that of the tungsten carbide counter-sample.

ACKNOWLEDGEMENTS

This work was produced as part of the project implemented within the framework of project-oriented education – PBL, in the XI competition under the Excellence Initiative – Research University program, at the Silesian University of Technology.

BIBLIOGRAPHY

1. K. Chen, Yiting Pan, G. Tang, D. Liang, H. Hu, X. Liu, Z. Liang, Facile fabrication of TiN coatings to enhance the corrosion resistance of stainless steel, *Surface and Coatings Technology* 494 (2024) 131450.
2. M. Staszuk Investigations of CrN+Cr₂O₃/TiO₂ coatings obtained in a PVD/ALD hybrid method on austenitic 316L steel substrate, *Vacuum* 207 (2023) 111653.
3. S. Indupuri, P. Sai Kiran, R. Kumar, Ch. Satish, A. Kumar Keshri, High-temperature tribological behavior of plasma sprayed GNPs-reinforced YSZ coating over 316L stainless steel, *Materials Today Communications* 41 (2024) 110451.
4. M. Staszuk, D. Pakuła, Ł. Reimann, A. Kloc-Ptaszna, K. Lukaszewicz, Structure and properties of the TiN/ZnO coating obtained by the hybrid method combining PVD and ALD technologies on austenitic Cr-Ni-Mo steel substrate, *Surfaces and Interfaces* 37 (2023) 102693.
5. V.J.S.N. Prasad, F. Mayanglambam, P.N.V.V.L. Primila Rani, Pamu Dobbidi, Silver-doped ZrO₂-TiO₂ nanocomposite coatings on 316L stainless steel for enhanced corrosion resistance and bio applications, *Surface and Coatings Technology* 493 (2024) 131203.
6. A.F. Yetim, H. Tekdir, K. Turalioglu, M. Taftali, T. Yetim, Tribological behavior of plasma-sprayed Ytria-stabilized zirconia thermal barrier coatings on 316L stainless steel under high-temperature conditions, *Materials Letters* 336 (2023) 133873.
7. <https://www.ebmia.pl/wiedza/porady/obrobka-porady/stal-316l-1-4404/> (access: 22.12.2024)
8. <https://blog.vaportech.com/what-is-pvd-coating-an-intro-to-physical-vapor-deposition-other-thin-film-deposition-technologies> (access: 04.11.2024)
9. S.A. Naghibi, K. Raeissi, M.H. Fathi, Corrosion and tribocorrosion behavior of Ti/TiN PVD coating on 316L stainless steel substrate in Ringer's solution, *Materials Chemistry and Physics* 148 (2014) 614-623.
10. M. Soleimani, A. Fattah-alhosseini, H. Elmkhah, K. Babaei, O. Imantalab, A comparison of tribological and corrosion behavior of PVD-deposited CrN/CrAlN and CrCN/CrAlCN nanostructured coatings, *Ceramics International* 49 (2023) 5029-5041.
11. The Editors of Encyclopedia Britannica. "Tribology | Physics." *Encyclopedia Britannica*, 7 June 2017, www.britannica.com/science/tribology.



31th January 2025
Gliwice, Poland

DEPARTMENT OF ENGINEERING MATERIALS AND BIOMATERIALS
FACULTY OF MECHANICAL ENGINEERING
SILESIA UNIVERSITY OF TECHNOLOGY

INTERNATIONAL STUDENTS SCIENTIFIC CONFERENCE

Development of a computer model and simulation of three-point bending test using the Gleeble 3800 simulator

Michał Masoń ^a, Wojciech Borek ^b

^a Student of the Silesian University of Technology, Faculty of Mechanical Engineering, Department of Mechanical Engineering and Machine Design

email: mm304152@student.polsl.pl

^b Silesian University of Technology, Faculty of Mechanical Engineering, Department of Engineering Materials and Biomaterials

email: wojciech.borek@polsl.pl

Abstract: In this article, the design and numerical verification of a specialized fixture for three-point bending tests conducted on a Gleeble 3800 are presented. The fixture was initially conceived as a digital model and is designed to meet ISO 14125 standards, enabling precise specimen clamping under various conditions. Finite element analysis was used to evaluate stress and strain distributions, ensuring the fixture's structural integrity and accurate test results.

Keywords: three-point bending test; Gleeble 3800 simulator; finite element analysis (FEA); numerical simulation; fixture design

1. INTRODUCTION

The phenomenon of the diversity of materials, their unique characteristics, and properties accompanies us at every step. From everyday objects such as smartphones and cars to advanced space technologies, we encounter a variety of substances everywhere, whose characteristics determine their application. Material properties are a set of physical, chemical, and mechanical characteristics that describe the behaviour of a material under various conditions. It is thanks to these properties that we can understand why steel is strong, glass is transparent, and rubber is elastic [1].

To fully understand the behaviour of engineering materials under various operating conditions and to select them optimally for specific applications, it is necessary to conduct a series of specialized tests. These types of tests aim to accurately determine the mechanical properties of materials, such as strength, hardness, ductility, or fatigue resistance. Due to the diversity of engineering materials and the wide range of their potential applications, many advanced research methods have been developed. Each of these methods allows for the determination of specific material parameters, providing engineers with the necessary information for designing and optimizing structures. Mechanical testing of materials is not only static tensile, compressive, or bending tests, but also more advanced dynamic tests that simulate the actual

operating conditions of materials in structures. Thanks to them, we can assess how the material will behave under cyclic loading, variable temperatures or aggressive environments [2].

2. RESEARCH METHODOLOGY

A detailed 3D computer model of the grip (Fig. 1) for mechanical tests according to ISO 14125 was developed which can be used only in Gleeble 3800 simulator. The model was adapted to the geometric constraints of the machine's clamps, ensuring adequate stiffness, stability, and secure clamping of the 56 mm long, 2.5 mm thick specimen with a 40 mm span. The optimal method of attaching the grip to the clamps was also determined. Necessary analyses and simulations were carried out [3-5].

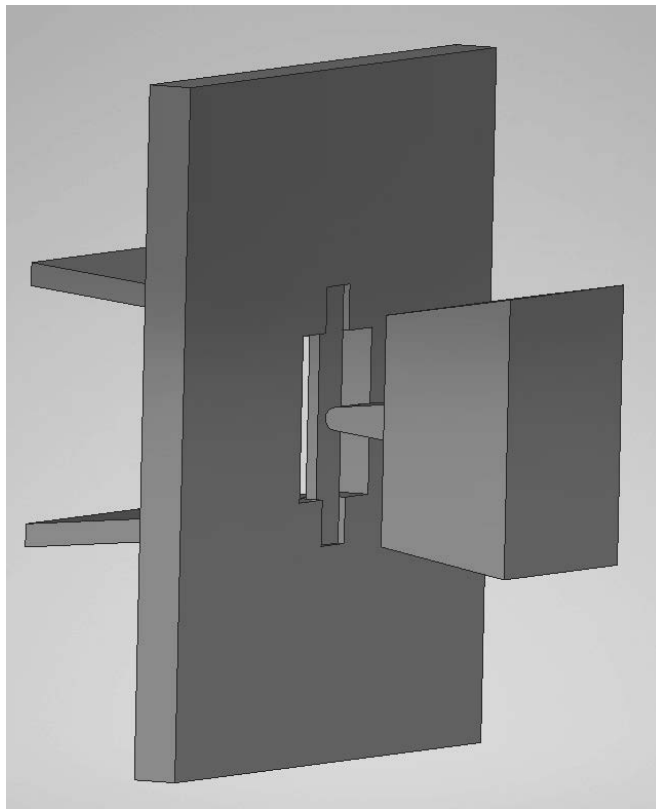


Figure 1. 3D assembly of the grip, jaw with pin, and specimen components

In accordance with ISO 14125, the support span was set to a ratio of 1:16. Subsequently, a numerical simulation of the bending process was conducted, focusing on the stress distribution analysis in the support area. To optimize the simulation process, degrees of freedom were reduced. The entire structure was made of S314L stainless steel [3, 4].

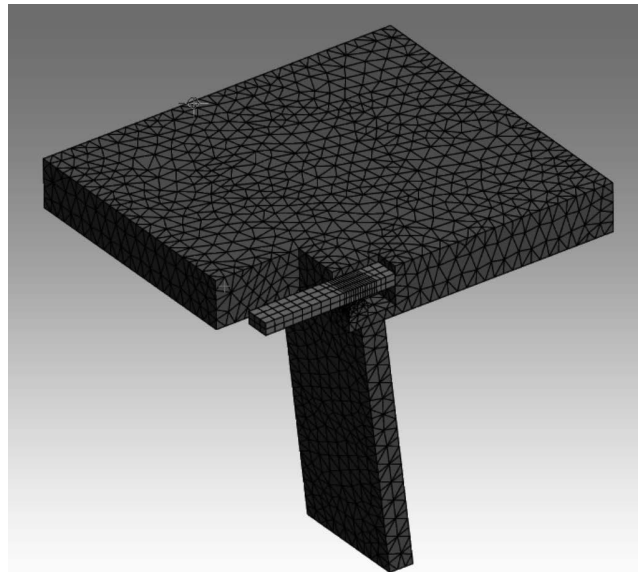


Figure 2. Finite element model

The mesh (Fig. 2) is non-uniformly refined, meaning that the size of the finite elements varies across the model. In regions where high stress or strain gradients are expected, such as at the support, the elements are smaller. Conversely, in areas with lower stress gradients, the elements can be larger. This discretization approach allows for more accurate results while simultaneously limiting the number of elements, which reduces computation time. Three-dimensional solid elements were used, providing a versatile tool for numerical analysis.

Subsequently, a simulation was conducted to obtain information about the model's behaviour under a displacement of 0.1 mm.

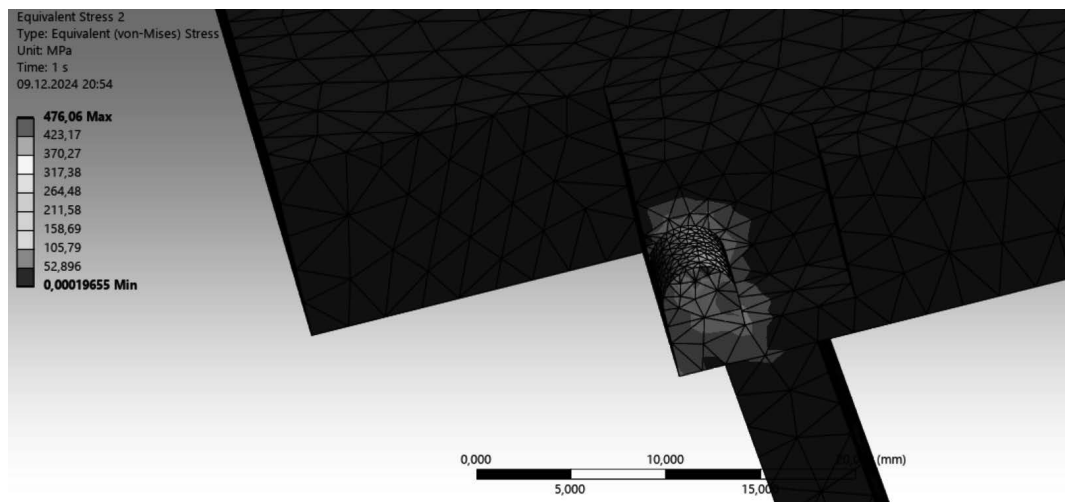


Figure 3. Equivalent stress at the supports in a three-point bending test

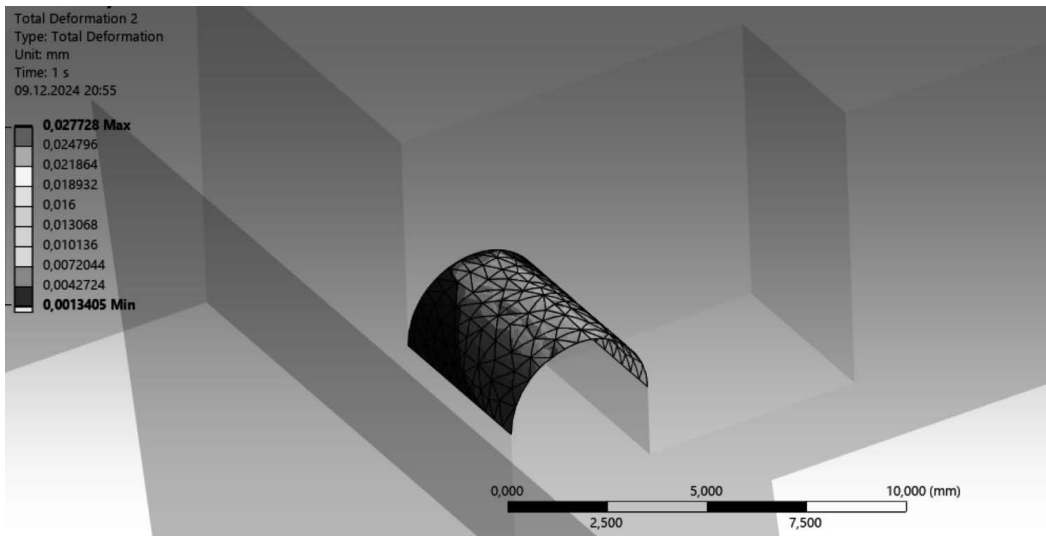


Figure 4. Total displacement of the supports during a three-point bending test

The highest stress values for the support during the three-point bending test (Fig. 3) concentrate in a narrow region, indicating stress concentration. This is a typical phenomenon at section changes, holes, or other geometric discontinuities. In this case, stress concentration likely occurs at the joint of the structural elements. The area with the highest stresses is most susceptible to damage. If the value of these stresses exceeds the material's strength, a fracture or other type of damage may occur. The support displacements (Fig. 4) are relatively small, indicating that they are sufficiently stiff to carry the loads. The largest displacements occur in the cylinder, suggesting it is the most loaded element of the structure, where the highest stresses also occur.

A similar simulation was conducted with a 10mm pin displacement for the previously mentioned scenario.

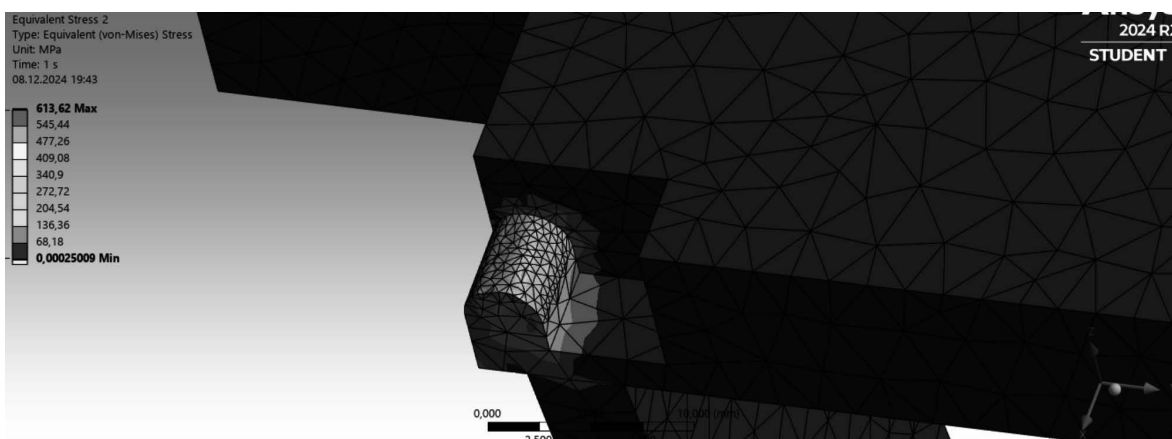


Figure 5. Equivalent stress at the supports in a three-point bending test

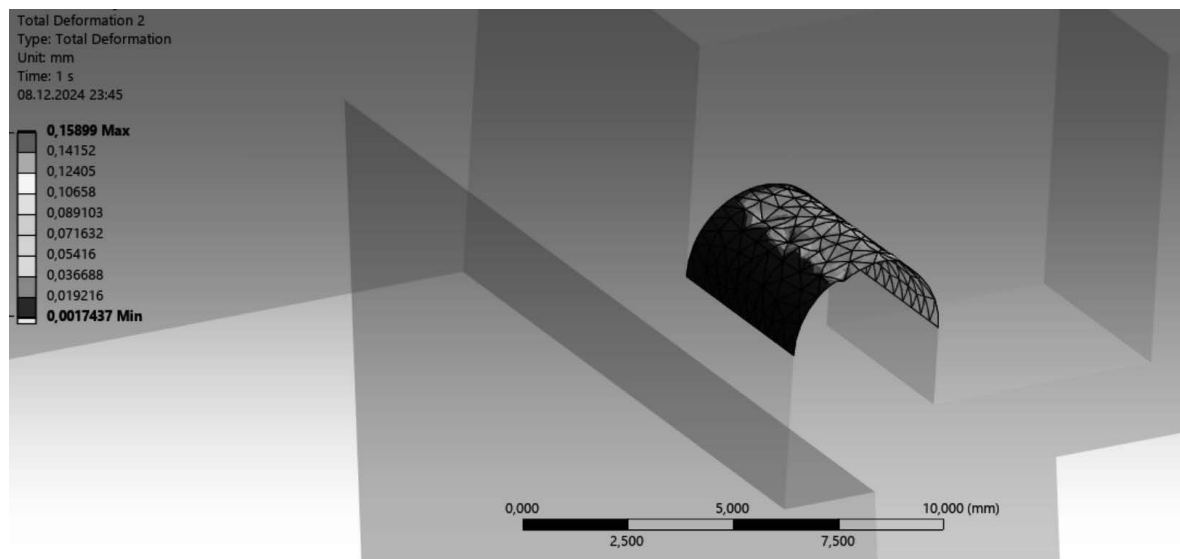


Figure 6. Total displacement of the supports during a three-point bending test

3. RESULTS

Table 1. Maximum and minimum stress and displacement at the supports

Displacement [mm]	0.1		10	
	max	min	max	min
max and min value [MPa]				
Equivalent stress [MPa]	476.06	0.00020	613.62	0.00025
Total displacement [mm]	0.0277	0.0013	0.159	0.0017

In Table 1 shown that increasing the displacement from 0.1mm to 10mm resulted in a significant increase in both maximum stresses and total displacement. The very low values of minimum stresses indicate that the support areas were practically unloaded during the test. Conversely, the maximum stress values suggest that the material was subjected to significant loads in these areas. The difference in total displacement for both displacement values is significant, confirming that larger deformations lead to greater overall sample deformations. Based on the above results, it can be concluded that the simulation was performed correctly.

4. CONCLUSIONS

The developed grip design meets the requirements of ISO 14125. Geometric measurements

allowed for the adaptation of the grip to the machine clamp limitations, while ensuring safe sample clamping. Correctly defined boundary conditions and an appropriately dense finite element mesh increased the accuracy of the simulation results. The use of model symmetry and non-uniform mesh refinement significantly reduced computation time without loss of accuracy. Increasing the pin displacement value results in an increase in stresses and strains in the sample. The simulation view shows a uniform distribution of these quantities throughout the structure. Such a stress state is beneficial for the sample's strength, as it minimizes the risk of local stress concentrations that could lead to premature material failure. Based on the simulation analysis, it was found that the most stressed area is the contact area between the support and the sample. With a maximum pin displacement of 10mm, the maximum support stress value was 613MPa. These stresses were distributed uniformly, with the least stressed points having a value of only 0.0025MPa. The tested structure exhibited high stiffness. Despite increasing the pin displacement by 10mm, the resulting structural deformations were small, indicating its high resistance to deformation. The maximum deformation, amounting to 0.159 mm, occurred at the contact point and gradually decreased to a minimum value of 0.0017 mm, confirming the uniform stress distribution throughout the structure. Based on the analysis of literature data and simulation results, it was concluded that the proposed design meets the requirements for a three-point bending test in the Gleeble 3800 simulator.

BIBLIOGRAPHY

- [1] Wiesław Żelasko. Właściwości materiałów i ich badanie. Politechnika Rzeszowska, data from 08.12.2024.
- [2] Mariusz Król, Zbigniew Brytan. Badania własności mechanicznych materiałów inżynierskich. Laboratoria Aparatura badania. LAB 3 (2018) str. 20-24.
- [3] <https://www.zwickroell.com/pl/branze/badanie-materialow/badanie-zginania/>
- [4] <https://www.zwickroell.com/pl/branze/tworzywa-sztuczne/termoplastyczne-i-utwardzalne-masy-formierskie/proba-3-punktowego-zginania-zgodnie-z-astm-d790/>,
- [5] "Kształtowanie struktury i własności materiałów inżynierskich z wykorzystaniem symulatora obróbki cieplno-plastycznej Gleeble 3800", Instytut Materiałów Inżynierskich i biomedycznych Politechniki Śląskiej, Prace studenckich kół naukowych, 2014r, Gliwice

Technologies for the production of carbon fiber components in the automotive industry

Kamil Mazelanik, Bogusław Ziębowicz

Faculty of Mechanical Engineering, Department of Engineering Materials and Biomaterials, Silesian University of Technology, Konarskiego 18A , 44-100 Gliwice, Poland;
email: kamimaz708@student.polsl.pl; boguslaw.ziebowicz@polsl.pl

Abstract: The article discusses the technologies for the production of carbon fiber components, which are widely used in the automotive industry. Carbon fiber, with its exceptional mechanical properties such as high strength and low weight, is used in the construction of components that require high durability and precision. The methods for producing composites, such as wet laminating, vacuum molding, the RTM method, and prepreg technology, are analyzed. The importance of experience and precision in the production process is emphasized, and the potential of carbon fiber in modern industry is presented.

Keywords: carbon fiber, wet laminating, vacuum molding, RTM, prepreg, composites, automotive industry.

1. INTRODUCTION

Carbon fiber is a material with unique mechanical properties such as high strength, stiffness, and low weight, making it ideal for applications in the automotive, aerospace, and sports industries. Its history dates back to the late 19th century when Thomas Edison first used carbon fiber in light bulbs. Today, it is used across a wide range of industries utilizing advanced technologies.



Fig. 1. Carbon fiber car hood of the Toyota GT86.

The aim of the article is to analyze the methods of manufacturing carbon fiber components, their advantages, disadvantages, and potential applications in industrial practice.

1. Carbon Fiber and production process

Carbon fiber is a composite material composed of thin fibers made almost entirely of carbon atoms (92-99%). The residual atoms that may be present are oxygen, associated with the processes of carbonization and stabilization. These fibers have a unique structure in which carbon atoms form microscopic crystals arranged parallel to the fiber axis, resembling graphite. Fibers with a high modulus of elasticity have a more regular and parallel arrangement of crystallites. Additionally, if there are amorphous areas in the fiber structure arranged irregularly, these parts of the fibers are more flexible.

The production of carbon fiber is a complex process that can be divided into several key stages:

1. Chemical Stabilization of the Precursor:

In this process, the fiber undergoes oxidation, forming a stable chemical structure ready for further carbonization. The most commonly used precursor is polyacrylonitrile (PAN), which is processed in a controlled atmosphere with oxygen at a temperature of around 200–300°C.

2. Carbonization:

During carbonization, the fibers are subjected to very high temperatures (1000–3000°C) in an oxygen-free environment, which removes atoms other than carbon, such as hydrogen, oxygen, or nitrogen. This results in almost pure carbon fiber, which gains its exceptional mechanical properties due to this process.

3. Surface Treatment:

The fibers are lightly oxidized or etched with chemicals to improve their adhesion to the resin in the composite.

4. Finishing:

The fibers are coated with special substances (e.g., sizing) that facilitate further processing and enhance their compatibility with various resins.

2. METHODS OF PRODUCING CARBON FIBER COMPONENTS

2.1 Wet Laminating

Wet laminating is one of the most cost-effective methods for producing carbon fiber components, primarily used in low-volume and prototype production. The process involves manually laying carbon fiber fabric in a properly prepared mold, wetting it with resin, and removing excess resin using tools. The laminate cures at room temperature or slightly higher, making this method simple and economical. However, the lack of vacuum pressure limits the mechanical properties of the produced components. Mold preparation plays a crucial role in the quality of the final product. The mold must be thoroughly cleaned (e.g., with acetone), coated with a release agent (such as wax or PVA), and possibly gel-coated, which improves the surface finish and composite resistance. After applying the required number of fiber layers, separated by resin, the laminate undergoes a curing process, during which the resin gels and hardens, achieving its final mechanical properties. During curing, an exothermic reaction may occur, especially in thicker laminates, which requires supervision to avoid overheating. Once curing is complete, the laminate is removed from the mold using plastic wedges to prevent

damaging the composite. Final finishing includes applying a clear coat and polishing, giving the component an aesthetic appearance.

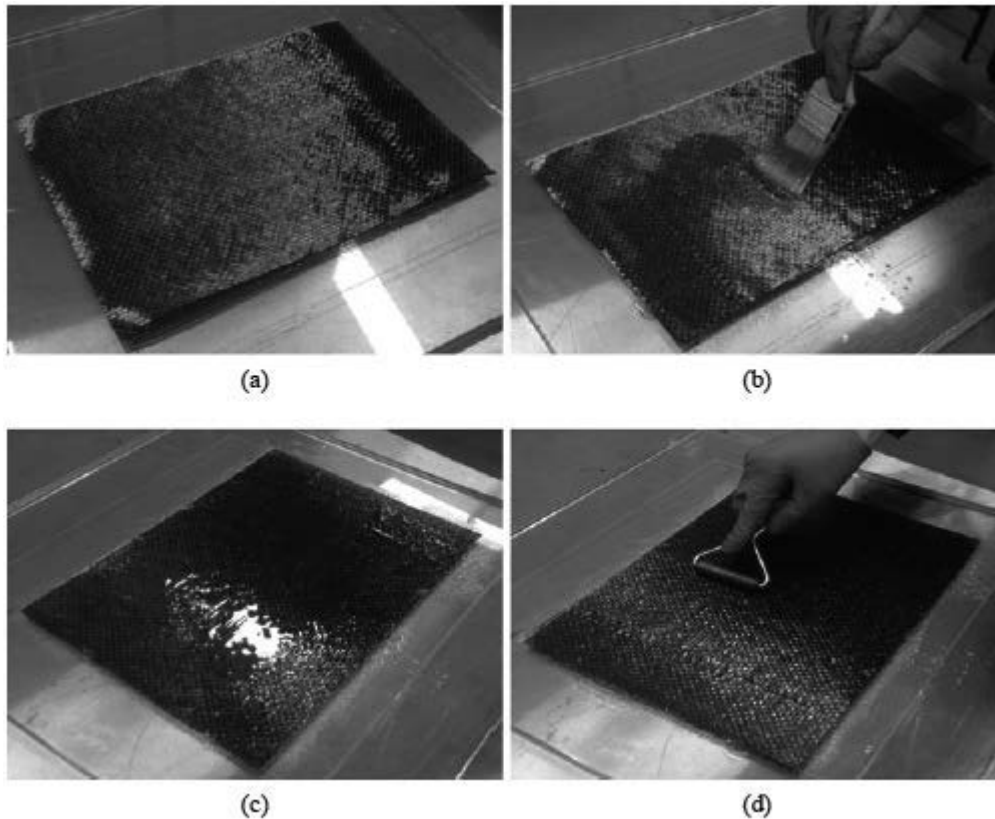


Fig. 2. Steps of wet lamination method: a) laying the first layer of carbon fiber; b) saturating with resin using a brush; c) excess resin on the surface; d) using a roller to remove air trapped in the resin.

In summary, the wet laminating method is a simple and versatile solution, but it requires experience to achieve high-quality components. The limitations of this technology include a lower fiber volume fraction and the inability to precisely control curing, making it less efficient compared to more advanced techniques such as vacuum molding or RTM.

2.2 Vacuum molding

Vacuum molding is an advanced technique for manufacturing carbon fiber components, which involves removing air and excess resin from the laminate using a vacuum pump. The process requires the use of additional materials such as release films, absorbent fabrics, and vacuum bags. Conducting the process under vacuum ensures better wetting of the fibers and reduces the number of voids in the composite. This results in a higher fiber volume fraction and better laminate consolidation compared to manual laminating.

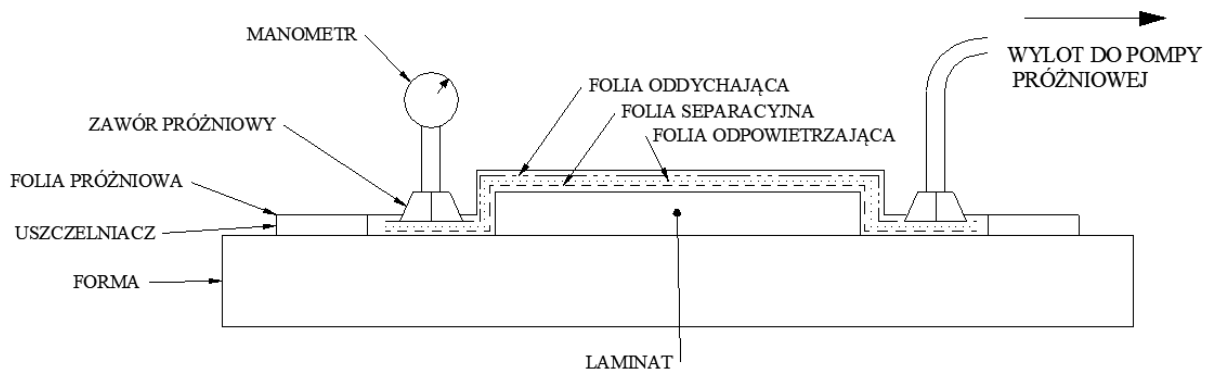


Fig. 3. Diagram of vacuum molding process.

A key step in the process is preparing a sealed vacuum bag using sealing tape, which allows for effective air extraction and the creation of a vacuum. This process can take several hours, depending on the size of the component. After the laminate has cured to a solid state, the equipment is removed, and the composite is separated from the mold using plastic wedges. The process may be supported by additional thermal treatment to accelerate the resin curing after the part has been formed. Vacuum molding is a technique that enables the production of high-quality composites by effectively removing air and excess resin, which reduces the number of voids and improves fiber consolidation. Additionally, it allows for achieving a higher fiber volume fraction, which translates to better mechanical properties of the laminate. The advantage of this method is the reduced emission of organic compounds during production. However, its drawbacks include higher costs associated with auxiliary materials and the need for skilled operators, which can affect production time and cost.

2.3 Resin Transfer Molding (RTM)

The RTM (Resin Transfer Molding) method involves placing several layers of fabric or preform in the lower part of a two-part mold, which is then closed. Resin is injected through a central inlet channel under pressure of 69–690 kPa, filling the spaces between the fibers and displacing the air through vents. The process can take place at room temperature or in an oven, depending on the type of resin and hardener used. The use of preforms is also possible, which allows for better molding of complex shapes and eliminates time-consuming material trimming.

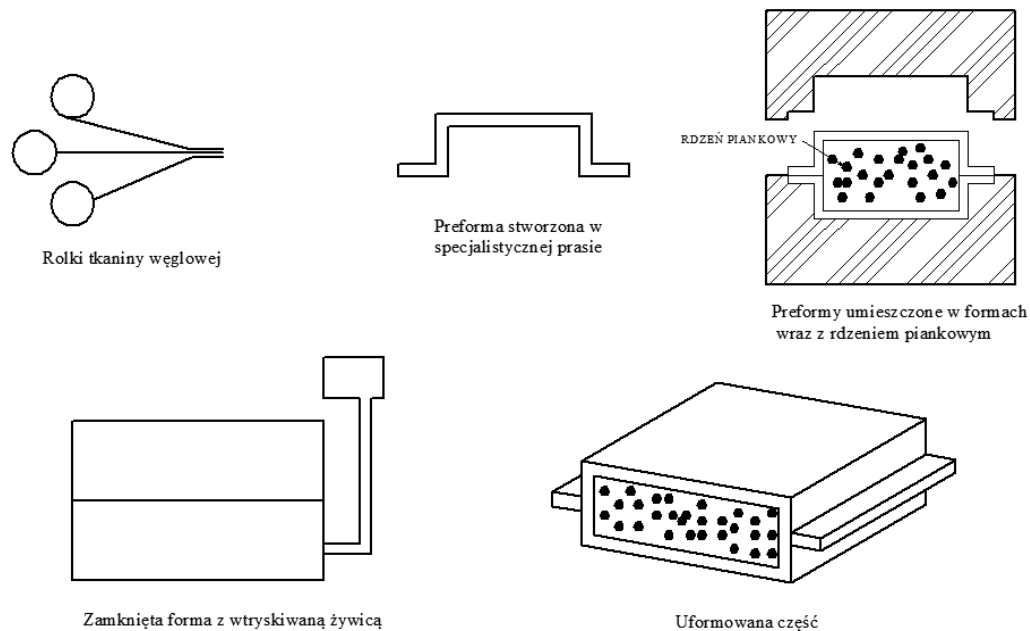


Fig. 4. Simplified diagram of the RTM (Resin Transfer Molding) process.

When using this method, voids may form in the composite due to uneven fiber permeability, which arises from differences in the fiber structure and orientation. High resin flow rates can lead to the formation of pores within the fibers, while low flow rates result in voids between them. The permeability of the composite depends on the type of fabric – for random fibers, it is about $1 \times 10^{-9} \text{ m}^2$, and for unidirectional fabrics with a high fiber content, it is approximately $1 \times 10^{-11} \text{ m}^2$. The RTM method enables the production of parts with high precision, uniformity, and complex shapes. It is an effective method for larger production runs, allowing controlled resin flow and a high fiber volume fraction. However, its drawbacks include high mold and equipment costs, the need for precise process parameter control, and the risk of defects if the fibers are not sufficiently wetted.

2.4 Manufacturing Components Using Prepregs

Prepreg molding is a precise method for manufacturing composites that uses carbon fiber pre-impregnated with epoxy resin, known as prepreg. Prepregs, which are partially cured materials, are stored in freezers for 3-12 months. After being removed from the freezer, they are thawed for several hours, cut to the desired shape, and then used. At room temperature, they become sticky and easy to handle. Heating them during placement helps conform them to the mold. Prepregs are characterized by high precision in fiber orientation, which ensures high-quality composites with low porosity (about 1%).



Fig. 5 Preimpregnate pre-soaked in resin.

Additional thermal curing, in an autoclave under pressure, allows for the elimination of air bubbles and ensures material uniformity. This additional curing occurs within a constant temperature range of 60-180°C. The advantages of the prepreg method include exceptional precision in fiber orientation, low composite porosity, and high-quality control. The drawbacks are higher material costs and the need for storage of prepregs in freezers and careful preparation before use.



Fig. 6. Components prepared for heat curing in an autoclave

3. SUMMARY

The production of carbon fiber components is a multi-stage process that requires the proper selection of manufacturing methods depending on the intended use and the design specifications of the element. An analysis of the technologies reveals that each method has its advantages and limitations, which determine their application. Due to its unique properties, carbon fiber enables the creation of components with very low weight and high strength simultaneously. In particular, in the automotive industry, where the goal is to reduce vehicle weight and increase energy efficiency, carbon fiber-based composites provide invaluable solutions. In the future, advancements in manufacturing and recycling technologies may allow

for even broader use of this material, making it one of the cornerstones of modern engineering technologies.

BIBLIOGRAPHY

- [1] Chi Zhang, Dajiang Zheng, Guang-Ling Song, Yang Guo, Ming Lui, Effect of the Microstructure of Carbon Fiber Reinforced Polymer on Electrochemical, *Journal of The Electrochemical Society*, Vol. 165/10, 2018, 647-656.
- [2] A. Öchsner, L. F. M. da Silva, H. Altenbach, *Advanced Structured Materials*, Springer, 2012
- [3] W. Hall, Z. Javanbakht, *Design and Manufacture of Fibre Resin Composites*, Springer, 2021
- [4] W. Królikowski, *Polimerowe kompozyty konstrukcyjne*, Wydawnictwo Naukowe PWN, Warszawa 2018.
- [5] A. Boczkowska, G. Krzesiński, *Kompozyty i techniki ich wytwarzania*, Oficyna Wydawnicza Politechniki Warszawskiej, Warszawa 2016.
- [6] H. Lee, K. Neville, *Handbook of epoxy resins*, McGraw-Hill, 1981.
- [7] Moon Koo Kang, Woo Il Lee, H. Thomas Hahn, Formation of microvoids during resin-transfer molding process, *Composites Science and Technology*, Vol. 60, Issues 12–13, 2000, 2427-2434.
- [8] K. Potter, *Resin Transfer Molding*, Chapman & Hall, 1997.
- [9] K. Mikucka, I. Eliaz, M. Czerwiński, Porównanie zastosowania zaawansowanej technologii wytwarzania kompozytów z włókna węglowego prepreg i technologii infuzji na masę elementów oraz możliwości produkcyjne, *Materiały 52. Międzynarodowego Seminarium Kół Naukowych w Olsztynie*, Wydawnictwo Naukowe FNCE, 2023, 457-472.
- [10] K. Trębacki, A. Królicka, Wpływ struktury materiałów kompozytowych na właściwości mechaniczne, *Bezpieczeństwo i Ekologia*, Vol. 9, 2017, 129-131.



31th January 2025
Gliwice, Poland

DEPARTMENT OF ENGINEERING MATERIALS AND BIOMATERIALS
FACULTY OF MECHANICAL ENGINEERING
SILESIA UNIVERSITY OF TECHNOLOGY

INTERNATIONAL STUDENTS SCIENTIFIC CONFERENCE

Korózna odolnosť nehrdzavejúcich ocelí po plazmovej nitridácii

Erik Meliš^a, Viera Zatkaliková^a

^a Žilinská univerzita v Žiline, Strojnícka fakulta, Katedra materiálového inžinierstva, Univerzitná 8215/1, 010 26 Žilina, Slovak Republic
email: melis2@stud.uniza.sk, viera.zatkalikova@fstroj.uniza.sk

Abstrakt: Príspevok sa zaoberá koróznou odolnosťou austenitických nehrdzavejúcich ocelí s povrchovou úpravou - plazmovou nitridáciou. Teoreticky popisuje nehrdzavejúce ocele, definuje koróziu, koróznou odolnosť, typy korózie a podáva základné informácie o nitridovaní a druhoch nitridovania.

Kľúčové slová: nitridácia, koróziivzdorná oceľ, plazmová nitridácia, korózia, bodová a jamková korózia

1. ÚVOD

Korózia je bežný samovoľný jav, ktorý je vidieť všade na svete. Je to dej, pri ktorom materiál degraduje vplyvom vonkajšieho prostredia a stráca svoje mechanické aj fyzikálne vlastnosti. Tento dej sa dá spomaliť, nie však zastaviť a to pomocou rôznych povlakov (niklovanie), použitím vhodných materiálov (nehrdzavejúce ocele) alebo chemicko-tepelným spracovaním ako je napríklad nitridovanie, ktoré slúži na zlepšenie tvrdosti a odolnosti voči opotrebeniu.

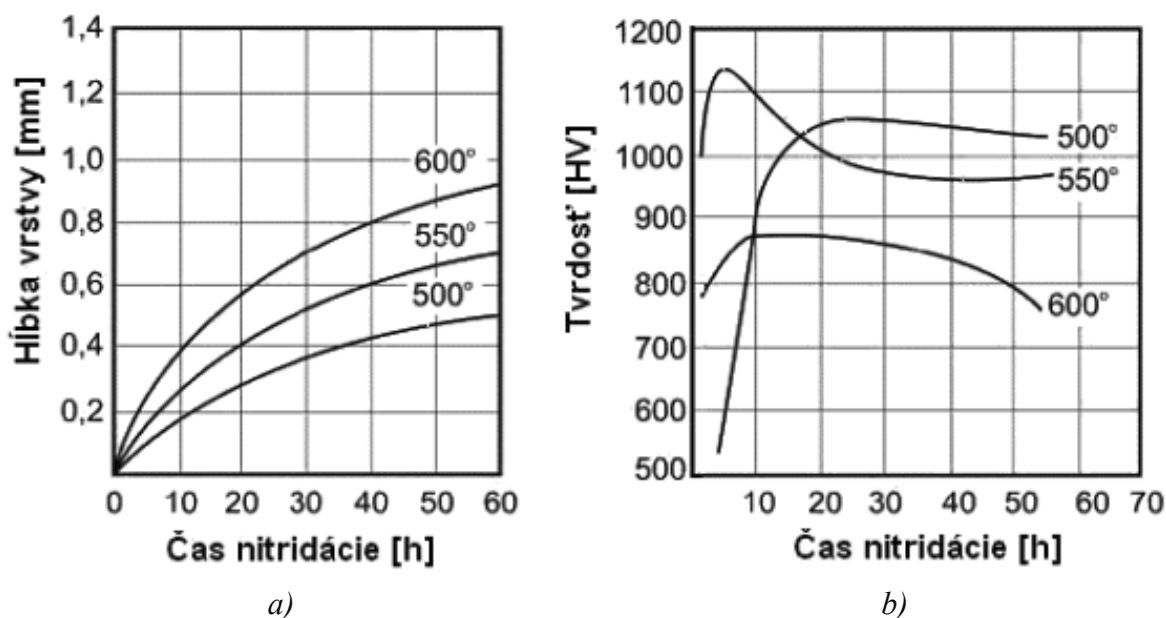
V tomto článku je vysvetlený pojem nitridovania a prehľad rôznych metód nitridácie. Osobitná pozornosť je venovaná plazmovej nitridácii, ktorou budú ošetrené vzorky v rámci experimentálnej časti projektu. Plazmová nitridácia je široko využívaná v priemysle, vrátane potravinárskeho a automobilového odvetvia.

2. NITRIDOVANIE

Nitridovanie je jedným z procesov chemicko-tepelného spracovania, ktorého podstata je v nasýtení povrchov ocelí a liatin dusíkom. Dusík, ktorý prenikne do ocele vytvára od určitej teploty nitridy v povrchovej vrstve a tým zlepšuje jej povrchovú tvrdosť. Nitriduje sa v kvapalnom alebo plynnom prostredí a pomocou plazmy [1].

Počas nitridácie v plyne atomárny dusík vznikne termickou disociáciou čpavku na nasycovacom povrchu [2]. Nitridy legujúcich prvkov a aj nitridy železa sa vytvárajú vďaka dusíku. Nitridácia v soľnom kúpeli sa vykonáva v zmesiach kyanátov a kyanidov ich následným

rozkladom. V rámci posledných rokov sa začala využívať plazmová nitridácia, ktorá začala používať ionizovaný dusík získaný elektrickými výbojmi.



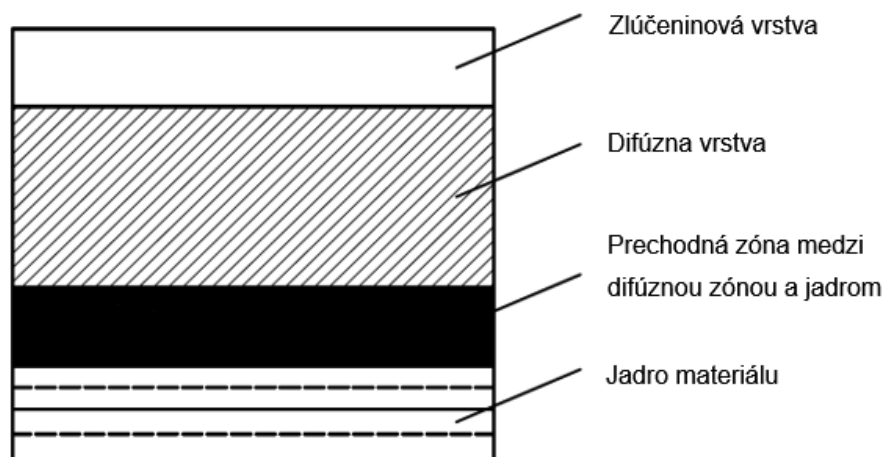
Obr. 1 Závislosť hrúbky a) a tvrdosti b) nitridovanej vrstvy od času pre rôzne teploty nitridácie
 Figure 1. Dependence of the thickness a) and hardness b) of the nitrided layer on time for different nitriding temperatures

O nitridovaní hovorí norma STN ISO 42 0004. Pri nitridovaní nie je hlavným prvkom uhlík, ako pri iných tepelných spracovaniach ocelí, ale hlavným prvkom je dusík [3]. Atomárny dusík má schopnosť prenikať cez absorpčnú vrstvu nitridov, pri zvýšenej teplote mriežky kovu a difundovať ďalej do ocele. Dusíka je vo vzduchu 80 %, ale tento dusík je v podobe dvojatómových molekúl a zlučuje sa veľmi problematicky s ťažkými kovmi [3]. Dusík, ktorý difunduje do povrchovej vrstvy ocele zlepšuje tvrdosť hlavne pri oceliach obsahujúcich hliník a chróm.

Po nitridovaní už nenasleduje žiadne ďalšie tepelné spracovanie.

Základnými faktormi, ktoré majú vplyv na výsledky nitridácie sú zloženie ocele, čas a teplota nitridácie a tiež tepelné spracovanie pred ňou. Teplota pri nitridácii sa pohybuje pri bežnom procese pri teplote pod A_{c1} v intervale 470 - 580 °C s dĺžkou trvania od 12 - 95 hodín, čo vedie k nadmernej spotrebe energie a nízkej efektívnosti výroby v priemyselných aplikáciách [1]. Preto sa skrátenie doby spracovania a zlepšenie účinnosti nitridácie stáva hlavnou výzvou pre povrchových inžinierov a výskumníkov [4]. V súčasnosti sa najčastejšie volí časový rozsah 24 - 72 hodín (obr. 1).

Nitridovaná oceľ odoláva veľmi dobre únavovým lomom, pretože únavový lom vzniká až pod vrstvou a prípadné povrchové chyby nemajú v dôsledku nitridovania žiadny vplyv na únavu komponentov [5]. Povrchová vrstva sa skladá z dvoch hlavných štruktúrnych častí: bielej (zlúčeninovej) vrstvy a difúznej vrstvy (obr. 2).

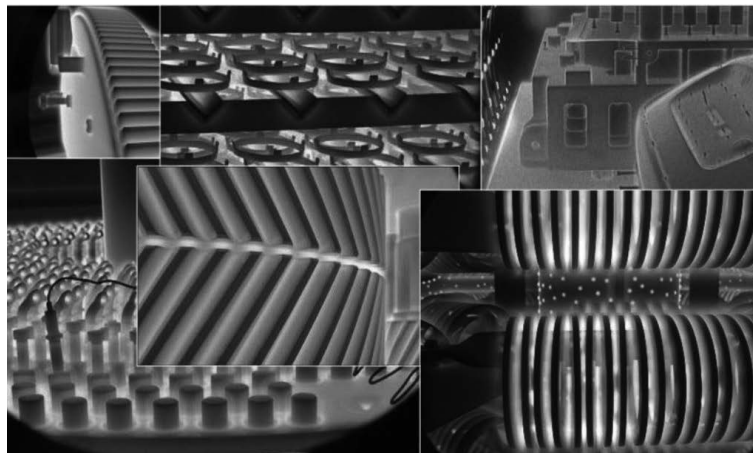


Obr. 2 Znáznornenie zloženia nitridovanej vrstvy
 Figure 2. Illustration of the composition of the nitrided layer

2.1 Plazmová nitridácia

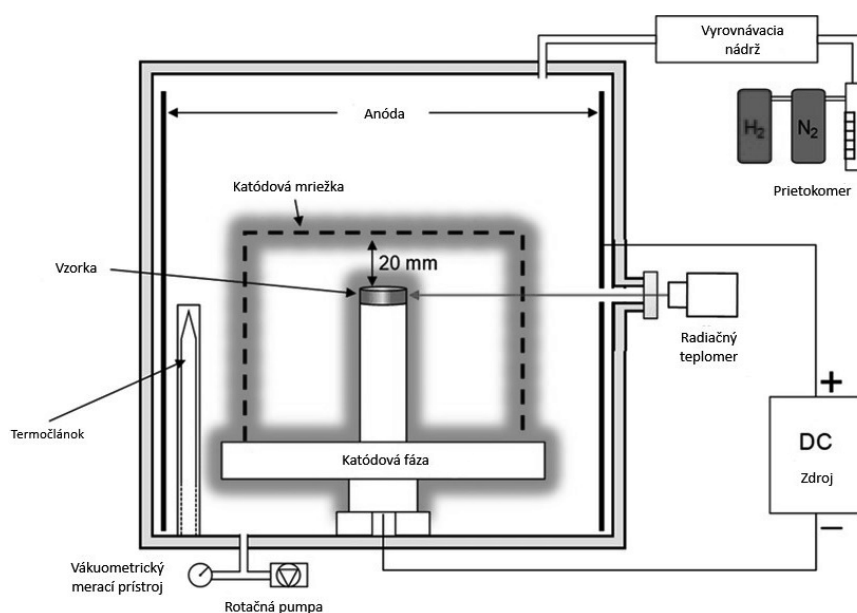
Plazmová nitridácia sa vykonáva v plazme, teda v ionizovanom plyne, ktorý obsahuje ióny a elektróny generované pri kolíziách neutrálnych častíc s elektrónmi. Je podmienená prítomnosťou atomárneho dusíka na povrchu materiálu [6]. Súčiastky sú vložené izolovane vo vákuovej nádobe (recipiente) a zapojené ako katóda. Recipient je zapojený ako anóda. Pri procese nitridácie je potrebné udržiavať tlak zriedenej zmesi plynov NH_3 , NH_3+N_2 , N_2+H_2 v rozpätí 0,1 - 1,5 kPa [1]. Medzi anódou a katódou musí byť vysoké napätie 400 - 1000 V.

V dôsledku vytvoreného elektrického poľa dochádza k ionizácii a štiepeniu plynnej atmosféry na plazmu. Kladné ióny s vysokou kinetickou energiou dopadajú na katódu (obr. 4). Kinetická energia sa pri náraze mení na tepelnú, čo spôsobuje zahrievanie nitridovaných komponentov. Plazmová nitridácia sa bežne vykonáva pri teplotách v rozpätí 500-600°C. Nečistoty sa z povrchu súčiastky odstránia iónovým bombardovaním po uplynutí nastaveného času nahrievania a tlakovania nádoby. Súčiastky počas nitridácie majú fialovú farbu (obr. 3).



Obr. 3 Vzhľad súčiastok počas plazmovej nitridáci
 Figure 3. Appearance of components during plasma nitriding

Aby mali častice plynu dostatok kinetickej energie na zrážku so súčiastkou, plazmové procesy prebiehajú vo vákuu, vďaka ktorému majú súčiastky malé deformácie a dosahuje sa vyššia rýchlosť nasycovania a proces má žiaduce účinky na ochranu životného prostredia a vysokú mieru ekonomickosti [7]. V rámci procesu nitridácie plyny reagujú s časticami ocele a vytvárajú vrstvu odolnú voči opotrebeniu. Táto vrstva môže pozostávať z gama (γ) primárneho Fe_4N (nitrid železa) alebo epsilon (ϵ) Fe_{2-3}N (nitrid železa) v závislosti od podielu každého plynu v % v danom prostredí. Okrem zvýšenia odolnosti voči oteru, sa vylepšuje aj únavová pevnosť a znižuje koeficient trenia. Cyklus prebieha 2 - 72 hodín, obvykle dosiahne vrstva 0,0508 - 0,6096 mm. Nízkoлегované ocele sa všeobecne spracovávajú dlhšiu dobu [8].



Obr. 4 Schéma procesu plazmovej nitridácie

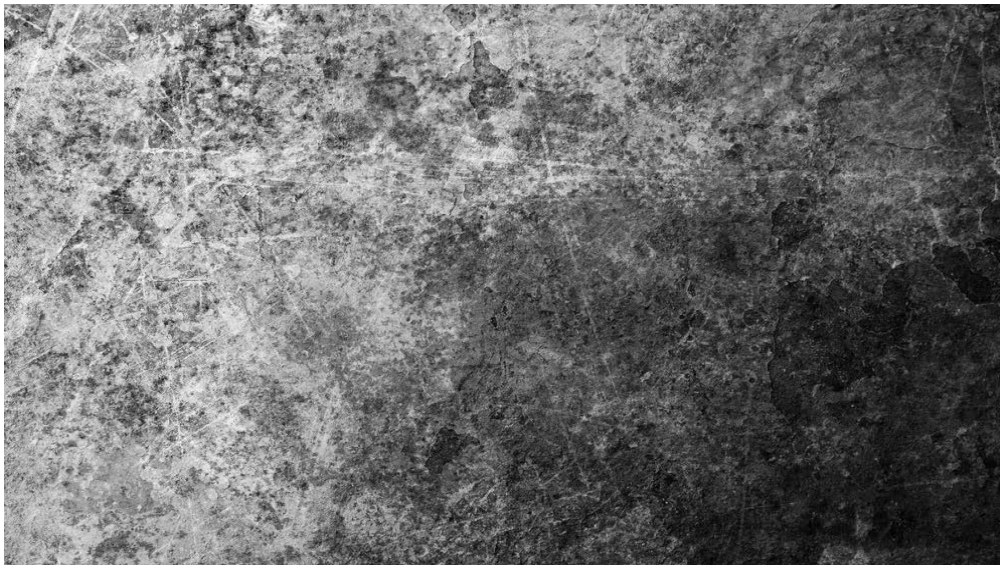
Figure 4. Scheme of the plasma nitriding process

3. KORÓZIA

Pod pojmom korózia si predstavujeme nežiadúce interakcie materiálu a prostredia, ktoré samovoľne vedú k postupnému zhoršeniu alebo až úplnej strate ich pôvodných vlastností u kovov, nekovových organických alebo anorganických materiálov [9, 10]. Korózia predstavuje postupnú degradáciu materiálu vplyvom životného prostredia, vedúcu k trvalým zmenám v jeho mechanických, chemických a fyzikálnych vlastnostiach. Korózii pomáhajú k vzniku agresívne prostredia, ktoré pôsobia fyzikálno-chemicky alebo chemicky a znehodnocujú materiál [9, 10]. Do okruhu korózie zaraďujeme aj deje, ktoré vedú k narušeniu materiálu, pri ktorých má kľúčový význam pôsobenie chemických procesov.

Korózia vzniká v kvapalných, plynných a aj dokonca tuhých prostrediach, ktoré sú denne vystavené rôznym environmentálnym faktorom. Znaky korózie sa preukazujú vzhľadom, rozmerovými a hmotnostnými úbytkami dosahujúcimi hodnotu 1-5% celkovej hmotnosti, pevnosťou, zmenou štruktúry materiálu [11].

V užšom zmysle sa korózia týka len kovových materiálov. Najznámejšia forma korózie je hrdzavenie. Keď dôjde k hrdzaveniu, kovový povrch sa pokryje charakteristickou oranžovo-hnedou škvrnou (obr. 5).



Obr. 5 Korózia na oceleovej platni
Figure 5. Corrosion of steel plate

Koróziu môžeme rozdeliť podľa mechanizmu na chemickú a elektrochemickú (obr. 6), podľa vzhľadu na rovnomernú a nerovnomernú. Poznáme aj rozdelenie podľa rozhodujúceho korózneho činiteľa na koróziu pod napätím a na únavovú koróziu.



Obr. 6 Schéma rozdelenia korózie
Figure 6. Corrosion distribution diagram

3.1 Chemická korózia

Chemická korózia je porušenie kovových materiálov vplyvom chemického pôsobenia vonkajšieho nevodivého prostredia. Najčastejšie sa prejavuje pôsobením suchých plynov, produktov horenia a v kvapalných neelektrolytoch, ako sú benzín a nafta [12]. Je heterogénnou chemickou reakciou kvapalného alebo plyného prostredia s kovmi. Pri tomto druhu korózie vzniká na fázovom rozhraní kov - korózne prostredie vrstva korózných spodín nového chemického zloženia [10]. Dané vlastnosti závisia od teploty, štruktúry kovu, chemického zloženia, stability (rozkladajú sa alebo sú stabilné) a objemu spodín, ktoré zapríčiňujú ďalší priebeh korózie povrchu kovu, pretože chránia, resp. nechrania povrch pred ďalším priebehom korózneho procesu. Najrozšírenejšou chemickou koróziou, je korózia plynmi (oxidačne alebo redukčne pôsobiacimi), obvykle pri vysokých teplotách. Hlavným faktorom ovplyvňujúcim rýchlosť korózie v plynach je homogenita vrstvy spodín [10]. Difúzia je často rozhodujúca pri vzniku hrubých vrstiev korózných spodín.

3.2 Elektrochemická korózia

Elektrochemická korózia je narušenie kovových materiálov vplyvom vzájomného elektrochemického pôsobenia s okolitým elektricky vodivým prostredím [9]. Hlavným predpokladom je vytvorenie tzv. katódových a anódových miest na kove, ktorý koroduje, preto jej vytvorenie je závislé od vonkajších a vnútorných faktorov kovu. Prebieha pri spoločnom pôsobení kovov s vodou, elektrolytmi, vlhkým vzduchom, kyselinami, roztavenými soľami a lúhmi a vodnými roztokmi soli. Elektrochemická korózia je závislá od pravidiel elektrochemickej kinetiky. Elektrický prúd je vytvorený pri korózne reakcii a veľká časť elektrického prúdu sa premieňa na teplo. Vodivým spojením dvoch kovov v koróznom prostredí sa môže vytvoriť korózny makročlánok [9]. V danom prípade sa anódová reakcia vzťahuje na menej ušľachtilý kov, avšak nie je možné vylúčiť jej priebeh na oboch kovoch.

Koróziu rozdeľujeme na rôzne druhy. Druhy a tvary korózneho napadnutia zistené na metalografickom výbruse sa porovnávajú so schémami normy STN 03 8137, slúžiacej k metalografickému vyhodnocovaniu korózneho napadnutia kovov [13].

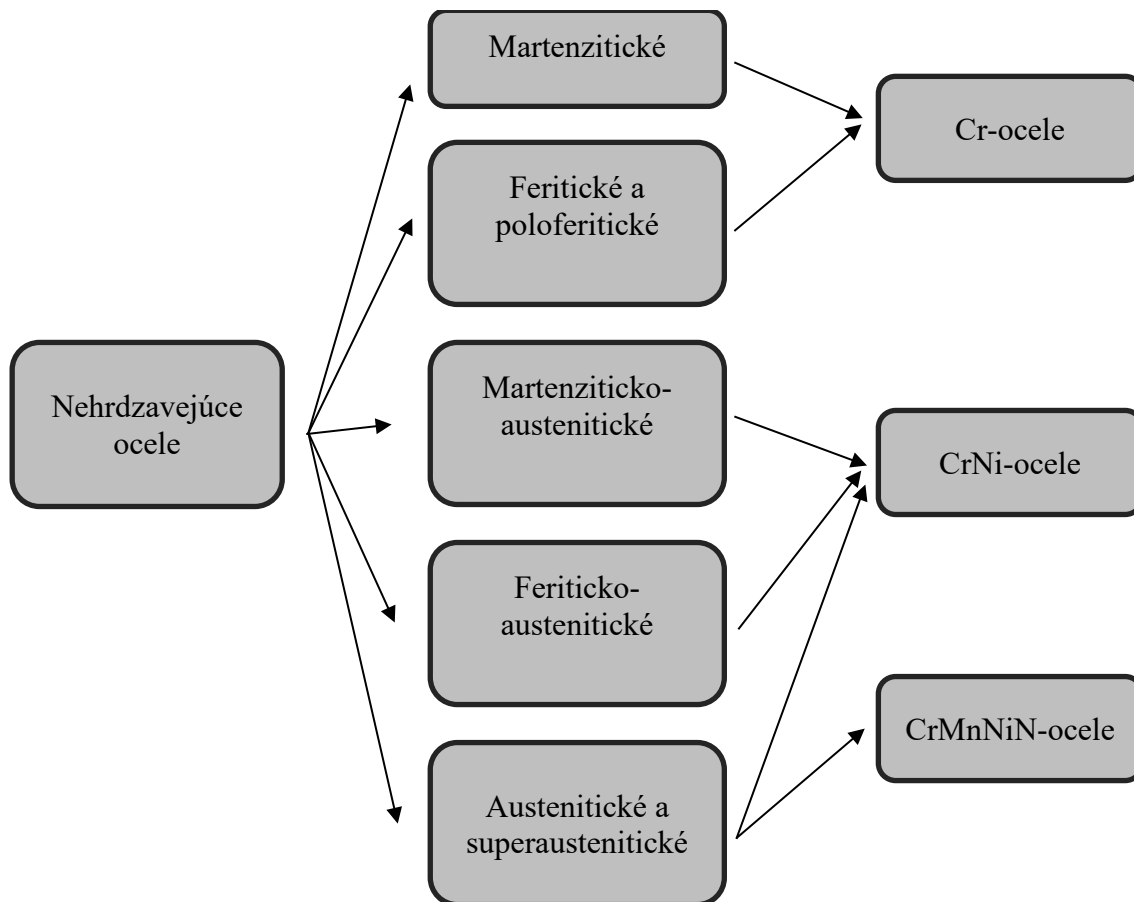
4. NEHRDZAVEJÚCA OCEĽ

Nehrdzavejúca oceľ (slangovo nerez, nerezová oceľ alebo nehrdzavejúca oceľ) je vysokolegovaná oceľ so zvýšenou odolnosťou voči chemickej aj elektrochemickej korózii. Korózna odolnosť je založená na schopnosti tzv. pasivácie povrchu železa. Nehrdzavejúce ocele sa zaraďujú do triedy 17. Skladajú sa aspoň z 11,5 % chrómu a vrchnou hranicou chrómu 30 % [11]. Chróm poskytuje odolnosť voči korózii a tvorí ochrannú oxidačnú vrstvu na povrchu ocele. Tvorbu pasivačnej vrstvy podporuje aj nikel, ktorý súčasne zvyšuje odolnosť proti redukčným kyselinám. Molybdén zvyšuje odolnosť proti bodovej korózii a proti pôsobeniu chloridov.

Nehrdzavejúce ocele rozdeľujeme podľa štruktúry do rôznych skupín (obr. 7). Podľa chemického zloženia sú to ocele chrómové, chrómnikové a chrómmangánové, ktoré môžu obsahovať ešte ďalšie zliatinové prvky ako molybdén, kremík, meď, titán, niób, dusík a pod.

Jednou z kľúčových vlastností nehrdzavejúcej ocele, ktorá zabezpečuje jej rozsiahle využitie, je schopnosť odolávať korózii. Odolnosť nehrdzavejúcej ocele voči korózii je úzko spojená s tvorbou povrchovej pasívnej vrstvy, čo je tenká, rovnomerná a stabilná vrstva oxidu chrómu na

povrchu materiálu [10]. Vytvorenie a vlastnosti tejto pasívnej vrstvy sú posilnené zvýšením obsahu chrómu a pridaním ďalších prvkov, ako sú molybdén a dusík.



Obr. 7 Rozdelenie nehrdzavejúcich ocelí podľa štruktúry a legujúcich prvkov
Figure 7. Classification of stainless steels according to structure and alloying elements

POĎAKOVANIE

Príspevok vznikol v rámci riešenia spoločného slovensko-poľského projektu Project Based Learning ako výsledok spolupráce medzi Politechnikou Slaskou, Gliwice a Žilinskou univerzitou v Žiline a projektov KEGA č. 004ŽU-4/2023 a KEGA č.009ŽU-4/2023.

BIBLIOGRAFIA

1. GÁBRIŠOVÁ Z. a BRUSILOVÁ A., Tepelné spracovanie – Návod na cvičenia, 2019 https://www.sjf.stuba.sk/buxus/docs/docs/edicne/el_publ/Gabrisova__Brusilova_Tepelne_spracovanie_Navody_na_cvicenia_na_CD_1.pdf.
2. PULC, V., HRNČIAR, V., GONDÁR, E. Náuka o materiáli. 1.vyd. Bratislava: [1] <http://www.sjf.tuke.sk/inmf/NW/moznosti/nitridovanie.html>.

3. ZÁBAVNÍK V. a BURŠÁK M., Materiál, tepelné spracovanie, kontrola kvality. Strojnícka fakulta TU Košice 2004. ISBN 80-8073-159-4.
4. WANG B., SUN S., GUO M., JIN G., ZHOU Z., FU W., Surface and Coatings Technology. Study on pressurized gas nitriding. 2015. 60-64, volume 279 .
5. TOTTEN G., Steel heat treatment, 200.6
6. IŽDINSKÁ Z., Nitridovanie Strojnícka fakulta STU. 2011.
7. PALCUT M. a ŠPOTÁK M., Otázky a odpovede. 2014.
8. KORECKÝ et al. 1951. NITRIDOVANÍ POVRCHOVÉ TVRZENÍ OCELI DUSÍKEM. PRAHA. 2018 ISBN 658.153 :[338.45 (47)].
9. HADZIMA, B. – LIPTÁKOVÁ, T., 2008. Základy elektrochemickej korózie kovov, Žilina, EDIS, ISBN 978-80-8070-876-4.
10. LIPTÁKOVÁ T., Bodová korózia nehrdzavejúcich ocelí. 2009 .
11. SKOČOVSKÝ P., BOKUVKA O., KONEČNÁ R. a TILLOVÁ E.: Náuka o materiáli pre odbory strojnícke. 2006. ISBN 80-8070-593-3.
12. ŠVAČ V. a KOVÁČ J., 2009. Korózia kovov a protikorózna ochrana. 2012.
13. KUCHARIKOVÁ L., TILLOVÁ E. a BELAN J., Kontrola kvality materiálov, Návody na cvičenia. 2021. ISBN 978-80-554-1782-0.



31th January 2025
Gliwice, Poland

DEPARTMENT OF ENGINEERING MATERIALS AND BIOMATERIALS
FACULTY OF MECHANICAL ENGINEERING
SILESIA UNIVERSITY OF TECHNOLOGY

INTERNATIONAL STUDENTS SCIENTIFIC CONFERENCE

Predictive Maintenance on Medium Voltage Cable Production Extrusion Machine

¹Cemal Meran, ²Berranur Ceker, ²Sezai Kunan, ²Murat Mat, ³Koksal Ilhan

¹Prof.Dr., Pamukkale University, Faculty of Engineering, Department of Mechanical Engineering, Denizli, Turkey,
cmeran@pau.edu.tr

²Student, Pamukkale University, Faculty of Engineering, Department of Mechanical Engineering, Denizli, Turkey

³Nexans Turkey Industry, R&D Center, Denizli, Turkey

Abstract: Maintenance techniques and applications are becoming increasingly significant in enhancing the efficiency of industrial production processes and ensuring uninterrupted operations. Failures in machinery lead to production downtime and disruptions, which increase operational costs and negatively impact a company's reputation. In this study, predictive maintenance practices were implemented on an extruder machine used in a cable production line. After initial measurements, detailed analyses and calculations were performed, leading to the replacement of faulty machine components and the completion of maintenance procedures. Subsequent measurements revealed the positive effects of the maintenance on the machine's efficiency and performance. Additionally, the costs and environmental impacts of the maintenance process were evaluated, examining its economic and ecological benefits through cost analysis and carbon footprint calculations. The findings of this study demonstrate that predictive maintenance plays a crucial role in extending machine life and reducing energy consumption.

Keywords: Predictive maintenance, vibration analysis, spectrum form, wave form.

1. INTRODUCTION

The main purpose of this study is to demonstrate that predictive maintenance offers a more rational, efficient, and cost-effective alternative compared to traditional breakdown-based and periodic maintenance strategies. Unexpected machine failures in industrial settings lead to high costs and production losses, causing disruptions in operational processes. Therefore, the development and optimization of maintenance strategies are critical not only for reducing costs but also for achieving environmental sustainability goals.

This study aims to systematically integrate predictive maintenance practices into extruder machines used in cable production. In the initial phase, the current condition of the machines will be identified through parameters such as vibration, temperature, and electrical

consumption, while potential failure sources—such as imbalance, mechanical looseness, and coupling misalignment—will be analyzed. The collected data will be thoroughly examined using spectrum analyses and waveform interpretations, enabling the early detection of abnormalities and potential failures in the machines.

These analyses will not only assess the condition of the machines but also contribute to the optimization of maintenance planning. Additionally, periodic measurements will facilitate trend analyses and electrical energy consumption calculations, enabling the monitoring of changes in machine performance.

The study aims to demonstrate the effectiveness of predictive maintenance practices and contribute to reducing the carbon footprint. By promoting early intervention and planned maintenance processes, it seeks to enhance production efficiency and help businesses maintain their competitive edge.

2. PREDICTIVE MAINTENANCE

The predictive maintenance approach is a strategy that enables intervention in systems by monitoring and analyzing potential failures before they occur. This approach predicts the timing of failures using specific monitoring methods, minimizing the need to replace parts before they break down. As a result, it reduces spare parts and inventory costs. Predictive maintenance aims to minimize downtime caused by failures, thereby reducing production losses.

The advantages of predictive maintenance include minimizing maintenance costs, extending the operational lifespan of machinery, maximizing machine efficiency rates, and preventing unplanned downtime and failures. Let us illustrate several studies from the literature on predictive maintenance as an example.

Aydın and Meran (2018), predictive maintenance methods applied in cement plants, the devices used, and field application examples were detailed. Weekly vibration measurements were carried out using mobile measurement devices, particularly on critical equipment such as the Rotary Kiln-1 Flue Gas Fan. During the periodic measurement on June 2, 2017, changes were observed in the bearing measurement trends of the flue gas fan. Spectrum measurements on the motor-side bearing revealed the formation of peak and harmonic frequencies corresponding to the bearing outer race failure frequency. Upon examining the demodulation graphs, it was clearly demonstrated that damage development had begun in the outer race of the bearing. [1]

Saleem et al. (2012), the concept of "Deformation Shape of the Shaft" (DSS) was used to detect imbalance in the rotating components of a rotor machine. They demonstrated that changes in the deformation shape indicate the presence of imbalance in the shaft. To conduct the study, tests were carried out on a machine fault simulator under various imbalance conditions. As a result, it was concluded that imbalance in rotor machines causes a significant increase in vibration, which occurs due to the rise in centrifugal force. [2]

Özbay (2002) studied a system consisting of a motor, coupling, disc, and bearing. Under normal operating conditions of the system, he collected vibration values at specified measurement points and then created artificial faults in the experimental setup to take measurements again at those points. In his comparisons, he observed that the vibration values increased as expected. [3]

3. MATERIAL AND METHODS

In line with the scope of the study, detailed performance measurements of the machine were conducted both before and after maintenance. Maintenance activities were carried out based on the identified faults. The measurements were taken in radial (vertical and horizontal) and axial directions while maintaining constant motor speeds. The measurement directions and locations are shown in Figure 1. These data were analysed to compare the machine's condition before and after maintenance. The motor speeds were determined by considering the operational limits and speeds used in the factory's production processes, ensuring that measurements were conducted under consistent parameters. This approach enabled a more accurate evaluation of the maintenance activities' impact on machine performance and provided valuable insights for preventing potential efficiency losses in the production process.

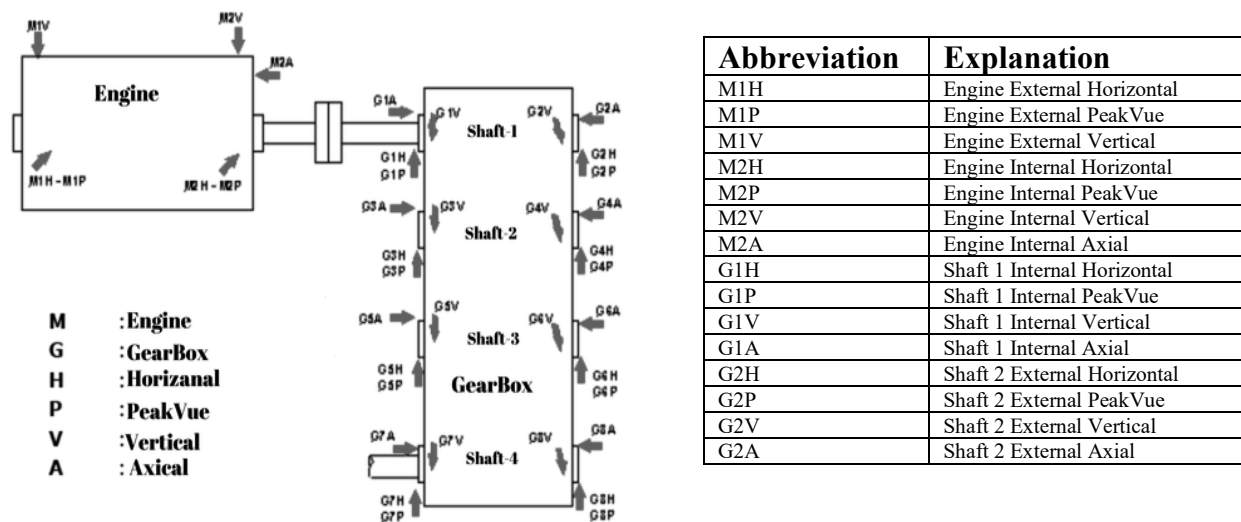


Figure 1. Schematic representation of the measurement directions (M: Engine (Motor), G: Gear, H: Horizontal, V: Vertical, A: Axial, P: PeakVue)

In our study, the machine used is the IK 34 main extruder, located at the Nexans factory and employed in cable production. It is primarily responsible for producing the outer sheath or insulation material of the cable. The main extruder processes the primary plastic coating material, which protects the cable from external factors and provides electrical insulation. The machine and its components are illustrated in Figure 2.

As shown in Figure 3, the initial vibration measurements were conducted with the SKF Microlog GX series CMXA 70 analyzer. The SKF Microlog GX analyzer was used for initial measurements to collect data from machinery and equipment. The device supports two-channel, multi-route, or non-route data collection. It was preferred in our factory due to its ease of use and performance. With its FFT analyzer, it enables easy spectral/phase measurements. It allows fast data collection in the field for FFT spectrum and phase measurements. [4]

The second vibration measurements were performed using the Emerson AMS 2140 analyzer, as shown in Figure 4. The AMS 2140 analyzer was used for second measurements to

collect vibration data and perform analysis on machinery and equipment. The AMS 2140 features simultaneous four-channel plus phase data collection and peak detection capabilities, which serve as the earliest indicators of bearing and gearbox degradation.

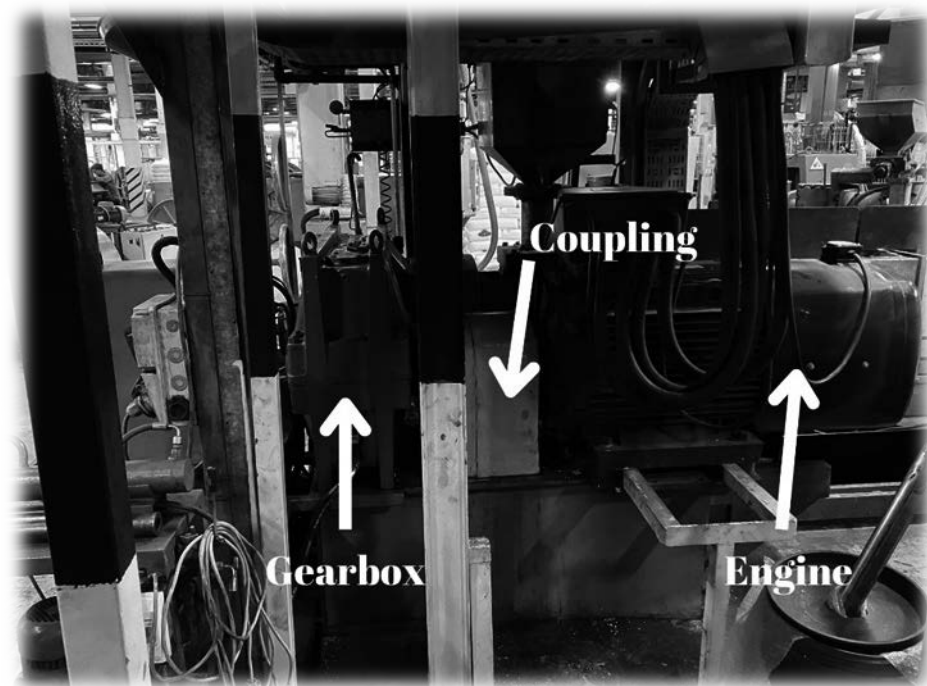


Figure 2. Machine area where the measurements were made



Figure 3. SKF Microlog GX seriesi CMXA70



Figure 4. Emerson AMS 2140

4. RESULTS AND DISCUSSION

The first measurements were taken before maintenance, the second measurements were taken after maintenance and they are compared. The measurements and comparison are presented in *Table 1*. In the measurements taken before and after maintenance, care was taken to ensure that measurements were conducted under the same conditions in order to maintain the consistency of the measurement points and the motor operating speeds. Analysis of the results of the first measurements revealed high amplitude values in the bearings and gears of the first bearing (*figure 5*). Based on this observation, it was determined that maintenance actions

should be carried out during the first scheduled downtime to ensure the sustainability of machine performance and improve efficiency.

During the planned maintenance, which involved stopping the machine, the accuracy of the signals obtained upon opening the bearing covers was verified. The inspection revealed damage to the bearings and fractures in the input gear. The bearings were replaced, and since the input gear is an integral part of the shaft (integral gear), its replacement was postponed to a later maintenance period.

Following the maintenance, the second set of measurements showed a significant reduction in the amplitude values. However, since the input gear was not replaced, the current condition of the gear continued to cause the amplitude values to remain at elevated levels. Replacing the gear is expected to further reduce these high amplitude values and ensure the efficient operation of the machine.

Machine ID	Measurement ID	Date of 1st Measurement	Date of 2nd Measurement	1st Measurement values	2nd Measurement values
İK34	M1H	10.10.2024	30.11.2024	1,924 mm/s	1,219 mm/s
İK34	M1V	10.10.2024	30.11.2024	0,960 mm/s	0,677 mm/s
İK34	M2H	10.10.2024	30.11.2024	1,813 mm/s	1,265 mm/s
İK34	M2V	10.10.2024	30.11.2024	1,799 mm/s	1,356 mm/s
İK34	M2A	10.10.2024	30.11.2024	1,459 mm/s	,917 mm/s
İK34	G1H	10.10.2024	30.11.2024	3,047 mm/s	,878 mm/s
İK34	G1V	10.10.2024	30.11.2024	4,377 mm/s	1,296 mm/s
İK34	G1P	10.10.2024	30.11.2024	3,244 G's	0,038 G's
İK34	G1A	10.10.2024	30.11.2024	2,197 mm/s	1,325 mm/s
İK34	G2H	10.10.2024	30.11.2024	1,803 mm/s	1,084 mm/s
İK34	G2V	10.10.2024	30.11.2024	2,291 mm/s	1,186 mm/s
İK34	G2P	10.10.2024	30.11.2024	2,216 G's	0,373 G's
İK34	G2A	10.10.2024	30.11.2024	1,880 mm/s	1,231 mm/s
İK34	G3H	10.10.2024	30.11.2024	2,120 mm/s	1,110 mm/s
İK34	G3V	10.10.2024	30.11.2024	1,939 mm/s	1,071 mm/s
İK34	G3A	10.10.2024	30.11.2024	1,264 mm/s	1,211 mm/s
İK34	G4H	10.10.2024	30.11.2024	2,236 mm/s	0,835 mm/s
İK34	G4V	10.10.2024	30.11.2024	3,223 mm/s	0,759 mm/s
İK34	G4A	10.10.2024	30.11.2024	1,823 mm/s	2,044 mm/s

Table 1. The vibration measurement test results

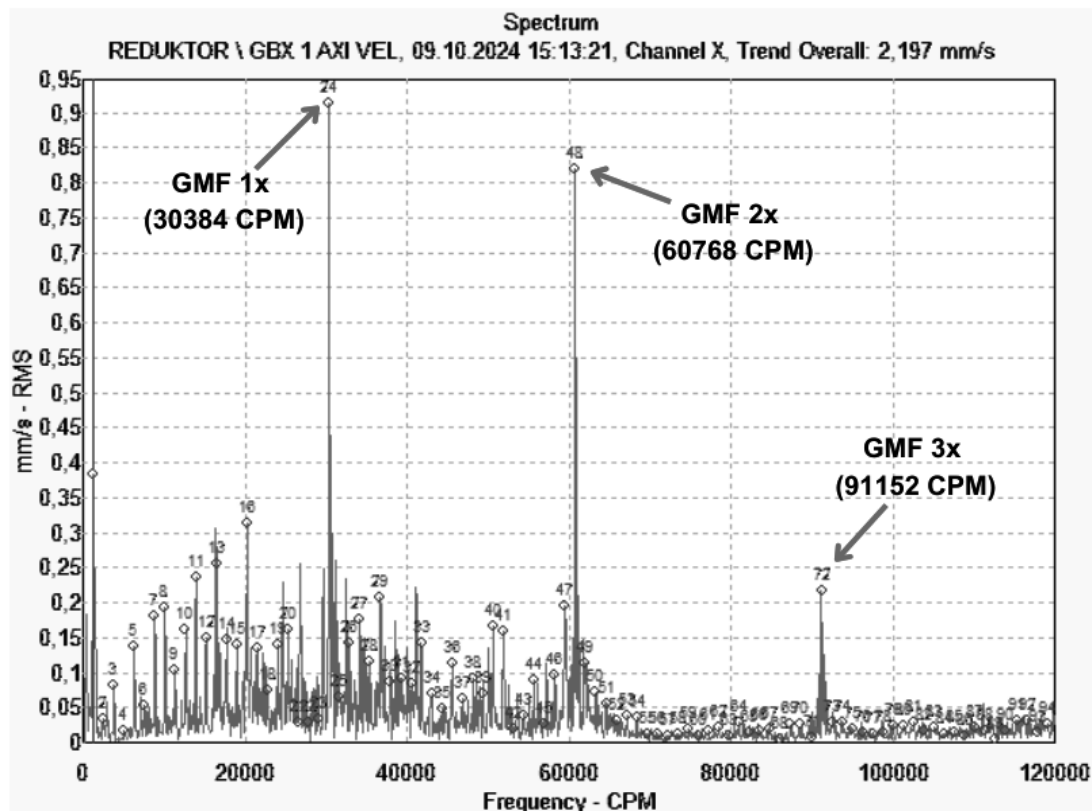


Figure 5. The spectrum graph for first measurements taken on the gearbox

Following the initial measurements, it was determined that the measurement values of our machine were above the standard values. Detailed analyses and calculations led to the conclusion that the gear on the input shaft of the gearbox might be broken and the bearing cage could be disintegrated. Based on these findings, a maintenance plan was created, and the machine was stopped for the necessary maintenance work. After the maintenance, verification procedures were carried out, and the analyses were confirmed to be correct, as verified by the images shown in Figure 6. and Figure 7.



Figure 6. Broken gear



Figure 7. Damaged bearing cage

After the maintenance, the repeat measurements taken from the motor and gearbox data showed a significant decrease in the amplitude values (Table 1.). This development indicates that the maintenance work was effective and resulted in a substantial improvement in the overall system performance. However, since the gear is an integral gear, the gear replacement has not been carried out yet, and as a result, the broken signals persist. The gear replacement has been postponed to a later date as part of the planned maintenance strategy. On the other hand, after the bearing replacement, a notable reduction in the signals was observed, and some signals were completely eliminated. The spectrum and waveform graphs obtained from the second measurements are shown in Figure 8. This clearly demonstrates the effectiveness of the bearing replacement and the improvement in the system. The accuracy of the interventions has been further confirmed by monitoring the vibration levels and overall performance of the system. At the same time, the electricity consumption of the line was analyzed at the same line speeds before and after maintenance and is shown in Table 2.

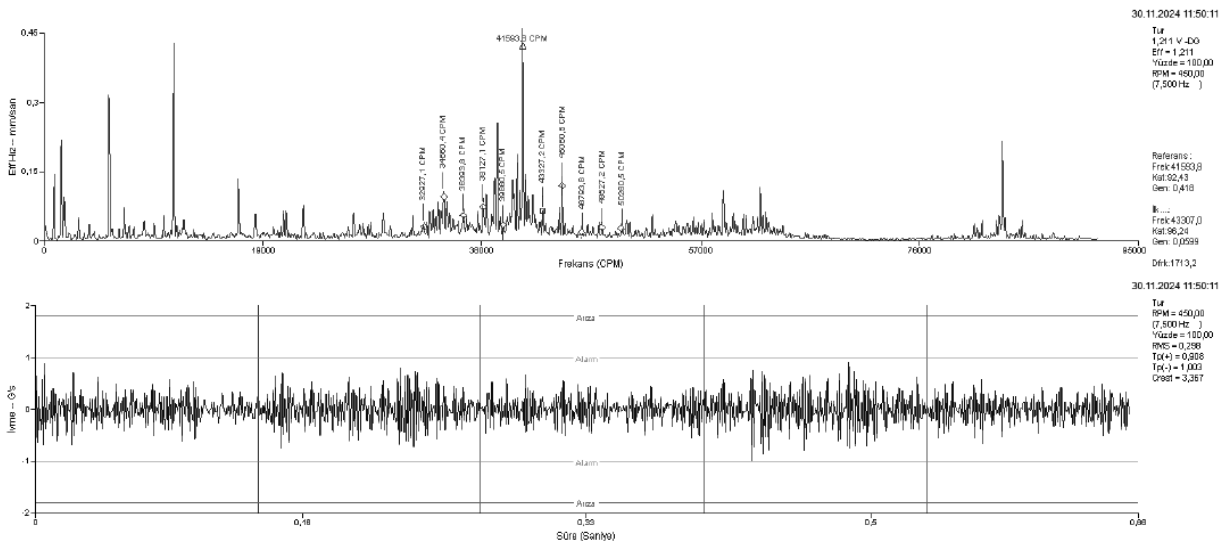


Figure 8. The spectrum and wave form graphs for second measurements on the gearbox

Table 2. Comparison of electricity consumption before and after maintenance

Line Speed m/min	Amper(A)		Engine revolution min ⁻¹	
	Before Maintenance	After Maintenance	Before Maintenance	After Maintenance
60	198,7	197,3	1266	1266

As can be seen from Table 2, although there are no significant differences in energy consumption before and after maintenance, when considering all the machines in the factory, it is clear that non-negligible values have emerged. These small differences can lead to significant energy consumption in large-scale production processes, resulting in substantial cost increases. Furthermore, this increased energy consumption contributes to higher fossil fuel use, which in turn increases the carbon footprint, causing a negative impact on the environment. In the long term, failure to prevent such waste can harm the company’s sustainability goals. Air pollution

may also worsen as a side effect of this increased energy consumption, posing serious threats to both the environment and public health. Therefore, implementing measures to increase energy efficiency not only reduces costs but also helps the company fulfill its environmental responsibility by reducing its environmental impact.

5. CONCLUSION

Many companies view the maintenance of machines used in production processes as an unnecessary cost and often prefer to postpone these tasks. However, maintenance not only ensures that machines operate efficiently and healthily, but also significantly contributes to improving product quality and preventing operational disruptions such as unexpected downtime. When maintenance is neglected, the continued operation of the system can lead to failures in other components of the machine and may also negatively affect production quality. Therefore, neglecting maintenance can result not only in machine failures but also in costly repairs and production interruptions.

Vibration analysis, one of the predictive maintenance techniques, has become an indispensable method for detecting and addressing machine faults at very early stages. In this study, through measurements taken before and after maintenance on our machine, the analysis and calculations conducted from the spectrum and waveform graphs obtained via vibration analysis are practically demonstrated on an extrusion machine in a cable production line. The key is to regularly monitor vibration amplitude trends, take measurements, and intervene beforehand based on this data, ensuring that limit values in standards are not exceeded. In this way, machines can operate healthily, allowing faults to be detected early, and preventing potential disruptions and costly repairs.

It should not be forgotten "What gets measured, gets managed." (Peter Drucker)

REFERENCES

- [1] Aydın, G., & Meran, C. (2018). *Çimento sektöründe kestirimci bakımla arıza teşhisi ve önlenmesi*. Mühendis ve Makina, 59(692), 48-67.
- [2] Saleem, A., Dıwakar, G., Satyanarayana, M.R.S., "Detection of Unbalance in Rotating Machines Using Shaft Deflection Measurement During Its Operation" IOSR Journal of Mechanical and Civil Engineering (IOSR-JMCE) ISSN: 2278-1684 Volume 3, Issue 3 P8-20, 2012
- [3] Özbay, A., "Predictive Maintenance and its Applications in Industry", Yüksek Lisans Tezi, Çukurova Üniversitesi Fen Bilimleri Enstitüsü, Adana, 99s, (2002).
- [4]Dereoğlu, F. (2020). Kağıt Üretim Sistemindeki Kurutucu Silindir ve Sirkülasyon Fanının Kestirimci Bakım Tekniği ile Arıza Takibi ve Titreşim Analiziyle Tespiti (Yüksek Lisans Tezi). Kocaeli Üniversitesi, Kocaeli



31th January 2025
Gliwice, Poland

DEPARTMENT OF ENGINEERING MATERIALS AND BIOMATERIALS
FACULTY OF MECHANICAL ENGINEERING
SILESIA UNIVERSITY OF TECHNOLOGY

INTERNATIONAL STUDENTS SCIENTIFIC CONFERENCE

Predictive Maintenance on Rod Break Down Machine

¹Cemal Meran, ²Aysenur Kabukcu, ²Dilruba Yavas, ²Mustafa Furkan Orha, ³Fatih Oztekin

¹Prof.Dr., Pamukkale University, Faculty of Engineering, Department of Mechanical Engineering, Denizli, Turkey, cmeran@pau.edu.tr

²Student, Pamukkale University, Faculty of Engineering, Department of Mechanical Engineering, Denizli, Turkey

³Nexans Turkey Industry, R&D Center, Denizli, Turkey

Abstract: Predictive maintenance aims to prevent unexpected breakdowns, reduce maintenance costs, and enhance production efficiency by continuously monitoring machines and predicting potential failures in advance. This strategy plays a critical role in increasing operational efficiency and extending equipment lifespan, particularly in the manufacturing sector.

In this study, predictive maintenance practices were carried out on a coarse wire drawing machine, selected as a pilot in the cable industry, through vibration analysis. The primary aim of the study was to assess the current condition of the machine and identify potential failures. Using vibration measurements, gear faults, mechanical looseness, and bearing defects were identified, with these issues being concentrated in the gearbox. The results were evaluated in accordance with ISO 10816-3 standards, and the applicability of predictive maintenance in the sector was examined in detail within this context.

Keywords: Predictive Maintenance, Vibration Analysis, Mechanical Looseness, Current Analysis

1. INTRODUCTION

In the cable production industry, with rapidly advancing technology and increasing energy demands, losses and breakdowns during the production process reduce machine efficiency, disrupt production workflows, and increase operational costs. Regular and effective maintenance is crucial to ensure that machines operate continuously and efficiently. Predictive maintenance stands out as a key strategy to meet this need, extending the lifespan of machines while ensuring they operate at maximum efficiency.

There are a limited number of studies on predictive maintenance of wire drawing machines in the literature. Novelo and Chu (2022) investigated the detection and prediction of mechanical failures through vibration analysis in a nut production factory in Taiwan. In their study, analytical techniques such as fast Fourier transform, empirical mode decomposition, and shock response spectrum were applied to a six-die nut production machine. The research demonstrated that optimizing maintenance schedules could enhance production volume and quality [1]. Alcelik and

Kam (2020) investigated the effects of vibration analysis on shaft bearing systems. According to the study's findings, misalignment increases vibration levels, leading to additional static and dynamic loads on the bearings, which in turn reduces system performance [2]. Ranieri et al. (2018) evaluated the applicability of vibration analysis in engine and transmission systems in a study conducted within the automotive sector. The results indicated that this method achieved an accuracy of over 85% in fault detection and reduced operational costs by 20% [3]. Martinez and Lopez (2017), in a study conducted at a textile factory, reported that predictive maintenance practices reduced the failure rate of weaving machines by 35% and decreased unplanned downtimes from 120 hours to 40 hours annually. This improvement resulted in annual savings of \$75,000 [4]. Bose and Sharma (2011) evaluated predictive maintenance practices in power plants through a study conducted on a 2 MW gas turbine. Cracks in the turbine blades were detected early using vibration analysis, resulting in savings of \$350,000. Additionally, the operational lifespan of the turbine was extended by 15% [5]. Peng and Chu (2004) examined the applicability of vibration analysis in high-cost systems such as wind turbines. Their findings revealed that vibration analysis plays a critical role in the early detection of rotor imbalance and gear failures, increasing system reliability by 25% [6].

Literature reviews indicate that predictive maintenance has been addressed across various industries, but studies focusing on wire drawing machines in the cable industry are limited. Therefore, this study aims to explore the potential benefits of applying predictive maintenance practices to wire drawing machines.

2. PREDICTIVE MAINTENANCE

It is a type of maintenance that evaluates the operational status of machinery and equipment, assesses the results of measurements and analyses, and takes necessary precautions and planning when adverse conditions are detected. In predictive maintenance, specialized devices are used to perform observations and measurements. By monitoring the condition of a machine or component and utilizing the collected data, this approach determines the most appropriate time for maintenance. This results in fewer downtimes, reduced labor and cost losses, and extended equipment lifespan, allowing for greater utilization. Since the cause of the failure is identified in advance with this method, less time is spent during maintenance. As intervention occurs before a machine breaks down, it can be reactivated without production halting or delays in deliveries. This method ensures better continuity in production processes.

Methods used in predictive maintenance include infrared thermography, oil analysis, ultrasonic monitoring, motor current monitoring, and vibration analysis. [7].

Vibration analysis identifies machine faults at the frequency level. Faults produce vibrations at specific frequencies, which can be used for fault detection. Imbalances cause increased vibrations at a frequency equal to the machine's rotational speed (1x). Gear faults generate distinct vibrations at multiples of the gear mesh frequency, depending on the number of gear teeth. Bearing faults, on the other hand, exhibit high-frequency vibrations, with damage to the inner or outer races causing vibration peaks at specific frequencies. Coupling misalignments typically manifest as increased vibrations at 2x or 3x the rotational frequency. By analyzing vibration data in this way, machine faults can be detected early, and maintenance needs can be identified in a timely manner.

3. MATERIAL AND METHODS

This study was conducted to implement predictive maintenance practices on the TC-10 coarse wire drawing machine located at Nexans Turkey Industry and Trade Inc.'s Denizli Cable Factory. The materials used included the TC-10 wire drawing machine and the Emerson AMS 2140 vibration measurement device. The TC-10 performs copper wire drawing, where an 8 mm diameter copper wire is reduced to as thin as 1.75 mm upon exiting the machine. The machine has 750 km/day production capacity, which translates to approximately 8.64 meters of wire being drawn per second. During the wire drawing process, the machine operates at a speed of 1518 rpm, drawing 217 amperes of current and requiring 265 kW of motor power. **Figure 1** shows the image of the wire drawing machine used for the measurements.



Figure 1. Rod copper break down machine

In this study, the focus area for measurements was the motor and gearbox section of the machine. **Figure 2** shows an image of the motor and gearbox. The mains frequency was fixed at 50 Hz, and all measurements were conducted at this constant frequency.

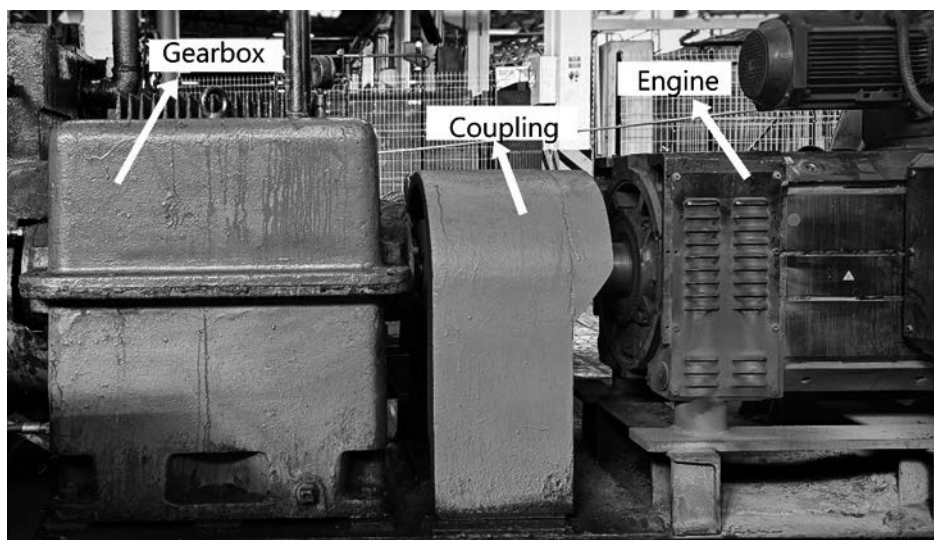


Figure 2. Gearbox and motor section of the measured TC-10 machine

Measurements were taken from a total of 16 different points, covering the radial (vertical and horizontal) and axial directions at the motor's input and output points as well as the gearbox's input and output points, to fully analyze the vibration behavior of the machine. The representation of these points on the system is shown in **Figure 3**.

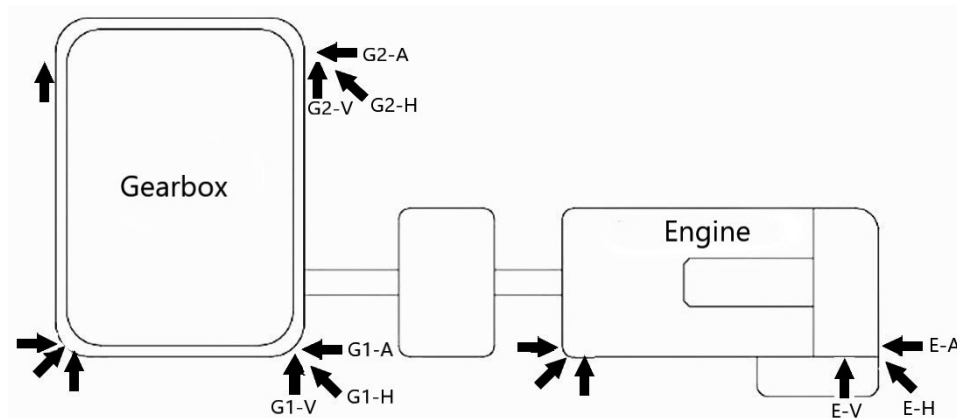


Figure 3. Vibration measurement points. A: axial V: vertical H: horizontal G: gearbox E: engine

The collected data was analyzed using PeakVue Technology, developed by Emerson. PeakVue is an advanced vibration monitoring method that enables rapid and reliable analysis of the health status of rotating machinery. Unlike traditional vibration analysis, which typically focuses on RMS (root mean square) values of the signal, PeakVue analyzes the peak values of the signal. This approach allows for a clear detection of sudden impacts or irregularities, making it particularly effective in identifying mechanical issues, lubrication deficiencies, or wear in rotating equipment such as bearings, gears, and pumps. **Figure 4** illustrates the moment of measurement at the horizontal axis of the gearbox's input section using the vibration measurement device.

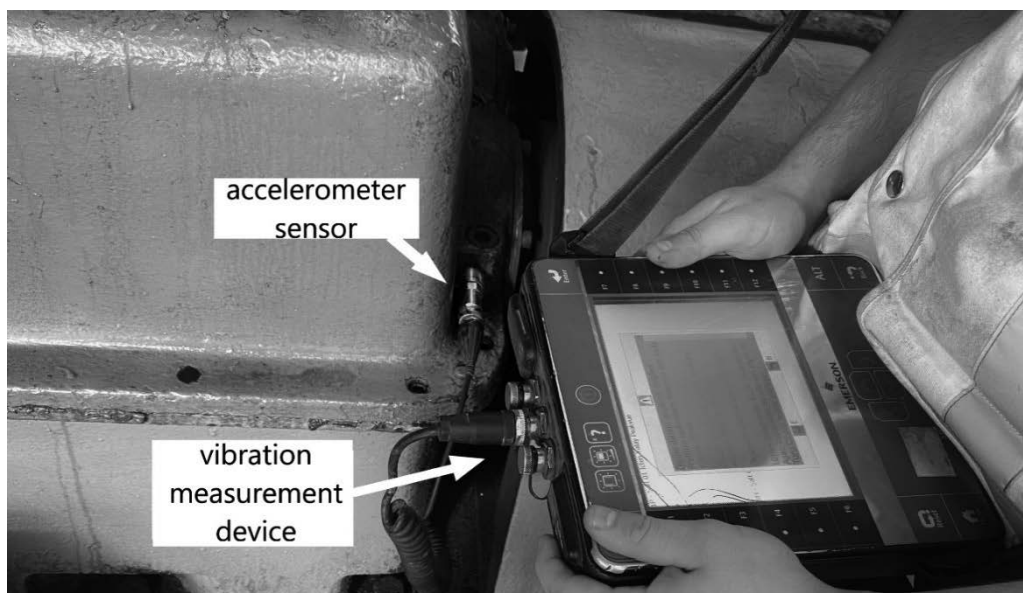


Figure 4. Vibration measurement from the horizontal axis at the inlet of the gearbox

4. RESULTS AND DISCUSSION

Although there was no definitive information about the existing issues at the outset, the current condition of the machine was evaluated based on the analyses performed, and potential solutions to the identified issues were discussed.

The results obtained from the spectrum and time-wave graphs of the motor's rear vertical measurement are presented in **Figure 5**. According to the findings, the highest peak in the motor's rear vertical measurement graph was observed at the 6x frequency component, indicating a potential for broad-band mechanical looseness at the base of this frequency. As a medium-sized machine with a 265 kW motor, it was assessed that the motor has a flexible structure due to its feet not being anchored and fixed to concrete.

According to ISO 10816-3 standards, the vibration velocity thresholds for flexible, medium-sized machines are set at 2.3 mm/s for the warning level, 4.5 mm/s for the alarm level, and 7.1 mm/s for the danger level. The measurement data from the motor's rear vertical axis are below these threshold values, and measurements from other axes also remain similarly below the standard limits.

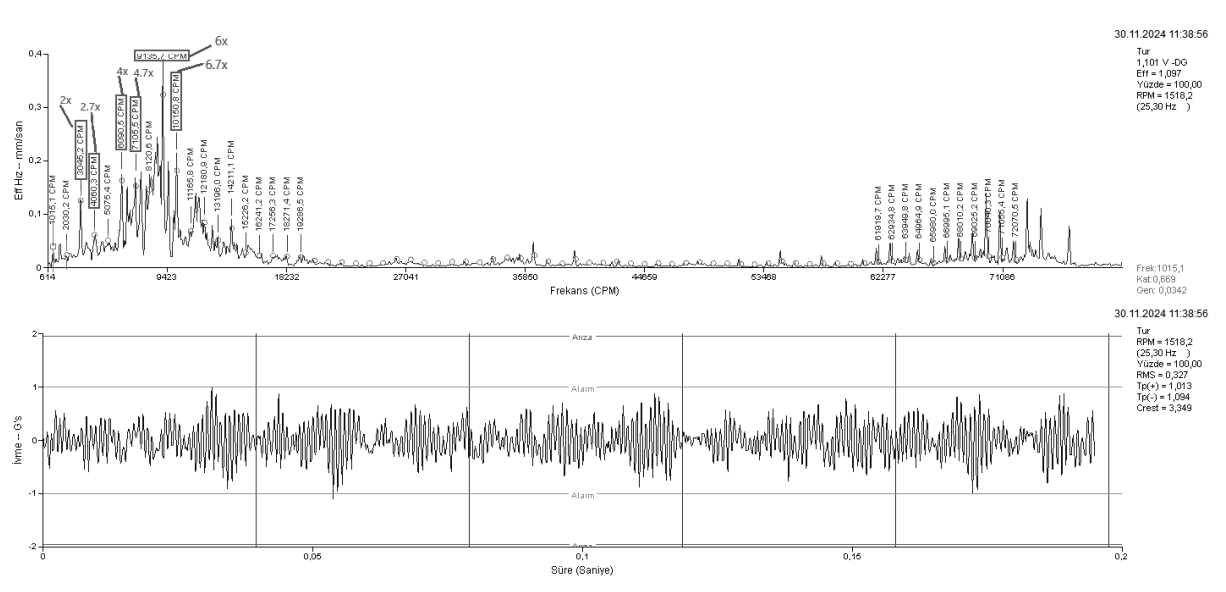


Figure 5. Engine rear vertical measurement spectrum and time-wave form

The gearbox measured consists of two stages. The operating principle of this gearbox is similar to that of a 4-speed transmission system. While shaft 1 remains stationary, shaft 2 moves along the x-axis and can shift through four stages with the assistance of a hydraulic fluid.

The spectrum and time-wave graphs for the horizontal input measurement of the gearbox's first stage are shown in **Figure 6**. According to the findings, significant mechanical looseness, likely originating from the bearings, was identified at low CPM (Cycles Per Minute) value ranges. Since the system contains only a 6316-type bearing, it is considered that this bearing may be contributing to the looseness issues. Regarding gear damage, for the second gear with an input RPM (Revolutions Per Minute) of 1518 and an output RPM of 1012, the CPM value for the gear pair Z=36 and Z=54 (Z=number of teeth) was calculated to be approximately 55,000, indicating potential damage. Similarly, for the fourth gear with an input RPM of 1518 and an output RPM of 1659, the CPM value for the gear pair Z=47 and Z=43 was found to be approximately 71,000, suggesting a high probability of damage in the fourth gear set.

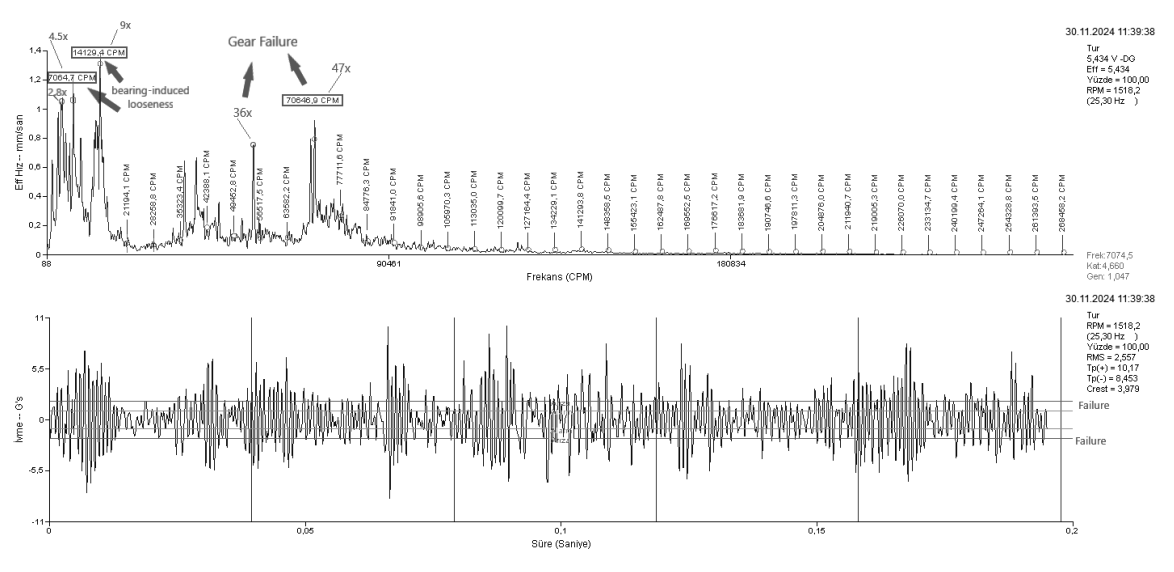


Figure 6. Reducer 1st stage input horizontal measurement spectrum and wave-time form

The spectrum and time-wave graphs for the horizontal input measurement of the gearbox's second stage are shown in **Figure 7**. According to the findings, the narrower CPM (Cycles Per Minute) range defined for the second stage (0–10,000) was more effective in identifying bearing faults. The 6316-type bearing, located at the input side of the second shaft, is considered to have a potential for damage in both its inner and outer races. However, this possibility could not be definitively confirmed due to a lack of precise alignment with the CPM values.

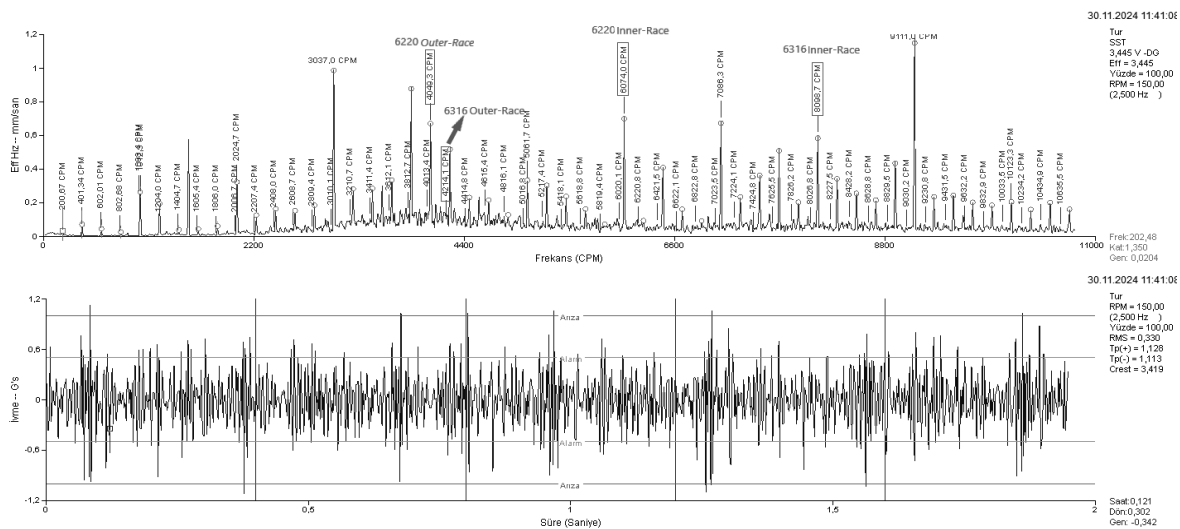


Figure 7. Reducer 2nd stage input horizontal measurement spectrum and wave-time graph

On the other hand, the 6220-type bearing, positioned at the output side of the second shaft and associated with the second gear, was observed to have a high likelihood of severe damage in both its inner and outer races. These faults were clearly visible in the vibration graph, indicating an urgent need for maintenance on these bearings. Additionally, other peak values observed in the

graph were inconsistent with the CPM values calculated. Therefore, assuming these peaks indicate faults could lead to misleading conclusions.

5. CONCLUSION

Many enterprises continue to produce without checking whether the machines they use in the production line are working properly. Mechanical looseness, axial misalignment and unbalance in production lines are among the most important factors that need to be monitored frequently. As the system operates with unbalanced, it can both cause other parts of the machine to fail and reduce product quality. In addition to these, it has been seen in the study that even the slightest unbalancing will increase production costs due to significant electricity consumption.

Vibration analysis is of indispensable value today in detecting and controlling machine failures at much earlier stages. This study explains how primary gear and bearing faults can be detected using a vibration measurement device and spectrum analysis. It is essential to take measurements regularly and compare them with baseline values to ensure that the threshold limits are not exceeded

In the study, it was determined that continuing operation with the damaged gear pair in the 4th gear and the 6220-type bearing is not considered safe for the machine. Therefore, maintenance planning should be carried out as soon as possible, and the necessary faults should be addressed promptly.

REFERENCES

- [1] Novelo, X. E. A., & Chu, H. Y. (2022). Application of vibration analysis using time-frequency analysis to detect and predict mechanical failure during the nut manufacturing process. *Advances in Mechanical Engineering*, 14(2), 16878132221082758.
- [2] Alçelik, N., & Kam, M. (2020). Dönen makinelerde aksel kaçıklık ve dengesizliğin titreşim analizi. *Bilecik Şeyh Edebali Üniversitesi Fen Bilimleri Dergisi*, 7(100. Yıl Özel Sayı), 256-269.
- [3] Ranieri, L., Cannarozzo, L., & Micelli, F. (2018). Vibration analysis in automotive applications: Fault diagnosis in motor and transmission systems. *Journal of Mechanical Science and Technology*, 32(3), 1121–1132.
- [4] Martinez, P., & Lopez, R. (2017). Predictive Maintenance in Textile Industry: A Case Study. *Journal of Industrial Automation and Maintenance*, 15(2), 345-356.
- [5] Bose, A., & Sharma, P. (2011). Cost Savings Through Predictive Maintenance in Gas Turbines. *Energy Systems Engineering Quarterly*, 9(2), 90-98.
- [6] Peng, Z. K., & Chu, F. L. (2004). Application of the wavelet transform in machine condition monitoring and fault diagnostics: A review with bibliography. *Mechanical Systems and Signal Processing*, 18(2), 199–221.
- [7] Ceyhan, H., & Kasapbaşı, M. C. (2022). Üretim sistemlerinde makine öğrenmesi ile kestirimci bakım uygulaması ve modellemesi. *Avrupa Bilim ve Teknoloji Dergisi*, (33), 167-175.



31th January 2025
Gliwice, Poland

DEPARTMENT OF ENGINEERING MATERIALS AND BIOMATERIALS
FACULTY OF MECHANICAL ENGINEERING
SILESIA UNIVERSITY OF TECHNOLOGY

INTERNATIONAL STUDENTS SCIENTIFIC CONFERENCE

Production of Cable That Changes Color at 60 °C Temperature

¹Cemal Meran, ²Kaan Kucuk, ²Ali Cagin Hatipoglu, ³Omer Eren

¹Prof.Dr., Pamukkale University, Faculty of Engineering, Department of Mechanical Engineering, Denizli, Turkey, cmeran@pau.edu.tr

²Student, Pamukkale University, Faculty of Engineering, Department of Mechanical Engineering, Denizli, Turkey

³Nexans Turkey Industry, R&D Center, Denizli, Turkey

Abstract: This thesis focuses on the use of thermochromic pigments as additives in cables by using their ability to change color with temperature. This will make it easier to recognize the cables in the event of a possible short circuit and to take precautions without preventing bigger dangers. For this, pigment that changes color at 60 degrees Celsius was used. The experiments in this thesis were carried out with the help of the R&D centers of Nexans Turkey Industry in Denizli. The test parts were carried out in the heat treatment laboratory at Pamukkale University with the help of engineering faculty lecturers. As a result of these experiments and tests, it was determined that the thermochromic pigment was used as an additive in the most cost-effective way and the amount was sufficient.

Keywords: Cable, Thermochromic, Coloring Pigment, PVC

1. INTRODUCTION

Cable, a metallic conducting wire covered with an insulating material used in the transmission of electric current. Url 1. The cables, which are defined in this way and have an important place in our lives, are protected from external factors thanks to their insulating sheaths.

Paints are used for many different purposes, such as protecting, beautifying, highlighting or drawing attention to or stimulating the materials they cover. Increasingly, new ideas and applications are developing in the coloring process. One of them is the ability to change color due to taste or needs.Url 2. Color-changing dyes or pigments are almost ubiquitous colorants and have many different functions. They can have different stimuli and respond differently. For example, the type of dyes defined as thermochromic dyes have properties such as changing color at a certain temperature, becoming colorless or revealing its color. The aim of this thesis is to use thermochromic pigments to make cables change color at the desired temperature. In this way, it will be possible to easily observe the damaged or potentially damaged areas by changing color depending on the temperature due to short circuit or any other reason. A target temperature of 60 C was chosen as the target temperature, which is slightly below the temperatures that the cable is required to withstand.

During the study, it will be important to find the appropriate thermochromic dye that can change color at 60 degrees and mix it in the compound in appropriate proportions.

In this project, unlike the common usage areas of thermochromic pigments, it is to ensure that electrical appliances such as mouse, charger, kitchen appliances, which we use everywhere to make life easier, are noticed by changing the color of that cable by heating in case of any short circuit. In this way, it prevents any dangerous situations such as fire, cable melting, etc. by seeing the danger in advance and preventing it. In this context, by conducting the necessary research and some experiments, we evaluated its suitability and cost and tried whether it can be used in our lives.

2. CABLE ADDITIVES AND COLORING PIGMENTS

A cable is a device that transmits electrical energy, connects two electrical devices and consists of one or more cores. Cable structures, except for special cables, generally consist of two main parts.

1. Conductor part: A wire or bundle of wires, consisting of one or more wires and not insulated, used to transmit electrical energy. The most common materials used for conductors are copper and aluminum.

2. Insulator part: The substance that electrically insulates the conductor. The most common materials used for insulators are thermoplastic insulators (PVC, PET), tires and paper. ^{Url 3.}

The recipe for the insulating part of the cable can be in different mixtures according to the need. Likewise, the substances added according to the need may vary. Their main components are usually polymers. This component constitutes the majority of the mixture. In addition, additives such as plasticizers, antioxidants, fillers, colorants, flame retardants, lubricants, mixing modifiers, stabilizers can be used according to the need.

Pigments are used as colorants in many different industries such as plastics, textiles and food. They give color to dyes and also add durability to the product and extend its life. Used as additives, these pigments determine the color of the final product.

Color-changing pigments change color depending on different environmental factors, giving the product an aesthetic appearance. Materials produced with these pigments change their color depending on the temperature change in the environment or in response to the light they are exposed to. In addition, depending on the area of use, they not only beautify the appearance but also provide different functions. Their application areas are quite wide and for example; temperature indicators, sensors, color changing inks, plastic industry and textile industry, safety markings, etc. It is also used in many different sectors.

Thermochromic pigments are pigments that change color according to the ambient temperature as an external stimulus. Upon reaching certain activation temperatures, these pigments change color in response and return to their original state when the temperature drops below the activation temperature. The way they change color can be from colored to colorless, from colorless to colored and from one color to one other color. Some types even have a certain range, e.g. 60 degrees activation, ± 15 degrees activation and flexibility in reversibility.

Reversible thermochromic dyes are classified into 2 different sections in the field used in the PVC industry.

1. Standard Thermochromic Pigment: These are generally the thermochromic pigments mentioned in the first part. When they reach the activation temperature, they lose their color and become colorless. When the ambient temperature drops below the activation level, they

return to their former color.

2. Reverse Thermochromic Pigment: These pigments work exactly opposite to the standards. When the ambient temperature is below the activation temperature, they look colorless, when they reach the activation temperature, their color is revealed. When it falls below the activation degree, they lose their color again and become colorless.

Most thermochromic pigments are based on the rearrangement of chemical bonds in their molecular structure upon temperature change. These pigments are encapsulated in microcapsules before application. When heat is applied to a thermochromic microcapsule, the structure of the thermochromic material inside the microcapsule changes and thus the color is lost. On cooling, the microcapsule's internal material structure reversibly returns to its original state and the microcapsule gains color. Url 4.

These chemical structure changes occur in 3 ways in thermochromic pigments. These are;

1. Proton Transfer: It is the occurrence of proton transfer with temperature change. This leads to a rearrangement of the chemical bonds of the pigment's molecules, resulting in a color change.

2. Hydrogen Bonding: Color change occurs when hydrogen bonds are broken or formed. These bonds affect the structural stability and color changing properties of the pigment.

3. Electron Distribution: Redistribution of electrons occurs in pigments when the temperature increases. This changes the optical properties of the pigment so that the absorption and reflection of light is different.[5]

3. MATERIAL AND METHODS

The experimental work was carried out at Nexans Turkey Industry in Denizli. After the production materials were received, they were taken to the production room and all processes were carried out in the extruder machine. The extruder machine is shown in Figure 1.

The test phase was carried out in the furnace in the Heat Treatment Laboratory in Pamukkale University Mechanical Engineering Faculty of Engineering, shown in Figure 2. The main cable material was supplied by Nexans and the thermochromic material by Nanorenk co. The pigments sent as samples are of two different types: black standard thermochromic and pink reverse thermochromic. The degree of activation is the same for both pigments at 60°. The dosage recommendation for thermochromic pigments is between 0.5% and 2% for PVCs.

Firstly, the mixtures were weighted according to the mixture ratios with a precision balance to prepare the mixtures in the room for production. Then the mixtures were put into bags and mixed. The recipe of our mixture, which is the cable material, is as follows; PVC Resin (powder) 40%, Calcite (filler) 40%, Stabilizer 4%, Plasticizer 16%. The addition amounts of thermochromic pigments to this mixture are as follows; black pigment was added at a rate of 1% and pink pigment at a rate of 2% in accordance with the guide.



Figure 1. Extruder Strip Sample Production Machine of NEXANS Company



Figure 2. Heat treatment furnace

The reason for adding different amounts is to observe whether it influences the material produced. The mixture was mixed by hand for about 10 minutes by closing the mouth of the bag and homogenization was ensured. Then the mixture was put into the extruder and production was started as a strip. The strip coming out of the machine came out in different colors because it was hot in the first state. As can be seen in Figure 3a and 3b, the black pigmented strip came out of the machine as white, and the pink pigmented strip came out of the machine in the first state by showing its color, that is, dark pink.



a) Black Strip



b) Pink Strip

Figure 3. Views of band extrusion from the extruder

4. RESULTS AND DISCUSSION

The produced strip was observed at different temperatures in the furnace in the laboratory to be used in the test phase and it was checked whether there was a change. With this experiment, the condition of our material at the activation temperature was observed and its effects were examined. The tested temperatures started from room temperature (about 25°) to 65 degrees, which is slightly above the activation temperature of 60 degrees. The test was performed with one black and one pink sample. The temperatures shown step by step in Figure 4 were

photographed at 25 degrees (a), 40 degrees (b) , 50 degrees (c), 55 degrees (d), 58 degrees (e), 60 degrees (f), 62 degrees (g) and 65 degrees(h) respectively.

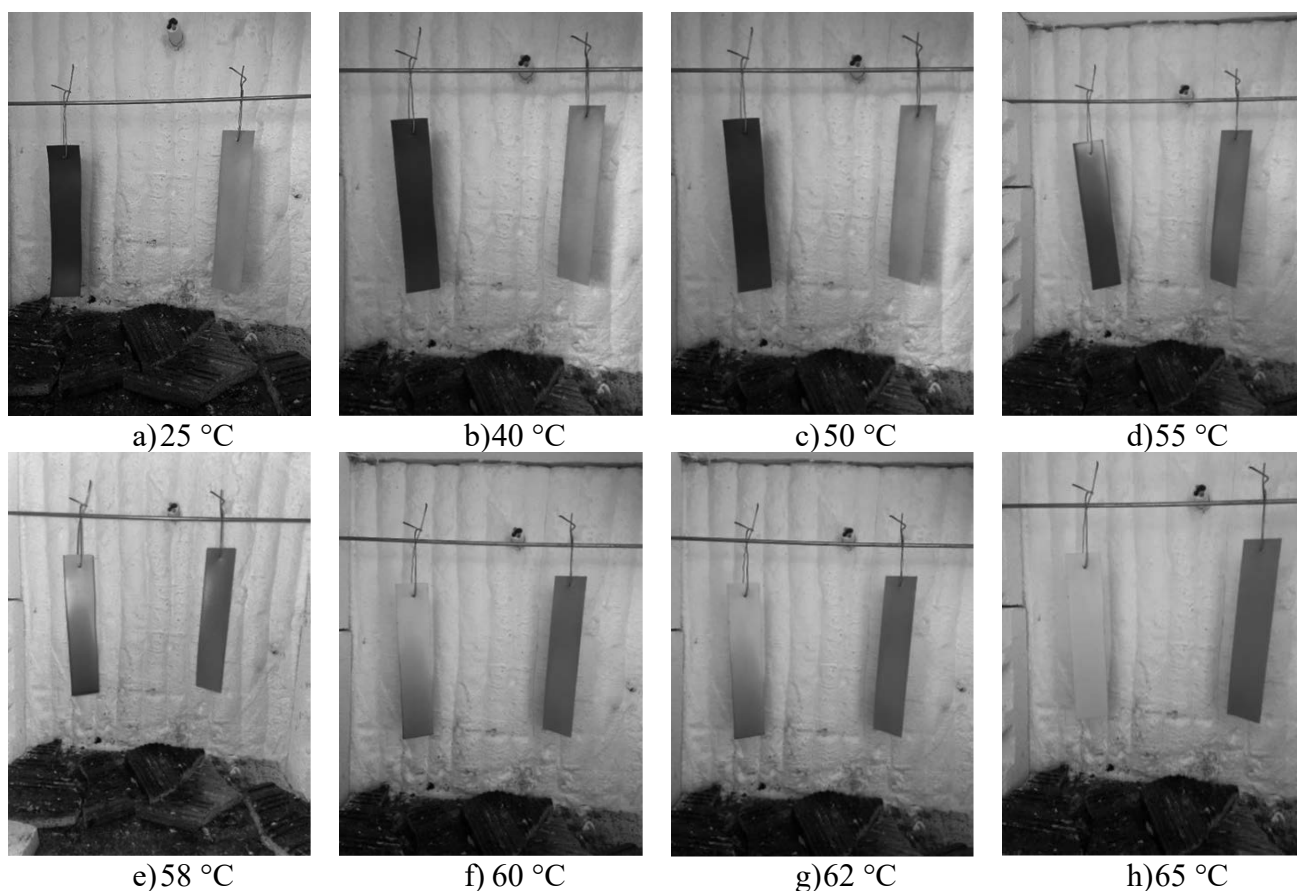


Figure 4. The view of color changing of polimer depend on temperature

As expected as a result of the above observations, no change was observed in our samples at room temperature, Figure 4a. At 40°C, the same image was obtained with room temperature, Figure 4b. However, due to the attachment of the samples with wires at the temperatures we made in the oven, the temperature was homogeneously distributed, but openings occurred, which are thought to be due to the thermal conductivity of the wires. For example, when we examined their condition at 50°C, we saw that the color of the samples started to change from the corners, Figure 4c. When we observed their condition below 55°C, we found that these color changes increased a little more, Figure 4d. As we approached the degree of activation, we started to observe the results we expected. The situation below 58°C shows a result that supports this statement, Figure 4e. When we reached 60°C; although not a complete transformation, we observed that we reached a satisfactory and noticeable change, Figure 4f. In the 62°C and 65°C observations, we can say that the color change was completed with very close results, Figure 4g and Figure 4h. This shows that the properties of our pigment fully serve its intended use and will give the necessary warning in a timely manner if used.

When the opened oven at 65°, we started to observe directly and saw that both samples reacted very quickly and returned to their original state at the end of 90 seconds. At $t=0s$, It was seen that they started to recover quickly from the corners, Figure 5a. When the looked at $t=30s$ and

$t=60$ s, it was seen that first half and then all of the black sample was restored, while the pink sample was fully restored around $t=90$ s, Figure 5b-d.

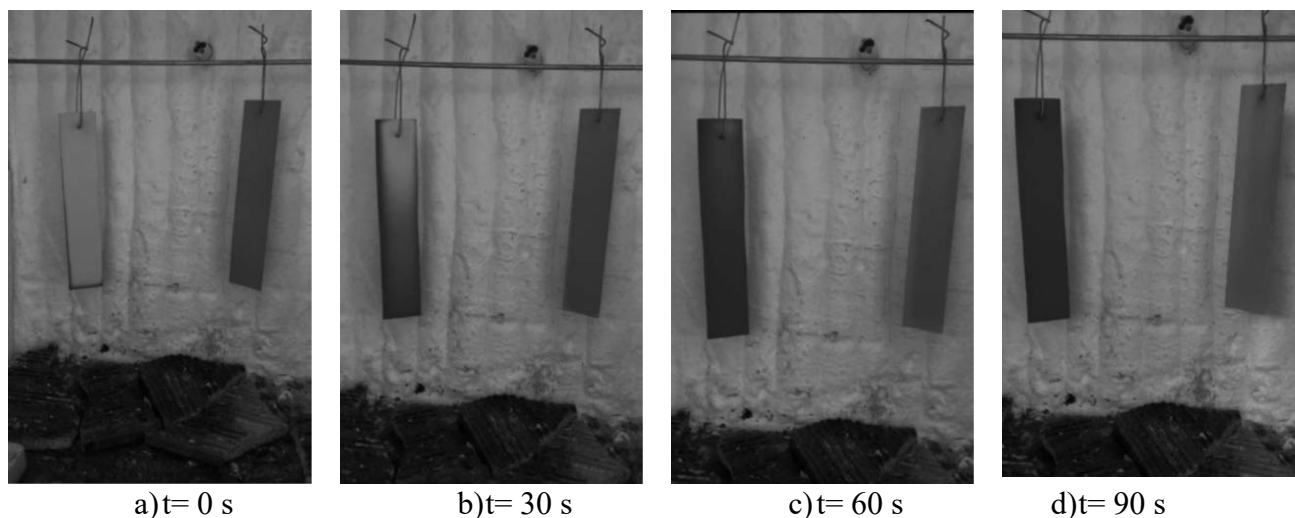


Figure 5. The view of color changing of polimer depend on time

5. CONCLUSION

Although the data obtained at the end of the experiment was sufficient, it proved that thermochromic pigment can be used in different areas of our lives and that it can have different functions other than aesthetic and pleasant appearance for us in areas such as security and precaution. The experiment showed that it can be successful in the field of detecting and preventing short circuits in cables and served as a pioneer in future studies. Despite the very small amounts added to the mixture, the thermochromic pigment showed its effect quite adequately. This is considered to be a method that can be used considering the benefits it will provide from the cost phase of the thesis.

According to these results, it was obtained the same results at the activation temperature regardless of the amount of pigment added to the mixture. It seen that the amount only affects the vividness and brightness of the color and that there will be a time delay in the recovery time that will not be important. In terms of cost, it may say that the most suitable one may vary according to the desired tone, but these pigments work for their purpose in an economical way. Considering that this method acts as an insurance and saves other costs, it is believed to be a method that should be used.

REFERENCES

- [1] Url 1 <https://tr.wikipedia.org/wiki/Kablo>
- [2] Url 2 <https://turkchem.net/renk-degistiren-maddeler>
- [3] Url 3 <https://www.sektorumdergisi.com/kablo/>
- [4] Url 4 <https://www.arcacolours.com/thermochromic-pigments/>
- [5] Bamfield, P. (2001). "Thermochromic Materials." In *Chromic Phenomena: Technological Applications of Colour Chemistry* (pp. 113-130).



31th January 2025
Gliwice, Poland

DEPARTMENT OF ENGINEERING MATERIALS AND BIOMATERIALS
FACULTY OF MECHANICAL ENGINEERING
SILESIA UNIVERSITY OF TECHNOLOGY

INTERNATIONAL STUDENTS SCIENTIFIC CONFERENCE

Modelowanie układu nóż stożkowy – uchwyt nożowy do urabiania skał

Wojciech Mikolejko ^a, Piotr Cheluszka ^b, Agata Śliwa ^a, Jarosław Mikula ^a

^a Silesian University of Technology, Faculty of Mechanical Engineering, Department of Engineering Materials and Biomaterials

email: Wojciech.mikolejko@polsl.pl, Agata.sliwa@polsl.pl, Jaroslaw.mikula@polsl.pl

^b Silesian University of Technology, Faculty of Mining, Safety Engineering and Industrial Automation, Department of Mining Mechanization and Robotization

email: Piotr.cheluszka@polsl.pl

Streszczenie: Przedmiotem analizy był nóż znajdujący zastosowanie do urabiania skał kombajnami górniczymi, stosowanymi przy drażeniu tuneli oraz eksploatacji złóż surowców mineralnych. Nóż oraz uchwyt nożowy zaprojektowano i zestawiono w programie SolidWorks, a następnie przygotowano model do analizy w oprogramowaniu Ansys. Przygotowano siatkę elementów skończonych, odebrano stopnie swobody, dodano właściwości kontaktu na odpowiednich powierzchniach elementów oraz założono ruch obrotowy.

Abstract: The subject of the analysis was a rock – cutting pick, which is used in the cutting of rock with shearers and roadheaders used in tunneling and mining of natural resource deposits. The pick and pick holder were designed and compiled in SolidWorks, and then a model was prepared for analysis in Ansys software. A finite element mesh was prepared, degrees of freedom were taken away, contact properties were added on the relevant surfaces of the components and rotational motion was assumed.

Keywords: Ansys, MES, nóż kombajnowy, symulacja

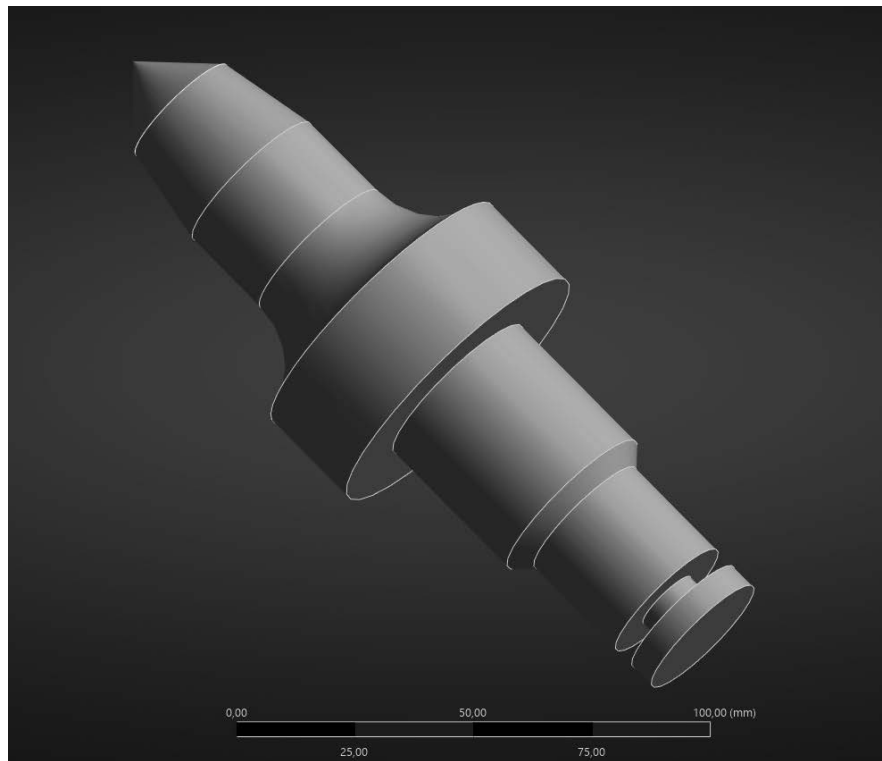
1. WSTĘP

Noże kombajnowe (rys. 1) są kluczowymi elementami górniczych maszyn urabiających wykorzystywanych w budownictwie i górnictwie do mechanicznego urabiania skał, drażeniu tuneli w różnorodnych warunkach geologicznych oraz w robotach wybierkowych. Do maszyn tych należą kombajny ścianowe stosowane w procesie wydobywania surowców mineralnych, takich jak węgiel kamienny czy inne surowce naturalne oraz kombajny chodnikowe stosowane szeroko do drażenia wyrobisk korytarzowych w kopalniach podziemnych oraz tuneli. Ich podstawowym zadaniem jest urabianie skał na zasadzie skrawania. Noże te osadzone są w uchwytach nożowych przyspawanych do pobocznic organów roboczych maszyn urabiających. Noże kombajnowe składają się z korpusu trzonka wykonanego z wysokiej jakości stali oraz ostrza z węglików spiekanych, które charakteryzują się wysoką twardością i odpornością na

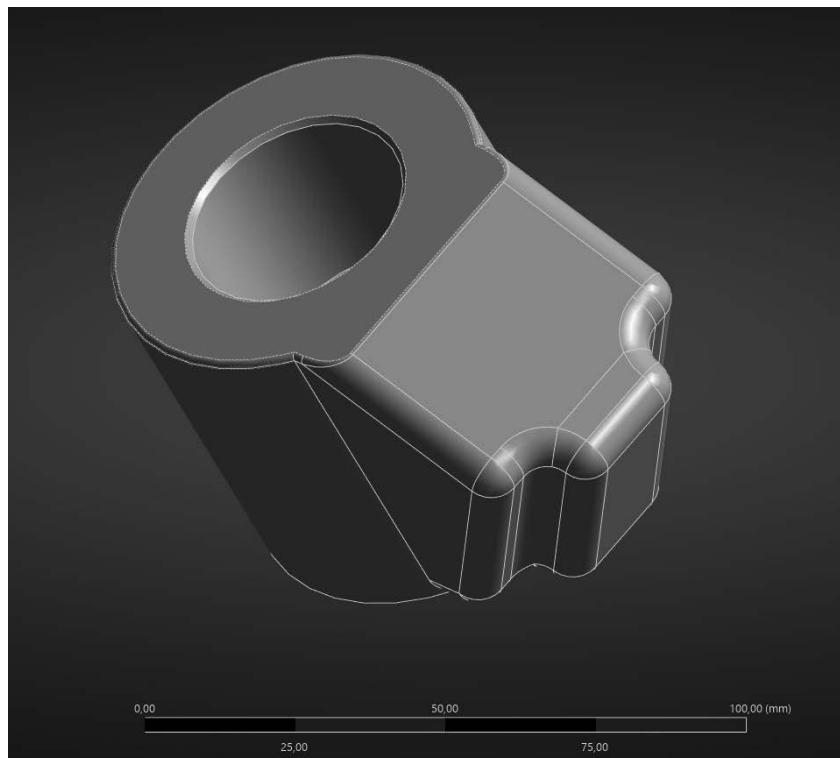
ścieranie. Proces łączenia wkładek z węglików spiekanych z trzonkiem noża odbywa się poprzez lutowanie twarde, co zapewnia trwałość i wytrzymałość narzędzia. Odpowiednie rozmieszczenie i ustawienie kątowe noży pozwala na efektywne urabianie materiału skalnego. Wysoka jakość wykonania oraz regularna kontrola stanu technicznego noży są kluczowe dla zapewnienia ciągłości i efektywności procesu wydobywczego. Wytwarzanie noży kombajnowych obejmuje zaawansowane technologie takie jak walcowanie poprzeczne, obróbka cieplna trzonków oraz technologie spiekania odpowiednio dobranych proszków na bazie węglików wolframu i kobaltu. Zastosowanie tych metod pozwala na uzyskanie narzędzi o wysokiej wytrzymałości i odporności na trudne warunki pracy w górnictwie. Podczas eksploatacji noże kombajnowe są narażone na intensywne zużycie ścierno-erozyjne oraz wykruszanie węglików spiekanych oraz zmęczenie termiczne, co może prowadzić do obniżenia skuteczności ich działania. Dlatego istotne jest monitorowanie stanu technicznego noży oraz ich regularna wymiana w celu utrzymania optymalnej wydajności kombajnu. Noże kombajnowe stanowią nieodzowny element wyposażenia maszyn górniczych, determinując efektywność i bezpieczeństwo procesu wydobywczego oraz oczekiwane postępy drażenia wyrobisk korytarzowych oraz tuneli. Ich konstrukcja, materiały użyte do produkcji oraz technologie wytwarzania są kluczowe dla zapewnienia wysokiej jakości i trwałości tych narzędzi w trudnych warunkach pracy pod ziemią [1-5].



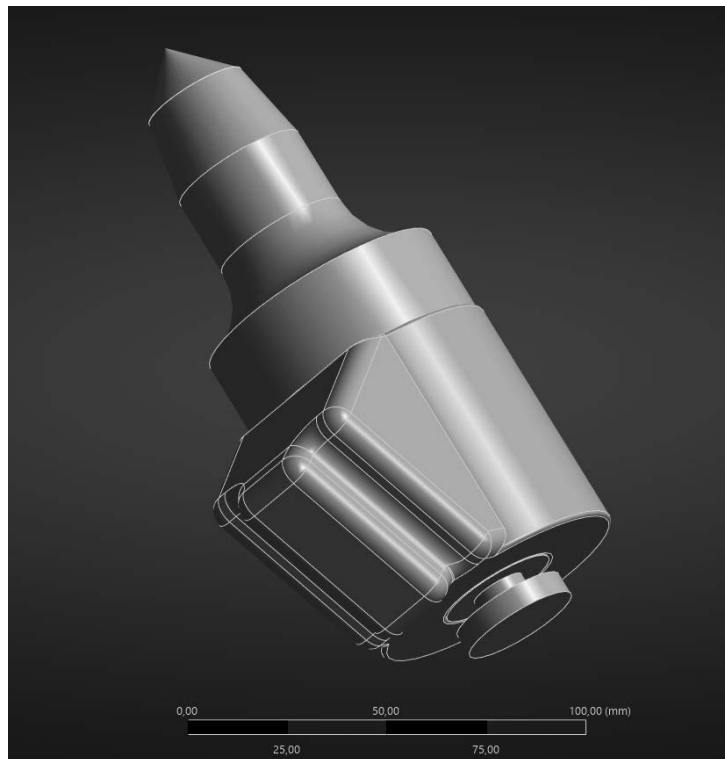
Rys. 1. Przykład noża stożkowego stosowanego w kombajnach tunelowych wraz z uchwytem montażowym [Opracowanie własne].



Rys. 2. Model noża kombajnowego zaprojektowany w programie SolidWorks [Opracowanie własne].



Rys. 3. Model uchwytu noża kombajnowego zaprojektowany w programie SolidWorks [Opracowanie własne].



Rys. 4. Model noża kombajnowego spozycjonowanego w uchwycie [Opracowanie własne].

Metoda Elementów Skończonych (MES, ang. Finite Element Method, FEM) jest jedną z najczęściej stosowanych technik numerycznych do analizy i rozwiązywania problemów inżynierskich oraz fizycznych. Jej wszechstronność umożliwia modelowanie skomplikowanych geometrii, analizę naprężeń, przepływów cieczy, transferu ciepła oraz wielu innych zjawisk występujących w mechanice, budownictwie, termodynamice czy elektrotechnice. Metoda elementów skończonych polega na rozbiciu ciągłej dziedziny, takiej jak konstrukcja mechaniczna, na dyskretne, mniejsze fragmenty zwane elementami skończonymi. Każdy z tych elementów reprezentowany jest przez zestaw funkcji aproksymujących (funkcje kształtu), które opisują rozkład wielkości fizycznych w jego wnętrzu. Podstawowym krokiem w MES jest sformułowanie równań różniczkowych problemu, które następnie przekształca się w układ równań algebraicznych. Rozwiązanie tego układu pozwala na wyznaczenie przybliżonych wartości szukanych wielkości w węzłach siatki dyskretnej. Etapy analizy w MES:

- modelowanie geometryczne: definiowanie geometrii badanego obiektu.
- podział na elementy (meshowanie): tworzenie siatki elementów skończonych, która jest kluczowa dla dokładności obliczeń.
- definicja warunków brzegowych i obciążeń: określenie obciążeń zewnętrznych, sił, temperatur lub innych wielkości wpływających na obiekt.
- rozwiązanie: obliczenie rozkładów pól, takich jak naprężenia, odkształcenia czy przepływ energii.
- analiza wyników: wizualizacja i interpretacja wyników w formie map konturowych, wykresów czy animacji.

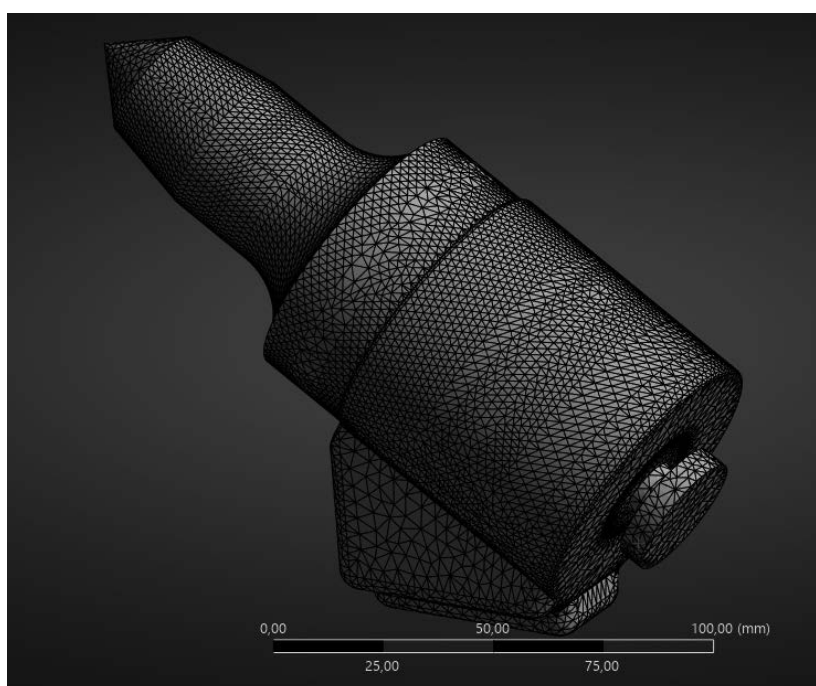
Metoda Elementów Skończonych znajduje zastosowanie w wielu dziedzinach inżynierii i nauki, m.in.: mechanice konstrukcji: analiza naprężeń, odkształceń i stabilności konstrukcji stalowych, betonowych czy kompozytowych, termodynamika: badanie przewodzenia ciepła,

wymiany ciepła w elementach oraz procesów chłodzenia, mechanice płynów: symulacje przepływów cieczy i gazów w kanałach, rurociągach oraz otwartych zbiornikach, biotechnologia: modelowanie struktur biologicznych, takich jak kości czy implanty, przemysł lotniczy i samochodowy: projektowanie aerodynamiczne oraz analiza wytrzymałości komponentów. Do zalet zastosowanie MES należą między innymi: możliwość analizy złożonych geometrii i warunków brzegowych, wszechstronność w zakresie różnych dziedzin fizyki, dostępność nowoczesnych narzędzi i oprogramowania (ANSYS, Abaqus, COMSOL).

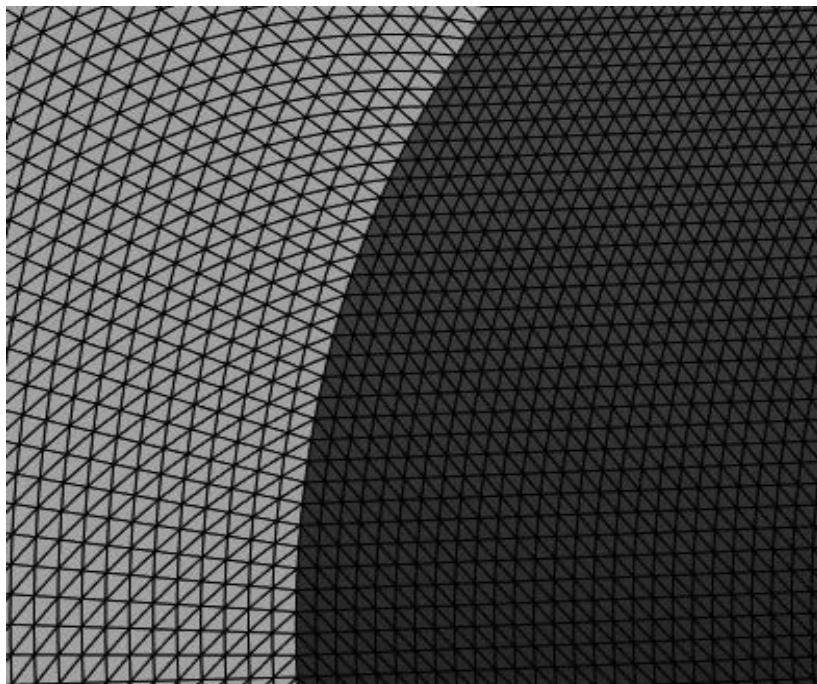
Do ograniczeń metody elementów skończonych należy zaliczyć: wysokie wymagania obliczeniowe dla skomplikowanych modeli, konieczność dokładnego przygotowania modelu oraz definiowania warunków brzegowych, wyniki są zależne od jakości siatki i parametrów modelowania [6-10].

2. METODYKA BADAWCZA

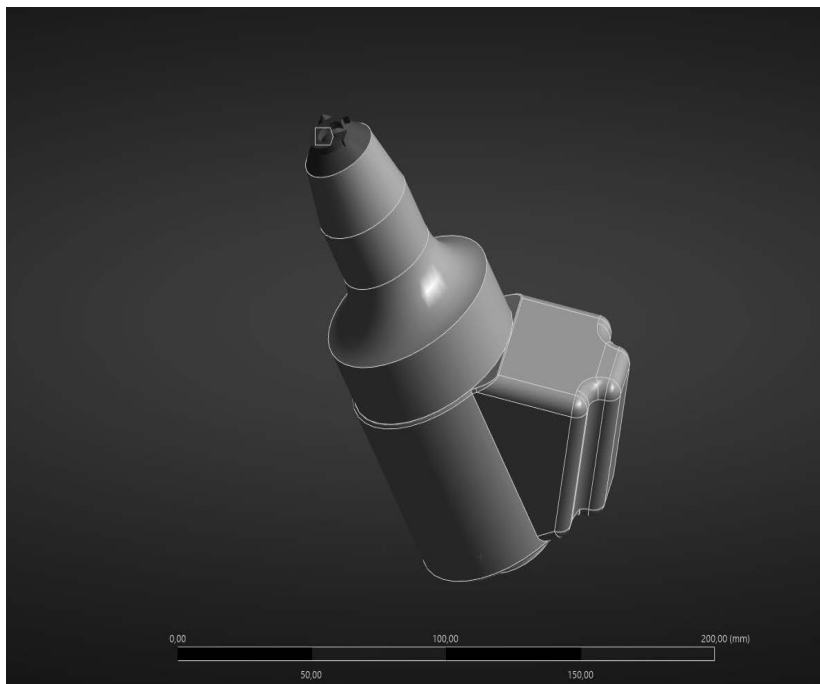
Pierwszym krokiem było zamodelowanie noża i uchwytu nożowego, a następnie spozycjonowanie noża w jego gnieździe (rys. 2 – 4) w programie SolidWorks. Dalej tak przygotowany model zaimportowano do środowiska programu Ansys. Tam z kolei przygotowano siatkę elementów skończonych (rys. 5-6) o rozmiarach: 2 [mm] na powierzchni kontaktowej noża, 5 [mm] na pozostałych jego powierzchniach, 3 [mm] na powierzchni kontaktowej uchwytu nożowego i 5 [mm] na pozostałych jego powierzchniach. Kolejnym etapem było wprowadzenie noża w ruch obrotowy względem jego osi podłużnej w wyniku przyłożenia do jego ostrza momentu obrotowego (rys. 7). Ostatnim krokiem było przygotowanie powierzchni kontaktowych pomiędzy nożem, a gniazdem (rys. 8), zastosowano kontakt typu „frictional” ze współczynnikiem tarcia typowym dla pary cieńej stal – stal $\mu=0,2$. Celem pracy była budowa poprawnie działającego modelu, układu nóż stożkowy – uchwyt nożowy. Model ten będzie stanowił podstawę do ustalenia warunków koniecznych do zapewnienia rotacji noża podczas procesu urabiania skał.



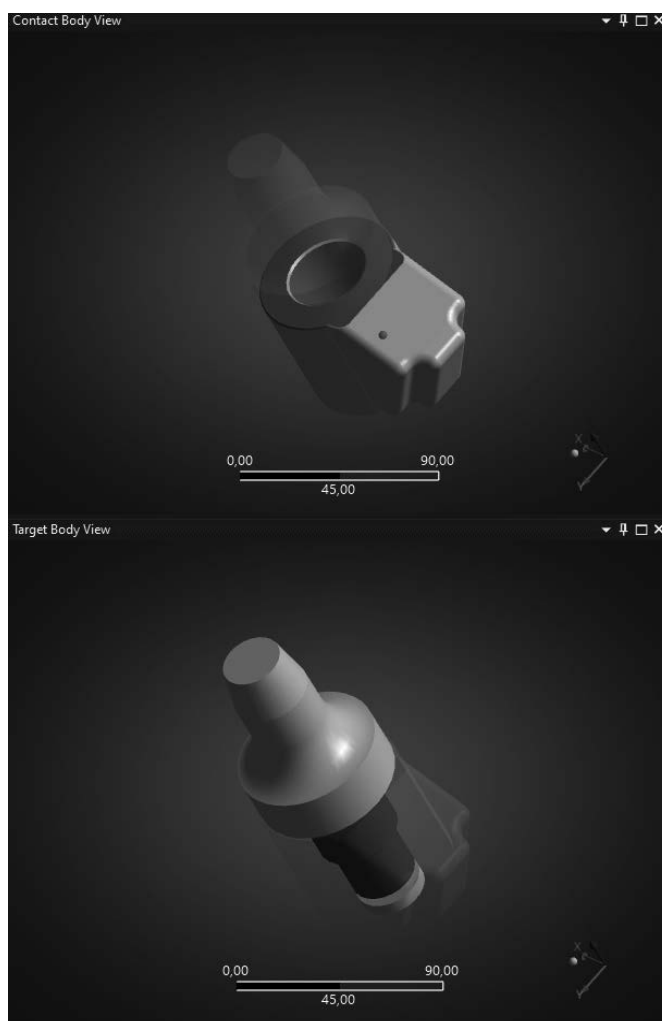
Rys. 5. Model z nałożoną siatką elementów skończonych wykonany w programie Ansys.



Rys. 6. Powierzchnia kontaktowa z nałożoną siatką elementów skończonych wykonana w programie Ansys.



Rys. 7. Model z oznaczonym miejscem przyłożenia momentu obrotowego wykonany w programie Ansys.



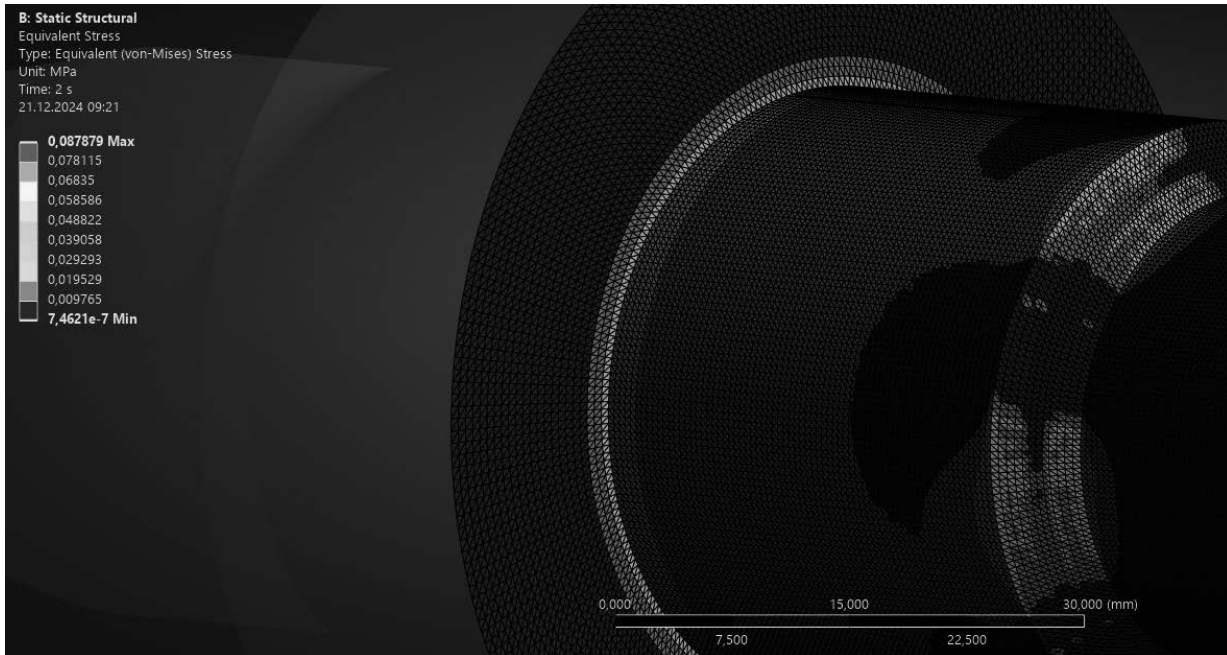
Rys. 8. Powierzchnie kontaktowe modelu wykonane w programie Ansys.

3. PODSUMOWANIE

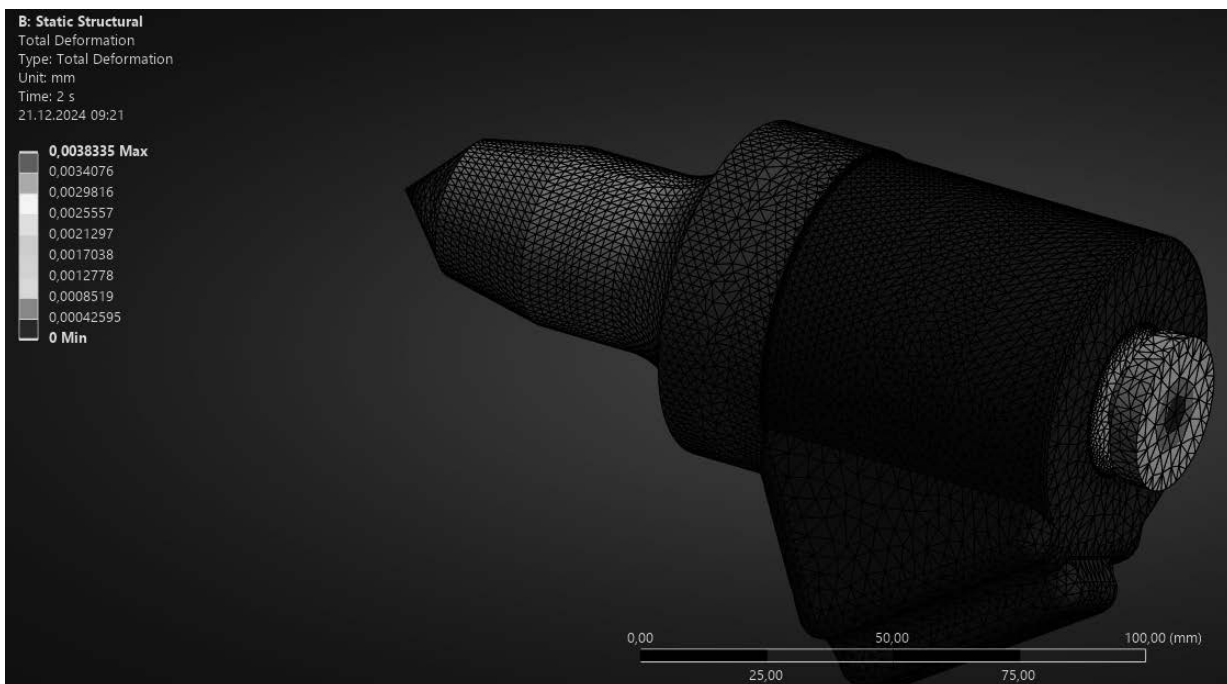
Opracowany model symulacyjny w środowisku Ansys pozwala na badanie stanu naprężenia i odkształcenia w trzonku noża oraz jego współpracy z gniazdem w uchwycie nożowym. Zamodelowane warunki brzegowe pozwalają na swobodny obrót noża względem uchwytu co jest warunkiem równomiernego zużycia jego ostrza. Model ten stanowi punkt wyjścia do określenia warunków niezbędnych dla zapewnienia obrotu noża w trakcie urabiania skał. Zbadanie możliwości obrotu noża w trakcie urabiania wymaga uwzględnienia rzeczywistego stanu obciążenia noża. W wyniku przeprowadzonego eksperymentu numerycznego uzyskano wykresy rozkładu naprężeń w miejscach kontaktowych (rys. 9) oraz przemieszczenia (rys. 10). Rysunek 9 przedstawiający mapę naprężeń wykazał ich koncentrację w obszarze sfazowania, związanego z stopniowaniem średnicy trzonka noża oraz na kołnierzu oporowym noża, w miejscu jego osadzenia na powierzchni czołowej uchwytu nożowego. Przemieszczenia przedstawione na rysunku 10 wskazują na obrotowy charakter pracy noża, co potwierdza prawidłowe założenia modelu.

Tab. 1. Wyniki rozkładu naprężeń zredukowanych na powierzchniach kontaktowych.

	Time [s]	<input checked="" type="checkbox"/> Minimum [MPa]	<input checked="" type="checkbox"/> Maximum [MPa]	<input checked="" type="checkbox"/> Average [MPa]
1	1.	1,5396e-006	9,7661e-002	6,1992e-003
2	2.	8,808e-008	9,3733e-002	6,0547e-003



Rys. 9. Rozkład naprężeń zredukowanych na powierzchniach kontaktowych noża.



Rys. 10. Rozkład przemieszczeń noża osadzonego w gnieździe.

LITERATURA

1. Cheluszka. P., Mięka S., Mięka J., Fries J.; „Improving the operational durability of tangential-rotary picks for rock cutting with central spraying and hydrodynamic rotation.” *Scientific Reports* | (2024) 14:12946 | <https://doi.org/10.1038/s41598-024-63733-1>
2. Mirski Z., Piwowarczyk T.; „Kombajnowe noże obrotowe zbrojone węglkami spiekanyymi w przemyśle wydobywczym.” *Transport Przemysłowy i Maszyny Robocze*. Wydawnictwo HMR-TRANS Sp. z o.o. 2011
3. <https://www.gfn.com.pl/noze-kombajnowe>
4. <https://mas.pl/produkty-dla-gornictwa/czesci-podzespoly-i-materialy-do-produkcji-urzadzen-gornicznych/narzedzia-urabiajace-noze-kombajnowe/>
5. Cheluszka. P., Mięka S., Mięka J.; „Wykorzystanie zgniotu powierzchniowego do polepszenia trwałości eksploatacyjnej trzonek noży kombajnów górniczych.” *Przegląd górniczy* nr 12, 2019.
6. Zienkiewicz, O. C., Taylor, R. L. *The Finite Element Method: Its Basis and Fundamentals*. Elsevier, 2005.
7. Bathe, K. J. *Finite Element Procedures*. Prentice Hall, 1996.
8. Reddy, J. N. *An Introduction to the Finite Element Method*. McGraw Hill, 2006.
9. Hughes, T. J. R. *The Finite Element Method: Linear Static and Dynamic Finite Element Analysis*. Dover Publications, 2000.
10. Cook, R. D., Malkus, D. S., Plesha, M. E. *Concepts and Applications of Finite Element Analysis*. John Wiley & Sons, 2002.



31th January 2025
Gliwice, Poland

DEPARTMENT OF ENGINEERING MATERIALS AND BIOMATERIALS
FACULTY OF MECHANICAL ENGINEERING
SILESIA UNIVERSITY OF TECHNOLOGY

INTERNATIONAL STUDENTS SCIENTIFIC CONFERENCE

Analiza rozkładu naprężeń występujących w ciernym układzie hamulcowym

Mateusz Musialik^a, Alan Nowak^a, Łukasz Mann^b, Daniel Pella^c, Amadeusz Dziwis^d, Wojciech Mikolejko^d, Agata Śliwa^d

^a Uczniowie Zespołu Szkół Technicznych i Ogólnokształcących „Mechanik” w Tarnowskich Górach

email: musialmati123321@gmail.com, nowakalan685@gmail.com

^b Nauczyciel Zespołu Szkół Technicznych i Ogólnokształcących „Mechanik” w Tarnowskich Górach

email: l.mann@mechaniktg.pl

^c Student Politechnika Śląska, Wydział Mechaniczny Technologiczny,

email: dp316755@student.polsl.pl

^d Politechnika Śląska, Wydział Mechaniczny Technologiczny, Katedra Materiałów Inżynierskich i Biomedycznych

email: amadeusz.dziwis@polsl.pl, wojciech.mikolejko@polsl.pl, agata.sliwa@polsl.pl

Streszczenie: W niniejszym artykule przedstawiono wyniki statycznej analizy wytrzymałościowej pary ciernej występującej w tarczowym układzie hamulcowym. W tym celu wykonano model tarcza-okładziny, a następnie wykonano symulację komputerową wykorzystując program SolidWorks.

Abstract: In the following article the static strength analysis of friction pair occurring in the disc brake system was presented. For this purpose, the disc-lining model was made and then, using SolidWorks, the simulation was carried out.

Słowa kluczowe: pary cierne, hamulec tarczowy, symulacja, SolidWorks

1. WSTĘP

Jednym z najważniejszych systemów bezpieczeństwa w przemyśle samochodowym jest układ hamulcowy pojazdów. Z tego względu stawiane są mu bardzo rygorystyczne wymagania i kryteria oceny. System hamulcowy samochodu musi zapewniać [1]:

- zatrzymanie samochodu na dystansie nie przekraczającym maksymalnej dopuszczalnej długości drogi hamowania,
- możliwość regulacji prędkości samochodu w zależności od warunków ruchowych,

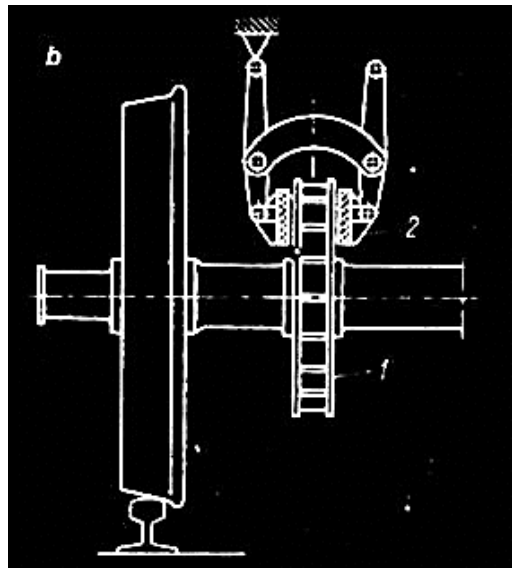
Z punktu widzenia inżynierii materiałowej kluczową rolę odgrywają pary cierne występujące w hamulcach. W przypadku elementów hamulców dobór odpowiednich materiałów warunkuje bezpieczeństwo pojazdu, redukcję masy pociągu w wyniku obniżenia

masy hamulców, polepszenie odporności korozyjnej oraz własności trybologicznych. Istotną cechą materiałów na pary cierne jest współczynnik cieplny, ponieważ elementy hamulców pracują w wysokich temperaturach, w pociągach osiągających nawet 800°C [1].

W kolejnictwie najczęściej stosowane są hamulce cierne. Podstawowymi typami hamulców ciernych są hamulce klockowe, tarczowe, i szynowe. W hamulcach klockowych i tarczowych para cierna tworzona jest przez element obrotowy wraz z mogącym się do niego dociskać w miarę potrzeby drugim elementem ciernym, połączonym przegubem z ramą wózka lub nadwozia pojazdu [2]

W hamulcach tarczowych (rys. 1) elementem obrotowym pary cierniej jest specjalna tarcza, osadzona na stałe na zestawie kołowym. Z tą tarczą współpracują szczęki pokryte okładziną cierną. Okładzina cierna przenosi siłę tarcia z tarczy obrotowej na oś koła zestawu. W pojazdach szynowych, ze względu na ciągły wzrost prędkości jazdy w celu uzyskania wymaganej drogi hamowania, stosuje się hamulec tarczowy jako hamulec zasadniczy [2-3].

Do niewielu wad hamulca tarczowego zalicza się brak możliwości kontroli stanu pary cierniej tarcza-okładzina w całym procesie eksploatacji.



Rys. 1. Schemat hamulca tarczowego, 1 – element obrotowy, 2 – element dociskający

Fig. 1. Disc brake scheme, 1 – rotary component, 2 – pressing component

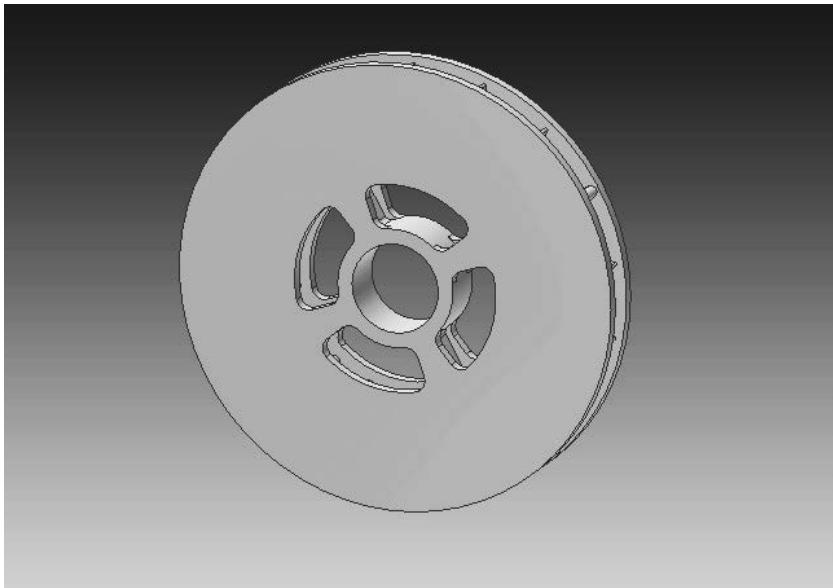
2. MODEL CAD

Modele tarczy hamulcowej (rys. 2) oraz okładziny (rys. 4) wykonane zostały w programie AutodeskInventorProfesiona. Posługując się operacjami, w jakie wyposażone jest oprogramowanie, zamodelowano odpowiedni kształt tarczy wraz z systemem wentylacji a także uproszczony model okładziny. Projekt zakłada prostotę elementu, mającą na celu usprawnienie procesu wytwarzania i obróbki tarczy.

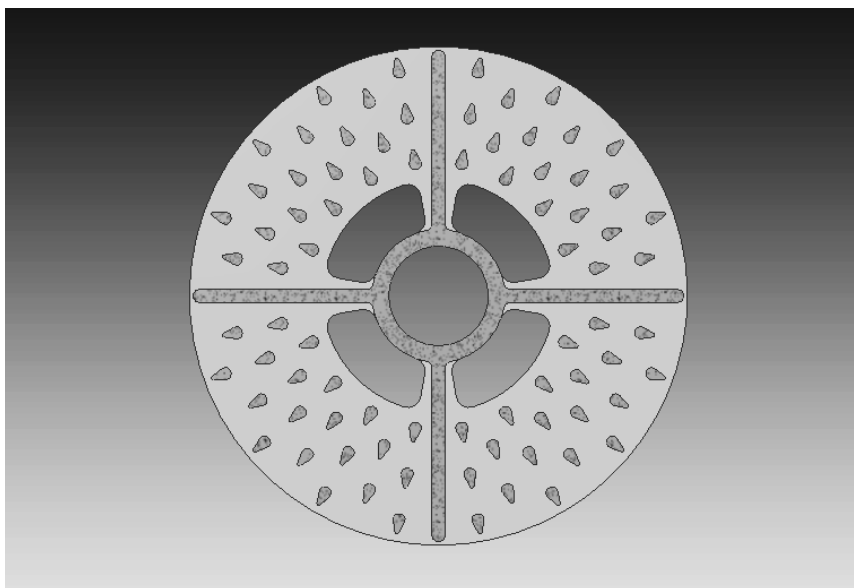
Funkcję wentylacyjną pełnić mają poprzeczne elementy łączące płyty tarczy (rys. 3), charakteryzujące się aerodynamicznym kształtem, który ma usprawniać przepływ powietrza i chłodzenie detalu. Wykorzystanie podobnego kształtu prętów znaleźć można np. w patencie

nr US 4865167 A z 1987 r. czy patencie nr US 20090272609 A1 z 2009 r. Odpowiednie rozmieszczenie elementów wentylacyjnych pozwala na lepsze chłodzenie tarczy, a tym samym wydłużenie czasu jej eksploatacji. Rozwiązanie to w porównaniu z klasycznymi kanałami wentylującymi umożliwia obniżenie masy tarczy przy jednoczesnym polepszeniu przepływu powietrza wewnątrz tarczy.

Stosowanie otworów jest jednym z podstawowych sposobów obniżania masy elementów, wskazuje na to wiele patentów, m.in.: EP 0085361 A1 z 1983 r., US 20070181389 A1 z 2007 r., US 7066306 B2 z 2006 r.

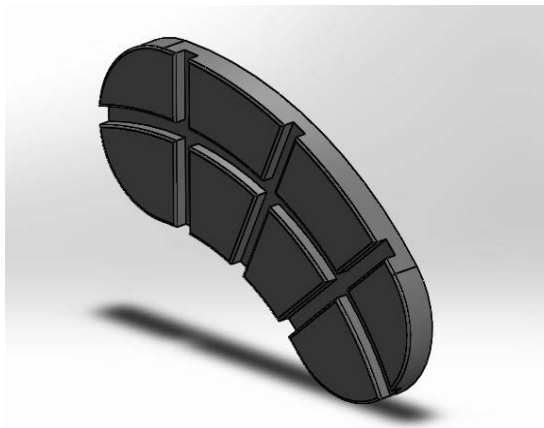


Rys. 2. Model 3D tarczy hamulcowej
Fig. 2. Model of the brake disc



Rys. 3. Przekrój modelu tarczy
Fig. 3. Section model of the brake disc

W celu dodatkowego ograniczenia masy tarczy wykonano cztery otwory przy kołnierzu tarczy, które wzmocnione zostały poprzez dodanie żeber. Okładzinę tarczy zamodelowano w oparciu o nowe wymagania dla okładzin ciernych hamulców tarczowych pojazdów kolejowych, określających m.in. cechy geometryczne okładzin oraz procedury homologacyjne [4]. Przyjęto powierzchnię kontaktową okładziny równą 200 cm^2 . Kształt okładziny odpowiadać miał geometrii tarczy. W kontaktowej części okładziny zastosowano rowki, mające na celu usprawnienie chłodzenia elementu.

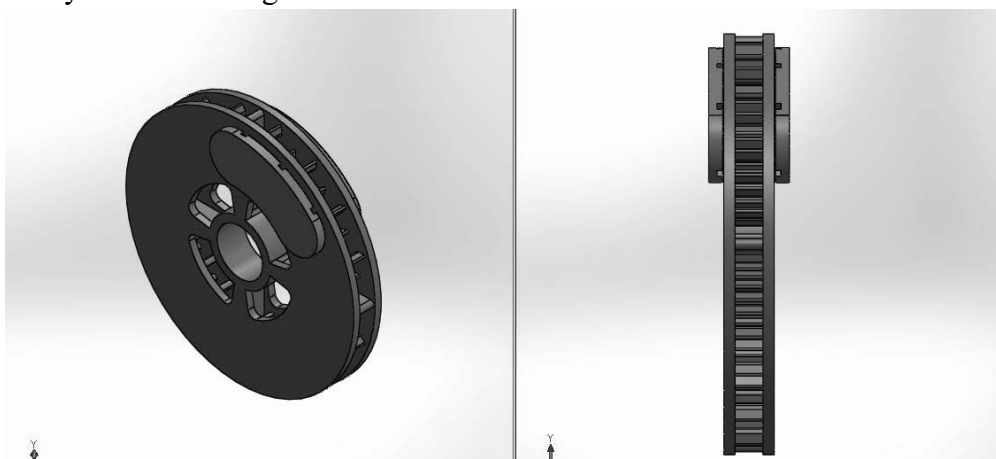


Rys. 4. Model okładziny

Fig. 4. Model of the brake pad

3. SYMULACJA WYTRZYMAŁOŚCIOWA

Statyczną analizę wytrzymałościową wykonano z wykorzystaniem narzędzi dostępnych w programie SolidWorks 2015 – dodatku SolidWorks Simulation. W symulacji rozważany był układ tarcza – dwie okładziny (rys. 5). Celem symulacji było określenie naprężeń występujących w układzie, ewentualnych odkształceń elementów oraz stwierdzenie ogólnej wytrzymałości zamodelowanego rozwiązania. W analizie przyjęto, że tarcza wykonana jest z żeliwa szarego, natomiast okładziny ze staliwa węglowego. Założono również współczynnik tarcia między powierzchniami kontaktowymi wynoszący 0,35. Wartość ta uznawana jest za najbardziej optymalną dla par ciernych hamulca tarczowego [5]. Łączna masa układu elementów wynosi ok. 140 kg



Rys. 5. Złożenie tarczy hamulcowej z okładzinami

Fig. 6. Brake disc and pads assembly



Rys. 6. Umocowania oraz obciążenia zewnętrzne przyjęte w analizie
Fig. 6. Constants and applied forces

Tarcza została umocowana wykorzystując nieruchomą geometrię na wewnętrznej ścianie kołnierza (rys. 6). Ma to w uproszczeniu symulować przytwierdzenie tarczy do piasty. Siła przyłożona do każdej z okładzin wynosiła 25kN. W literaturze wartość ta odpowiada sile potrzebnej do zatrzymania pociągu. Analizę rozpoczęto poprzez wygenerowanie siatki bryłowej o rozmiarze elementu 17.4666 mm oraz tolerancji 0.87333mm (rys. 7).



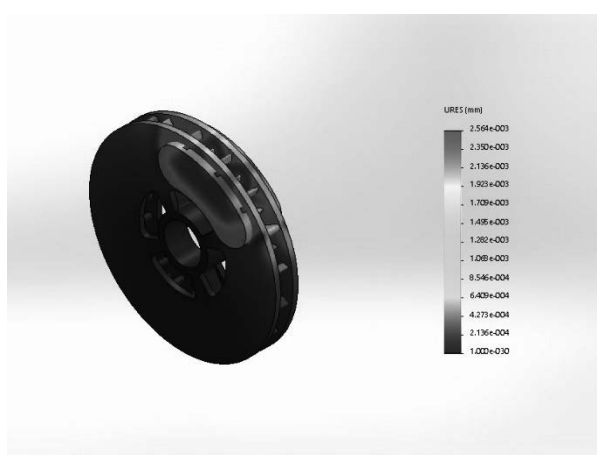
Rys. 7. Złożenie po wygenerowaniu siatki
Fig. 7. Assembly with generated mesh

8.1. Wyniki symulacji

W tabeli 1 zostały zestawione punkty maksymalnych i minimalnych naprężeń, przemieszczeń oraz odkształceń występujących w rozważanym układzie okładzina-tarcza. Na rysunkach 8-10 przedstawiono graficzną prezentację przemieszczeń, odkształceń oraz naprężeń zredukowanych wg Missesa, które występują w układzie tarcza-okładziny podczas hamowania.

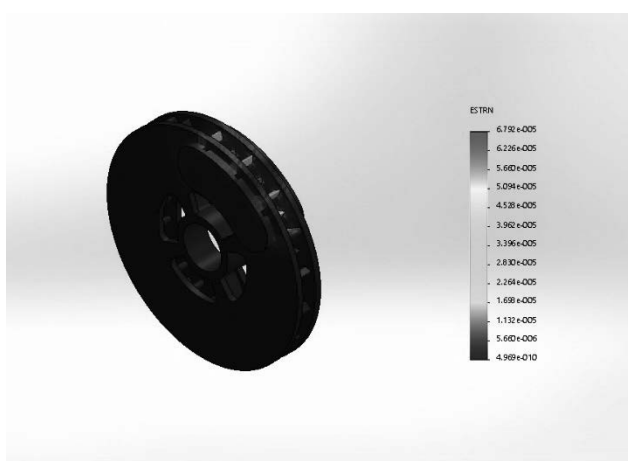
Tabela 1. Punkty maksymalnych i minimalnych naprężeń, przemieszczeń oraz odkształceń
 Table 1. Points of maximum and minimal stresses, static displacements and deformations

Nazwa	Typ	Min	Max
Naprężenie1	VON: Naprężenie zredukowane wg Misesa	18.8177 N/m ² Węzeł: 50732	6.54892e+006 N/m ² Węzeł: 54009
Nazwa	Typ	Min	Max
Przemieszczenie1	URES: Wypadkowe przemieszczenie	0 mm Węzeł: 328	0.00256367 mm Węzeł: 85457
Nazwa	Typ	Min	Max
Odształcenie1	ESTRN: Odształcenie równoważne	4.9691e-010 Element: 32829	6.79185e-005 Element: 796



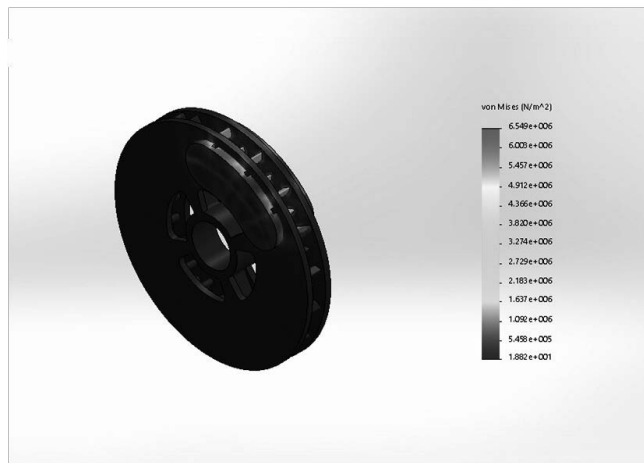
Rys. 8. Graficzna prezentacja przemieszczeń występujących w układzie tarcza-okładziny podczas hamowania

Fig. 8. Graphic representation of displacement occurring in brake disc-pads setup during braking



Rys. 9. Graficzna prezentacja odkształceń występujących w układzie tarcza-okładziny podczas hamowania

Fig 9. Graphic representation of deformations occurring in brake disc-pads setup during braking



Rys. 10. Graficzna prezentacja naprężeń zredukowanych wg Missesa występujących w układzie tarcza-okładziny podczas hamowania

Fig. 10. Graphic representation of Von Mises stresses occurring in brake disc-pads setup during braking

4. WNIOSKI

Przeprowadzona statyczna analiza wytrzymałościowa pozwala stwierdzić, że elementy spełniają postawione przed nimi wymagania eksploatacyjne. Występujące naprężenia są bardzo niskie, a materiał wybrany na tarczę posiada wystarczające własności wytrzymałościowe. Sama konstrukcja tarczy hamulcowej umożliwia prawidłowe przenoszenie naprężeń oraz nie ulega odkształceniu. Analiza nie wykazała żadnych deformacji elementów, a więc konstrukcja jest dostatecznie wytrzymała.

Zamodelowane elementy nie powinny ulegać deformacjom ani pęknięciom, które wykluczałyby je z użytku. W wyniku symulacji układu tarcza – okładzina można stwierdzić, że elementy te wytrzymają warunki eksploatacyjne i naprężenia występujące w układzie w wyniku działania sił hamujących.

5. PODSUMOWANIE

Hamulce są jednym z najważniejszych systemów bezpieczeństwa w samochodzie, których zadaniem jest regulowanie prędkości pojazdu w zależności od warunków ruchowych, a przede wszystkim zatrzymanie samochodu na dystansie krótszym niż maksymalna dopuszczalna długość drogi hamowania. Kształt tarczy oraz okładzin zamodelowano w oprogramowaniu CAD i modele te poddano statycznej analizie wytrzymałościowej. Zaproponowane rozwiązanie spełniło postawione wymagania, pozostawiając miejsce dla dalszej optymalizacji postaci konstrukcyjnej. Przy dalszej analizie należałoby uwzględnić również wpływ temperatury, która mogła by wpłynąć niekorzystnie na wytrzymałość podzespołów.

LITERATURA

1. Kukulski J., Badania stanowiskowe tarczy hamulcowej, *Prace Instytutu Kolejnictwa* 148 (2015) 47-49.
2. Gruszewski M., Wybrane zagadnienia eksploatacji hamulca tarczowego, *Technika transportu Szynowego, Technika Transportu Szynowego* 6-7 (1995) 84-86.
3. Kalinkowski A., Orlik A., *Wagony kolejowe i hamulce*, Wydawnictwo Komunikacji i Łączności, Warszawa, 1981.
4. Osiak A., Nowe wymagania dla okładzin ciernych do hamulców tarczowych pojazdów kolejowych, *TTS Technika Transportu Szynowego* 7-8 (2003) 54-63.
5. Sawczuk W., Wprowadzenie do zjawisk nieliniowych występujących w strefie kontaktu okładziny ciernej z tarczą hamulcową pojazdów szynowych, *Logistyka* 3 (2015) 4310-4316.

